RECENTS PROGRES
EN GENIE DES PROCEDES

No.79
Volume 15 - 2001

Tracers and tracing methods

RECENTS PROGRES EN GENIE DES PROCEDES

Une collection dédiée aux Congrès tenus en France dans le domaine du Génie des Procédés

Directeurs de la collection:

Georges Grévillot et Alain Storck
Laboratoire des Sciences du Génie Chimique- CNRS
Ecole Nationale Supérieure des Industries Chimiques
Nancy, France

Editeur:

Société Française de Génie des Procédés
(Membre de la Fédération Européenne de Génie Chimique)
1, rue Grandville BP 451, 54001 Nancy cedex, France

Diffuseur:

Technique et Documentation-Lavoisier
14, rue de Provigny 94236 Cachan cedex, France

La collection est référencée dans les bases de données bibliographiques:
Pascal-INIST et Chemical Abstracts Service (CAS)

Derniers numéros parus:

Volume-année	N°	Titre	
Volume 13-1999	63	Matériaux divisés	250 p
	64	Product engineering and chemical engineering now	624 p
	65	Process engineering fundamentals	342 p
	66	Heat, mass and momentum transfers-I	452 p
	67	Heat, mass and momentum transfers-II	308 p
	68	Separations	522 p
	69	Tools for process understanding and control	434 p
	70	Process / system engineering	576 p
	71	Specific processes and technologies	570 p
	72	La simulation: quelques aspects en Sciences pour l'Ingénieu	233 p
Volume 14-2000	73	Prospective en expérimentations: quelques aspects en SPI	120 p
	74	Intégration des membranes dans les procédés	358 p
	75	Fluidization-I	400 p
	76	Fluidization-II	292 p
Volume 15-2001	77	Science et technologie des poudres	590 p

Tracers and tracing methods

Editor

Jean Pierre Leclerc
Laboratoire des Sciences du Génie Chimique
CNRS-ENSIC
Nancy
France

2001

Proceedings of:

First International Congress
Tracers and tracing methods
29-31 mai 2001
Nancy
France

ISBN 2-910239-00-4 (collection)
ISBN 2-910239-53-5 (N°79)

FOREWORD

The first congress on "*Tracers and tracing methods*" took place in Nancy in November 1998. It was a successful national event with more than 100 participants and 65 presentations. It has now been extended at the international level. The objective of this second congress is to present the current status and trends on tracing methods and their applications. It will give the opportunity to people from different fields to exchange scientific information and knowledge about tracer methodologies and applications. The target participants are the researchers, engineers and technologists of various industrial and research sectors: chemical engineering, chemistry, environment, food engineering, bio-engineering, geology, hydrology, civil engineering, iron and steel production, etc.

Two sessions are planed to cover both fundamental and industrial aspects:

A) Fundamental development

- Tomography, tracer camera visualization and particles tracking
- Validation of Computational Fluid Dynamics (CFD) simulations by tracer experiments and numerical Residence Time Distribution (RTD)
- New tracers and detectors or improvement and development of existing tracing methods
- Data treatments and modeling
- Reactive tracer experiments and interpretation

B) Industrial applications

- Geology, hydrogeology and oil field applications
- Civil engineering, mineral engineering and metallurgy applications
- Chemical engineering
- Environment
- Food engineering and bio-engineering

The program includes 5 plenary lectures, 23 oral communications and around 50 posters.

The diversity of the studies and the good scientific level demonstrate clearly the importance of this field both from the academic and industrial points of view. We wish this congress to become a traditional international event.

I wish to express my deep thanks to everybody who contributed to the success of this event and specially to the scientific comity, to all the participants and to the staff of the CPIC (Centre de Perfectionnement des Industries Chimiques).

Leclerc Jean-Pierre
Scientific coordinator

SOMMAIRE

A - Fundamental development

A1 • TOMOGRAPHY, TRACER CAMERA VISUALIZATION AND PARTICLES TRACKING

A2 • VALIDATION OF COMPUTATIONAL FLUID DYNAMICS SIMULATIONS BY TRACER EXPERIMENTS AND NUMERICAL RESIDENCE TIME DISTRIBUTION

B - Industrial application

B1 • GEOLOGY, HYDREOLOGY AND OIL FIELD APPLICATIONS

B4 • ENVIRONMENT

A - Fundamental development

A A1 - TOMOGRAPHY, TRACER CAMERA VISUALIZATION AND PARTICLES TRACKING

AN ATTEMPT AT SPECT TOMOGRAPHY ON A PACKED COLUMN

Ph. Bandelier[1], Ph. Berne[2], V. Blet[3], S. Legoupil[4], F. Narp[2]

[1] DTEN/GRETh, CEA/Grenoble - 17 rue des Martyrs - 38054 Grenoble Cedex 9 - France
[2] DTEN/SAT, CEA/Grenoble - 17 rue des Martyrs - 38054 Grenoble Cedex 9 - France
[3] LETI/DTS, CEA/Grenoble - 17 rue des Martyrs - 38054 Grenoble Cedex 9 - France
[4] LIST/DIMRI/SIAR, CEA/Saclay - 91191 Gif-sur-Yvette Cedex - France

Abstract. Application of Single Photon Emission Computed Tomography (SPECT) to a packed column is presented. Liquid flow is monitored at two levels of the column, using ^{99m}Tc as a tracer. Two-dimensional activity maps can be reconstructed, showing some channelling of the liquid at the surface of the walls. Activity histories can be computed as a function of time, in 24 regions of interest in the cross section of the column.

INTRODUCTION

Single Photon Emission Computed Tomography [SPECT] is a technology which has been developed over the last decades to assist medical diagnosis. What makes SPECT so important, compared to other non invasive medical imaging, is the ability to image the metabolism of specific organs. SPECT (and Positron Emission Tomography, PET) is known to give a functional image of an organ while X ray scanner gives a structural image of the organ (since a few years, functional Magnetic Resonance Imaging - MRI - also has the ability to give functional images). For refined analysis or for research purposes, both methods are used for complementary features, which defines multi modal imaging. For example, brain for a given cognitive task is imaged both with PET and MRI to localize which area of the brain is stimulated. For statistical studies, the MRI image allows to match the examined brain to a "standard" brain. The calculated deformation is then applied to the PET image in order to improve the localization of regions involved in the cognitive task. In SPECT, medium life isotopes are injected and a gamma camera collects single photon gamma rays emission. The image of the distribution of the tracer inside the organ is computed from many projections at different angles around the body.

Similarly, tracers have been used for many years to monitor particular parameters in an overall industrial process by the Residence Time Distribution [RTD] approach. Such estimations are fundamental in industrial applications like cracking tower process, mixing process, oil in machinery, ... Compared to literature in the medical field, very few papers about PET or SPECT deal with applications in industry. Industrial PET has been developed by Parker [1], Hawkesworth [2], Heritage [3] and Van Den Bergen [4] to monitor oil lubricant in an engine, oil absorption in sand or velocity profiles in a nozzle. Some of these applications are not true PET in the sense of the medical community but much more Computer Assisted Radioactive Particle Tracking [CARPT]. The potential of Industrial SPECT [ISPECT] has been well described by Anderssen [5] but applications remain very

poor. At the industrial scale, Jonkers [6] has used for Shell Laboratories a mobile gamma camera to analyse various problems in situ (fluidization, gasification and bunker flow). Once again, no reconstruction was applied here, but cylindrical symmetry was supposed. The application closest to ISPECT in the sense of the medical community has been developed at a laboratory scale by one of the authors in 1997 [7]. It has been applied at industrial scale under confidential agreement in a French nuclear power plant. The following activities are potential applications for ISPECT:

1. Mixing of liquids and gases,
2. Movement of fluids in machinery,
3. Composition of mixtures,
4. Granular flow characteristics.

In this paper, a second application of this ISPECT system is reported. It deals with a packed column, which has been previously studied through the use of classical radioactive tracer techniques. The aim was primarily to study the radial distribution of liquid flow in the packing.

EXPERIMENTAL SET-UP

The column is a 30-cm-diameter glass column packed over 3.6 m. It works countercurrently and it is filled with Raschig Ralu Flow 25 random packing made of polypropylene (Figure 1 - successive positions of the SPECT device are also indicated).

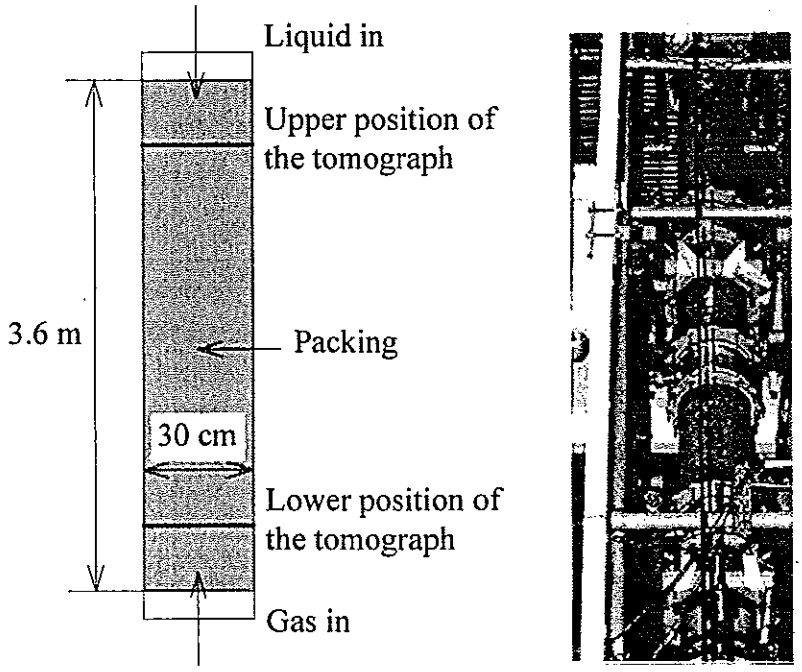

Figure 1. Schematic diagram and photograph of the packed column

Bed porosity is 95 ± 1 %. Water and air flowrates range from 0.5 to 2 and from 100 to 300 m^3/h respectively. Water flowrate is monitored by an electromagnetic flow meter and air flowrate by a hot wire probe.

The hydrodynamic properties of gas and liquid flow have already been investigated with a set of 12 classical nuclear detectors [8]. Some axial evolution of dispersive properties (especially at the bottom of the column, near the gas distributor) was demonstrated. Little information on the radial distribution of fluxes could however be obtained - hence the attempt at SPECT reported here.

METHODS

1. Two-dimensional SPECT

The SPECT device is based on 36 collimated detectors (Figure 2). Detectors include 38x19 mm BgO scintillators, high voltage and energy discriminator. All experiments were carried out with linear parallel hole lead collimators (80 mm length, 16 mm aperture). Six projections of the image are collected around the object with 6 measurements in each projection.

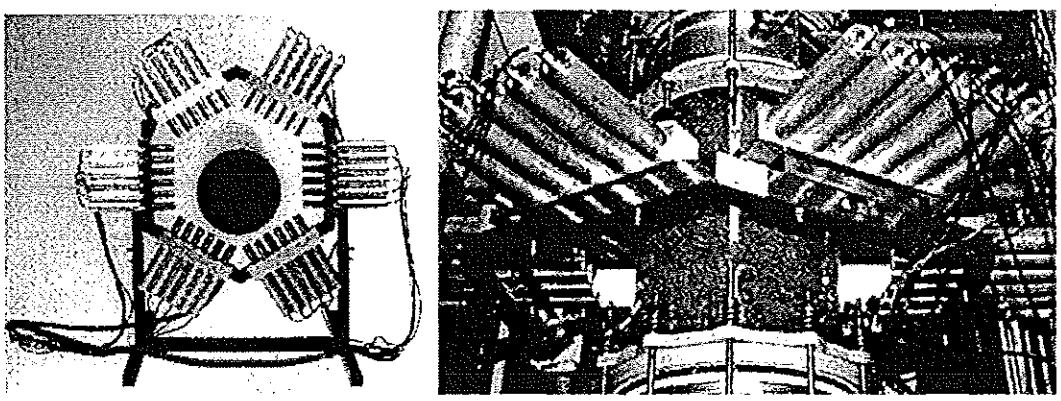

Figure 2. A view of the tomographic device and its position on the column

The tracer distribution is estimated from projections by a reconstruction technique. The projection process can be set as following. Let us decompose the image to reconstruct on a N^2 matrix. Let x_j denote the unknown intensity of pixel j. Let y_i denote the measurement in the i^{th} detector. If C_{ij} represents the probability that a photon emitted from pixel j is detected in detector i then it arises:

$$y_i = \sum_{i=1}^{N^2} C_{ij} x_j \qquad (1)$$

and for the set of measurements, in matrix notation:

$$y = Cx \qquad (2)$$

where y is the set of measurements, x is the set of unknown intensities and C is the projection matrix of the system. The aim of computed tomography is to inverse equation (2) providing that matrix C is a sufficient approximation of the projection process. Matrix C includes solid angle, gamma scattering, attenuation, lead

penetration and detector response. The estimation of the projection matrix is described below. The method used to inverse (2) is based on a statistical algorithm that takes into account the statistical nature of photon detection.

The Expectation Maximization [EM] method is an iterative algorithm for computing maximum likelihood estimates [9]. In the tomography problem, the algorithm maximizes the probability that experimental data yield the reconstructed image at the n^{th} iteration.

The reconstructed image is an estimation of the activity in each pixel j. The relationship between measured activity and tracer mass is given by:

$$\lambda_j = \alpha_j V_j c_j \tag{3}$$

where λ_j is the count rate in subregion j (counts/second), α_j is the counting efficiency proportionality, constant for all subregion j (counts/s/g), V_j is the volume of subregion j (cm^3) and c_j is the concentration of tracer in subregion j (g/cm^3). Since α_j and V_j are constants, λ_j is directly proportional to the tracer mass in pixel j.

Dynamic acquisition is obtained by selecting a counting period ΔT, and then storing all the counts that occur during ΔT. ΔT should be defined such that it matches the highest frequencies to be scanned. The injected activity is defined so that the average number of photons detected in each sample is sufficient to compute low noise images. The reconstructed values are given by:

$$x_j(t_k) = \int_{t_k}^{t_k+\Delta T} \lambda_j(t).dt \tag{4}$$

2. Calculation of the transport matrix

For an accurate estimation of the projection matrix, the different processes governing photons interactions with matter must be correctly simulated. A Monte Carlo software, MARILIN1, has been developed for this purpose. MARILIN1 simulates the response of a scintillation detector to a radioactive line source in a cylindrical pipe. For each detector, the projection matrix is modelled by a set of 12 parameters. The parameters a_i minimize the objective function given by:

$$J(a) = \sum_i \frac{\left(C(M_i) - F(a, M_i)\right)^2}{\sigma_i} \tag{5}$$

where M_i defines the point source locations, $C(M_i)$ is the probability computed at M_i, $F(a,M_i)$ is the response of the model and σ_i the error on $C(M_i)$. The parameters a_i are estimated by an optimisation process over 173 simulated line sources (figure 3). As we consider 2D distribution, the C_{ij} values are estimated for pixels of infinite height.

Maximum uncertainty over the estimated probabilities is 5 %. For a uniform tracer distribution in the pipe the error on the count rate is below 2 %. Figure 3 presents the matrix C for one detector. On the picture are also superimposed the simulated values which match the model.

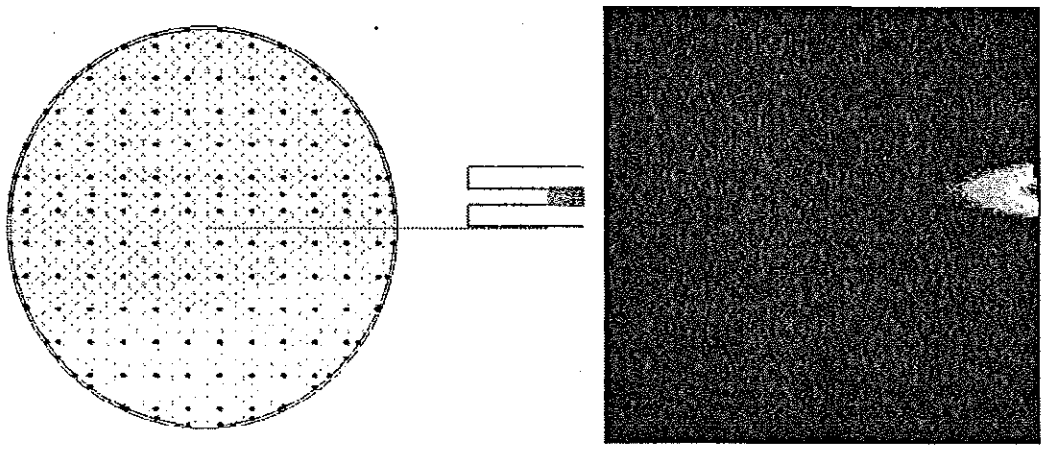

Figure 3. Position of line sources for computation of transport matrix. Illustration of the transport matrix of a detector

RESULTS

1. Operating conditions

Two tests were made in the conditions: Q_{air} = 200 m^3/h, Q_{water} = 2 m^3/h. The SPECT device was successively located at the positions depicted on Figure 1 (upper position for Test 1, lower position for Test 2). The idea was to investigate the axial evolution of liquid flow distribution in column cross section.

Only the liquid phase was traced, with Technetium 99m (half life: 6 hours, γ energy: 141 keV, emission probability 89 %) supplied by a Mo-Tc generator. Injected activity was about 1.9 GBq/50 mCi. This relatively large amount of activity allowed to get count rates in the 10^3-10^4 counts-per-second range, in spite of heavy collimation of the detectors.

The radioactive wave inside the column was simultaneously monitored by a set of six classical nuclear detectors, located at four levels along the column. Signals from these detectors allowed to check reproducibility between tests 1 and 2. Also, they were used to corroborate raw signals from the 36 detectors in the SPECT system.

2. Two-dimensional activity maps

Recorded count rates were high enough to allow good quality reconstruction of the 2D instantaneous activity maps in the cross-section of the tomograph. Total (time and space integrated) count rates differed by about 15 % for top and bottom positions. This difference can be attributed to some non-reproducibility in the tracer injection procedure. The time-averaged activity maps for the two positions are presented Figure 4. The color map is set up between 0 and the maximum value in the images. The distance between the 2 SPECT tomographs is 2.5 m. The sampling time is 0.5 s. The estimated spatial resolution is 4.5 cm and 3.0 cm respectively in the middle and on the edge of the column.

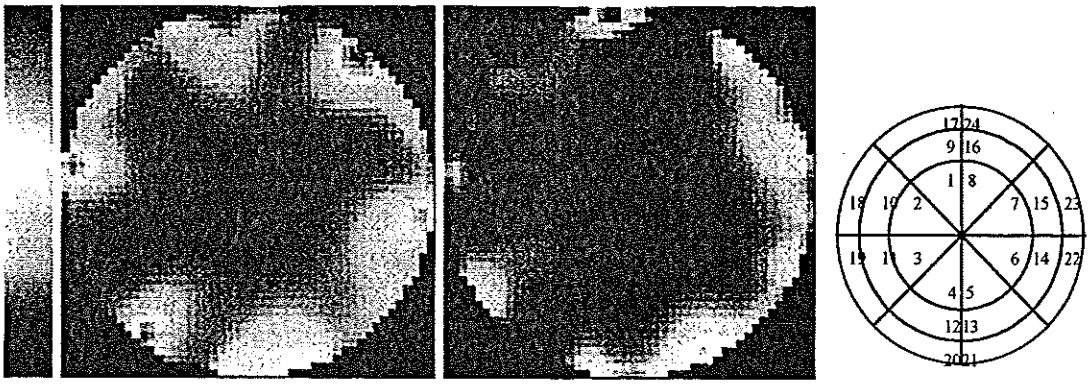

Figure 4. Average computed activity maps for positions top (l) and bottom (r). ROIs numbering

Some amount of water channelling is clearly visible at the wall, and indeed confirmed by visual observation of the column. Visual inspection suggests that this effect is more marked in the upper cross-section.

A more quantitative way of examining this phenomenon is as follows. For a given position of the tomograph, pixel-wise time-averaged activity is plotted under the form of an histogram indicating the number of pixels in each count range. Standard deviation (sigma) of this histogram (or rather the ratio of standard deviation to average) is a measure of tracer maldistribution : if the flow of tracer was spatially uniform, the same amount of activity would transit through all the pixels and the resulting histogram would reduce to a single sharp peak. On the contrary, spatial maldistribution of the tracer produces some widening of the histogram. Such histograms are depicted on Figure 5 for both positions of the tomograph.

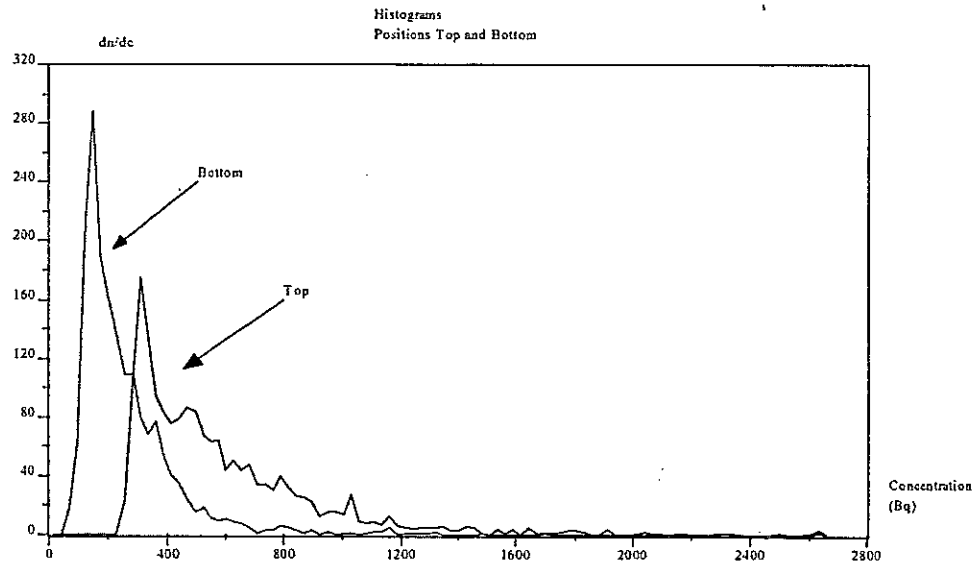

Figure 5. Histograms of the average activity maps presented figure 4

The histograms exhibit a clearly sharper distribution of activities at the bottom position (sigma/average =0.84) compared to the top position (sigma/average=1.18), hence more uniform tracer distribution in the bottom part, which confirms visual observations on the activity maps . We believe this type of quantitative criterion is a valuable contribution of the tomographic technique.

3. Activity histories in selected Regions Of Interest

The maps on Figure 4 do supply interesting information on liquid flow inside the column, but some more data can be extracted from the SPECT experiment by focusing on Regions Of Interest (ROIs). The principle is to divide column cross-section into a small number of regions in which pixel activity is space-intergrated, so as to compute ROI-averaged activity histories as a function of time. This procedure has been applied to our results by selecting three concentric rings (central - actually a disc - middle and external) and dividing each ring into eight identical sectors. Column cross-section is therefore divided into 24 regions (see Figure 4); ring widths have been selected so that the area of all the regions are identical. An example of tracer concentration histories is presented on Figure 6 for a few ROIs in each ring and for each position of the SPECT device.

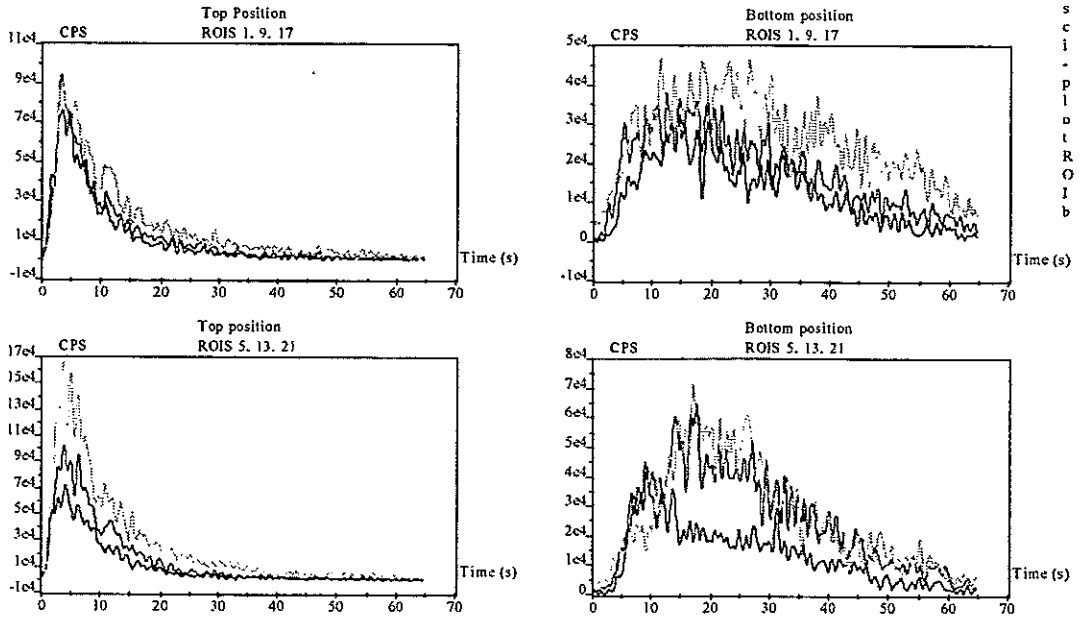

Figure 6. Activity histories in selected ROIs

These curves clearly demonstrate regions of radial symmetry (see ROIs 1, 9 and 17) and asymmetry (ROIs 5, 13,21), the latter being associated with water trickling along the wall.

CONCLUSIONS

The following results were achieved by tracing the liquid phase:

- good quality tomographic images could be obtained and revealed preferential passages of liquid, especially in the uppermost cross-section,
- a method using histograms has been proposed for quantitative appreciation of these flow maldistributions,
- activity histories in 24 ROIs could be computed for each position of the tomograph, with reasonable precision,
- examining ROI activity histories allows to determine regions of radial symmetry and asymmetry.

Further developments should involve tracing of the gas phase (a difficult enough job because of high gas velocity) and application of the technique to a packed column in industrial conditions.

REFERENCES

[1] Parker, D.J. and al., *Industrial positon based imaging: principles and applications*, Nuclear Instr. and Methods in Physics Research, (1994), 348(2).

[2] Hawkesworth M.R. and al., *Nonmedical applications of a positron camera*, Nuclear Instr. and Methods in Physics Research, (1991), 310.

[3] Heritage, J. and al., *An imaging system for radioactive tracing of lubricants in automative components*, IMechE (1985).

[4] Van den Bergen, E.A., Jonker, G., Strijckmans, K. and Goethals, P., *Industrial applications of positron emission computed tomography*, Nucl. Geophysics, 3 (1989), 407-418.

[5] Anderssen, R.S. and Gates, D., *The potential of SPECT Technology for industrial Non-Destructive Testing*, Non-destructive testing – Australia, (1994), 31(5).

[6] Jonkers, G., Van Den Bergen, E.A., and Vermont, P.A., *Industrial applications of a gamma ray camera system – 1.* Qualitative studies, Applied Radiation, Isotopes, 41 (1990), 1023-1031.

[7] Legoupil, S., *Tomographie d'émission gamma à partir d'un nombre limité de détecteurs, appliquée à la visualisation d'écoulements*, PhD, Rapport CEA-R-5855, ISSN 0429-3460.

[8] Blet, V., Berne, Ph., Chaussy, C., Perrin, S., Schweich, D., *Characterization of a packed column using radioactive tracers*, Chem. Eng. Sci., 54 (1999), 91-101

[9] Lange, K. and Carson R., *EM reconstruction algorithms for emission and transmission tomography*, Journal of computer assisted tomography, (1984), 8(2).

THE USAGE OF Sm-153 AS A SINGLE PARTICLE RADIOTRACER TO MEASURE TANGENTIAL CIRCULATION TIME OF GRANULAR MATERIAL IN A STIRRED HORIZONTAL VESSEL

G. van Kranenburg[1], S. Mutsers[2], J. Konings[3*]

[1]DSM Research, BC-PT, PO Box 18, NL-6160 MD Geleen, The Netherlands
[2]DSM Research, PO-PT, PO Box 18, NL-6160 MD Geleen, The Netherlands
[3]DSM Services, MPS-RAS, PO Box 18, NL-6160 MD Geleen, The Netherlands
*Author for correspondence (jack.konings@dsm.com)

Abstract. Within the framework of a research project, carried out at DSM Research, to characterize a horizontal stirred vessel with an axial stirrer, the mean tangential circulation time (TCT) of the granular material was investigated with the aid of a single radioactive particle.

Horizontal stirred vessels are frequently used for mixing different types of granular solids, for example fertilizers. The mean tangential circulation time is one of the important parameters that characterize the tangential mixing quality. Unlike most radiotracer experiments, where a huge amount of single particles (molecules) is applied to a process, a single radioactive particle was added to the test-rig. By detecting the passage of the radioactive particle through a narrow detection window a sample of the TCT distribution was gathered. By acquiring data of many passages of the particle the TCT distribution is formed. By means of simple mathematics the mean TCT and its standard deviation (σ) is calculated from the collected samples of the TCT distribution

Moreover the single radioactive particle represents a perfect dirac-impuls (the radioactivity is always injected correctly, no dispersion) and there is almost no need to correct the gathered data (like decay, background raises and/or tailing).

As radioactive tracer, Sm-153 was used. Sm-153 was chosen because of its easy shielding and high (NaI) detection efficiency due to its low gamma energy (103.2 and 69.7 keV), relative long half-life ($T_{½}$=46.27 h) and high neutron activation yield. Radioactive particles were produced by mixing Sm_2O_3 with plastic and moulding it into thin plates with varying thickness. From these plates grains were punched out with varying diameter (ranging from about 0.25 to 1 mm). The grains were irradiated with neutrons in the research reactor (IRI) of Delft University, The Netherlands to produce an activity ranging from 1 to 10 MBq. During several weeks nearly 100 experiments and TCT determinations were carried out. During the experiments the radioactive particle size (for validation reasons), the stirrer geometry, the filling height of the granular material and the stirrer revolution time were varied. The presented radiotracer method to determine the mean tangential circulation time (TCT) and its standard deviation has proven to be highly suitable. The requested parameter can be measured in a relative short time, with a minimum of radioactivity and cost effective.

Introduction

The probably most common application of a radiotracer in industry is the determination of a Residence Time Distribution (RTD). In a typical experiment a radiotracer is applied to a process stream at the entrance of the system under investigation as a pseudo-Dirac impulse. The radiotracer is transported jointly with the process stream through the system, mostly a vessel of some kind. In here, the process stream interacts with the properties of the vessel, which results in a certain time distribution of the radiotracer at the exit of the vessel.

However, in certain types of vessels the content is transported in more than one direction (not only from entrance to exit). One type of vessel in which the content is

transported in two directions is a horizontal vessel with an axial stirrer. Mass transport takes place from entrance to exit (axial) and around the stirrer (tangential).

Within the framework of a research project, carried out at DSM Research, to characterize the mixing quality of horizontal vessels with an axial stirrer, the granules tangential circulation time was investigated. The results of this investigation are to be used as an input parameter for modeling-software used to optimize the performance of this type of solid mixers. Up until recently the granular tangential circulation time was visually estimated and assumed to be in the order of 10 to 20 or more seconds in the test-rig.

Measuring principle

Because only the mean tangential circulation time (TCT) was of interest the test-rig was operated batch wise. It was partially filled with a single type of granular solids (grains with a mean diameter of about 0.5 mm). As a consequence of the rotating axial stirrer the grains are circulated around the central axis.

Hence the mean tangential circulation time (TCT) is a function of :

- stirrer revolution time
- stirrer geometry
- granular solids filling height

Unlike most radiotracer experiments, where a huge amount of single particles is used, this method cannot or only with great difficulties be applied to this case. A short time after applying the radiotracer to the test-rig it would be fully mixed over the tangential and radial content thus making data evaluation very difficult. Moreover one had to apply new radiotracer every experiment and empty the test-rig between experiments thus making it very labour intensive and costly.

An alternative method to perform a radiotracer experiment is to use a single particle (in stead of many) and carry out the experiment many times (in stead of once).

In our case this would mean that we had to apply just one radioactive particle to the test-rig, which would behave like the rest of the solid grains. By detecting the particle every time when it passes through a narrow axial detection window, between the stirrer axis and the vessel wall, we would get many samples of the TCT distribution.

By applying just one radioactive particle to the test-rig had also the advantage that many experiments could be carried out successively and thus limiting the total amount of radioactivity, labour and costs.

Moreover the single radioactive particle represents a perfect dirac-impuls (no need to worry to inject the radioactivity correctly) and there is almost no need to correct the collected data (like decay, background raises and/or tailing, integration areas).

Radiotracer

As radioactive tracer, Sm-153 was used. Sm-153 was chosen because of its easy shielding ($\mu/\rho_{lead,\ 100\ keV}$~0.49 m^2/kg) and high detection efficiency due to its low gamma energy (103.2 and 69.7 keV), relative long half-life ($T_{½}$=46.27 h) and high neutron activation yield (σ_{th}=206 barn, σ_{epi}=3141 barn).

To produce a radioactive grain Sm_2O_3 was mixed with plastic and moulded into thin plates with varying thickness. From these plates grains were punched out with varying diameter. The resulting grains looked very similar to the real solid grains and their diameter ranged from about 0.25 to 1 mm.

The grains where irradiated with neutrons in the research reactor (IRI) of Delft University, The Netherlands and transported within a few hours after irradiation to DSM Research. The resulting activities ranged from 1 to 10 MBq.

Measurement set-up

For the detection of the radioactive particle two industrial 2"x2" NaI detectors (Berthold Sz-5 D1 50/50) were used. Lead was used to give the detectors a narrow detection window (see figure 1) and also to reduce the background of the detectors (not drawn in figure 1). Lead was also used to fill up the stirrer axis to prevent possible double detection of the particle during one circulation.

In order to eye-witness the movement of the product in the vessel during operation the entire vessel was made of perspex. The stirrer was driven by an electromotor, which was electronically controlled by a PLC.

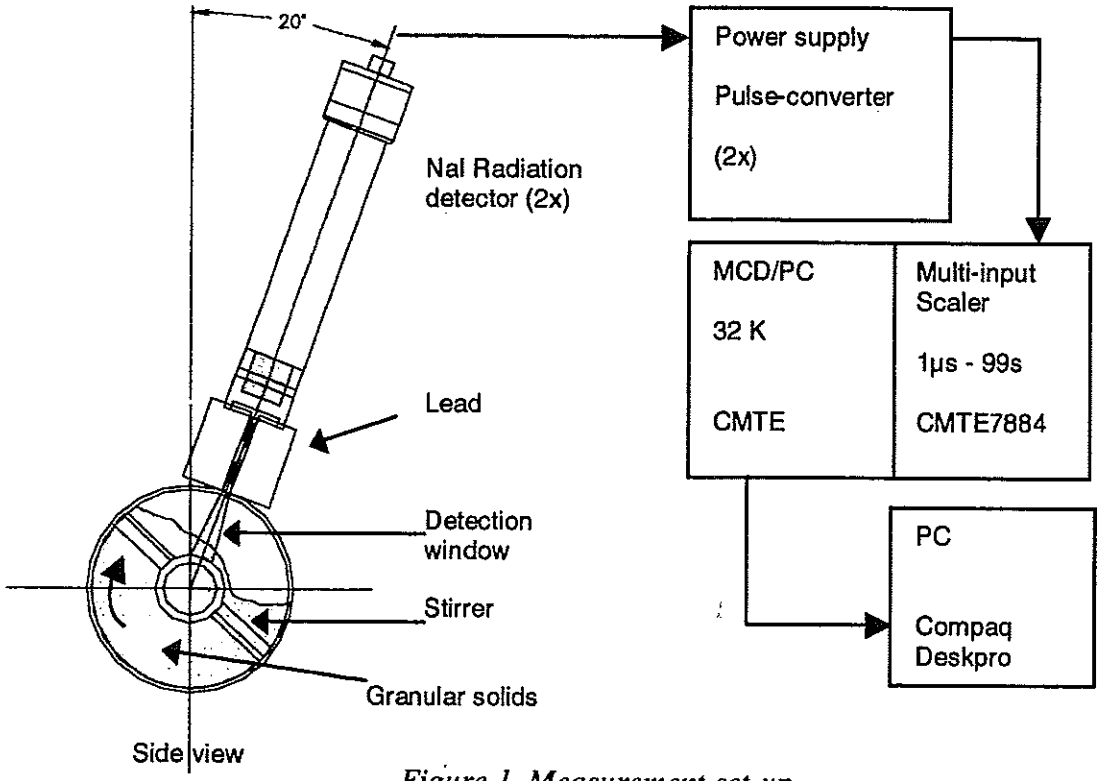

Figure 1. Measurement set-up

The signals of the two detectors were measured separately with a multi-input scaler coupled to a 32 KB multichannel data processor (8192 data points/detector). The dwell-times used, during experiments, ranged from 0.1 to 0.2 s. A standard PC was used to read the data buffer of the data processor and store the data to file.

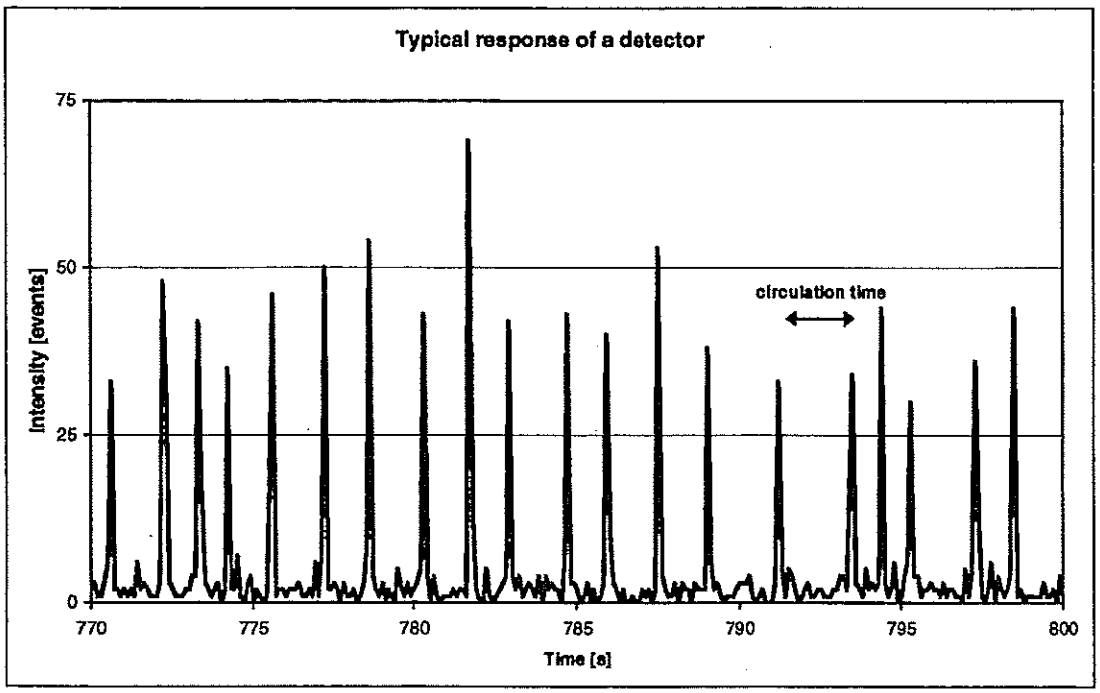

Figure 2. Typical detector response.

Figure 2 shows a typical detector response during an experiment. To process and reduce the collected data a small utility was written in Borland Pascal to extract the time differences between two passages of the radioactive particle and store this information in a standard ASCII file. MS Excel was used for further data evaluation (calculation of mean tangential circulation time and its standard deviation) and presentation.

Validation

The presented measuring principle depends on the single detection of the radioactive particle per circulation. It was of great importance to validate this behavior. As already mentioned much effort was taken to prevent possible double detection with the extensive use of lead to shield the detectors.

To validate the single detection per circulation behavior a sealed Cs-137 radioactive source was fixed on one of the stirrer paddles. Cs-137 emits radiation with a gamma energy of 661.6 keV which is much more penetrable than that of Sm-153.

With an empty test rig the stirrer was activated at a large circulation time and several TCT distributions were collected using a dwell-time of 0.025 s. Afterwards every collected TCT distribution was related to the expected TCT (see figure 3). If there would be "radiation leaks" a distinguishable peak would emerge at time index 0.5 indicating that the stirrer axis was insufficiently shielded or a more or less continuous spectrum would emerge between time index 0 and 1 indicating a poor performance of the detection window.

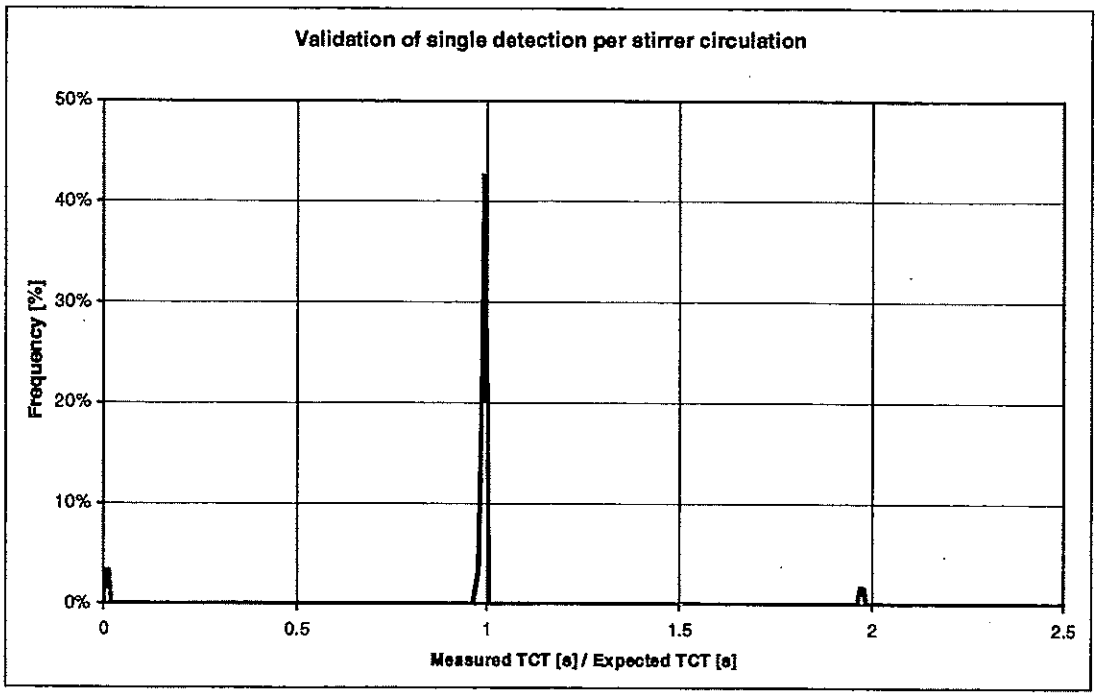

Figure 3. Result of a validation experiment.

As one can see (in figure 3) there is a very clear peak (area>95%) at time index 1 with a very small relative standard deviation (~1%) with no sign of any activity near time index 0.5 or even between time index 0 and 1.

The two small peaks at time index 2 and near zero are a result of the used small dwell-time. Because of this it is not impossible that the used algorithm to extract the TCT can miss a passage completely resulting in a small peak at time index 2 or interpret a single passage as two separate ones resulting in the dwell-time itself. Both effects can easily be corrected for or simply cannot occur during the experiments.

Experiments

During several weeks nearly 100 experiments were carried out using about 10 different radioactive particles. During the experiments the following parameters were varied :

- *particle size*

the size of the radioactive particle was varied from 0.25, 0.5 up to 1 mm diameter to validate that the particle size and its dissimilar weight had no or a neglectable influence on the TCT distribution

- *stirrer geometry*

two different stirrer geometries (A and B) were used

- *product filling height*

per stirrer geometry the test-rig was loaded with three different masses of the same granular solids resulting in three different filling heights (low, medium and high)

- *stirrer revolution time*

the stirrer revolution time was varied between small (high rpm), medium and large (low rpm)

MS Excel was used to calculate the mean TCT and its standard deviation and to correlate them to the above-mentioned varied parameters.

A typical result of several TCT distributions is presented in figure 4.

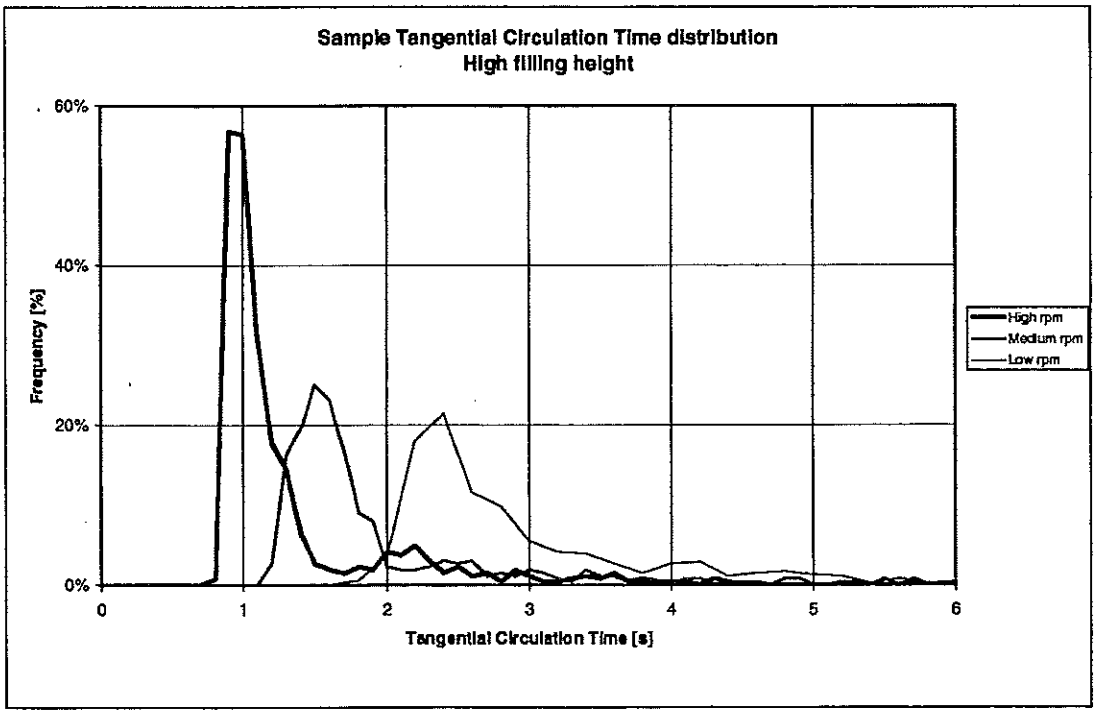

Figure 4. A typical result of TCT distributions at different stirrer revolution times.

After data evaluation it could be concluded that there was a neglectible (<5%) influence of the particle size and weight (in the range from 0.25 to 1 mm) on the TCT distribution.

Furthermore it proved to be beneficial to express the TCT and its standard deviation relative to the stirrer revolution time thus resulting in a relative TCT and standard deviation.

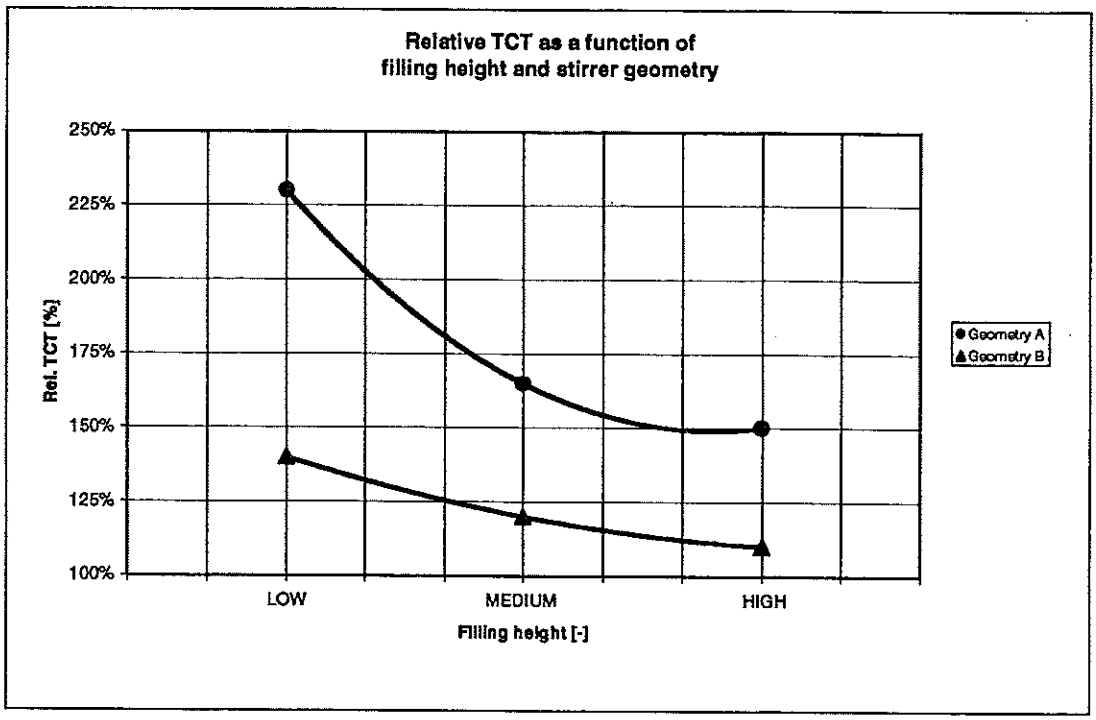

Figure 5. Overall view of the measured data

Figure 5 shows an overall view of the measured data regarding to the relative TCT. A similar picture can be draw for the relative standard deviation.

The data points were used to calculate 2nd order polynomials which served as an input for the modeling-software.

As one can see, the mean TCT for a type A stirrer is highly influenced by the filling height of the reactor. The filling height has only a moderate influence when a type B stirrer is used.

To visualize the tangential mixing behavior of the test-rig it is assumed that the tangential mixing can be modeled as a number of perfect mixers in series. The number (n) of perfect mixers in series is given by :

$$n = \frac{TCT^2}{\sigma^2} \qquad (1)$$

As one can see (in figure 6) the tangential mixing quality of the type A stirrer performs almost independent of the filling height (n=4). The type B stirrer depends highly on the granular solids filling height. It approaches near plug flow for high filling heights (6<n<30). This behavior also surprised the engineers.

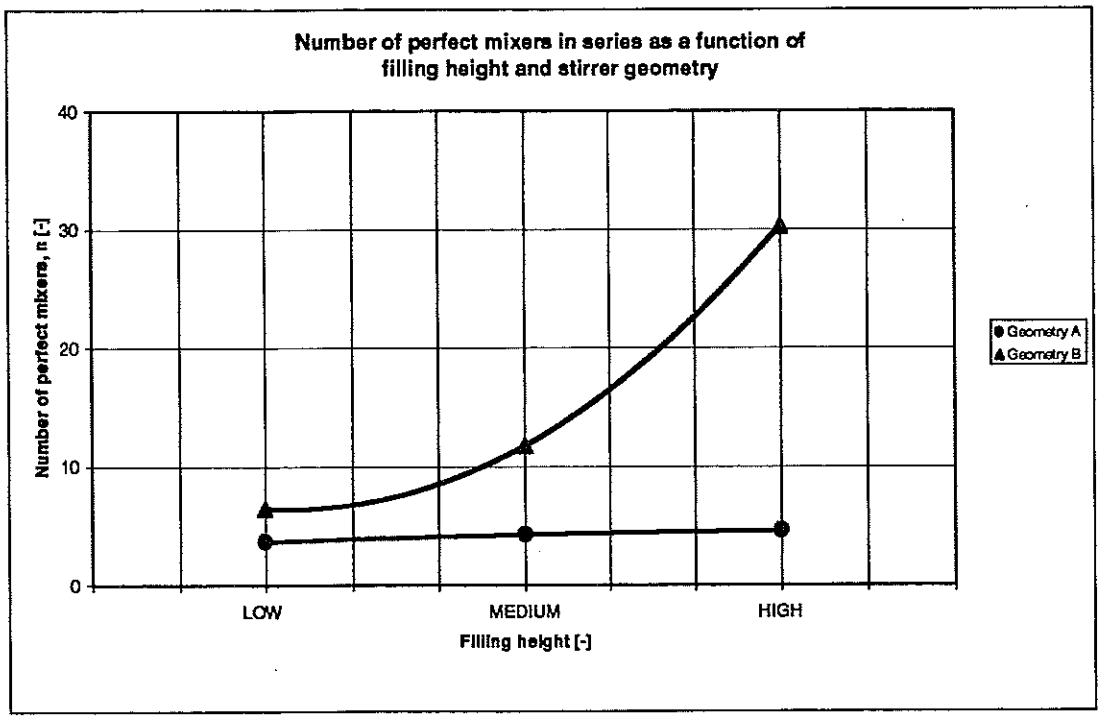

Figure 6. Number of perfect mixers in series

Conclusion

The presented radiotracer method to determine the tangential circulation time (TCT) and its standard deviation has proven to be highly suitable. The requested parameter can be measured in a relative short time, with a minimum of radioactivity and cost effective.

Furthermore the experiments resulted in an information yield, which was bigger than expected almost without any extra effort.

NUMERICAL PARTICLE TRACKING AND VISUALIZATION OF DEAN VORTICES

R. Moll[1], D. Veyret[2], P. Moulin[1], F. Charbit[1]

[1]Laboratoire d'Etudes et d'Applications des Procédés Séparatifs (LEAPS – E.A. 884), ENSSPICAM, Université de St Jérôme, Avenue Escadrille Normandie Niemen, 13397 Marseille cedex 20, France.
[2] Institut Universitaire des Systèmes Thermiques Industriels (UMR 6595) 5, rue Enrico Fermi, 13453 Marseille cedex 13, France.

Abstract. New hydrodynamics in membrane filtration processes could yield interesting enhancement in performance. In order to reduce fouling and polarisation concentration, helical membrane geometries were studied, which generate secondary flows called Dean vortices. The efficiency of the Dean vortices has been clearly demonstrated in several membrane applications (ultrafiltration, microfiltration, pervaporation,...). The performance enhancement comes from complex hydrodynamics phenomena that require further investigations. A 3-D numerical simulation of the flow and the particle path, coupled with laser visualisation results, allowed to quantify several parameters as components of the shear stress tensor. In the case of a solution (without particle), the simulation results clearly show that experimental enhancements observed are due to the wall shear stress in the helical geometry of the membrane. In the case of suspension (with solid particles), an additional increase of the permeate flux has been observed as the feed concentration increases. This cannot be explained by means of the same argument alone. Thus we present new simulation results dealing with tracers introduced in the same flows and the same geometries : they make it possible to investigate and discuss the consistency of the different observations and the interpretations derived.

INTRODUCTION

In membrane separation processes, due to the convective flow of permeation, a build up of retained compounds occurs at the membrane wall. This results in polarisation concentration, which is a concentration gradient near the membrane, or in membrane fouling [1]. These two phenomena reduce the membrane performance, especially the permeate flux. A modification of the hydrodynamics by means of new module design significantly may enhance the permeate fluxes [2]. In standard crossflow filtration it is established that an increase of the wall shear stress is sufficient to reduce the build-up of retained matter. No doubt that helical hollow fibre is the simplest of these new designs ; it generates secondary flows called Dean vortices. Such modules enhance permeate fluxes in various membrane separation processes such as microfiltration, ultrafiltration, nanofiltration and pervaporation. This new design is particularly attractive because it only require to turn hollow fibres initially straight into helical forms. In addition, the increase in pressure drop remains reasonable. Though in this case, the mass transfer enhancement is linked to the wall shear stress differences between straight and helical tubings, the mechanism of this mass transfer is not yet thoroughly understood. For example, concentration effects described hereafter are still surprising and require further investigations.

In order to improve the precise description of the complex hydrodynamics involved and that of its positive effects on separation performance, previous laser visualisation experiments and new numerical simulations were considered. These two approaches are basically different whence they provide different points of view for identical systems. We present results of both types which give insights into experiments which seemed inconsistent.

NUMERICAL SIMULATION

The mathematical model consists in solving the Navier-Stokes and continuity equations for a 3D steady, laminar flow of an incompressible homogeneous and Newtonian fluid [3]. The algorithm, which is based on the finite element method, is the use of a projection method in order to approximate the solution of the equations. In the case studied herein, attention is restricted to rigid, non-permeable bounded walls, the mesh is refined close to the walls in order to take into account strong variations of the velocity components. The inflow velocity has a parabolic profile, while the outflow is set free. In order to post-process the results, the global three-dimensional velocity field obtained is transformed into a local co-ordinates system, where (Oxy) is defined by the section studied and (Oz) is orthogonal to this section. From this system we can represent the axial and radial velocities, and calculate the local shear stress. From the same velocity field obtained all across the helix, we can track either numerical tracers or spherical solids particles with a Fortran subroutine. This post-treatment consists in injecting at the inlet cross section, a tracer or a number of identical spherical particles characterised by their diameter and density. The injection points are equally distributed in the inlet section (Fig. 1a) and particles are submitted to the flow, gravity and drag forces, despite their small diameter. Particle-particle and wall-particle interactions will not be considered in this study. Simulation results will then be considered for fully developed velocity distributions and for different Reynolds numbers. In the geometry we choose 360 given sections shared every two degrees and we represent the positions of tracers/particles in those successive sections. So, the result of this post treatment gives, after each narrow time step, the spatial co-ordinates of tracer particles, which are also transformed in the local co-ordinates system mentioned above (Fig. 1b). This geometric representation needs to be fulfilled by an another one which takes into account the residence time distributions. In this aim, we draw the inverse of the residence time vs. the position in the final section (after 2 laps). This is unusual but as much as, different particles are submitted to different speeds and trajectories while crossing the geometry, it point out the differences between faster (low residence time or high averaged speed) and slower particles (high residence time or low averaged speed)

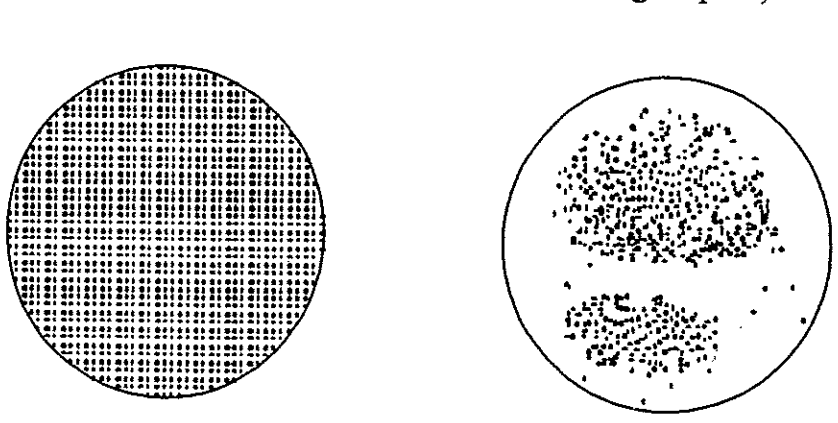

Figure 1a. Injection points in the inlet section. Figure 1b. Position of tracer after 10s in the outlet section (Re = 40, d_i = 3.2 mm, d_s = 20 mm, pitch = 30 mm)

LASER VISUALISATION

The experimental set-up used was developed by Moulin et al. [4], in the aim of giving qualitative and quantitative information about the structure of the flow. The way they were collected is now important to remember to discuss the interpretations derived. A permanent flow is created in a straight or helical glass tube. The fluid considered is an aqueous suspension of polystyrene particles (about 40 μm in diameter) with a density close to that of water (d = 1,0132). A semi-cylindrical mirror associated with a laser is used to make a laser plane that lights up a section of the tube. A video system visualises the fluid going through that plane. A data record system memorises and post-processes the intensity of each pixel of the image. Then the average light intensity of several successive images is calculated for each pixel. The post-treatment program is optimised : given that the exposure time is larger than the particle residence time in the laser plane, the intensity of each pixel is related to number of particles that pass through the laser plane at that location during the exposition time.

RESULTS & DISCUSSION

1. Velocity and wall shear stress

Several Reynolds numbers have been investigated in each of the two geometries. The results obtained by both methods in both geometries are compared at fixed given operating conditions.

1.1. Straight tube

Both methods give similar results. The same velocity profile is obtained, which would also result from the analytical solution of the system of equations.

1.2. Helical tubes

The efficiency of the visualisation experimental set-up was checked by determining the transition Reynolds number between laminar and turbulent flows. Our simulation results were checked by comparing wall shear stress values to those previously published for helical tubes. In any case, predicted results were obtained. Moreover, it can be seen as well by the laser visualisation as by the numerical simulation, that the rotation vortex centre moves towards the inner side of the coil at increasing Reynolds number. For each Reynolds number and for each section considered, numerical results show the variations of each component of the velocity (axial v_z; radial v_x, v_y) vs. the angle for a coiled tube at the closest row of nodes near the wall. The maximum velocity is located around the extrados of the tube (i.e. 180° position). All over the cross-section the radial component velocity is lower than the axial component. Figure (2) presents τ_w wall shear stress vs. angular position for a torus. The wall shear stress calculated for a straight tube is also plotted in order to emphasise the increase of the wall shear stress due the secondary flow. Between 66° and 296° the wall shear stress is higher than that obtained in a straight tube. The maximum value is reached at 180° and the wall shear stress is symmetrical about this

value. The average wall shear stress is calculated as $\tau_w = 4.05$ Pa which is in perfect agreement with that given by Mishra *et al.* [5] correlation : $\tau_w = 4.1$ Pa.

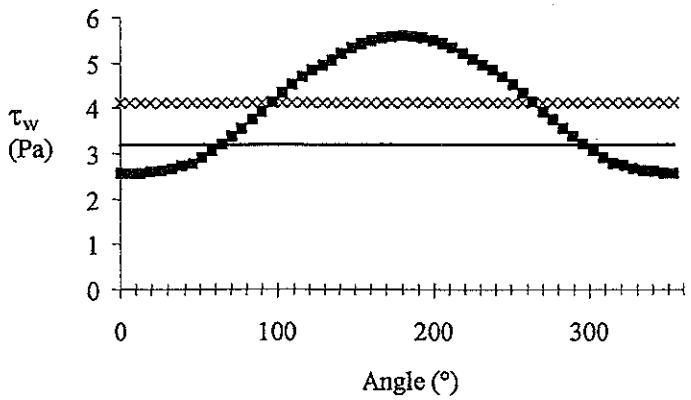

Figure 2. Variation of the wall shear stress vs. the angular position. (■) Present study, (x) Mishra et al., (-) straight tube), (Torus, Re = 400, De = 52, d_i = 1 mm, d_c = 60 mm, water, ρ = 1000 kg.m^{-3}, $\mu = 10^{-3}$ Pa.s)

1.2.1. Wall shear stress and mass transfer : case of a solution

Figure (3) presents, ratio values of the average wall shear stress in a coiled tube over that in a straight tube versus Reynolds number. Ratios of experimental permeate fluxes obtained in coiled tubes over those obtained in straight tubes are also plotted on the same diagram, dealing with the removal by pervaporation of volatile organic compounds from water. The corresponding curves are identical. Obviously, Dean vortices increase the wall shear stress in the same extent as they enhance permeate flux. Naturally, this first result is restricted to membrane processes characterised by low permeation fluxes such as the removal of volatile organic compounds (VOC) from water by pervaporation [6] or oxygenation of water [7]. Finally, simulation results yield analogous conclusions as experiments : enhanced wall shear stress and enhanced flux are strongly correlated.

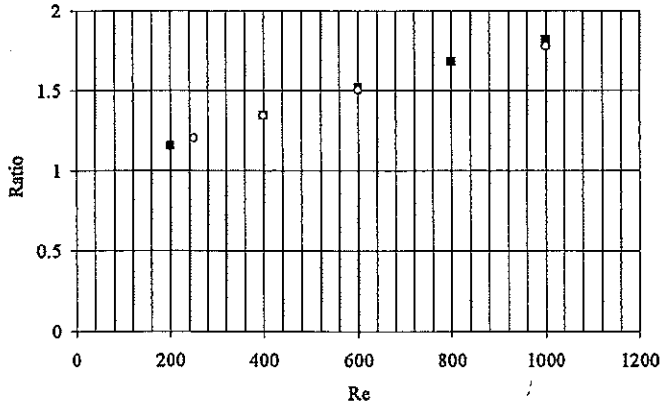

Figure 3. Comparison between numerical simulation and experimental membrane studies vs. Reynolds number((O) simulation results $\tau_{helical}/\tau_{straight}$;(■) removal of VOC with helical pervaporation modules :$J_{helical}/J_{straight}$)

1.2.2. Wall shear stress and mass transfer : case of a suspension

In the case of suspension, as the feed concentration increases the enhancement due to Dean vortices is more pronounced. Given that the wall shear stress is now constant this cannot be explained as above mentioned. More, Manno et al. [8] have predicted from viscosity measurements in baker yeast suspensions, that the higher the feed concentration, the lower the wall shear stress ratio between a helical and a straight tube at given velocity. The gain effect of the Dean vortices on the permeate flux should then decrease at increasing concentration. Yet, experimental results clearly show the opposite. The same unexpected behaviour was observed in the case of bentonite suspension. More, ultrafiltration of baker's yeast at 150 g/L has been performed with lower wall shear stress than that in straight tube : vortices obtained in helical tube yield much higher permeate fluxes ; improvement factors were up to 4. The wall shear stress alone cannot account for the mass transfer improvement.

The aim is now to give new insights into these surprising observations by comparing laser visualisation results previously presented with results obtained from numerical simulations involving tracers and particles

2. Residence time and trajectories

At Reynolds numbers higher than 2600 the observed outlines provided by laser visualisation corroborate the axial velocity distribution obtained from simulation. The conclusions deduced from both approaches above mentioned are consistent as in the case of straight tubes, i.e. the intensity of the images obtained by laser visualisation corresponds to the velocity distribution in the liquid obtained from the numerical simulation. However, since membrane processes usually operate with lower Reynolds numbers ($Re < 2000$), the influence of Dean vortices should be preferably investigated in this experimental range ; unfortunately the two investigation methods apparently diverge under these conditions. The maximum intensity determined by laser visualisation (Fig. 4a) corresponds to the centre of each vortex found by numerical simulation results ; meanwhile the maximum axial velocity is invisible at the extrados (i.e. 180° position) (Fig. 4b). At these low Reynolds number, there is obviously a discrepancy between the laser visualisation and the numerical simulation.

Those differences might stem from different origins :

- Particles might move to low shear stress area close to the centre of the Dean vortices meanwhile a few of them still pass near the wall ; as a result, the particle concentration would be modified in a cross section, decreased near the wall whence the solvent mass transfer would be increasingly improved.
- Otherwise, the flow could be higher at the centre of each vortex and the improvement of mass transfer would not be due to a local concentration modification.

The question to be discuss in light of the different results is then whether a segregation occurs or not. According to the assumption of no segregation, solid particles are equally distributed over a cross section and the high light intensity measured by laser visualisation, which is proportional to a number of particles enlighted during the exposition time could be due to a high volumetric flow. In contrast, velocity field calculated from numerical simulation only accounts for

instantaneous velocities, and thus is independent of residence time. To calculate the local values of flow rate let us now study the behaviour of tracers in a helical tube.

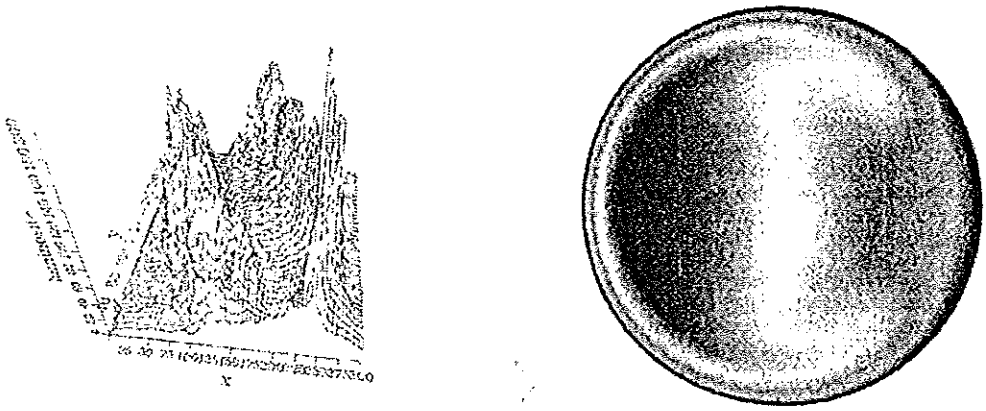

Figure 4a. Profile obtained by laser visualisation. Figure 4b. Velocity profile obtained by numerical simulation (Re = 1627, di = 3.2 mm, d_s = 20 mm, pitch = 30 mm)

2.1. Tracers

Basically each numerical tracer is continuously tracked during it residence time in the system, which allows us finally to draw different trajectories depending on the location of injection point and on Reynolds number. For the sake of clarity, different trajectories projected are presented in Figure 5a. and 6a. Due to the pressure gradient between the extrados (180°) and intrados (0°) the trajectories representation are not restricted to single points as in straight tube. At low Reynolds number we can observe that tracer injected far from the centre of the vortices have longer trajectories than those of tracers injected near a vortex centre. Taking into account the residence time, the flow rate values present two maxima located at the centre of each vortex. Even if in these areas the value of instantaneous velocity is not maximum (Fig. 4b.). Tracer simulation shows that the volumetric flow is greater at the centre of each vortex.

At higher Reynolds number (Fig. 6a), the local flow is deeply modified : the centres of the vortices move towards the inner side of the coil. Consequently, the flow representation is modified and turns into a C-letter-like form (Fig. 6b) joining the centres of the vortices and passing at the extrados side. This is in agreement with the laser visualisation.

In turbulent flow, results obtained by laser visualisation and numerical simulation are similar as above mentioned and the maximum value of volumetric flow is precisely located at the extrados of the coil.

Thus, the results obtained by laser visualisation and by numerical tracer simulation are in total agreement at any Reynolds number studied. This suggests that the laser visualisation gives as expected information on flow structure. The mass transfer improvement does not seem to be due to the concentration modification.

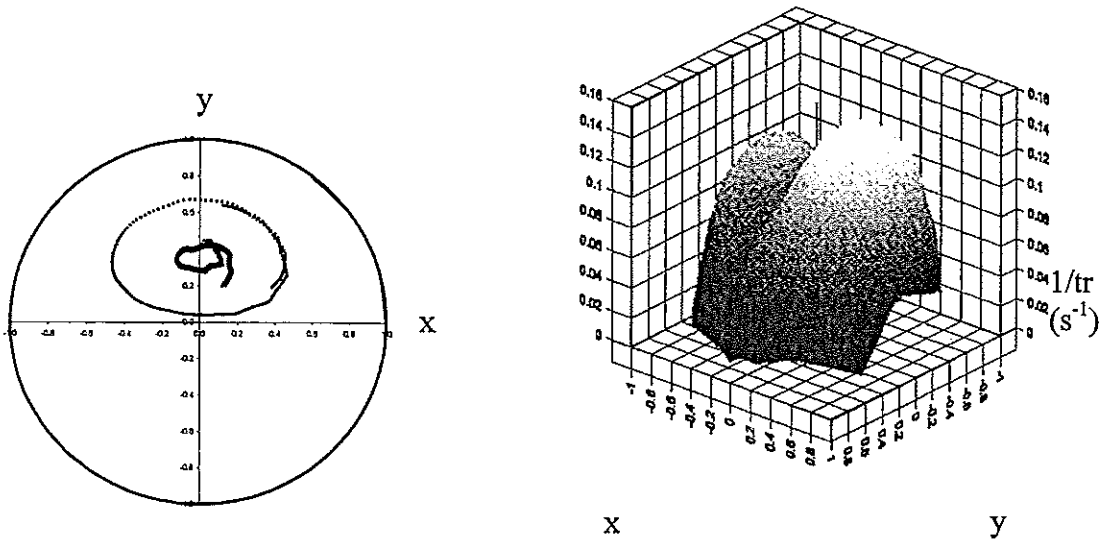

Figure 5a. Representation of the successive position (adimensional co-ordinates) for two tracers through the geometry. Figure 5b. Representation of the inverse of the residence time vs. the location (adimensional co-ordinates) in the outlet section. (Re = 40 ,d_i = 3.2 mm , d_s = 20 mm , pitch = 30 mm)

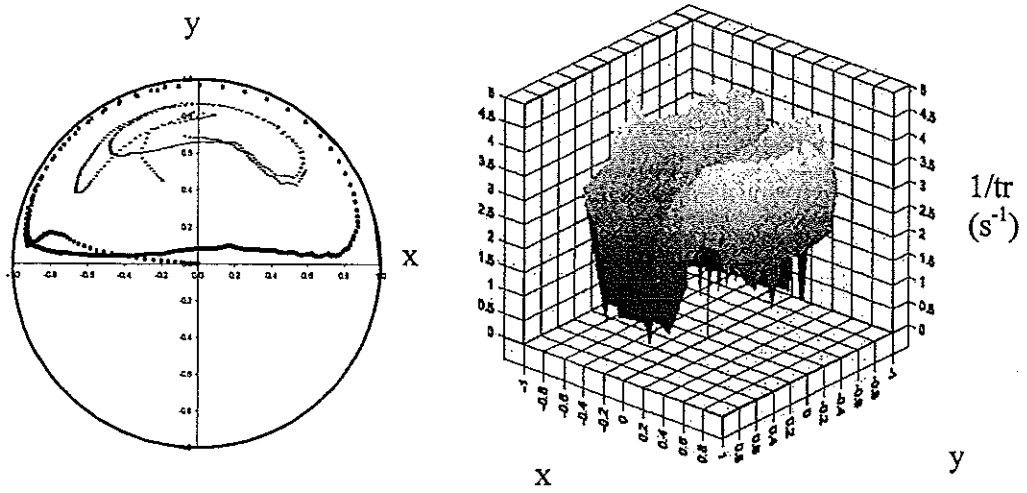

Figure 6a. Representation of the successive position (adimensional co-ordinates) for two tracers through the geometry. Figure 6b. Representation of the inverse of the residence time vs. the location (adimensional co-ordinates) in the outlet section. (Re = 1627 ,d_i = 3.2 mm , d_s = 20 mm , pitch = 30 mm)

2.2. Particles

We are now improving a particle simulation in order to strengthen the tracer simulation. Usual concentrations encountered in ultrafiltration processes (3-150 g/L) are higher than those considered in the frame of the laser visualisation (1.8 g/L) here discussed. Particle-fluid interactions should then be taken into account in order to rationalise the results. We studied variations of some physical properties of particles

(density, diameter, etc...). The first results are similar to those obtained by tracer simulation.

CONCLUSION

In this paper two methods have been used to understand the effect of Dean vortices on flux improvement in different membrane processes : a laser visualisation and a numerical simulation.

In the case of solutions and low permeation fluxes, the enhancement of wall shear stress obtained by numerical simulation in a helical tube accounts for the enhancement of permeate flux obtained in helical pervaporation membrane.

In the case of a suspension, the permeate flux enhancement seems more complex. At usual Reynolds numbers, the numerical approach clearly shows that the maximum velocity is located at the extrados of the coil. In contrast, laser visualisation shows under the same conditions, a maximum flow distribution including the centre of the Dean vortices and the same observations are deduced from numerical tracking. However, given that the residence time is lower at the centre of each vortex the different points of view are conciliated : the volumetric flow is higher in these areas.

We are at the present extending our simulation to high particle concentrations and to porous walls in order to precisely explain the mass transfer enhancement, which could be generated by new design for ultrafiltration membranes.

Acknowledgements : This work was performed in the framework of the FEDER objective (Contrat n° 17165).

REFERENCE

[1] Aimar, P., Sanchez V., Belg. J. Food Chem. Bio., 44 (1989), 203-214.
[2] Winzeler, H. B. and Belfort G., J. Membrane Sci., 80 (1993), 35-47.
[3] Moulin P., Veyret D., Charbit F., J. Membrane Sci., 183 (2001),149-162.
[4] Moulin, Ph., Serrano K., Serra C., Rouch J.C., Clifton M.J., Aptel P., Colloque de Mécanique des Fluides Expérimentale de Toulouse, C.E.R.T., Toulouse (1995).
[5] Mishra, P., Gupta S.N., Ind. Eng. Chem. Proc. Des. Dev., 18 (1979), 130-142.
[6] Schnabel S., Moulin P., Nguyen Q.T., Roizard D., Aptel P., J. Membrane Sci., 142 (1998), 129-141.
[7] Moulin P., Serra C., Rouch J.C., Clifton M.J., Aptel P., J. Membrane Sci., 114 (1996), 235-244.
[8] Manno P., Moulin P., Rouch J.C., Aptel P., Sep. Pur. Tech. 14 (1998), 175-182.

VARIATION OF THE FEED LOCATION AND IMPELLER SPEED IN A STIRRED TANK USING PLANAR LASER INDUCED FLUORESCENCE (P.L.I.F.)

A. Fall, O. Lecoq, R. David

Powders and Processes Center, Ecole des Mines d'Albi-Carmaux (E.M.A.C.), UMR CNRS 2392
Campus Jarlard, 81013 ALBI CT cedex 09, FRANCE

Abstract. The first stage of precipitation is generally the contacting of two reactive liquids which react quasi instantaneously and yield insoluble product. In the precipitation vessels it is essential to select the best position of the feed tubes, and stirrer speed in order to control the particle size distribution.

This study deals with a qualitative investigation of the mixing of two water feed streams in a 20 dm^3 continuous stirred tank from concentration and mixing index measurements. These measurements are carried out with Planar Laser Induced Fluorescence (PLIF). The influence of the following operating parameters are studied: feed location, stirrer speed and flow rate.

INTRODUCTION

Solid particles obtained by precipitation (reaction crystallization) in industry are generally produced in suspension in mechanically stirred tanks, in static mixers or in jet mixers. In these processes two liquid streams are put into contact but in a more or less controlled way.

Precipitation supersaturations originate from a chemical reaction and thus are very higher than in classical crystallization [1]. The first stage of this process is the contacting of two reactive solutions generally fed in a double jet operation. Then, these solutions react and yield the insoluble product. Furthemore, the effects of contacting and mixing conditions of reactants play an essential role on the nucleation and crystal size distribution [2]. Thus, the local mixing and contacting efficiency, which depend on the feed point location and stirring speed, control the particle size distribution, crystal nature and morphology. Indeed, if the mixing of both reactants is imperfect, in the stirred tank, the concentration pattern will not be homogeneous and supersaturations heterogeneities will be created. Consequently, nucleation and crystal growth rates will vary in the mixer from one point to another.

As a mixing model, we used the fluorescence properties of a solution mixed with pure water in a transparent tank, which is crossed by a planar laser sheet. During the first moments of mixing, the mixing of the two tracers is similar to the mixing of two reagents in ionic precipitation. Actually, there is no significant consuption of the reactants during the first seconds of mixing, owing to the small size of nuclei produced and to the time scales of the crystal growth which are much larger than those of nucleation [3]. As a result, mixing in ionic precipitation can be characterized by studying the mixing of two inert tracers, or the mixing of a single tracer in solution with pure solvant, each fluid being injected by two separate feed tubes.

The laser sheet visualization method has been used by [4], and developed in a 20 dm^3 mechanically stirred tank by Houcine et al. [5] and adapted at the pilot scale by Marcant et al. [6]. The laser induced fluorescence technique (L.I.F.), which is non-intrusive, can contribute to optimize the geometry of the mixers, the feed rates or the positions and shape of the injectors. It is based on the stimulation of fluorescence by laser and the measurement of the emitted light. Previous workers have used a CCD camera [4 - 6], a photomultiplier [7], and a line scan camera [8]. They measure the fluorescence hight intensity, respectively in a plane, at a point, and along a line. The planar laser induced fluorescence technique (P.L.I.F.) allows one to characterize mixing in any plane crossing the flow defined by the laser sheet. This technique is based on the fluorescence of organic substances induced by laser sheet and coupled with image analysis. The originality of this study, compared to previous works [4 - 6], lies (a) in the fact that the laser sheet is very thin (down to 100 μm), (b) the camera is much more sensitive, and finally (c) more powerful tools are used for image processing.

The aim of this paper is to check the influence of parameters like the feed point location, and the stirring speed on the contacting and mixing of two liquid feed streams by this method.

MEASUREMENT TECHNIQUE AND EXPERIMENTAL SET-UP

1. Principle

Several organic molecules in solution, like rhodamine B exhibit a fluorescence phenomenon when they are stimulated by laser light. For low tracer concentrations, the intensity of fluorescence is proportional to the local concentration of tracer and to the power of the incident laser light. The fluorescence is emitted with a wavelength of about 590 nm higher than the laser's one of 520 nm. Its intensity is filtered and monitored by a high sensitive video camera.

2. Procedure

The first set measurements are performed to establish the grey level images in the following cases:

- The tank is filled with water and the laser is switched off. It provides for the grey level field of the background: $NG_{ob}(x,y,t)$,
- Then the stirred tank is filled with a fluorescent tracer solution. Its concentration is the mixing concentration during the experiment in the completely homogeneous state C_{mp}. It yields the grey level field $NG_{C_{mp}}(x,y,t)$ corresponding to the perfect mixing images,
- Finally, two water feed streams (one containing the fluorescent tracer, the other only water) are fed in the stirred tank, yielding the grey level field: $NG(x,y,t)$.

For a diverging laser sheet, Houcine et al. [5] derived the relations:

- Between the instantaneous local concentration of tracer and the grey level $NG(x,y,t)$ of the image:

$$C(x,y,t) = \frac{NG(x,y,t) - \overline{NG_{ob}}(x,y)}{\overline{NG_{Cmp}}(x,y) - \overline{NG_{ob}}(x,y)} C_{mp} \qquad (I)$$

Where $\overline{NG_{ob}}(x,y)$ and $\overline{NG_{Cmp}}(x,y)$ are the average grey levels of the background and the perfect mixing, respectively.

•Between the grey level $NG(x,y,t)$, the power of light source (laser) P_0 and the tracer local concentration $C(x,y,t)$:

$$NG(x,y,t) = KP_0C(x,y,t)\exp\left[-\left(\varepsilon_i L + \varepsilon_e L'\right)C_{mp}\right] \qquad (II)$$

Where ε_i and ε_e are the extinction coefficients of incident laser light and emitted fluorescence light, L is the depth of penetration of the laser beam into the tracer solution, L' is the optical path length of the fluorescent light in the tracer solution, K is a constant grouping physical and geometrical parameters.

Equation (I) takes into account the average attenuation of the intensity along the optical path, approximately identical for $NG_{Cmp}(x,y)$ and $NG(x,y,t)$. The equation (II) is intended to determine the operating conditions of tracer and power favorable to obtaining a proportionality and a great sensitivity between the grey level and the fluorescent dye concentration.

3. Experimental

The scheme of the apparatus used in this work is shown in figure 1. The experiments are carried out in a standard type stirred tank of a 20 dm^3. The cylindrical vessel of internal diameter T = 290 mm is placed inside a square vessel filled with water in order to reduce problems associated with refraction by curved surfaces. Both vessels are made of a transparent material: optical quality Altuglass (PMMA). Four baffles of width T/10 and thickness T/100 are provided at intervals of 90° against the wall of the inner tank. The six bladed Rushton turbine in altuglass is coupled to a stainless steel shaft which has an external diameter of 10 mm. The impeller diameter and bottom clearance are equal to H/3, where H represents the height of the liquid in the tank. The other dimensions of the tank are represented in figure 2. The optical device includes a laser diode, with an emission wavelength of 520 nm and with a maximum power P_0 of 2W. When crossing the diaphragm, the laser beam is focused by a mirror and is spread out into a very thin sheet (down to 100µm) using a POWELL lens. A CCD camera, of total exposure time 35 ms, fitted with a sharp cut-off high pass filter at 570 nm takes 9 images per second. It gives high image resolutions down to ten micrometers, with images of 1280×1024 pixels encoded on 65536 grey levels. The camera and the laser are jointly assembled on a vertical and horizontal displacement system. This device is controlled by a computer with a total displacement of 540 mm and a repeatability of 0.1 mm. Two reservoirs continuously supply the tank with two incoming feed tubes (of internal diameter 6 mm). The feed points are situated on the vertical plane tangent to the impeller. In this plane, there is no significant orthogonal average velocity [9]. The tracer

concentration (40 $\mu g.dm^{-3}$) is selected in the range of linearity betwen concentration and grey level, [10]. The fluorescence images are recorded with FlowManager®-Dantec software and then processed in Aphelion®-Adcis images analysis software with specific developed macros.

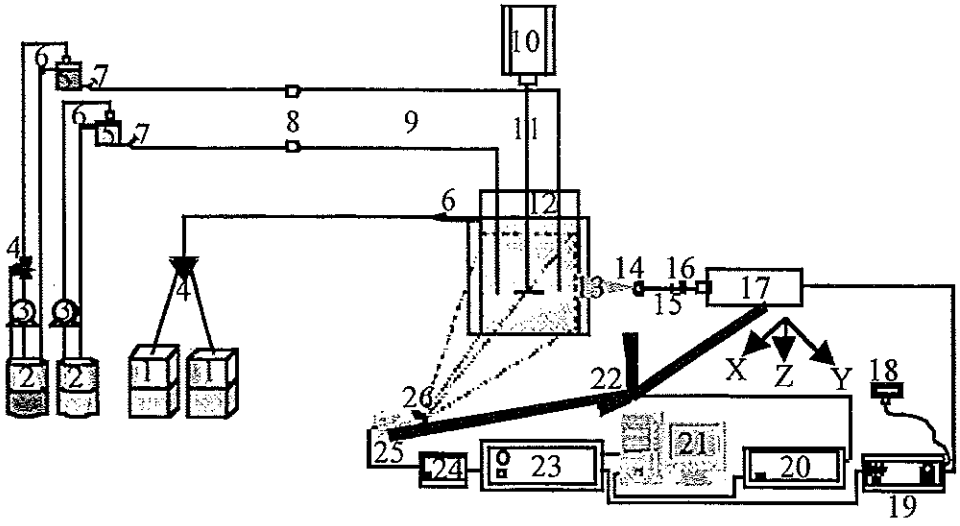

Figure 1: Experimental set-up: 1. Storage tanks, 2. Feed tanks, 3. Pumps, 4. Valves, 5. Reservoirs, 6. Outlet, 7. Taps, 8. Flow meters, 9. Feed tubes, 10. Motor, 11. Stirrer, 12. Mixing tank, 13. Laser sheet, 14. Powell lens, 15. Mirror, 16. Diaphragm, 17. Laser diode (power 2W at 520 nm), 18. Control module, 19. Internal diode power supply, 20. Displacement remote control, 21. Computer, 22. Displacement system, 23. Processor, 24. Video power supply, 25. CCD camera, 26. High-pass filter.

4. Operating conditions

The following parameters are investigated:

•The feed point location: the three different locations of feed point (figure 2), are:

(pos1) = 1: 50 mm under the stirrer,

(pos2) = 2 : in the disk plane of the turbine,

(pos3) = 3: 50 mm above the stirrer.

In these points, the stirring speed is fixed at N = $3s^{-1}$ and the flow rates is $Q_1 = Q_2 = 1.5\ dm^3.min^{-1}$.

•The stirring speed: the four stirring speeds are N = 0 s^{-1}, 3 s^{-1}, 6 s^{-1}, 9 s^{-1}. In this configuration, the tank is continuously supplied with equal flow rates $Q_1 = Q_2 = 1.4\ dm^3.min^{-1}$ and the feed location is the (pos2) (figure 2).

•The flow rates: the tank is continuously supplied with four flow rates $Q_1 = Q_2 = 0.6\ dm^3.min^{-1}$, $1.2\ dm^3.min^{-1}$, $1.8\ dm^3.min^{-1}$, $2.4\ dm^3.min^{-1}$. In these cases, the stirring speed is fixed at N = 2 s^{-1}, and the feed location is the (pos2) (figure 2).

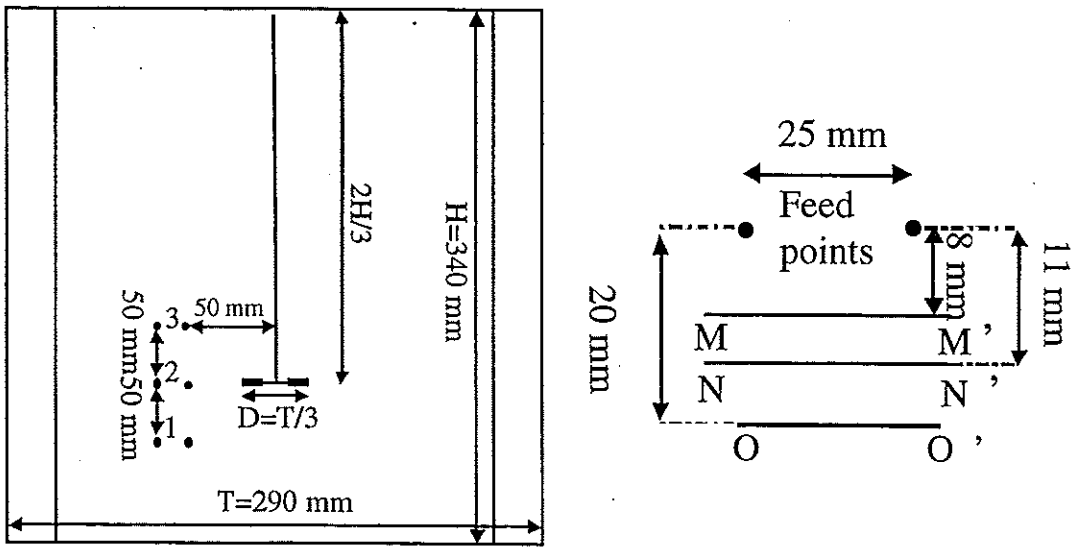

Figure 2: Mixing tank : T : The internal diameter or the tank, H : The height of the liquid in the tank, special measurements lines MM' = NN' = 60 mm, OO' = 50 mm.

For a quantitative exploitation of the results, three measurement lines MM', NN', OO' respectively have been chosen at different relative distances from the feed points (figure 2).

RESULTS AND DISCUSSIONS

Before starting the experiments in the continuous stirred tank, we have to determine the range of the linear response between the grey level and the tracer concentration. The linearity is observed up to 40 $\mu g.dm^{-3}$ ($8.35\ 10^{-8}$ $mol.dm^{-3}$), [10]. For larger concentrations the response of the grey level becomes non-linear because of the exponential term of the equation II. This result is in agreement with those obtained by [5], who used a laser power of 1.4 W. The linear response between the laser power and the response was also checked up to 2 W power [10].

The first results obtained point out the possibility to realise a quantitative analysis of mixing phenomenon using the reduced concentration, given by the equation (I) and the mixing index defined by the equation (III) in the case of two species A and B [11].

$$\alpha_{AB}(x,y,t) = 1 - \left| \frac{C_A(x,y,t) - C_B(x,y,t)}{C_A(x,y,t) + C_B(x,y,t)} \right| \qquad \text{(III)}$$

In the case of a tracer water solution (A) and pure water (B), the equation (III) becomes, with the tracer concentration $C_A(x,y,t)$:

$$\alpha_{AB}(x,y,t) = 1 - \left| \frac{C_A(x,y,t) - C_{A_0}}{C_A(x,y,t) * (2 * f - 1) + C_{A_0}} \right| \qquad \text{(IV)}$$

where $\bar{f} = \frac{Q_A}{Q_A + Q_B}$, Q_A and Q_B are the flow rates in feed tube A and B respectivelly.

1.Feed point location

Figures 3 and 4 show a plot of the reduced mean concentation $\frac{\bar{C}(x,y)}{C_{mp}(x,y)}$ and mean mixing index $\bar{\alpha}(x,y)$ along a line NN' at 3 different locations (figure 2). One of the feed tubes the right one containing water is closer to the blades passing. This explains the asymmetry of the two feed streams at pos2 position. The reduced mean concentation varies between 0 and 2 and the mean mixing index between 0 and 1, corresponding to the feed stream of water and fluorescent tracer respectively. Perfect mixing is reached for the values 1 of both variables. The results of $\bar{\alpha}(x,y)$ and $\frac{\bar{C}(x,y)}{C_{mp}(x,y)}$ for the positions pos1 and pos3 are very close, and further more these positions are considerably less mixing effective when compared to the position pos2. In fact, the average velocity generated by the stirrer is much lower at pos1 and 3 (about 0.15 $m.s^{-1}$) than for pos2 (0.67 $m.s^{-1}$) at N = 3 s^{-1}, when compared with jet initial velocity (0.8 $m.s^{-1}$) at $Q_1 = Q_2 = 1.5$ $dm^3.min^{-1}$.

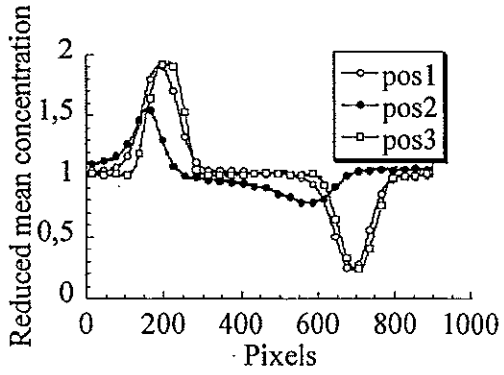

Figure 3 : Variation of reduced mean concentration along a line NN' at 3 different positions : 1 (pos1), 2 (pos2), 3 (pos3). N = 3s^{-1} $Q_1 = Q_2 = 1.5$ $dm^3.min^{-1}$.

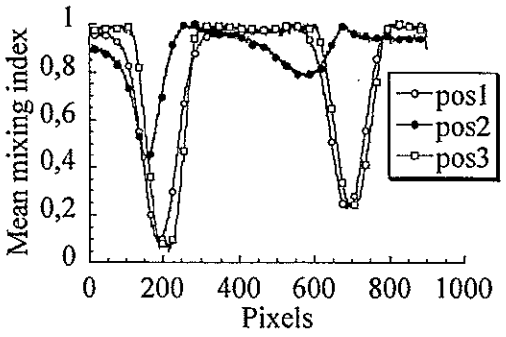

Figure 4 : Variation of mean mixing index along a line NN' at 3 different positions : 1 (pos1), 2 (pos2), 3 (pos3). N = 3s^{-1} $Q_1 = Q_2 = 1.5$ $dm^3.min^{-1}$.

2.Stirring speed

Figures 5 and 6 represent the evolution of reduced mean concentration and mean mixing index, respectively as a function of stirring speed along a line OO'. At low stirring speed, there is no effect on the incoming jets. From N = 3 s^{-1}, corresponding to the turbulent flow (Reynolds number Re = 28000) these both variables are detached compared to N = 0 s^{-1} and tend to 1 (perfect mixing). These results clearly emphasize the mixing efficiency as the stirrer speed increases.

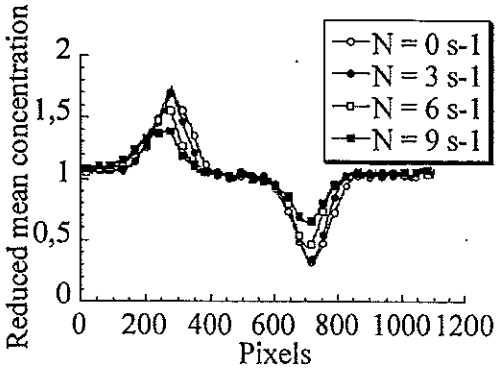

Figure 5 :Reduced mean concentration as function of the stirrer speed along a line OO' at the pos2 position (feed flow rates $Q_1 = Q_2 = 1.4\ dm^3.min^{-1}$)

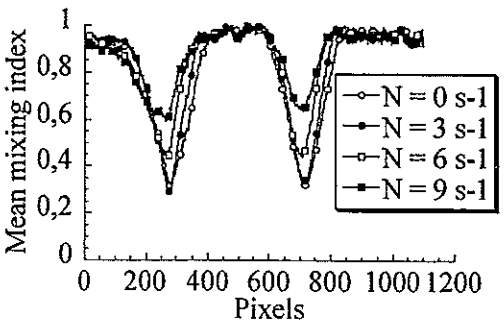

Figure 6: Mean mixing index as function of the stirrer speed along a line OO' at the pos2 position (feed flow rates $Q_1 = Q_2 = 1.4\ dm^3.min^{-1}$)

3.Feed flow rates

Evolutions of the reduced mean concentration and mean mixing index as function of the feed flow rates along a line MM' at the pos2 position are given in figure 7 and 8 respectively. These 2 variables are not significantly influenced on the incoming jets at high feed flow rates ($Q_1 = Q_2 = 1.2\ dm^3.min^{-1}$, $1.8\ dm^3.min^{-1}$, $2.4\ dm^3.min^{-1}$). But they are considerably marked for $Q_1 = Q_2 = 0.6\ dm^3.min^{-1}$ corresponding to a jet initial velocity of $0.33\ m.s^{-1}$, much lower compared to average velocity generated by the stirrer $0.45\ m.s^{-1}$ for pos2 at $N = 2\ s^{-1}$. Therefore, the jet motion is preponderant at $Q_1 = Q_2 = 1.8\ dm^3.min^{-1}$ and $2.4\ dm^3.min^{-1}$, whereas the flow pattern induced by the stirrer is determinant at the lowest flow rate.

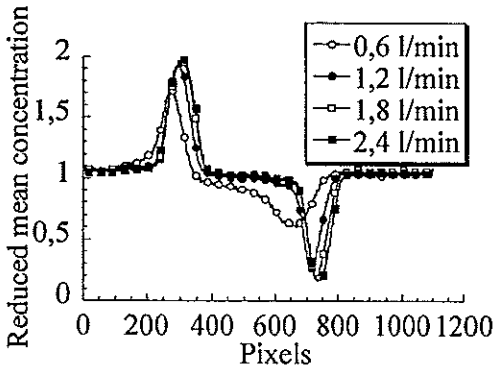

Figure 7 : Reduced mean concentration as function of the flow rate along a line MM', pos2, $N = 2\ s^{-1}$

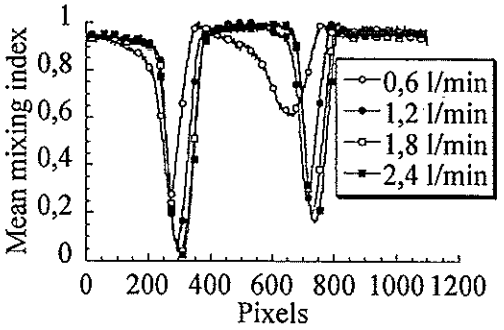

Figure 8 : Evolution of mean mixing index along a line MM', pos2, $N = 2\ s^{-1}$

CONCLUSION

Planar laser induced fluorescence (P.L.I.F.) technique is a powerful non intrusive tool for rapid measurement of mixing characteristics. It was applied to mean

concentration and mixing index qualitative measurements in a stirred tank reactor, continuously fed with a tracer solution and pure water. This technique allows characterization of the local state of mixing by reduced mean concentration $\frac{\overline{C}(x,y)}{C_{mp}}$ and mean mixing index $\overline{\alpha}(x,y)$. The influence of impeller speed, feed point locations and flow rates have been studied. The results clearly show that the two feed streams are not symmetrical. This is due to the fact that one of them (here: the right one) is closer to the passing blades. The following conclusions may be drawn from these results:

- Except in the feed jets the quality of mixing is almost perfect: $\frac{\overline{C}(x,y)}{C_{mp}}$ and $\overline{\alpha}(x,y)$ are both close to 1,
- In the feed jets center lines the reduced mean concentration tends to 1 with increasing impeller speed, as well as the mean mixing index. The evolution of $\frac{\overline{C}(x,y)}{C_{mp}}$ and $\overline{\alpha}(x,y)$ for the positions pos1 and pos3 is almost identical, whereas the mixing proceeds much better for the pos2 position (where the jet is in the radial discharge zone of the impeller). The effects of the jets on both variables are particulary marked above 1,2 l/min, and are almost independent of flow rates in that range.

REFERENCES

[1] Villermaux J., David R., *Effet du micromélange sur la précipitation*, Journal de Chimie physique, 85 (2), (1988), 273-279

[2] Marcant B., David R., *Experimental Evidence for and Prediction of Micromixing Effects in Precipitation*, AIChE Journal, 37 (11), (1991), 1698-1710

[3] David R., Marcant B., *Prediction of Micromixing Effects in Precipitation : Case of double-jet Precipitators*, AIChE Journal, 40 (3), (1994), 424-432

[4] Mahouast M., *Mesure des champs de concentration et de température dans un réacteur agité par traitement des images de la fluorescence induite par une nappe laser*, Récent Progrès en Génie des Procédés, 24, (1993), 53-60

[5] Houcine I., Vivier H., Plasari E., David R., Villermaux J., *Planar laser induced fluorescence technique for measurements of concentration fields in continuous stirred tank reactor*, Experiment in Fluids, 22, (1996), 95-102

[6] Marcant B., Seidlitz F., Plasari E., Villermaux J., *Direct measurements of generalized mixing model parameters by laser sheet visualization*, Récent Progrès en Génie des Procédés, 11 (51), (1997), 349-356

[7] Gaskey S., Vacus P., David R., Villermaux J., André J.C., *A method for study of turbulent mixing using fluorescence spectroscopy*, Experiment in Fluids, 9, (1990), 137-147

[8] Distelhoff M.F.W., Marquis A. J., *Scalar mixing in the vicinity of two disk turbines and two pitched blade impellers*, Chemical Engineering Science, 55, (2000), 1905-1920

[9] Kemoun A., *Caractérisation expérimentale de la structure de l'écoulement dans une cuve agitée : Mélange*, Thèse de doctorat INPL, Nancy-France, (1995)

[10] Fall A., Lecoq O., David R., *Characterization of mixing in a stirred tank by Planar Laser Induced Fluorescence (P.L.I.F.)*, International Symposium on Mixing in Industrial Processes (I.S.M.I.P.4), Toulouse-France, 14-16 May 2001

[11] Ablitzer C., *Etude de la formation de poudre dans des jets coaxiaux réactifs*, Thèse de doctorat INPG, Saint-Etienne-France, (1999)

THE USE OF ELECTRICAL CAPACITANCE TOMOGRAPHY TO STUDY THE AXIAL AND RADIAL SOLIDS LOADINGS UP A CFB-RISER

C. Vandewalle[1], K. Smolders[2] and J. Baeyens[1]

[1] Katholieke Universiteit Leuven, Chemical Engineering Department, de Croylaan 46, B-3001 Heverlee,
[2] Universiteit Antwerpen, Institute for Environmental Studies, Universiteitsplein 1, B-2610 Antwerpen

Abstract. The determination of the solids hold-up and local solids fluxes is of paramount importance in the study of the hydrodynamics of a two phase flow. Several techniques have been used during the past decades, either as invasive methods (probes, non-isokinetic sampling etc) or non-invasive methods (pressure gradients, X-ray photography, tomography etc). The authors used electric capacitance tomography (ECT) to measure the solids hold-up in the riser of a circulating fluidized bed.

INTRODUCTION

The determination of the solids hold-up and local solid fluxes is of paramount importance in the study of the hydrodynamics of a two-phase flow. Several techniques have been used during the past decades (Table 1). These methods can be classified in two groups, depending on their possible disturbance of the two-phase flow. During a detailed investigation of the hydrodynamics of Circulating Fluidized Beds (CFBs), the authors studied the solid loading profiles using several techniques, including ECT (electrical capacitance tomography). The text below summarises the initial important findings and data treatment.

Table 1: Methods for measuring solids hold-up and local solids fluxes

Method	Property obtained	Reference
Pressure gradient over the riser	pressure gradient, bed density profile, voidage profile, slip velocity	[1 - 7]
Quick-closing valves	voidage profile	[8, 9]
Capacitance probes	local voidage	[10 – 12]
X-ray photography	radial solids density profile	[13]
Non-isokinetic sampling	radial profiles of solids mass flux	[14, 15]
Optical fiber probe	solids density profile, cluster length and density, local particle concentration	[16 –19]
High-speed video camera	plugs and slugs, particle motion at the wall	[8, 20]
Video camera with optic fiber micrograph probe	shape and transformation of clusters, radial and axial distribution of clusters	[21]
TSI fiber optic probe laser doppler velocimeter	local particle velocity	[18]
Laser sheet technique	3D flow visualisation of suspension	[22]

EXPERIMENTAL LAYOUT

1. The Circulating Fluidized Bed

The circulating fluidized bed consists mainly of two parts: the riser where particles are transported upwards, and the recycle loop, needed to convey the particles back to the bottom of the riser. The CFB used in most experiments is shown in Figure 1. A similar CFB, of ID 150 mm, was also used. The riser is built of three sections of perspex for a total height between distributor and top of 6.47 m. The exit of the riser is very sudden and sharp, which will have an influence on the solids hold-up. To minimise electrostatic effects, the riser and all other parts of the CFB are electrically grounded.

Air from a Roots-type blower is fed to the riser through a metal gauge distributor. To prevent clogging of the distributor by oil or dirt, the air is filtered. The distributor and windbox can be disconnected from the riser for easy cleaning.

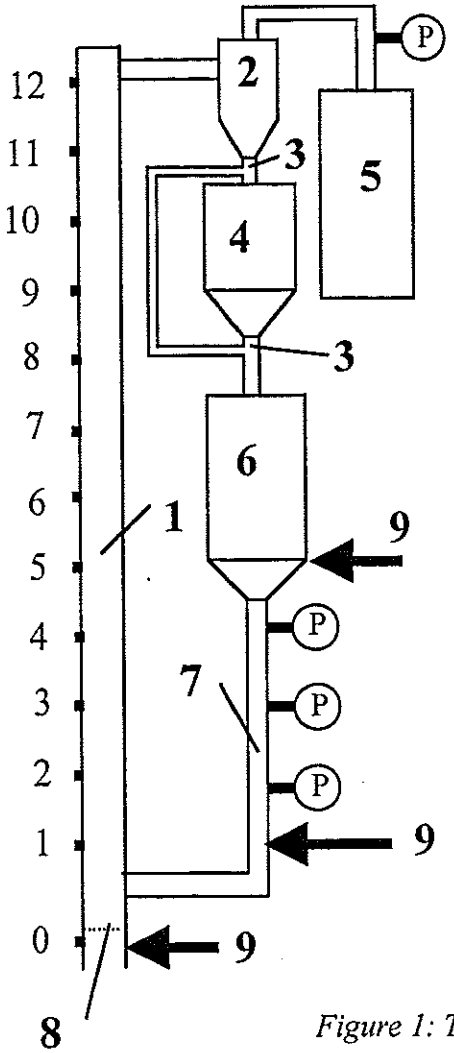

1. Riser
2. Cyclone
3. Diverter valve
4. Measuring bed
5. Bag filter
6. Slow bed
7. L-valve
8. Metal gauge distributor
9. Air from Roots blower

Figure 1: The circulating fluidized bed

At the exit of the riser, solids are separated from the air by a high efficiency Stairmand cyclone, followed by a bag filter. Almost all particles are collected by the cyclone (>99% efficient). The bag filter only traps the ultrafines, which are periodically returned to the unit. The fluidized bed in the recycle loop of a CFB is needed to create a pressure build-up, which compensates the pressure drop of riser and cyclone. It can be constructed as a fluidized standpipe or as a fluidized bed ('slow bed') with a diameter larger than the other parts of the recycle loop, thus also providing particle storage. In our system, the particles discharged from the cyclone first pass through a measuring bed and then in a slow bed. The slow bed has an I.D. of 0.29 m and a height of 1.30 m. In most of the experiments, the height of the slow bed is between 0.6 and 0.9 m. The bed is fluidized at a superficial velocity just in excess of U_{mf} by air introduced through a tubular distributor with 2 mm I.D. orifices facing downwards. The fluidizing air of the slow bed leaves the bed through a pipe at the top into a bag filter for dust removal. Particles can also be fed into the CFB through the slow bed. For the controlled recycle of solids into the riser, several systems can be used. Some authors use a downward inclined pipe with a mechanical slide valve to control the solid flow. The non-mechanical valves (J-, V- and L-valve) are very popular, as they only need an airstream to control the solid flow. The most important advantages are that no moving parts which can block or become eroded and that a gas seal is created, so that no gas from the riser is leaking to the recycle loop. In our system, the recycle of solids from the slow bed to the riser is controlled by a 63.5 mm I.D. L-valve of 2.3 m vertical and 0.75 m horizontal length. The air is supplied to the L-valve at 17 cm above the elbow.

2. Solids used

A rounded sand and a spent catalyst were used. Properties are given in Table 2. Average particle sizes were determined by Malvern laserdiffractometry. Bulk and absolute densities were separately measured. A 100 μm sand was used in the 0.15 m ID set-up.

Table 2: Properties of powders used in experiments

	Sand	FCC
particle size d_p (μm)	90	70
particle density ρ_p (kg/m_)	2600	1700
90%-range (μm)	75-150	50-130
bulk density ρ_b (kg/m_)	1400	1000

3. Measurements

The gas velocity in the riser was determined by measuring the pressure drop across a standard orifice plate, placed in the line before the distributor. The solids circulation rate leaving the cyclone is measured by diverting the solids to the measuring bed for a given time, using a valve between the measuring and the slow bed. The difference in height of the bed surface of the slow bed is measured. This difference is kept small (maximum 7 cm) to minimise the influence on the CFB system. Measured solids are returned into the loop whilst in operation. The mass of the solids in the

measuring bed and hence the solids circulation rate can be determined by:

$$M = \rho_b A_{SB} \Delta L_{SB} \tag{1}$$

M is the mass of the solids collected in the measuring bed (kg), ρ_b the bulk density (kg/m_), A_{SB} the cross-sectional area of the slow bed (m_), ΔL_{SB} difference in height of slow bed surface (m). Calibration tests have validated the use of eqn. (1).

Pressure tappings were installed at various heights in the riser (every 0.5 m), over the L-valve, over the bag filter and after the cyclone. To prevent ingress of powder into the measuring lines, the pressure tappings were provided with a glasswool plug. The measuring lines were fixed onto a T-piece, connected respectively to a water manometer and a solid state pressure transducer. The transducers were linked to a personal computer via an A/D converter. Pressure measurements across the bag filter and the cyclone were needed to check the behaviour of both. Pressure gradients along the height of the riser ($\Delta P/\Delta L$) were determined.

Each set of experiments was preceded by the determination of the pressure drop across the distributor. Pressure drops were recorded at several gas velocities without solid flux. If the gas/wall friction can be neglected, the pressure drop across tapping 0 and 1 (Figure 1) is equal to the pressure drop across the distributor. The pressure drop, caused by gas-wall friction is given by:

$$\Delta P_g = 4 f_g \frac{\rho_g U? L}{2 D} \tag{2}$$

ΔP_g is the pressure drop caused by gas-wall friction (Pa), ρ_g the gas density (kg/m_), L the total height of the riser (m), D the riser or bed diameter (m), U the superficial gas velocity (m/s). The friction factor f_g can be calculated from the Blasius equation:

$$f_g = \frac{0.079}{Re^{0.25}} \qquad \text{for } 4000 < Re < 10^5 \tag{3}$$

Re is the Reynolds number ($= \rho_g U D/\mu$) with μ the gas viscosity (Pas).

The pressure drop between pressure tappings 0 and 1 is within approximately 1% of the pressure drop across the distributor [23]. A fitting of the pressure drop across the distributor ΔP_{distr} resulted in the expected equation:

$$\Delta P_{distr} = aU^2 \tag{4}$$

As the distributor can be clogged during the experiments, cleaning was periodically performed. Every new set of experiments was preceded by the

measurement of the pressure drop across the distributor. The pressure drop barely changed, even after cleaning.

MEASUREMENTS OF THE SOLIDS LOADING

1. Generalities

Within the methods of measuring the solids loading, both non-invasive and flow-disturbing methods can be used. The disturbing methods are characterised by some devices that enter the riser and hence disturb the flow of gas and particles, e.g. quick-closing valves, probes ... Probes include optical probes (which 'see' the particle flow in the core of the riser), probes to measure the electric capacitance of the flow and suction probes. The use of these methods is detailed elsewhere [23, 24, 25] and is not dealt with in the present paper. Non-invasive methods do not obstruct the particle flow profile and are therefore preferred.

2. Non-invasive methods: pressure gradients

Measuring the pressure gradient to determine the solids hold-up is the easiest and most widely used method that does not influence the two-phase flow at all. Provided the change in pressure gradient with height is small, it has been demonstrated by Louge and Chang [26] that the mean solids volume fraction in the riser may be calculated directly from the riser pressure gradients, assuming negligible acceleration and friction effects:

$$\left(1-\bar{\varepsilon}\right)=\frac{-\Delta P}{\Delta L}\sqrt{\frac{1}{\rho_p g}} \qquad (5)$$

$\Delta P/\Delta L$ is the pressure gradient (Pa/m), $\bar{\varepsilon}$ the average voidage, ρ_p the particle density (kg/m_), g the gravitational constant (m/s_).

To verify the conditions stipulated by Louge and Chang [26], the acceleration and friction losses were calculated [23]. For most experiments carried out, these calculated losses were less than 5% of the total pressure drop and hence only of minor influence. Typical experimental axial profiles of pressure and solids concentration are given in [23] and corresponds with the data of previous publications [1,2,4, ...]. All figures attest to the high solids concentrations that can be maintained in the riser at velocities that are a multiple of those normally employed in bubbling beds of the same solids. The voidage is not uniform, with a sharp decrease at the bottom of the riser and a gradual reduction higher up and towards the exit of the riser. Increasing the solid flux or decreasing the gas velocity results in an increase of the solids concentration and this mainly in the bottom part of the riser.

3. Non-invasive methods: the tomographic techniques

Tomography regroups several techniques, all however with the objective to visualise the internal structure of an object or system in a two- or three-dimensional way. It is even possible to study the dynamic properties of processes.

The different techniques applied/applicable in chemical engineering processes and research are summarised in Table 3 below.

Table 3: Different tomographic techniques and their application in chemical processes and research

Method	Property obtained
Nuclear, transmission (X-ray, gamma-ray, neutron)	- imaging multiphase flow and mixing of particles in fluidized beds - non-destructive testing (NDT)
Nuclear, emission (photon, positron)	- imaging particle mixing - non-destructive testing (NDT)
Nuclear, dispersion (neutron, Compton gamma-ray)	- determination of volume fractions in liquid/gas flow
Optical, transmission	- imaging flow profiles - flame analysis
Optical, emission (infrared)	- remote temperature sensing - plasma analysis
Acoustical, reflection	- imaging two-phase flow
Acoustical, sound wave analysis	- imaging cavities - remote sensing of temperatures in furnaces - determination of velocity profiles
Acoustical, diffraction	- imaging flow profiles - non-destructive testing (NDT)
Microwave, diffraction	- remote temperature sensing - robot distance sensing - non-destructive testing (NDT)
Nuclear magnetic resonance	- determination of velocity profiles
Electrical, capacitancy	- imaging two-phase flow and particle flow in fluidized beds, downcomers etc.
Electrical, resistance	- imaging hydrocyclone flow and mixing - geophysical exploration
Electrical, impedancy	- no references until now

All techniques operate according to similar principles:

- a signal is emitted by a source; this signal can be of e.g. electromagnetic, nuclear, acoustical, electrical or other nature;
- depending upon the contents of the studied object, this signal will undergo changes according to physical principles;
- the signal is then detected;
- the difference between emitted and detected signal is a function of the magnitude of the physical property influenced by the signal;
- a 3D picture is obtained by either rotating the object or by installing several detectors;
- a computer transforms the signal response according to a appropriate algorithm.

MEASUREMENTS OF THE SOLIDS LOADING

1. Layout

A number of electrodes (16) is placed around the riser of the CFB. Each electrode is used as an emittor. A 15V, 200 Mhz signal is applied to the electrode and the capacitance is measured between the source and the 15 other electrodes. Thereafter, another electrode (e.g. N°2) is activated and capacitancies with electrodes 3 to 16 are measured. In doing so, n(n-1)/2 independent measurements are made. The computer thereafter transforms data into density profiles. The data treatment occurs in "real time" and results are illustrated in density profiles at a given height. During the research at the University of Bradford, tests were done on measuring radial profiles by an electric capacitance tomography system developed by UMIST. Figure 2 shows the experimental set-up with 16 electrodes fixed around the CFB-column.

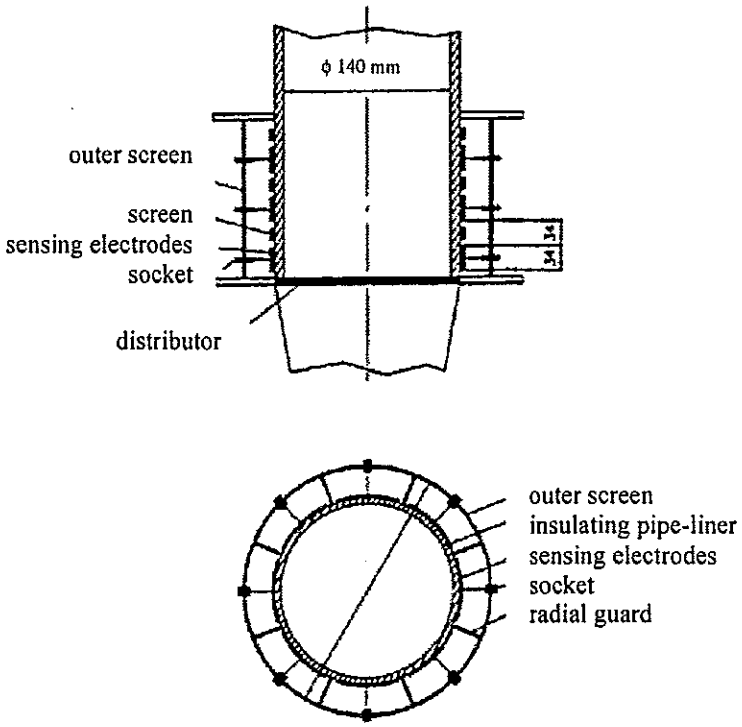

Figure 2: Layout of the ECT-application

2. Results and discussion

Experiments at different superficial velocity and solids' flux were examined. Combined conditions are illustrated in Table 4. Illustration of the tomographic imaging is given in Figs 3 to 5, taken resp. at the indicated conditions. Similar results were obtained at locations higher up the riser.

Table 4: Combined conditions of the experimental tomographic tests

U (m/s)	G (kg/m .s)
3.05	13
3.28	22
3.60	27
3.71	36
3.91	32
4.27	50
4.54	31
4.70	52
4.88	42
4.9	35
4.9	62
5.85	75
5.87	43

The results of ECT-measurements confirm the existence of a dense phase at the wall and a dilute core in the centre of the riser. The influence of the solid flux and the gas velocity can be noticed: the density at the wall increases with increasing solid flux and decreasing gas velocity. At higher gas velocities, the annulus is smaller and the gradient in the solid voidage across the annulus is greater. When descending in the riser, the negative flow rates in the annulus increase whereas the core diameter decreases. The average solids density also increases in the same direction. The observations stress the value of the core-annulus approach for the solids flow up a riser in a CFB. These findings were confirmed by invasive measurements using a non-isokinetic probe [15, 23].

Since the density of the core zone is lower than the lowest current detection limit of the ECT-installation, ECT can at present only be consired a qualitative tool to study local solids hold-up and not yet adapted for quantitative results. Since our preliminary tests, UMIST has improved its ECT-installation, which will lead to reliable quantitative results in the future. The most important advantages are its real time nature, non-obstructive measuring method and the possibility to use it at high temperatures and pressures as it is fixed outside the riser.

Figure 3: Tomography (U = 5.85 m/s & G = 75 kg/m_s)

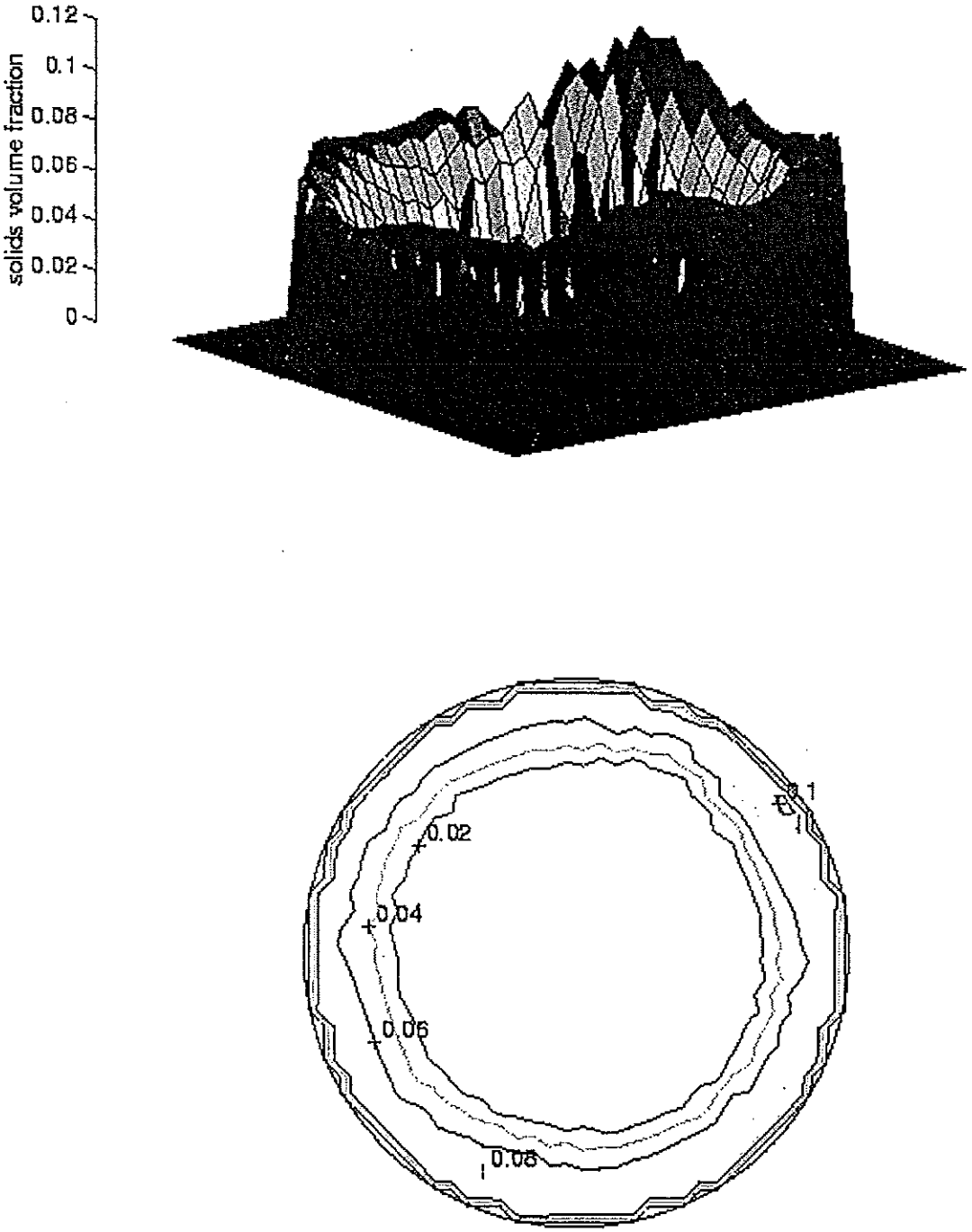

Figure 4: Tomography (U = 5.87 m/s & G = 43 kg/m_s)

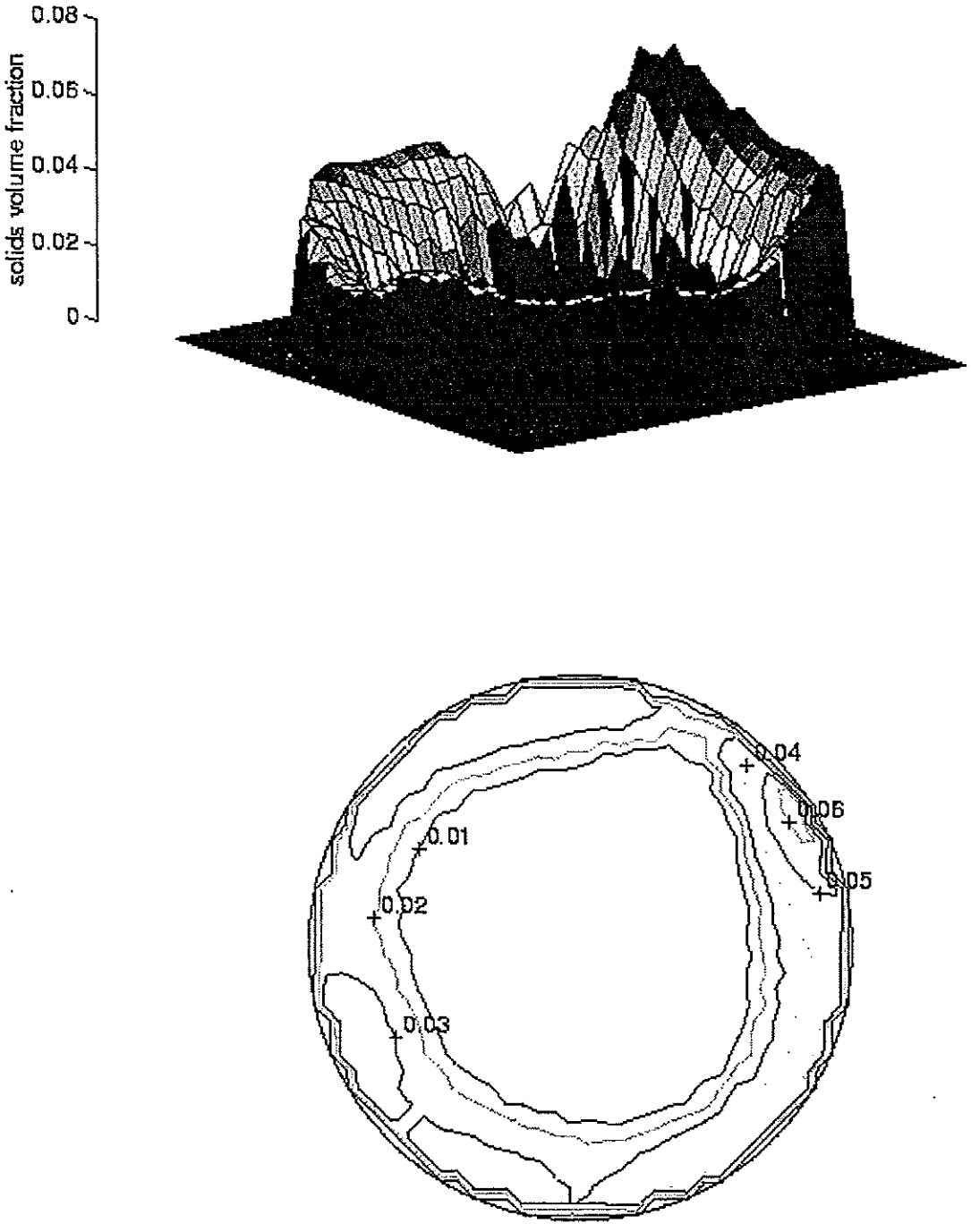

Figure 5: Tomography (U = 3.76 m/s & G = 36 kg/m_s)

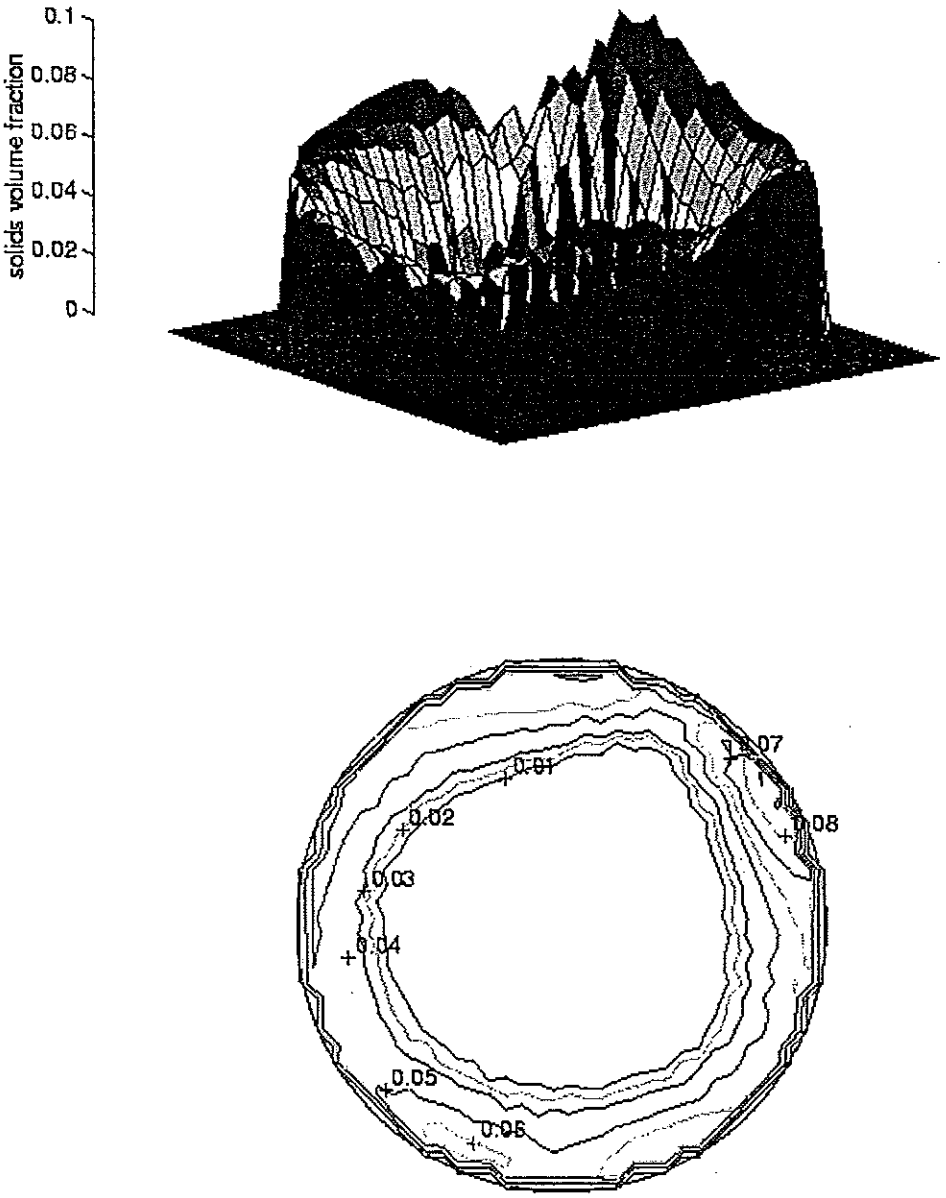

CONCLUSIONS

The study of the hydrodynamics of a two-phase flow targets the determination of the solids hold-up and local solids fluxes. Both non-invasive techniques (pressure drop measurements, electric capacitance tomography (ECT) and invasive methods (tribo-electric probe, non-isokinetic probe) can be used to characterised axial and radial solids hold-up in the riser. The denser bottom zone and the dilute phase higher up the riser were observed by pressure drop measurements, while the existence of a core/annulus flow was confirmed by the measurements with the ECT-system.

REFERENCES

[1] Yerushalmi J., Cankurt N.T., Powder Technol. 24, (1979) 125.
[2] Takeuchi H., Hirama T., Chiba T., Biswas J., Leung L.S., Powder Technol. 47, (1986) 195.
[3] Arena U., Marzocchella A., Massimilla L., Malandrino A., Powder Technol. 70, (1992) 237.
[4] Hirama T., Takeuchi H., Chiba T., Powder Technol. 70, (1992) 215.
[5] Mori S., Liu D., Kato K. , Kobayashi E., Powder Technol. 70, (1992) 223.
[6] Wong R., Pugsley T., Berruti F., Chem. Eng. Sci. 47, (1992) 2301.
[7] Glicksman L.R., Hyre M., Woloshun K., Powder Technol. 77, (1993) 177.
[8] Arena U., Cammarota A., Pistone L., *Circulating Fluidized Bed Technology*, P. Basu (Ed.) Pergamon Press, Toronto, (1986) 119.
[9] Van der Ham A.G.J., Prins W., Van Swaaij W., AIChE Symp. Series 89 (296) (1992) 53.
[10] Hartge E.-U., Rensner D. Werther J., *Circulating Fluidized Bed Technology II*, P. Basu and J.F. Large (Eds.), Pergamon Press, (1988) 165.
[11] Brereton C.M.H., Ph. D. Thesis, University of British Columbia, Vancouver, Canada (1987).
[12] Riley C.A., Louge M., Particulate Science Technol. 7, (1989) 51.
[13] Weinstein H., Shao M., Schnitzlein M., *Circulating Fluidized Bed Technology*, P. Basu (Ed.), Pergamon Press, Toronto, (1986) 201.
[14] Rhodes M.J., Laussman P., Villain F., Geldart D., *Circulating Fluidized Bed Technology II*, P. Basu and J.F. Large (Eds.), Pergamon Press, (1986) 155.
[15] Rhodes M.J., Laussman P., Powder Technol. 70, (1992) 141.
[16] Ishii H., Horio M., Adv. Powder Technol. 2, (1) (1991) 25.
[17] Horio M., Ishii H. , Nishimuro M., Powder Technol. 70, (1992) 299.
[18] Wang Z., Bai D. and Jin Y., Powder Technol. 70, (1992) 271.
[19] Zhou J., Grace J.R., Qin S., Brereton C.M.H., Lim C.J., Zhu J., Chem. Eng. Sci. 49, (1994) 3217.
[20] Rhodes M.J., Mineo H., Hirama T., Powder Technol. 70, (1992) 207.
[21] Li H., Xia Y., Tung Y. , Kwauk M., Powder Technol. 66, (1991) 231.
[22] Horio M., Kuroki H., Chem. Eng. Sci. 49, (1994) 2413.
[23] Smolders K., Ph. D. Thesis, Katholieke Universiteit Leuven, Belgium (1999).
[24] Smolders K., Baeyens J., to be published in Powder Technol. (2001).
[25] Smolders K., Baeyens J., Powder Handling and Processing 9, (1997) 123.
[26] Louge M. Chang H., Powder Technol. 60, (1990) 197.

PARALLEL FLOW ASYMMETRIES DUE TO NON-UNIFORM TEMPERATURES INVESTIGATED BY TRACER TECHNIQUES

R. Žitný and J.Thýn

Czech Technical University in Prague, Department of Process Engineering, Technická 4,
166 07 Prague 6 , CZECH REPUBLIC

Abstract. The effect of flow asymmetry was observed experimentally in lateral parallel channels of continuous direct ohmic heater. While the flow in parallel channels is uniform at isothermal conditions, one stream may be delayed and even stopped or reversed if the temperature differences between channels are too high in case of heating. The effect can be explained by buoyancy and theoretical analysis predicts existence of two solutions, symmetric and asymmetric distribution of flowrates, which can be stable within a certain range of temperatures and flowrates. Integral model, based upon momentum and heat balances has been suggested with the aim to predict influence of heater geometry, fluid properties and operational parameters (flowrates, intensity of heating) upon the RTD of parallel laminar flows. The model takes into consideration also the cross-flow between the main parallel streams. This "zonal" model enables to calculate residence time distribution (RTD) of the heater and results predict that the effects of asymmetries upon RTD is significant. Therefore the measurement of RTD characteristics seems to be promising method for detection of the parallel flow asymmetries. Experimental verification was based upon a) flow visualisation (injection of a coloured tracer and monitoring the tracer by Canon MV-100 camera), b) measurement of temperature profiles (11 thermometers Pt100), and on c) stimulus response experiments using KCl as a tracer for conductivity methods (2 Pt conductivity probes) and Tc99 as a radioisotope tracer (collimated scintillation detectors). Results confirm predicted influence of operational parameters and geometry (diameter of channels) on the stability of flow.

INTRODUCTION

Parallel flows are typical for many important apparatuses of process industries, e.g. flows in shell&tube or plate heat exchangers, heaters, reactors. Sometimes flow irregularities, instabilities or just only non-uniform distribution of flow in parallel channels occur. These undesirable phenomena can be caused by natural convection if the apparatus operates at non-isothermal conditions, which is typical for heat exchangers or heaters.

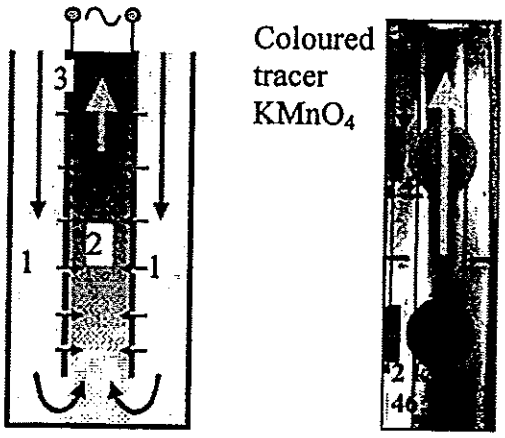

Figure 1. Continuous ohmic heater (scheme and photograph showing asymmetry of flows). 1-lateral channels;2-central channel,3-electrodes.

The effect of flow asymmetry was observed experimentally in lateral parallel channels of continuous direct ohmic heater, with two planar electrodes (electrical current flows directly through the heated liquid), see Fig.1. Liquid enters the top of heater and flows downwards through two rectangular channels where liquid is preheated only by warm electrodes. At the bottom of heater the two parallel streams join and liquid flows upward in a nearly uniform electrical field between electrodes (distance 0.036 m, voltage 220 V, 50 Hz). In order to suppress the electrode fouling, a perforation of electrodes was suggested, assuming that the cold cross-flow could displace overheated substance moving slowly along the electrode surface.

While the flow in parallel channels is uniform at isothermal conditions, a nonuniform distribution of flowrate and different temperature profiles exist in parallel channels at heating and also the cross flow is changed. These phenomena can be explained by the effect of buoyancy and can be detected by measuring of RTD.

STABILITY OF NON-ISOTHERMAL PARALLEL FLOWS

Parallel laminar flows in lateral channels of continuous ohmic heater are symmetric only at isothermal conditions. In case of heating, one stream is delayed and even stopped or reversed if the temperature increase is too high. This phenomenon can be explained by buoyancy.

A similar situation occurs in a simpler and probably more frequent case when two vertical parallel streams are separated by wall having a constant temperature T_e, see Fig.2.

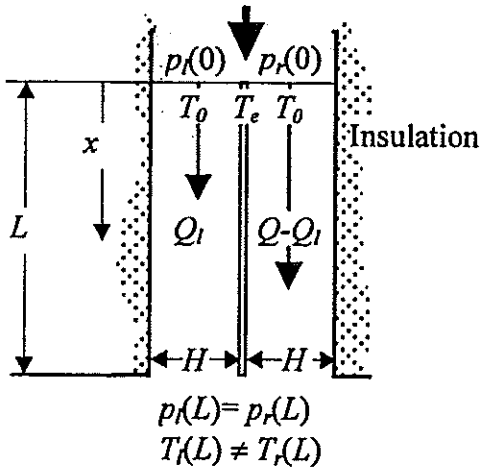

Figure 2. Parallel flows heated by wall at constant temperature T_e.

The analysis is based upon the fact that the pressure difference $p(L)$-$p(0)$ must be the same in the left and in the right channel at a steady state. We shall consider only two contributions to the pressure difference: the first represents viscous forces (written for flowrate Q_l [$m^3.s^{-1}$] in the left channel)

$$p_f(0) - p_f(L) = \frac{12\mu L f}{BH^3} Q_l \qquad (1)$$

where B, H [m] are dimensions of rectangular cross-section (depth and width of channel respectively), and f equals 1 for laminar flow between plates or

$$f = \frac{1}{1 - \frac{192H}{\pi^5 B} \sum_{n=1,3,5,..} \frac{1}{n^5} tgh \frac{n\pi B}{2H}} \tag{2}$$

for fully developed laminar flow in a rectangular channel B x H.

While the viscous component of pressure $p_f(x)$ decreases in the direction of flow, the hydrostatic pressure $p_b(x)$ increases. Assuming linear temperature dependence of density (coefficient proportionality β [K^{-1}]) and an exponential temperature profile $T_l(x)$,

$$\frac{T_l - T_e}{T_0 - T_e} = e^{-\frac{\alpha B}{\rho_0 c_p Q_l} x} \tag{3}$$

i.e. assuming a constant value of the heat transfer coefficient α [$W.m^{-2}.K^{-1}$] and heat capacity c_p [$J.kg^{-1}.K^{-1}$], the contribution of hydrostatic pressure can be expressed as

$$p_b(0) - p_b(L) = -\rho_0 g \int_0^L [1 - \beta(T_l - T_0)]dx = \rho_0 gL\{1 + \beta(T_0 - T_e)[1 - \frac{Q_l \rho_0 c_p}{\alpha BL}(1 - e^{-\frac{\alpha BL}{Q_l \rho_0 c_p}})]\} \tag{4}$$

This expression can be approximated by

$$p_b(0) - p_b(L) = -\rho_0 gL[1 + \beta(T_0 - T_e)\frac{\alpha BL}{2Q_l \rho_0 c_p}] \tag{5}$$

for high heat capacity of stream $Q\rho_0 c_p$ and for low value of heat transfer coefficient α.

Summing pressure differences corresponding to the friction forces (1) and buoayant forces (5) we can express equilibrium of forces in the left (lower index l) and right (index r) channel by equation

$$\frac{12\mu Lf}{BH^3} Q_l - \rho_0 gL[1 + \beta(T_0 - T_e)\frac{\alpha BL}{2Q_l \rho_0 c_p}] = \frac{12\mu Lf}{BH^3} Q_r - \rho_0 gL[1 + \beta(T_0 - T_e)\frac{\alpha BL}{2Q_r \rho_0 c_p}]. \tag{6}$$

It is obvious that this equation is always satisfied by symmetric solution $Q_l = Q_r$, nevertheless another, asymmetric, solution can exist too

$$Q_l Q_r = (T_e - T_0)\frac{g\alpha\beta B^2 H^3 L}{24\mu f c_p} \tag{7}$$

Eq.(7) can be rearranged to a dimensionless form by introducing the total flowrate Q and the ratio $\psi = Q_l/Q$

$$\psi(1 - \psi) = (T_e - T_0)\frac{g\alpha\beta B^2 H^3 L}{24\mu f c_p Q^2} = \mathbf{R} \tag{8}$$

The Eq.(8) predicts, that the asymmetric solution (i.e. distribution of flowrates satisfying balance of forces) can exist only if $\mathbf{R}$<1/4. For higher values of

dimensionless parameter **R** the balance of forces cannot be satisfied giving rise flow reversals or other form of flow instabilities.

An important question appears whether and when the symmetric and asymmetric flow is stable. Let us assume a small disturbance of flowrate $Q_l+\delta Q$, $Q_r-\delta Q$, i.e. slightly increased flowrate in the left channel and decreased in the right channel. Then the pressure differences in the left and in the right channel are changed by increments (see Eq.(6))

$$\delta p_l = [\frac{12\mu Lf}{BH^3} - (T_e - T_0)\frac{g\alpha\beta BL^2}{2Q_l^2 c_p}]\delta Q, \qquad \delta p_r = [-\frac{12\mu Lf}{BH^3} + (T_e - T_0)\frac{g\alpha\beta BL^2}{2Q_r^2 c_p}]\delta Q \quad . \tag{9}$$

In the case that $\delta p_l > \delta p_l$ the pressure at the inlet to the left channel would be higher than the pressure in the right channel and this difference induces transversal flow towards the right channel. This redistribution of flow acts against the disturbance δQ, which means that the flowrates Q_l, Q_r will be stable if $\delta p_l - \delta p_l > 0$ for $\delta Q > 0$, i.e.

$$\frac{1}{\mathbf{R}} = \frac{24\mu f c_p Q^2}{g\alpha\beta L B^2 H^3 (T_e - T_0)} > \frac{Q^2}{2}(\frac{1}{Q_l^2} + \frac{1}{Q_r^2}) = \frac{1}{2}(\frac{1}{\psi^2} + \frac{1}{(1-\psi)^2}) . \tag{10}$$

This inequality leads to the conclusion that the symmetric flow (ψ=0.5) will be stable if

$$\frac{1}{\mathbf{R}} > 4 . \tag{11}$$

Example, corresponding to the geometry of lateral channels of the direct ohmic heater in Fig.1: B=0.08 m, H=0.008 m, L=0.56 m, flowrate of water Q=32 ml/s, ρ=1000 kg.m^{-3}, β=0.00093 K^{-1}, c_p=4200 J.kg^{-1}.K^{-1}, μ=1 mPa.s, estimated α=150 W.m^{-2}.K^{-1}. Temperature difference T_e-T_0 calculated from (11) using these parameters is approximately 10 ^{0}C, while flow asymmetries were observed within the range of heating power 1.8÷2.5 kW with corresponding water temperature increase 13÷18 ^{0}C in experiments. The deviation between prediction (11) and experiment could have been expected, because temperature of electrodes is not uniform and first of all is lower than the temperature of heated water.

The inequality (10) can be used for assessment of asymmetric solution (8) as well:

$$\frac{1}{\mathbf{R}} > \frac{1}{2}(\frac{1}{\psi^2} + \frac{1}{(1-\psi)^2}) = \frac{1-2\mathbf{R}}{2\mathbf{R}^2}, \qquad \mathbf{R} > \frac{1}{4} \tag{12}$$

In view of the fact that the asymmetric solution exists only for **R**<1/4, the stability requirement **R**>1/4 cannot be satisfied and asymmetric solution cannot be stable.

ZONAL MODEL OF PARALLEL AND CROSS-FLOWS

Continuous heater with perforated electrodes exhibits also rather complicated behaviour, because the cross flow through perforation is a decreasing function of heating power. The reason can be also found in buoyancy effects.

Geometry of two lateral channels (denoted by indices l,r) and central channel (c) is shown in Fig.3.

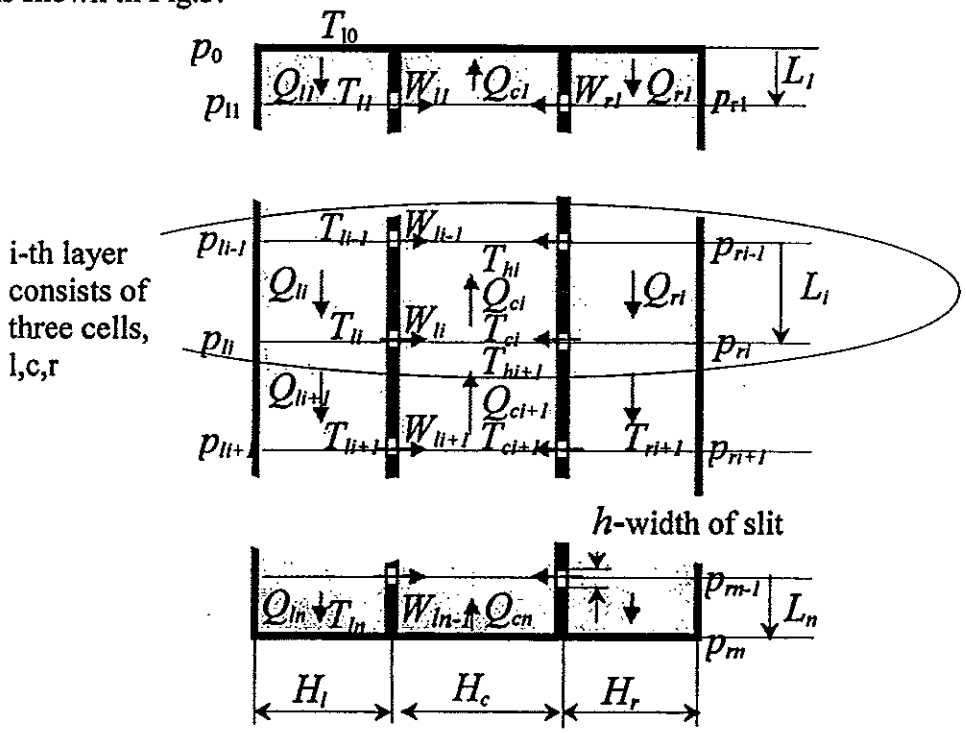

Figure.3.Zonal model

The following analysis is based upon integral balances of control volumes formed by sections of heater between slits in perforated electrodes. It is assumed, that the flow inside these volumes is fully developed, laminar and only in the axial direction.

Continuity equation can be written for each cell inside lateral channels

$$Q_{li} = Q_{l0} - \sum_{j=1}^{i-1} W_{lj} \qquad Q_{ri} = Q_{r0} - \sum_{j=1}^{i-1} W_{rj} \qquad \text{i=1,2,...,n} \tag{13}$$

and for the central channel

$$Q_{ci} = Q_{li} + Q_{ri} = Q_{l0} + Q_{r0} - \sum_{j=1}^{i-1} (W_{lj} + W_{rj}) \qquad \text{i=1,2,...,n} \tag{14}$$

Heat balance enables to estimate temperatures within the cells. Axial temperature profiles in lateral channels are assumed continuous, while the axial temperature profile are characterised by steps corresponding to injection of colder liquid in the places where electrodes are perforated. The heater is assumed to be thermally insulated therefore the balances of enthalpy in lateral channels give (written only for the left channel as an example)

$$\rho c_p Q_{li}(T_{li} - T_{li-1}) = \alpha_l L_l B(T_{ci} - T_{li}) \tag{15}$$

The axial temperature profile in the central channel is described by the step change at the interface between control volumes (mixing with lateral streams, cross-flow)

$$Q_{cl}T_{cl} - Q_{cl+1}T_{hl+1} = W_{ll}T_{ll} + W_{rl}T_{rl} \tag{16}$$

while the temperature change inside the cell is given by

$$\rho c_p Q_{cl}(T_{hl} - T_{cl}) = L_l B[-\frac{\alpha_l}{2}(T_{cl} + T_{hl} - T_{ll} - T_{ll-1}) - \frac{\alpha_r}{2}(T_{cl} + T_{hl} - T_{rl} - T_{rl-1}) + \kappa_l \frac{\Delta U^2}{H_c}] \tag{17}$$

where the last term describes volumetric heat source (κ_i [S.m^{-1}] is electrical conductivity of liquid and ΔU [V] voltage).

Pressure distribution is determined by hydraulic losses and by gravity. Hydraulic losses and buoyancy can be calculated using the same method as previously, giving axial profiles of pressure in lateral channels (written again for the left channel only)

$$p_{ll} - p_{ll-1} = \rho_0 g L_l[1 - \beta(\frac{T_{ll-1} + T_{ll}}{2} - T_0)] - L_l f_l Q_{ll} \qquad \text{i=1,2,...n} \tag{18}$$

and in the central channel

$$p_{cl} - p_{cl-1} = \rho_0 g L_l[1 - \beta(\frac{T_{cl} + T_{hl}}{2} - T_0)] + L_l f_c Q_{cl} \tag{19}$$

where $$f_l = \frac{12\mu f}{BH_l^3}, \qquad i = l,r,c \cdot \tag{20}$$

Combining continuity equation with Eqs.(18-19) we can eliminate internal pressures and express the pressure at an arbitrary cell in terms of pressure p_0 at inlet and volumetric flowrate Q_{l0} at inlet

$$p_{ll} - p_0 = \sum_{j=1}^{l} \{\rho_0 g L_j[1 - \beta(\frac{T_{lj-1} + T_{lj}}{2} - T_0)] - L_j f_l (Q_{l0} - \sum_{k=1}^{j-1} W_{lk})\} \cdot \tag{21}$$

Mention the fact that not only the inlet pressures, but also the pressures at the bottom should be the same $p_{ln} = p_{rn}$, giving the following relationship between inlet flowrates in the left and in the right lateral channel Q_{l0}, Q_{r0}:

$$\frac{\rho_0 g\beta}{2}\sum_{j=1}^{n} L_j(T_{lj-1} + T_{lj} - T_{rj-1} - T_{rj}) = L(f_r Q_{r0} - f_j Q_{l0}) + \sum_{j=1}^{n} L_j \sum_{k=1}^{j-1}(f_l W_{lk} - f_r W_{rk}) \cdot \tag{22}$$

The crossflow is related to the pressure differences between lateral and central channels. When calculating hydraulic resistance the two components are considered: Pressure drop corresponding to viscous forces which is proportional to $f_w = 12\mu fl/(Bh^3)$ and pressure drop corresponding to acceleration of liquid (Bórda's losses):

$$p_{ll} - p_{cl} = \frac{\rho W_{ll}^2}{2(Bh)^2} + f_w W_{ll} \tag{23}$$

This quadratic equation enables to express the flowrate as a function of pressure difference

$$W_{li} = \frac{(Bh)^2}{\rho}\left(-f_w + \sqrt{f_w^2 + \frac{2\rho(p_{li} - p_{ci})}{(Bh)^2}}\right) \tag{24}$$

Iterative solution can be as follows: Flowrates at inlet (or ratio of flowrates Q_{l0}/Q_{c0}) are selected as an initial approximation. Cross-flows W_{li} W_{ri} are also estimated, for example as zero. Flowrates in cells are calculated from continuity equation (13-14). Knowing flowrates the complete temperature profiles are calculated from (15-17). Pressures are calculated from Eq.(18-20) and (23), giving improved values of cross-flow. New ratio of flowrates at inlet is calculated from Eq.(22), and all previous steps are repeated several times.

This model forms a basis for development of spatially localised RTD (Residence Time Distribution) model. Each cell in Fig.3 is described by a subsystem of one to five ideally mixed tanks, and flow-rates at inlets to these subsystems (including cross-flows) are given by preceding analysis. Thus it is possible to describe the spatial distribution of concentration of tracer as a function of time. Initial conditions (concentration of trace inside the heater) is zero, and inlet concentration at entry to lateral channels can be an arbitrary function of time (delta function or experimentally determined stimulus function). Resulting system of ordinary differential equations is integrated numerically.

It is true that approximation of tracer dispersion in convective laminar flow by a model formed by ideally mixed tanks is rather crude and cannot properly describe details of flow near walls. However, the model is simple and comparison with experiments indicates that the errors of calculated residence times are acceptable.

RTD EXPERIMENTS AND RESULTS

Experiments were performed with different thickness of lateral channels (H_l=H_r= 18, 11 and 7.8 mm). Temperature at lateral channels was recorded by two Pt100 probes and optical fibre probes Nortech TP-21-M02 which prove to be a sensitive indicator of flow instabilities, however results have not completely evaluated yet. Visualisation using $KMnO_4$ as a colour tracer indicates that the asymmetric flow could exist within a certain range of operational parameters, see the following table:

H [mm]	Q [ml/s]	$\Delta T_{exper.}$ [K]	T_e-T_0 Eq.(11)	Flow pattern	Evaluation
8	76	20	58	symmetric, stable	agree
8	65	22	42	asymmetric	acceptable
8	39	31	15.3	unstable	agree
18	83	14	14	symmetric, stable	acceptable
18	72	17	10.3	asymmetric ?	Eq.(11) unstable
18	68	18	9.2	unstable	agree

Residence time distribution was identified by using KCl and Tc-99 as a tracer [4]. Results obtained with these tracers are very similar, however the radioisotope is a better tracer at heating because solution of Tc99 has no effect upon direct ohmic heating (this is not true for solution of KCl which increases power and temperature when passing between electrodes).

Selected results of RTD measured in the system with narrow and wide lateral channels with and without heating and simulation by presented model for different width of perforation *h* are shown in Figs. 4a, b, c and d.

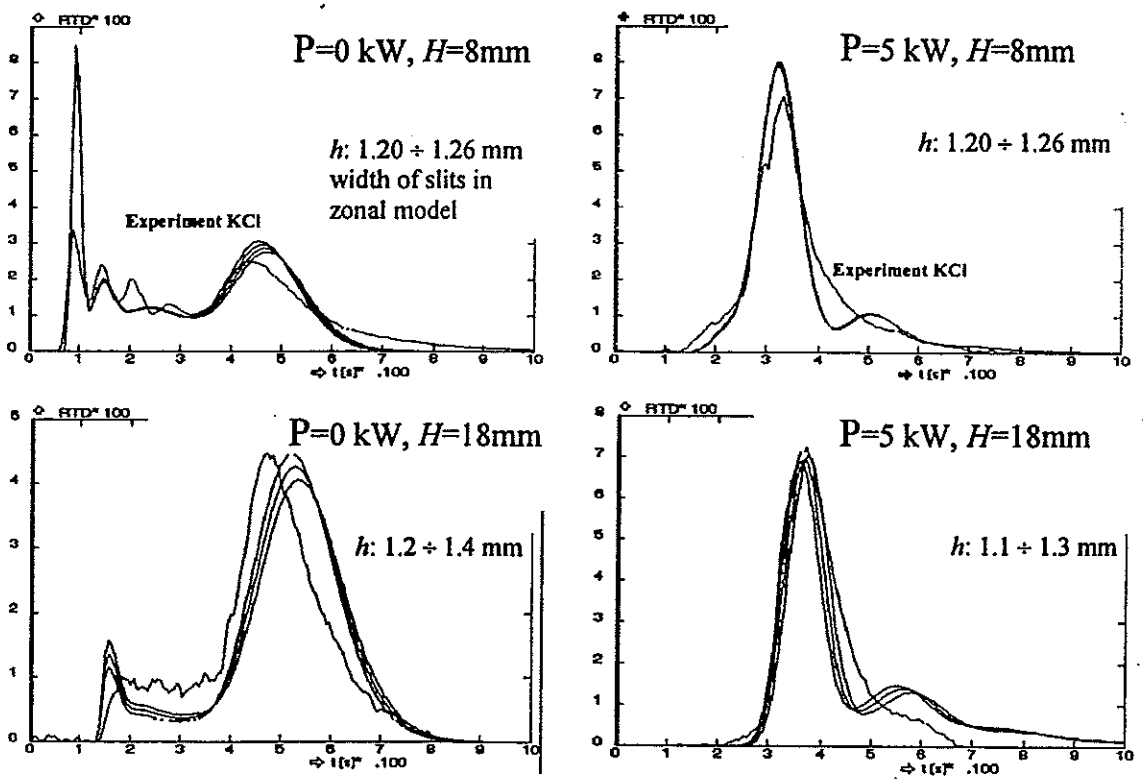

Figure 4. Experimental and simulated RTD for direct ohmic heater with perforated electrodes with different width h of perforation. Conductivity method.

CONCLUSION

Buoyancy has undesirable effects in heaters with downwards oriented parallel flows (non-uniform distribution and instability of flow), which can be suppressed by

- Decreasing width of channels (this is the most efficient way)
- Increasing viscosity
- Cross-flow (perforation of walls) has also positive effect improving stability.

This research has been subsidized by the Research Project of Ministry of Education of the Czech Republic J04/98:21220008

REFERENCES

[1] Žitný,R.,Šesták, J., Dostál M., Zajíček M., *Continuous direct ohmic heating of liquids,* International Conference CHISA'98 , Prague, 23-28 August (1998)

[2] Žitný,R., Thýn, J., *Verification of CFD predictions by Tracer Experiments,* International Conference CHISA'2000, Prague, 28 - 31 August (2000)

[3] Thýn, J., Žitný, R., Klusoň, J., Čechák,T.,*Analysis and Diagnostics of Industrial Processes by Radiotracers and Radioisotope Sealed Sources,* Ed. ČVUT, Prague (1999)

[4] Žitný,R., Thýn, J.,*Parallel flow asymetries in continuous heaters,* CVUT Workshop 2001, Praha, 14-16 February (2001)

SCANNING BY LASER TOMOGRAPHY OF THE ACTIVE ZONE OF AN ULTRASONIC REACTOR AT HIGH FREQUENCY

E. Valette, E. Gonze, Y. Gonthier

Laboratoire de Génie des Procédés, ESIGEC, Université de Savoie, 73376 Le Bourget-du-Lac, France

INTRODUCTION

The general objective of this work is the optimisation of an ultrasonic reactor allowing the degradation of the organic compounds present in industrial wastewater. To this end, it's necessary to study the movements of the fluid due to the sonication in order to determine the participation of ultrasound to the mixing of the solution. This work concerns the determination of the velocity field in a batch reactor. These results are linked with the results of micro-mixing.

EXPERIMENTAL ULTRASONIC MATERIAL

The experimental set up is composed of an ultrasonic transducer with a transducer of 4 cm diameter, stuck under a stainless steel plate, connected to a high frequency generator (500 kHz, 200 W), and fixed at the bottom of a 10 L reactor vessel. The preliminary experiments are carried out in batch conditions with a sonicated volume of 5 L. The effective power is 100 W (efficiency of 50 %).

TOMOGRAPHY

The laser tomography is a mode of visualization, which consists of lighting with a laser a fine slice of a flow that is beforehand sown with markers (0-24 µm Rilsan particles). A camera connected to a computer containing an acquisition card allows the achievements of several images of this slice. They are then treated to cartography the velocity field.

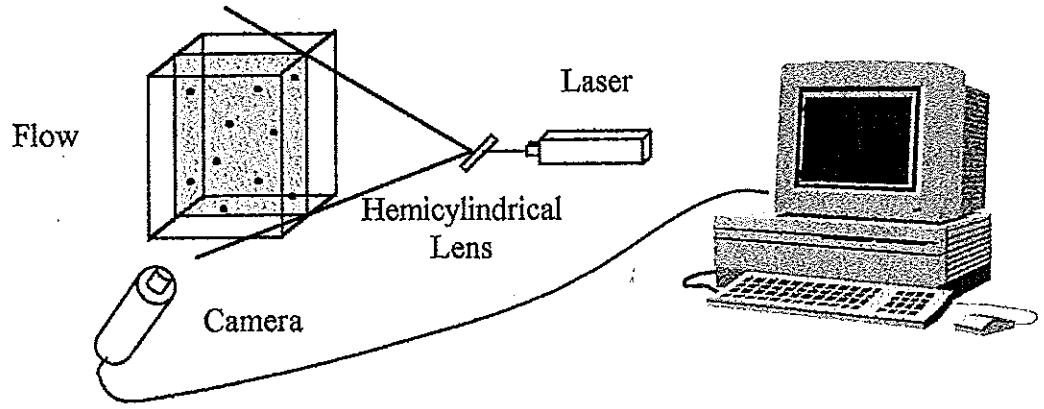

Figure 1. Experimental set up

The examination is done by Particles Images Velocity (PIV), which is currently used in fluid mechanics [1]. Its principle is based on the following of some particles in a zone of the flow resulting from a preliminary image division. This method leads to a measurement of the velocity field according to a regular grid.

RESULTS

The following results represent a velocity field cartography along a radius of the reactor. This work concerns only the half of the reactor because of the symmetrical flow.

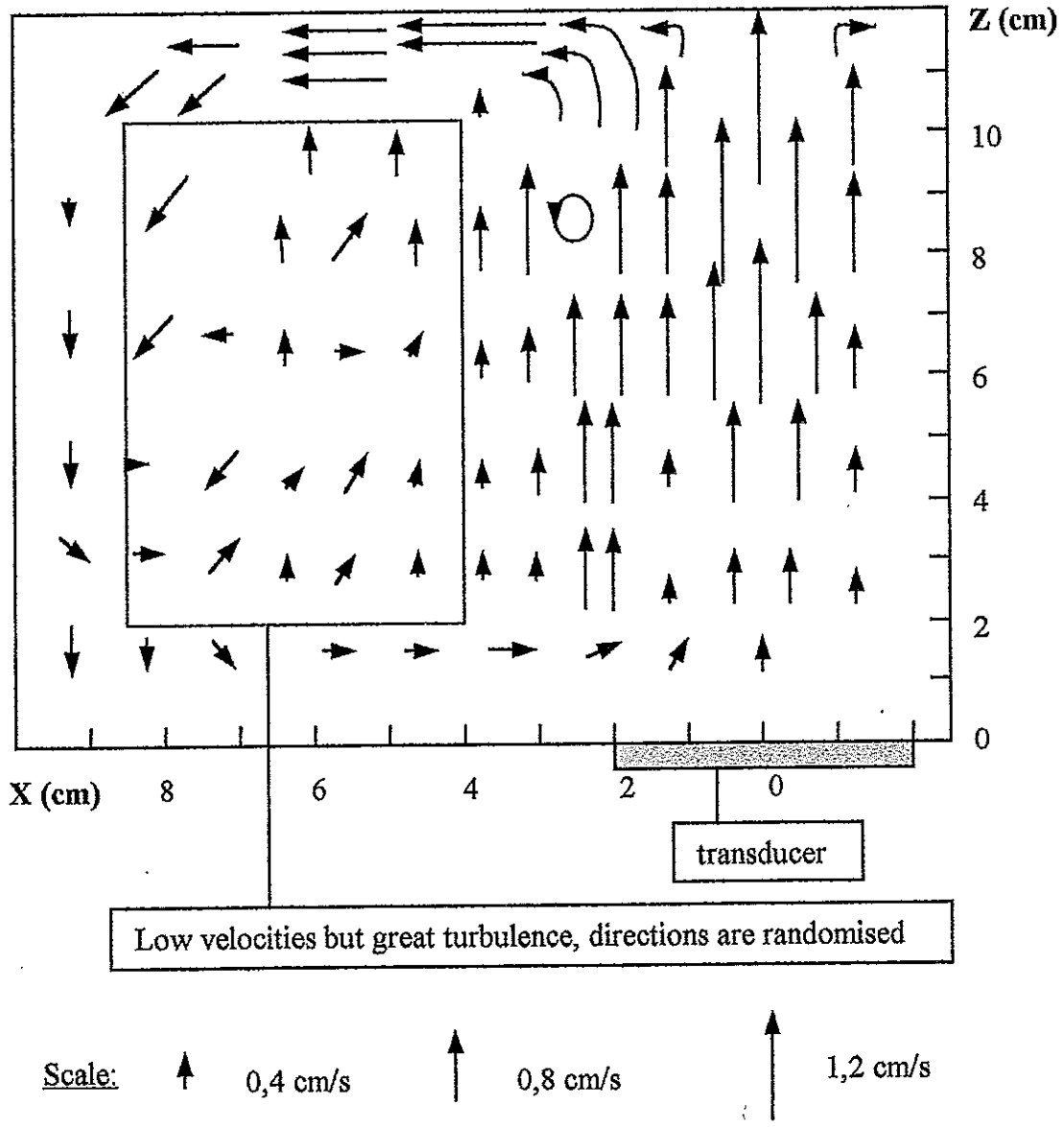

Figure 2. Velocity field obtained with an ultrasonic power of 200 W

The general flow is a large whirlpool which goes up near the center of the vessel above the transducer, and flows down along the walls.

Blue area in the figure 2 is not an interesting input area in a continuous running. The best place is located just above the transducer.

The following graph presents the values of the velocity gradients in the reactor. The values range between 0,2 $cm.s^{-1}$ (red) and 2,0 $cm.s^{-1}$ (purple).

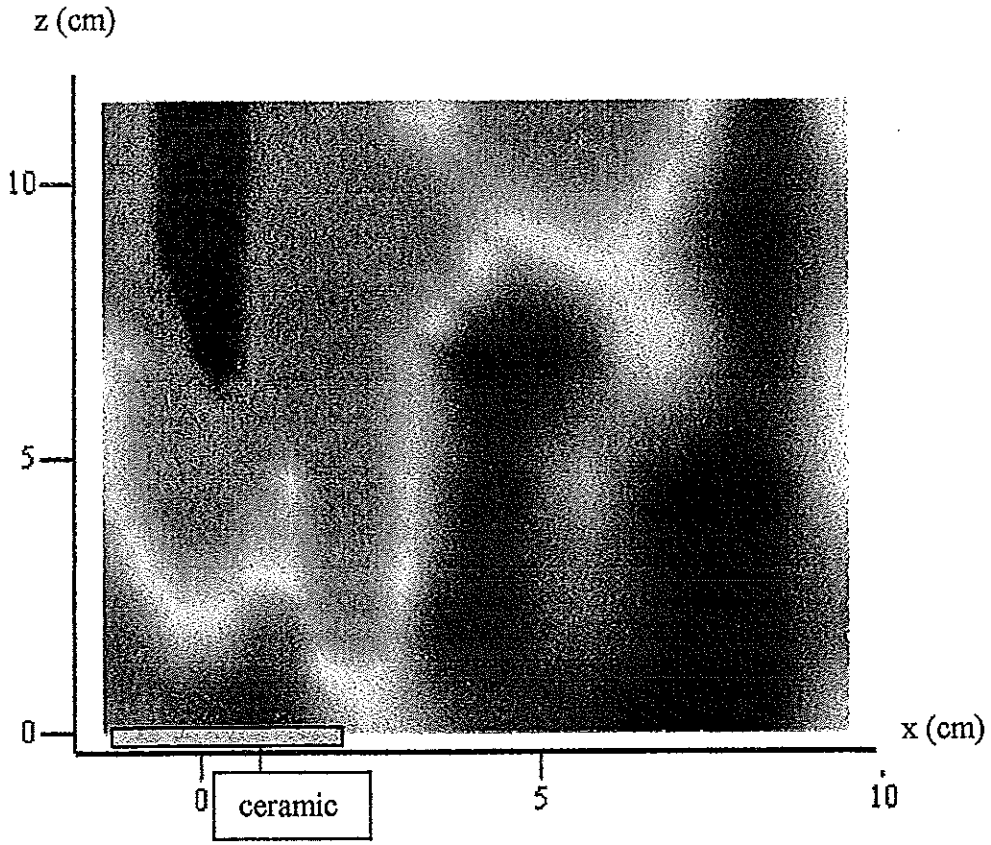

Figure 3 . Velocity field in the reactor (P=200 W)

The mean value of the velocity is about 1 $cm.s^{-1}$ and the greatest values ($2cm.s^{-1}$) are above the transducer. These velocities rise when the free area of the liquid is reached.

These results match with those obtained with a chemical method (two parallel and competing reactions) [2,3] which allows to characterise micro-mixing as can be seen in the following graph. The main difference is in the central part of the reactor where exists a medium micro-mixing whereas there are low velocities. This is due to the fact that micro-mixing is characterized by two major phenomena. The first corresponds to the value of local velocity, and the second corresponds to the turbulence (shearing). Thus it's logical to find a significant micro-mixing when velocities are high, and a medium micro-mixing when there are low velocities but a significant shearing of.

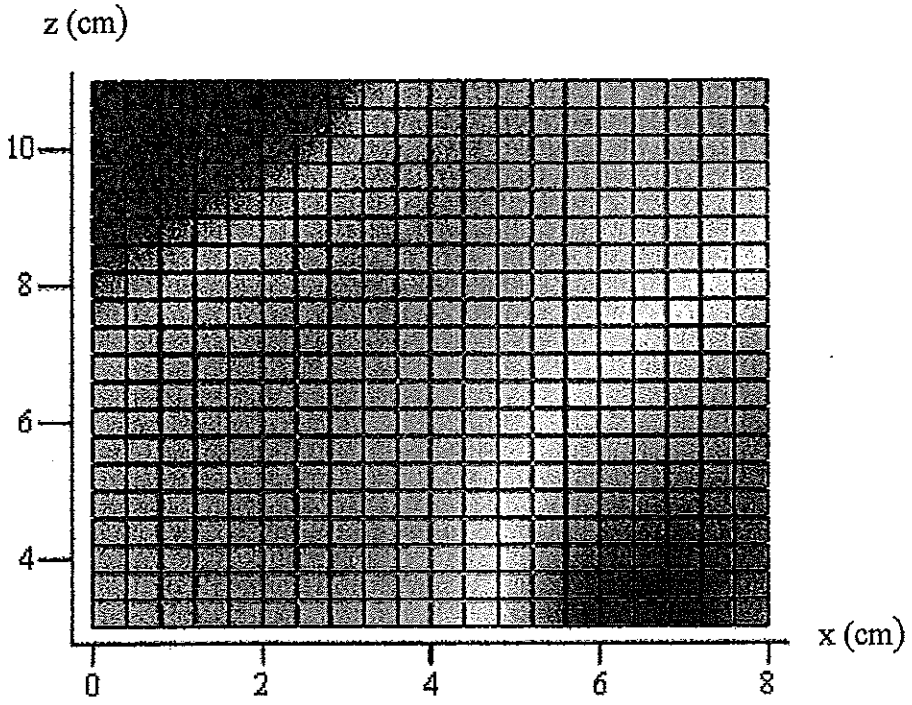

Figure 4 . Characterization of micro-mixing in the reactor (P=200 W)

An run has been carried out at 100 W and it gives similar results, with lower velocities yet.

Flow in different layers of 2 cm high above the transducer are calculated to underline the velocity rising when the free area of the liquid is reached. Results obtained at 100 W and 200 W are matched too. Flow for the first and the last layers are not calculated as they correspond to a horizontal flow.

Table 1. Mean flow by layers of 2 cm high in the 0-4 cm radius area that corresponds to the area where velocities are strictly rising

Flow ($cm^3.s^{-1}$)	Layer (cm)	100 W	200 W
Q	2<h<4	5,0	6,5
Q	4<h<6	5,9	8,1
Q	6<h<8	7,0	9,5
Q	8<h<10	8,0	14,1
Mean Q	2<h<10	6,5	9,5

An increase from 100 W to 200 W leads to a rise of 50 % on the average flow in the studied area.

There is a significant increase of the flow with the height. Consequently, a central flow with a distributed supplying is obtained. This observation is important because Gondrexon, through a measure of the residence time distribution, shown

that this behaviour was similar to a stirred tank reactor [4]. From a hydrodynamic point of view, there are no differences between these two models (Villermaux [5]). However the results found in the study of micro-mixing don't confirm this model.

Flow corresponding to the return area near the walls have been calculated too. Velocities are lower than that above the transducer, however the area is much more important (9<R<10 cm). Thus flow is significant, almost four times greater than the previous (0<R<4 cm).

Table 2. Mean flow in the 9-10 cm diameter area

	Layer (cm)	100 W	200 W
flow ($cm^3.s^{-1}$) for 9<R<10 cm	2<h<10	28,2	31,5

These results allow to calculate the flow between the 4 and 9 cm radius area where velocities are low and where it's difficult to give a sharp direction. Flow balance : $\sum Q_i A_i = 0$ (Q=flow in $cm^3.s^{-1}$ and A=area in cm^2), leads to :

Table 3. Mean flow in the 8-18 cm diameter area

	Layer (cm)	100 W	200 W
flow ($cm^3.s^{-1}$) for 4<R<9 cm	2<h<10	6,6	6,9

As can be seen with these previous figures, the major difference between a 100 W and a 200 W running is located just above the ceramic.

CONCLUSION

Velocities induced by ultrasounds are low, only a weak ratio of the electric power input is used in kinetic energy. The maximum value is 2,0 $cm.s^{-1}$. But, taking into account the velocities distribution in the vessel, it behaves overall like a perfectly stirred tank reactor.

REFERENCES

[1] Chouvellon Myriam : Etude tomographique d'un micromélange dans un réacteur à ultrasons traitant des eaux industrielles ; Université J. Monnet de Saint-Etienne, 2000

[2] Guichardon. P : Caractérisation chimique du micromélange par la réaction iodure-iodate, thèse INPL, Nancy, 1996

[3] Monnier. H : Effets des ultrasons sur le micromélange ; Institut National Polytechnique de Toulouse, 1997

[4] N. Gondrexon, V. Renaudin, C. Petrier, M. Clement, P. Boldo, Y. Gonthier, A. Bernis, Experimental study of the hydrodynamic behaviour of a high frequency ultrasonic reactor, Ultrasonics Sonochemistry, 5 (1998), 1-6

[5] J. Villermaux, Génie de la réaction chimique – Conception et fonctionnement des réacteurs, 2°édition, Lavoisier Tec. Et Doc., Londres, Paris, New-York, 1993

CARPT Dynamic Bias Studies: Evaluation of Accuracy of Position and Velocity Measurements

A. Rammohan, A. Kemoun, M. Al-Dahhan, M. Dudukovic, F. Larachi[1]

Chemical Reaction Engineering Laboratory, 1 Brookings Drive, Washington University, St.Louis, MO-63130. [1]Department of Chemical engineering , Quebec, Laval, Sainte Foy, Canada G1K 7P4

Abstract. The Computer Automated Radioactive Particle Tracking (CARPT) technique has been extensively used to characterize multiphase flows at high volume fractions of the dispersed phase in a variety of multiphase reactors such as bubble columns, risers and fluidized beds, etc [1-3]. In CARPT a neutrally buoyant radioactive tracer particle is introduced in the flow and followed as a function of time. The particle trajectory information obtained from such tracking is further processed to obtain the Eulerian velocity fields in the flow of interest. Amongst other factors (like size of tracer, fluctuation statistics) the accuracy of the velocity measurements from CARPT also depends on the rate at which the particle trajectory information is sampled. It is particularly important to quantify the distortion of the dynamic bias brought about by improper selection of the sampling frequency in reconstructing tracer positions and velocities. The current work thus evaluates the accuracy of the velocity measurements obtained from CARPT as a function of the *sampling frequency*. For the purpose of illustration, CARPT experiments have been performed in a stirred tank by placing the radioactive tracer particle at the impeller tip. Particle trajectory information was obtained over a range of rotational speeds (100-750 rpm corresponding to Impeller tip speeds ranging from 35 cm/s to 2.62 m/s) at different sampling frequencies (ranging from 10-200 Hz). From the trajectory information the particle velocities were obtained using the CARPT reconstruction algorithms. For each rpm, plots of reconstructed velocity vs. sampling frequency were made. These enable us to establish the proper *de-biasing* procedures by selecting the appropriate data sampling rate for a particular velocity. A Monte-Carlo based model has been developed which permits *a priori* evaluation of the extent of dynamic bias thus providing guidance in setting the appropriate data sampling rate for different velocities. This study is expected to be of considerable use when implementing the CARPT technique in industrial systems where such detailed experimental analysis of technique's accuracy will be both cumbersome and time consuming.

1. Introduction

The Computer Automated Radioactive Particle Tracking (CARPT) technique has been extensively used to characterize multiphase flows at high volume fractions of the dispersed phase in a variety of multiphase reactors such as fluidized beds, bubble columns, etc. [1-3]. Recently the technique has been applied to characterize complex liquid swirling flows in stirred tanks [4-5]. Detailed analysis of the results [6] revealed that the CARPT data obtained in stirred tanks was missing velocity and turbulence information in comparison with similar data obtained using other techniques, *e.g.*, LDA. Possible sources for loss of this information were identified to be size of radioactive tracer, statistical nature of the photon emission process and the rate at which the CARPT data is sampled. In this work the error introduced into CARPT measured positions and velocities due to the data sampling rate will be quantified experimentally and numerically (using a Monte Carlo based model). In the following section the nature of this error is discussed in detail.

In the CARPT technique two kinds of measurements are performed. The first called 'static measurement' is performed for calibrating the data acquisition process. During calibration the radioactive tracer is placed at several hundred known locations and the scintillation detectors register the number of counts (typically 256 samples acquired @ 50 Hz). A calibration map for each detector is then generated by plotting the mean of these 256 samples at each point against the distance of that point from that detector. A typical calibration curve is shown below in Fig. 1.

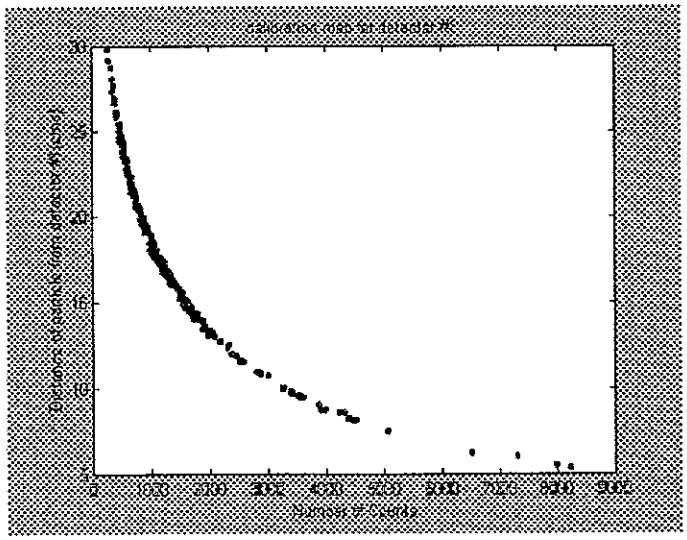

Figure 1. Calibration Map for detector #1

Once the calibration map has been generated for each detector, then the second kind of measurement 'dynamic measurement' is performed. For dynamic measurements the CARPT tracer particle is thrown into the flow field whose fluid dynamics is to be characterized. As the tracer starts moving with the fluid, the photons emitted by the radioactive tracer are then registered by each detector after every τ seconds (corresponding to sampling rate $f_{sample}=1/\tau$). The counts' vector acquired at each sampled instant is then fed into the calibration curve for that detector to find out the corresponding distance of the tracer from that detector given below by Eq. 1.

$$d_{tracer}^{ith\,detector} = f\left(C_{ith\,detector}\right) \tag{1}$$

Knowing the distance of the tracer from each detector the tracer co-ordinates can be computed [3]. The dynamic bias issue is that when the particle is in motion the count registered by the ith detector at a certain location $\left(x_P(t,t_o), y_P(t,t_o), z_P(t,t_o)\right)$ in the reactor will strongly depend on the past particle trajectory, the fluid velocity along the particle path and the rate at which the photon counts are registered by that detector. Hence, the mean count registered by the ith detector when particle is kept stationary $C_{stationary}^{i^{th}\,detector}\left(x_P, y_P, z_P\right)$ will be different from the instantaneous count $C_{dynamic}^{i^{th}\,detector}\left(x_P(t,t_o), y_P(t,t_o), z_P(t,t_o)\right)$ registered by the ith detector as the particle moves to the point $\left(x_P(t,t_o), y_P(t,t_o), z_P(t,t_o)\right)$. Hence when the tracer is in motion the distance estimated from the static calibration measurements (1) will be different from the real distance of the tracer. The concept is illustrated below (Fig. 2).

It can be seen from Fig. 2 that as the fluid velocity increases for a fixed sampling rate or as the sampling rate decreases for a fixed fluid velocity the greater will be the deviation of the dynamic measurement from the static measurement. In this work we have quantified the error introduced in the reconstructed particle position and the particle velocity for different sampling rates and fluid velocities experimentally.

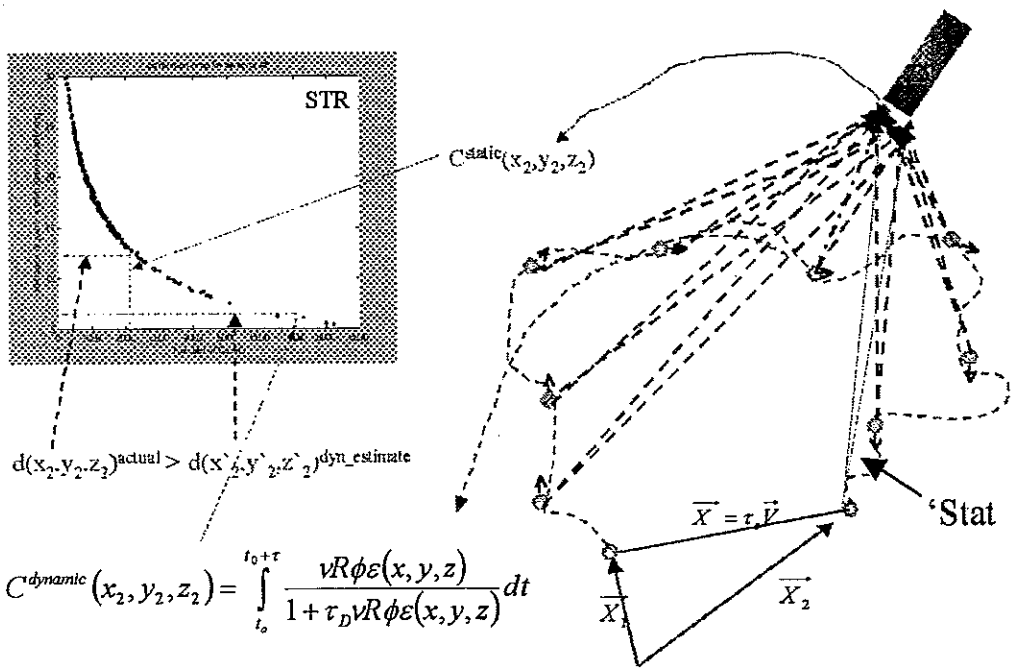

Figure 2. Cartoon illustrating the concept of 'Dynamic Bias' issue

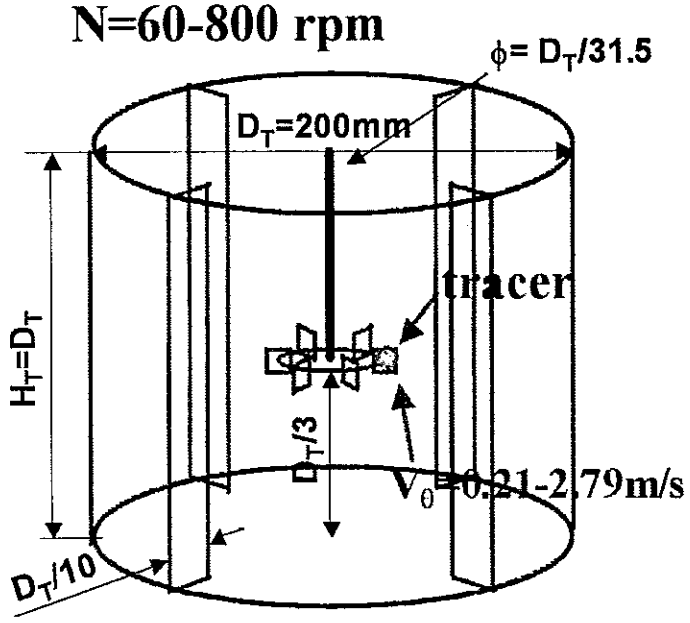

Figure 3. Dimensions of stirred tank reactor

2. Experimental details

To quantify the dynamic bias, the errors introduced due to the flow following capability of the tracer must be uncoupled from CARPT measurements. Further, the tracer must follow a known trajectory with known velocity to be able to compare the experimental results and quantify the error. Hence, the tracer was placed at the tip of a Rushton turbine in the stirred tank (Fig. 3). The impeller speed varied from 60–800 rpm corresponding to tangential velocities 2.8–21 cm/s. At each impeller speed the

photon counts were registered by each of the 16 detectors surrounding the tank (details in [4-5]). Data was acquired at 200 Hz. The dynamic measurements were preceded by static calibration ones resulting in calibration curves as in Fig. 1.

Impeller speeds were monitored with a high-precision magnetic tachometer (speed variations <1%). The raw count data generated from these experiments were sub-sampled to obtain raw count data corresponding to slower acquisition rates: 25, 50, 100 Hz. Raw data from different sampling frequencies were used in CARPT reconstruction [1] to estimate tracer trajectories at various sampling rates and impeller speeds. The technique used to quantify the dynamic bias is outlined below.

3. Details of numerical technique

A Monte Carlo model developed earlier [7] has been extended to simulate the dynamic bias in CARPT. Theoretically, the photopeak counts C recorded by a detector during an interval T from a point tracer of strength R placed at a (x,y,z) inside a the stirred tank can be expressed by the following relationship [8-9]:

$$C = T\nu R\phi\varepsilon / \left(1 + \tau\nu R\phi\varepsilon\right) \tag{2}$$

$$\text{where } \varepsilon = \iint_{\Omega} \frac{\vec{r}\,\vec{n}}{r^3}\left(1 - e^{-\mu_D d}\right) e^{-\mu_R(e_R - e_{shaft}) - \mu_{shaft} e_{shaft} - \mu_W e_W}\, d\Sigma \tag{3}$$

ν is the number of γ-rays emitted per disintegration, ε is the total detector efficiency, τ is the dead time, ϕ is the photopeak fraction, r is the distance between source and point P on the detector surface, e_R, e_{shaft}, e_W the γ-ray flight length in the tank, across the shaft, and the tank wall (Fig. 4.), d the crystal thickness in r direction, Ω solid angle subtended by the detector surface, n is an external unit vector locally normal to dΣ. μ_R, μ_{shaft}, μ_w, μ_D are the total linear attenuation coefficients of tank inventory, stainless steel impeller shaft, tank wall and detector material, respectively.

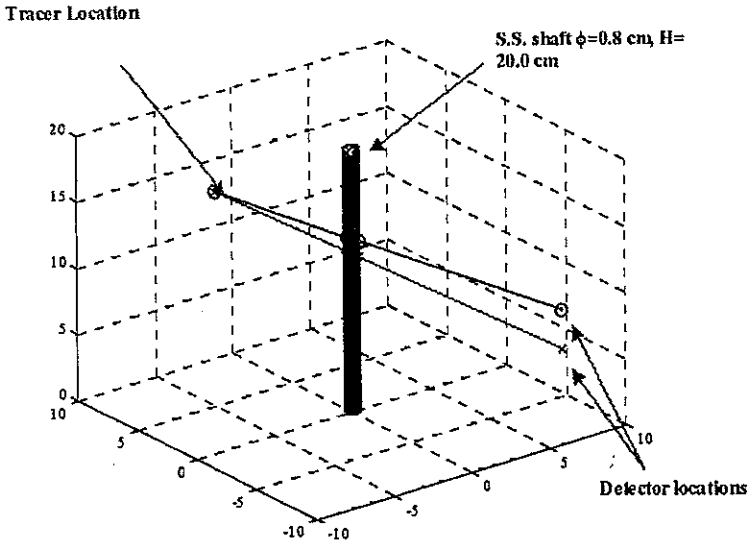

Figure 4. Modeling internals using Monte Carlo simulation

It is in the computation of the efficiency ε that the Monte Carlo procedure is used. Out of N photons emitted by the tracer only a certain fraction of them will intersect the detector. The direction of each photon is picked at random using a rectangular random number generator and depending on the direction cosines of the photons it can be checked whether or not a particular photon will intersect the detector. This fraction of the total photons intersecting the detector surface, by definition is the solid angle subtended by the detector at the location of the tracer. The advantage of using a Monte Carlo integration is that the error decreases with the increase in number of photon histories tracked as $N_{history}^{-1/2}$. Tracking 1000 photon histories provides a reasonably accurate estimate of the detection efficiency [7]. The first step in the Monte Carlo simulation is to estimate the parameters of the model (2) i.e. R, τ, μ using the calibration data or the static measurements discussed in section 2. Then the next step is to verify that the model can be used to simulate the counts registered by the detectors for each known calibration point. A sample parity plot of the simulated versus measured calibration counts for detector #1 (Fig. 5) suggests reasonably good predictions by the model.

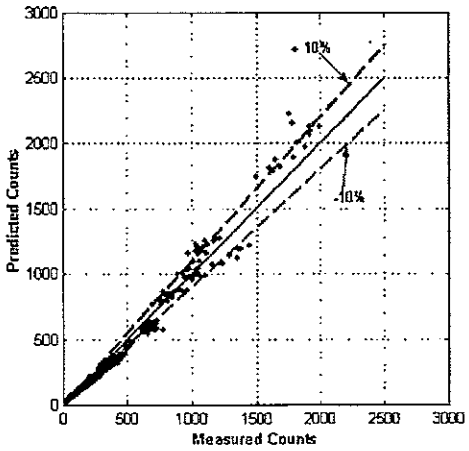

Figure 5. Parity plot of predicted vs measured calibration counts registered by detector #1

The next step in using the model is to feed into Eq. 2 a known *circular* tracer orbit (corresponding to a certain impeller speed) $\vec{X}(t)$ sampled at a frequency $f_{sample}=1/\tau$ to generate a dynamic estimate of the count registered by the ith detector i.e. $C_{dynamic}^{i^{th}\,detector}\left(x_P(t,t_o), y_P(t,t_o), z_P(t,t_o)\right)$ as :

$$C^{dynamic}\left(\vec{X}(t_0+\tau), i\right) = \int_{t_o}^{t_0+\tau} \frac{\nu R \phi \varepsilon(x,y,z)}{1+\tau_D \nu R \phi \varepsilon(x,y,z)} dt \qquad (4)$$

This equation is handled numerically as:

$$C^{dynamic}\left(\vec{X}(t_0+\tau), i\right) = \sum_{k=1}^{N_{small}} C_k\left(\vec{X}\left(t_0+\frac{k}{N_{small}}\tau\right), i\right) \qquad (5)$$

The value of the integral does not change for values of N_{small}>20. Thus Eqs. 4, 5 are used to numerically generate a raw count file corresponding to the dynamic CARPT measurements. These are then fed into a Monte Carlo based tracer rendition

algorithm [1] to estimate the tracer trajectory and velocity for different sampling rates and impeller speeds. In the following sections the experimental results are discussed and some preliminary results from the simulations are outlined.

4.Results and discussions

4.1 Variation of radial bias with data acquisition rate

Fig.6 shows the variation of radial bias $r_{reconstructed}$-r_{actual} with sampling rate at various impeller speeds. For all impeller speeds and sampling frequencies the bias is always negative i.e. the reconstructed radial particle position is always underestimated. Further, for a given impeller speed the radial bias is minimum within a certain optimal data sampling rate window. The window shifts to the right with increasing speeds i.e. at lower impeller speeds (26 –52 cm/s) the bias tends to be small within 25 –50 Hz while for higher speeds (1.05 – 2.79 m/s) it tends to be minimum within 75 – 125 Hz. For all speeds the bias becomes independent of the sampling rate beyond 200 Hz. As the data acquisition rate increases the number of photon counts registered by a detector decreases and therefore the resolving capability of the detector deteriorates. Hence there would seem to be an inherent upper limit on the data sampling rates fixed by the resolving capability of the detectors. Given that, the lower limit on the sampling frequency seen from Fig. 6 would correspond to the desired minimum frequency below which the dynamic bias effects become important. That one should anticipate such limits as shown later theoretically.

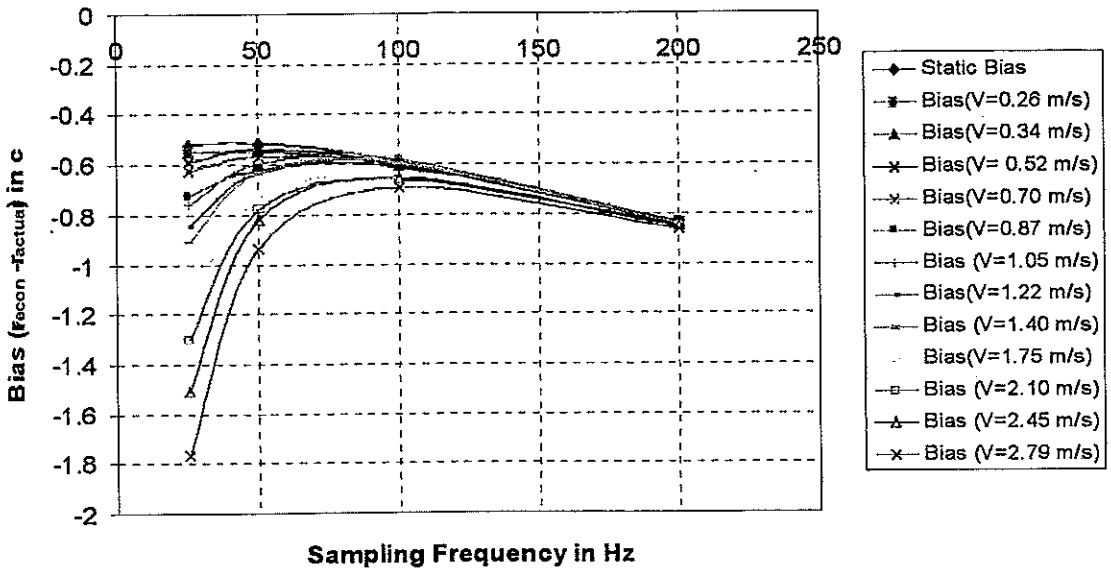

Figure 6. Variation of radial bias with data sampling rate (Vtip=0.21 - 2.79 m/s)

4.2 Determination of optimal data acquisition rate

Based on the reconstructed orbits, the tracer azimuthal velocity has been computed using CARPT algorithms [3]. Variation of the dimensionless azimuthal velocity (V_θ/V_{tip}) with sampling frequencies for different impeller tip speeds is shown in Fig. 7 which shows variations similar in nature to Fig 6. Ideally estimated dimensionless velocities must be equal to 1. The figure shows that at all data acquisition rates and

for all impeller speeds the velocity is underestimated. The velocity bias is found to be minimum in a certain optimal sampling window. The bias at lower sampling rates is found to become higher with increase in impeller speeds. Beyond a certain sampling rate (200 Hz) the bias becomes independent of the sampling rate.

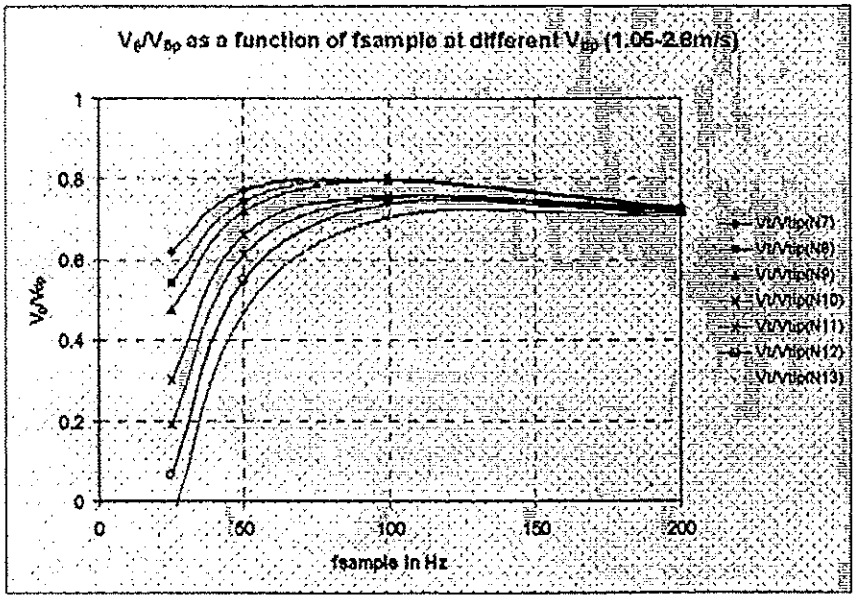

Figure 7. Variation of estimated V_θ/V_{tip} vs data sampling rate ($V_{tip} = 1.05 - 2.79$ m/s)

The estimates of bias shown above have contribution from the statistical fluctuations due to the nature of the photon emission process. The different contributions to the bias observed can be thought of as shown below in Fig. 8.

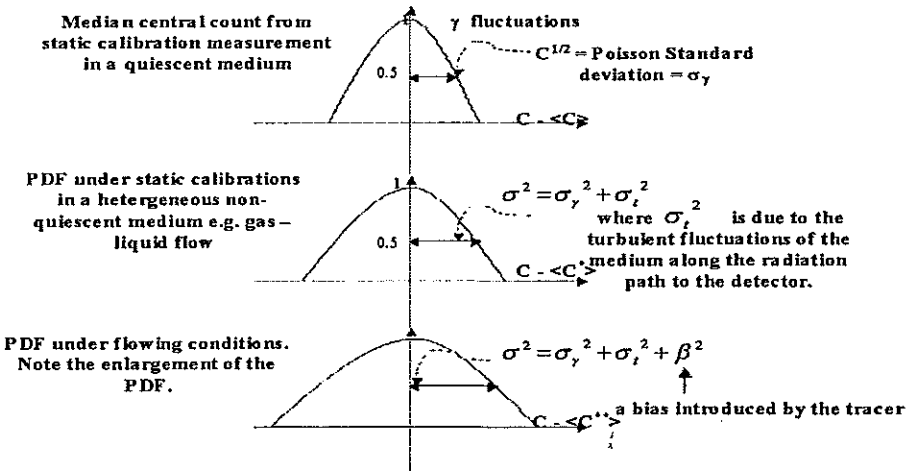

Figure 8. Errors in CARPT due to nature of experimental technique

In the current experiment the medium was quiescent and hence the final data are corrupted only by the static bias and the dynamic bias. Subtracting the static bias contribution from the velocity estimates suggests that the dynamic bias is of the

order of 14 –30 % (with increasing velocities). This would seem to be a considerable loss of information due to the dynamic bias effects.

4.3 Limits on sampling rates

The analysis below will help explaining the results reported in sections 4.1 and 4.2.

The optimum sampling frequency to capture a certain velocity is bounded between f_{smin} and f_{smax}. f_{smin} would be the minimum frequency with which one would need to sample the data to ensure that the dynamic count at a certain location is as close as possible to the static count registered at that point. This criterion will ensure that the tracer velocity will be captured reasonably accurately. This frequency is decided by the following relationship:

$$\frac{\left|C^{dynamic}(x_2,y_2,z_2)-C^{static}(x_2,y_2,z_2)\right|}{\sqrt{C^{static}(x_2,y_2,z_2)}}<<1 \qquad (6)$$

f_{smax} is the maximum frequency with which one can sample the data beyond which the statistical nature of the emission process makes it meaningless to acquire photons. An estimate of this maximum frequency can be obtained as follows:

$$1/\Delta t = V_x/\Delta x \qquad (7)$$

The LHS of Eq. 7 is maximum if V_x is maximum and Δx is minimum. Maximum V_x is the maximum expected velocity in the system. The smallest measurable displacement is the CARPT resolution in x-direction. An estimate of Δx is [1]:

$$\Delta x = 1/\left(S\sqrt{C}\right) \qquad (8)$$

$$C = \Gamma_D R/f_s \qquad (9)$$

where S is the CARPT sensitivity. Substituting Eqs. 9 and 8 into Eq. 7 yields:

$$f_{s\,max} = V_x S\sqrt{\Gamma_D R/f_{s\,max}} \qquad (10)$$

Therefore, the maximum sampling frequency becomes:

$$f_{s\,max} = (\Gamma_D R)^{1/3}(V_x S)^{2/3} \qquad (11)$$

V_x is the maximum velocity we wish to capture, R is known, S is a complex function of the detector arrangement (Γ_D), relative location of the tracer in the column with respect to the detector arrangement and several other factors [10]. An estimate of S is obtainable from [10] where distributions of S for different detector configurations and locations of tracers are given. The maximum mean sensitivities are around 3 %/mm. By virtue of spatial dependence of S and V_x, the sampling frequency f_s depends on (x,y,z). Estimates of f_{smax} can be made using the sensitivity calculated at the (x,y,z) where the maximum velocities are expected for a particular detector - tracer arrangement. For the stirred tank set-up, this maximum velocity is expected at the impeller tip which is near the column center. The calculations predict $f_{smax} \approx 600$ Hz whose order of magnitude is comparable to the maximum sampling rate observed experimentally.

f_{smin} observed experimentally would then be an estimate of the appropriate frequency to capture a certain velocity. At lower f_s error due to the statistical nature of the photon emission is lower than at higher f_s. Hence, a lower-estimate obtained experimentally is a reasonable estimate of the desired frequency.

5. Conclusion

The dynamic bias effect has been quantified experimentally. The results suggest that an optimal sampling frequency window exists. Further the appropriate sampling frequency tends to differ from region to region in the tank depending on local flow conditions. This suggests that CARPT data should be acquired at the highest experimentally possible sampling frequency. Then the data must be reprocessed at different optimal frequencies in different zones based on a physical understanding of the flow being investigated. The preliminary results obtained from the numerical simulations are very encouraging. This will enable us to develop the ability to estimate optimal f_S *a priori* for any reactor configuration to capture velocities accurately. This will be of considerable use when the CARPT technique has to be implemented in large industrial reactors where performing such experimental studies is both cumbersome as well as time consuming.

References

[1] Chaouki, J., Larachi, F. and Dudukovic', M.P., Elsevier, Amsterdam (1997).

[2] Devanathan, N., Moslemian, D., Dudukovic', M.P., *Chem. Eng. Sci.*, 45(1990), pp. 2285-91.

[3] Degaleesan, D.Sc., St. Louis, Missouri (1997).

[4] Rammohan, A.R., Kemoun, A., Al-Dahhan, M.H., and Dudukovic', M.P., A Lagrangian description of flows in stirred tanks via Computer Automated Radioactive Particle Tracking (CARPT), *Chemical Engineering Science*, 56(2001), pp.1-11.

[5] Rammohan, A.R., Kemoun, A., Al-Dahhan, M.H., and Dudukovic', M.P., Characterization of Single Phase Flows in Stirred Tanks Via Computer Automated Radioactive Particle Tracking (CARPT), *Proceedings of the Fourth International Symposium on Mixing in Industrial Processes, ISMIP4, Tolousse*, France, May 14th – 16th (2001).

[6] Rammohan, A.R., Characterization of flow patterns in stirred tank reactors, *A proposal presented to the Sever Institute of technology*, Washington University, St.Louis, U.S.A (2000).

[7] Larachi, F., G. Kenedy and J.Chaouki, A γ-ray Detection System for 3-D Particle Tracking in Multiphase Reactors, *Nucl. Instr. And Meth.*, A338 (1994), pp.568-576.

[8] Tsoulfanidis, N., *Measurement and detection of Radiation*, McGraw Hill, New York (1983).

[9] Moens, L., J. De Donder, X.L. Lin, F. De Corte, A. De Wispelaere, A. Simonits and J. Hoste, Calculation of the absolute peak efficiency of the gamma ray detectors for different counting geometries, Nuclear Instrumentation and methods, 187 (1981), pp.451 – 472.

[10] Roy, S., D.Sc., St.Louis, Missouri (2000).

STUDY OF TWO POWDERS MIXTURE BY AN ORIGINAL IMAGE PROCESSING METHOD

A-L. LE COËNT, A. RIVOIRE, S. BRIANÇON, M. TAYAKOUT and J. LIETO

Laboratoire d'Automatique et de Génie des Procédés (LAGEP). UMR CNRS 5007 UCB Lyon 1 et ESCPE-Lyon; Bât. 308G, 43 Bd du 11 Nov. 1918, 69622 Villeurbanne Cedex. FRANCE.

Abstract. This study shows an original method to follow the blending of two powders in a classical reactor, under different agitation conditions. This technique implies a continuous images recording followed by an adequate analysis. It is a non intrusive method which avoids sampling and therefore process interruption and sample preparation necessary otherwise. However, the image analysis is not evident and needs several steps. The simple application of the box-counting method on the synthesis on real images did not lead to any satisfying results because of the lack of variation of the D coefficient between different images with a variable homogeneity. The box-counting method was then associated with an erosion treatment, leading to an interesting parameter to characterise the mixture homogeneity. This parameter is the variation of the fractal dimension of the image, from the initial crude image to the final completely eroded one.
The first results showed that the mixing is completely homogeneous after 40s of agitation. In fact, a pseudo homogeneity is achieved much more rapidly (t<20s) but subsequent images show that aggregates still remain in the reactor. These first results are satisfying and the method will now be applied to the mixing of the two powders under different operating conditions and also to the blend of the two powders and one viscous liquid to simulate the chemical reaction evolution. The final aim is to link these results on the mixing homogeneity and the solid/solid contact times with the reaction kinetics.

INTRODUCTION

The aim of this work is to investigate the mixture of two powders (A and C) and one liquid (B). These reagents are involved in a chemical reaction between the powder A and the liquid B, the second solid acting as a catalyst. The reaction is initiated through a solid-solid contact. The obtained mixture is brought into contact with the viscous liquid in the reactor. This non-homogeneous system is studied in a well-characterised reactor allowing the use of different mixers adapted for this media : an anchor-style impeller and helical ribbons. The resulting blends and the associated contact times are strongly related to the kinetic parameters. This paper deals with the visualisation of the blending of the two powders using an image processing technique in order to quantify the mixing in the reactor. This is a fast and accurate method for characterising the powder blend.

1. Image acquisition

The mixture of the two powders A and C are examined in a model reactor made of glass compatible with an optical analysis. Figure 1 shows the impeller-vessel system used in this study.

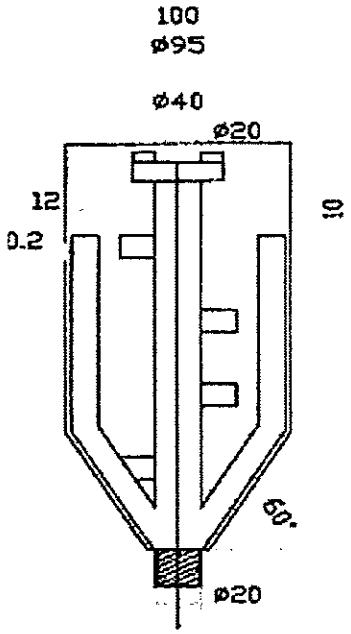

Figure 1: Schematic representation of the reactor and anchor-style impeller.

This glass stirred vessel is similar (volume, shape, configuration) to the stainless steel reactor in which the chemical reaction takes place. This is an one liter cylindrical vessel, with a cone-shaped bottom well suited for draining a viscous material.

The two powders are introduced into the reactor in different quantities corresponding to the optimum conditions for the chemical reaction. Therefore, the volume ratio A/C is about 30. For this study, the two powders need to be optically differentiated. This is not the case of the two real powders which are both white. Therefore, we choose to use the powder A such as it is and to replace the powder C by a model coloured powder with the same characteristics, especially density and mean size. The blend of the reagents is followed with a high-resolution tri CCD camera which allows to captur blur-free, clear images of fast moving objects. This colour video camera is coupled with a computer. The powder A is first introduced in the vessel and then the powder C. The system is then mixed and about 10 images, subsequently processed, are taken per second. These images represent a part of the mixture immediately behind the vessel glass wall. Each image corresponds to an area of the vessel of about 0.0025 m_.

2. Image analysis

In this study, we are using an image processing in order to characterise the mixture of the two powders in a glass reactor by fractal properties. Indeed, the time profile of an image fractal dimension presents information on the degree of mixing.

2.1. Image treatment

The images are analysed using the box-counting method which is employed to perform the fractal image analysis of binary images. The obtained coloured images were processed with the Scion Image® software.

In order to eliminate any defaults associated to a non-uniform lighting, we subtract to each image an initial image representing only the white powder A. The coloured images are then converted to binary ones with objects pixels having a level value equal to 255 and background pixels set to 0. Finally, the images are thresholded and analysed.

2.2. Box-counting method

The principle of the box-counting procedure is the following [1-3]. The image is divided into boxes of length r and the number of boxes Nr containing at least a number of pixels having a level value of 255 is counted. This procedure is done several times with variable r values. The fractal dimension D is given by a power law as shown in equation (1), so it can be determined by the slope of the line representing log Nr versus log r.

$$Nr = A\,r^{-D} \tag{1}$$

The box-counting method is used to evaluate D, which provides information on the degree of homogeneity of the distribution of powder C in the reactor.

This method allows to follow the homogeneity of the mixture without interrupting the mixing process and does not need any sample preparation. Indeed the classical methods for describing the progress of mixing are to withdrawn several samples of powder from various regions of the reactor [4]. A physical or chemical analysis allows then to determine the composition of the sample. However, this intrusive technique can disturb the mixture structure and thus the samples can be unrepresentative of the mixture. These problems are not encountered with the image analysis techniques which are not destructive. However, it should be mentioned that the images taken by the camera concern only a reduced area of the reactor just behind the glass wall and this area has to be considered as representative of the whole blend. This is the main drawback of this method: we cannot get any image of the bulk. The box-counting procedure was used by Akiyama *et al* [5-6] to study the solids mixing in two-dimensional vibrating particle beds. They characterised by fractal properties the convective motion and mixing of the particles within vertically vibrating beds. The fractal dimension was used to characterise the evolution of mixing along the bed height. So they showed that the rate of mixing is the highest in the middle of the bed.

2.3. Procedure

The first part of the work deals with the analysis method with reference images created by computer. The influence of the number of pixels, their size and their distribution (agglomeration...) are investigated to study the influence of the dispersion quality on the results of the analysis. The aim is to achieve a calibration of the analysis method in order to use it later to quantify the dispersion of the real images.

3. Results

Synthesis image are first created by computer in order to study the influence of the pixels number on the fractal coefficient D. The reference images dimension is 100*100 pixels.

3.1. Influence of the pixels number on the reference images

We applied the box-counting method to the reference images containing more and more pixels and we examined the representative plots of log Nr versus log r for each of these images. We have established that 500 pixels at least are necessary to obtain a straight line. Figures 2 and 3 show respectively an image of 500 pixels and the corresponding log Nr – log r curve.

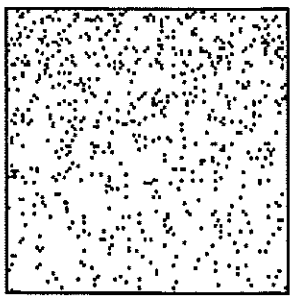

Figure 2: Reference image of 500 pixels.

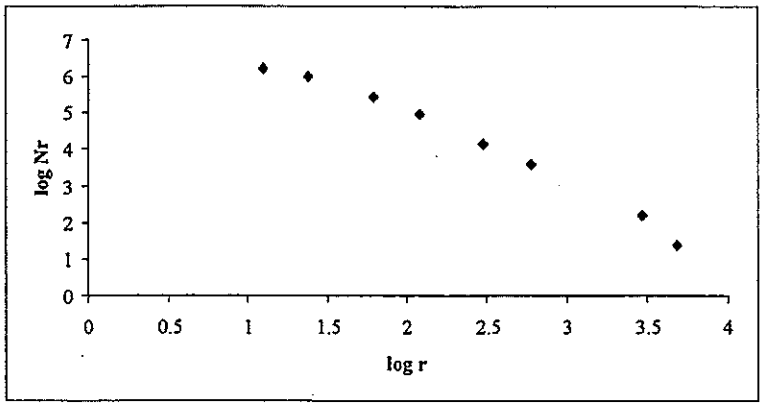

Figure 3: Relationship between Nr and r for a 500 pixels reference image.

Therefore, the relationship between Nr and r on log coordinates is linear if the number of pixels is large enough (>500). However, in this study, the number of pixels which represents the powder C particles depends on the volume ratio of the two powders A and C brought into contact. This ratio is equal to 30. Therefore, a synthesis image representative of the real mixture needs to contain about 325 black pixels for an image containing 10000 pixels. Meanwhile, the particles C are four times bigger in diameter than the particles A. Therefore, the pixels which correspond to the powder C must to be agglomerates of 4 pixels and we can work on reference images with points of 4 pixels in size.

3.2. Reference images with points of 4 pixels

The influence of the pixels distribution in the image on the variation of the D coefficient has been investigated.

3.2.1. Homogeneous repartition of pixels

Synthesis images were produced with an homogeneous distribution of points on the entire surface of the image or only on a part of this surface. Different cases were studied, with points present only on a half or a quarter of the image. The representative plots of log Nr versus log r are always a straight line. The coefficient D is the same in all the cases. This means that this is not an appropriate variable to represent the distribution of points on an image.

3.2.2. Influence of the agglomerate size

We made reference images with agglomerates of different sizes and intermediate images between an heterogeneous and homogeneous mixture. Figures 4 and 5 show an example of these images.

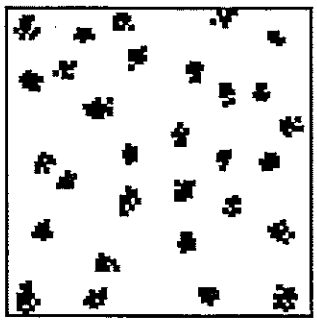

Figure 4: Image with small agglomerates

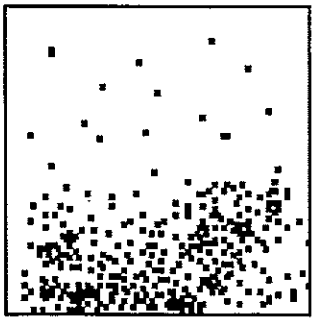

Figure 5: Intermediate image

The D coefficient varies in these two cases between 1.5 and 1.6. We conclude that it is not a discriminant parameter in that case either.

3.2.3. Results and discussion

As seen previously, the value of the D coefficient does not significantly vary according to the homogeneity degree of the image. To get more pertinent information, we decided to study the variations of this coefficient when the images

are modified by an erosion process. The erosion implies a regular decrease of the points size: it is possible because the points of these images are represented by 4 pixels.

We evaluated the variation of the D coefficient between the initial and the eroded images and found that this variation was depending on the degree of homogeneity of the initial image.

It was brought to the fore that the ratio $\frac{\Delta D}{D}$ can take 3 values according to the homogeneity degree of the mixture :

- $\frac{\Delta D}{D}$ is less than 40 % if the mixture contains big agglomerates.
- $\frac{\Delta D}{D}$ is between 40 and 50 % if the mixture contains small agglomerates.
- $\frac{\Delta D}{D}$ is larger than 60 % for homogeneous mixture.

We conclude that the ratio $\frac{\Delta D}{D}$ allows to differentiate a mixture containing small or big agglomerates or an homogeneous mixture.

However, the value of $\frac{\Delta D}{D}$ is the same if the pixels are set on the entire surface of image or only on a fraction of it. Therefore the distribution of the points on the surface cannot be studied by this way.

3.3. Real images

The obtained mixing images are thresholded in order to eliminate the background noise. These are then treated the same way as the reference images. The only difference is that the number of erosions is now equal to 5 from the initial image until no point remains on the image.

Figures 6 and 7 represent the mixture at t = 5s (initial mixture) and t = 100s (final mixture) respectively.

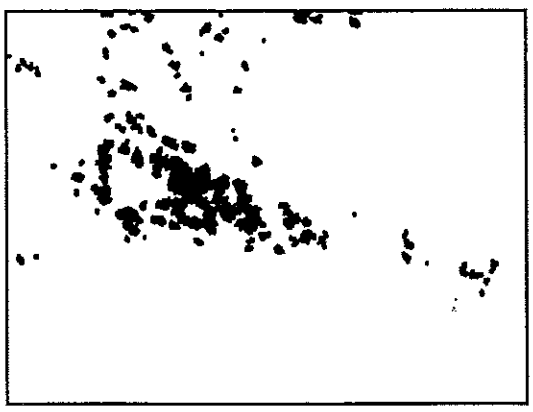

Figure 6: Real mixture at t = 5s after threshold and treatment.

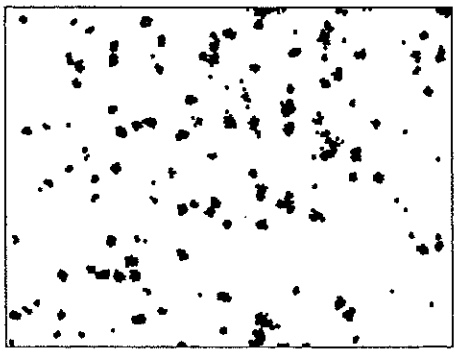

Figure 7: Final mixture (t = 100s) after threshold and treatment.

3.4. Results

As with the synthesis images, we investigated the evolution of the ratio $\frac{\Delta D}{D}$ between the initial real image and the 5 times eroded image.

At the beginning of the mixing (t = 5s), $\frac{\Delta D}{D}$ is equal to 20 %. This low value is in agreement with the obtained ratio for a reference image containing big agglomerates (about 40%, see § 3-2-3).

At the end of the mixing (t = 100s), $\frac{\Delta D}{D}$ is equal to 61 %. It corresponds to results obtained with synthesis image for an homogeneous mixture. For each real image, we obtained a linear evolution of D versus the number of erosion and we defined p as the slope of this straight line.

Figure 8 shows the evolution of this slope p with time obtained from images taken regularly from the beginning of mixture (t = 5s) to the end (t = 100s).

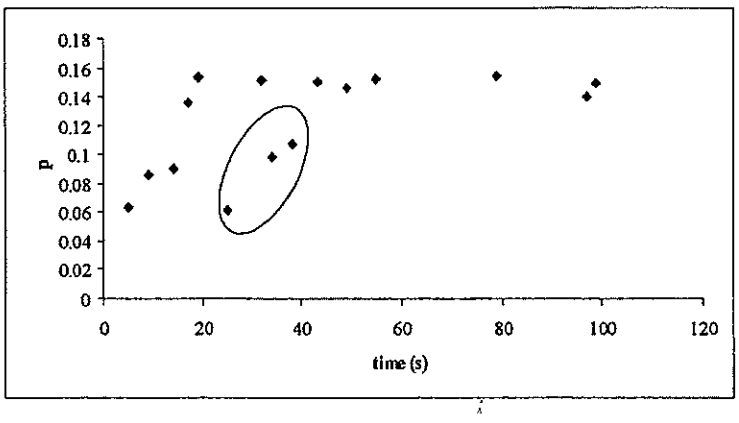

Figure 8: Time profile of p.

We found out that p increases at the beginning of the mixing and then rapidly becomes stabilised after about 40s of fluctuations. These fluctuations are due to the

heterogeneity of the mixture. Indeed, this method do not allow to differentiate between an homogeneous distribution on a part of the surface and an homogeneous distribution on the whole image. The breakings in the p time profile (surrounded points, Figure 8) could be explained by this default of the method: the image taken at t = 20s presents a pseudo homogeneous distribution on a part of the surface so that the slope p is about the final value. In fact, some agglomerates still remain and appear on the next image, leading to an important decrease of the slope p. This phenomenon is selfrepeated for the next images until t = 40s. After t = 40s, the mixing can be considered as completely homogeneous, when the slope p reaches a stable value (about 0.16).

CONCLUSION

In this study, the visualisation of the blending of two powders is investigated using an image processing technique. The obtained images are analysed using the box-counting method. In a first step, we tried to calibrate the image analysis method by applying it on well defined images created by a computer. This first part of the study showed that only images with enough points can be analysed by the box-counting method. This condition is necessary to achieve the fractal dimension of the image, deduced from the evolution of log Nr versus log r. Fortunately, the number of points on real images corresponds to this criterion. We also brought out that the crude information deduced from a simple treatment of the initial images do not allow to conclude about the homogeneity of the points distribution. In a second step, our method implies successive erosions of the points and box-counting applications, to study the variation of the fractal coefficient D. We found that the time profile of the variation of the fractal coefficient D versus the erosion number is representative of the homogeneity degree into the reactor and we decided to adopt this variation as a characteristic number.
This method will now be used to quantify the blending in the reactor for different mixing rates and different mixers. The two powders mixture will also be brought into contact with more and more viscous liquids in order to simulate the viscosity increase of the mixture during the chemical reaction. This should lead to the resulting blend and the associated contact times which will be coupled to the kinetic parameters.

REFERENCES

[1] Kraft, R., Fractals and dimensions, http://www.edv.agrar.tu-muenchen.de , (1995)
[2] Kraft, R., Kauer, J., Estimating the fractal dimension from digitized images, http://www.edv.agrar.tu-muenchen.de , (1995)
[3] Aker, E., http://www.fys.uio.no/eaker/thesis , (1997)
[4] Fan, L. T., Chen, Y.M., Lai, F.S., Recent developments in solids mixing, Powder Technol., 61 (1990), 255-287
[5] Akiyama, T., Aoki, K., Iguchi, T., Nishimoto, K., A fractal property of vertically vibrated beds of granules, Chem. Eng. Sci. 51 (1996), 3351-3353
[6] Akiyama, T., Iguchi, T., Aoki, K., Nishimoto, K., A fractal analysis of solids mixing in two-dimensional vibrating particle beds, Powder Technol., 97 (1998), 63-71

A A2 - VALIDATION OF COMPUTATIONAL FLUID DYNAMICS SIMULATIONS BY TRACER EXPERIMENTS AND NUMERICAL RESIDENCE TIME DISTRIBUTION

TRACER EXPERIMENTS – A WAY TO VALIDATE COMPUTATIONAL FLUID DYNAMIC SIMULATIONS IN AN AGITATED VESSEL.

G. Delaplace[1], C. Torrez[2], C. André[2], J.-C. Leuliet[1]

[1]Institut National de la Recherche Agronomique (I.N.R.A), Laboratoire de Génie des Procédés et Technologie Alimentaires (LGPTA), 369 rue Jules Guesde, B.P. 39, 59651 Villeneuve d'Ascq Cédex, France

[2] Hautes Etudes Industrielles (H.E.I.), Laboratoire de Génie des Procédés, 13 rue de Toul, 59046 Lille Cedex, FRANCE

Abstract. In this paper, numerical simulation of flow field involving highly viscous fluids into a stirred tank was conducted by means of a commercial available fluid dynamic (CFD) software package (FLUENT). A rounded bottom vessel equipped with an atypical helical ribbon impeller was used as mixing equipment. The reliability of the numerical procedure was demonstrated on the basis of a comparison of the numerical results with power consumption measurements and tracer experiments. Measured and simulated values of power consumption were obtained for both Newtonian and non-Newtonian fluids. Tracer experiments were only carried out with Newtonian fluids and consist in comparing axial circulation time data obtained by experimental methods (flow follower and conductivity techniques) to predicted values calculated by CFD approach. Close agreement between the two set of data was obtained. Finally, dispersion of a clustered tracers was performed using CFD approach and the homogenisation process was analysed. It is shown that computational tools are able to provide the volume fraction of the agitated liquid which has achieved the degree of homogeneity required. These approaches are likely to have a significant impact in the close future to get an idea of mixing efficiency of various mixing systems.

INTRODUCTION

Mixing highly viscous fluids in agitated vessel is one of the oldest and of the most common processing operation encountered in the food and chemical industries. For these industries, the purpose of mixing operations could be quite different. For example, the requirement could be to ensure good homogeneity inside the vessel or/and to improve heat and mass transfer.

A large number of impellers can be used for the mixing duty. The impeller geometry chosen depends on the operating conditions such as the agitation speed and the rheological behaviour of the fluids. The design of industrial mixing equipment is based mainly on the analysis of macroscopic quantities such as power consumption, and/or mixing characteristics (mixing and circulation times) obtained by correlating tracer experiments data. Although tracers and tracing methods have provided us lot of basic information about the vast variety of mixing devices and have represented a real progress in this field, it is widely admitted that tracers experiments (black box data) are sometime not adequately adapted to investigate and understand locally the complex hydrodynamics inherent to industrial mixers. Moreover, it is recognised that these experimental methods does not always provide an efficient pathway to scale-up or scale down mixing equipment. In this area, perspectives offered by advanced computational fluid dynamics (CFD) seem very interesting.

Although numerical approaches provide very powerful method for the analysis of the mixing flow pattern, lack of experimental validations can lead to drastic errors. In this way, tracer experiments can still be very useful. One objective of this work is to demonstrate how tracer experiments can be used to validate CFD simulations and to improve understanding of the mechanisms responsible for homogenisation and transport processes in mixing vessel.

In this paper, homogenisation process of highly viscous Newtonian fluids in an industrial agitated vessel (34 litres) equipped with an atypical helical ribbon impeller (Figure 1) was attempted numerically. Using a commercially available fluid dynamic software package (FLUENT), the velocity field generated by the agitator in the tank has been first performed, then trajectories of a few clustered tracers have been computed and their dispersion with time have been analysed .

The reliability of the numerical procedure was demonstrated on the basis of a comparison of the numerical results with experimental data in several ways. First for various Newtonian and non-Newtonian fluids, measured and numerically calculated values of power consumption were reported. Then numerically calculated values of axial circulation times were compared with those measured by tracer experiments. Experimental circulation times data were obtained by two different methods: the flow follower technique and the conductivity method. Numerical values of axial circulation time are deduced from the knowledge of both computed values of axial velocities through an horizontal plane and the volume of liquid in the tank.

EXPERIMENTAL APPARATUS AND METHOD

1. Mixing system investigated

A sketch of the mixing system investigated (atypical helical ribbon impeller and rounded bottom of the vessel) is shown in Figure 1. The dimensions of the mixing system are also reported in Figure 1.

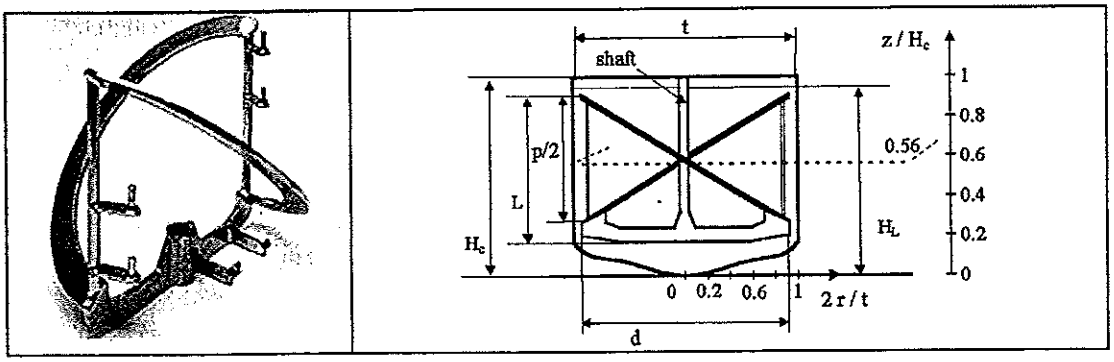

Figure 1. Picture of the agitator (PARAVISC®, Ekato) and scheme of the mixing equipment studied. (vessel diameter, t =0.346 m, impeller diameter, d =0.320 m; blades width, w =0.032 m, impeller pitch, p = 0.560 m; impeller height, L= 0.340 m tank height, H_c = 0.443 m). Dotted lines refer to the horizontal plane (z / H_c =0.56) taken as reference to compute numerical values of axial circulation times .

Very few data are available for the helical ribbon impeller studied. Indeed this non standard helical impeller has two particularities: firstly, it is equipped with an anchor at the bottom in order to avoid the formation of a stagnant zone; secondly the size of the pitch ratio p/d (p/d=1.7) is greater than with a typical double helical ribbon mixer ($0.5 < p/d < 1.2$). During all the experiments, the volume of liquid was kept constant and equal to $34 .10^{-3}$ m^3 which corresponds to a liquid depth, H_L of 0.409 m.

2. Fluids

Several Newtonian liquids and a shear-thinning fluid were prepared to ascertain numerical results. The Newtonian fluids were mixture of glucose syrups with various water concentrations (1350 kg.m^{-3} $< \rho < 1420$ kg.m^{-3}). The shear-thinning fluid was 3% w/w guar gum solution ($\rho = 1000$ kg.m^{-3}).

The rheological properties and densities of the test fluids were obtained at the same temperature as that encountered in the mixing equipment. Rheological properties of the test fluids were measured in classical controlled rotational speed concentric cylinders (Contraves-Rheomat 30). The shear rates range vary from 0 to $500s^{-1}$. For the shear-thinning fluid, Krieger and Maron [1] corrections were applied to correct the expression for the wall shear rate obtained with Newtonian fluids Rheological behaviour of shear-thinning fluids was described by a power-law equation over the entire range of shear rate ($\mu_a = k\,\dot{\gamma}^{n-1}$ - *n=0.113 - k=197.9 Pa.s^n).*

3. Numerical simulation of the velocity distribution

The numerical tools and solution procedure used by the commercial CFD finite volume software (FLUENT) to determine the fluid velocity profiles inside the vessel are well known [2] and will not be repeated in details here. In the following part, only details about the mixing system modelling options will be given. An unstructured mesh of 453,238 tetrahedral cells has been built to represent the vessel.

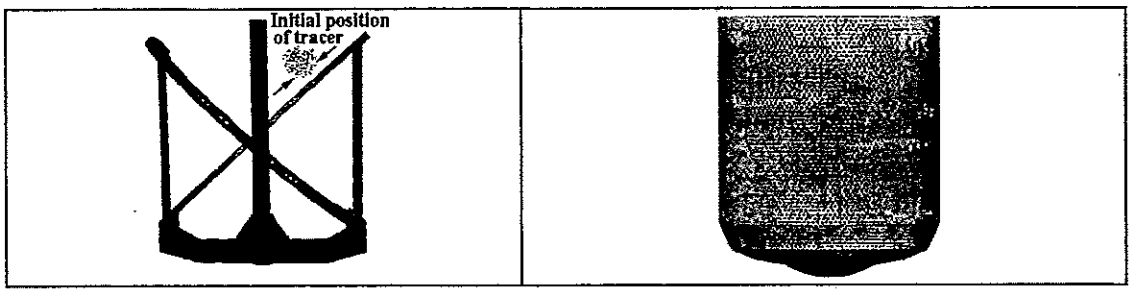

Figure 2. Mesh of the agitator [PARAVISC®, Ekato] (on the left) and of the rounded bottom vessel studied (on the right). Initial position of clustered tracers used for numerical simulation of dispersion is also reported (left figure).

Note that the geometry of the mixing system used for simulation is very similar to the experimental equipment. The rounded bottom of the vessel has been accurately duplicated. Only additional parts of the impeller used to fix scrapers haven't been meshed (Figure 2).

The boundary conditions at the impeller shaft and at the vessel walls were those derived assuming the no-slip condition. At the free surface, the boundary conditions were modeling by requiring that there is no normal velocity and zero normal gradient for all variables. A rotating reference frame was used to perform the simulation.

4. Treatment of experimental and numerical data

4.1. Power consumption for Newtonian and non-Newtonian fluids

A strain gauge torquemeter, in the range of 0 to 100 N.m was used to measure experimentally power consumption. The rotational speed of the impeller was measured by using a digital tachometer. For numerical approach, assuming that the power consumption supplied by the impeller is exclusively consumed as viscous dissipation of energy inside the vessel, we calculated the total power consumption P in the vessel by the summation of energy consumed in each volume control, throughout the vessel

$$P = \sum_i \mu_{a_i} \dot{\gamma}_i^{\,2} V_i \tag{1}$$

where $\mu_{a_i}, \dot{\gamma}_i, V_i$ are respectively the apparent viscosity, the shear rate and the volume of the agitated fluid contained in cell i. For each cell, $\dot{\gamma}$ was deduced from the second invariant of rate of the deformation tensor $\overline{\overline{\Delta}}:\overline{\overline{\Delta}}$

$$\dot{\gamma} = \sqrt{\frac{1}{2}\overline{\overline{\Delta}}:\overline{\overline{\Delta}}} \tag{2}$$

4.2. Axial circulation times for Newtonian fluids

Experimental axial circulation times data t_c were obtained by two different methods: the flow follower technique and the conductivity method.

For conductivity method, the tracer pulse injected has the same physical properties as the fluid in the tank (temperature and composition) with an additional quantity of Nacl at a concentration of 100g/l. It has been shown that addition of salt has a negligible influence on tracer density and viscosity. Both tracer injections of 72ml and of 500ml have been carried out. The incorporation is performed with the help of a pneumatic system with pistons (Type DACO, PCM DOSYS).

Details about probe position and location of injection area are given elsewhere [3-5]. Experiments were carried out and observed with the helix pumping upward (counter-clockwise direction of rotation)

When the passage of a freely suspended particle in a vessel is monitored (flow follower technique), t_c is the average time taken by a particle to cross a given reference plane two times in the same direction.

On the other hand, when probe methods are used, the axial circulation time t_c is defined as the time between two subsequent peaks on the response curve.

For numerical approach, axial circulation times are deduced from the knowledge of both the value of axial circulation flow rates Q_{ax} through an horizontal plane and the volume of liquid V in the tank:

$$t_c = V/Q_{ax} \tag{3}$$

Axial circulation flow rate Q_{ax} is deduced from the numerical values of axial velocity u_{ax} of each cell i contained in the reference horizontal plane:

$$Q_{ax} = \frac{1}{2}\sum_i \left| u_{ax,i} \right| A_i \tag{4}$$

where A_i is the cross section area of cell i contained in the horizontal plane chosen. For this work, the horizontal plane taken as reference to predict numerical values of circulation times were located at $z = 0.248$ m above the bottom of the tank (which are equal to z / H_c=0.56 - Figure 1).

5. Dispersion of clustered tracers

Homogenisation process generated by our agitator was investigated by computing the trajectories of clustered tracers contained in a sphere of 0.0265 radius (267 cells) and launched at the upper part of the vessel (Figure 2). In order to represent the evolution with time of the degree of mixing in the vessel, tracer concentration in each volume control was recorded at various time step and numerical values of concentration fluctuations have been used to determine mixing times at 50, 75, 90, 95, 97 and 99%. Mixing times at *x%* was defined as the time at which fluctuation of concentration in each volume control was less than *(1-x%)* of the final concentration

RESULTS AND DISCUSSION

1. Reliability of numerical method

1.1. Power consumption for Newtonian and non-Newtonian fluids

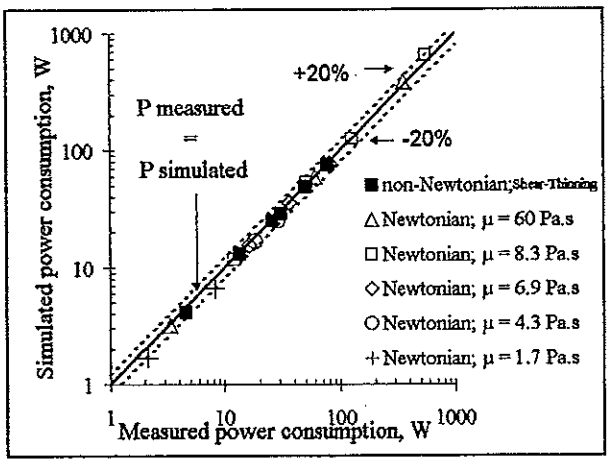

Figure 3. Power consumption data obtained numerically and experimentally when mixing Newtonian liquids (1.7 Pa.s<μ<60 Pa.s) and a shear-thinning fluid (n=0.113 – k=197.9 Pa.s^n) under laminar regime (0.17<Re<80) at different impeller rotational speeds (2.73rev/s<N<0.06 rev/s).

Figure 3 shows, for test fluids, the comparison between experimental and numerical results of power consumption *under isothermal conditions*. Even for strong shear-thinning fluid ($n < 0.3$), relative errors between experimental and numerical results have always been found less than 15%.

1.2. Axial circulation times, t_c for Newtonian fluids

Experimental results of axial circulation times for our mixing equipment are shown in Figure 4 (on the left). Results are plotted as the product of impeller rotational speed, N and axial circulation time, t_c as a function of Reynold number $Re=\rho Nd^2/\mu$. Note that each axial circulation time obtained by conductivity method (left figure) is the result of a tracer injection and in this case t_c is deduced from the average period of the tracer response curve.

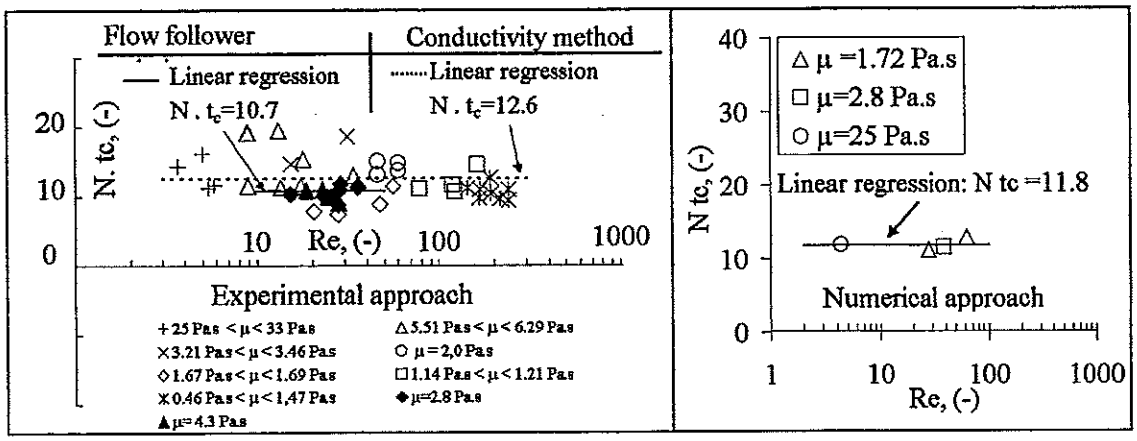

Figure 4. Axial circulation times data obtained experimentally (on the left) and numerically (on the right) for the mixing system investigated using various Newtonian fluids. Note that symbols which appear on this figure refer respectively to experimental data (on the left) (white symbols - conductivity method; black symbols - flow follower method) and to computed values obtained by CFD (on the right).

Experimental approaches show that the product $N.\ t_c$ is constant in the laminar flow regime. Using the least square method, we obtained, for $10<Re<40$, $N.t_c=10.7$ by flow follower technique and we obtained, for $3<Re<250$, $N.t_c=12.6$ by conductivity method. These experimental values of axial circulation number are qualitatively in agreement with those reported in the literature for typical double helical ribbon impellers: $N.t_c$ between 5 and 25 [4]. It is difficult to make a more precise comparison with other helical ribbon agitators because the circulation number is dependent both on the mixing system and in a certain extent on the experimental technique used to measure it [4-5].

Figure 4 (on the right) also shows results of axial circulation times obtained numerically for $4 < Re < 60$. As expected, the product $N.t_c$ is also constant. $N.t_c=11.8$. This value of the product $N.t_c$ is qualitatively in agreement with those obtained experimentally. Indeed the distribution of axial circulation time obtained by flow follower method is large and probe measurements give axial circulation time

data measured at one point in a flow system, so the accuracy of numerical results seems quite acceptable.

All these results regarding the power consumption and axial circulation times for various test fluids prove that numerical simulation method has sufficient reliability to predict flow behaviour of highly viscous fluids in such mixing system, especially under laminar regime and isothermal conditions.

Note that axial circulation times obtained numerically are not based on the computation of tracer trajectories (Lagrangian approach) but deduced from the numerical velocity field (Eulerian approach) through an horizontal plane. This has been chosen deliberately. Indeed, it is well known that, for Newtonian fluids and a given mixing system, mixing time is not only dependent on impeller rotational speed and on the position of the sensor used to detect quality of mixing. Other additional factors such as the area of injection, tracer quantity and way used to incorporate tracer (shape of clustered tracers, initial velocity of the tracers) have also a strong influence on mixing times data. Unfortunately, for numerical approach, it is very difficult to define or/and to duplicate all the operating conditions encountered during tracers experiments. For example, experimental injections of tracer take place close to the free surface of the agitated vessel. Numerically, duplicate similar way of injection, is a major difficulty since to make easier numerical model, no normal velocity is generally assumed at the free surface. Moreover, when highly viscous fluids are injected by a pneumatic system equipped with pistons, it is very difficult to define the shape of clustered tracers and their initial velocity at the time they incorporate the agitated fluid. Unfortunately these data are required for numerical approach and can generate important errors to calculate trajectory of tracer and consequently to determine axial circulation times.

2. Dispersion of tracers

An example of numerical results obtained for dispersion of clustered tracers with the helical agitator studied (N=0.75 rev/s, ρ =1396 kg/m^3, μ=1.76 Pa.s) is presented in Figure 5. For this test, molecular diffusivity of the viscous media is 2.88 10^{-5} m^2/s.

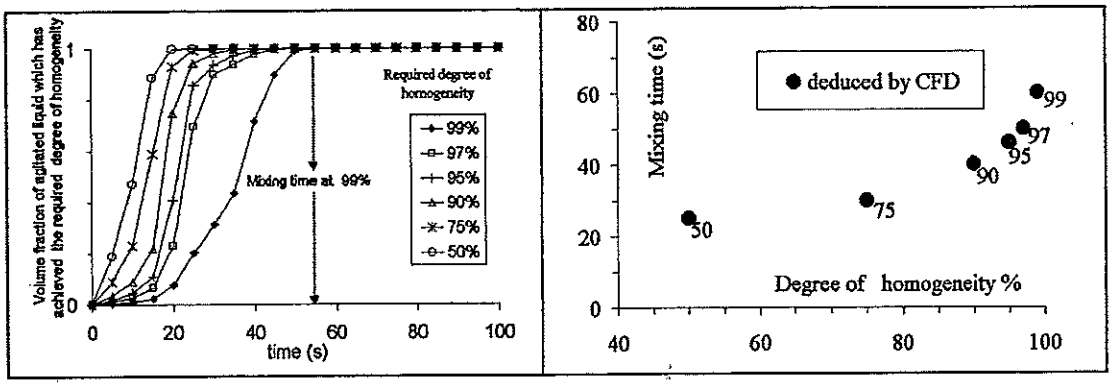

Figure 5. Evolution with time of the volume fraction of the agitated Newtonian liquid which has achieved the required degree of homogeneity (on the left). Numerical values of mixing times at 50%, 75%, 90%, 95%, 97%, 99% (on the right) obtained after tracer injection (78 ml) for the mixing system investigated.

Figure 5 (on the left) shows during an homogenisation process, for various degree of homogeneity, the evolution with time of percentage of viscous media which has achieved the fixed degree of homogeneity. Note that tracer is incorporated at initial time. Even if one must also keep in mind that changing the quantity or/and the initial position of the tracer may affect the results, figure 5 (left part) gives an idea of the dispersion potential of the helical ribbon agitator tested.

Mixing times make sense only in the case of well-mixed system. So, mixing times must be defined as the time at which all elements of fluid (or all control volumes) satisfy the fixed degree of homogeneity. In this work, numerical approach allows such determination of mixing times as shown in Figure 5. Results of figure 5 (on the right) show that there is no simple relation of proportionality between the mixing time and the degree of homogeneity: The mixing time increases quick faster when the required level of homogeneity is higher. It is clear that knowledge of an accurate state of mixing in the whole volume of the tank can be very helpful to gain a better understanding of numerous industrial homogenisation processes.

CONCLUSION

In this work, first a three-dimensional resolution of the flow equations in a mixing vessel has been conducted by CFD approach and tracer experiments have been carried out to validate numerical results. Then trajectories of a few clustered tracers have been computed. It has been shown that drop dispersion calculation gives an idea of local mixing time, ie mixing time relevant to the region of the tank volume considered and consequently it becomes possible to obtain new criteria (knowledge of intensity of segregation at any point in the tank) to study the global stirring performances of a given mixing system. It is now clear that the science of mixing will benefit a lot from numerical simulation in a close future. CFD simulation allows a thorough analysis of the flow pattern in such way that it enables us to assess preferential mixing zones, dead zones caverns. It will be also possible to modify the agitator's geometry to improve mixing efficiency. Increasing number of numerical simulations open new perspectives for tracer applications. Indeed, at the state of the art, it is indispensable that numerical results were compared with experimental measurements and tracer experiments are interesting tools to ascertain numerical results. In particular, theirs use seems essential when numerical studies deal with complex mixing systems with non-Newtonian liquids as encountered in industry.

REFERENCE

[1] Krieger, I.M., Maron, S.H., J. of Appl. Phys., (25), 1, (1954) 72-75.

[2] Patankar S.V. *Numerical heat transfer and fluid flow*. Series in Computational Methods in Mechanics and Thermal Sciences, Mc Graw Hill, New york, (1980).

[3] Delaplace, G., Dieulot, J.Y., Leuliet, J.C., Brienne, J.P., The Can. J. of Chem. Eng., 77 (1999) 447-457.

[4] Delaplace, G., Leuliet, J.C., Relandeau, V., Exp. in Fluids, 28 (2000) 170-182.

[5] Delaplace, G., Belaubre, N., Leuliet, J.C., Dieulot, J.Y., Récents Progrès en Génie des Procédés, 12, 61, (1998) 273-278.

VALIDATION OF A LAGRANGIAN TRAJECTORY CALCULATION ALGORITHM BY COMPARISON WITH AN EXPERIMENTAL RESIDENCE TIME DISTRIBUTION

J. Pruvost[1], J. Legrand[1], P. Legentilhomme[1]

[1]GEPEA-UMR.MA, University of Nantes, CRTT-IUT, BP 406, 44602 Saint-Nazaire Cedex, FRANCE.

Abstract. The knowledge of the flow-field can be very useful in reactor design and optimization. Providing information about displacement and trajectories of reactive elements, such characterization is of primary interest to better understand the process running. Results are deduced from Computational Fluids Dynamics or experimental measurements. But, for complex-type flow such as the swirling decaying flow, numerical simulation are difficult to achieve and trajectories have to be calculated using velocity-field measurements. This problem is rather simple if a Lagrangian formulation is employed, and the difficulty results then in expressing turbulence effect on calculated trajectories, and especially the set-up of structured eddies. Fluctuations are thus not pure random functions, but they are linked to turbulence spatial correlation. A method is presented in this study and then employed to calculate trajectories of elementary fluid particles in a swirling decaying flow, using hydrodynamical characteristics obtained by Particle Image Velocimetry (PIV) investigation. Results are finally verified by determining the Residence Time Distribution (RTD) using the trajectory calculation algorithm. A comparison with an experimental RTD confirms the efficiency of the method to determine trajectories in the swirling decaying flow.

INTRODUCTION

Trajectories can give useful information on chemical processes. But, they remain difficult to measure with accuracy. Visualization techniques like injection of colouring agent or particle tracer (glass, polystyrene beads or fog) only provide a global estimation of trajectories. Another solution is to use Computational Fluid Dynamics (CFD) to model the flow under study. The velocity-field can then be determined and it is trivial to deduce elementary fluid trajectories [1]. But, when the flow exhibits a complex behavior, flow modeling becomes very difficult, especially in turbulent flow regime, and an experimental investigation is often needed.

Recent experimental velocity measurement techniques like Laser Doppler Anemometry (LDA), hot-wire or Particle Image Velocimetry (PIV), are now able to provide with accuracy the main hydrodynamical characteristics as, for example, instantaneous components of the velocity-field. Trajectories of elementary particles can then be deduced by integrating the velocity-field. As often applied in CFD [2-4], a Lagrangian formulation can be used. Trajectories are determined step by step by calculating successive positions of the fluid element, P, by:

$$P(t+\Delta t) = P(t) + u\Delta t \qquad (1)$$

where Δt is a time step to determine and u the instantaneous velocity.

If the Reynolds decomposition of the instantaneous velocity is used in equation (1), the path of an elementary fluid particle can be written as:

$$P(t+\Delta t) = P(t) + (U + U')\Delta t \qquad (2)$$

where U is the mean value of the velocity, and U' the fluctuating one.

Mean statistical characteristics of the flow, like mean velocity components, turbulent intensities or velocity correlations can be experimentally measured. If the mean velocity distribution is known in equation (2), difficulty remains in the determination of the fluctuating velocity U' due to turbulence. This can be solved by introducing a mathematical modeling of the fluctuating velocity. But, turbulence cannot be considered as a pure random phenomenon in complex flows, and attention must focus on spatial turbulence correlations to represent effects of the eddies on trajectories [2]. This approach was retained for a swirling decaying annular flow.

This flow is induced in an annular geometry by a tangential inlet which appears to be of rather simple design to create such hydrodynamics [5]. A schematic representation of the geometry is given in Figure 1. This kind of flow exhibiting three dimensional motion and increasing turbulent intensities compared with that obtained in a purely axial flow is found to be an efficient way to enhance heat or mass transfer phenomena [6-8]. The swirl motion is created at the inlet of the device and then decays freely along the flow path, involving a very disturbed and complex flow behavior [9-11]. A numerical simulation of such a flow remains difficult to achieve. An easy way to investigate this particular flow is to employ the PIV measurement technique to provide main hydrodynamical characteristics. A previous study has shown how to get, using this method, the turbulence length scale and the three components of the mean velocity and turbulent intensity [12]. In the present study, experimental PIV measurements are used to determine trajectories using equation (2). Because the swirling flow is not axisymmetric, a three-dimensional calculation method is needed. Next, the RTD is experimentally determined, and finally compared to the simulated one, obtained using the trajectory calculation algorithm.

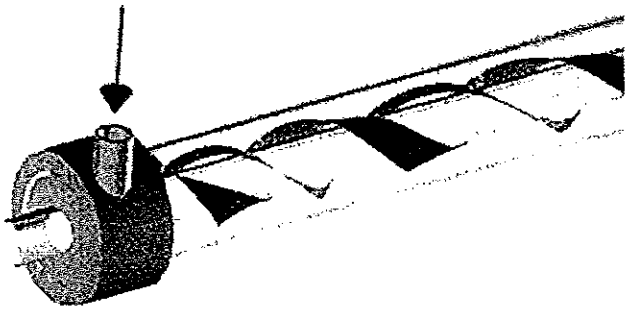

Figure 1. Schematic representation of the swirling flow

EXPERIMENTAL SET-UP

The hydraulic test rig used for the experimental investigation has been previously described in Pruvost et al. [12]. It consists in an annular test section (Figure 1) made of two concentric Plexiglas tubes having a total length of 1.5 m. The internal radius of the outer cylinder, R_o, is 50 mm, the outer radius of the inner tube, R_i, equal to 20 mm. The diameter of the tangential inlet is 30 mm, equal to the annular gap width, e, corresponding to pure swirling flow according to Legentilhomme &

Legrand [7]. The outlet of the annulus is of axial type, so as to not disturb the flow. For all the experimental measurements, the water flow rate is Q = 1.27 m^3/h corresponding to a mean axial velocity in the annulus, $\overline{U}$, of 5 cm/s and a Reynolds number, Re, equal to 3000, where Re is calculated by :

$$Re = \frac{2\,e\,\overline{U}}{\nu} \tag{3}$$

All needed hydrodynamical characteristics described in this study were obtained using the PIV measurement technique. The PIV set-up and the investigation method is described in Pruvost et al. [12]. But, PIV cannot provide information about the flow-field on the entire geometry and, in order to calculate trajectories with a Lagrangian formulation, each hydrodynamical parameter has to be determined for successive locations of the elementary fluid particle. Authors have shown how a neural network method using Radial Basis Functions (RBF) can be used to obtain a mathematical expression defined on the whole domain of each one of these characteristics using experimental PIV results [13]. The application of this technique allows the determination of hydrodynamical properties such as the mean velocity-field and turbulent intensities on the entire geometry.

Mean velocities and turbulent intensities calculated using PIV instantaneous results are defined by:

$$U_x = \frac{1}{N}\sum_{i=1}^{N} u_{xi}\,,\quad U_r = \frac{1}{N}\sum_{i=1}^{N} u_{ri}\quad,\quad U_\varsigma = \frac{1}{N}\sum_{i=1}^{N} u_{\varsigma i} \tag{4}$$

$$T_x = \frac{\sqrt{\frac{1}{N}\sum_{i=1}^{N}(u_{xi}-U_x)^2}}{\overline{U}}, T_r = \frac{\sqrt{\frac{1}{N}\sum_{i=1}^{N}(u_{ri}-U_r)^2}}{\overline{U}},\quad T_\varsigma = \frac{\sqrt{\frac{1}{N}\sum_{i=1}^{N}(u_{\varsigma i}-U_\varsigma)^2}}{\overline{U}} \tag{5}$$

To achieve stable results, 200 PIV acquisitions were necessary for mean values, and 1000 for turbulent intensities.

MATHEMATICAL MODELING OF THE VELOCITY FLUCTUATIONS

Trajectories calculation is often used in two-phase flow modeling [2, 4, 14-16]. According to these studies, the fluctuating velocity has to be carefully considered to achieve accurate results. Some mathematical formulations of this time-dependent parameter are available [2, 16]. The simplest one is to use a pure random function of Gaussian type with its root mean square linked to turbulent intensity:

$$U'(P) = q(P) \tag{6}$$

where q(P) is a gaussian distributed random function determined for the location P.

For an anisotropic three-dimensional turbulence, this is expressed by :

$$\begin{cases} U_x'(x,r,\xi) = q_x(m_x,\tau_x) = q_x\left(0,\overline{U}\,T_x(x,r,\xi)\right) \\ U_r'(x,r,\xi) = q_r(m_r,\tau_r) = q_r\left(0,\overline{U}\,T_r(x,r,\xi)\right) \\ U_\varsigma'(x,r,\xi) = q_\varsigma(m_\varsigma,\tau_\varsigma) = q_\varsigma\left(0,\overline{U}\,T_\xi(x,r,\xi)\right) \end{cases} \tag{7}$$

where m and τ are respectively the mean and the root mean square of the Gaussian random function calculated for each velocity component.

But, approximating the fluctuating velocities by a pure random phenomenon leads to a loss of information, especially about turbulence correlations which cannot be neglected in duct flows [17]. Thus, it was chosen to consider turbulence correlations in the fluctuating velocity determination, the formulation of which corresponds to the weighted sum of a random term calculated using equation (7) and another one introducing the correlation expression [2]:

$$U'(P+\Delta P) = c_{cor}U'(P) + c_{rand}q(P) \quad (8)$$

where c_{cor} and c_{rand} are weighting parameters to be determined linked respectively to the correlation and the random terms.

Parameters c_{cor} and c_{rand} depend on the type of flow under study, and especially of the turbulence correlation obtained. As shown in a previous study [12], PIV technique is well-adapted to the measurement of spatial correlations.

Spatial correlations values can be obtained using PIV for both axial and radial velocity components, along the axial and radial coordinates. Spatial correlations are defined by:

$$f_{x,r,\xi}(l_x) = \frac{\overline{U_x'(x,r,\xi)U_x'(x+l_x,r,\xi)}}{\overline{U_x'(x,r,\xi)^2}} \quad (9) \qquad g_{x,r,\xi}(l_x) = \frac{\overline{U_r'(x,r,\xi)U_r'(x+l_x,r,\xi)}}{\overline{U_r'(x,r,\xi)^2}} \quad (10)$$

$$f_{x,r,\xi}(l_r) = \frac{\overline{U_x'(x,r,\xi)U_x'(x,r+l_r,\xi)}}{\overline{U_x'(x,r,\xi)^2}} \quad (11) \qquad g_{x,r,\xi}(l_r) = \frac{\overline{U_r'(x,r,\xi)U_r'(x,r+l_r,\xi)}}{\overline{U_r'(x,r,\xi)^2}} \quad (12)$$

where $\overline{\ }$ represents time average value, $f_{x,r,\xi}(l_x)$ is the axial correlation of the axial velocity component, $g_{x,r,\xi}(l_x)$ the axial correlation of the radial velocity component, $f_{x,r,\xi}(l_r)$ the radial correlation of the axial velocity component and $g_{x,r,\xi}(l_r)$ the radial correlation of the radial velocity component.

Figure 2 shows an example of experimental correlation calculated using PIV, fitted by a Gaussian type function [17]. Such functions only depend on one fitting parameter, called the integral length scale L defined by :

$$F(l) = exp\left(-\left(\frac{l}{L}\right)^2\right) \quad (13)$$

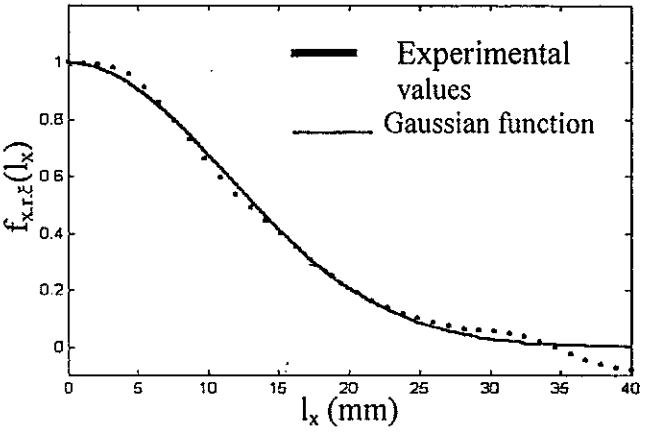

Figure 2. Example of spatial correlation

A previous PIV investigation has been made to determine correlations on the whole domain and the integral length scale was calculated for each correlation. Results have shown that length scales can be considered as axisymmetric. Values are only function of axial and radial coordinates of the geometry. An example of distribution of L_{fx}, the length scales obtained for the axial correlation of the axial component, is given in Figure 3.

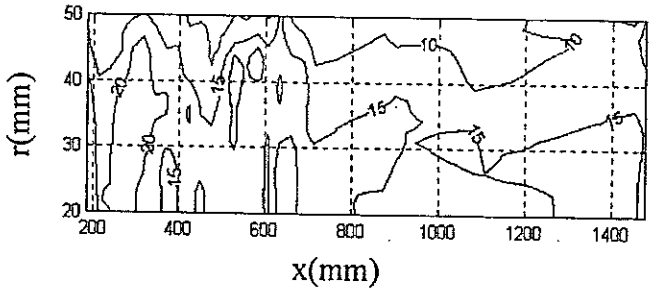

Figure 3. Example of distribution of the integral length scale L_{fx} (unit : mm)

By using equation (13), parameters c_{cor} and c_{rand} are given by [2, 16] :

$$c_{cor} = exp\left(-\left(\frac{\Delta P}{L}\right)^2\right) \quad \text{and} \quad c_{rand} = \sqrt{1 - exp\left(-\left(\frac{\Delta P}{L}\right)^2\right)} \tag{14}$$

Finally, it may be notified that this method does not apply to the circumferential velocity, because PIV technique cannot provide measurement of linked spatial correlations. It was chosen to consider an additional hypothesis which is to conserve turbulent energy, K, when determining velocity fluctuations. After axial and radial fluctuating velocities have been calculated, the following equation is used for the circumferential fluctuating velocity:

$$U_\varsigma' = \sqrt{\left|\overline{U}^2 K - U_x'^2 - U_r'^2\right|} \tag{15}$$

As explained by Ormancey & Martinon [16], trajectory calculation considering length scales effect involves further hypothesis. In equation (14), the integral length scale is determined for the starting position of the fluid particle. But, when this one moves away, the influence of the spatial correlation term decreases, until the velocity fluctuation becomes only a random function. A way to take into account this fact is to introduce an arbitrary value which gives the maximum length that can be covered by the fluid particle before the current position is redefined as the new initial point for the spatial correlation. Different values can be found, ranged between L/2 and 3L/2 [2, 16]. Because this data can only be defined arbitrary, the L/2 value was chosen to consider with accuracy the spatial correlation by frequently renewing the determination of the integral length scale. The final algorithm is:

1 - Definition of the starting location
While the fluid particle stays in the geometry
2 - Determination of integral length scales for the current position
While the distance covered is less than L/2
2-a - Determination of hydrodynamical characteristics for the current position using the neural network results (Mean velocities, Turbulent intensities)
2-b - Determination of fluctuating velocities using equations (14) and (15)
2-c - Determination of the next position using equation (2)
End
End

TRAJECTORIES CALCULATION

1 Trajectory algorithm results

In the Lagrangian formulation of equation (1), the time step Δt has to be specified. This value was determined by studying the influence of this parameter on the mean residence time of the fluid element in the cell and trajectories were found to be not dependent on the time step if a minimal value of 0.01 s is chosen. This value was thus retained.

An example of trajectories is shown in Figure 4. The rotating motion involved around the inner cylinder is easily seen on the three-dimensional representation. Plane projection of the trajectory show the complex behavior of the flow. Elementary particle displacements appear to be very disturbed, due to the set-up of large eddies. This fact explains the efficiency of the swirl flow which appears to create a three-dimensional motion, where mixing conditions are greatly improved [6, 8]. The trajectory calculation algorithm is a useful tool to understand the flow effect on trajectories and then on the history of fluid particle in this device.

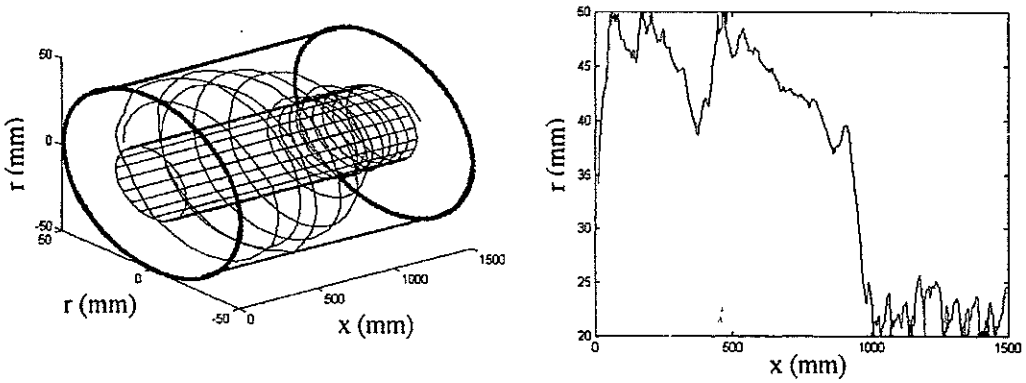

Figure 4. Example of trajectory obtained (Left : 3D representation ; Right : Axial-Radial plane projection)

2 Experimental validation of the trajectory calculation algorithm

Trajectories calculation is validated by comparing numerical results to the experimental determination of the RTD. A conductimetric method was employed using a two-measurement probes technique [18]. Probes were set at inlet and outlet of the annulus. NaCl tracer solution is injected before the inlet probe. Each probe is connected to a conductimeter giving a signal proportional to the NaCl concentration.

In order to determine the RTD using the trajectory calculation algorithm, a set of 15000 trajectories was calculated with an initial starting point located in the inlet of the annulus. The time needed for each elementary fluid particle to reach the outlet gives the RTD. But, the inlet signal is not a perfect impulsion of Dirac type. To get an accurate representation of the real injection conditions, the low dispersion of the tracer at the inlet probe was simulated by dividing the inlet distribution in time intervals, as shown in Figure 5. The set of calculated trajectories was next randomly re-allocated following the divided inlet distribution and the resulting calculated outlet time distribution. Results are given in Figure 5.

RTD determined with the trajectory calculation algorithm and the experimental one are close to each other, showing the efficiency of the trajectories determination. The algorithm is able to represent the complex hydrodynamical particles dispersion in the turbulent swirling flow. Figure 5 shows that the calculation algorithm provides some trajectories having long residence time, greater than 60 s. This occurs when some elementary fluid particles remain successively in recirculation areas of the swirling flow and near walls, as shown by the example of Figure 4. An elementary fluid particle can stay for a long time at this location, increasing the resulting residence time. But, only 5% of trajectories have a residence time longer than 60 s, and only 1% greater than 80 s. Furthermore, the conductimetric method is not enough sensitive to allow measurement of very little amount of tracer in solution, as it occurs at the end of the experimental RTD-curve. The long residence time is thus difficult to observe experimentally. In conclusion, the trajectory calculation algorithm can be considered to be accurate, compared with experimental results.

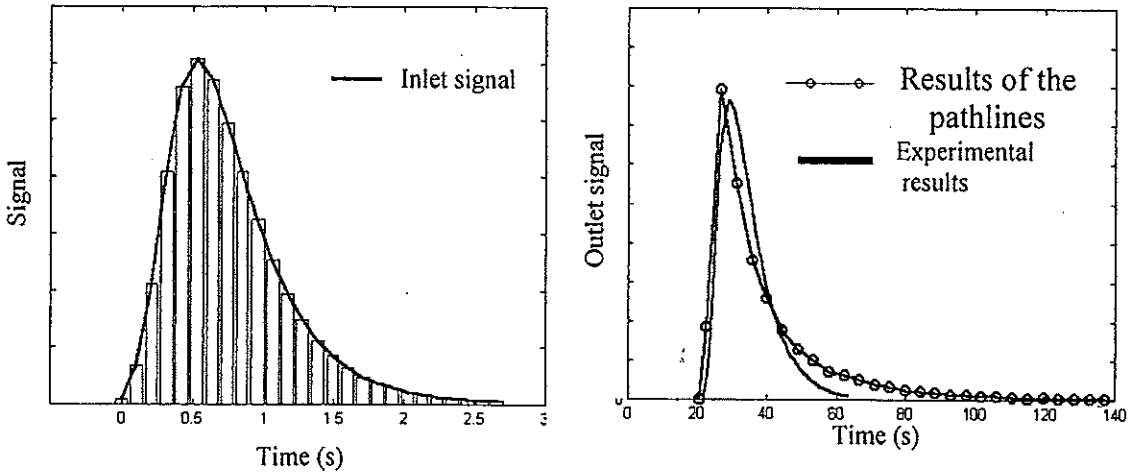

Figure 5. Validation of the Lagrangian trajectory calculation algorithm by comparison with experimental RTD (left : inlet signal ; right : outlet signal)

CONCLUSION

A Lagrangian method has been used to calculate trajectories of elementary fluid particles in a swirling decaying flow. This flow is characterized by the set-up of large eddies, preventing fluctuation velocities to be approximated by a pure random phenomenon. This characteristic of the complex behavior of the swirling flow was simulated by considering integral length scale of turbulence measured using PIV when determining the fluctuating velocities. The Lagrangian model described was verified by comparing results to an experimental measurement of the RTD, showing the efficiency of the retained method.

The technique allows the determination of trajectories of elementary fluid particles using experimental results measured by PIV. Trajectories are very difficult to measure when the flow is complex, especially for the three-dimensional motion involved by the tangential inlet which prevents from a direct determination of trajectories. The model appears helpful to optimize processes involving swirling decaying flows. Such hydrodynamics remain difficult to understand and characterize, despite they appear as an efficient way to enhance transport phenomena in chemical reactors with a rather simple design. The trajectory model can lead to a better control of swirl reactor.

REFERENCES

[1] Farias Neto, S.R., Legentilhomme, P., Legrand, J., Comp.Meth.Appl.Mech.Eng., 165 (1998), 189-213.
[2] Berlemont, A., Desjonqueres, P., Gouesbet, G., Int.J.MultiphaseFlow, 16 (1990) 19-34.
[3] Chen, X.Q., Pereira, J.C., Int.J.Num.Meth. Flow, 26 (1998), 345-364.
[4] Domgin, J.F., Huilier, D., Burnage, H., Gardin, P., J.HydraulicRes., 35 (1997), 473-490.
[5] Gupta, A., Lilley, D.G., Syred, N., *Swirl Flow*. Energy and Engineering Sciences Series, Abacus Press (1984).
[6] Legentilhomme, P., Legrand, J., J.App.Electro., 20 (1990), 216-22.
[7] Legentilhomme, P., Legrand, J., Int.J.HeatMassTrans., 34 (1991), 1281-1291.
[8] Legentilhomme, P., Aouabed, H., Legrand, J., Chem.Eng.J., 52 (1993), 137-147.
[9] Aouabed, H., Legentilhomme, P., Nouar, C., Legrand, J., J.App.Electrochemistry, 24 (1994), 619-625.
[10] Aouabed, H., Legentilhomme, P., Legrand, J., Exp.Fluids, 19 (1995), 43-50.
[11] Legrand, J., Aouabed, H., Legentilhomme, P., Lefèbvre, G., Huet, F., Exp. Therm.Fluid Sci., 15 (1997), 125-126.
[12] Pruvost, J., Legrand, J., Legentilhomme, P., Doubliez, L., Exp.Fluids, 29 (2000), p. 291-301.
[13] Pruvost, J., Legrand, J., Legentilhomme, P., Submitted to J. FluidsEng. (2000).
[14] Berlemont, A., Chang, Z., Gouesbet, G., Flow,Turb.Comb., 60 (1998), 1-18.
[15] Chen, X.Q., Pereira, J.C., Int.J.HeatMassTransf., 39 (1996), 441-454.
[16] Ormancey, A., Martinon, J., Phys.Chem.Hydro., 5 (1984), 229-244.
[17] Hinze, J.O., *Turbulence*. McGraw-Hill Book Co (1959).
[18] Legentilhomme, P. & Legrand, J., Can.J.Chem.Eng., 73 (1995), 435-443.

HYDRODYNAMIC DIAGNOSIS OF A SHELL-AND-TUBE HEAT EXCHANGER USING TRACERS - COMPARISON OF GLOBAL AND LOCAL APPROACHES

M. Albaric[1], C. Jallut[2], P. Bandelier[1]

[1]GRETh – CEA/Grenoble, 17 rue des Martyrs 38054 Grenoble cedex 9, France
[2]LAGEP, Université Claude Bernard – ESCPE – CNRS, UMR 5007, 43, Bd du 11Novembre 1918, 69622 Villeurbanne cedex, France

Abstract. The global performances of heat exchangers are lowered by flow maldistribution. Furthermore, fouling increases in the dead zones and the residence time may be increased. Such phenomena can induce degradation of heat-sensitive products. In any case, the consequences are higher operating costs and lower quality products. It is thus important to be able to diagnose the hydrodynamic state of a heat exchanger while it is running. In this paper, we present two diagnosis methods, a global approach and a Computational Fluid Dynamics approach, based on the comparison between tracer experiments and numerical models. Furthermore, it is interesting for a given geometry, to compare these two techniques. An hydrodynamic study of a shell-and-tube heat exchanger will illustrate these questions.

INTRODUCTION

The global performances of heat exchangers are lowered by flow maldistribution. The origins of maldistribution are numerous: *mechanical causes* (due to the design of the tubes and the heads), *causes induced by the process of the heat transfer itself* (freezing or fouling may lead to a modification of the friction factors), *causes related to the nature of the flow* (for example, the *two phase flows* are very difficult to distribute uniformly) [1].

Some of the consequences are: decreasing global efficiency of the equipment, increasing fouling in the dead zones, longer residence time resulting in degradation of heat-sensitive products.

In any case, extra costs of operation due to energy loss and a lower quality of the end product occur. Consequently, it is important to be able to diagnose the flow distribution in heat exchangers as they are running, so as to detect faults like bypasses, fouled channels, dead zones and so on.

In this paper, we present two diagnosis methods, a global approach [2-6] and a Computational Fluid Dynamics approach, based on the comparison between tracer experiments and numerical models.

THE EXPERIMENT

1. "DAVY" test loop

"DAVY" test loop was built to perform hydrodynamic studies by using tracer experiments. Heat exchangers (plate or shell-and-tube) as well as their elements like plate, tubes, heads... can be studied. The fluid used is water.

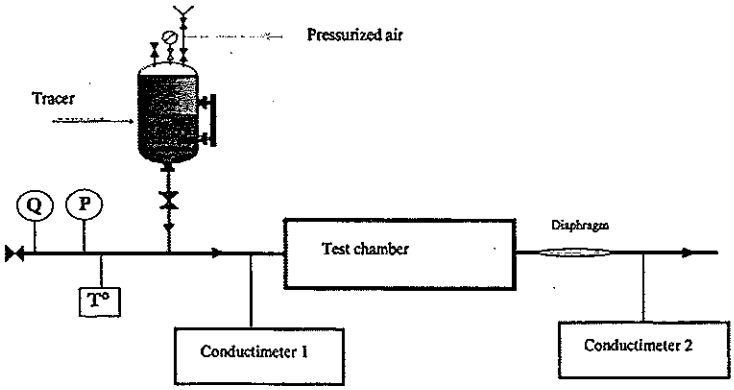

Figure 1 "DAVY" test loop

"DAVY" test loop is equipped with tracer injection, measurements and data acquisition systems. There is also a test chamber where the system to be studied is placed (Figure 1).

The tracer used is a pressurized salt solution. The injection signal (Dirac, Heaviside or pseudo random signal) and the quantity of injected tracer is controlled by an electric valve. To ensure an homogenous mixing of the tracer along the cross section of the tube, the salt solution is injected against the flow at the inlet and a diaphragm is placed at the outlet.

The variation of the electrical conductivity of the industrial water is used to detect the presence of tracer. Two conductimeters are used at the inlet and the outlet of the test chamber. It is possible to record the time evolution of the signal at the inlet and the outlet of the studied system.

Pressure, global flow rate and temperature are also measured. The water temperature is supposed to be constant in the whole system.

2. Presentation of the heat exchanger

The studied heat exchanger is a shell-and-tube heat exchanger. We present here the results concerning the tube side hydrodynamics.

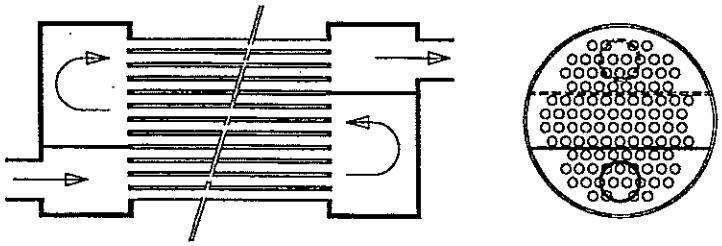

Figure 2. Diagram of the shell-and-tube heat exchanger

It's a 102 tube shell-and-tube heat exchanger divided into 3 channels. The internal diameter of the tubes is 14 mm, the step between each tube is 20 mm and the length of the tubes is 3500 mm.

The diameter and the depth of the two heads are respectively 275 mm and 185 mm.

THE GLOBAL APPROACH

1. The principle

The flow and the mixing phenomena in the heat exchanger are described using global methods. Danckwerts [4] developed this approach for chemical reactors system. It is based on a statistic description of the flow in the system [5].

Tracer experiments leads to the measurement of the Residence Time Distribution (RTD) of the fluid in the system. A model can be designed to represent the experimental RTD. A time domain fitting allows to estimate the parameters of the model and to give a diagnosis of the flow [6].

2. The phenomenological model proposed for the tube side flow

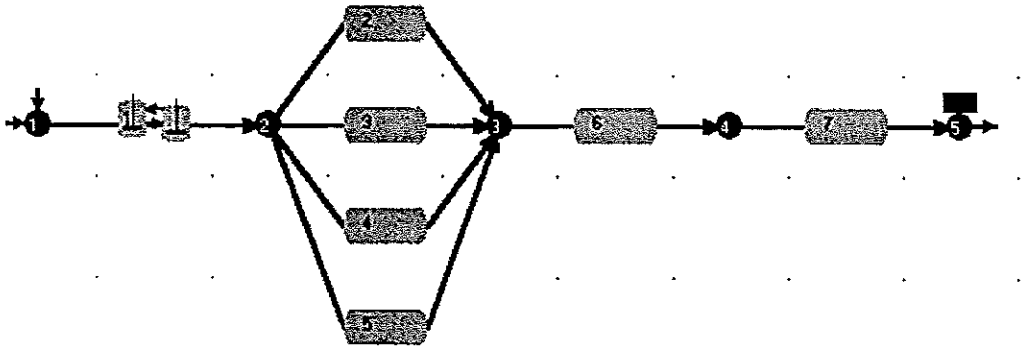

Figure 3.The phenomenological model

The phenomenological model was built with DTS (PROGEPI ENSIC) software [7]. It is divided into three parts:

- The flow in the two heads is modelled by a serie of CSTR with backmixing. The flow is supposed to be identical in each head.
- The flow in the first channel is modelled by four parallel "plug flows". It is considered that the flow distribution is none uniform, according to the position of the tubes.
- The flows in the second and the third channels are modelled by two « plug flows » in series. It is considered that the flow distribution is uniform after the first head.

The model proposed is a three-parameter model :

- **Tau**, the residence time of the fluid in the two heads.
- **J**, the number of CSTR.
- **Alpha**, the back-mixing flow rate.

All the other parameters can be estimated with the experimental data.

3. The parameter estimation

By using "DAVY" experimental data, a parametric estimation of the model has been made from tracer experiments performed on a heat exchanger free of any defect (Figure 4).

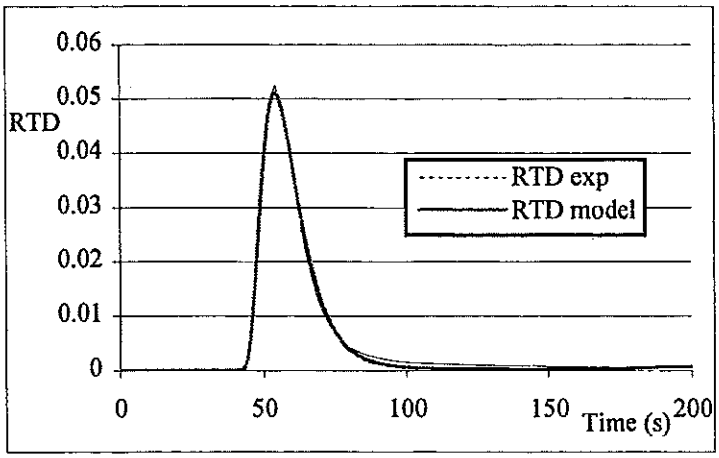

Figure 4. Comparison Model – Experiment for Q_l=5 $m^3.h^{-1}$

This initial behavior is a reference for future maldistribution detections. For example, if we consider a heat exchanger with a by-pass flow maldistribution in the two heads, the response is dramatically changed (Figure 5). A new parameter optimisation could enable to quantify the defect.

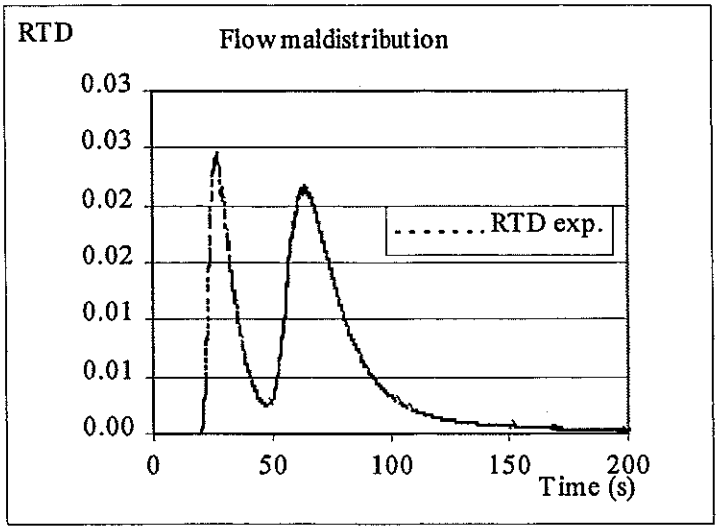

Figure 5. By-pass for Q_l=5 $m^3.h^{-1}$

THE COMPUTATIONAL FLUID DYNAMIC APPROACH

On an other way, we modelled the shell-and-tube heat exchanger (see Figure 2) with a Computational Fluid Dynamics software named FLUENT. From this detailed model, the Residence Time Distribution (RTD) curve can also be simulated.

1. The equations

The turbulent flows are modelled by the Reynolds equations:

$$\frac{\partial U_i}{\partial t}+U_i\frac{\partial U_i}{\partial x_i}=-\frac{1}{\rho}\frac{\partial P}{\partial x_i}+\frac{\partial}{\partial x_j}\left[\nu\left(\frac{\partial U_i}{\partial x_j}+\frac{\partial U_j}{\partial x_i}-\frac{2}{3}\delta_{ij}\frac{\partial U_l}{\partial x_l}\right)\right]+\frac{\partial}{\partial x_i}\left(\overline{-u_i'u_j'}\right) \quad (1)$$

U_i is the average velocity ($m.s^{-1}$)
u_i' represents the fluctuation of the velocity ($m.s^{-1}$)
P is the average pressure (Pa)

The Reynolds stresses : $\left(\overline{-u_i'u_j'}\right)$ are modelled with the empirical Boussinesq hypothesis. To close and to solve this equations system, we use a standard (k-ε) model. It gives good results for a large range of velocity and was created for pipe flows with high Reynolds number and with an homogenous and isotropic turbulence.

2. The boundaries conditions

The boundaries conditions are :

- Inlet velocity : v=0.5 $m.s^{-1}$ (Reynolds number is about : Re~32000)
- Outlet pressure : P=0 bar

The wall condition is standard. More precisely, a linear profile is used in the viscous layer, then a logarithmic one.

3. The velocity and the pressure fields

To ensure the quality of the results, it is interesting to consider different points.

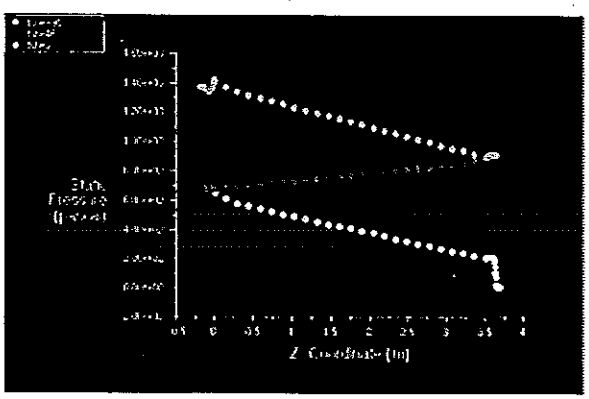

Figure 6. Pressure evolution over the three channels

The Figure 6 shows the evolution of the pressure over the three channels of the heat exchanger. The linear decrease of the pressure along a tube is verified. Moreover, the pressure losses are in the range of these expected for a straight pipe and are about 440 Pa. The evolution of the pressure along a straight pipe verifies the relation:

$$\Delta P=\lambda.\frac{\rho.L.V^2}{2.D} \quad ; \quad (2)$$

P is the pressure (Pa), λ the friction coefficient, ρ the fluid density ($kg.m^{-3}$), V the velocity ($m.s^{-1}$), D the diameter of the tube (m) and L the length of the tube (m).

For turbulent flow λ is calculated with the following relation :

$$\lambda = \frac{0.316}{Re^{1/4}} \qquad (3)$$

Re is the Reynolds number.

The pressure step at the inlet and the outlet of the heat exchanger are linked to the singularities induced by the two heads. Furthermore, at the outlet, the effect of the boundary condition can be seen (P=0 bar).

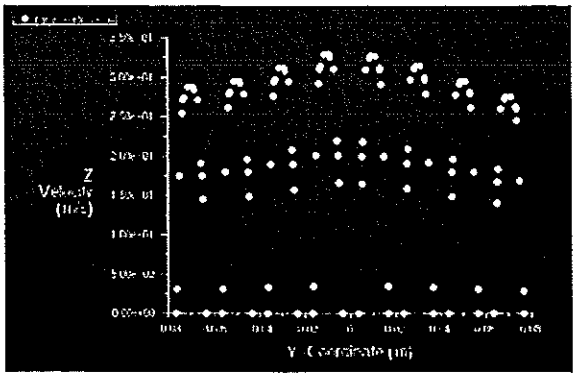

Figure 7. Velocity field on the first channel

The velocity field of the Figure 7 is located on the second row of the tubes of the first channel. It shows that, according to the hypothesis assumed for the global approach, the flow distribution is not uniform. In fact, the flows through the tubes, which are in front of the inlet (see Figure 2), are greater. But, the mixing in the head homogenises the flow distribution. It can be seen on the Figure 8.

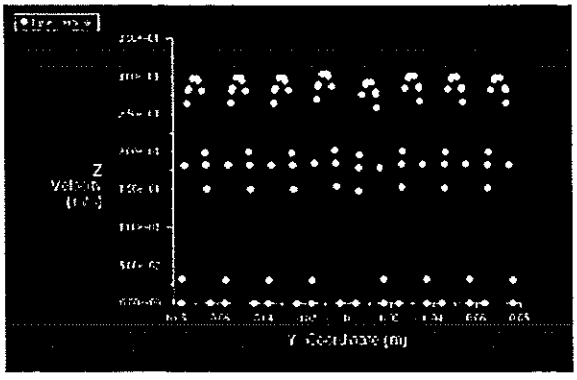

Figure 8. Velocity field on the third channel

This velocity field is located in the third channel at the opposite side of the one of the Figure 7. The flow distribution is homogeneous.

The Reynolds number in the tubes is about 4000. It corresponds to a transition towards a turbulent flow. That's why it is difficult to compare the velocity fields to those expected for a turbulent flow. The velocity field of the Figure 7 and 8 are close to a laminar velocity field.

4. The simulated Residence Time Distribution from the CFD model

To calculate the RTD curve, we use the velocity and the pressure field determined over the points of the mesh and we solve the equation of a passive tracer. At time t=0, a heaviside signal of the tracer is imposed at the inlet of the heat exchanger. The response is calculated over the oulet area by recording the evolution of the mass fraction of the tracer with time. The RTD curve is obtained by numerical derivation.

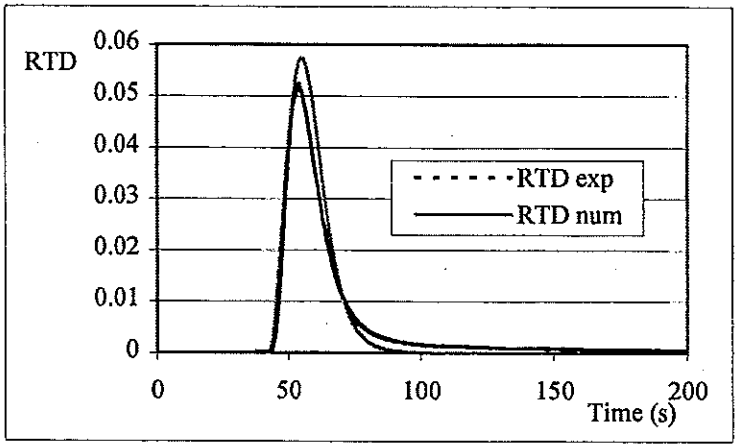

Figure 9. Comparison between numerical RTD. and experimental RTD.

The Figure 9 shows that the CFD model of the heat exchanger gives results close to experimental RTD. It could be interesting to identify the modifications to bring to the model in order to fit the experimental Residence Time Distribution curve, which is supposed to be free of defects.

- The numerical results depend on the mesh of the heat exchanger. So, it is really important to make an accurate mesh and to ensure a good path of the information along the geometry, especially between the tubes and the heads.
- The numerical results depend on the turbulence model used. So, is the choosen model really the best one?
- The unique links with the experiment are the boundaries conditions. Perhaps, they could be the first parameter to be changed to fit the experimental RTD curve.

An other problem is that the geometry used is an "ideal" or "perfect" geometry wich is also free of defects. If the difference between experimental and simulated RTD is too important, for example if there is a by-pass, a new complete modelisation could be necessary. Such a new modelisation would lead to the diagnosis of the system.

The time costs are bigger for this approach than for the global one, especially in terms of geometry building, mesh building and time calculation.

On the one hand, the objectives of making a diagnosis are perhaps far away. On the other hand, it is really interesting to see precisely the evolution of the flow. It could be a good way to diagnose and to locate maldistribution induced by the geometry of the heat exchanger like dead zones.

CONCLUSION

Depending on the information to be collected and the complexity of the flow, one of the two approaches , global or CFD, may prove more appropriate.

Whatever the method, it will require a parameter estimation from the tracer experiments by using an optimisation technique. The results of this optimisation will lead to a diagnosis by matching estimated parameters to their expected values for a faultless heat exchanger. The optimisation is performed according to:

- the boundary conditions and/or grid for the CFD approach ;
- the parameters of the model for the global solution.

For complex geometry, it becomes difficult to carry out a realistic grid, in which case implementing the "CFD" approach will be more difficult.

REFERENCES

[1] Lalot S., Florant P., Lang S.K., and Bergles A.E., *Flow maldistribution in heat exchanger*, Applied Thermal Engineering, 19 (1999), 847-863.

[2] Ros S.; Jallut C.; Grillot J.M.; Amblard M., *A transient test technique for the heat transfer coefficient measurement in a corrugated plate heat exchanger channel based on frequency response and residence time distribution*, Int.J.Heat Mass Transfer, 38 (1995),1317-1325

[3] Levenspiel O., *Tracer curves and the residence time distribution*, Chem.Eng.Science. 25 (1970), 1611-1613.

[4] Danckwerts P.V., *Continuous flow systems. Distribution of residence times*, Chem.Eng.Science, 2 (1953), 1-13.

[5] Villermaux J., *Génie de la réaction chimique. Conception et fonctionnement des réacteurs*, Lavoisier Tec & Doc, 2ème édition, (1993), 1-448.

[6] Roetzel W. and Xuan Y., *The effect of Core Longitudinal Heat conduction on the transient behavior of multipass shell and tube heat exchangers*, Heat transfer engineering, 14 (1993), 52-61.

[7] Leclerc J.P., *DTS: un logiciel d'aide à l'élaboration de modèles d'écoulement dans les réacteurs*, Revue de l'Institut Français du Pétrole, 50 (1995), 641-656.

USING PEPT TO STUDY THE FLOW PATTERN OF A 22 LITRE DRAFT TUBE CRYSTALLISER

M.D. de Jong[1,2,†], G.S.M. van Beuzekom[2,3], Z.I. Kolar[3], H.J.M. Kramer[1], and B. Scarlett[2]

[1] Laboratory for Process Equipment, Faculty of Design, Construction and Production, Delft University of Technology, Leeghwaterstraat 44, 2628 CA, Delft, THE NETHERLANDS
[2] Section Particle Technology, Faculty of Applied Sciences, Delft University of Technology, Julianalaan 136, 2628 BL, Delft, THE NETHERLANDS
[3] Interfacultary Reactor Institute, Delft University of Technology, Mekelweg 15, 2629 JB, Delft, THE NETHERLANDS

Abstract. Using the Positron Emission Particle Tracking (PEPT) radiotracer technique, the flow pattern of a 22 litre Draft Tube Crystalliser (DTC) was investigated. Previous research had led to the development of 3D CFD flow models of this vessel, which sofar remain unvalidated. The goal of this research is to validate those models on a macroscale level. PEPT is based on the coincidental detection of a pair of collinear 511 keV gamma quanta originating from a positron-election annihilation by two LFOV position-sensitive gamma cameras. The original ammonium sulphate system was replaced by a glass spheres/water slurry for practical reasons; the spheres (ρ is 2650 kg/m^3) had an approximately equal particle size distribution and volume concentration as the ionic system under steady-state conditions (at 50°C and 0.1 bara, x_{50} is 650 μm, volume fraction is 0.09). Two types of neutrally buoyant tracer particles containing the positron emitter ^{64}Cu (half-life: 12.7 h; obtained from neutron irradiation of ^{63}Cu) were prepared: one with a density of water (diameter: 8 mm), and one with a density of the glass beads (diameter: 650 or 1000 μm). After irradiation to 20 MBq activity, they were put into the stirred vessel (750 rpm) containing either the glass/water slurry, or plain water. The particles were refreshed after 14 hours and reached optimum activity at 14.8 MBq. For quantitative validation, 3 tracer particles were used per experimental setting. After processing, coincidental data yield ensemble-averaged velocity fields. The previously computed CFD flow fields correspond very well with the measured data, except in areas where the resolution of PEPT is low (near the stirrer, due to the high velocities in its vicinity). Several confusing aspects of the simulations, such as fluid recirculation above the stirrer, were found to be genuine phenomena. A qualitative difference between slurry and non-slurry flow could be established.

INTRODUCTION

Crystallisation, the formation of a solid phase from a liquid one, is the second most commonly applied separation technique in chemical process industry. It combines low energy consumption, high product purity and mild process conditions. However, due to its inherent two and sometimes multiphase nature, it is a difficult process to study and understand. A very important problem is the fact that the crystals are never equal in size (and shape): a range of sizes, known as the *Crystal Size Distribution* or CSD, is formed. This CSD typically spans up to 3 orders of length: from μm to mm. One of the consequences of this broad size range is a strong *two-way coupling* between crystals and liquid. On the microscale, crystals grow as a function of supersaturation and temperature, whose local instantaneous values are determined by macroscale transport phenomena, and may vary considerably

† Current address: Shell Global Solutions International B.V., SRTCA/OGNL-OGUF, P.O. Box 38000, 1030 BN, Amsterdam, The Netherlands

throughout the entire vessel. Crystals will therefore grow at different rates depending on their location. On the other hand, the macroscale is influenced by the crystals through transport properties such as viscosity and density. Crystalliser models have to take this two-way coupling into account by quantifying the flow patterns and the interaction between crystals and liquid within the crystalliser vessel. This can be done either by measurements or by a priori calculations.

Previous work by DE JONG (see [1] and [2]) led to the development of a 3D, single phase *Computational Fluid Dynamics* or CFD model of a 22 litre *Draft Tube Crystalliser* or DTC, and a 3D, two phase CFD model of a 150 litre *Forced Circulation Crystalliser* or FCC. (Both crystallisers are maintained by the UNIAK project: an ongoing research effort to study the design and control of industrial crystallisers.)

Unfortunately, despite numerous advances CFD has not yet reached the point where its results can be taken as definitive; validation is still required, especially when it concerns two or multiphase flow. Even though the computed flow patterns of the DTC and FCC devices seemed 'reasonable' (correct general flow pattern, correct average velocities) despite several 'oddities' (large recirculation above an impeller), this does not constitute a succesful validation. However, it proved to be very difficult to measure flow data inside these vessels: the experimental conditions are harsh (saturated ammonium sulphate solutions at 50°C and 0.1 bara and a crystal volume fraction of approximately 0.09) and the vessels are inaccessible to many types of standard flow measurement devices. Eventually, radiotracers were investigated, as various authors (MOSLEMIAN [3], LARACHI [4], to name but a few) were able to succesfully determine flow patterns in difficult flow environments. A promising new radiotracer technique is *Positron Emission Particle Tracking* or PEPT, which has the distinct advantage over other radiotracer trechniques that the tracer location reconstruction is independent of the medium being traced.

The goal of this research is to measure the macroscale flow patterns of the 22 litre DTC using PEPT and compare them against the previously obtained CFD results, validating the latter.

POSITRON EMISSION PARTICLE TRACKING

1. The General Principle

PEPT is based on the coincidental detection of a pair of 511 keV gamma quanta originating from a positron-election annihilation. Provided the photons are not scattered along their travel path, they and their point of origin will lie on a (nearly[†]) straight line. Should those photons be detected by two separate and oppositely facing position-sensitive detection devices, it is possible to construct a *line* between the two detection points. The point of annihilation is then somewhere along the line. In theory it is possible to determine this location by measuring the very small

[†] Even though in reality the angle between the two photons is somewhat less than 180 degrees due to the conservation of momentum of both positron and electron (≈ 0.6 degrees), in this discussion the deviation is assumed to be 0.

difference in detection time (order of 1 ns), but as our equipment is unable to do this, we are faced with the situation depicted in Figure 1: the point of annihilation could be anywhere along the line.

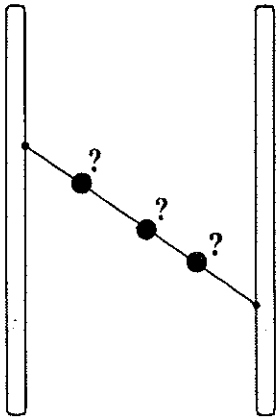

Figure 1. Single line yields no point of annihilation.

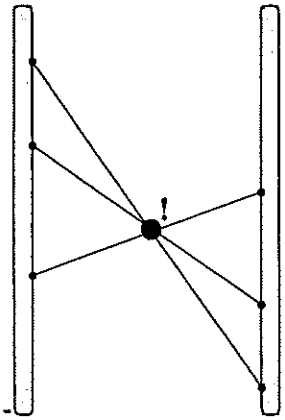

Figure 2. Intersection of several lines yields point of annihilation.

The solution to this problem is depicted in Figure 2: if more lines (resulting from more annihilation events) are drawn, they will intersect at a certain point in space. This point is the most probable location of the origin of the annihilation events. Should the positrons only travel a short distance before they are annihilated (which on average is indeed the case), the intersection point is then equal to the point where the positrons themselves were generated–in a tracer particle, for example.

The above works very well if the positron emitter–from here on designated as the tracer particle–is stationary. If the tracer is moving, the lines are displaced and will not intersect in a point, but rather an elongated sphere: the particle's location is then determined by a confidence region. This region becomes larger as the particle's speed increases, or the production rate of lines decreases.

The result of the technique is a string of tracer locations (with some uncertainty) as a function of time, from which ensemble averaged velocity fields and number residence plots can be computed. It should be kept in mind that the computed trajectory deviates from the real trajectory, as the tracer locations are connected by straight lines rather than the curved ones followed by the tracer. If the tracer velocity is continously increased, there will come a point where the difference between computed and actual travelled distance becomes too great: the technique is then no longer usable. This value is strongly dependent on the setup and tracer activity; in our system it is approximately 2 – 2.5 m/s.

Finally, the size of the uncertainty region determines the resolution of the technique; flow phenomena with a characteristic size smaller than this region will not be resolved. This value is once again strongly dependent on the type of setup (especially the quality of the gamma detection devices): in our case the resolution cannot be made smaller than 6.5 mm. It is therefore impossible to use our setup for the study of micro- or even mesoscale flow structures, which have characteristic sizes of approximately 0.05 and 0.5 mm, respectively.

2. Comparison with Other Techniques

For flow validation studies, the traditional employed techniques are *Laser Doppler Anemometry* or LDA and *Particle Image Velocimetry* or PIV. Both offer far more insight into the smaller flow scales than PEPT does, but when one is not really interested in these structures both techniques yield a lot of interesting, but essentially superfluous data. Since the CFD models of DE JONG [1] only convey macroscale information (and are in fact degraded considerably before being applied to crystalliser process models), PEPT appears a more logical choice.

PEPT can be applied with equal ease to single phase flow or concentrated slurry studies, unlike LDA and PIV which rely on the experimentally difficult trick *refractive index matching*. Several authors (PARKER [5], BROADBENT [6], and STELLEMA [7]) have succesfully applied PEPT to difficult flow systems like powder shear mixers and fluidized beds. Since crystallisation processes fall into the category of concentrated slurry systems (crystal volume fractions of 0.25 are not uncommon!), PEPT appears once again to be a more logical choice.

EXPERIMENTAL SETUP AND PROCEDURE

1. The Crystalliser Vessel

The original 22 litre DTC vessel proved to be unsuitable for our PEPT experiments: its stainless steel design which allows it to be operated under vacuum scatters and absorbs too much radiation. Therefore a perspex 1:1 copy was built using as little material as possible. The design mimicks the original in every way: an outer tube (height: 850 mm, internal diameter: 232 mm, wall thickness: 4 mm) encloses an inner tube (the *draft tube*; height: 602.5 mm, inner diameter: 154 mm, wall thickness: 3 mm) equipped with four symmetrically arranged baffles (height: 575 mm, width: 10 mm). The stirrer (three-bladed marine type impeller, diameter: 136 mm, pitch: 25 degrees) protudes from the bottom of the vessel. Like the original, the bottom is shaped like a torus to ease the transition of the downward flow in the annular region (the *downcomer*) to an upward flow in the draft tube.

The use of perspex means that evaporative crystallisation can not be performed anymore. Not only are there considerable mechanical problems (forces due to vacuum, corrosiveness of ammonium sulphate solutions), but a changing CSD in the setup makes interpretation of the slurry flow fields extremely difficult, as the CSD changes faster than PEPT can construct a flow field image.

The ionic salt was therefore replaced with glass beads (ρ: 2650 kg/m^3) with an approximately equal size distribution to that of the ammonium sulphate system under nominal steady state conditions (crystal volume fraction: 0.09, x_{50}: 650 µm, x_{90}: 1200 µm, heat input: 120 kW/m^3; see NEUMANN [8]). This results in the weight fractions listed in Table 1:

Table 1. Glass bead size distribution.

Sieve fraction [µm]	Weight fraction [%]
290–420	24
400–520	29
500–750	24
650–900	17
850–1230	6

on a total mass of 6.5 kg. The remainder of the vessel is filled with tap water to a total volume of 22 litres. The stirrer speed is set at a constant 750 rpm.

2. The Scintillation Cameras

The gamma detection devices are two *Large Field-of-View* or LFOV scintillation cameras with NaI(Tl) monocrystals as the scintillating medium. The crystals have a diameter of 380 mm and a thickness of 9.5 mm. Both are optimised for the detection of ^{99m}Tc, which emits gamma radiation at a far lower energy of 141 keV. The intrinsic detection efficiency of these cameras for positron annihilation radiation is therefore rather low: taking everything into account, only 4% of all perpendicularly incident 0.511 MeV gamma quanta are registered at this energy. In order to boost the efficiency of the system, STELLEMA [7] chose to register the scintillations having an energy between 100 and 340 keV as well; the idea being that these scintillations are the result of genuine 511 keV quanta having an incomplete interaction with the crystal. To reduce the uncontrolled contribution of Compton scattered photons having an energy within the mentioned range, *graded absorbers* were mounted in front of the cameras. A special software filtering algorithm subsequently removed nearly all remaining so-called *corrupt events*. STELLEMA was able to double the location reconstruction frequency (from 8 s^{-1} to 17 s^{-1}) as a result of the above procedure at no cost to the location accuracy (specified at 10 mm). It was decided to adopt his approach in this research.

Upon registering a scintillation on each camera, a coincidence circuit determines whether the event constitutes a coincidental detection; if this is the case, the cameras are queried for the (x, y)-position of the scintillation. (For further information, see STELLEMA [7]).This information and the time at which the event occurred is written to a file for reconstruction analysis. The data rate (at nominal tracer activity) is approximately 55 MB/h.

Since the setup is larger than the cameras, only a part can be studied at a time. Three *regions of interest* or ROI were identified: below the stirrer, above the stirrer, and the top of the draft tube, to investigate the transition from upward to downward flow. The stirrer is not included because of the expected high velocities in this region. The figures below show the setup and the cameras in upper position.

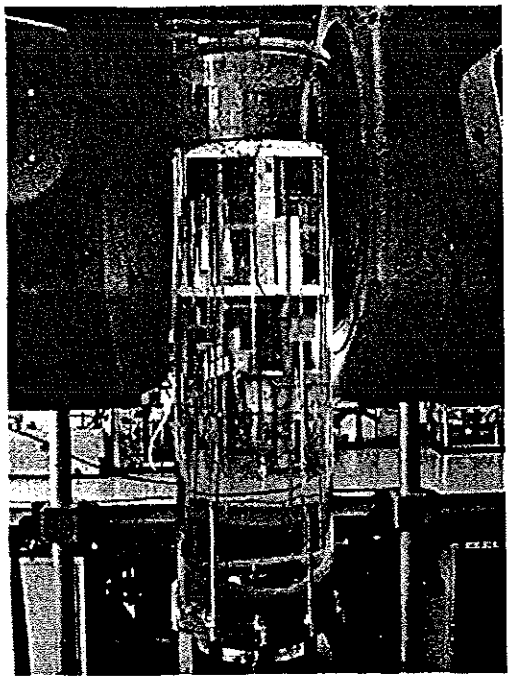

Figure 3. Side-on view of the setup.

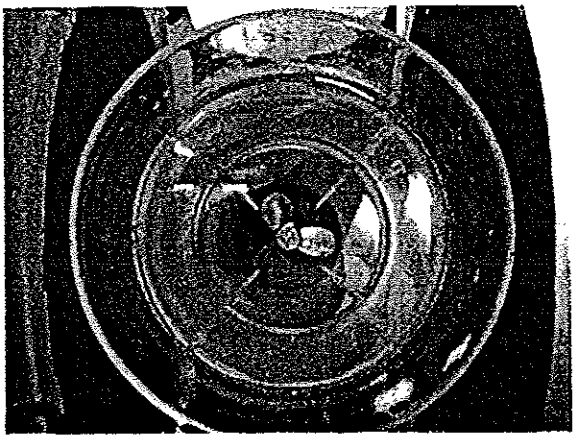

Figure 4. Top view of the setup.

3. The Tracer Particles

Like STELLEMA [7], we used ^{64}Cu as the positron-emitting radionuclide. The isotope is prepared by irradiating natural copper containing approximately 70% ^{63}Cu with thermal neutrons obtained from the nuclear reactor of IRI at Delft University of Technology. ^{64}Cu has a half-life of 12.7 h; the positron decay path to ^{64}Ni is taken in approximately 20% of all cases. The other decay paths produce either low-intensity X-rays or beta radiation; both have little influence on the technique.

About the only disadvantage to using ^{64}Cu is the high density of copper: 8900 kg/m^3. Neutrally buoyant particles must therefore contain substantial amounts of a lighter material. Two types of tracer particles were developed: a *solution tracer* having a density equal to that of water, and a *slurry tracer* having a density equal to that of the glass beads. The solution tracer is a foamed polystyrene bead with a pure copper core and a diameter of 8 mm. This (admittedly large) size means that the particle is a tracer for the *average* rather than the *instantaneous* fluid flow pattern, and that results near walls (and thus the entire downcomer) cannot be treated as conclusive. The slurry tracer is a melt of a special low-Na content glass with sufficient copper to make the density equal to that of the beads. This tracer was available in two sizes, 650 and 1000 μm, meaning that these tracers are completely representative for their size class.

Both tracers were irradiated to an initial activity of 20 MBq, and refreshed once their activity dropped below 10 MBq. The optimum activity is around 14.8 MBq, corresponding to a coincidence detection rate of 3000 s^{-1}. A quantitative validation is obtained after tracing three particles; tracing two or less results in a more qualitative picture.

4. The Reconstruction Algorithm

The camera hardware produces a list of (x_1, y_1)-(x_2, y_2)-t data, which have to be transformed into a list of (x, y, z)-t tracer locations. As outlined in subparagraph 2, the algorithm must also remove corrput events as much as possible. We used the method described by PARKER [5] in a modified form:

1. Select N sequential coincidences, and compute the pairwise intersection point of all possible (N_i, N_j) line combinations.
2. Compute the average intersection point A from these intersection points.
3. Compute $d_i(A, N_i)$, $\langle d \rangle$, and σ_d.
4. Discard every line N_j with $d_j > k \cdot \sigma_d$.
5. If the remaining number of lines is larger than $f \cdot N$, go back to step 1 using the remainder; otherwise A is the estimated tracer location.

The above algorithm works by removing those lines of a set which lie furthest away from the average midpoint. It has the advantage of being fast and reasonably accurate in removing corrupt events, although it is not as advanced as the original method. Based on experiments with stationary and slow-moving tracer particles, we fixed N at 200, and f at 0.15; these averaged values resulted in the smallest deviation between computed and known tracer location for all locations and speeds. k we chose to be 1.4 as this seemed to yield better convergence than PARKERs original value of 1.2.

After the reconstruction algorithm has finished, the *voxel algorithm* converts the tracer locations into ensemble averaged velocity fields. Using the previously reconstructed locations, it tracks the particle on a grid of cubic elements (10 mm x 10 mm x 10 mm) overlaying the vessel geometry. The *ensemble averaged velocity* of the tracer in a particular voxel then follows from

$$\langle \mathbf{u} \rangle = \frac{1}{n} \sum_i \mathbf{u}_i \,.$$

5. Experimental Procedure

Two types of experiments were carried out: the first employed a solution tracer in a single phase (plain water) flow, the second employed a slurry tracer in a glass beads/water mixture. The precise details for the single phase experiments can be found in Table 2, for the two phase experiments see Table 3.

Table 2. Single phase experiments.

Stirrer speed	Tracer type	ROI	Duration
750 rpm	solution (foamed PS)	top	3 x 14 h
750 rpm	solution (foamed PS)	above stirrer	3 x 14 h
750 rpm	solution (foamed PS)	bottom	3 x 14 h

Table 3. Two phase experiments.

Stirrer speed	Tracer type	ROI	Duration
750 rpm	slurry (glass; 650 μm)	top	1 x 14 h
750 rpm	slurry (glass; 650 μm)	bottom	1 x 14 h
750 rpm	slurry (glass; 1000 μm)	top	1 x 14 h
750 rpm	slurry (glass; 1000 μm)	bottom	1 x 14 h

As can be concluded from the above tables, the two-phase experiments are qualitative in nature due to their short duration, caused by a number of experimental problems.

Data were gathered real-time, and later stored on CD for convenience. Each block of 14 hours fills approximately 1 CD. An Athlon-based PC reconstructed the tracer movements at a speed of approximately 90 minutes per CD.

RESULTS AND DISCUSSION

Only a small selection of the large amount of experimental results can be presented here. For more information the reader is referred to DE JONG [2].

1. Single Phase Flow Results

In Figure 6 the ensemble averaged velocity field for the bottom ROI can be seen. Even though the fluid seems to stop moving once it reaches the line $y = 30$ cm, this is not the case in reality: the tracer particle at that point leaves the measuring volume enclosed by the cameras, becoming more or less 'invisible'. The effect of using a large tracer particle can be clearly seen near the draft tube: at some points it seems as though fluid is passing *through* the wall. Therefore, the vectors immediately next to a wall are qualitative at best. The same holds for the vectors near the stirrer: the velocities in this area exceed the upper limit of the system, and are thus the result of a significant amount of trajectory shortcutting.

Figure 5 depicts the velocity fields of the same area (but only of the left half) as calculated by DE JONG [1]. The resemblance between the two figures is striking. The large recirculation above the stirrer as predicted by the CFD model, long thought to be a numerical artefact of the simulations, is seen to be a genuine phenomenon. The location corresponds very well with that measured by PEPT, although the simulation predicts that it reaches closer to the stirrer. It can also be seen that the fluid moving away from the stirrer has a significantly higher radial component than is shown in the measurements: it illustrates the trajectory shortcutting mentioned earlier very clearly. Finally, even though it is hard to see in the measurements, the existence of the small eddy underneath the tip of the stirrer is also confirmed.

Even though work is still in progress to compare simulation and measurement on a more quantitative level, it is unlikely that major differences will be discovered; the general characteristics will remain as they are. It seems justified to conclude that the single-phase CFD model has been validated on a macroscale level.

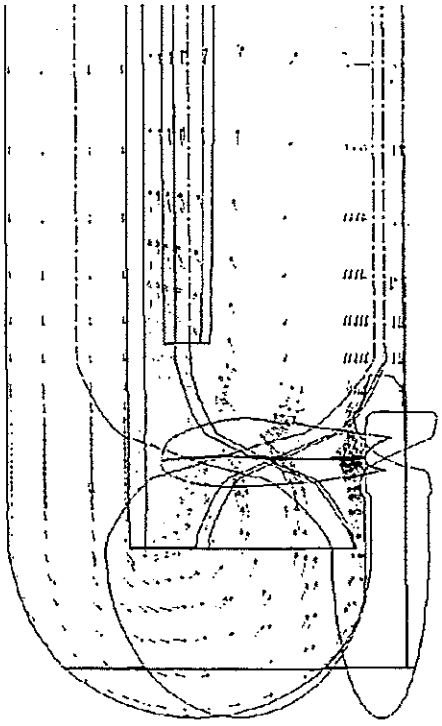

Figure 5. Axial velocity field of half the CFD model of the 22 litre DTC vessel.

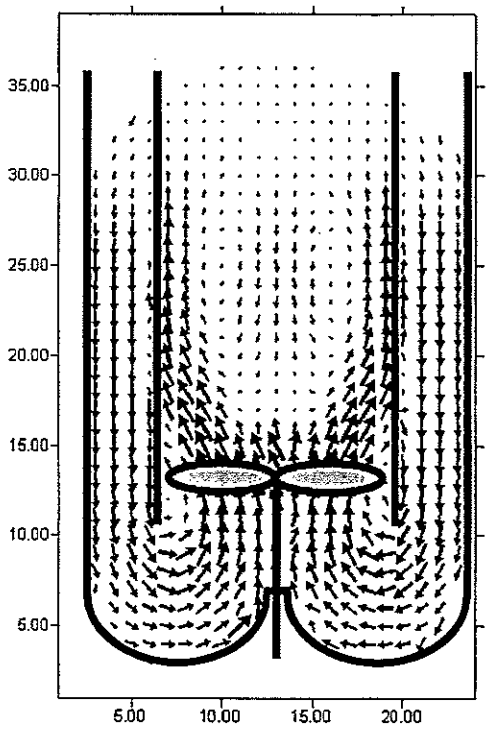

Figure 6. Axial velocity field in bottom ROI for single phase flow with a solution tracer. Axes in cm.

2. Two Phase Flow Results

Figures 7 and 8 depict the flow patterns of the bottom ROI for each of the two tracer sizes. Since they are based on a single 14-hour set of coincidental data, care must be taken not to interpret them quantitatively. Even so, they already show interesting differences between themselves and Figure 6. The most important difference is the near-absence of high-velocity vectors in the curvature of the bottom next to the stirrer axis. This clearly illustrates that the heavy glass beads are slow to move up, a direct effect of gravity holding them back. Also, compared to the flow pattern of the 650 μm tracer, the flow pattern of the larger particle seems to have shifted a small distance downwards. This indicates that small and large particles have different flow behaviour. However, without further data it is impossible to tell for certain. Finally, it is quite remarkable that even a heavy 1000 μm tracer particle follows the recirculation pattern.

No CFD flow fields exist to compare these data to. Even so, to our knowledge they are the first measurements of slurry flow fields in this type of vessel, and are therefore unique and important in their own right.

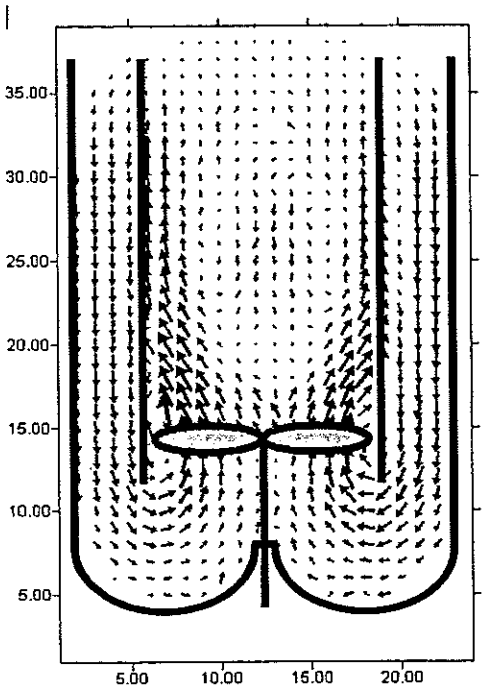

Figure 7. Axial velocity field in bottom ROI for slurry flow with a 650 μm tracer. Axes in cm.

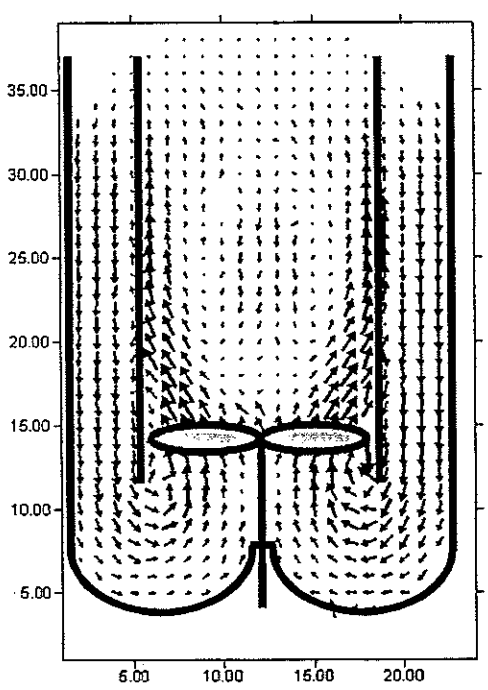

Figure 8. Axial velocity field in bottom ROI for slurry flow with a 1000 μm tracer. Axes in cm.

CONCLUSIONS

The radiotracer technique PEPT was presented and applied to the study of the flow pattern of a 22 litre DTC vessel. Despite the relatively low resolution of PEPT, it is possible to measure the single phase macroscale flow patterns as was illustrated by the excellent agreement between these measurements and CFD simulations. It was also shown that PEPT can be applied with equal ease to the measurement of flow fields in concentrated glass bead suspensions, which has never been done in this type of vessel before. PEPT is therefore a valuable and versatile technique to study the flow behaviour of this type of equipment.

Acknowledgements. Akzo Nobel, BASF, Bayer, DOW, DSM, DuPont de Nemours, Purac and the Netherlands Technology Foundation (STW) are acknowledged for their financial support of the UNIAK-3 research programme. Also, a *big* thank you to Sander Balthussen, André van den Bosch, Wim den Hollander, Aris de Rijke and Tona Verburg, without whose continued support in all matters constructional, mechanical, computational, electrical and radioactive, this research project would never have gotten to the point where it is today.

Symbol list

A	Average intersection point	t	Time [s]
N	Number of lines in a set [-]	u	Velocity vector [m/s]
d(a, b)	Distance from a to b [m]	x, y, z	Coordinates [m]
f	Fraction [-]	σ	Standard deviation
k	Selection constant [-]	1, 2	**Indices:** Camera number
n	Number of passages through a voxel	i, j	**Indices:** General counters

Cited literature

[1] Jong, M.D. de, R.E. Breslau, A.M. Neumann, H.J.M. Kramer and B. Scarlett, *Proceedings of the World Conference on Particle Technology III* (1998), Brighton, UK

[2] Jong, M.D. de, *Modelling, Validating and Applying the Hydrodynamics of Industrial Crystallisers*, Ph.D. thesis, to be published

[3] Moslemian, D., N. Devanathan and M. Dudukovic, *Rev. Sci. Instrum.*, **63** (1992), 4361–72

[4] Larachi, F., G. Kennedy and J. Chaouki, *Nucl. Instr. and Methods A*, **338** (1994), 568–74

[5] Parker, D.J., C.J. Broadbent, P. Fowles, M.R. Hawkesworth and P. McNeil, *Nucl. Instr. and Methods A*, **326** (1993), 592–607

[6] Broadbent, C.J., J. Bridgwater and D.J. Parker, *Chem. Eng. J.*, **56** (1995), 119–25

[7] Stellema, C.S. *Radiotracers for Gas/Solids Flows in (Interconnected) Fluidized Beds*, Ph.D. thesis, Delft University of Technology, Delft, The Netherlands (1999)

[8] Neumann, A.M., *Characterizing Industrial Crystallisers of Differnt Scale and Type*, Ph.D. thesis, Delft University of Technology, Delft, The Netherlands (2001)

MULTIDIMENSIONAL SIMULATION OF AIR FLOWS AND RESIDENCE TIMES DISTRIBUTION IN A VENTILATED ROOM

L. Ricciardi, J.C. Laborde

Institut de Protection et de Sûreté Nucléaire, Département de Protection et d'Etude des Accidents,
Service d'Etudes et de Recherches en Aérocontamination et en Confinement
CEA/Saclay – Bât. 383 – 91191 Gif-sur-Yvette Cedex, France

Abstract. We propose to assess the ability of a Computational Fluid Dynamics (CFD) code to simulate air flows in a ventilated room. This assessment is performed through the calculating of the room Residence Times Distribution curve. Several simulations are carried out with the CFX code on two experimental facilities. In the first one, the influence of various parameters is studied, an experimental curve being used as a reference. For the second one, the RTD curve is calculated by prediction for different air supply and exhaust configurations.

INTRODUCTION

Prevention of radiological hazards in ventilated rooms of nuclear facility requires knowledge of potential contamination transfers and therefore characterization of air flows. For this purpose, it is common to use an experimental method that relies on determining the room Residence Times Distribution (RTD): the response of a pulse injection of tracer gas at the room inlet can highlight the presence of short circuits, recirculations and dead zones.

However, only overall information is provided by an experimental RTD curve. One solution for obtaining more local information on the flow may be brought by using a multidimensional CFD code. Such a tool can also be used to study air flows in a global way according to different ventilation configurations, without the need of experimental tracing.

We propose in this paper to assess, through the RTD computation, the pertinence of using a CFD code to simulate air flows in a ventilated room. The simulations presented here were carried out with the commercial code CFX-4.3 [1].

METHODOLOGY

We assume that the flow in room is an isothermal (20°C), incompressible and turbulent air flow. The aeraulics equations solved are the incompressible time averaged Navier-Stokes equations (Reynolds equations). The turbulence model used by default is the standard k-ε model (1^{st} order). Transport of helium is governed by a classical convection-diffusion equation with source term.

Since air flows in room are not affected by a weakly concentrated tracer gas, the calculating of RTD is carried out in two steps:

1) a stationary computation yields the steady state aeraulics field,

2) a transient computation just simulates the transfer of helium in room after its injection; this approximation has been confirmed by a computation solving the transient aeraulics field as well.

SENSITIVITY STUDY ON A FIRST FACILITY

1. Presentation of the study

The first experimental facility, depicted Figure 1, is a 100 m^3 ventilated room incorporating two vertical ducts (one for blowing and one for exhaust), of rectangular section 0.4m×0.5m, practically diagonally opposed. Each duct comprises two openings (one in upper position and one in lower position) which can be opened or closed arbitrary, allowing the study of various ventilation configurations.

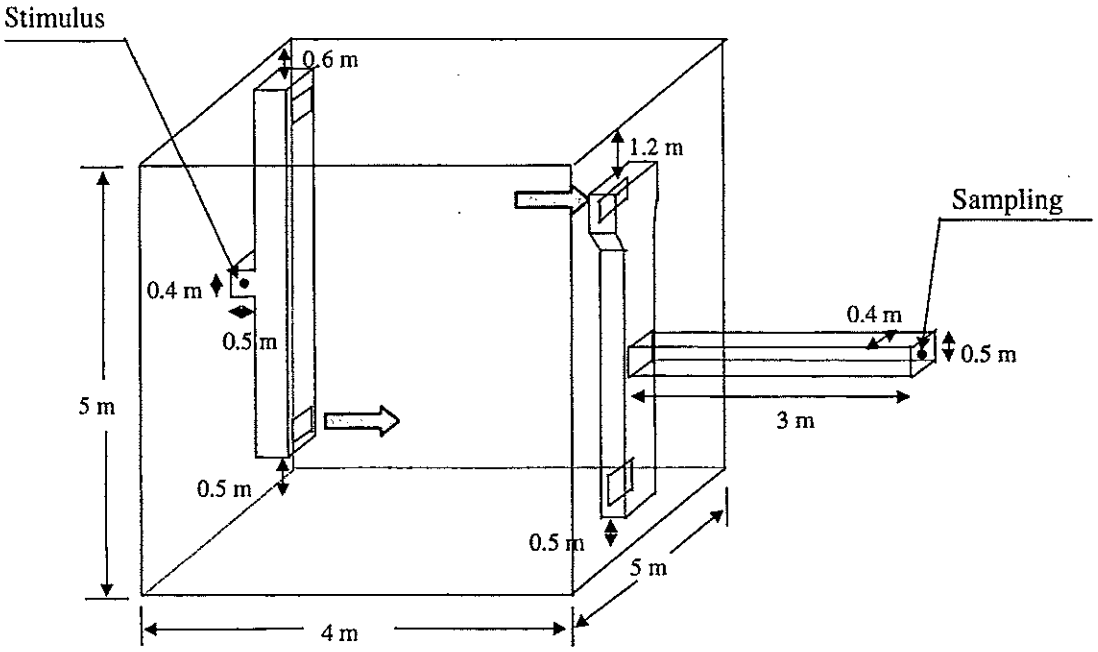

Figure 1. Geometry of the first experimental facility

The configuration studied here corresponds to a blowing in the lower part and an exhaust in the upper one. The flow rate, measured by a tracing gas method, is equal to 1000 $m^3.h^{-1}$. An experimental response curve at the room outlet, after pulse tracer gas (helium) release at the inlet, is available in this configuration. The injection time of helium is estimated to 5 s. The volume injected, calculated by integration of the RTD curve, is equal to 6.6 l.

The modeled geometry corresponds to the real one presented in Figure 1. The boundary conditions at the domain inlet are Dirichlet conditions on the air velocity U_{in}, the turbulent kinetic energy k_{in} and the turbulence dissipation rate ε_{in}: $U_{in} = 1.4\ m.s^{-1}$, $k_{in} = 1.5\ (I.U_{in})^2$ and $\varepsilon_{in} = k_{in}^{1.5}/(0.3\ L)$ with I the turbulent intensity (set to 4%) and L the dissipation length (hydraulic diameter of the duct).

At the domain outlet, atmospheric pressure is set and Neumann conditions are applied on the transported variables. These conditions require a fully developed flow, which is respected at the exhaust duct extremity.

The injection of helium is realized by introducing during 5 s a mass source term at the inlet which corresponds to the experimental volume of helium.

2. Sensitivity studies

Several RTD curve calculations have been performed on this facility, in order to study the sensitivity of various parameters. If each multidimensional modeling is a particular case which requires *a priori* its own sensitivity study, this study may allow to set computational parameters for analogous configurations. It may also allow to identify sensible experimental parameters, that therefore must be precisely known.

The different simulation results shown in this part have been obtained with the following default conditions: "coarse" grid, time step 0.1 s, turbulence model k-ε, exhaust flow rate 1000 $m^3.h^{-1}$, punctual injection of helium at the inlet section center during 5 s. For each sensitivity study, the modified parameters are specified.

Influence of time step

The RTD curves obtained with time step values varying between 5 s and 0.1 s are plotted in figure 2. It can be seen that, except time step of 5 s (which is equal to the time injection), the influence of time step is weak. It must be noted that the iterations number per time step required for convergence is lower than 10; therefore, CPU times are relatively short (12 min with dt = 1 s to simulate 500 s of physical time).

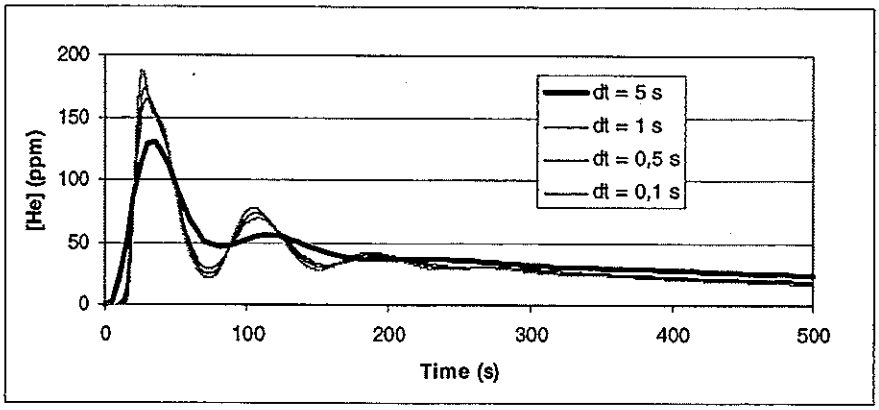

Figure 2. Influence of time step

Influence of grid

Two grids have been generated: a "coarse" grid (50 000 cells from 10 to 30 cm) and a finer grid (141 000 cells from 5 to 15 cm). In both cases, the constraint imposed near the wall by the high Reynolds number turbulence models is respected: $y^+>12$ with $y^+ = u^*\Delta y/\nu$ where u^* is the wall friction velocity, Δy the distance away from the wall and ν the cinematic viscosity.

Figure 3 shows that convergence is practically achieved with the coarser grid. Therefore, an order of magnitude of 10 cm for the minimum mesh size (generally near the wall) seems sufficient in a first approximation.

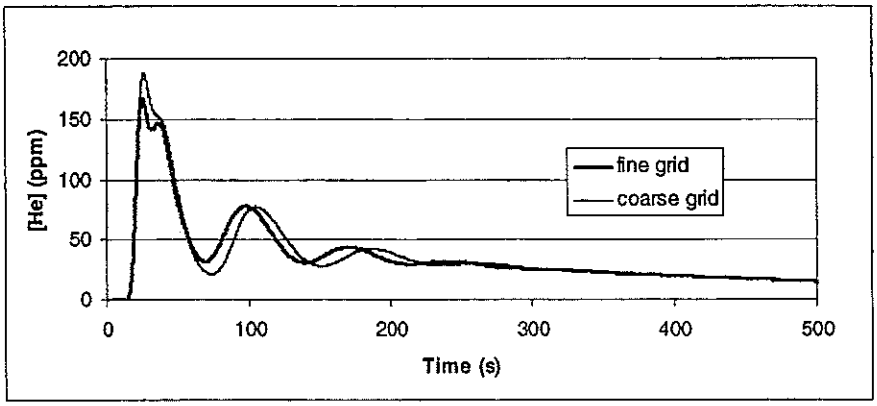

Figure 3. Influence of grid

Influence of turbulence model

If standard k-ε model is the most turbulence model used in industrial applications, it is not necessarily the most appropriated in this case. Other turbulence models have been therefore tested: the RNG k-ε model and the 2nd order "Reynolds Stress" model. Figure 4 shows that the behaviour of the two 1st order models is almost identical and that the RTD curve obtained with these models is closer to the experimental curve. In particular, the main three peaks, that correspond to a short circuit followed by recirculations, are well reproduced. Nevertheless, relatively important differences in frequency and amplitude can be observed compared to the experimental curve.

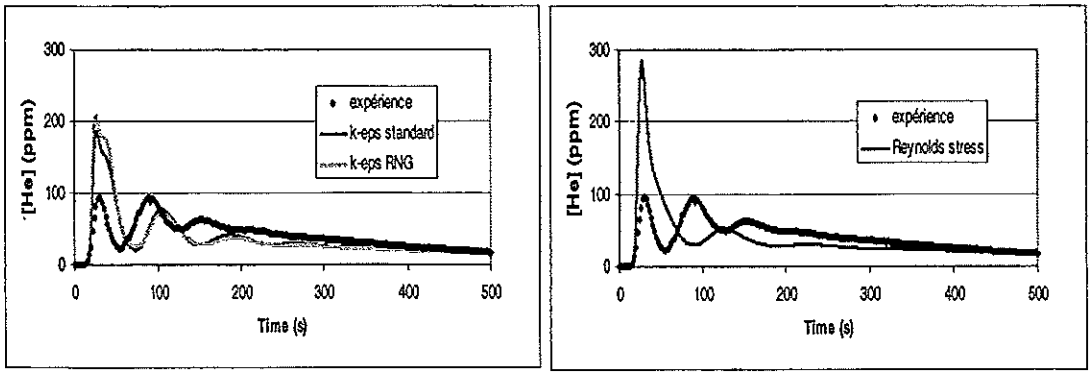

Figure 4. Influence of turbulence model

Influence of flow rate

The exhaust flow rate has been measured by tracing, with an uncertainty between 10 and 20 %. Therefore we attempt to evaluate the sensitivity of this parameter. Figure 5 shows the RTD curves obtained with a flow rate equal to 1000, 1100 and 1200 $m^3.h^{-1}$. It can be seen that the more the flow rate increases, the more the oscillations frequency (corresponding to recirculations in the room) increases. A satisfactory comparison in frequency is thus obtained with a 1200 $m^3.h^{-1}$ flow rate (with the coarse grid). However, differences still remain in amplitude, especially on the first peak. It can be noted that such differences have already been observed by Berne et al. [2].

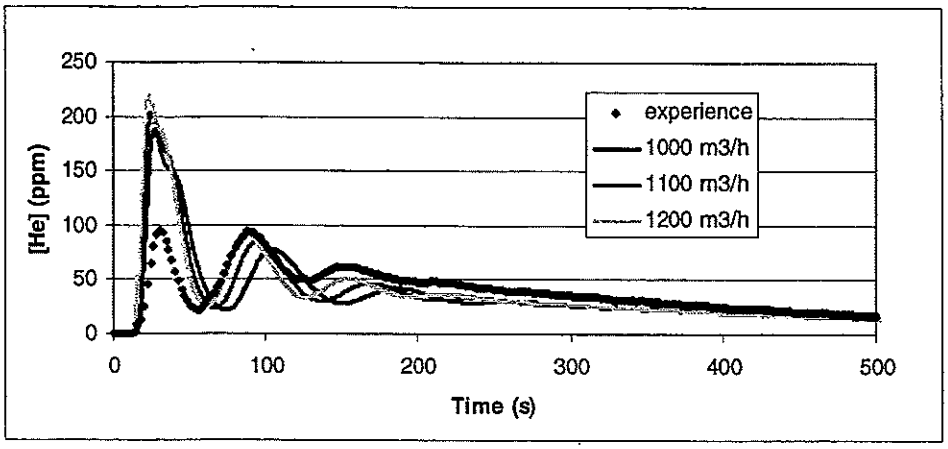

Figure 5. Influence of flow rate

Influence of injection method

In addition to an uncertainty on the flow rate, an uncertainty exists about the homogeneity of the helium concentration at the blowing duct outlet. The comparison of the RTD curves obtained with punctual and uniform injections (Figure 6) shows an influence of the injection method, mainly on the first peak amplitude which is closer to the experimental one in the case of uniform injection. The comparison with the experimental curve is thus globally satisfactory in this case.

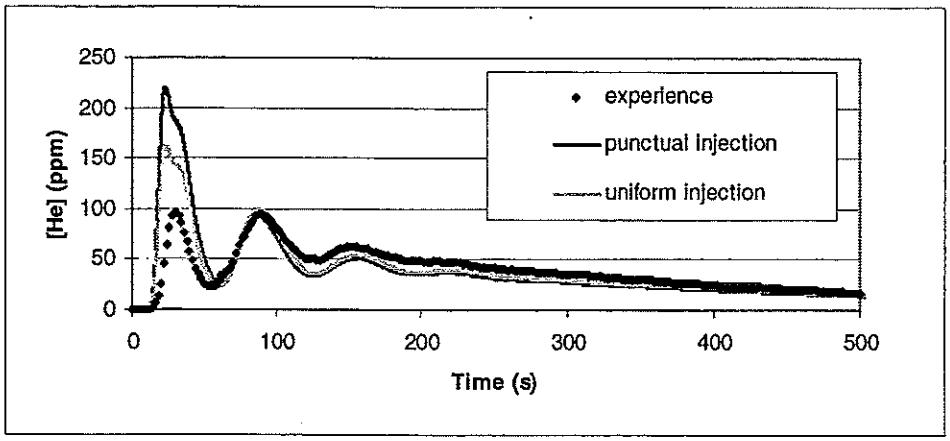

Figure 6. Influence of injection method ($Q=1200\ m^3/h$)

Influence of injection time

Computations have been performed with an injection time of 1 s and 10 s, for a same quantity of helium injected. The RTD obtained are identical to the one obtained with an injection time of 5 s. Therefore it seems that the injection time, negligible compared to the air change time, has not influence. Nevertheless, it must be recalled that the dynamic of injection itself is not modeled.

SIMULATIONS ON THE SECOND FACILITY

1. Presentation of the study

The second facility studied, referred to as CEPIA, is a 36 m^3 experimental chamber intended for examining the representativeness, in a ventilated room, of personal sampling with regard to the ambient sensors [3]. Comprising eight openings of 8cm×16cm on the walls and one opening of 8cm×28cm on the ceiling (Figure 7a), this facility was designed to allow various air blowing and exhaust configurations: each opening can be closed or opened as blowing or exhaust opening.

In addition to the room, it appears useful to represent the outer pipes comprising one general inlet for the whole blowing and one general outlet for the whole exhaust, in order to simulate various ventilation configurations. The modeled geometry is shown in Figure 7b.

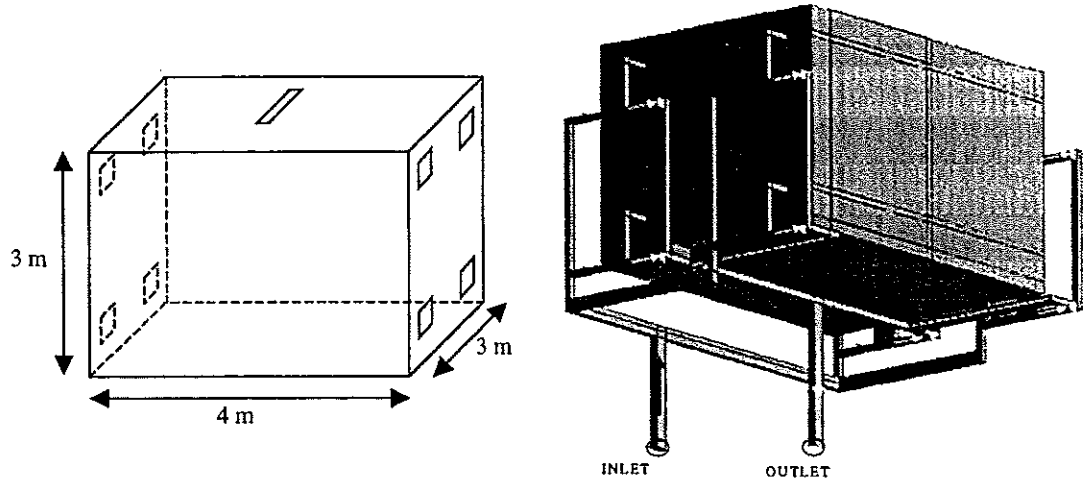

Figure 7. CEPIA room (a) and modeled geometry (b)

The grid used comprises 37 000 cells from 8 to 15 cm. The boundary conditions are the same as in the first study: Dirichlet conditions at the general inlet and Neumann conditions with imposed pressure at the general outlet. The flow rate is equal to 108 $m^3.h^{-1}$, namely 3 air changes per hour.

The injection of helium is realized as in the first study, by introducing a source term at the general inlet. The quantity of helium introduced has been evaluated to obtain a maximal concentration of 100 ppm volume in the case of a continuous stirred tank reactor (CSTR). The helium concentration is recorded at the general outlet.

2. Results

Six configurations of ventilation have been simulated. Only the most significant results are presented here. It must be noted that these simulations have not been yet compared with experimental results. We attempt to assess, through the computation of RTD, the ability of a CFD code to simulate by prediction the air flows in a ventilated room for different conditions of ventilation.

Configuration 1

In this configuration, blowing is carried out through the four upper openings, and exhaust through the four lower ones. The flow mixing is therefore important, as shown by the visualization of stream lines on Figure 8a. This mixing can also be seen on the RTD curve presented in Figure 8b, which is close to the RTD curve of a continuous stirred tank reactor.

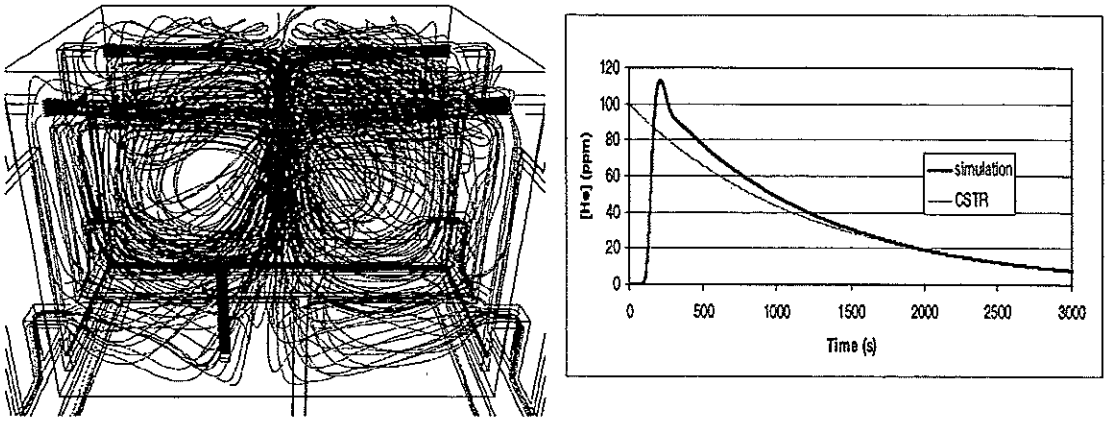

Figure 8. Configuration 1: stream lines (a) and RTD curve (b)

Configuration 2

This time, blowing is carried out through two upper openings, and exhaust through the two opposite lower ones. The RTD curve depicted Figure 9b shows a first peak corresponding to a short circuit, a part of helium being evacuated without mixing in the room. Then, the two oscillations seem to indicate the presence of recirculations. Finally, the decreasing slope, analogous to the CSTR one, corresponds to the room air change. The visualization of stream lines on Figure 9a confirms this analysis.

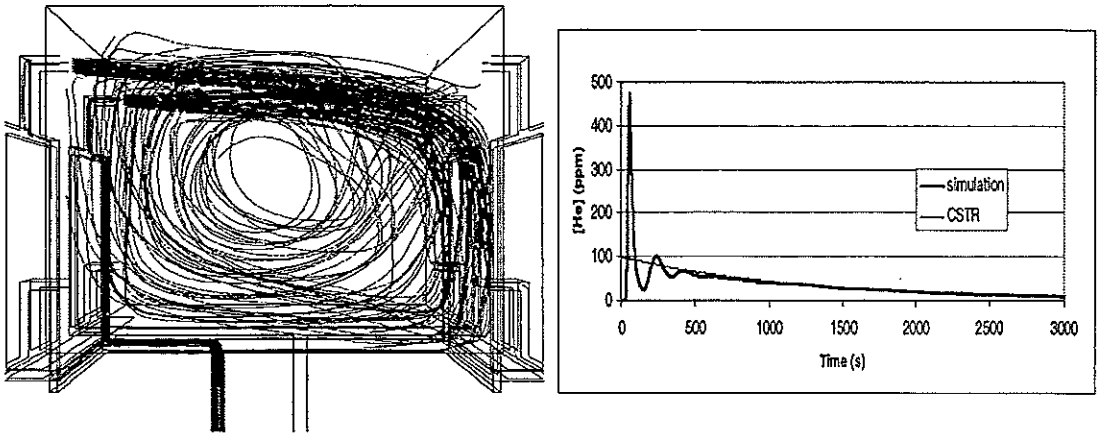

Figure 9. Configuration 2: stream lines (a) and RTD curve (b)

Configuration 3

The last illustration corresponds to a blowing through the ceiling and an exhaust through the four openings in the lower part. The form of the RTD curve obtained, shown in Figure 10b, is similar to the previous case one. The amplitude of the first peak, corresponding to a short circuit, is however twice greater, since the helium

leaves the room through four exhaust openings instead of two, for a same exhaust flow rate (Figure 10a).

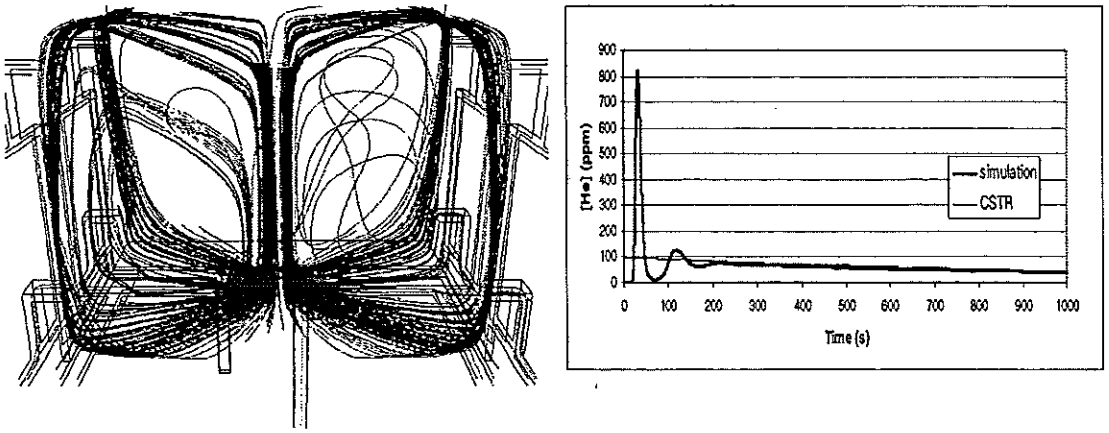

Figure 10. Configuration 3: stream lines (a) and RTD curve (b)

CONCLUSION

The sensitivity studies performed on the first facility allowed to come out several important conclusions about the influence of computational and experimental parameters. Moreover, the general form of the RTD curve has been reproduced quite well, even though some differences remain about the amplitude of the curve, in particular on the first peak.

For the second application, even though comparison between simulation and experimental results must be waited for, the computation results obtained by prediction are qualitatively encouraging.

In conclusion, the use of a CFD tool seems to describe properly the general trend of air flows in a ventilated room. Nevertheless, it must be recalled that, on the one hand this assessment has only dealt with a RTD curve, and on the other hand that the results precision, as for any calculation code, depends on the experimental data precision (flow rate, geometry, potential leakage, etc.).

REFERENCES

[1] CFX-4.3 Solver, AEA Technology, Harwell

[2] Berne Ph., Blet V., *Assessment of the systemic approach using radioactive tracers and CFD*, 6th International Conference on Air Distribution in Rooms, Roomvent (1998)

[3] Fauvel S., Witschger O., *A test room for studying area and personal sampling*. J. Aerosol Sci., 31 (2000), S781-S782.

RTD : A USEFUL STEP TO DEFINE SYSTEMIC MODELS FROM CFD INFORMATION – APPLICATION TO INDUSTRIAL OZONATION TANKS FOR DRINKING WATER TREATMENT

C. de Traversay[1], F. Luck[1], D. Wolbert[2], A. Laplanche[2]

[1] Anjou Recherche - Vivendi Water, Chemin de la digue, BP 76, 78603 Maisons Laffitte Cedex, France
[2] ENSCR, Ecole Nationale Supérieure de Chimie de Rennes, Av. du Gal Leclerc, 35000 Rennes Beaulieu, France

Abstract. Computerised fluids Dynamics (CFD) software can be used to determine the hydraulic behaviour of ozone contactors and to simulate Residence Time Distributions (RTD). With this information, a strategy to build systemic models was developped. That is an association of elementary reactors such as Completely Stirred Tank Reactor (CSTR) or plug flow reactor. A comparison of RTD obtained by CFD and by tracer experiments was completed to validate the results given by CFD.

INTRODUCTION

Modelling the performances of a process with a complex chemical and/or biological mechanism requires knowledge of its hydrodynamics. This can be achieved by defining a systemic model of the reactor. Computerised Fluid Dynamics (CFD), which describes the hydrodynamic behaviour of a reactor and simulates Residence Time Distribution (RTD), can be an useful tool for the design of the systemic model.

The objective of this paper is to suggest a strategy to build the systemic model from the CFD results for full-scale ozone contactors in drinking water treatment. In order to validate the results given by CFD, RTD obtained by CFD and by tracer studies are compared.

BACKGROUND

To meet the requirements imposed by more stringent European and American drinking water regulations, the operation of ozone contactors is becoming increasingly complex. Indeed in many cases several objectives sometimes conflicting must be simultaneously fulfilled by ozonation : improved disinfection, oxidation of pollutants, reduction of ozonation by-products (bromate, by-products of pesticides). Therefore the design and the monitoring of ozonation reactors must be optimised with the help of ozonation reactor modelling.

The accurate modelling of an ozonation stage demands knowledge about kinetics as well as the hydrodynamics of the contactor. Two methods are available to characterise the hydrodynamic behaviour of reactors :

- tracer studies obtained by experiment give access to general flow information using RTD measurement ;
- Computerised Fluid Dynamics (CFD) provides the necessary information to understand the hydrodynamics of complex geometries. CFD is a computer-based methodology used to solve the fundamental equations of fluid flow : the Navier-Stokes equations. Using CFD, the hydrodynamic behaviour of a reactor can be described and RTD simulated. The RTD calculation involves the transient simulation of a non reacting specie propagating with water from the inlet to the outlet.

Information on hydrodynamics from RTD only is too broad for the modelling of the ozonation stage. Another approach is the combination of the kinetic model with CFD. The main drawback of this solution is the computation time, which is proportionate to the number of equations and to the grid size. In water treatment, the size of the contactor can be very large (from a few m^3 to several thousand m^3). As the sensitivity of the predicted results depends on the meshing cell size, it is important to have an accurate mesh, and then the time needed for the solution can be quite important. For a large number of equations to solve, including the kinetic reactions (around 50 for the ozonation stage), it takes too long to calculate the results (several days). Moreover, varying on the operating conditions to study the influence on the results becomes prohibitive.

That is why another approach investigated to combine hydrodynamics and kinetics : the systemic model. A systemic model is a combination of ideal reactors such as plug flow or Completely Stirred Tank Reactor (CSTR). It represents the flow inside the contactor but it gives less information than CFD on the flow pattern. The modelling of the ozonation stage can be achieved by using a tool resolving kinetic reactions on a systemic model. The main advantage of a such tool is the computation time which is relatively short (a few minutes). Nevertheless the systemic model has to be as accurate as possible. The definition of the systemic model can be done from the CFD hydraulic information, if CFD gives realistic results. This requires validation against experimental data. The local measurement of the liquid velocity is very difficult and expensive to do in an industrial ozone contactor. Most methods, such as Particle Image Velocity (PIV), have been developed for pilot units. The easiest way to validate the CFD results is the RTD, by comparison between experimental RTD and numerical RTD.

COMPARISON BETWEEN EXPERIMENTAL RTD AND NUMERICAL RTD

1. Presentation of the full-scale ozone contactor

The contactor (figure 1) consists of three main chambers (400 m^3 each) designed to maintain a reaction time. Water depth is about 6.8 m and operating liquid volume is approximately 1100 m^3. The water flow rate is about 8300 $m^3.h^{-1}$ and the Theoretical Hydraulic Retention Time (THRT) is around 8 min.

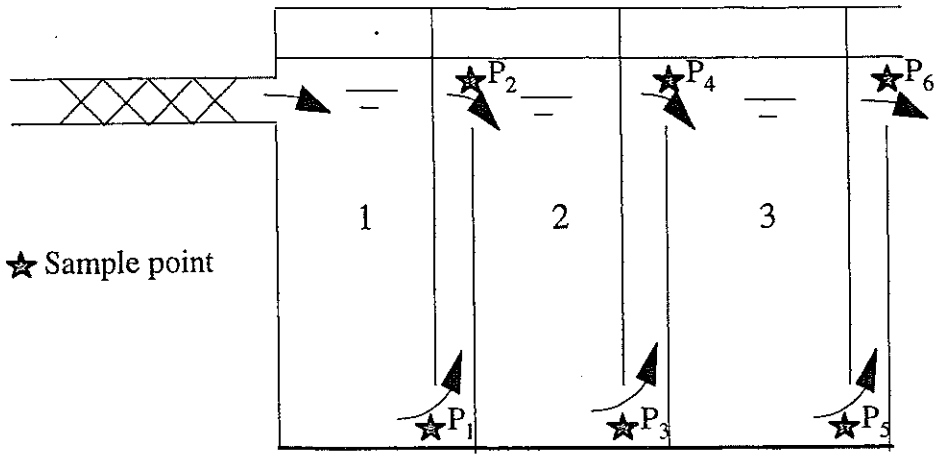

Figure 1. Section of the contactor

2. CFD results

The hydrodynamic behaviour of the reactor can be accessed with CFD software. This gives a description of the velocity field in steady state conditions with single-phase flow (figure 2) and the turbulent kinetic energy distribution (figure 3).

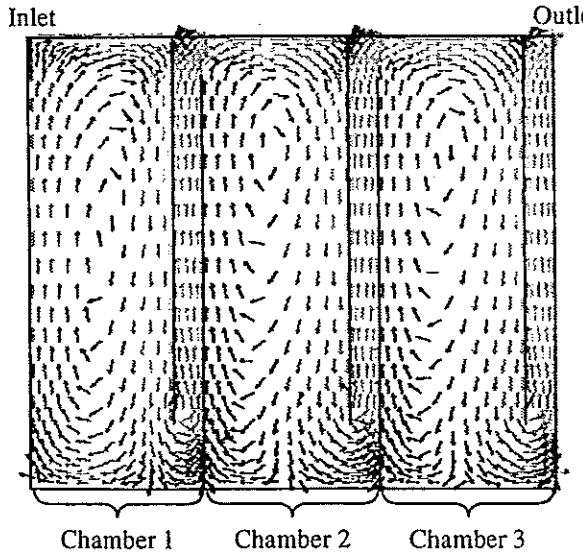

Figure 2. Velocity field

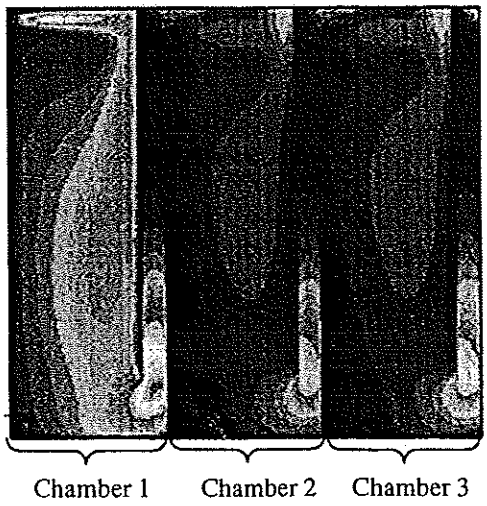

Figure 3. Turbulent kinetic energy distribution

The velocity field serves to locate the three back-mixing zones (one in each compartment) and to estimate the direct-flow and recycling flow volumes with respect to the incoming flow rate.

RTD obtained by CFD is presented in figure 4.

The CFD results can then be used to define the systemic model.

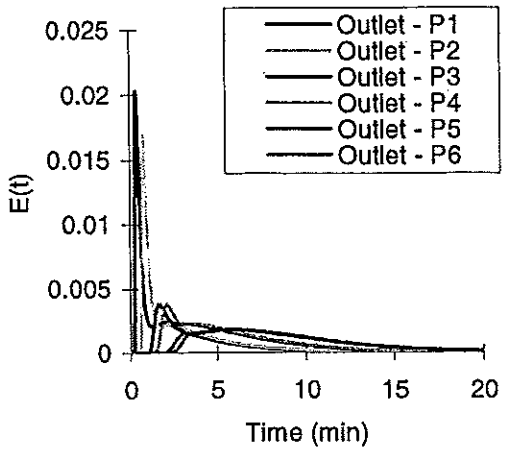

Figure 4. RTD at the under and over baffles

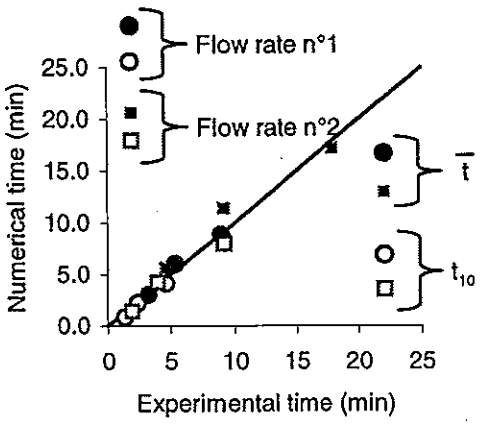

Figure 5. Comparison of $\bar{t}$ and t_{10} from CFD and tracer experiments for two flow rates at the outlet of the different chambers

3. Comparison with experimental RTD

Even if experimental RTD is a quite laborious and expensive operation, this step is the simplest way to validate the CFD results. Once the validation step is completed for an application, CFD can be used without doing further tracer experiments.

Experimental and modelled RTD curves have been compared on the following variables [1] :

- $\bar{t}$ which is the average time or the centroid of the distribution, this gives the location of distribution ; $\bar{t}$ must be compared to the THRT, calculated by dividing the volume by the flow rate. If there is a significant difference between $\bar{t}$ and THRT, there exists a dead zone or a short-circuit.
- t_{10} which represents the time for which 10 % of the fluid has left the contactor. This parameter is quite important because the disinfection efficiency criteria of an ozone reactor is based on it.

The comparison of simulated and experimental RTD results for an ozone contactor are presented in figure 5.

The deviation between experiment and modelling is less than 5 % : the numerical solution is representative of the real life situation.

PROTOCOL

1. Description of the protocol

A protocol was developed to link the different data given by CFD for an elementary unit of volume (part of the reactor). The CFD simulations can be obtained by using general commercial CFD computer packages. The results presented in this paper were obtained using the Fluent commercial computer code which is recognized throughout the world. Fluent resolves the flow equations using the finite volume approach. Theoretical and numerical background is readily available [2].

From the velocity fields, the recycling zone can be located inside the reactor and the parallel flows can be visualised. The flows through the reactor can be characterised in terms of volume and flow rates, and then residence times since CFD is able to give velocity in each point of the mesh and volume for each elementary cell of the mesh.

From this information, the systemic model is then developed according to figure 6 [3]. Optimisation of the model parameters is realized with numerical RTD using software which calculates the RTD from the systemic model [4].

The ideal reactors arrangement is based on the turbulent kinetic energy distribution. The inlet, the change of flow direction and the outlet of chambers correspond to high turbulent energy. These parts of the reactor will correspond to predominately CSTRs. For the zones of equivalent turbulent kinetic energy, each CSTR will be associated to a plug flow reactor.

2. Application of the protocol to full scale ozone contactor

Analysis of the RTD of the main compartments and between the narrow baffles indicates that there is a flow dispersion inside each zone of the reactor.

Velocity fields show that there is a recycling flow in each main chamber. Nevertheless, there is only one peak in the RTD. So, each main compartment can be represented by a direct zone associated with a recycle zone. Characteristics of each zone deduced from CFD are given in table 1.

Table 1. Characteristics of direct zone and recycle zone for each chamber

	Chamber 1		Chamber 2		Chamber 3	
	Direct zone	Recycle zone	Direct zone	Recycle zone	Direct zone	Recycle zone
Flow rate ($m^3.s^{-1}$)	4.766	2,452	3,662	1,348	3,670	1,356
Volume (m^3)	164.2	174,0	203,8	134,4	204,2	134,0
THRT (s)	34	71	56	100	56	99

The flow between the narrow baffles tends towards plug flow behaviour according to the velocity field and the RTD, with no parallel flow.

Each zone can be represented by an association of a series of CSTR and a plug flow reactor. The unknown parameters (numbers of CSTR in each zone) can be determined by optimising the RTD of the systemic model to the numerical RTD.

Table 2. Systemic parameters for each main chamber

	Chamber 1		Chamber 2		Chamber 3	
	Direct zone	Recycle zone	Direct zone	Recycle zone	Direct zone	Recycle zone
Number of CSTR	2	3	3	2	2	6
τ_{CSTR} (s)	26	71	46	100	46	79
τ_{PF} (s)	10	0	13	0	20	20

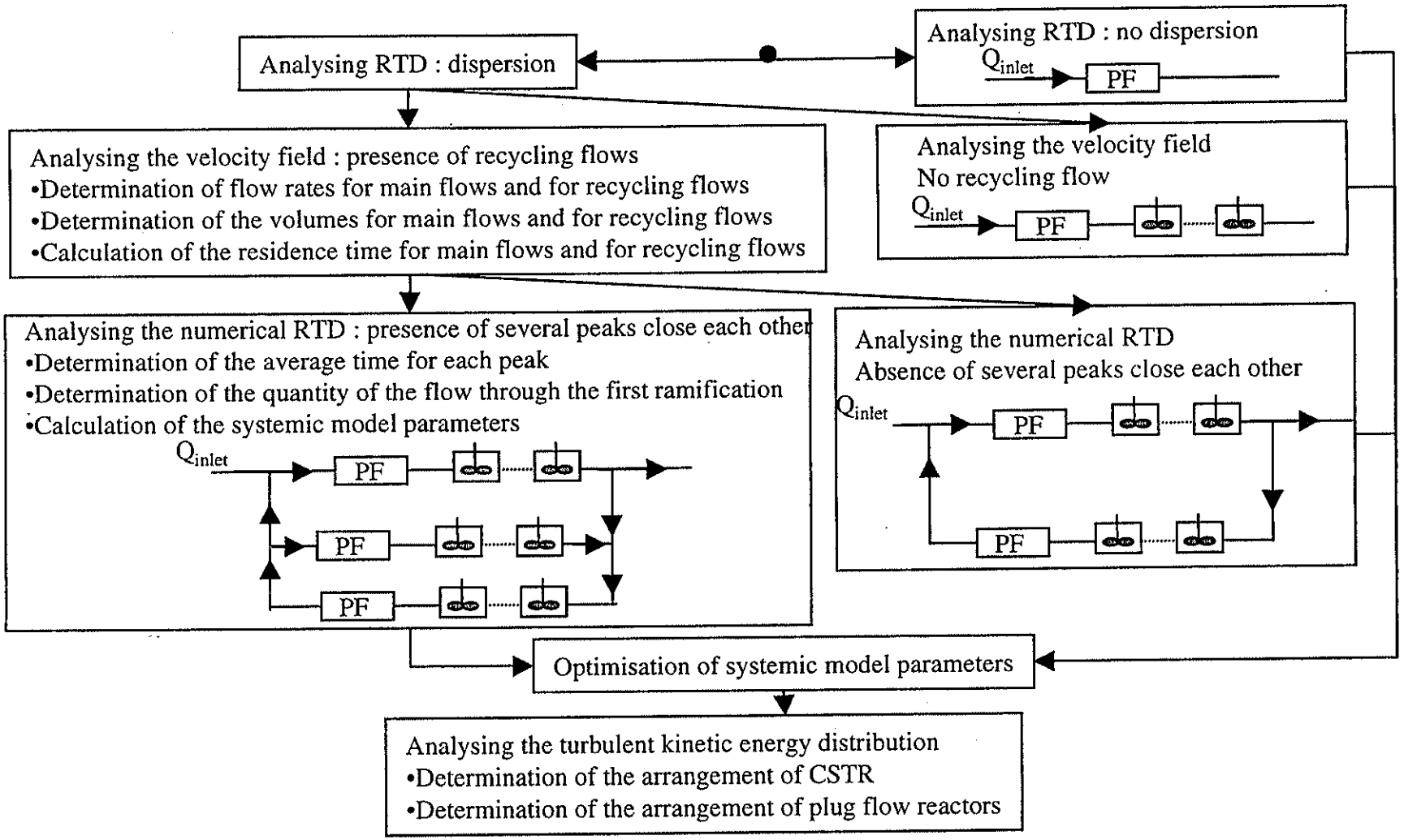

Figure 6. Strategy to connect CFD results to systemic model

The arrangement of CSTR and plug flow reactor is defined by analysing the turbulent kinetic energy distribution. High turbulent kinetic energy zones, corresponding to CSTRs, are located at the inlet of the narrow baffles, while plug flows correspond to less turbulent flows. The final systemic model is represented on figure 7.

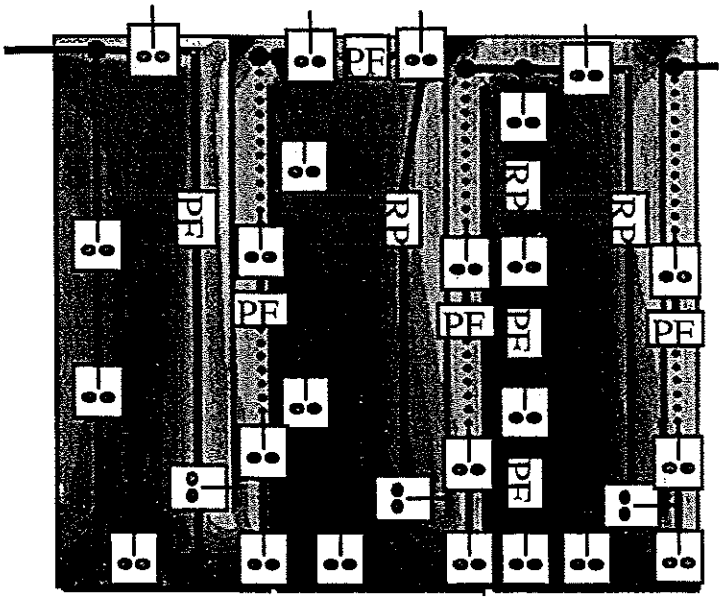

Figure 7. Systemic model for the full-scale ozone contactor

Figure 8 presents the RTD obtained by CFD and the RTD of the systemic model.

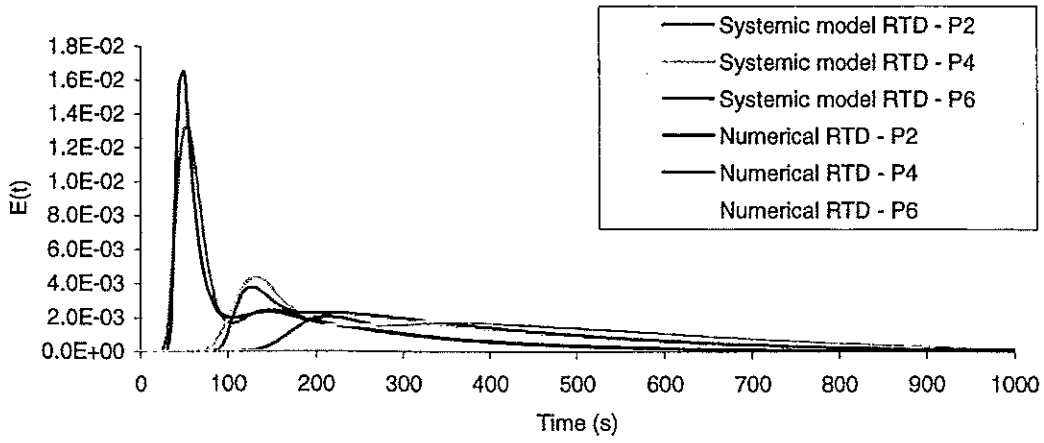

Figure 8. Comparison between the systemic model RTD and numerical RTD for the full-scale ozone contactor

CONCLUSION

For the modelling of large reactors with complex chemical mechanisms, systemic models are the easiest to use. CFD is too time consuming to allow the modelling of the ozonation stage and RTD is not sufficient because the information it gives is too broad. The definition of a systemic model has to take into account more accurate information that can be deduced from RTD. The present study shows that CFD is a useful tool to improve knowledge of the hydrodynamics. It allows development of the systemic model, without doing experiments, which are expensive and quite difficult to implement. Nevertheless, experimental RTD can be used to validate CFD results on large contactors. RTD are correctly described with the simulation of a tracer injection and CFD gives an accurate description of the velocity fields.

REFERENCES

[1] LEVENSPIEL O. (1962) Chemical Reaction Engineering. Ed. John Wiley & Sons

[2] FLUENT User's guide, Release 5, August 1998, Fluent Inc., Vol. 4 Chapter 19

[3] de TRAVERSAY C. (2000) De la mécanique des fluides numérique à l'approche systémique : application aux réacteurs d'oxydation en potabilisation. Thèse de l'université de Rennes.

[4] LECLERC J. P., DETREZ C., BERNARD A., SCHWEICH D. (1995) DTS : un logiciel d'aide à l'élaboration de modèles d'écoulement dans les réacteurs. Revue de l'Institut Français du Pétrole, 50 (5) 641-656

AIR FLOW DISTRIBUTION IN VENTILATED ROOM : RTD MODEL SYNTHESIS BASED ON SIMULATED ANNEALING AND CFD

P. Floquet[1], C. Laquerbe[1], J.C. Laborde[2], S. Soares[2], L. Pibouleau[1] et S. Domenech[1]

1 Laboratoire de Génie Chimique (LGC) UMR CNRS/INP/UPS 5503
ENSIACET 18, Chemin de la Loge
F31078 Toulouse Cedex 4

2 Institut de la Protection et de la Sûreté Nucléaire (IPSN) – DPEA/SERAC
CEA Saclay
F91191 Gif-sur-Yvette Cedex

Abstract. This communication presents the main principles of an approach, which is based on RTD theory and gives an illustration of its potential extension to ventilation problems. The general solving strategy adopted, consisting in a two-level dissociated treatment of parametric identification and structural identification of models. The comparison between experimental residence time distribution curves recorded on a ventilated laboratory enclosure and the simulated ones shows a good agreement. For this problem, a comparison with results obtained from a Computational Fluid Dynamics (CFD) tool has been performed.

INTRODUCTION

The control of the airborne contamination transfers linked to operators protection and to facilities safety is a key feature in nuclear industry, particularly to prevent radiological risk. So, it is necessary to have tools in order to assess airborne contamination transfers inside a ventilated enclosure. In this framework, a systemic approach based on Simulated Annealing combined with Computer Fluid Dynamics (CFD) aims at interpreting Residence Time Distribution (RTD) in a room. The goal of the systemic approach is to build a model from a combination of elementary systems representing basic ideal flow patterns (perfect mixed flow, plug flow,...). The adjustment of the model lies on the comparison of the response to a stimulus injected into the model with an experimental tracer emission performed in ventilated room inlet. The general solving strategy adopted, consists in a two-level dissociated treatment of parametric identification and structural identification of models [1]. Then, a comparison with results obtained from CFD tool can be performed.

MELANIE

A real ventilation room (100 m3), the laboratory enclosure called MELANIE(CEA Grenoble) and represented Figure 1, has been used to illustrate this mixed approach, that gives an illustration of its potential extension to various problems. Inside this room, various air flows and residence time distributions by either changing the position of blowing and exhaust openings (near the floor or near the ceiling), or modifying the exhaust flow rate, can be obtained [2]. The configuration studied here

corresponds to an exhaust flow rate equals to 1100 m3/h at 20°C, and to the classical location of blowing and exhaust opening in nuclear ventilation applications (blowing in the upper part of the room and exhaust in the lower part). For this configuration, identifications have been performed using the experimental response of this system from an impulse release of helium used as tracer gas.

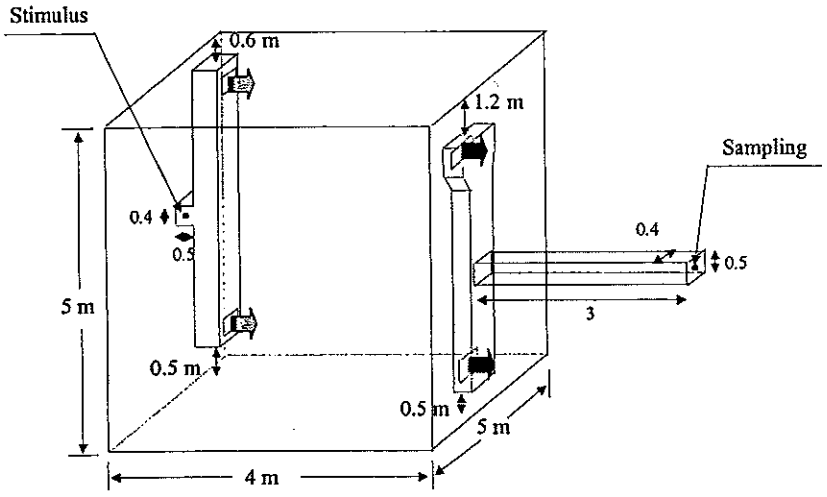

Figure 1. : MELANIE Laboratory Facility

IDENTIFICATION PROCEDURE

The global methodology adopted for the development of a computational package allowing the synthesis of RTD model structures is constituted by a master problem performing the structural identification of the models and a slave problem performing classical least square parametric identification. The problem of discrimination of the various schemes is solved by a stochastic procedure based on Simulated Annealing (SA). The implementation of this algorithm previously presented [3] is not detailed here. Figure 2 shows the experimental impulse response and the identification curve (obtained by IDTS "Identification de Distribution de Temps de Séjour" package). Identifications have been realized with Simulated Annealing (SA) procedure. The best structure obtained and physically near from the real behavior is represented on Fig.3. The comparison between the experimental curve and the simulated one is quite satisfactory (Figure 2).

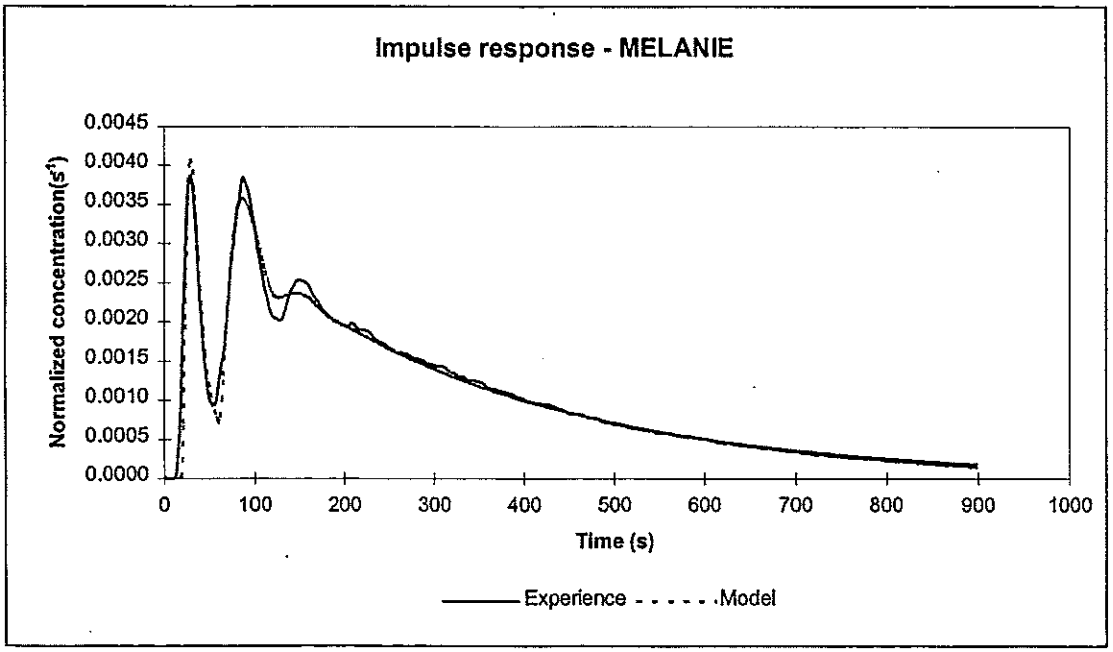

Figure 2 : Experimental and model impulse response for MELANIE enclosure

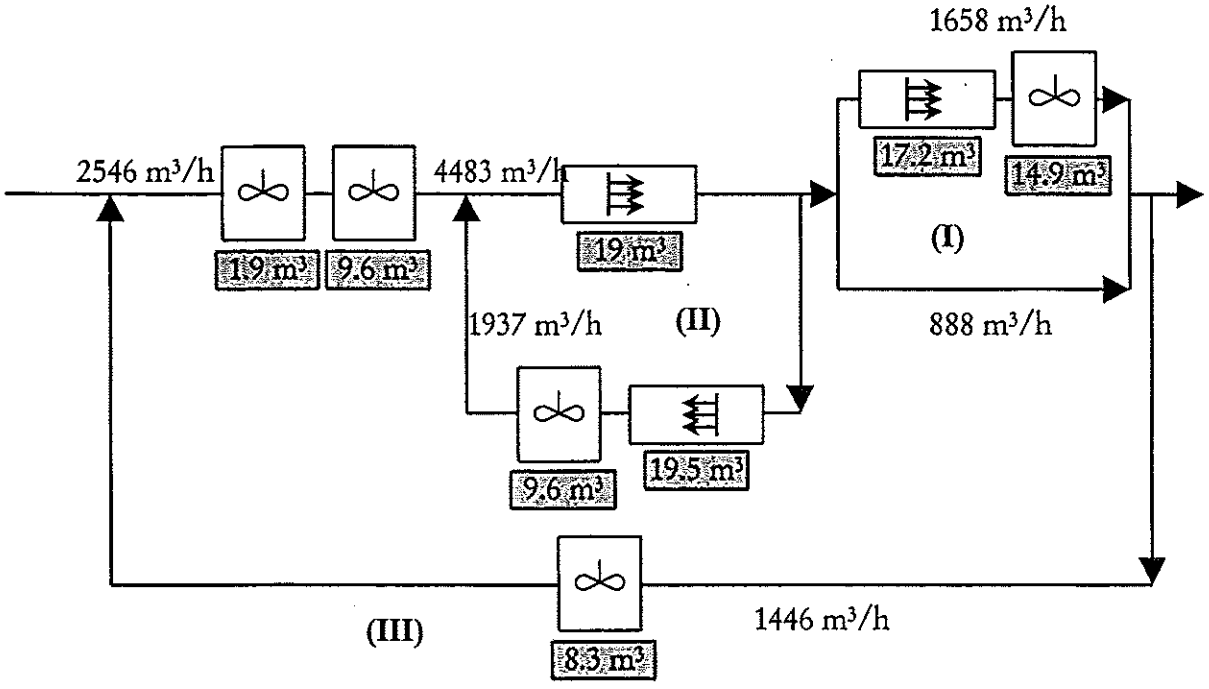

Figure 3 : Best structure obtained by IDTS procedure

CFD PROCEDURE

To verify that this model can represent the reality of the air flow in the room, a complementary study has been carried out. The model proposed by IDTS is analysed by comparing the flow patterns induced by this structure and those calculated by 3D predictive numerical simulations performed by the Flovent™ code. The helium transfers inside the ventilated enclosure have been simulated and are reported Figure 4 at various times. With those informations, it is possible to locate the main parts constituting the RTD model (Figure 3).

- Figure 4.a., obtained 20s after the beginning of a continuous release of helium inside the ventilated room, shows a small part of the blowing flow rate passing quickly into the exhaust opening. This phenomenon corresponds to the first peak on the experimental RTD curve, and can be generated by the branch n°I of the structure obtained by IDTS (Figure 3).

- Figure 4.b. illustrates a secondary recirculation near the exhaust opening, that appears on the RTD curve after 40s with a second peak. This can be related to the recycling branch n°II in Figure 3.

- After t=100s, Figure 4.c. illustrates a main recirculation loop from the exhaust opening the blowing one. This phenomenon could be located in the branch n°III of the structure (Figure 3).

- Finally, around t=300s and after (Figure 4.d.), the tracer has filled all the volume of the cell, and its change involves the classical exponential decrease on the RTD curve.

Figure 4.a : Evolution of helium released inside MELANIE (t=20s)

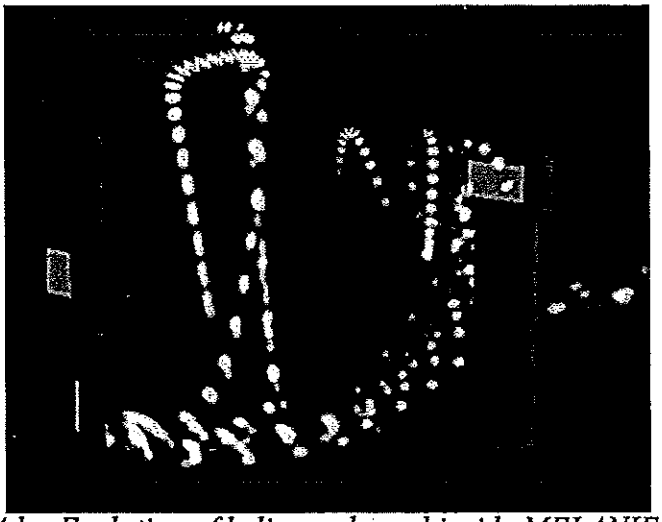

Figure 4.b : Evolution of helium released inside MELANIE (t=40s)

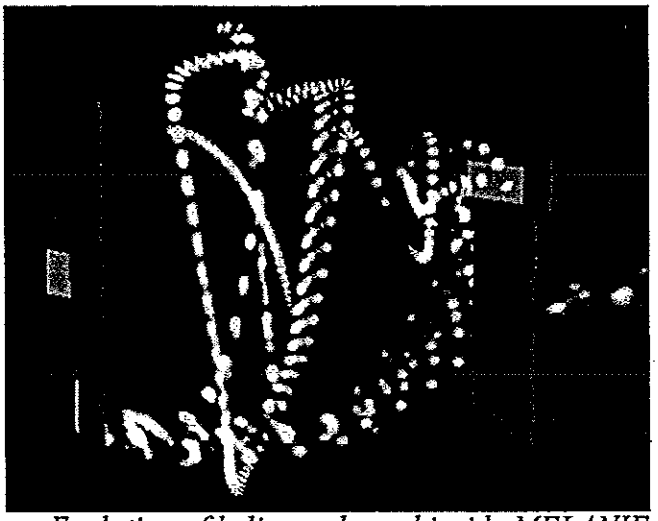

Figure 4.c : Evolution of helium released inside MELANIE (t=100s)

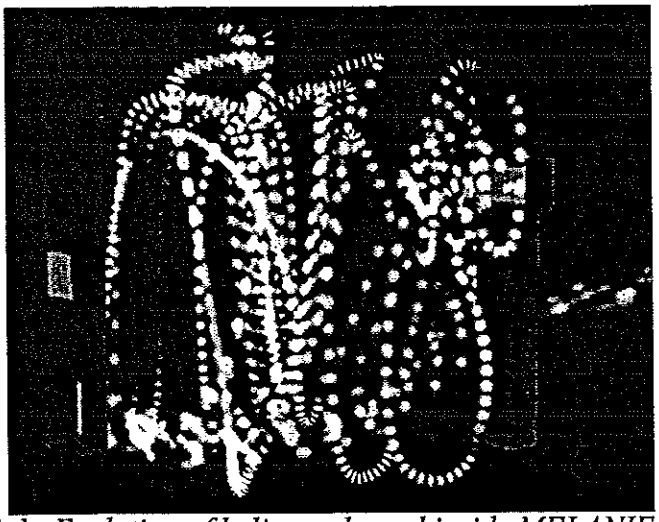

Figure 4.d : Evolution of helium released inside MELANIE (t=300s)

These results show how the two different tools constituted by the IDTS code and a CFD code can be used to analyse the air flow distribution and the associated contaminant transfers in an industrial ventilated enclosure.
The structure of the model represented in Figure 3 has been also applied to various configurations of the ventilation system of the cell MELANIE: different exhaust flow rates (1100 m^3/h, 2200 m^3/h and 3000 m^3/h) and different positions of blowing and exhaust openings (4 different configurations tested). For each ventilation configuration studied, only with an identification of the operating parameters (volumes of CSTRs and PFRs, flow rates) of the structure given Figure 3, it has been verified that this model can represent quite satisfactorily the various corresponding RTD curves.

Once a RTD model is proposed by the IDTS code, it can be used as part of safety studies to simulate the contaminant transfers after an accidental release in one determined region of the structure. Indeed the contamination propagation can be simulated in all regions present in the model structure for a release in a given region.

CONCLUSION

The computational package presented in this communication constitutes an useful and innovative tool to elaborate residence time distribution models in order to characterise flow patterns and associated transfers. The computational package includes various components: a simulation tool, a parameter identification tool for models with fixed structures, but also a structure generator very useful in the conception step.
Validation and qualification of IDTS software has been carried out. The complementarity between the systemic and the CFD approaches has also been illustrated.
This CAD tool seems to have useful applications not only in industrial ventilation but also in more classical chemical engineering fields or other domains which commonly use the analysis of residence time distribution curves, especially when

the enclosure structure is unknown. This point is particularly original compared with previous works cited in introduction.

BIBLIOGRAPHY

[1] Drecourt S., Laborde J. C., Domenech S. Floquet P. et Laquerbe C.,
Développement d'un outil de calcul appliqué à la caratérisation d'une ventilation par traçage et basé sur l'approche systémique, Communication « Traceurs et méthodes de traçage » in « Récents Progrès en Génie des Procédés » Ed. J. P. Leclerc et G. Grevillot, Vol 12, n° 61, pp. 49-55, 1998

[2] Espi E.,
Prévision des transferts de contamination en cas d'incendie dans un local ventilé ,
Ph-D thesis, INP Toulouse, 2000

[3] Laquerbe C., Laborde J.C., Floquet P., Pibouleau L. and Domenech S.,
Identification of parametric models based on RTD theory – Application to safety studies in ventilated nuclear enclosures , Escape 8, Bruges (Belgium), 24-27 May 1998, Computers Chem. Engng, Vol 22S, p. S347-S354, 1998

APPLICATION OF RTD AND CFD FOR FLUE GAS IRRADIATION REACTOR INVESTIGATION

A.G. Chmielewski[1], J. Palige[1], A. Dobrowolski[1], A. Owczarczyk[1], A. Rozen[2]

[1]Institute of Nuclear Chemistry and Technology, Dorodna 16, 03 – 195 Warsaw, POLAND
[2]Warsaw Technical University, Chemical and Process Engineering Faculty, Waryńskiego 1 00 – 645 Warsaw, POLAND

Abstract. Power plant for flue gas desulfurization and denitrification with electron beam technology application is in implementation stage. Experimental and theoretical studies have proved that mixing conditions and multistage irradiation is essential for high NO_x removal efficiency. Gas flow structure for electron accelerators switch on and switch off was determined. Radiotracer tests have been performed on the pilot plant installation (20000 Nm^3/hour) using Br – 82, in form of methyl bromide, as a gas tracer. Paralelly to radiotracer experiments study using computational flow dynamics were performed. Comparison of the results obtained during both methods application is discussed.

INTRODUCTION

More and more environmental pollution has become a serious problem. The electron – beam (EB) process has been succesfuly applied for pollutant destruction and for their removal from gas, liquid and solid phase of the matter. One of the radiation process, successfuly demonstrated in many laboratories, pilot plant facilities and in last time in industrial scale, is reduction of SO_2 and NO_x pollutants from flue gases emitted during fuel combustion in electrical power and heat production [1].

When high energy electrons – about 800 keV – are applied for flue gas irradiation, quantities of free radicals and free atoms are generated in a primary process as a result of ionisation and dissociation. During the process stoichiometric quantitie of NH_3 is added. SO_2 and NO_x are oxidised in water presence to H_2SO_4 and HNO_3.

In the third stage, the intermediate products react with ammonia to form ammonium sulphate and ammonium nitrate. The dry powdery ammonium salts are then collected by the filtering units and can be used after as a fertiliser. In optimal conditions, an amount of 5 kGy is required for 95 % removal efficiency of SO_2 and 7 kGy for 70 % removal of NO_x. Total duration of all radiation reactions is less than 1s.

PILOT PLANT FACILITY INSTALLED IN WARSAW POWER STATION KAWĘCZYN

The pilot plant for flue – gas treatment by EB application has been installed in Power Station Kawęczyn in Warsaw. The flow capacity through the installation is up to 20000 Nm^3/h. The installation is equipped with two EB accelerators.

These accelerators, which can provide 50 kW EB power each with energy 500 – 700 keV, were installed in a series within the reaction vessel. The main objectives of the research carried out at the pilot plant were:
- test of all parts of the installation;
-optimisation of the process parameters;
- preparation of the industrial – scale facility design.

The principal new elements introduced to the construction of radiation chamber were:
- cascade double irradiation;
- longitudinal irradiation of the gas (the beam is scanned along the chamber axis).

From the chemical engineering point of view the radiation chamber presents the gaseous continnous flow tube chemical reactor. In such installation the efficiency of chemical reactions strongly depends on mixing conditions and flow structure of gas phase inside of the reactor. For this reason two series of radiotracer experiments, one for accelerators switched off and second for accelerators switched on were carried out. Using the Br – 82 in methyl bromide form for gas labelling, the residence time distribution (RTD) of gas in installation for different technological conditions were determined. The tracer distribution in different points of installation were measured by collimated scintillation detectors located along the installation outside the tube for gas transportation and reaction vessel. The principal scheme of installation with accelerators A1, A2 and detectors localisation indication is presented in Figure 1.

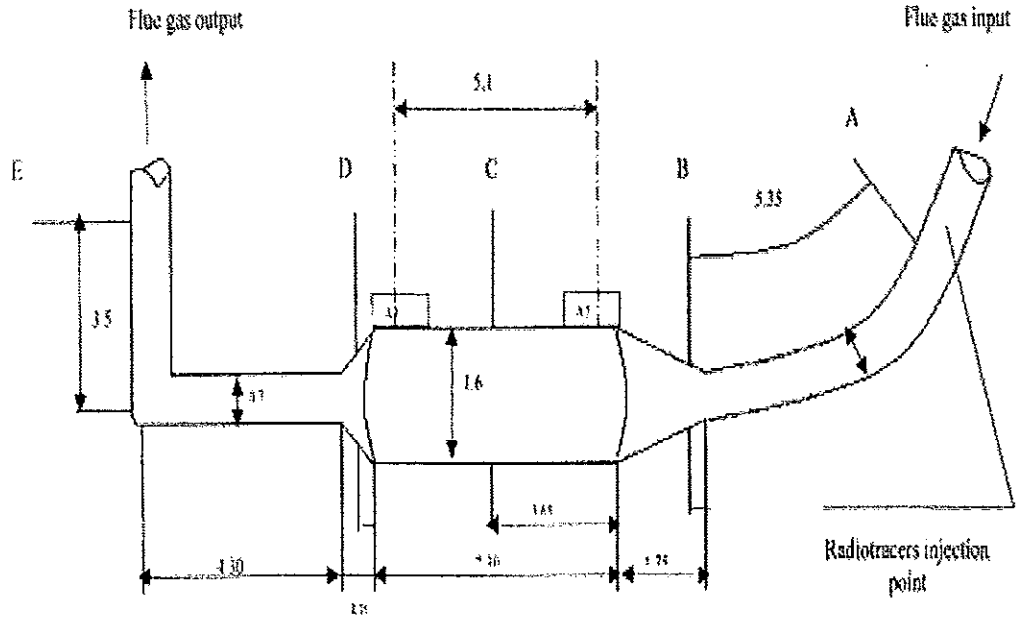

Figure 1. Principal scheme of installation for flue gas irradiation A1, A2 – accelerators; A, B, C, D, E – detectors.

RADIOTRACER EXPERIMENT

In total seven experiments were carried out. During the experiment No 1 the conditions of radiotracer investigations were established. In next experiments radiotracer Br – 82 activity was 70 MBq, time discretisation for data acquisition – 100 ms. Total duration of experiment – about 20 s.

Experiments 2, 3, 4 and 5, 6, 7 were carried out for accelerators switched off and switched on respectively. Technological parameters of installation during the experiments are presented in Table1.

Table 1. Technological parameters of installation

Experiment	2	3	4	5	6	7
Temperature (°K)	341	341	356	345	341	337
Flow rate (Nm^3/h)	5300	10400	15000	14940	10262	5028
Real flow rate (m^3/s)	1.83	3.61	5.43	5.24	3.56	1.72

Mean gas pressure in installation – 99kPa. Total volume V_{BD} = 16.9 m^3, V_{AE} = 22.4 m^3. For accelerators switched off the signals in measuring points B, C, D were registered. In experiment 5, 6, 7 (accelerators switched on) only the signals in points A and E could be measured (due to the huge scattering X – radiation around the installation). All the signals were processed using standard RTD procedures (in MATLAB software) i.e background subtraction, filtration, extrapolation, moments calculations (mean residence time, variance). Comparison of theoretical and mean residence time gives the portion of installation volume with flow stagnation Vd.

The gas flow between B – D sections of reaction vessel was modelled by serie of two piston flow regions with axial dispersion connected with region of flow stagnation. The principal scheme of the proposed model is presented in Figure 2.

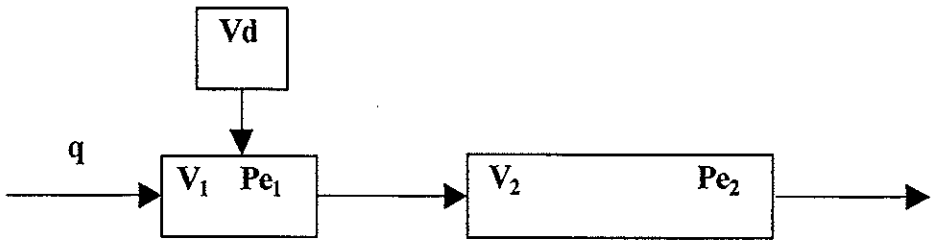

Figure 2. Flue gas flow RTD model

q is volumetric flow rate of flue gas in reactor chamber (m^3/s), Vd volume of flow stagnation (m^3), V_1 volume of dispersion model open – open (m^3), Pe_1 Peclet number for model open – open, V_2 volume of dispersion model open – closed (m^3), Pe_2 Peclet number for model open – closed.

The model parameters were optimised by comparison of experimental signals in point D with experimental signals in point B convoluted with impulse characteristic of proposed model. The comparison for experiments 2, 3 and 4 are presented in Figure 3.

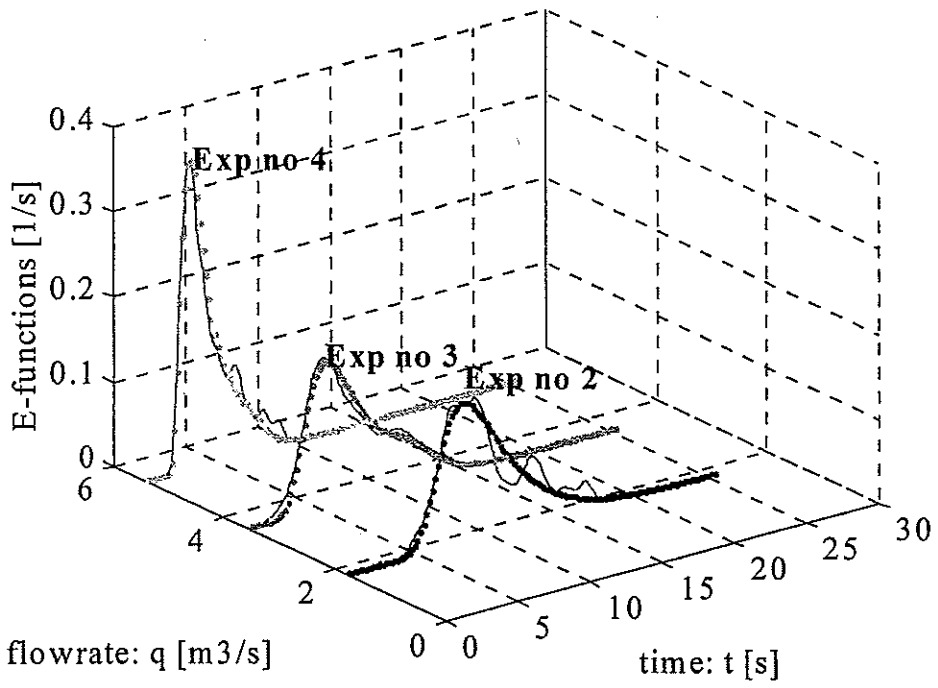

Figure 3. Comparison of experimental and model curves in outlet of installation – point D.

The results of flow parameters calculations from experimental curves and optimal model parameters are presented in Table 2.

Table 2. Gas flow characteristics and model parameters.

Experiment	TT	MRT	NDV	Pe_1	Pe_2	V_1	V_2	Vd
2	9.2	7.2	0.13	48	7.5	4.9	8.8	3.2
3	4.7	4.4	0.17	15.7	10.7	4	11.9	1
4	3.1	2.8	0.16	168	11.5	4.5	12	0.4

TT is teoretical residence time (s), MRT mean residence time (s), NDV non dimensional variance, Pe Peclet number, V volume (m^3).

The proposed , simple model, seems to be more or less adequate to physical reality of gas flow in installation. We observed the decrease of flow stagnation volume with increase of flow rate. The relations between V_1 and V_2 volumes are stable. Unfortunately the values and relations of Pe_1 and Pe_2 are not reasonable.

It can be connected with omission of radial dispersion or with irregularities in tracer injection.

CFD CALCULATIONS

Taking into account, that RTD model proposed for gas flow description is chosen more or less arbitrary, the CFD methods were used for flow structure testing. As a first step the flow with accelerators switched off was investigated. In this case we have axialy symetrical gas flow in reaction tube without heat sources so it means that it is 2D problem. For dry flue gas composition N_2 – 80.5 %, O_2 – 8.5 %, CO_2 – 11 % and traces of SO_2, NO_x the viscosity coefficients were calculated. The data concerning gas density (kg/m^3), viscosity (Pa.s) and Reynold's numbers (Re) in experiments are presented in Table 3.

Table 3. Gas properties and Re numbers in experiments

Experiment	Density	Viscosity.10^5	Re
2	1.044	1.938	78840
3	1.043	1.936	154700
4	0.992	1.983	216200

Using numerical software FLUENT 5.4 the system of appropriate Navier – Stokes (NS) and continuity equations for turbulent, incompressible gas flow were solved. For Reynold's turbulent stress determination and closure of equations system the standard model k - ε was used [2]. The method of finite volume with variable mesh size (smaller near the wall and bigger in center) was applied. The velocity fields and streamlines obtained in all experiments were similar. As an example the velocity field in experiment 3 is presented in Figure 4.

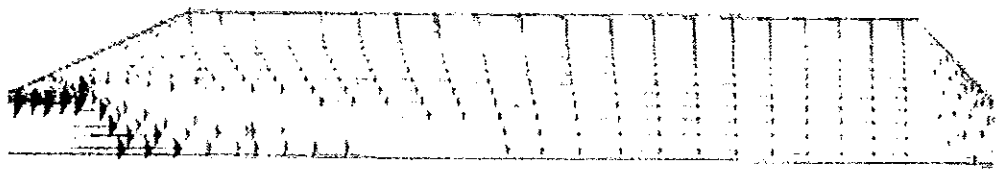

Figure 4. Velocity field obtained by CFD in experiment No 3.

In all cases the back flow near the wall of tube in the initial part of reactor is observed. Volume of this region is about 2.2 m^3. The velocity of gas is distributed uniformly in all reactor cross section only after one third of installation length. Using the Discrete Random Walk (DRW) technique (about 100000 particles injection) the RTD curves were calculated for different cross section of reactor.

The comparison of experimental and CFD RTD curves for part of reactor between B and D sections is presented in Figure 5.

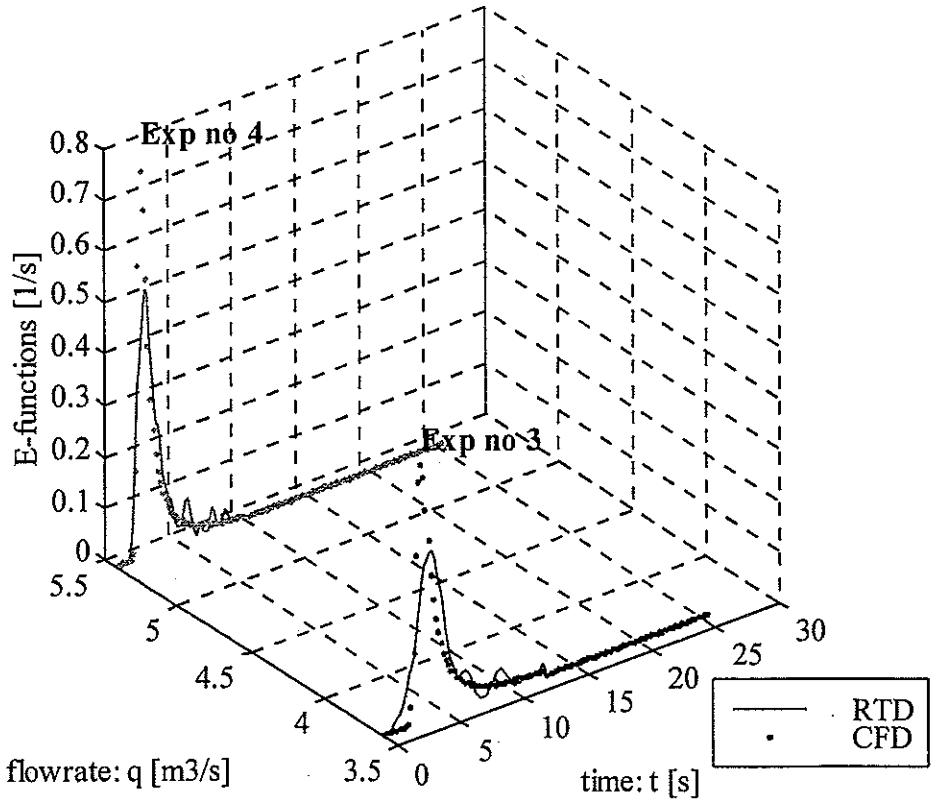

Figure 5. Comparison of RTD curves experimental and CFD for B – D part of reactor.

For identification of radial dispersion matter the injection of tracer in axis of inlet tube were simulated. The trajectories of gas particles were calculated. The results confirmed the importance of radial dispersion of tracer in initial part of reactor and necessity to take into account an exchange of mass between "dead" and active volumes of installation.

Actually the second step of CFD calculations for accelerators switch on is realised. In this case we have the gas flow in tube in presence of two heat sources, so the problem is non symetrical and 3D. Authors expect to explain the influence of accelerators operation on gas mixing conditions. From radiotracers experiments the disappearance of dead volume was observed. The results of this calculations will be presented later.

REFERENCES

[1] Chmielewski, A.G., Zimek, Z., *Nuclear technology for cleaning coal emissions*, The Environmental Challenges of Nuclear Disarmament, Ed. Kluwer Academic Publishers, (2000), 139 – 148
[2] Peyret, R., Taylor, T.D., Computational Methods for Fluid Flow, Springer – Verlag, (1983)

VISUALIZATION AND NUMERICAL SIMULATION OF CURRENT'S STRUCTURES IN FRONT OF THE WATER INTAKES OF THE LAROUSSIA DAM

Z. Hafsia[1] and K. Maalel[2]

[1] and [2] ENIT. Laboratory of Hydraulic and Environemental Modelization. B.P. 37. Belvedere, 1002, Tunisia.

Abstract. Three-dimensional currents structure analysis in the vicinity of water intakes of the Laroussia dam are based on visualization experiments on hydraulic model and numerical simulations of the flow's hydrodynamics. The study domain was discretized according to non orthogonal curvilinear grid and hydrodynamic equations are solved using the PHOENICS code (Parabolic Hyperbolic Or Elliptic Numerical Integration Code Series). The turbulence of the flow is modelised by a constant turbulent viscosity that is determined by comparing the visualized and simulated currents structure. The reduction of the upwelling of the bottom toward MCB water intake under the effect of an approach-channel is confirmed by visualized and simulated currents structure.

INTRODUCTION

The Laroussia dam is located on the low valley of the Medjerda stream. Its normal water level is fixed to 37.50 m. This dam permits to satisfy the water demand of three intakes (Figure 1) : the hydroelectric power station (C), the Great-Channel (GC) and the Medjerda-Cap-Bon (MCB) deriving respectively a maximum discharge of 50 m^3/s, 13 m^3/s and 16 m^3/s. The GC and MCB intakes allow to satisfy irrigation and drinking water demand. Since 1989, an islet of mud deposits has been observed in front of the MCB intake and an important quantities of deposits have been recorded along MCB channel.

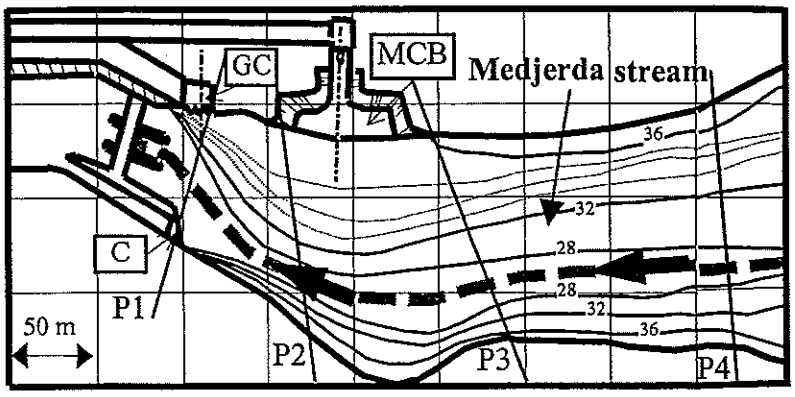

Figure 1. Location in plan of three water intakes of the Laroussia dam.

To identify and thereafter analyze the effects of currents structure in the observed mud deposits, visualization experiments on an hydraulic model with fixed bed have been realized. This approach allows to overcome the difficulties to reproduce the movement of suspension particles in hydraulic model with mobile bed [3].

To overcome the costs and delays of construction and exploitation of hydraulic models, often very large, several computational fluid dynamics (CFD) code have been used simultaneously to hydraulic model studies for waterworks design (spillway, energy dissipation basin, intake structures) and to verify the efficiency of the proposed sediment control devices [1 and 8]. However, the predetermination of the three-dimensional currents structure in the complex geometric configurations remains confronted to certain difficulties associated to the grid generation of the study domain and to the definition of boundary conditions.

Qualitative analysis of the visualized and simulated flow structure in the Laroussia dam reservoir, allows to explain the main causes of mud deposits in front of the MCB intake and therefore to propose a sediment control device in order to reduce the entrance of muds in the MCB channel.

DESCREPTION OF THE HYDRAULIC MODEL AND BASIC EQUATIONS OF THE MATHEMATICAL MODEL

1- Hydraulic model

It is a fixed bed model constructed on a rectangular experimental channel having 12.18 m long, 2.00 m wide and 0.6 m depth. In a turbulent free surface flows, it is essential to satisfy the similarity of the volume forces (inertia and gravity) and surface forces (viscous and turbulent shear stress). Therefore, it is necessary to conserve the same Froude number and Reynolds number in the hydraulic model and on the field scale. For a given relative roughness, it is sufficient to conserve the same flow regime on the model and the prototype, for roughly turbulent flow [7]. This implies that the Reynolds number is at least equal to 1400 according to Henderson, and that the Froude similarity is also satisfied. A distorted hydraulic model is adopted to take into account these limitations and the imposed dimension of the experimental channel. This distortion, defined as the ratio of the vertical scale ($h_r = 1/25$) to the horizontal scale ($L_r = 1/100$), is taken equal to $\Delta = h_r/L_r = 4$. The visualization experiments are realized in the normal operating flow conditions : the three Laroussia dam gates are closed and water reservoir level is maintained fixed to its normal level, 37.50 m. The derived discharge through each water intake is taken equal to the maximal discharge.

2. Mathematical model

The hydrodynamic model is based on mass and momentum conservation equations. For a steady flow and incompressible fluid and by choosing covariant velocity components as independent variables, these equations is written as [2] :

$$(g^{jk} U_k)_{;j} = 0 \qquad i = x, y, z \tag{1}$$

$$\rho (g^{jk} U_i U_k)_{;j} - \rho(\nu + \nu_t)\left(g^{jk} U_{i;k}\right)_{;j} = -p_{;i} \qquad i = x, y, z \tag{2}$$

with, U_i : covariant velocity components; ρ : water density; ν : kinematic viscosity of fluid; ν_t : turbulent viscosity; g^{jk} contravariant metric tensor; (;) covariant derivatives.

According to the number of transport equations considered to determine the turbulent viscosity field, different types of turbulence models are distinguished : with zero, one or two transport equations [10]. In the case of the Laroussia dam reservoir, we adopted a constant turbulent viscosity model. This implies that the turbulence is dissipated where it is produced.

Boundary conditions of the three-dimensional hydrodynamic model given by equation (1-2), concern the definition of inflow, outflow, the rigid wall, free surface conditions. At the inlet, longitudinal velocity component is assumed to have a uniform distribution determined by the corresponding inlet discharge (the discharge ratio is equal to Q_r = 1/12500). At the MCB intake exit, the horizontal velocity components are fixed from results of the depth-averaged two-dimensional hydrodynamic model [6]. We adopted the classical conditions with logarithmic profile of the streamwise velocity as conditions on the bottom and lateral walls of the reservoir. The free surface is treated as a rigid wall without friction.

In PHOENICS code, the transport equations is discretized by the finite volume method. The algorithm for treatment of pressure-velocity coupling is the SIMPLEST algorithm based on a sequence of prediction-correction of pressure and velocity fields until the balance of mass and momentum are satisfied [9].

ANALYSIS OF THE FLOW STRUCTURE

1. Upwelling and interaction of currents before modification

Photo 1 shows the visualized bottom current, obtained using the fluoerescine, from the right bank of the cross profile P4 in the case of the MCB intake opening with its maximum discharge, Q = 1.3 l/s (16 m^3/s on the prototype). After the bottom current ascention along the right bank, these currents are derived by the MCB intake with a less marked curvature far away from this intake. The comparison between experimental and numerical results shows that the streamlines for $\nu_t = 5\ 10^{-5}$ m^2/s have the tendency to better reproduce the curvature of these streamlines. Hence, the zone covered by these currents is the same that the observed one (figure 2).

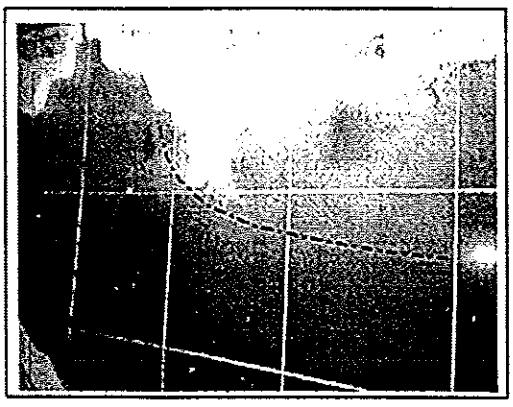

Photo 1. Bottom currents upwelling from profile P4 (Q_{der} = 1.3 l/s).

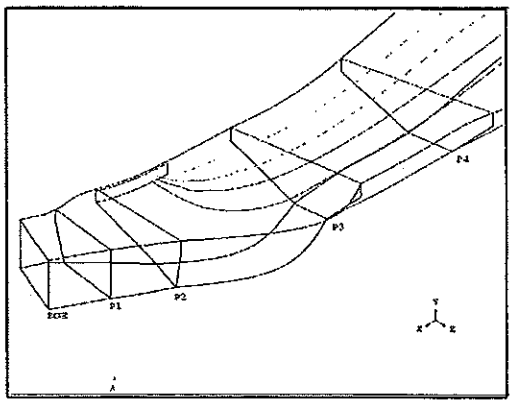

Figure 2. Simulated bottom currents from profile P4 (Q_{der} = 1.3 l/s).

Photo 2 shows bottom currents in front of the MCB intake, visualized using grains of potassium permanganate. The upwelling of these currents along the length of the MCB intake crest, fixed at 34.84 m, explains the sediments entrance in the MCB channel. The analysis of surface currents shows the existence of two recirculation zones on the two sides of the two gates of MCB intake.

The visualized bottom currents, using the permanganate of potassium, when the GC intake is opened are represented in photo 3. These currents is deviated by the GC intake with no recirculation zone. The visualized surface currents showed that these currents are also deviated by the GC intake with no recirculation zone. These results are confirmed by hydraulic model studies achieved by Combes in 1953 : the shape and orientation of the GC intake lead to a correct alimentation conditions [4].

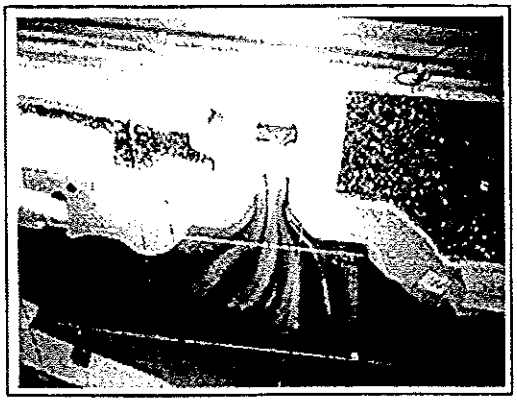

Photo 2. Bottom currents upwelling in vicinity of the MCB water intake (Q_{der} = 1.3 l/s).

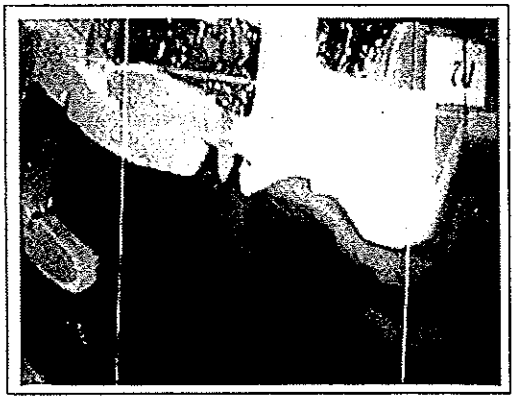

Photo 3 : Bottom currents upwelling in vicinity of the GC water intake (Q_{der} = 1.0 l/s).

Relative to the individual opening of each intake, the interaction of bottom currents between the MCB and GC intakes results in a modification of the streamlines curvature in the adjusting zone of these two intakes (photo 4). The observations on the hydraulic model show that this interaction zone is a stagnation zone (or a deposit zone). Figure 3 represent four streamlines in the vicinity of the MCB and GC water intakes coming from the profile P4. The three streamlines Lc(F), Lc(RD) and Lc(RG) come respectively from the mid-width of the bottom and the mid-height of the right bank and the left bank of the cross profile P4. The fourth streamline Lc(RG') comes from slightly below the Lc(RG'). The two streamlines Lc(RD) and Lc(F) are deviated toward the MCB intake and they are not influenced by the opening of the GC intake. Under the effect of the GC intake, Lc(RG) is deviated by this intake, whereas Lc(RG') is deviated by the MCB intake. The comparison between the visualized and simulated currents, for a turbulent viscosity $\nu_t = 5\ 10^{-5}\ m^2/s$, shows that the general tendency of bottom currents is comparable and that the interaction between this two intakes is limited to the adjusting zone between the two intakes (figure 3).

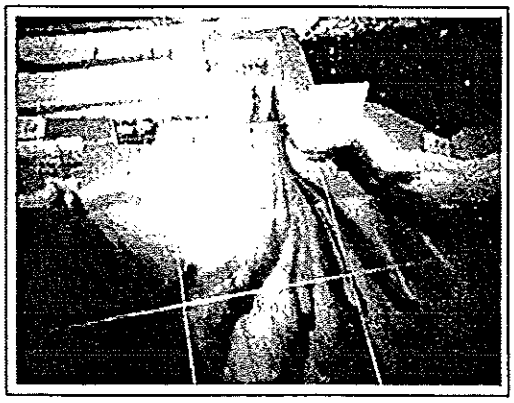

Photo 4. Bottom currents interaction in vicinity of the MCB and GC water intakes (Q_{der} = 2.3 l/s).

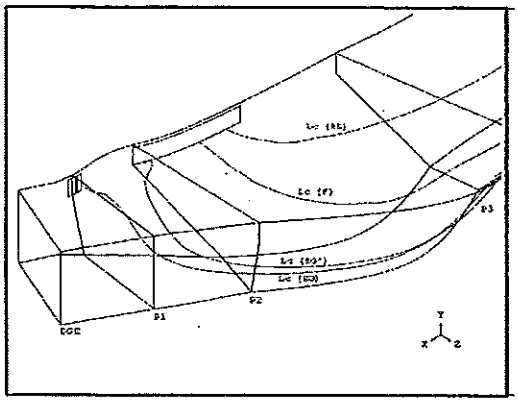

Figure 3. Simulated currents structure (Q_{der} = 2.3 l/s).

For other working cases of the Laroussia dam intakes, other interaction mechanisms of surface and bottom currents are observed.

2. Currents structure modification

To reduce the entry of muds in the MCB channel, it is therefore primordial to modify the direction of bottom currents, which transported a high proportion of sediment, in order to reduce their upwelling toward the MCB intake. In this purpose, three alternatives of training walls are studied. Results of the visualized and simulated currents permitted to develop a comparison criteria between these three alternatives [5]. The retained alternative consists in a training wall opened by its downstream extremity. By a rigorous choice of the shape of the MCB intake, a new alternative device that consists in an approach-channel implanted at the entrance of the MCB intake (photo 5).

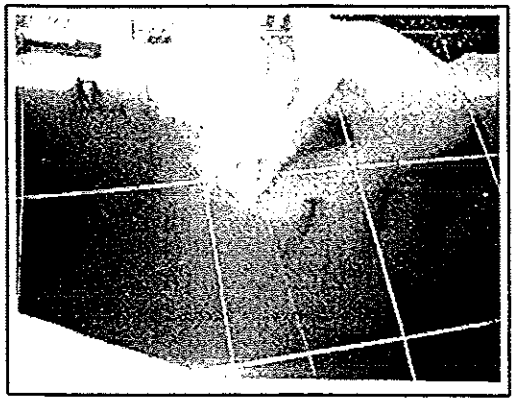

Photo 5. Reduction of the bottom currents upwelling (Q_{der} = 1.3 l/s).

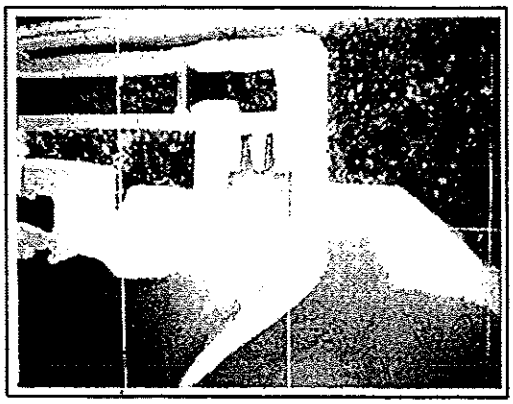

Photo 6. Surface currents structure (Q_{der} = 1.3 l/s).

Under the effect of this approach-channel, the visualized bottom currents in the vicinity of the MCB intake show a well marked reduction of the bottom currents upwelling toward this intake (photos 5 and 2). Photo 6 shows surface currents in the vicinity of the MCB intake, visualized by using a powder of milk. The analysis of the structure of this currents shows that no recirculation or detachment zone is recorded to the entrance of MCB intake.

These results are confirmed by analyzing secondary currents structure on the cross profile P3 situated upstream of the MCB intake (the location of this profile is presented in Figure 1). Figure 4 shows these current's structure in the case of the MCB opening. Without sediment control device, the secondary currents on the right side bank, in which the MCB intake is located, are ascending toward the MCB intake. These current's direction is inversed under the effect of the approach-channel.

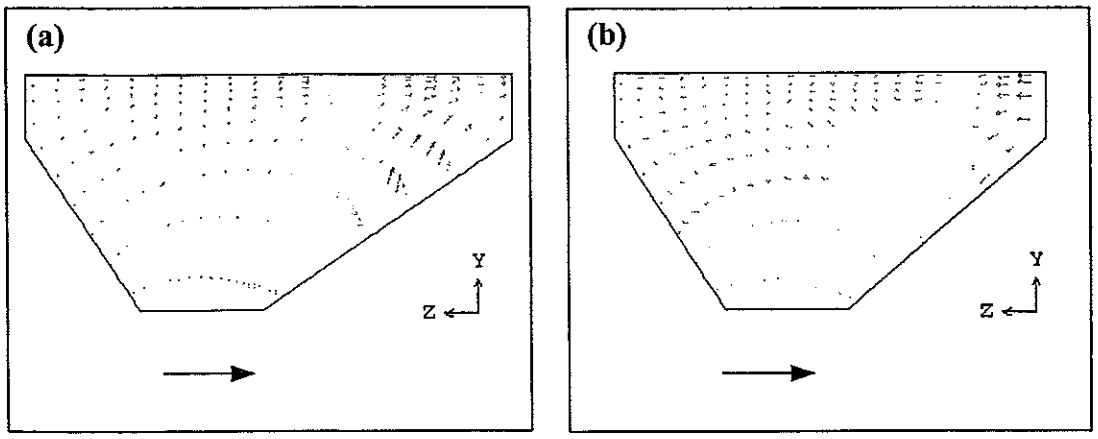

Figure 4. Simulated secondary currents structure on the cross profile P3 upstream of the MCB intake (Q = 1.3 l/s).
a) Without sediment control device. b) With approach-channel.

This inversion is expected to reduce bottom currents upwelling toward the MCB intake and therefore the entrance of muds in this intake. Their effect extend along a distance of about 0.31 m upstream of the MCB (corresponding to 31 m on the prototype). This approach-channel also favorizes the MCB intake alimentation by water coming from nearby the dam which is much clear due to the very low velocity in this region.

CONCLUSION

In accordance with visualized currents structure on the hydraulic model of the Laroussia dam, the numerical simulations replicate correctly the bottom currents upwelling toward the MCB water intake as well as the interaction zone, when MCB and GC intakes is opened simultaneously. The reduction of the bottom currents upwelling under the effect of an approach-channel is associated to the secondary current inversion at the upstream of the MCB intake. This inversion has for consequence to reduce the entrance of sediments in the MCB channel.

REFERENCES

[1] Atkinson, E. - Predicting the performance of sediment control devices at intakes. OD/TN 41 (1989).
[2] Beale, S. B. – Fluid flow and heat transfer in tube banks. Thesis submitted for the degree of Doctor of Philosophy. Imperial College (1992).
[3] Bouvard, M. - Barrages mobiles et ouvrages de dérivation à partir de rivières transportant des matériaux solides. Eyrolles (1984).
[4] Combes, G. et Beranger, J. - Barrage de Taullerville -El Aroussia. Définition des ouvrages (1953).
[5] Hafsia, Z. et Maalel, K. - Simulations numériques en 3-D des écoulements au voisinage de la prise d'eau Medjerda-Cap-Bon. Choix d'une variante d'aménagement. Accepté pour publication à la Septième Conférence Annuelle de la CFD. Halifax, Canada, 30 mai-1er Juin (1999).
[6] Hafsia, Z. et Maalel, K. - Three-dimensional hydrodynamic model coupled with depth averaged two-dimensional model : Case of the Medjerda-Cap-Bon water intake. 8th International PHOENICS User Conference 17-21 may (2000).
[7] Henderson, F.M. - Open channel Flow. Macmillan (1966).
[8] Higgs, James A. - Folsom Dam Spillway Vortices Computational Fluid Dynamic Model Study. Water Resources Research Laboratory (1997). http://ogee.do.usbr.gov/jhiggs/folsom/
[9] Patankar, S.V. - Numerical heat transfer and fluid flow. Hemisphere Publishing Corporation (1980).
[10] Schiestel, R. - Modélisation et simulation des écoulements turbulents. Hermes (1993).

A A3 - NEW TRACERS AND DETECTORS OR IMPROVEMENT AND DEVELOPMENT OF EXISTING TRACING METHODS

MODELING AND ON-LINE MEASUREMENT OF OVERALL AND LOCAL RESIDENCE TIME DISTRIBUTIONS IN EXTRUDER REACTORS

Guo-Hua HU

Laboratoire des sciences du génie chimique, CNRS-ENSIC-INPL, 1 rue Grandville, BP 451, 54001 Nancy Cedex, France. hu@ensic.inpl-nancy.fr

Abstract. Today, screw extruders are important reactors in the polymer industry. This paper reports some of the progresses in modeling and on-line measurement of overall and local residence time distributions (RTD) in extruder reactors. They are important for process design, diagnosis, optimization and control.

INTRODUCTION

Screw extruders are the most important polymer processing equipment. Over the last two decades, they have gradually been transformed to chemical reactors, owing to joint efforts of chemical and mechanical engineers. This new type of chemical reactor, called extruder reactor or reactive extruder, has many distinct features and advantages compared to classical reactors and is particularly suited to highly viscous chemical systems such as solventless polymerization [1-2]. Extruder reactors have become important reactors in the polymer industry to supplement classical ones. They are used to perform tasks classical polymerization reactors would not be able to do in a suitable fashion [1-2]. They also have begun to invade more and more areas which long belong to classical polymerization reactors. The use of screw extruders as chemical reactors to deliberately perform chemical reactions of polymers or polymerizable monomers is commonly called reactive extrusion.

Residence time distribution (RTD) is an important process parameter for continuous reactors. This parameter is not easy to obtain theoretically nor experimentally for extruder reactors . The difficulty in modeling the RTD in a (single or twin) screw extruder compared with a classical chemical reactor results mainly from complicated geometry of the flow path and complicated thermal and rheological properties of polymers. Thus the RTD in an extruder reactor is often obtained by measurements. Most of the time, only the overall RTD of the extruder from its hopper (the main entrance) and the die (the main exit) is measured. A reactive extrusion process is often an integration of a certain number of more or less interdependent and sequential unit operations along the extruder reactor length such as solids feeding, solids conveying, melting/plastification, mixing, reaction, side feeding, devolatilization, pumping and shaping. This is particularly so for modern twin screw extruder reactors. Their individual unit operations are more or less well demarcated by special mixing and/or pressure consuming elements. Therefore, it is important to know not only the overall RTD of the entire extruder reactor but also the local RTD of each of these functional zones in order to optimize the process. Unfortunately, local RTDs are usually difficult to obtain by measurements.

The aim of this paper is to report some of the progresses in modeling and measurement of the overall and local RTDs in twin screw type extruder reactors made in the author's laboratory.

MODELING OF OVERALL AND LOCAL RTDs

A statistical theory for residence time distribution

Flow mechanisms passing through screw channels and boundaries between screw elements in series in particular are often very complicated. Thus development of RTD models in screw extruder reactors remains difficult. This is particularly so for twin screw extruder reactors. To simplify the problem, a statistical theory for RTD is elaborated and then used to develop RTD predictive models in extruder reactors [3-7]. The basis of the theory is that for flow passing through the junction or boundary of a system composed of two elements in series, if fluid particles leaving the first element have the same probability to occupy a given position at the entrance of the second one, the RTDs in these two elements are statistically independent of each other. Then the overall RTD can be calculated from the individual RTDs using a statistical method [3]. Consider a system consisting of n statistically independent elements connected in series of which the residence time density functions are $f_1(t)$, $f_2(t)$, ..., $f_n(t)$ (Figure 1).

Element 1 $f_1(t)$	Element 2 $f_2(t)$	.....	Element n-1 $f_{n-1}(t)$	Element n $f_n(t)$

f(t)

Figure 1. n elements in series.

The overall f(t) and the individual ones are related, in the Laplace domain, by

$$\bar{f}(s) = \bar{f}_1(s)\bar{f}_2(s).....\bar{f}_n(s) \tag{1}$$

or in the convolution time domain by

$$f(t) = \int_0^t f_1(\tau_1)\int_0^{t-\tau_1} f_2(\tau_2)...\int_0^{\tau_{n-3}-\tau_{n-2}} f_{n-1}(\tau_{n-1})f_n(\tau_{n-2}-\tau_{n-1})d\tau_{n-1}...d\tau_2 d\tau_1 \tag{2}$$

For a combination of two elements, equation 2 reduces to:

$$f(t) = \int_0^t f_1(\tau)f_2(t-\tau)d\tau \tag{3}$$

As discussed in [3], the statistically independent RTDs in elements in series physically implies that perfect two-dimensional mixing (radial mixing) exists at the junction or boundary between any two adjacent elements so that fluid particles at this location are totally randomized. In order words, the residence time that a particle acquires in the first element has no bearing on its residence time in the second element.

Validation of the statistical theory for RTD in extruder reactors

Before using the above statistical theory for modeling RTD in extruder reactors, one first has to verify its validity and applicability. The key question is whether there are locations along the extruder length where two-dimensional perfect mixing is achieved. It is experimentally confirmed that such locations do exist and correspond to those of high shear, elongational or squeezing mixing elements such as kneading discs and calender gaps [3-7]. The latter are able to randomize fluid particles over the entire sections so that equation (2) or (3) is applicable. Three types of extruder reactors are subjected to verification: a single screw extruder and two different counter-rotating twin screw extruders (CRTEX): intermeshing and non-intermeshing. For the single screw extruder and the intermeshing CRTEX, a long die having a long cylindrical channel is used to measure the RTD in the screw and long die combinations. A short die is used as an adapter to measure the RTD of the single or twin screw (the volume of its channel is very small so that the residence time in it is negligible). The overall RTDs in the screw and long die combinations, f(t), and those in the screws, $f_1(t)$, are measured. That in the long die, $f_2(t)$, is calculated. Figures 2a and 2b show that there is a good agreement between the measured f(t) and that predicted by the statistical theory, i.e., equation (3). This implies that fluide elements at the junction between the die and the single screw tip or between the die and the twin screw tip are well mixed so that the statistical theory applies.

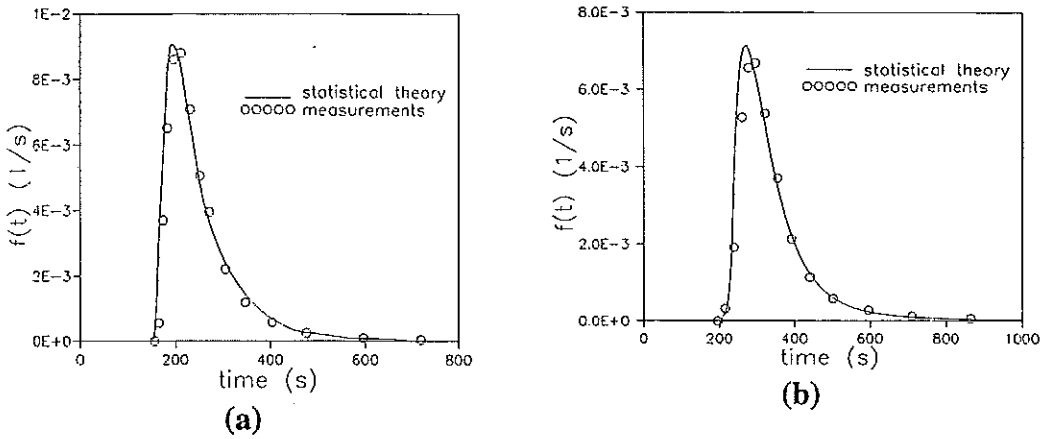

Figure 2. Comparison between the RTD functions predicted by equation (3) and the measured ones. (a) single screw and long die combination; (b) twin screw and long die combination.

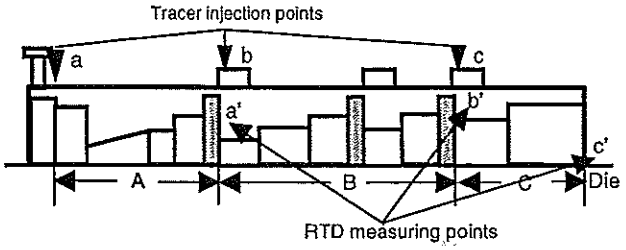

Figure 3. Locations for the tracer injection and tracer response measurement; and division of extruder reactor zones.

The non-interemshing CRTEX has screw diameter of 20 mm and a length/diameter ratio of 72. It is divided into three zones, A and B et C (Figure 3).

They are separated by two compounders. The RTD functions in these three zones are obtained by a tracer technique. For example, tracer injection at point a and its response measurment at point a' allows to obtain the RTD in zone A. The statistical theory and the experiment are in excellent agreement for the combination of A and B zones (Figure 4a) and that of A, B and C zones (Figure 4b). This shows that compounder induced mixing is strong enough for the statistical theory to be valid.

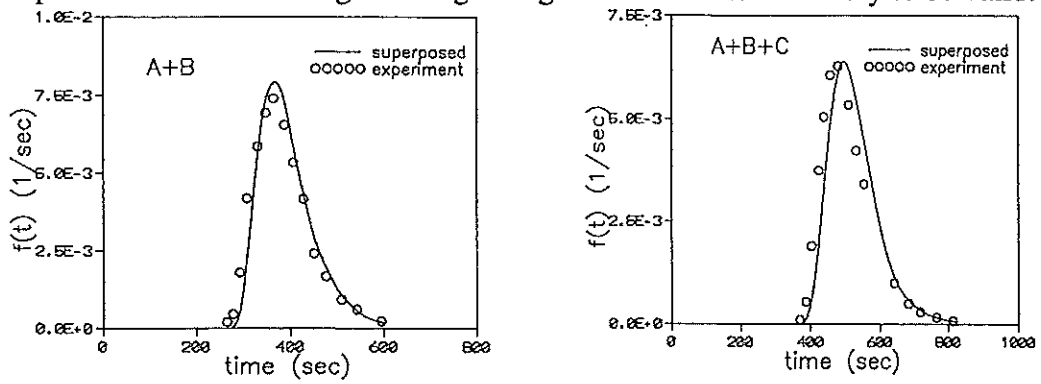

(a) (b)

Figure 4. Comparison between the RTDs predicted by the statistical theory and measurements. (a) A and B zone combination; (b) A, B and C zone combination.

Development of RTD predictive models for extruder reactors

Two different types of CRTEX are considered: intermeshing (Figure 5a) and non-intermeshing (Figure 5b). An intermeshing CRTEX can be treated as being consisting of C-chambers connected in series. Every single C-chamber is considered as an element, and leakage flows at the boundaries of each pair of elements are assumed to be totally randomized by squeezing forces due to the screws rotating in opposite directions. A non-intermeshing CRTEX can be either staggered or matched. Here the matched screw configuration is examined. The entire extruder is composed of individual turns of screw connected in series because there is an interaction area (apex area) between every turn of the screw channel. Strong mixing exists in the apex area, where discontinuity of the flow fields develop. If the flow is sufficiently randomized in these areas, the RTD functions in any two adjacent turns of the screw channels are independent of each other and the overall RTD in the extruder can be calculated from the RTDs of the individual turns of screw channel.

If the screw curvature is neglected, the C-chambers of the intermeshing CRTEX and the individual turns of the non-intermeshing one can be treated as straight rectangular channels. The RTD function in each straight rectangular element can be calculated using the following analytical expression developed originally for a single screw extruder [8]:

$$f(t)dt = \frac{3\xi\left[1-\xi+\sqrt{1+2\xi-3\xi^2}\right]}{\sqrt{1+2\xi-3\xi^2}}d\xi \qquad (4)$$

$$t(\xi) = \left[\frac{l}{3V_b\left(1+Q_p/Q_d\right)}\right]\frac{3\xi-1+3\sqrt{1+2\xi-3\xi^2}}{\xi\left[1-\xi+\sqrt{1+2\xi-3\xi^2}\right]} \quad 2/3 \le \xi \le 1 \qquad (5)$$

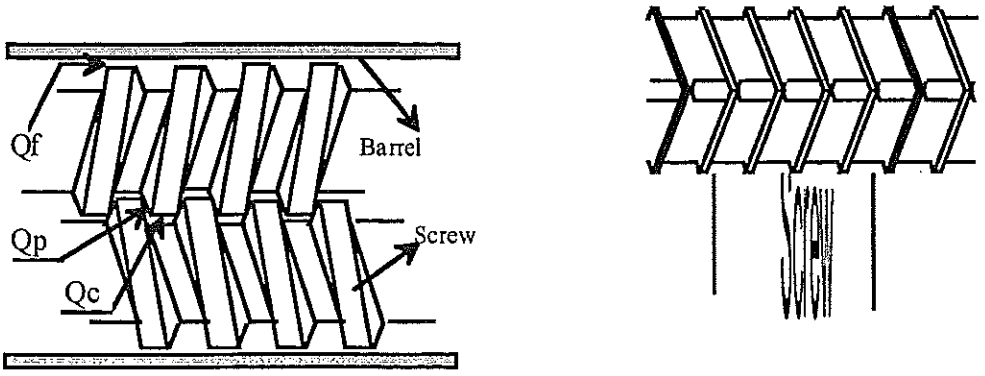

(a) (b)

Figure 5. Two different types of CRTEX and associated leakeage flows. (a) intermeshing; (b) non-intermeshing.

The above RTD models describe very well experimental results for both the intermeshing and non-intermeshing CRTEX (Figure 6). It should be pointed out that the success of these models is mainly attributable to the incorporation of the statistical theory. The use of this theory only requires perfect two-dimensional mixing at chosen boundaries for division of elements, which can be met in screw extruders of which the flow channels are usually very long and narrow. By virtue of such flow channels, two-dimensional perfect mixing can be readily achieved at the locations of high shear, elongational or squeezing mixing elements such as kneading discs, calender gaps, apex areas and compounders so that fluid particles at these locations can be distributed randomly across the entire sections to which equation (2) or (3) can be applied. By contrast, three- dimensional perfect mixing is much more difficult to achieve in screw extruders just because of the long and narrow nature of the screw channels.

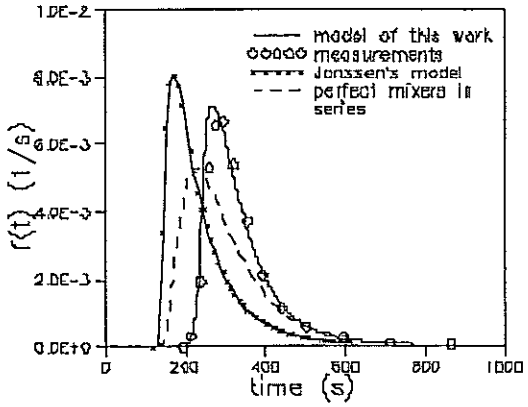

Figure 6. Schematic representation of two different counter-rotating twin screw extruders and associated leakage flows. (a) intermeshing; (b) non-intermeshing.

ON-LINE MEASUREMENT OF OVERALL AND LOCAL RTDs

Tracer Selection

Strictly speaking, a measured distribution is that of the tracer particles or molecules themselves. In order for the measurement to reflect accurately the RTD of the fluid stream of interest, the tracer should have exactly the same flow properties as the molecules or particles it represents, and yet it is sufficiently different in some

nonflow attribute that it can be detected by an analytical instrument. Three antracene tracers (Figure 7) of very different thermomechanical properties are tested in a co-rotating self-wiping twin screw extruder using polystyrene as polymer model system. It is found that as as large as the difference of dispersion among the three tracers may be, it could not be reflected in the measured RTD [9].

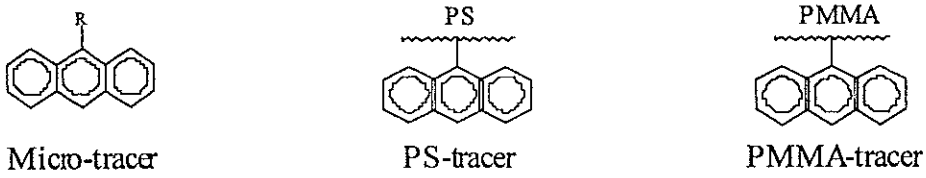

Figure 7. Three tracers of very different thermomechanical properties

On-line measurement

Determination of the RTD can be done either off-line or on-line. The second approach has many advantages over the first one as it is much less tedious and time-consuming. Also it provides real time information about the RTD, which is important for process design, diagnosis, optimization and control. A fluorescence monitoring device is constructed to measure in real time the RTD function in screw extruders [10]. Its centerpiece is an optical fiber probe capable of transmitting optical excitation energy to the processed flow stream and detecting the subsequent fluorescence emission (Figures 8). The source of fluorescence emission is an antracene bearing substance (Figure 7). In addition to its reliability (Figure 9) and great sensitivity to fluorescence emission and ease of implementation on an extrusion line, this device can be used to monitor and diagnose in real time subtle variations of an extrusion operation including reactive extrusion.

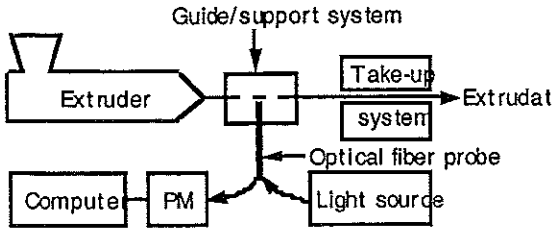

Figure 8. A schematic diagram of the fluorescence monitoring device for on-line measurements of the overall RTD (PM is a photomultiplier) in an extruder reactor.

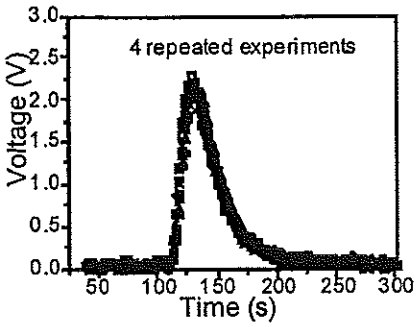

Figure 9. Illustration of the reliability in terms of reproducibility of the fluorescence monitoring device with 4 repeated overall RTD measurements under the same conditions.

Local RTDs in sequential zones of extruder reactors

The above one-line RTD measurement device can also allow to obtain local RTDs in extruder reactors, which are very important for process diagnosis, optimization and/or control. For illustration purpose, consider a simple screw profile consisting of three main zones: solids conveying, melting (KB) and pumping (Figure 10). The RTD functions, $f(t)$, $f_b(t)$ and $f_c(t)$, can be obtained when the device is implemented at the die exit and the tracer is injected at the hopper, just before the melting zone and just after the melting zone, respectively (Figure 10a). The use of the statistical theory, equation (3), allows to obtain local RTDs in the solids conveying, $f_1(t)$, and the melting zone,

$f_2(t)$ (Figure 10b). In principle, the above device can be implemented inside the barrel all along its length. Attempts were made to place a silica optical probe just before and after the melting zone [10]. It turned out that the probe did not last long because of severe thermomechanical conditions (high temperature, high pressure and high shear). Also the signals obtained were very noisy.

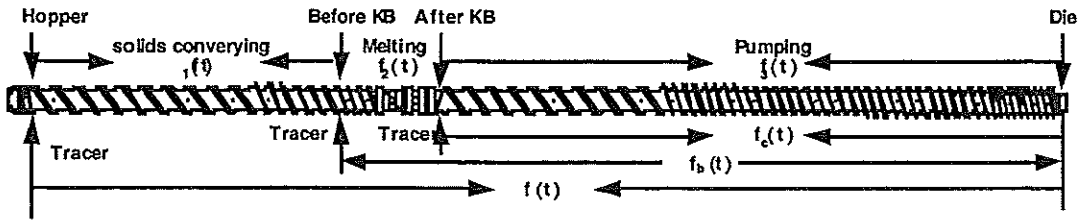

Figure 10. Screw profile of a co-rotating self-wiping twin screw extruder and various tracer injection points for determining local RTDs.

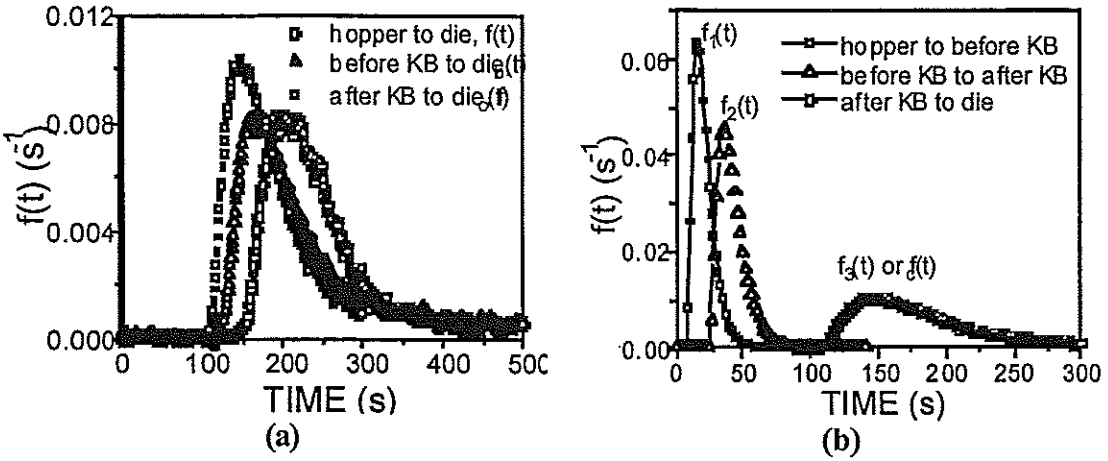

Figure 11. (a) Measured RTDs in three different zones: from hopper to die, f(t); from "before KB" to die, $f_b(t)$; from the after KB to die, $f_c(t)$; (b) Local RTDs in three different zones calculated using the statistical theory: from hopper to before KB, $f_1(t)$; from before KB to after KB, $f_2(t)$; from after KB to die, $f_3(t)$.

CONCLUDING REMARKS

Various issues concerning modeling and on-line measurement of overall and local residence time distributions in various types of screw extruder reactors are discussed. Progresses made in various theoretical and technical aspects are useful for design, diagnosis, optimization and control of reactive extrusion processes. Nevertheless, more work is necessary.

REFERENCES

[1] Hu, G.H., Lambla, M., "Fundamentals of reactive extrusion: An overview", chapter 6 (pages 345-400) of the Encyclopaedia "*Materials Science and Technology*", ed. R. W. Cahn, P. Haasen and E.J. Kramer, Vol. 18 "Processing of Polymers", ed. H.E.H.H. Meijer, VCH, Munich (1997).

[2] Hu, G.H., "Reactive Polymer Processing: Fundamentals of Reactive Extrusion", a chapter of the Encyclopaedia "*Materials Science and Technology*", ed. R. W. Cahn, P. Haasen and E.J. Kramer, Vol. "Processing of Polymers", ed. H.E.H.H. Meijer, VCH (2001).

[3] Chen, L., Hu, G.H., "Application of a statistical theory to residence time distribution", *AIChE. J.*, 39 (1993), 1558.

[4]. Chen L., Pan, Z., Hu, G.H., "Residence time distribution in screw extruders", *AIChE. J.*, 39 (1993), 1455.
[5] Chen, L., Hu, G.H., Lindt, J.T., "Residence time distribution in non-intermeshing counter-rotating twin screw extruders", *Polym. Eng. & Sci.*, 35 (1995), 598 - 603.
[6] Hu, G.H., Kadri, I., "A novel on-line technique for measuring the residence time distribution in screw extruders", *Proceedings of the 13th Polymer Processing Society European Regional Meeting* (August 19-21, 1997), Gotherburg, Sweden
[7] Guo-Hua HU, "Issues concerning the residence time distribution in screw extruders: Tracer Selection; On-Line Monitoring and Multiphasic Polymeric Systems.", *Polymer reaction engineering, DECHEMA monographs*, 137 (1998), 577-586, Wiley-VCH Verlag GmbH.
[8] Pinto, G, Tadmor, Z., "Mixing and residence time distribution in melt screw extruder", *Polym. Eng. Sci.*, 10 (1970), 279-288.
[9] Hu, G.H., Kadri, I., "Preparation of macromolecular tracers and their use for studying the residence time distribution of polymeric systems", *Polym. Eng. Sci.*, 39 (1999), 200.
[10] Hu, G.H., Kadri, I., Picot, C., "On-line measurement of the residence time distribution in screw extruders", *Polym. Eng. Sci.*, 39 (1999), 930.
[11] Yu, Q., unpublished doctorate work, EAHP-Université Louis Pasteur de Strasbourg, France (1997).

SYNTHESIS OF A 5'-OH DEOXYNUCLEOSIDE FLUORESCENT PHOTOLABILE PROTECTING GROUP

C. Muller[1], M.L. Viriot[1], M.C. Carré[1]

[1] Département de Chimie Physique des Réactions, UMR 7630 CNRS-INPL, Groupe ENSIC, 1 rue Grandville BP 451, 54001 Nancy Cedex, FRANCE

Abstract. A fluorescent photolabile group, based on coumarin and MeNPOC was synthesized to protect 5'-OH terminal function of thymidine (T). Photodeprotection under a 365 nm irradiation was performed, then photochemical and photophysical properties were studied. Photocleavage is not affected by the fluorophore, but the deprotection quantum yield is slightly lowered. Fluorescence properties of the probe due to the coumarin structure are remained during and after irradiation, which is satisfying for the application required, i.e., the *in situ* synthesis of DNA microchips.

INTRODUCTION

Over the past few years the fabrication of high-density DNA microarrays has been of central importance in the biotechnological field [1], especially for biological analysis and the development of new DNA sequencing methods. Within this context, we focused our research on the synthesis of 5'-hydroxyl terminal function protecting groups of deoxynucleosides, particularly useful in light-directed combinatorial synthesis. Since photolabile molecules are mainly used as nucleic acids or peptides protecting groups, we developed new ones with fluorescent properties.

Actually photolabile protecting groups, with a permanent fluorescent moiety may allow visualization of support grafting during *in situ* synthesis of oligonucleotides, and quantification of photocleavage after irradiation at 365 nm. Moreover these probes may encode for each deoxynucleoside if they do not show the same photophysical properties.

When we started this project, only scarce examples of fluorescent photolabile protectors were described in the literature [2]. Moreover the fluorophore used by Burgess et al. is a dansyl derivative whose absorption domain is around the irradiation wavelength (365 nm) and therefore it is not proper to our application. Despite some low photolytical efficiency rate and yield, these authors have enlarged their studies on the synthesis of nucleoside triphosphates with 3'-O-blocking photolabile fluorescent groups [3-4].

Two different approaches are possible to the achievement of these protecting groups (figure 1):

- the first one involves the synthesis of a photolabile molecule that shows intrinsic fluorescent properties, or liberate a fluorescent part after irradiation,

- the second one implies the binding of four different fluorophores to the same photolabile group, which facilitates the choice of the molecules because the two properties are not bore by the same group.

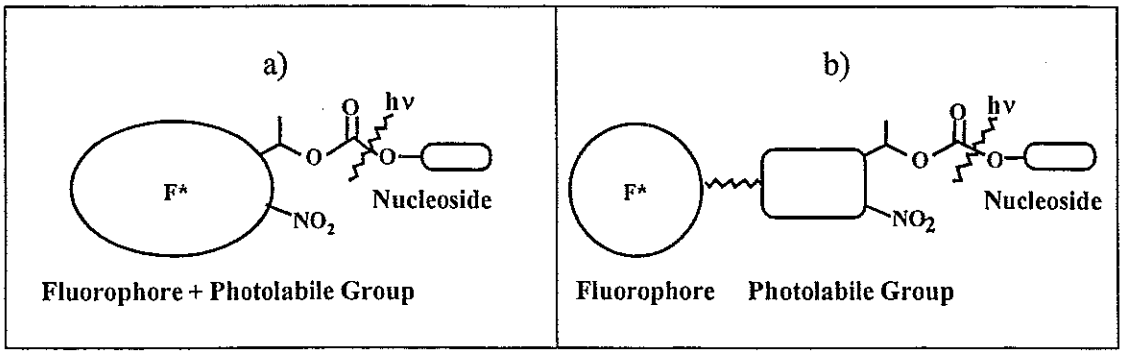

Figure 1. Description of the two syntheses pathways
a) a fluorescent photolabile molecule grafted to the nucleoside
b) a fluorophore coupled to a photolabile group grafted to the nucleoside

The synthetic pathway we followed to assess fluorescent photolabile groups is the second one, it has parallel with chemistry developed for solid-phase photolabile linkers [5]. Therefore we chose to use four fluorophores bound to the same photolabile group. As α-methyl-2-nitropiperonyloxycarbonyl group (MeNPOC) exhibits good photolytic properties in the DNA microarray application [6], it was chosen and modified to be grafted to the different fluorophores *via* an aminolinker. The fluorophores have been selected according to their absorption and emission wavelengths, which have to be higher than the photolytic one (λ = 365 nm).

Concerning the choice of fluorescent molecules, we first used a coumarin derivative, compound 3 on figure 2 (λ_{abs} = 427 nm, λ_{em} = 473 nm in MeOH/H_2O, 3/2, v/v) previously studied in our laboratory, to synthesize the following fluorescent photolabile protecting group Cou-AMNPEOC (4[(N-7'-diethylaminocoumarin-3'-carbonyl)-5"-aminopent-1"-yl-oxy]-5-methoxy-2-nitrophenyl-ethoxycarbonyl).

The protection of the 5'-OH terminal function of thymidine was performed with this new fluorescent photolabile protecting group. The photochemical deprotection of the deoxynucleoside was realized under a 365 nm irradiation and the following of the photolysis studied by HPLC. Photophysical properties were also studied to determine any modification of coumarin behaviour after photocleavage.

RESULTS AND DISCUSSION

1. Synthesis of the fluorescent photolabile deoxynucleoside Cou-AMNPEOC-T

The synthesis of the target molecule consisted of two branches that converged in the final step: the first branch concerned the photolabile part ; the second one consisted in transforming the fluorescent part. The different steps are pictured on figure 2.

1.1. Photolabile part

Starting from the commercial compound 3,4-methylenedioxyacetophenone (Lancaster), the photolabile moiety could be synthesized in a three steps sequence in 53% overall yield: electrophilic aromatic nitration was performed with concentrated nitric acid at 10-15°C ; the keto group was reduced with sodium borohydride in methanol, at 10°C ; finally, regioselective aromatic nucleophilic displacement with methoxide led to the compound 2, which was used in the fluorescent grafting reaction without any purification.

1.2. Fluorescent part

The basic structure of coumarin (compound 3) was obtained by a Knoevenagel condensation of commercial 4-diethylamino-2-hydroxybenzaldehyde and diethyl malonate in the presence of piperidine [7]. The ester function was removed by saponification with KOH. The amino part of a linker was coupled to the acid function leading to the compound 5, the primary terminal alcohol function of which was converted into bromide by treatment with CBr_4, PPh_3.

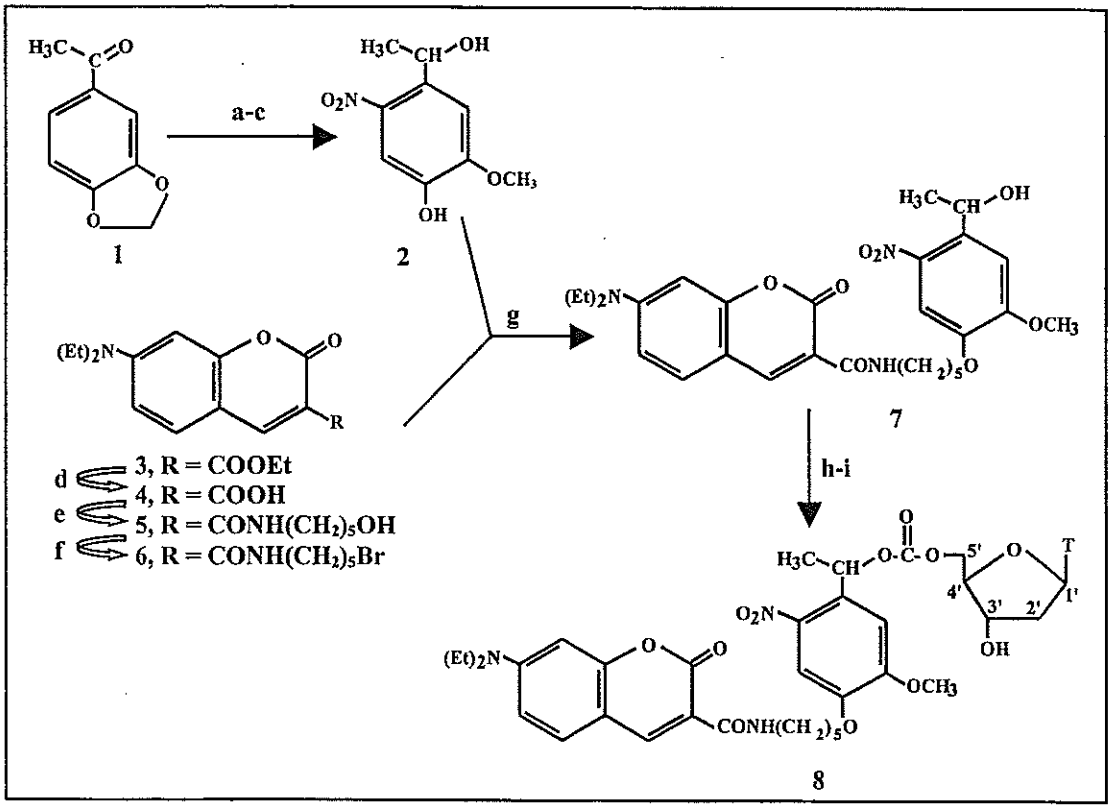

Figure 2. Synthesis of the fluorescent photolabile nucleoside Cou-AMNPEOC-T
a) 70% HNO_3, 10-15°C, 1 h, 68% ; b) $NaBH_4$, MeOH, 10°C, 4 h, 98% ;
c) Na, MeOH, DMSO, 80°C, 2 h, 80% ; d) KOH, EtOH/H_2O, 96% ;
e) $H_2N(CH_2)_5OH$, HOBT-DCCI, CH_2Cl_2, DMF, 0°C, 24 h, 90% ;
f) CBr_4, PPh_3, CH_2Cl_2, 0°C, 4 h, 90% ; g) K_2CO_3, DMF, 75% ;
h) $(Cl_3CO)_2CO$, CH_2Cl_2, 0°C, 4 h ;
i) Thymidine, Pyridine, 0°C, then at RT 24 h, 39%

1.3. Fluorescent photolabile deoxynucleoside Cou-AMNPEOC-T

Alkylation of the phenoxy function of the photolabile part with the brominated fluorescent derivative, realized in the presence of potassium carbonate in dimethyl formamide (DMF) led to the fluorescent photolabile group 7 with 75% yield.

The chloroformate was prepared from triphosgene in CH_2Cl_2 and then condensed on T dissolved in pyridine: the 5'-O-protected T, Cou-AMNPEOC-T (compound 8), purified on silica gel column chromatography, was obtained with 39% yield.

2. Photolysis study of the Cou-AMNPEOC-T

2.1. Photolysis conditions and HPLC analysis

Irradiation of protected thymidine was achieved in order to study both photochemical and photophysical properties of the fluorescent photolabile protecting group. The experimental parameters have been optimized as follows: a solution of Cou-AMNPEOC-T (72 µM, MeOH/water, 3/2, v/v) has been irradiated in a 2 mm pathlength quartz cuvette with a 500 W mercury arc lamp (Osram) at 365 nm, selected by a UG11 filter which gave a light intensity of 68 $mW.cm^{-2}$, determined by chemical actinometry: ferrioxalate and uranyl oxalate methods [8]. The photodeprotection *versus* time was followed by HPLC using a reverse phase column (5 µm C_{18}-silica, 4.6 mm internal diameter x 250 mm) eluated with a linear gradient of acetonitrile/0.1 M aqueous triethylammonium acetate, pH = 7.3 (5-80% over 25 min) at a flow rate of 1 mL. min^{-1} and monitoring of the eluant at 260 nm.

2.2. Photodeprotection rate and half-life determination

The new fluorescent photolabile group was subjected to irradiation at 365 nm. By HPLC analysis, we followed Cou-AMNPEOC-T and free thymidine concentrations variations *versus* irradiation time. In both cases we compared the results with the ones obtained after irradiation of the 5'-O-protected thymidine with MeNPOC, under identical experimental conditions.

Figures 3 and 4 represent respectively the decrease of Cou-AMNPEOC-T and MeNPOC-T parallel to the formation of free thymidine.

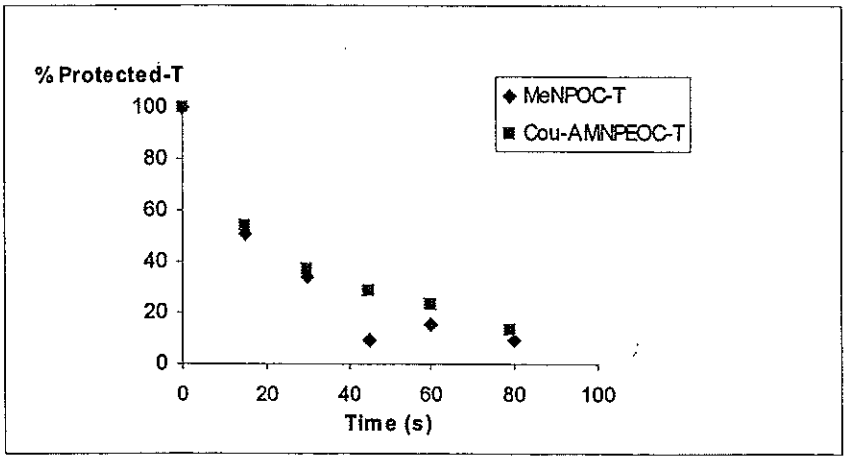

Figure 3. Photolysis of Cou-AMNPEOC-T and MeNPOC-T

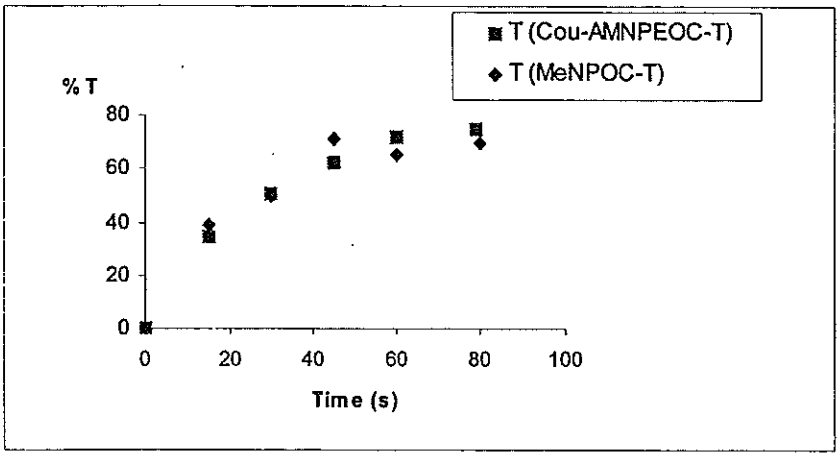

Figure 4. Free thymidine issued in the photolysis of Cou-AMNPEOC-T and MeNPOC-T

Comparison of the results obtained with Cou-AMNPEOC-T photolysis and MeNPOC-T photolysis is satisfying as the curves are similar.

If we focus on the photolysis reaction half-life (figure 5), determined by the exponential decrease of Cou-AMNPEOC-T during the photolysis, it remains almost unchanged by comparison with MeNPOC-T photolysis (table 1).

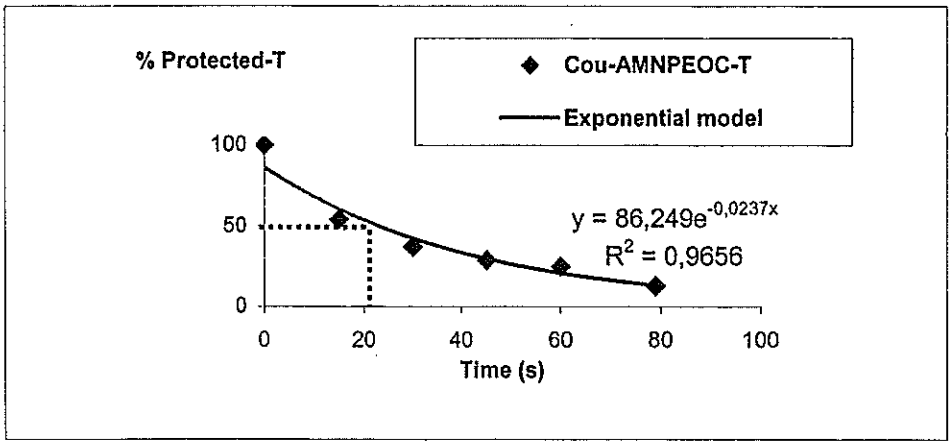

Figure 5. Half-life determined by exponential decreasing of Cou-AMNPEOC-T

However, if the compound Cou-AMNPEOC-T shows a stronger absorption than MeNPOC-T, its photolysis quantum yield ϕ is almost half time lower than MeNPOC-T's one, which implies that the photolysis is less efficient with the presence of the fluorophore. The coumarin when irradiated at 365 nm (results not shown) dissipated some energy into fluorescence pathway, which seems to compete with the photolysis reaction.

Table 1. Comparison of main photolytic data between MeNPOC-T and Cou-AMNPEOC-T

5'-O-protected thymidines	ε_{365} ($L.mol^{-1}.cm^{-1}$)	$t_{1/2}$ (s)	T (%, after 5 min)	ϕ (photolysis)
MeNPOC-T	3750	19	98	0,0075
Cou-AMNPEOC-T	6980	21	98	0,0041

MeNPOC: α-methyl-2-nitropiperonyloxycarbonyl ; Cou-AMNPEOC: (4[(N-7'-diethylamino coumarin-3'-carbonyl)-5"-aminopent-1"-yl-oxy]-5-methoxy-2-nitrophenylethoxycarbonyl) ; T: thymidine ; ε_{365}: molar extinction coefficient at 365 nm ; $t_{1/2}$: half-life ; ϕ: quantum yield.

2.3. Photophysical properties

Since fluorescent properties are important for the application required, we have studied the influence of grafting on the intermediate compounds implied in the synthesis of the deoxynucleoside protected with the fluorescent photolabile group. Table 2 and figure 6 present the influence of the nature of the substituant on the spectral molecular rotor characteristics: absorption and fluorescence properties decrease according to the steps of the grafting syntheses. In spite of this, the properties are conserved and the fluorophore still plays its labelling role.

Table 2. Effect of substituant on coumarin UV-visible spectral pattern ($MeOH/H_2O$, 3/2, v/v)

Coumarin derivative	ε_{425} ($L.mol^{-1}.cm^{-1}$)
Compound 3	37800
Compound 5	33000
Compound 7	24700
Cou-AMNPEOC-T 8	13700

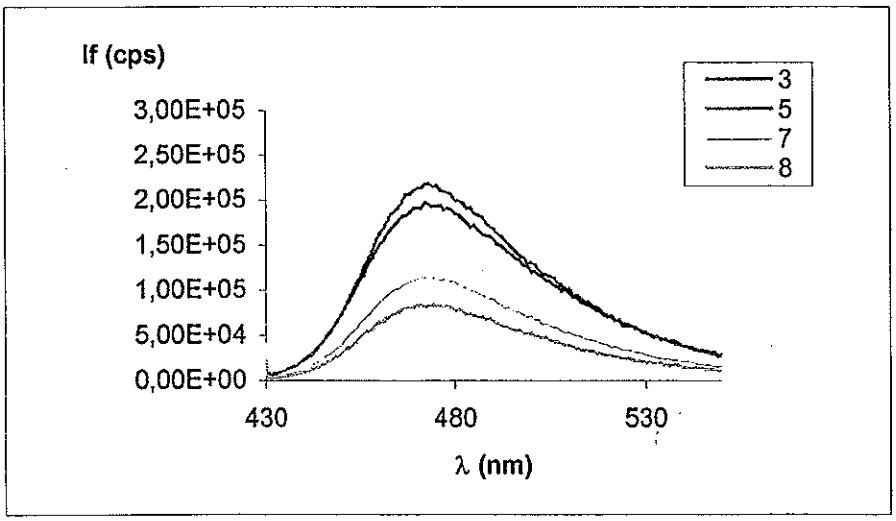

Figure 6. Fluorescence spectra of the coumarin derivatives (10^{-6} M, $MeOH/H_2O$, 3/2, v/v)

If we focus on the photophysical properties of the fluorescent photolabile probe before and after irradiation (figure 7), it appears that they are remained, the fluorescent part is not damaged or disturbed by the photolysis. We have also checked that irradiation at the fluorescence excitation wavelentgh (λ = 425 nm) *versus* time (during 7 min) does not cleave the photolabile part: HPLC analyses of aliquots (0.5, 1, 2, 7 min) do not show any significant change in the shape and integration of the peak corresponding to the starting fluorescent protected thymidine.

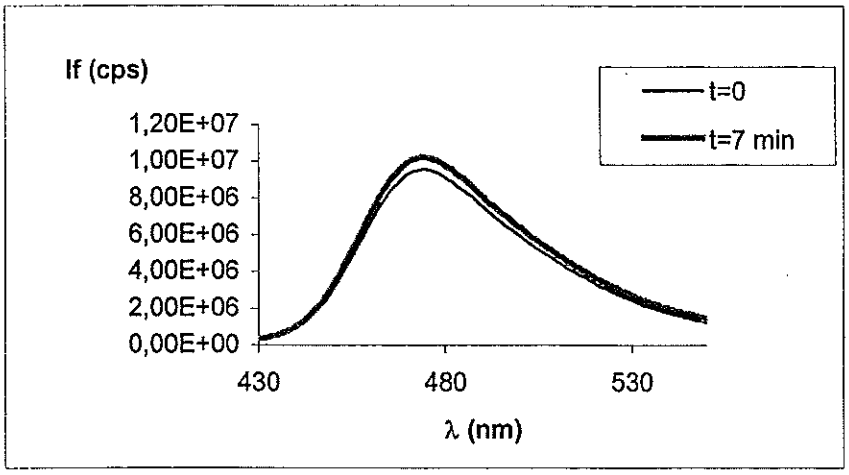

Figure 7. Fluorescence emission of Cou-AMNPEOC-T before and after 7 min of irradiation

CONCLUSION

The first fluorescent photolabile probe we synthesized shows very interesting properties, both on photophysical and photochemical points of view. Actually, even if the coupling of a fluorophore on a photolabile molecule lower the photolysis quantum yield by a factor of 2, the results are satisfying because specific behaviour of the two parts remains unchanged: the MeNPOC plays its photolabile role, whereas the coumarin derivative conserves its fluorescent properties during and after irradiation.

Synthesis of other fluorescent photolabile groups with different photophysical properties will allow the identification of each nucleoside on a large wavelength range. The characteristics of these probes are significant of very powerful tools not only for DNA microchips approachs, but also for many other applications in Biosciences [9].

ACKNOWLEDGEMENTS

CNRS (Genom program ; C. Muller, M.L. Viriot), INSERM (M.C. Carré), Région Lorraine (C. Muller) are acknowdged for their financial support.

REFERENCES

[1] Anderson R.C., McGall G., Lipschutz R.J., *Polynucleotide arrays for genetic sequence analysis,* Top. Curr. Chem., 194 (1998), 117-129

[2] Burgess K., Jacutin S.E., Lim D., Shitangkoon A., *An approach to photolabile, fluorescent protecting groups*, J. Org. Chem., 62 (1997), 5165-5168

[3] Welch M.B., Martinez C.I., Zhang A.J., Jin S., Gibbs R., Burgess K., *Syntheses of nucleosides designed for combinatorial DNA sequencing*, Chem. Eur. J., 5 (3), (1999), 951-960

[4] Welch M.B., Burgess K., *Synthesis of fluorescent, photolabile 3'-O-protected nucleoside triphosphates for the base addition sequencing scheme*, Nucleosides & Nucleotides, 18 (2), (1997), 197-201

[5] Lloyd-Williams P., Albericio F., Giralt E., *Convergent solid-phase peptide synthesis*, Tetrahedron, 49 (1993), 11065-11133

[6] McGall G.H., Barone A.D., Diggelmann M., Fodor S.P.A., Gentalen E., Ngo N., *The efficiency of light-directed synthesis of DNA arrays on glass substrates*, J. Am. Chem. Soc., 119 (1997), 5081-5090

[7] Van Gompel J., Schuster G.B., *Chemiluminescence of organic peroxides: intramolecular electron-exchange luminescence from a secondary perester*, J. Org. Chem., 52 (1987), 1465-1468

[8] Favaro G., *Actinometry: concepts and experiments*, Spec. Publ.-R. Soc. Chem., 225 (1998), 295-304

[9] Welch M.B., Martinez C.I., Zhang A.J., Jin S., Gibbs R., Burgess K., *Syntheses of nucleosides designed for combinatorial DNA sequencing*, Chem. Eur. J., 5 (1999), 951-960

EXPERIENCES WITH THE PERFLUOROCARBON TRACER ANALYSIS BY GC/NICI-MS IN COMBINATION WITH THERMAL DESORPTION

C.U. Galdiga[1], S.K. Hartvig[1], Ø. Dugstad[1], T. Bjørnstad[1,2] and T. Greibrokk[2]

[1]Institute for Energy Technology, P.O. Box 40, N-2027 Kjeller, Norway
[2] University of Oslo, Department of Chemistry, P.O. Box1033, N-0315 Oslo, Norway

Abstract. While thermal desorption in combination with gas chromatography and electron capture detection is a standard technique for the analysis of perfluorocarbon tracers in atmospheric samples today, the analysis of this type of compounds in reservoir gas is still based on sampling with gas cylinders. Air is - compared to reservoir gas - a rather "easy" sample matrix. Large volumes (litres) of air can be sampled on suitable sorbents until detectable amounts of perfluorocarbons are collected and analysed with gas chromatography. Interfering compounds are not present in most cases and electron capture detection is sufficient for this type of samples.

In contrast, reservoir gas consists mainly of a variable mixture of hydrocarbons. In addition volatile compounds with heteroatoms originated from the reservoir and halogenated compounds from the exploration activities may be present in interfering concentrations. The hydrocarbons reduce the capacity of the sorbent for the perfluorocarbons and hence the collectable amount of the tracers. The "non-hydrocarbon" compounds represent the chromatographic background. This background affects the detection limit and makes the identification and quantification by electron capture detection unreliable at trace concentrations.

Thermal desorption in combination with GC/NICI-MS (gas chromatography/negative ion chemical ionisation mass spectrometry) overcomes these drawbacks and enables the automated analysis of perfluorocarbon tracers in reservoir gas matrices at the femtoliter/liter concentration level with confident identification and quantification (picoliter/liter).

The intention of this article is to present this unique combination of analytical equipment. Real reservoir samples will show the enhanced performance of this new method in terms of sensitivity and tracer identification. Compared to the conventional technique the limit of detection is lowered by a factor of 100 for the perfluorocarbon tracer. Furthermore our experience with this new method during the first years after introduction will be discussed.

INTRODUCTION

High stability, chemical inertness and high detectability make perfluorocarbons, such as perfluorodimethyl cyclobutane (PDMCB), perfluoromethyl cyclopentane (PMCP), perfluoromethyl cyclohexane (PMCH), 1,2- and 1,3-perfluorodimethyl cyclohexane (1,2-/1,3-PDMCH), suitable gas tracers for a wide range of applications. Their use in atmospheric studies [1-4], marine surface studies [5], in house ventilation examinations [6], and in petroleum reservoir studies [7-9] has been reported.

In this range of applications determination of these compounds is well described in the literature, both on packed and on capillary columns. O`Mahony and co-workers [10] concluded in a review article that the majority of published methods used packed columns, while capillary columns have not been fully exploited for this purpose. In most cases a gas chromatograph equipped with an electron capture detector (GC/ECD) is used only. For sample matrices that contain interfering

compounds, such as reservoir gas, this may not be sufficient. Beside hydrocarbons, not visible with electron capture detection, other compounds containing heteroatoms like sulphur or oxygen are present with interfering concentrations. These compounds cause a high chromatographic background especially for systems with packed columns. Capillary columns have much better separation capabilities, but on the other hand only small sample volumes can be applied [11].

One way to eliminate matrix interferences is the catalytic treatment of the sample: Lagomarsino [12] reported the catalytic reduction of chlorofluorocarbons in atmospheric samples, while Senum et al. [13] described the catalytic combustion of the reservoir gas matrix prior to GC/ECD analysis. Another way to achieve a more selective detection is the use of NICI-mass spectrometry. Already in 1972, Dougherty et al. created negative ion mass spectra with methane or isobutane added to the ion source [14]. GC/NICI-MS has become very useful for the identification and quantification of compounds with high electron affinities such as dioxins or PCBs in environmental samples [15], but to our knowledge only Begley and co-workers in 1988 [16] have reported the use of NICI-GC/MS for perfluorocarbon tracer detection (in air samples) so far. One reason for that might be that PFT analysis on conventional capillary columns needs starting temperatures below 0 °C to achieve good chromatography [12,16,17]. On the other hand capillary columns are a "must" for the NICI-technique, which is very sensitive to system variations of e.g. the system pressure. Jet separators used for the connection of packed columns can introduce such system variations. However, the use of an Al_2O_3 porous layer open tubular (PLOT) column for perfluorocarbon tracer analysis avoids these problems and enables GC separation without cryogenic oven cooling [18].

Dietz and co-workers [19] reported the detection of PMCP and PDMCH in atmospheric samples in concentrations below the femtoliter/liter (10^{-15} L/L) range after selective tracer enrichment on adsorber tubes filled with activated carbon material followed by analysis with a packed column GC/ECD-system. Reservoir gases, however, represent a much more complex matrix, which may cause difficulties for selective tracer adsorption due to their competition for the "active sites" of the sorbent material. Even if the material is specific for perfluorocarbons, the high concentration of hydrocarbons in reservoir gas will replace the tracer molecules. Thus, large sample volumes (up to several liters), which are commonly used for air samples cannot be achieved with reservoir gas samples unless special, and in most cases unpractical, measures are taken (for instance large absorbent volumes).

Nevertheless, fully automated perfluorocarbon tracer identification in the 10^{-13} [L/L] range and reliable quantification in the 10^{-12} [L/L] concentration range will be demonstrated with thermal desorption, in combination with GC/NICI-MS.

EXPERIMENTAL

1.Analytical Equipment

The analyses have been performed on a GC/MS-system from Agilent consisting of a HP 6890 gas chromatograph with a HP 5973 quadrupole benchtop mass spectrometer. The separation was performed on an Al_2O_3 PLOT column. The mass spectrometer were operated in the NICI mode. Sample introduction was carried out

with an ATD 400 Thermal Desorption Unit from Perkin Elmer. A sketch of the instrumentation is shown in Figure 1. The detailed analytical conditions are described elsewhere [11,20].

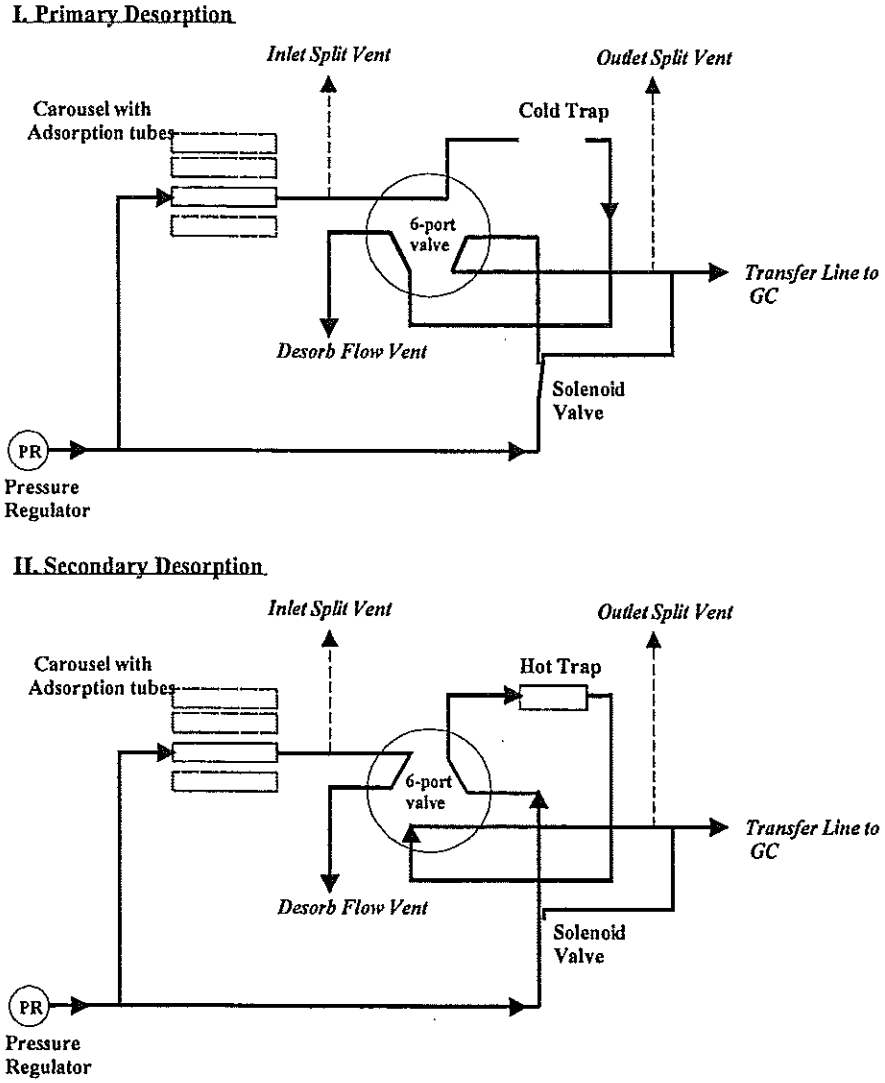

Figure 1. A sketch of the analytical set up, highlighting the two step operation of the Thermal Desorption Unit. Step 1: Primary Desorption of the perfluorocarbons from the adsorption tube and their trapping on the cold trap. Step 2: Secondary desorption by flash heating the trap and transfer of the tracers into the GC.

2. Gas Sampling

Stainless steel tubes (89 mm x 4 mm ID; supplier Perkin Elmer or Markes), filled with a molecular sieve, were used for perfluorocarbon trapping. Gas sampling was carried out with a sampling device as described in Figure 2.

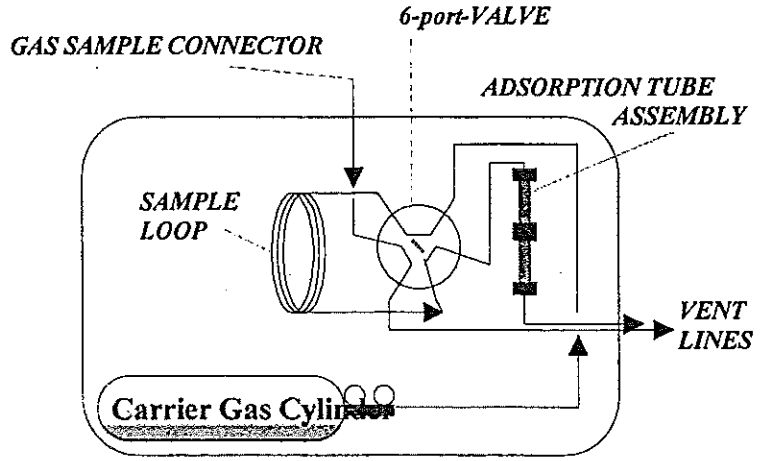

Figure 2. Device for Reservoir Gas Sampling on IFEs Adsorption Tubes. The sample loop - typical volume 20 mL - was flushed with the Reservoir Gas (Step 1). Then the 6-port-valve was switched and the carrier gas transfers the sample into the adsorption tube assembly (Step 2, shown).

3. Standard Preparation

Gas Standards were prepared by injecting dilutions of the perfluorocarbon tracers in hexane into stainless steel cylinders. The cylinder was then pressurised several times with the gas matrix of choice to about 10 to 15 bar. These tracer standards were checked against a commercial standard (Linde GAS) for accuracy.

DISCUSSION

The major aim was to enable confident perfluorocarbon tracer quantification and molecule specific identification at ultra low concentration levels. The analytical method described is based on a two step adsorption/thermal desorption process followed by NICI-GC/MS analysis (see Figure 1). Up to 50 adsorption tubes can be placed into the carousel. After loading into the carousel, the tube was connected to the flow line and the sample transferred with a two step procedure into the GC/MS.

Figure 3 shows typical selected ion recordings (SIR) of a reservoir gas sample, spiked with the tracers to give concentrations of about 6 x 10^{-13} [L/L]. The upper panel shows the SIR with the typical patterns of PMCP and the two isomers PDMCB (m/z 300). The intermediate panel shows the SIR of the PMCH (m/z 350), while the lower panel shows the selected ion recording of the PDMCH isomers with their typical patterns (m/z 400).

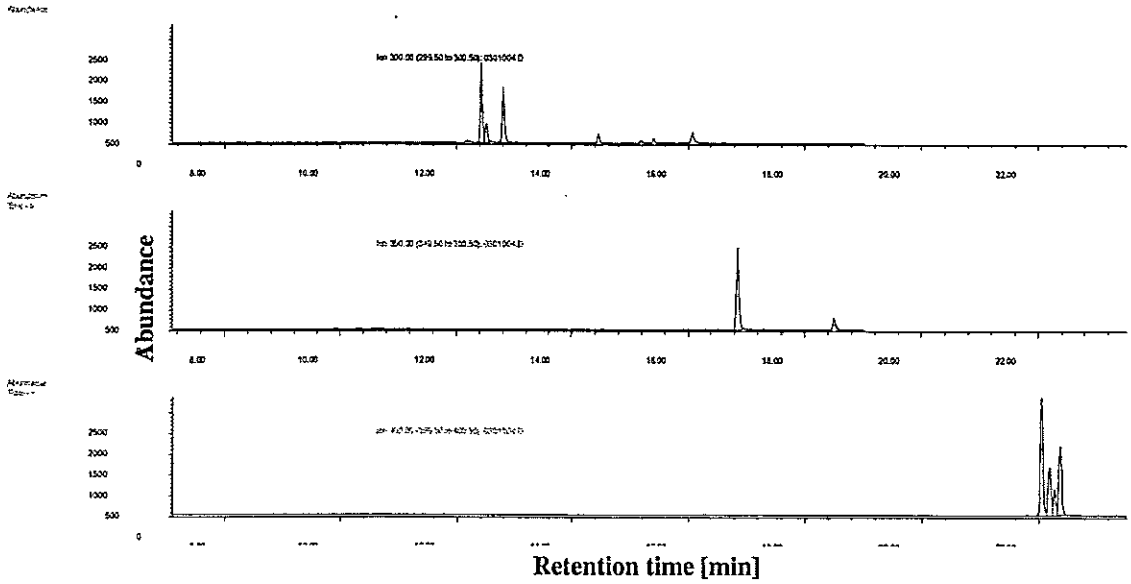

Figure 3. SIR of Perfluorocarbon tracers at about 6 x 10^{-13} [L/L] concentrations. Upper Panel: PMCP and PDMCB (2 isomers), mid panel: PMCH, lower panel: Isomers of PDMCH

The TIC-chromatogram (total ion current) of a reservoir sample containing PDMCB and PMCH in 10^{-12} [L/L] concentrations is shown in Figure 4. The corresponding chromatogram generated with the GC/ECD method is shown in Figure 5. While both tracers are easily detected and quantified with the GC/MS-system, both tracers are not detectable in the ECD chromatogram. The figures demonstrated that identification and quantification of the perfluorocarbons at the trace level is superior with GC/NICI-MS.

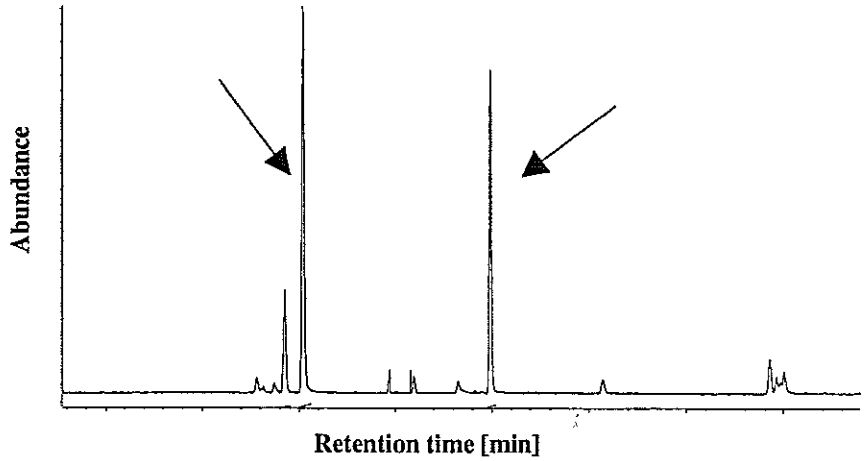

Figure 4. A TIC-chromatogram of a Reservoir Gas Sample containing PDMCB and PMCH in 10^{-12} [L/L] concentrations. PDMCB (2 isomers) and PMCH are easily detected and quantified.

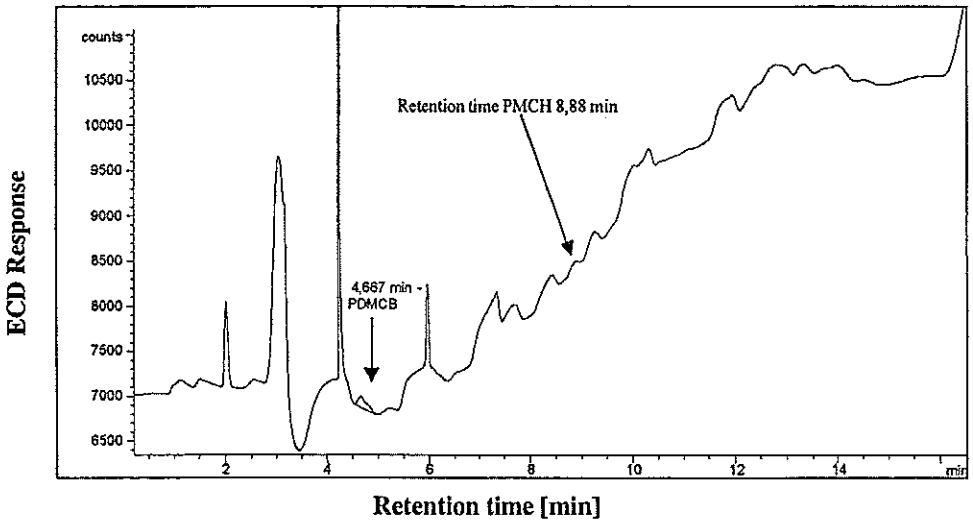

Figure 5. The GC/ECD chromatogram of the same Reservoir Gas Sample. PDMCB and PMCH are covered by the chromatographic background

Reservoir gas samples taken at different wells from one petroleum reservoir have been analysed both with GC/ECD and GC/NICI-MS. The samples contained either PMCP or PMCH. The samples were analysed three times on both systems. The standard deviation of all six analyses per sample was typically below 10 %. In Figure 6 the performance of both methods is compared: GC/ECD and GC/NICI-MS generate the same tracer concentrations in the examined samples.

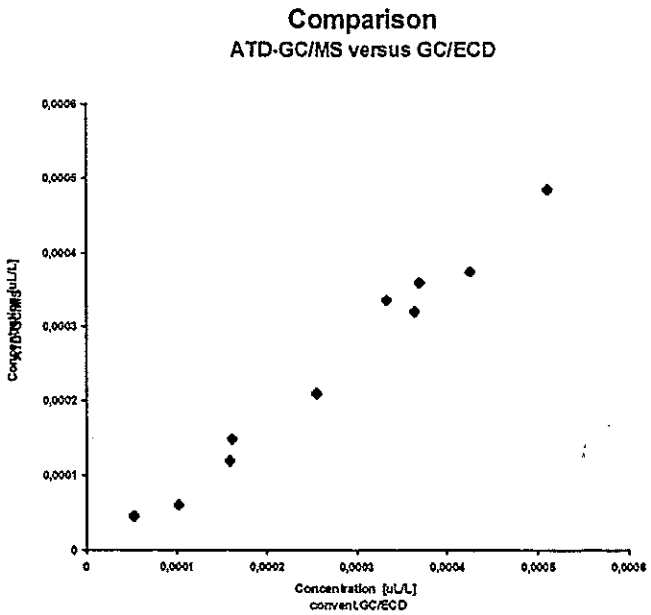

Figure 6. The diagram shows that GC/ECD and GC/NICI-MS generate the same tracer concentrations in the individual Reservoir Gas Samples

Quantification was based on external standard calibration. Standards with the perfluorocarbon tracers in concentrations ranging from 10^{-9} to 10^{-12} [L/L] were prepared. The calibration curves based on the selected ion recordings of the molecular ions showed a linear response within the selected concentration range. The linear coefficients were better than 0.999 for all tracer compounds.
In Table 1 calibration data generated with two independent sets of standards, based on a commercial standard (Linde) and a local standard respectively, are compared. The calibration coefficients are in a good agreement.

*Table 1. Comparison of calibration data from two different sets of independent standards: a commercial standard (Linde) and a local standard (a and b refers to Area = a*conc+b; R^2 from MS Excels linear regression function)*

	Standards from Linde			Standards prepared at IFE		
	a	b	R^2	a	b	R^2
PMCP	6,635E16	1,841E05	0,9998	6,595E16	6,454E04	0,9999
PMCH	7,763E16	2,737E05	0,9998	7,941E16	6,700E04	1,0000

The new method [20] was introduced in early 1999 and has completely replaced the former GC/ECD-method. As the adsorption tubes are not pressurised and do not contain flammable gas, there are no shipment restrictions. This in combination with the automation make it possible to analyse gas samples from all over the world with very short response times. Figure 7 shows a tracer response curve from a South American oil field. The typical measured concentrations ly in the range of 10^{-12} to 10^{-11} [L/L].

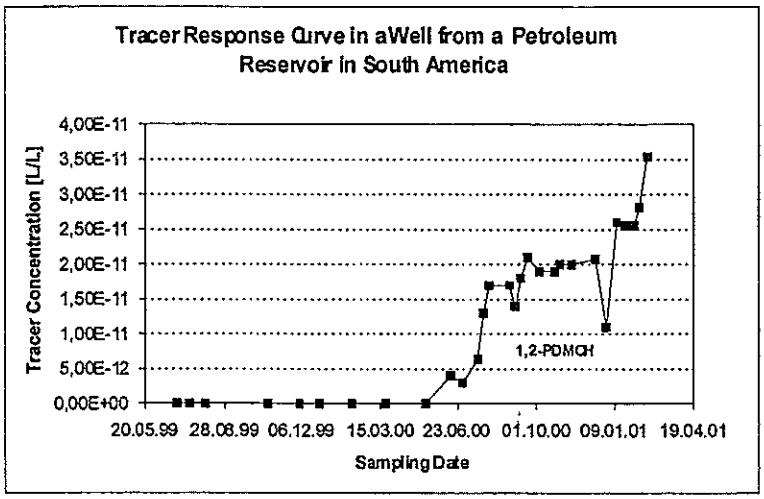

Figure 7. A tracer response curve of 1,2-PDMCH taken from a South American petroleum reservoir. The curve is not corrected for variations in the gas production.

CONCLUSIONS

The performance of a new analytical method for the ultra trace determination of perfluorocarbon tracers has been described. The new method is superior in terms of sensitivity and tracer identification. In addition, the use of adsorption tubes enables automated analyses and non-restricted gas sample shipment with express services or ordinary mail. Hence, analytical results, e.g. from Overseas Samples, can be reported in very short terms.

REFERENCES

[1] Lovelock, J.E., Ferber, G.J., Atmos. Environ. 16 (1982), 1467
[2] Lagomarsino, R.J., Raymond, J., Latner, N. J., Chromatogr. 595 (1992), 359
[3] Draxle, R.R., Dietz, R., Lagomarsino, R.J., Start, G., Atmos. Environ. 25A (1991), 2815
[4] Dietz, R., Spandau, D.J., Senum, G.I., D`Ottavio, T.W., Goodrich, R.W., 50th Anniversary 1938/1988: Division of Analytical Chemistry newsletter (1988)
[5] Upstillgoddard, R.C., Watson, A.J., Liddicoat, M., Anal. Chim. Acta 249 (1991), 555
[6] Menzies, K.T., Pong, C.M., Randel, M.A., 80th Annual Meet. of the Air Pollution Control Assoc. NY (1997)
[7].Kleven, R., Høvring, O., Opdahl, S.T, Bjørnstad, T., Dugstad, Ø., Hundere, I.A., Technical Paper SPE-35651, Calgary (1996)
[8] Dugstad, Ø., Aurdal, T., Galdiga, C., Hundere, I., Torgersen, H.J.T., Technical Paper SPE-56427 Houston (1999)
[9] Ljosland, E., Dugstad, Ø., Bjørnstad, T., Hundere, I.A., J. Pet. Sci. Eng. 10 (1993), 27
[10] O`Mahony, T.K.P., Cox, A.P., Roberts, D.J., J. Chromatogr. 637 (1993), 1
[11] Galdiga, C.U., Greibrokk,T., Chromatographia 46 (1997), 440
[12] Lagomarshino, R.J., J. Chromatogr. Sc. 34 (1996), 405
[13] Senum, G.I., Cote, E.A., Dòttavio, T.W., Dietz, R.N., Brookhaven National Laboratory Report BNL-42769 (1989)
[14] Dougherty, R.C., Dalton, J., Biros, F.J., Org. Mass Spectrom. 6 (1972), 1171
[15] Oehme, M., Fresenius J. Anal. Chem. 350 (1994), 544
[16] Begley, P., Foulger, B., Simmonds, P., J. Chromatogr. 445 (1988), 119
[17] de Bortoli, M., Pecchio, E., J.High Resolut. Chromatogr. & Chromatogr. Commun. 8 (1985), 422
[18] Ghaoui, L., Dessai, E., Wentworth, W.E., Weisner, S., Zlatkis, A., Chen, E.C.M., Chromatographia 20 (1985), 75
[19] Dietz, R.N., Goodrich, R.W., Cote, E.A., Wieser, R.W., Brookhaven National Laboratory Report BNL-33846 (1986)
[20] Galdiga, C.U., Greibrokk, T., Fresenius J. Anal. Chem. 367 (2000), 43

STUDY OF THE GAS HYDRODYNAMICS IN AN ANNULAR REACTOR.

G. Genin, E. Schaer, L. Falk, J.L. Houzelot, C. Favre

Laboratoire des Sciences du Génie Chimique
CNRS-ENSIC, B.P.451, 1 rue Grandville, 54001 Nancy Cedex, France

Abstract. Authors present a study of the hydrodynamics of an annular reactor used for gas-solid contact and reactions. These are preliminary results (fluid flow of the gas phase) of a detailed characterisation of this new type of reactors in term of particles flow and the study of mass exchange between phases. The measure of the residence time distribution of the gas has been achieved thanks to an original system using ozone as the tracer. Thanks to RTD experiments, a systemic flow model of the reactor, based on a Continuous Stirred Tank Reactor (CSTR) cascade, has been proposed. A CFD approach has also been achieved thanks to the code Fluent. Validation has been carried out by comparison of experimental and calculated RTD.

INTRODUCTION

The conveyors where solid particles circulate by pneumatic conveyance, essentially used for transport, can also be used as contactors for operations such as drying of solids, chemical reactions with catalytic solid or not. However, the residence times of the gas and of the solid are very short, so that transport reactor is limited to operations or reactions whose kinetics is not controlled by solid internal diffusion. The reaction must, for example, take place on the surface and the particles must be sufficiently small so that the internal transfers of matter are fastest as possible.
The improvement of the performances in such reactors should be done thanks to devices which ensure a more intense mixture, therefore of longer contact time between the solid and the gas phases.

Such gas-solid contactors have been proposed several years ago [1-2]. The annular reactor [3], which is the subject of this study, could improve the contact performance between gas and solid phases. It consists of an annular space located between two concentric tubes. The gas-solid suspension circulates of bottom to the top and enters the reactor tangentially. The gas and the solid follow an ascending helicoidal movement. Under the effect of gravity, the solid particles are " braked " compared to the rate of flow gas. This phenomenon allows a good exchange between gas and solid.

The objectives of this study are to present the experimental installation developed to determine the Residence Time Distribution of the gas phase within an annular reactor. Then a systemic modelling of this flow, and a CFD approach, carried out with Fluent and validated by comparing the experimental and numerical RTD, are presented.

EXPERIMENTAL APPROACH

1. Geometry of the reactor

The geometry of the reactor is presented in figure 1. The lower and higher parts where are located the inlet and outlet pipes are made in PVC. They are used as flanges of two concentric tubes of glass whose annular space constitutes the volume of the reactor. The input and the output are tangentially placed in order to ensure a helicoidal flow.

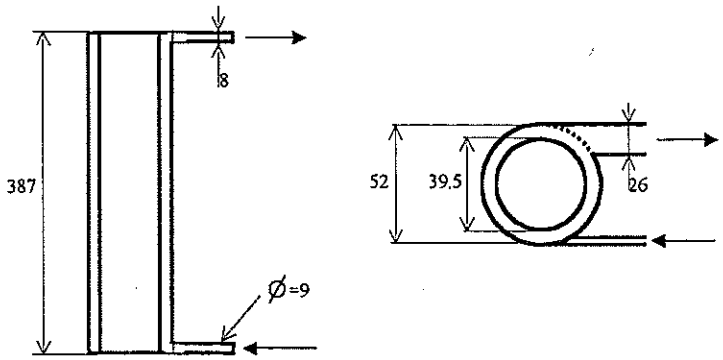

Figure 1 : Reactor dimension.

2. Detection system

The experimental set-up (figure 2) is fed out with oxygen. This one makes it possible to produce tracer gas (ozone) in a ozonor thanks to a strong potential applied between two electrodes. The flow of the vector gas is imposed by a mass volumetric regulator (MVR). The oxygen flow meter can feed the installation in a range going from 2.5 l/min to approximately 22 l/min. The ozone concentration in the carrier gas can reach using this system values up to 20000 ppm.

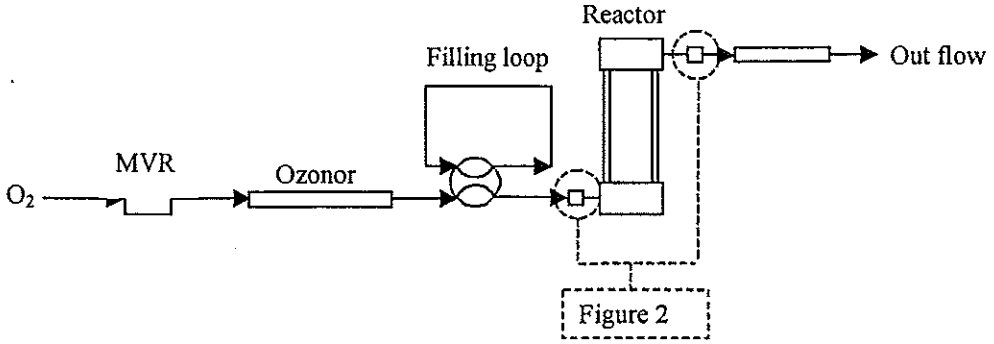

Figure 2: Experimental set-up.

The measure of ozone concentration is carried out by spectrophotometry in the ultraviolet ray at 253.7 nm. Indeed the coefficient of extinction of ozone passes through a maximum at this wavelength. From literature, typical value of the coefficient of extinction is 120 $m^3mol^{-1}m^{-1}$. The light intensity is then a function of the ozone concentration by the Beer-Lambert law in the linear field (weak concentration). This original system makes it possible moreover to follow the advance of the reaction of decomposition of ozone in the reactor if an adequate

catalyst is used for the solid phase transported [1]. The measurement of residence time of particles was also carried out using this system [4].

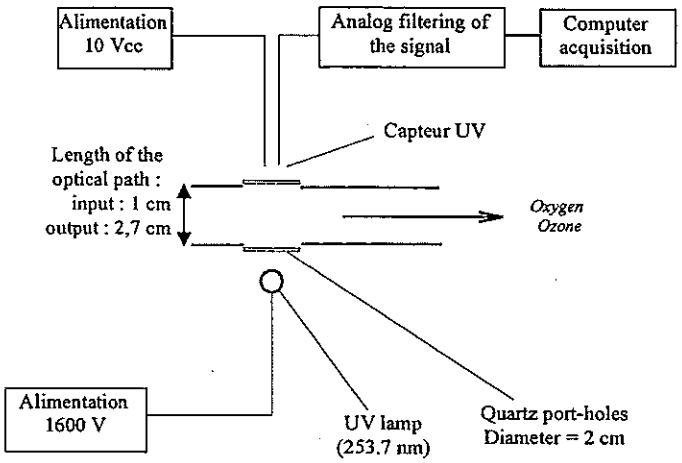

Figure 3 : Cell of ozone concentration measure (spectrophotometry UV method).

In practice, the measuring cells (figure 3), placed at the inlet and the outlet side of the reactor (figure 1), are each one made up by two quartz port-holes placed in opposite on the walls of the tubes. At the entry, the optical path is of 1 cm, and at output 2.7 cm. For each measuring cell, at the opposite side of the two port-holes is placed a spectral lamp UV mono-line at 253.7 nm. This lamp is supplied by an alternating voltage of 1600V. Behind the second port-hole is placed a photo diode made of silicon which is blind in the light of the day. It provides an output voltage in response to the luminous intensity from 0 to 2 Volts, this linearly. An interface of data acquisition makes it possible to obtain the curves of the intensities at the inlet and the outlet of the reactor with time.

3. Experimental results

The Residence Time Distribution of the gas phase has been experimentally determined by injecting pulse inputs of tracer and measuring outlet concentrations.

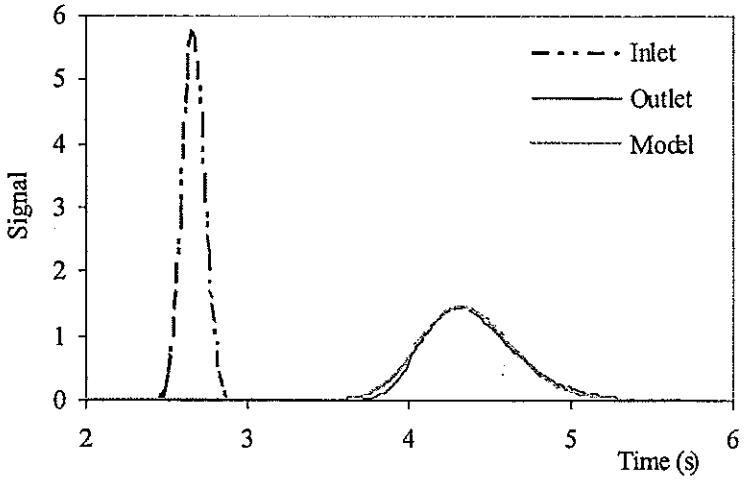

Figure 4 : Concentration curves at the inlet and outlet (Q_{O_2}= 19 l/mn)

Typical signals curves at the inlet and the outlet of the reactor are shown in figure 4. The mean residence time where then easily deduced, whereas the software DTS (which allows convolution calculations) has been used to model the annular reactor as a combination of ideal reactors.

SYSTEMIC APPROACH

1. Mean Residence Time

The variations of the mean residence time t_s in the annular reactor against the inlet Reynolds number Re_0 for several runs are presented in figure 5. The inlet Reynolds number is calculated according to :

$$Re_0 = \frac{\rho u d_0}{\mu} \qquad (1)$$

where ρ and μ are respectively the density and viscosity of the gas, u its speed in the inlet pipe and d_0 the inlet pipe diameter.

Beside the good concordance between the different experiment sets, one can remark that the mean residence time decreases against the inlet Reynolds number. Following the treatment developed by Lede et all. [5] for a cyclone reactor, the mean residence time of the gas phase in the annular reactor can here be described by :

$$t_s = 4725\, Re_0^{-1.06} \qquad (2)$$

as can be seen in figure 5.

The exponent –1.06 in equation (2) is not far from –1, which corresponds to a determinist and incompressible flow.

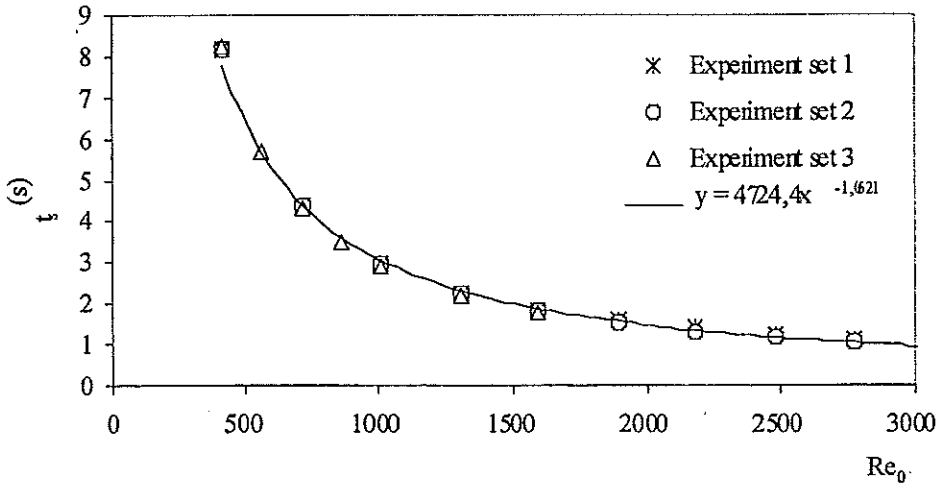

Figure 5 : Mean residence time against the inlet Reynolds number

2. Systemic flow model of the gas phase in the annular reactor

Since the RTD of the annular reactor approaches that of a plug flow reactor with axial dispersion (see figure 4), the tank-in-series model were used to account for the nonideality of our reactor. The DTS software has been used to convolute the inlet signal with the RTD of a series of J Continuous Stirred Tank Reactors (CSTRs) and to optimise (by comparison between the convolution integral and the experimental outlet signal) the number J of CSTRs in series.

For the same conditions as in figure 4, the experimental and modelled RTD are presented in figure 6. For large feed flow rates (i.e. the case of this figure), the agreement between experiment and model is very good.

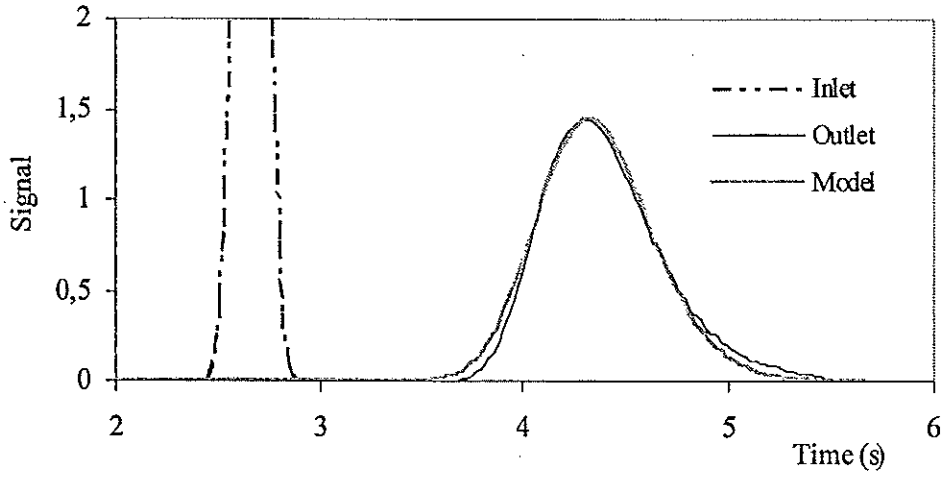

Figure 6 : Experimental and modelled RTD

We only had some difficulties to describe our experiments for very low feed flow rates (or inlet Reynolds below 1000) were diffusion effects are no more negligible. For such conditions, when the tracer no more reflect the material flowing through the reactor, the measured signal might not correspond to the RTD.

The variations of the number J of CSTRs in series against the inlet Reynolds number are presented in figure 7 for large inlet Reynolds numbers (above 1000).

The number J of CSTRs in series may vary significantly from one experiment set to one another. However, the value of J can be considered as almost constant, around 33, with the Reynolds number. The variation of J which might be seen in figure 7 is neither statistically significant nor, at first sight, physically relevant.

For the tanks in series model, the number J of stirred tanks is related to the mean residence time value and the variance μ_2 of the RTD.

$$J = \frac{\left(\bar{t}_s\right)^2}{\mu_2} \qquad (3)$$

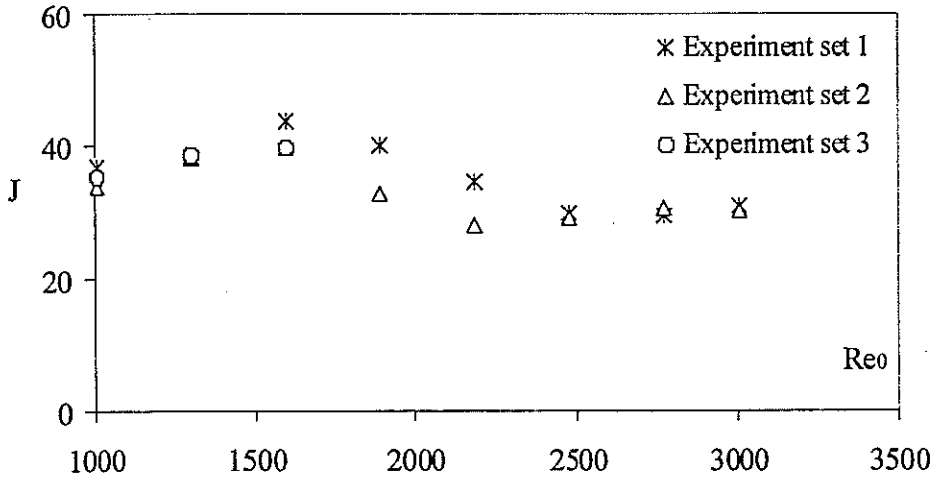

Figure 7 : Variation of the number of CSTRs in series against the inlet Reynolds number

For constant J value, this relation points out that the standard deviation varies linearly with the mean residence time, or in other words that the dispersion decreases when the flow rate increases.

CFD APPROACH

The full simulation of the flow field in the annular reactor has been computed thanks to the commercial CFD code FLUENT. Several flow configurations have been simulated corresponding to a low, a medium and a high flow rate. The Reynolds number at the inlet are respectively 423, 1860 and 2964. The validation of the calculations has been carried out by comparison of the simulated RTD with the experimental ones.

Figure 8 compares the experimental and the simulated outlet signals. For each calculation, the relative deviation of the moments between simulated and experimental RTD have been reported in Table 1. If the mean residence time values are virtually identical, the discrepancy is however much pronounced for the moments of higher order, particularly in the case at low Reynolds number. The experimental signal at this low flowing rate shows nevertheless a suspicious bump which is difficult to explain. Rigorously, the comparison between the experimental data and the calculation should have been done on experimental signals averaged over several sets.

The advantage of using a CFD code is not only the possibility of calculating a priori RTD but also its ability, compared to black box methods like RTD method, to visualize flow structures. Such structures may be evidenced by visualizing the trajectories of fluid particles which are considered as mathematical tracers with either mass or volume. Such trajectories have been illustrated in figure 9, for the three previous considered flow rates.

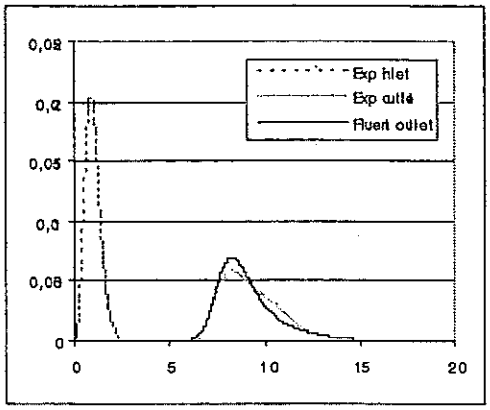

Q = 2.76 l/min

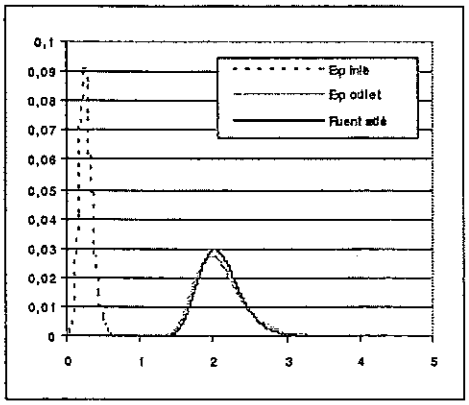

Q=12.14 l/min

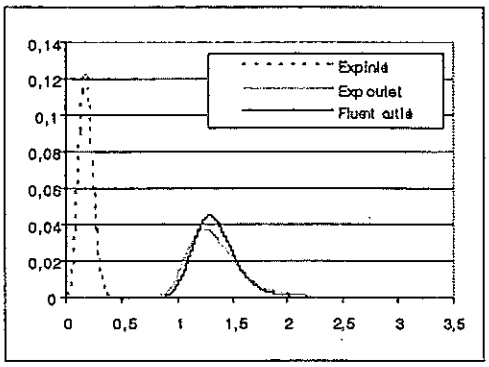

Q = 19.34 l/min

Relative deviation %	Residence time	Variance	Skewness	Kurtosis
Re = 423	0.6	19	155	155
Re =1860	0.7	13	6	4
Re = 2964	0.8	29	45	35

Table 1: relative deviation between simulation and experiments.

Figure 8 : Comparison of experimental and simulated response signals

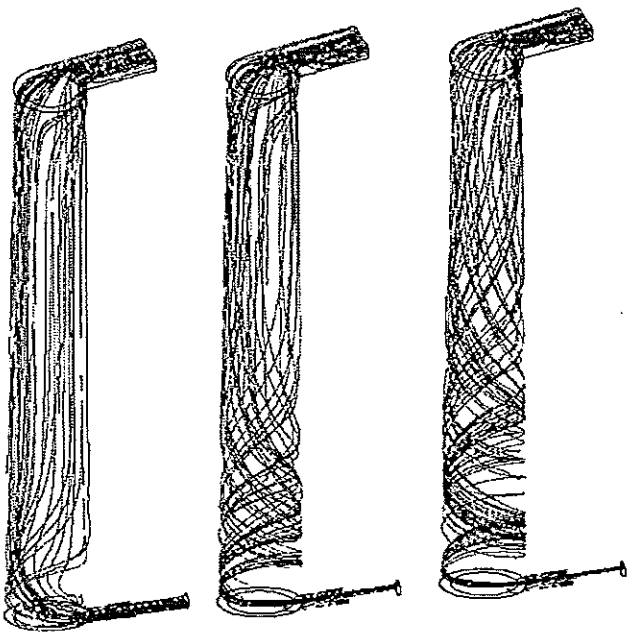

Re = 423 Re = 1860 Re = 2964

Figure 9 : Flow structures against the inlet Reynolds number

It can be clearly distinguished that the vortex effect in the annular reactor increases with the flow rate. In the considered flow rate range, the tangential flow structure occupies only a part of the complete volume of the annular reactors. At Re = 423, the vortex effect is almost inexistent, at Re =1860, one third of the reactor presents a strong tangential flow structure and at Re = 2964, the tangential region represents almost one half of the total volume of the reactor. The RTD signals do not show any particular characteristics from which this kind of flow structure may be deduced.

CONCLUSION

An original tracing method based on ozone as the tracer has been developped. Ozone presents two advantages which are its ability to be detected with non-intrusive optical method, and its ability to be used as a reactive tracer to determine RTD of solid particles. CFD technique has been used to compute RTD which have been compared with good accuracy to experimental data. Full simulation of the internal fluid flow allow to visualize specific flow structure which are not detectable with the systemic approach based on the tank in series model.

REFERENCES

[1] G. Genin, Contribution au développement d'un nouveau contacteur gaz-solide destiné à la mise en œuvre de réactifs pulvérulents, Thèse de l'INPL, 1999

[2] E. Schaer, Etude d'un nouveau réacteur de pyrolyse, DEA du LSGC-GRC ENSIC-INPL, 1992

[3] A. Kotro, Mesure de la distribution des temps de séjour d'un solide circulant dans un réacteur cyclone annulaire par une nouvelle méthode expérimentale, DEA du LSGC-GRC, ENSIC-INPL, 1993

[4] G. Genin, J.L. Houzelot, A. Kotro, G. Martin, Nouvelles méthodes de mesure des distributions de temps de séjour d'une phase solide transportée, Chem. Eng. J., 81 (2001), 301-6

[5] Lede, J., Li, H. Z., Villermaux, J., *Le cyclone réacteur : Partie I : Mesure directe de la DTS de la phase gazeuse – lois d'extrapolation*, Chem Engng J., 42 (1989), 37-55

A A4 - DATA TREATMENTS AND MODELING

EXPERIMENTAL EFFECT OF FLOW AND PARTICLE SIZE ON PARTICLE RTD IN A CONTINUOUS POWDER MIXER

K. Marikh [1], H. Berthiaux [1], V. Mizonov [2], R. David [1], E. Barantseva [2]

[1] Ecole des Mines d'Albi-Carmaux, UMR 2392-CNRS, Campus Jarlard, 81013 Albi cedex 9 (France).
[2] Ivanovo Sate Power Engineering University, Rabfakovskaya 34, 153 003 Ivanovo (Russia).

Abstract. Continuous powder mixers are now seen as an alternative to traditional batch mixing processes for many reasons, such as homogeneity stability. However, few researches have been done in this specific field. This work reports results concerning flow regimes and RTD experiments performed in such a mixer at pilot scale. Special attentions are devoted to the existence of different flow regimes and the randomness of RTD evaluation. The importance of tracer flow characteristics on RTD is also demonstrated, and highlights the possible presence of a stagnant zone.

INTRODUCTION – SCOPE

Many industries need to use the mixing of powders. For instance, pharmaceutical products have to be homogeneous at the scale of a tablet to be efficient. For different reasons, food, chemical and cement industries also have a great concern with this topic.

The major problem related to mixing of dry particulate solids is that nearly all mixing operations involve particles having different physical properties. As a consequence of these differences the mixtures are likely to exhibit some tendency to segregate. This negative effect may happen during mixing, or most likely in the subsequent handling of the mixed product. If the mixture is unsuitably transported, such as it is often the case in screw or vibrating conveyors, or stored near a vibration source, segregation can easily occur and disrupt a previous "good" mix. The main problem with segregation is that it is a source of differences in particle flowability, which is in turn influenced by many inter-related factors: particle size, shape, surface roughness, friction, ... These make segregation hardly quantifiable.

If the expected or measured segregating effects can cause problems, a system based on continuous mixing could be considered, mainly because product stability is better guaranteed that way. Knutsen et Landmo [1] have recently listed the advantages of continuous mixers:

- High capacity relative to size of mixer
- Relatively cheap with respect to capacity
- Low consumption of energy per unit mass or volume due to short residence times
- Suitable for materials with a tendency to segregate
- Possibility to have less segregation if the mixed material is used directly without any intermediate handling
- No need for large and expensive storage equipment after mixing
- Suitable for automation

Very few research has been carried out to characterize and model the particulate flow inside continuous mixers, despite of the fact that this is the very first step towards a better understanding of the link between particle flow and homogeneity at the outlet of the mixer. To make this effective, the concept of Residence Time Distribution (RTD), a chemical engineering concept introduced by Danckwerts [2], is of great help in order to treat dynamic data obtained form RTD experiments and further for technological improvement of such processes. It has been applied for various industrial processes involving particles (see for example [3]), whilst there seems to be no real deep investigations concerning the effect of solid tracer size on RTD [4].

The RTD possesses a theoretical background that emphasizes the role of complex flow modeling in the mixer, for example with the help of Markovian chains [5], down to the micromixing scale. In recent years, some authors have used the Markov chain approach to simulate RTD curves in many types of flow configuration [6]. Sometimes, this approach included chemically reactive systems, thus taking into account system properties and the related effects on RTD determination (double stochasticity).

On the other hand, RTD relies on an experimental method that consists of performing tracer experiments of particles in order to determinate RTD function and elaborate a clinical understanding of the systems dynamics. The measurement of RTD is derived from tracer out flow monitoring. These tracers are detectable by their specific properties. For instance: color, fluorescence, electrical charges and piezoelectric effects, etc.... The most interesting tracers include colored tracers, chemical tracers, magnetically marked particles and radioactive tracers. The general principle of determination involves injection at the system's inlet and further detection of the tracer's concentration. It is obvious that the tracer has to remain neutral with respect to the main (bulk) flow. In other words, a particulate tracer has to exhibit a flow behavior as close as possible to that of the bulk because any segregation tendency would cause a deviation from the main behavior and affect the main particle flow. Thus the measurement could be shifted.

The present work describes measurements of Residence Time Distributions carried out in a continuous powder mixer at pilot scale. Using different size fractions of the same tracer highlights the effect of tracer's size. It also reports results concerning the flow regimes that can take place in terms of hold-up variations for different operating conditions.

EXPERIMENTAL SET-UP AND EQUIPMENT

1. Pilot plant mixer

RTD and flow regimes experiments have been performed in a pilot scale continuous mixing apparatus GERICKE G500M (see figure 1), equipped with a high-level automatic control system, allowing carrying out multi-component mixtures with high dosage precision (loss-in-weight system). In such a process the ingredients are continuously fed into the mixer, mixed, and finally discharged by a gate with different openings. Loss-in-weight (gravimetric) feeders are used to ensure a constant mass flow rate value with very little oscillations due to the conveying screw effect, such as in volumetric feeding devices [7].

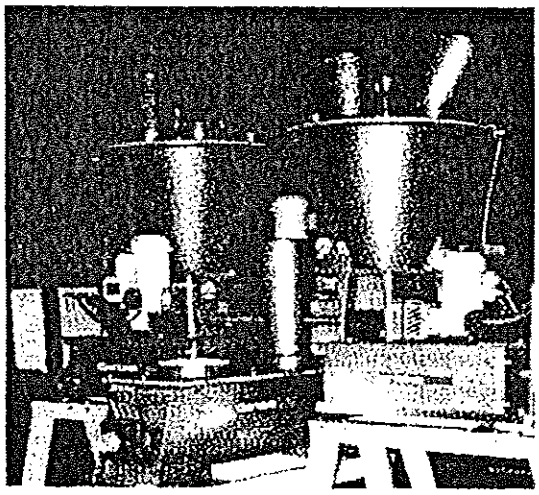

Figure 1. Continuous powder mixer pilot plant used in this work, showing the two gravimetric feeders, the inlet tube, the, mixing chamber and the outlet gate.

The mixing action is ensured by blades supported by a frame (radial mixing effect) while the whole bulk (couscous or semolina) is being transported by a screw to the outlet (see figure 2). A conveyor belt is placed at the mixer's outlet, from which several boxes allow taking consecutive samples continuously for further analysis.

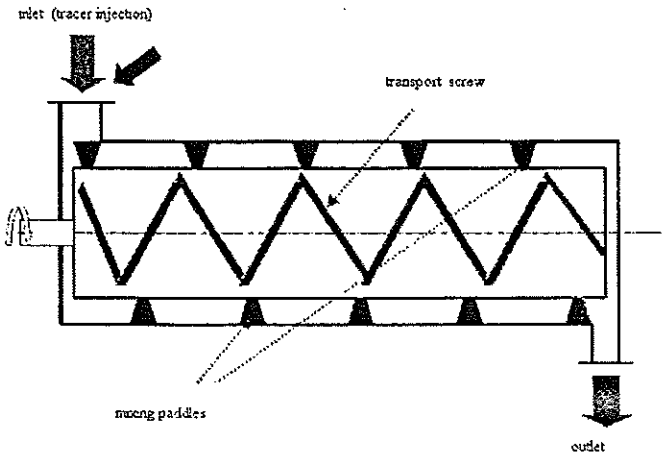

Figure 2. Mixing chamber configuration showing the transport screw and the mixing blades supported by a frame.

2. Operating conditions

Concerning the mixing of solids, geometrical configuration and dynamic properties of the continuous mixer, as well as physical and physicochemical properties of particles are important factors to get a homogeneous mixture. The mixture quality obtained in such a convective mixer is therefore mostly influenced by the speed of rotation of the mobile. For example, the use of high speed produces centrifugation of particles that would result in a further segregation effect [8].

On the other hand, the filling ratio f (or the hold up weight M) is also responsible for the general flow pattern and subsequent homogeneity. Too low filling ratio as well as too high ones may cause poor cross (radial) mixing because of reduced particle mobility, and it is expected that this mobility could readily be expressed from the moments of the RTD curves.

In the present case, filling ratio is a complex function influenced by many variables: the agitator's speed of rotation N, the overall mass flow rate Q, the section s of the outlet opening, and finally the mixed particle bulk characteristics that are always difficult to define and measure properly. This latter point makes difficult any attempt to a rigorous dimensional analysis. Nevertheless, for a definite particulate system, we could roughly say that homogeneity is controlled by Q, N and s. For instance, graphs showing the variations of the mass hold up with the mass flow rate for different discharge openings and speed of rotations are able to give a good picture of the mixer's flow regimes.

3. Particulate systems and tracer preparation

The main particles (bulk) used in this study are granulated semolina grossly spherical "couscous" previously sieved in the range between 1.6 mm and 2 mm. The method for tracer preparation was done by coloring some of these couscous particles by iodine adsorption, which is facilitated by the starch content of semolina, and further drying. It is expected that these colored (black) particles will follow also the flow pattern of the normal ones without any influence of particle size, shape and density (see figure 3). At this early point of the study, tracer detection was performed manually by separation of the black particles and further by weighing. It is obvious that image analysis could make this work less tedious.

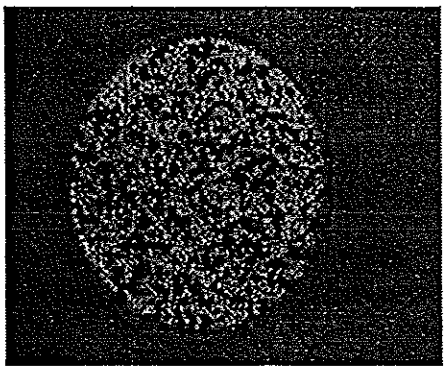

Fig.3: Sample of a mixture containing the bulk and the tracer (bulk particles colored in black by iodine adsorption).

A second tracer with different particle size (but same density) was also used to investigate whether size is essential or not. It consisted of non – granulated semolina with respect to the main flow particles sieved between 250 μm and 315 μm. With such a difference in size (~1/6), we are at the limit of natural percolation of the tracer with respect to the bulk (~1/7). Tracer detection could then be performed in a simpler way by sieving, and further weighing of the different fractions.

RESULTS AND DISCUSSION

1. Flow regimes and operating conditions

Figure 4 shows the evolution of the hold up weight M with mass flow rate, obtained for two different discharge openings, and within a range of rotation speed of the agitator between 2Hz and 20 Hz.

Inversion of the rotational sense of the mobile was not studied here, but it could contribute to retain more particles in the mixing chamber whose volume is almost equal to 24l. Mass flow rates superior to 120 $kg.h^{-1}$ could not be studied because it yet corresponds to the limit of correct loss-in-weight operation of the feeders (this would require a silo placed at the top of each of the feeders).

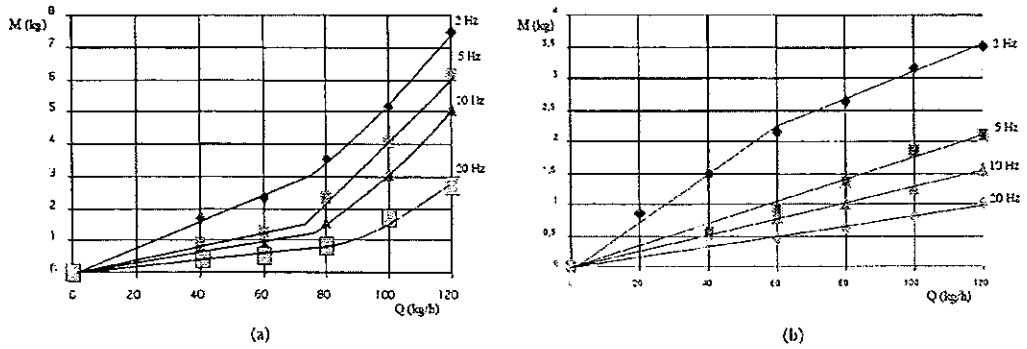

Figure 4. Hold up weight against mass flow rate for different discharge openings (a:nearly closed, b: open), showing the effect of the agitator's speed of rotation.

Table 1: Characteristics of the second flow regime

N (Hz)	2	5	10	20
Slope of M vs. Q	0.86	1.37	1.94	1.90
Exponent n	1.86	2.37	2.94	2.90

According to typical industrial rules, an efficient mixing condition occurs when the filling ratio is between 20% and 60%: this is only the case with the smallest discharge opening. Then, two different flow regimes depending on the mass flow ranges are evidenced. This is however clearer in figure 5 where ln(M/Q) is plotted according to ln(Q), the limit between the flow regimes being denoted by a change in slope :

- For $Q < 70$ $kg.h^{-1}$, whatever the speed of rotation, the hold up varies almost linearly with Q. As a consequence, the spatial residence time $\tau=M/Q$ is independent of the mass flow rate, and this should be confirmed by RTD experiments.
- For $Q>70$ $kg.h^{-1}$, the variation of the hold up with Q seems to follow a power law, the exponent n being also dependent on the speed of rotation N (see table 1). Also, for high values of N, n seems to reach an asymptotical value (~3).

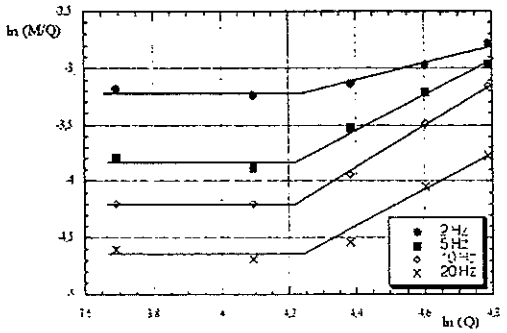

Figure 5. Logarithmic plot of space time (M/Q) against mass flow rate.

2. RTD determination

RTD experiments were performed by direct tracer pulse-injection at the inlet of the mixer during few seconds, the total tracer mass being 100 g. As mentioned above, consecutive samples were taken in the conveyor belt, just after the mixer's outlet. The total sample mass was approximately 250 g, each of these samples containing nearly 10 to 100 tracer particles. These numbers coupled with the sampling procedure and the stochastic nature of particle flow makes that RTD curves are –in essence- not reproducible. This important point, that has been recently commented by Fan et al. [9], can be observed in figure 6 where two RTD curves obtained under the same conditions are plotted.

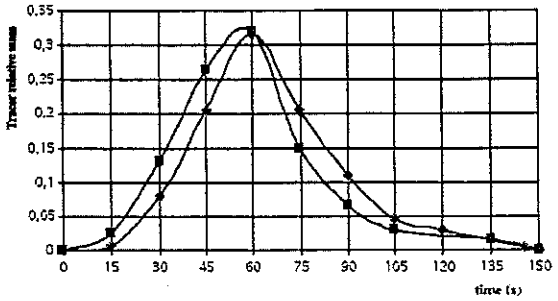

Figure 6. Example of two RTD curves obtained in the same flow conditions (Q=60 kg.h^{-1}, N=5 Hz, opening max)

The moments of both curves are reported in table 2, where it can be seen that these are quite close to each other. The spread of the curves seems to be quite important, which means that the particles cross over various regions in the mixer, resulting then in a probable good homogeneity. However, an important feature, which can be noted here, is that these curves exhibit a certain trail. This effect may be due to a stagnant zone, perhaps corresponding to the bottom part of the mixer where the blades may cause insufficient motion of the particles. A typical model for taking this into account is the series of perfectly mixed cells with material exchange with a stagnant zone, this latter being represented by an internal coefficient or a characteristic time [10].

Table 2. Characteristics of two RTD curves obtained in the same conditions

N° exp.	μ_1	μ_2	μ_3
1	59 s	4105 s^2	327406 s^3
2	63 s	4363 s^2	347967 s^3

3. Influence of tracer size

The possible presence of a stagnant zone is very problematic with respect to segregation during mixing. Such zones may become a "trap" for particles differing in size or in density for instance. This could perhaps lead to unstable flow patterns inside the mixer, or oscillating regimes, that could in turn lead to a dramatic increase or decrease of the hold-up, and finally result in to an overloading (or emptying) and a stop of the mixer.

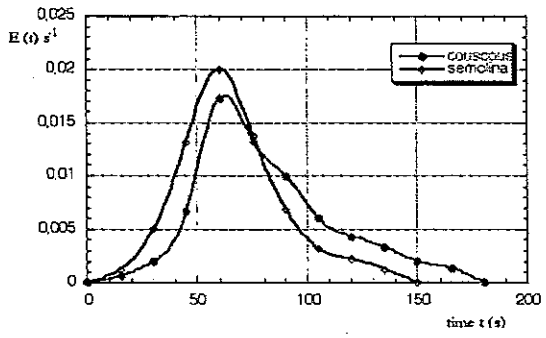

Figure 7. Comparison of the RTD curves obtained with tracers of different sizes

In order to have an insight onto this possible dynamic behavior, experiments in the same conditions as above were performed using "tracer" particles of a smaller size (semolina) than those of the bulk. The results are shown in figure 7 and are compared with those obtained previously with the "real" tracer. The semolina particles exhibit higher difficulties for leaving the mixer, as it can be seen in the earlier times. Also, the trail is much more important, which could be representative of a slower material exchange of the main flow with respect to the stagnant zone. Physically, this could be caused by an easier particle percolation through the mixer up to the stagnant zone, where smaller particles can hardly escape. Of course, this effect needs to be confirmed, perhaps by tracer injection directly at the bottom of the mixer. In any case, it seems that a major defect of such a mixer could be diagnosed from these RTD experiments, and perhaps corrected from a technological point of view. With respect to the moments of he RTD curves (see table 3), one important feature is that the centered moment seems to remain almost constant for both experiments. This could indicate that the number of cells in the series of the mentioned model is independent of the composition of the mix itself, the only effect of particle size being quantified by a characteristic time of mass transfer between the main flow and the stagnant zone.

Table 3. Characteristics of the RTD obtained for the two different tracers

	μ_1	σ^2/μ_1^2	μ_3
Colored couscous	65 s	0.134	404746 s^3
semolina	81 s	0.147	786526 s^3

CONCLUSIONS – PERSPECTIVES

In this work, investigations concerning the dynamics of the mixing process of solid couscous from the point of view of flow regimes and RTD experiments have been reported. For such an apparatus exhibiting a free surface of the particle flow, graphs showing the evolution of the spatial residence time with mass flow rates are very essential because different flow regimes effectively occur and are difficult to predict. We have also seen how crucial is the care taken of tracer characteristics. The use of a tracer of different size to that of the bulk can quickly lead to a misinterpretation of the RTD curves, and it is to be expected that shape and/or density differences could lead to the same conclusions. At this stage, it also seems that the skewness of the RTD curves could be a rather good indication of internal segregation tendency. For future investigations, the experimental part will now consist of performing RTD experiments in different flow regimes, and will probably require the use of image analysis for an easier data treatment. The presence of a possible stagnant zone remains also to be clarified via specific experiments. With respect to modeling, the effect of particle size on flow is to be taken into account on the RTD formulation, as well as its dramatic importance when mixing particles of different sizes. For instance, such models can be built up with the help of Markovian chains theory and typical classification laws [11].

REFERENCES

[1] Gisle F.Knutsen, Geir Ingvald Landmo, *Mixing of powders*, The Postec Newsletter, 15 (1996).

[2] Danckwerts P.V. Continuous flow systems: Distribution of Residence Times, Chem. Eng. Sci., 2, 1953, pp 1-13.

[3] Genin G., Houzelot J.L., Kotro A., Martin G. Nouvelles méthodes de mesure des distributions de temps de séjour d'une phase solide transportée, Chem. Eng. J., 2001, pp 301-306.

[4] Laurent B., Bridgwater J., Parker D.J. Motion in a particle bed agitated by a single blade, AIChE J., 46 (2000), pp 1723-1734.

[5] Mizonov V., Berthiaux H., Marikh K., *Application of the theory of Markovian chains to processes analysis ans simulation*, internal report, Albi (2000).

[6] Tamir A., *Application of Markov chains in chemical engineering*, Ed. Elsevier, Amsterdam (1998).

[7] Weinekötter R.,Reh L., *Continuous mixing of fine particles*, Part. Part. Syst. Charact, 12 (1995).

[8] Sinay Y., Tawashi R., *Etude modèle de mélanges solides-solides; facteurs dynamiques et géométriques*, Pham. Acta Helv., 47 (1971), 265-272.

[9] Fan L.T., Shen B.C., Chou S.T. Stochastic modeling of transient Residence Time Distributions during start-up. Chem. Eng. Sci., 50, 2, 1995, pp 211-221.

[10] Sardin M., Modélisation des interactions solide-liquide en milieu poreux naturel. Application au transport transitoire de solutés, stage CPIC «Méthodologie de la réhabilitation des sols pollés », Nancy, 1997.

[11] Berthiaux H., Espitalier F., Mizonov V. A Markov Chain Approach for Particle Classification Modeling (en russe). State of The Art and Future Potential of Energo-Technologies, Ivanovo (Russie), Juin 1999.

Z-TRANSFORM AND ADAPTIVE SIGNAL PROCESSING IN ANALYSIS OF TRACER DATA

L. Furman[1]

[1]Faculty of Physics and Nuclear Techniques, University of Mining and Metallurgy, Al. Mickiewicza 30, 30-059 Krakow, POLAND

Abstract. In the field of data processing the common practice is to interpret the tracer determined residence time distribution (RTD) of particles, through different arrangements of elementary models (plug flow, perfect mixer models, etc.). However, such analysis needs an *a priori* chosen arrangement of such models. The paper presents a competitive method based on adaptive system identification in z-transform domain, which may give better insight into flow patterns of a steady-state flow system. The general mathematical model (transfer function in z-domain) is created by adaptive algorithm using experimental data only. Then, utilising analysis of the mathematical structure and the knowledge of the investigated system, the deterministic flow model is constructed. The method also finds its application in data pre-processing: radiation background subtraction, fitting the "tail" of the RTD curve, de-convolution and on-line flow parameters identification. The application of the said modelling in interpretation of radiotracer data from recent studies in different industry sectors, is presented.

INTRODUCTION

The tracer determined residence time distribution (RTD) has been utilised in the analysis of many types of flow processes, including chemical reactors, hydro-transport in pipes, sewage systems and mineral industry operations. Many systems possess complex internal flow fields resulting from bypassing and stagnant zones (slow-moving flow regions, internal re-circulation). The approach most often used to model the mixing is the construction of a deterministic flow model. The main difficulty in using complex, descriptive flow models is the need to introduce adjustable parameters into the mathematical equations.

Continuous-time signals e.g. concentration of radiotracer, can be transformed to the complex frequency domain by Fourier or Laplace transforms. The obtained result gives additional insight into the operation of the investigated system. However, the recorded continuous–time function is transformed by the data collection process into a discrete-time function, with values being defined only for $t = nT$ (n an integer and T the sampling time). Its range is also discrete, brought about by digital counters. Therefore, we are now concerned with discrete-time systems.

1. Discrete-Time Signals and the z-Transform

The discrete time signals can also be represented by a Fourier transform (DFT). However, instead of using the more general relationship – Laplace transform, the z-transform is applied.

The z-transform, discrete-time analogue of the Laplace transform, can be introduced by setting up the relation between the complex s plane and the complex z plane:

$$z = exp\ (sT) \tag{1}$$

It may be simplified by sc. bilinear transformation:

$$s = \frac{2}{T}\frac{1-z^{-1}}{1+z^{-1}} \tag{2}$$

The definition of the z-transform $X(z)$ for any sequence of numbers (samples) x_n is given by

$$X(z) \overset{def.}{=} \sum_{n=0}^{\infty} x_n z^{-n} \tag{3}$$

In general, the variable z in (3) is a complex variable. The z^{-n} factor, associated with a particular sample x_n, represents a time delay of n sample intervals.

By taking the z-transform of the discrete time convolution relation, we can define transfer function $G(z) = Y(z)/X(z)$ where $X(z)$, $Y(z)$ are the z-transforms of input x_n and output y_n sequences.

A more general form of $G(z)$ is known as Infinite Impulse Response System (IIR) or recursive filter (a_n, b_n – constant filter coefficients):

$$G(z) = \frac{Y(z)}{X(z)} = \frac{a_0 + a_1 z^{-1} + \ldots + a_N z^{-N}}{1 + b_1 z^{-1} + \ldots + b_N z^{-N}} \tag{4}$$

Digital modelling (approximation) of real industrial processes utilises usually a recursive algorithm – the IIR system.

2. Adaptive Modelling

For derivation of the z-model for a given flow process an adaptive signal processing technique was chosen. In some applications it is advantageous to perform system identification adaptively rather then by using the classical least-squares modelling techniques, e.g. in real-time applications when system parameters change over the time or when the model is a part of an adaptive control process. It is expected that the method will simplify calculations enough to perform on-line modelling of flow systems.

The basic structure for adaptive system identification is illustrated in Figure 1.

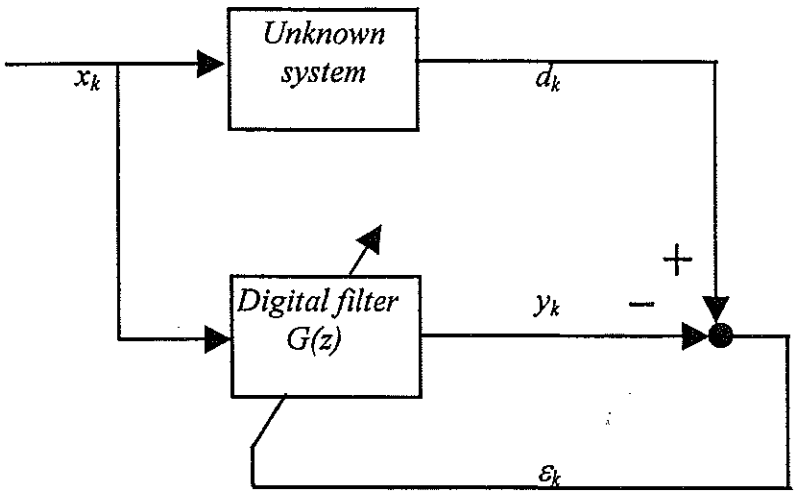

Figure 1. Adaptive system identification

In this case, we have the usual input and output sequences x_k, y_k and the time-varying transfer function describing their relationship $G(z)$. The "desired response" sequence d_k is the response of the unknown system to the input sequence. The error sequence ε_k is defined as the difference between the desired response and the actual response. It is used to control the adaptation of $G(z)$ (adjusting its coefficients).

$$\varepsilon_k = d_k - y_k \tag{5}$$

From many adaptive filtering algorithms, the SHARF - Simple Hyperstable Adaptive Recursive Filter [3] was chosen.

CHARACTERIZING FLOW PATTERNS FROM RTD

Physical interpretation of the obtained transfer function requires calculation of the inverse z-transform. However, the complicated, time-domain function is usually inconvenient for describing the mass transfer in a flow system. In this section, the suggested method of transfer function interpretation is presented.

The interpretation of the transfer function can be simplified using several simpler functions rather then a single complex one. One way is to decompose $G(z)$ into a product of first and second order functions:

$$G(z) = KG_1(z)\ldots G_S(z) = \prod_{i=1}^{S} G_i(z) \tag{6}$$

where

$$G_i(z) = \frac{\left(1 + a_i z^{-1}\right)}{\left(1 + b_i z^{-1}\right)} \qquad \text{or} \qquad G_i(z) = \frac{1 + a_{1i} z^{-1} + a_{2i} z^{-2}}{1 + b_{1i} z^{-1} + b_{2i} z^{-2}} \tag{7}$$

The system $G(z)$ is now factored into S subsystems $G_i(z)$ connected in series.
If $G(z)$ is written as a sum of terms obtained by a partial fraction expansion, we can then obtain the decomposition of $G(z)$ in parallel form:

$$G(z) = L + G_1(z) + \ldots + G_R(z) = \sum_{j=1}^{R} G_j(z) \tag{8}$$

Each term is of the form

$$G_j(z) = \frac{a_j}{1 + b_j z^{-1}} \qquad \text{or} \qquad G_j(z) = \frac{a_{1j} + a_{2j} z^{-1}}{1 + b_{1j} z^{-1} + b_{2j} z^{-2}} \tag{9}$$

The terms (7), (9) may be easily interpreted in time domain. Particularly, the first order terms may be identified as perfect mixer models, while second order terms may represent cascade of perfect mixers or a perfect mixer with dead volume.
For a given rational transfer function (system function), it is possible to identify several sets of cascade/parallel implementations that will realise the system. Some of these realisations are describing physical properties of the system. The model however, is not given *a priori* but somehow created by the adaptive algorithm.

Different elementary models commonly used to represent flow patterns of industrial systems in Laplace s-domain are given in Table 1 [4]. Together with them the appropriate mathematical models for a plug flow, perfect mixers and perfect mixers with dead volume in *z*-transform domain, are presented. To be consistent with commercially available software for RTD decomposition (e.g. "DTS", PROGEPI, Nancy), other, even well known flow models, having limited practical application are not considered. The elementary flow models were created using so called bilinear transformation. It has to be emphasised that the models obtained directly from definition (3) give perfect response to the impulse input (impulse invariant models); they are not suitable for cascade implementation. For modelling flow systems with recirculation the similar calculations as in Laplace transform domain have to be done.

Table 1. Bilinear Transformation Models

Model	Laplace transform $H(s)$	z-transform $G(z)$
Plug flow	$\exp(-\tau s)$	$z^{-\theta}$
Perfect mixer	$\frac{1}{1+\tau s}$	$\frac{1}{2\theta+1}\frac{1+z^{-1}}{1-\frac{2\theta-1}{2\theta+1}z^{-1}}$
N-perfect mixers in series	$\frac{1}{\left(1+\frac{\tau}{N}s\right)^N}$	$\left(\frac{N}{2\theta+N}\frac{1+z^{-1}}{1-\frac{2\theta-N}{2\theta+N}z^{-1}}\right)^N$
Perfect mixer with dead volume	$\frac{1+t_m s}{1+(\tau+t_m+\tau K)s+\tau t_m s^2}$ 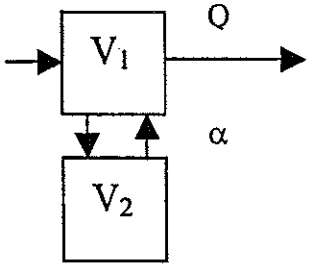	$\frac{a_0+a_1z^{-1}+a_2z^{-2}}{1+b_1z^{-1}+b_2z^{-2}}$ $a_0=(1+2\theta_m)/D$ $a_1=2/D$ $a_2=(1-2\theta_m)/D$ $b_1=(2-8\theta\theta_m)/D$ $b_2=(1-2\theta_m-2\theta-2\theta K+4\theta\theta_m)/D$ where $D=1+2\theta_m+2\theta+2\theta K+4\theta\theta_m$

τ - mean residence time MRT, T- sampling time, Q- flow rate, α - flow rate ratio, volume ratio $K=V_2/V_1$, $t_m=V_2/\alpha Q$, $\theta=\tau/T$, $\theta_m=t_m/T$

The models in *z*-transform domain are suitable for computer calculations; they enter the world of Digital Signal Processing (DSP). The theoretical work already done enabled creating elementary flow models in MATLAB® and LABVIEW™. The LABVIEW™ virtual instruments may be used then as building blocks in "G" -

graphical programming language. Also adaptive filtering procedure was implemented in LABVIEW™. However, the most important test of this new analysis technique is to examine its ability to enhance understanding of an actual physical process.

CASE STUDIES

1. Modelling of the Ball Mill

The exemplary, experimental study analysed is tracer experiment carried out on a ball mill where the grinding of copper ore takes place.
Ore samples were activated in a thermal neutron flux to produce the radioactive isotope ^{64}Cu – the natural tracer for copper. Also water solution of NH_4Br (^{82}Br) was applied as a tracer for water. Intensities of γ-rays from the tracer were measured by scintillation probes situated close to the mill's feed where also injection took place, and at the outlet. The injection was considered as an impulse function. Then, by applying DTS software, basic parameters such as MRT and separation coefficients of different components of ore were determined. The type of the RTD function (Figure 2) suggested the suitable model - series of perfect mixers with dead volume. The model consists of serially connected "plug flow" reactor and three perfect mixers with dead volume.

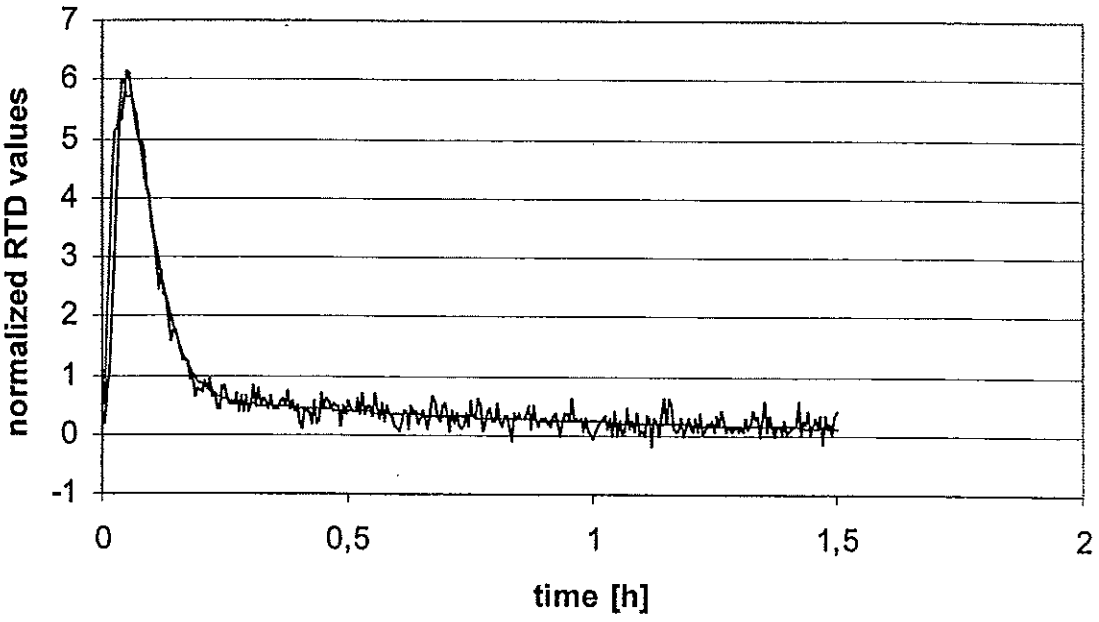

Figure 2. RTD function for sandstone ore and the z-model.

The obtained transfer function for sandstone ore in z-domain is:

$$G(z) = \frac{0.161 + 0.438z^{-1} + 0.246z^{-2} + 0.649z^{-3}}{[1-(-0.127 \pm 0.865j)z^{-1}](1-0.89z^{-1})^2} + \frac{0.098 + 0.27z^{-1}}{1-0.994z^{-1}} \quad (8)$$

The transfer function is already decomposed into two terms describing the main stream and the slow moving region. The first term with a double, positive root indicates $\tau = 5.2$[min], which agrees with the model optimised by DTS but time constants for dead volume differ remarkable because of differences in fitting the RTD tail part.

2. Background Subtraction and Tail Fitting

Thanks to the courtesy of PROGEPI-Nancy, the set of RTD functions from aerated sludge channel reactor pilot were used for testing quality of z-modelling. The feature of the most interest was sc. tail fitting in case of incomplete RTD recording and possibility of background evaluation. This could replace the fitting of exponential curve and/or subtracting a constant.

It is evident that the beginning part of the RTD function carries complete information on its type. When dealing with simulated data, the adaptive process of tail reconstruction can easily detect the correct solution. However, the experimental data, very often far from theoretical functions and with statistical fluctuations (noisy signal), may not always be appropriate for such "improvement".

In Figure 3 the background subtraction is presented. Adaptive filtering using first order filter enables identification either constant or altering backgrounds.

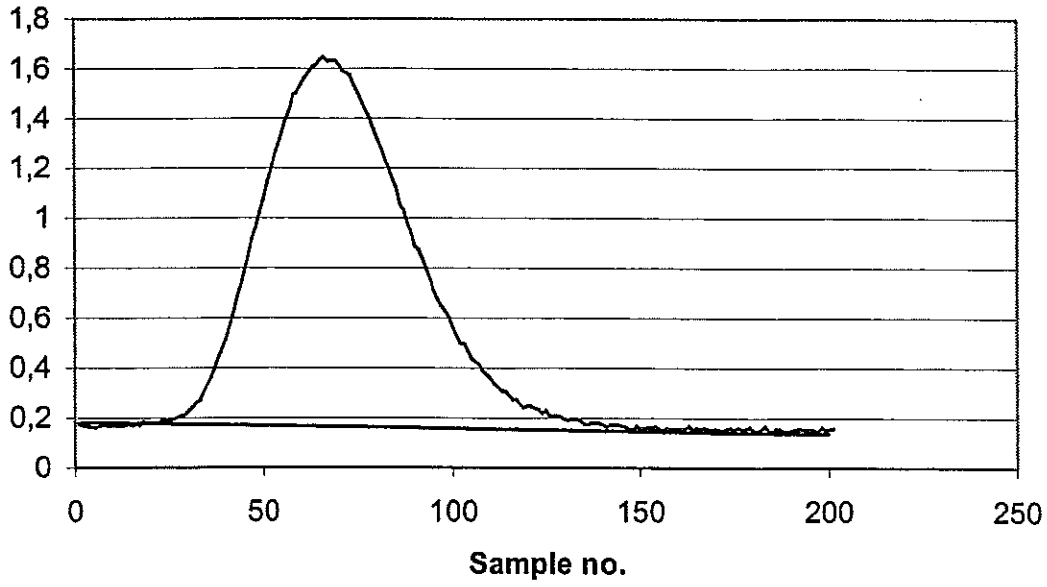

Figure 3. Background subtraction by adaptive filtering. Filter's parameters are a_0*=0.176,* a_1*=0.007,* b_1*=0.998.*

3. Real-Time Application

Setting the number of feedback filter coefficients b_n to zero (1), adaptive filtering procedure performs a simple Finite Impulse Response (FIR) model design. When coupling the adaptive software with data acquisition procedure it is possible to perform on-line z-modelling. The structure of the FIR filter requires usually more coefficients and operates slower then the appropriate IIR filter. However, this is not a case when, for instance, modelling solid state flow inside the pipes. Usually, the sc. plug flow dominates; it can be modelled by a simple z^{-n} delay, considerable reducing then the number of filter coefficients.

As a part of an international project devoted to exploitation of manganite nodules from the bottom of Pacific Ocean, the laboratory slip velocity measurements were performed [2]. The stones, Ø20-50 (mm), could be elevated to the surface by a water flow 3 (m/s) inside a Ø150 (mm) pipe. The laboratory installation, built at the Agriculture University in Wroclaw (Poland), consists of the pipeline in a form of a closed loop, with 7 (m) long vertical section. The labelled pebbles (^{82}Br tracer in a form of Hg_2Br_2) are circulating without passing through the pump blades, thus eliminating the solid state degradation.

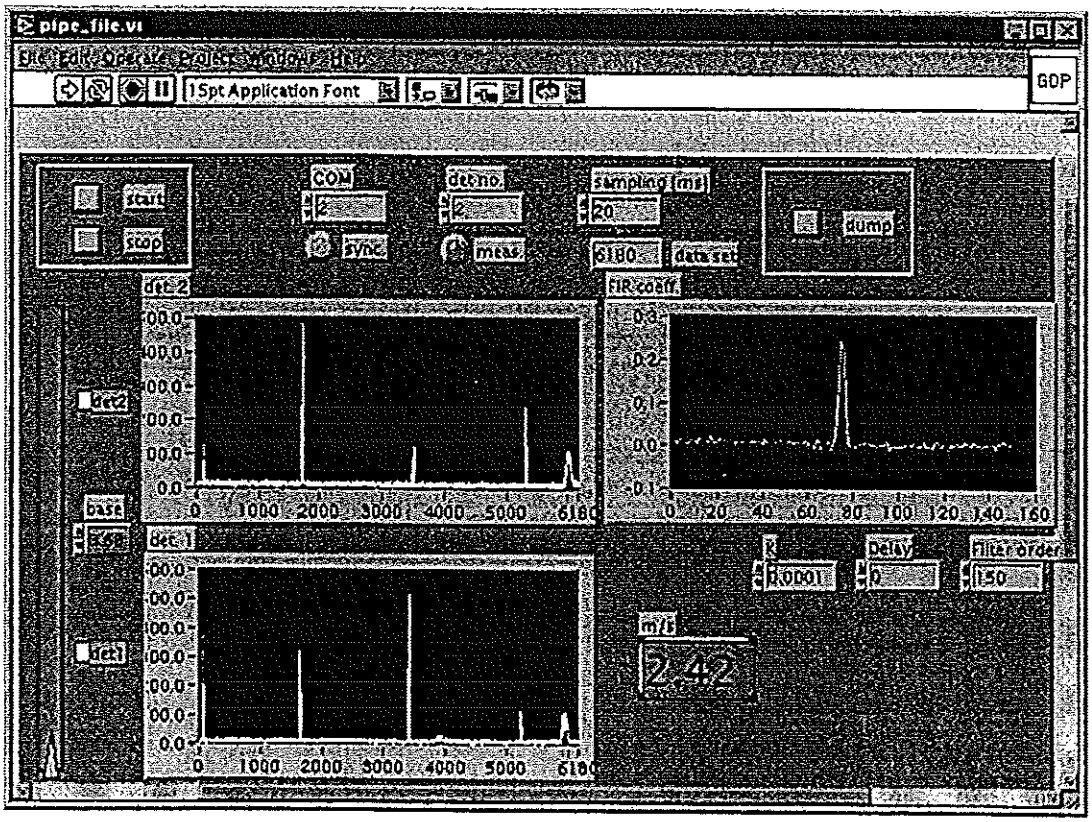

Figure 4. Front panel view of the data acquisition and adaptive filtering system. Exemplary diagram of FIR filter coefficients achieved by adaptive filtering of the data collected on hydro-transport installation after injection of a labelled pebble.

For a given measuring base 3.68(m), sampling time 20(ms) and the expected flow velocity of about 3(m/s), the estimated, relative error introduced to velocity

evaluation is about ±1.5(%). The diagram of FIR filter coefficients (Figure 4) shows the clear maximum, indicating delay of 76 samples between data collected by detector 1 and detector 2. Thus, the velocity of the pebbles is 2.42±0.03(m/s). The FIR filter follows velocity changes over the observation time. Wide peaks recorded by detectors (det.1 and det.2) result from simultaneous injection of the tracer for water (NH_4Br, ^{82}Br).

CONCLUSIONS

The *z*-domain is suitable for analysis of discrete-time tracer data. The adaptive derivation of the *z*-model and the proposed method of its interpretation provide a physical base for interpreting the RTD functions. In case of an *a priori* chosen arrangement of elementary models some information carried by RTD curve may be lost. The flow fields obtained from adaptive filtering of the RTD curve seem to be more realistic, even though we deal with a problem of non-uniqueness in transfer function interpretation. The elementary z-models (e.g. digital filters) may be used as building blocks for constructing a model of the entire process.
The unique features of adaptive filtering: background subtraction, "tail" fitting, and de-convolution may find application in data pre-processing.
When coupling the adaptive filtering software with data acquisition procedure it is possible to perform on-line velocity measurements of multiphase flows.

ACKNOWLEDGEMENTS

The author gratefully acknowledge the financial support of International Atomic Energy Agency (IAEA), Research Contract No.POL-10055 and the KBN – State Committee for Scientific Research, Research Grant KBN/HP_K460-XP/AGH/013/2000.

REFERENCES

[1] Furman, L., *Application of the z-Transform and Adaptive Signal Processing to Radiotracer System Analysis; Guidelines for z-model interpretation. Report of the First Research Co-ordination Meeting on Radiotracer Technology for Engineering Unit Operation and Unit Processes Optimization*, International Atomic Energy Agency (IAEA) Vienna, Austria, 20-23 April 1998, Annex 15.
[2] Sobota, J., Boczarski, S., Vlasak, P., Berman, V., *Preliminary Results of Slip Velocity Measurements in Vertical Pipeline During Coarse Particle Mixture Flow. 10th International Conference on Transport and Sedimentation of Solid Particles*, 4-7 Sept. 2000, Wrocław, Poland, (2000), 589.
[3] Stearns, S.D., & David, R.A., *Signal Processing Algorithms*. Prentice-Hall, Englewood Cliffs, New Yersey (1988)
[4] Zitny, R., Thyn., J., *Residence Time Distribution Software Analysis.User's Manual.* Computer Manual Series No.11, International Atomic Energy Agency (IAEA), Vienna (1996)

CHARACTERIZATION OF AN ELECTROCHEMICAL INDUSTRIAL SIZE FILTERPRESS REACTOR BY HYDRODYNAMIC AND MASS TRANSPORT STUDIES

Angel Frias-Ferrer[1], José González-García[1], Juan A. Conesa[2], Enrique Gadea-Ramos[3], Eduardo Expósito[1], Vicente García-García[1], Vicente Montiel[1] and Antonio Aldaz[1]

[1] Departamento de Química Física. Universidad de Alicante. Web: *http://www.leqa.ua.es*
[2] Departamento de Ingeniería Química. Universidad de Alicante.
[3] Departamento de Química Inorgánica. Universidad de Alicante.
Ap. correos 99, C.P.: 03080 Alicante (Spain)

Abstract. This work deals with the study of the influence of turbulence promoters in hydrodynamic and mass transport behaviour of a filter-press type electrolyser with 3250 cm^2 of electrode area (model REIM 3300 supplied by "I.D. Electroquímica") in undivided configuration.

A simple experimental arrangement was used to generate data from electrolytic conductivity measurements in a series of impulse-response experiments. The experimental curves has shown a strong influence of the presence or absence of turbulence promoters inside the reactor in the hydrodynamic behaviour. In previous papers, we used a new approach to analyse the different residence time distributions (RTD) in other smaller reactors. In those studies a new parameter, the turbulence factor, given as $N_\alpha\theta_\beta$, was defined and employed to classify the turbulence promoters. The model used in those papers assumes plug flow with dispersion and flow exchange with stagnant zones and uses three parameters: N_α, θ_β and Pe. N_α characterises the rate of exchange between the stagnant zones and the dispersed plug flow, θ_β is the ratio between volume in dispersed plug flow/total volume and Pe is the Peclet number. In this present work a new complication has been taken into account due to the presence of two peaks in the RTD curves. Then a model with two paths has been used in order to describe the hydrodynamic behaviour of this electrochemical industrial size filterpress reactor.

The optimised values of the parameters provided by the model give a plug-flow hydrodynamic behaviour with low axial dispersion for the reactor with turbulence promoters and more mixing for the empty configuration.

The classification obtained by electrochemical method (mass transport enhancement factor) for the turbulence promoters (plastic nets) is compared with the obtained from hydrodynamic study.

INTRODUCTION

As late as 2000 electrochemistry and the application of electrochemical reactors in the industry is not totally accepted and it is usually relegated to a secondary option in front of other more traditional techniques. One of the possible facts of this abandon would be the lack of a good knowledge of the hydrodynamic behaviour of these systems.

Real reactors never fully follow the idealised flow patterns. This deviation can be caused by channelling of fluid, by recycling of fluid, or by creation of stagnant regions in the vessel. In all these cases this type of irregular flow should be avoided since it always lowers the performance of the unit.

The problems of this type of nonideal flow are closely related with the losses of efficiency in systems at pilot-plat scale or at fully industrial scale. For this reason it is important to take into account the nonideal flow pattern inside the reactor in order to minimise the inefficiencies in the whole system.

One of the most usual methods for characterise system is the use of RTD (Residence Time Distribution) curves. An RTD curve shows how long the individual molecules of fluid stay in the vessel.

In this present work, a tracer substance is injected quickly into the flowing stream of fluid at the inlet of the reactor. A detector located at the reactor outlet detects the disturbance of the tracer as it exits the reactor. Signal is transmitted to a computer which displays the curve of concentration into a screen or saves it into a floppy disk.

This paper is focused on the study of an industrial scale electrochemical filter-press reactor and it is the continuation of other previous works [1-3].

EXPERIMENTAL SECTION

The electrochemical reactor was an industrial scale filter-press electrochemical cell (model REIM 3300 supplied by "I.D. Electroquímica"). The turbulence promoters used were very similar to those used in other works found in literature and its geometrical dimensions and view are shown in Figure 1 and Table 1. It is interesting to point out the characteristics of the turbulence promoters, such as the strands, apertures and mesh area, which are important aspects in the full characterisation of the turbulence promoters.

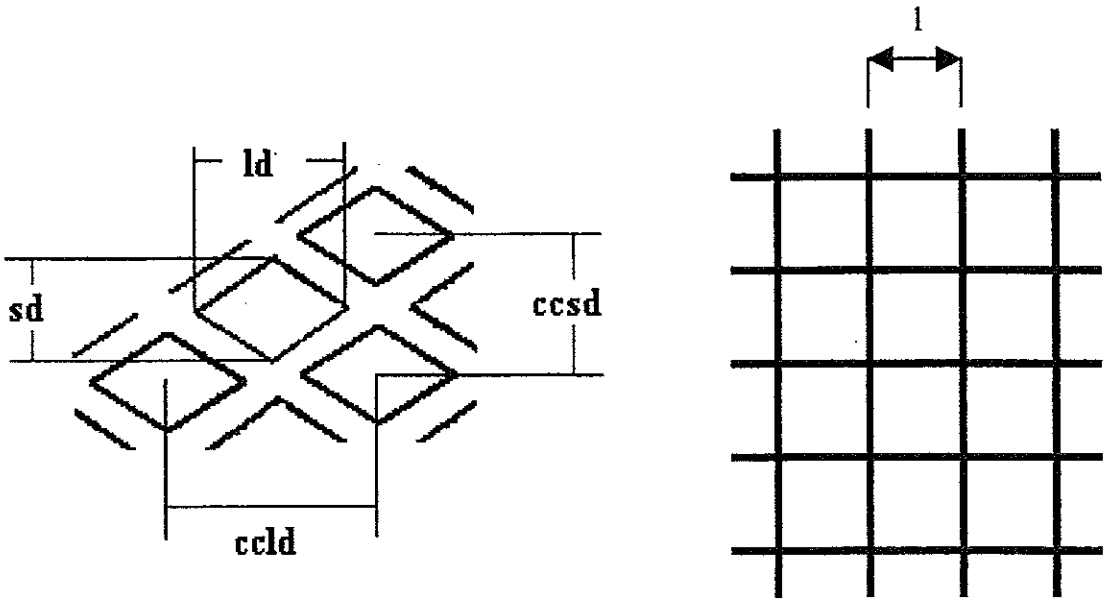

Promoter A Promoter B

Figure 1. Sketch of the parameters of the turbulence promoters. (Values in Table 1)

Table 1. Parameters of the turbulence promoters

Parameter	Promoter A	Promoter B
sd/ mm	4.5	
ld/ mm	6.6	
ccld/ mm	9	
ccsd/ mm	7	
Promoter thickness/ mm	2	1.4
l / mm		11
Porosity	0.73	0.72

The promoters were placed in the compartment (length 65 cm, width 50 cm, thickness 2.5 cm). The number of promoters was high enough to assure that, the compartment is completely occupied and the promoters cannot be moved away.

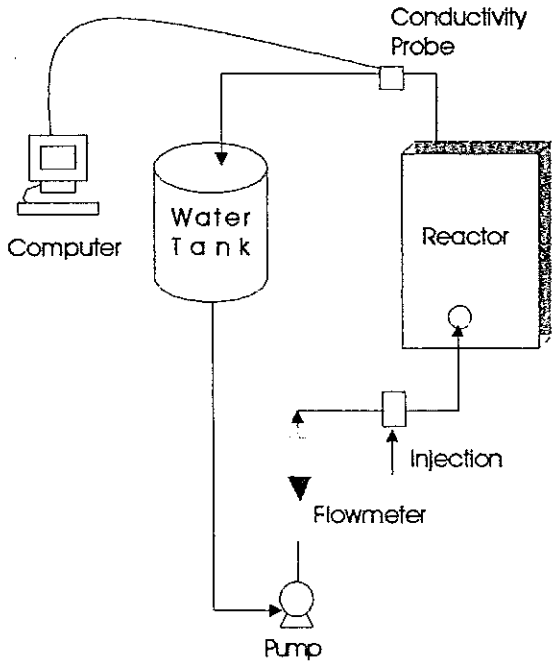

Figure 2. Diagram of the system

The solution was pumped into the reactor from one tank of 600 l. The flow rate was controlled between 300-800 L/h which means a lineal velocity for the fluid inside the reactor between 0.6-1.8 cm/s approx.

At the outlet a conductivity probe was placed inside the pipe to measure the conductivity. The signal was recorded and send to a computer where it is processed.

For each experiment the water tank was drained and filled again with water. The injection at the inlet of the reactor was 5 mL of saturated NaCl using a syringe. The injection was approximately half second long.

MATHEMATICAL MODEL

To develop a model for the observed behavior, different non-ideal flow models have been tested. These models are based on the combination of the dispersed plug-flow reactor model and models for stirred tank reactors in series.

In our case, and due to the existence of two peaks in the RTD, the model proposed considers two possible paths by where the electrolyte may flow. A scheme of this model is shown in Figure 2. This model is a modified version of the model used in other works [3].

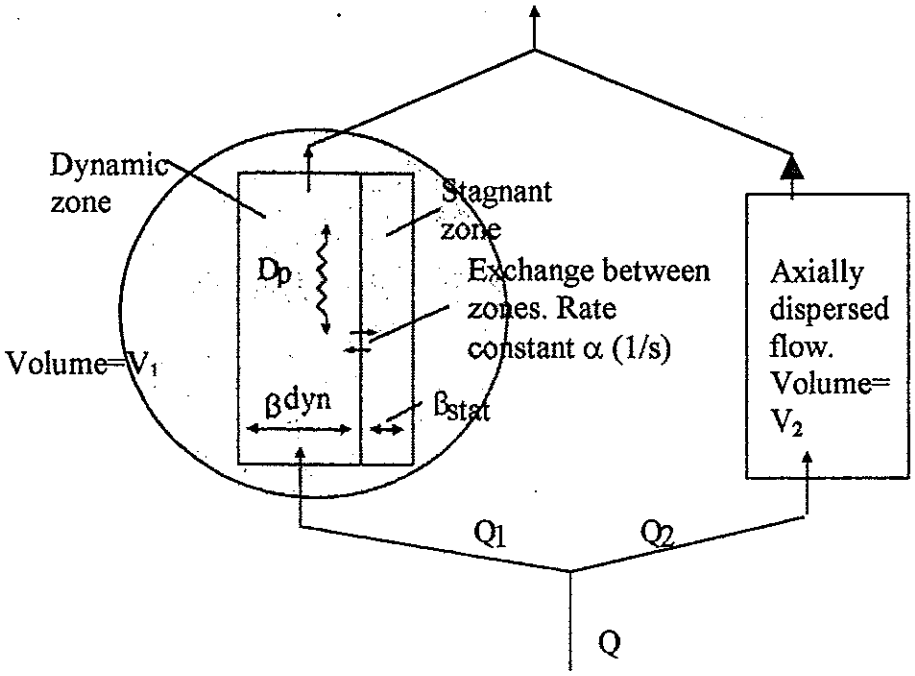

Figure 3: Model proposed

For one of the paths, (path 1, occupying a volume V_1) it is assumed that the electrolyte flows following a dispersed plug-flow model, and that exists a stagnant area. The electrolyte in the stagnant areas is slowly refreshed by the freely flowing electrolyte that can be considered in axially dispersed plug flow. The electrolyte hold-up in this zone, β_{tot}=m^3 liquid/m^3 column, is divided into a dynamic hold-up, β_{dyn} and a static or stagnant hold-up, β_{stat} (see Figure 3). The local rate of exchange between the dynamic (d) and static (s) hold-up is assumed to be proportional to the concentration difference in the dynamic and static phases, and it can be characterized by an exchange coefficient, α_m (s^{-1}), defined by,

$$\frac{number\ of\ moles\ exchanged}{m^3\ liquid \cdot \sec ond} = \alpha_m\,(c_d - c_s) \qquad (1)$$

where c_d and c_s are the concentrations in the dynamic and static phase respectively. α_m can be considered as the product of a mass transfer coefficient and the specific interfacial area between the flowing and the stagnant zones, k_La.
The model equations can be found from applying the mass balance equation and the results are:

$$\theta_\beta \frac{\partial C_d}{\partial} = \frac{1}{Pe_d} \frac{\partial^2 C_d}{\partial Z^2} - \frac{\partial C_d}{\partial Z} - N_\alpha (C_d - C_s) \qquad (2)$$

$$\left(1-\theta_\beta\right)\frac{\partial C_s}{\partial \theta} = -N_\alpha\,(C_s - C_d) \tag{3}$$

where Z=z/L, being L the total length of the reactor; $\theta_\beta=\beta_{dyn}/\beta_{tot}$; $N_\alpha=(\alpha_m \cdot L)/(\theta_\beta u_1)$; $Pe_d=(u_1 \cdot L)/D_d$; $\theta=t/\tau$, with $\tau=L/(\theta_\beta u_1)$; $C_s=c_s/c$; $C_d=c_d/c$. In this way, N_α is the number of mass transfer units for the mass exchange between the dynamic and the static phase, and Pe_d is the Peclet number for the dynamic phase.

For the other path (path 2, occupying a volume V_2), the dispersed plug-flow model, assuming a small dispersion grade is applied. The curve representing the distribution of residence times for path 2 (E_2) is:

$$E_2 = \frac{1}{2\sqrt{\frac{\pi}{Pe_2}}}\exp\left(-\frac{\left(1-\frac{t}{\tau_2}\right)^2}{\frac{4}{Pe_2}}\right) \tag{4}$$

In this equation, Pe_2 is the Peclet number for path 2; t is time from the injection of a tracer and τ_2 is the mean residence time for path 2.

Considering that the model proposed for path 1 may be applied to a volume V_1 that has a flow rate Q_1, and the model for path 2 may be applied to a volume V_2, with a flow rate Q_2, the total RTD is calculated using:

$$E = E_1\frac{Q_1}{Q} + E_2\frac{Q_2}{Q} \tag{5}$$

Where E_1 is the RTD curve for path 1 and it is obtained from the solutions of equations (2) and (3). The values that must be optimised are: τ_1, θ_β, Pe_d, N_α, τ_2 and Pe_2.

RESULTS

Figure 4 shows the RTD curves obtained for the promoter B at different values of Re and Figure 5 shows an example of the model fitting for one experimental data.

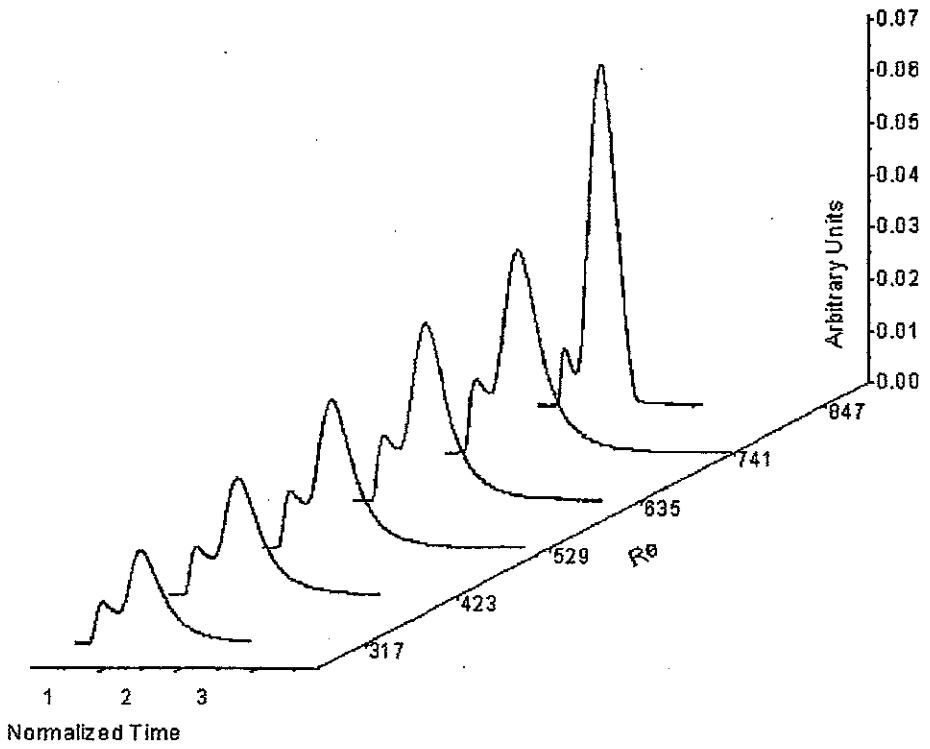

Figure 4. RTD curves for the reactor with promoter B

The optimized values of the parameters provided by the model give a plug flow hydrodynamic behaviour with low axial dispersion for the reactor with turbulence promoters (higher Pe and θ_β values than empty configuration) and more mixing for the empty configuration. It is also very interesting to highlight that the turbulence factor, $N_\alpha\theta_\beta$, (see Table 2) decreases as Re increases, showing the same behaviour that the mass transport enhancement coefficient obtained from electrochemical studies using the limiting current technique.

The classification obtained by electrochemical method for the turbulence promoters (plastic nets) A and B is the same than that obtained from hydrodynamic study: B > A > empty.

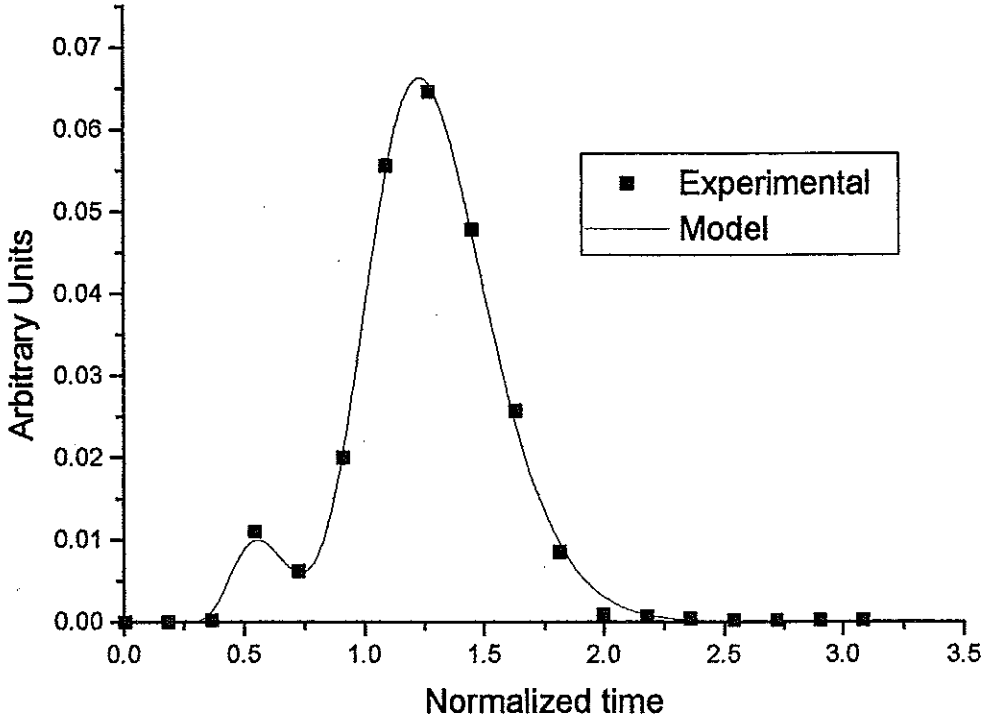

Figure 5. Example of model fitting with the reactor filled with promoter B. Re = 847

Table 2. Summary table

	Promoter A			Promoter B			Empty		
Re	θ_β	N_α	$N_\alpha \cdot \theta_\beta$	θ_β	N_α	$N_\alpha \cdot \theta_\beta$	θ_β	N_α	$N_\alpha \cdot \theta_\beta$
317	0.81	0.38	0.31	0.78	3.35	2.61	0.86	0.31	0.27
423	0.79	0.32	0.25	0.79	3.07	2.43	0.76	0.2	0.15
529	0.8	0.23	0.18	0.83	2.35	1.95	0.85	0.27	0.23
635	0.82	0.14	0.11	0.86	2.20	1.89	0.92	0.17	0.16
741	0.82	0.16	0.13	0.83	2.06	1.71	0.84	0.12	0.10
847	0.9	0.11	0.10	0.99	1.06	1.06	0.83	0.10	0.08

REFERENCES

[1] J. González-García, J. A. Conesa, J. Iniesta, V. García-García, V. Montiel, A. Aldaz, *Characterization of an electrochemical laboratory filterpress reactor by hydrodynamic and mass transport studies,* I. Chem.E. Symp. Ser. 145 (1999) 51-60.

[2] José González-García, Angel Frías, Eduardo Expósito, Vicente Montiel, Juan A. Conesa and Antonio Aldaz, *Characterization of an electrochemical pilot-plant filter-press reactor by hydrodynamic and mass transport studies,* Ind. Eng. Chem. Res. 39 (2000), 1132-1142.

[3] José Gonzalez-García, Vicente Montiel, Antonio Aldaz, Juan A. Conesa, José R. Perez and Guillermo Codina, *Hydrodynamic behavior of a filter-press electrochemical reactor with carbon felt as a three-dimensional electrode,* Ind. Eng. Chem. Res. 37 (1998), 4501-4511.

USING SOLUTES AS TRACERS FOR THE CHARACTERIZATION OF A LIQUID – LIQUID SEPARATION PROCESS : THE CENTRIFUGAL PARTITION CHROMATOGRAPH

L. Marchal[1], J. Legrand[1], A. Foucault[2]

[1]Laboratoire de Génie des Procédés-Environnement-Agroalimentaire, GEPEA - UMR-MA 1152
Université de Nantes - IUT de Saint-Nazaire, C.R.T.T. - B.P. 406
44602 SAINT-NAZAIRE CEDEX (FRANCE)
[2]CNRS-FRE 2314, Laboratoire Biochimie et Molécules Marines, IFREMER - BP 21105
44311 NANTES CEDEX 03 (FRANCE)

Abstract. Centrifugal Partition Chromatography is a chromatographic method that uses two immiscible liquid phases prepared by mixing two or more solvents or solutions. The flow patterns of the two phases in the instrument have an influence on the separation efficiency of the process. The characterization of this effect is obtained with a two-step tracing method:
1.study of the mobile phase hydrodynamic by residence time distribution analysis, using a solute with no affinity for the stationary phase;
2.mass transfer coefficient calculation by injection of a solute with a given partition between the two phases.
The chromatograph is modeled by a plug flow with axial dispersion for the mobile phase, and mass exchange with a stagnant volume corresponding to the stationary phase. The axial dispersion coefficient in the mobile phase is determined in function of process parameters and flow patterns.

INTRODUCTION

Centrifugal partition chromatography is a separation process based on the partitioning of solutes between two immiscible liquid phases. The apparatus consists of a series of cells connected by ducts in cascade and subjected to an important centrifugal field (see Figure 1). One phase is kept into the cells (the stationary phase) while the other one is pumped through it (the mobile phase). The separation process occurs in each cell when the two liquids are in contact.

According to their affinities for the two phases, the solutes have different retention times in the instrument. If K_D is the partition coefficient of a solute in a two-phase system, its retention time, Tr, is :

$$Tr = \frac{Vm}{Q} + K_D.\frac{Vs}{Q}$$

Vm is the mobile phase volume, Vs the stationary phase one and Q the volumetric flow rate of the mobile phase. When optimizing a mass transfer process like CPC, solvent selection, operating conditions and design criteria need to be carefully evaluated.

In CPC, the two-phase system is chosen in order to obtain distinct partition coefficients for the solutes to be purified, with values around one. As the two phases are liquid, they can be finely tuned using up to five solvents or solutions, giving then very selective systems. Physical properties of solvents (density, viscosity and interfacial tension) are also important parameters and must be taken into account.

Operating conditions are the mode of elution, i.e. the type of the mobile phase (upper phase UP or lower phase LP), the flow rate and the intensity of the centrifugal acceleration field.

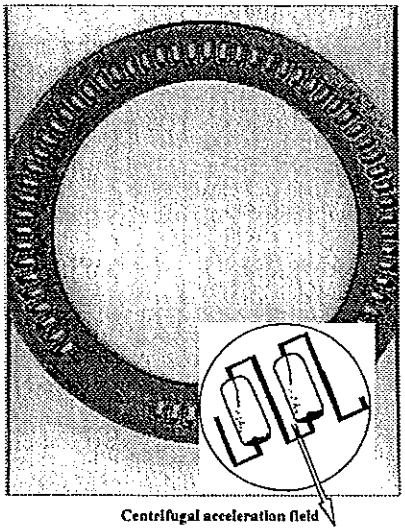

Figure 1. The stainless steel ring engraved with 66 cells ; the sketch represents the mobile phase, dark colored (the more dense one here) flowing through the colorless stationary phase.

The broadening of a solute peak, i.e. the loss of separation efficiency, may have different origins:

1.injection method;
2.off-column set-up (pipe fittings, valves, rotary seal joints) ;
3.duct shape (mobile phase flow) ;
4.flow patterns in each cell (volumes and behavior of both two phases).

The aim of this study is to consider each source of dispersion. Each point will be characterized using R.T.D. (residence time distribution) analysis, and flow pattern determination by video visualization, owing to a CPC prototype with the upper side transparent. The model used is based on chromatography modeling introduced by J. Villermaux [1], and applied to CPC by M. van Buel [2].

EXPERIMENTAL

As initially reported by Scott and Kucera [3], complete injection of a sample loop results in a non ideal injection concentration profile, with a broadening that has to be taken into account for the following steps of the model. To solve this problem, a two-points measurement method was employed. As often in chromatography, the UV absorption property of solutes was used to determine the R.T.D. The experimental setup consisted of two Spectra 100 UV detectors (ThermoQuest, San Jose, CA, USA), equipped with 0-3 mm, 0-4.6 µl, variable pathlength preparative scale LC flowcells. The first one was located just after the injection valve in order to record the input concentration profile, and the second one was downstream of the CPC column and for the output concentration profile. The solution was diluted in

order to respect the linear response domain of the UV detectors. Data were collected and discretized by a SA32 data acquisition system (AOIP, Evry, France), and exported onto a computer for the treatment.

An overview of the experimental setup is shown in (Figure 2).

A P4000 quaternary gradient pump equipped with inert assemblies (ThermoQuest), delivered a constant flow rate from 0.1 up to 30 ml/min. A 6-port injection valve, with a 240 µl loop in peek™ tubing (Polyetheretherketone), and a 4-port switching valve, both in peek™ material (Upchurch Scientific, Oak Harbor, WA, USA), were used for injection and selection of either "ascending" (less dense mobile phase) or "descending" mode (more dense mobile phase).

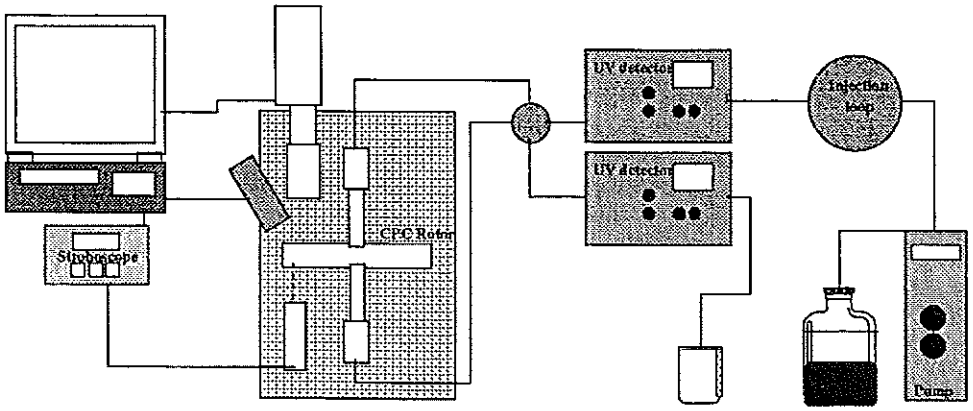

Figure 2. Overview of experimental setup, with the video equipment on the left, the visual CPC in the middle, and the injection-detection system on the right.

1. The visual CPC

The visual CPC is a prototype designed to visualize the flow pattern in each cell of a CPC column. The cells are engraved in a 5 mm thick steel ring (Figure 1) clamped between a steel plate and a glass ring of optical quality (Ediver, Rebais, France). A 0.05 mm thick Teflon® sheet was tightened on each side of the engraved ring to ensure a leakage-free rotor. There are 66 cells, nearly parallelepipedic (10x4x5 mm) connected by 0.8 mm width ducts. The rotor is connected through 1/16 in. peek™ tubing (Upchurch) and to 2 rotary seal joints (Tecmeca, Epernay, France).

The visual CPC rotor is driven by an asynchronous motor (Leroy Somer, Angoulême, France) allowing rotational speeds up to 3,000 rpm.

2. Video instrumentation

A slightly modified VideoStrobe system was used (Sysmat Industrie, St Thibault des Vignes, France), consisting of a TMC-9700 progressive scan CCD color camera (Pulnix, Sunnyvale, CA, U.S.A.) with an asynchronous shutter, two Phylec stroboscopic units (Sysmat) and a VLS7T optical speed sensor (Compact, Bolton, U.K.) which triggered both stroboscopes and camera. The camera was equipped with a 18-108 mm F 2.5 TV Zoom lens and connected to a CDM-810 multi-system converter (World Advanced Technologies, Toulouse, France), allowing NTSC/PAL/SECAM transcoding. Images were recorded on an HR-DD946MS video-recorder (JVC, Japan) monitored with a CPM1404 monitor (Hitachi, Japan).

3.Two-phase system and tracer

One two-phase system was used, made with two solvents, heptane and methanol (well-known system for the separation of fatty acids and lipids). Heptane and methanol were purchased from Carlo Erba (Rodano, Italy). The physical properties of each phase are summarized in Table 1. Heptane is partially miscible with methanol (miscibility 30% w./w.). Due to this miscibility, the two phases have similar densities and viscosities, and the interfacial tension is low (it was measured by the spinning drop method at 23°C [4]). The viscosities were calculated by pressure drop measurements in a capillary tube, preliminary calibrated with pure solvents.

Table 1. Physical properties of the 2-phase system at 22°C (except σ, at 23°C). UP: upper phase, LP: lower phase

System	ρ density UP (kg/m^3)	ρ density LP (kg/m^3)	Δρ density difference (kg/m^3)	σ interfacial tension *mN/m*	μ viscosity UP *cP*	μ viscosity LP *cP*
Hep/MeOH	684	756	72	1.16	0.47	0.65

The study is done in "descending" mode (the lower phase LP is the mobile phase) and potassium nitrate KNO_3 (R.P. Normapur® from Prolabo, Paris, France) is used as a tracer for RTD determination in the mobile phase, because it has no affinity with heptane ($K_D = 0$). KNO_3 has a maximum of absorption at a wavelength value of 220 nm (the spectrum was achieved with a UV/Vis spectrometer (ATI UNICAM UV2 series spectrometer, Cambridge, UK)).

FLOW PATTERNS

This system is studied for flow-rates in the 3-24 ml/min range and rotational speeds in the 400-2,400 rpm range (results are summarized in a flow chart - Figure 3, and are analyzed in [5]). Typically, the mobile phase enters the cell at the outlet of the duct, and an interface is created. Then the deformation of the interface between the two phases depends on the operating conditions. At the outlet of the cell, separation phase occurs with settling of the mobile phase. Thus, the mobile phase reaches the next cell by the connecting duct. Three main flow patterns are observed, in agreement with previous studies [6-7]:

1.jet or film stuck along the cell walls;
2.curvilinear film or curtain with oscillating instabilities;
3.atomization.

For each flow rate value, at low centrifugal acceleration fields (400-700 rpm, i.e. 18-56 g, where g=9.81 m/s^2 is the gravitational field), the mobile phase flows as two films along the cell walls. When the flow rate increases, one of the two films leaves the walls. Then, there is a transition zone, where the gravitational field becomes negligible (700-900 rpm, i.e. 56-93 g), the two films become unstuck, giving just one oscillating film, strongly deviated from the radial direction by the Coriolis force

[5-6]. The film length decreases with increasing the rotational speed, due to interfacial instabilities apparition, giving droplets often too small to be distinguishable on the video screen. For the lower flow rates, the film length decreases down to 0, and a cloud of droplets is formed. For the higher ones, Q > 15 ml/min, instabilities appear in the duct, giving suddenly an atomization shape.

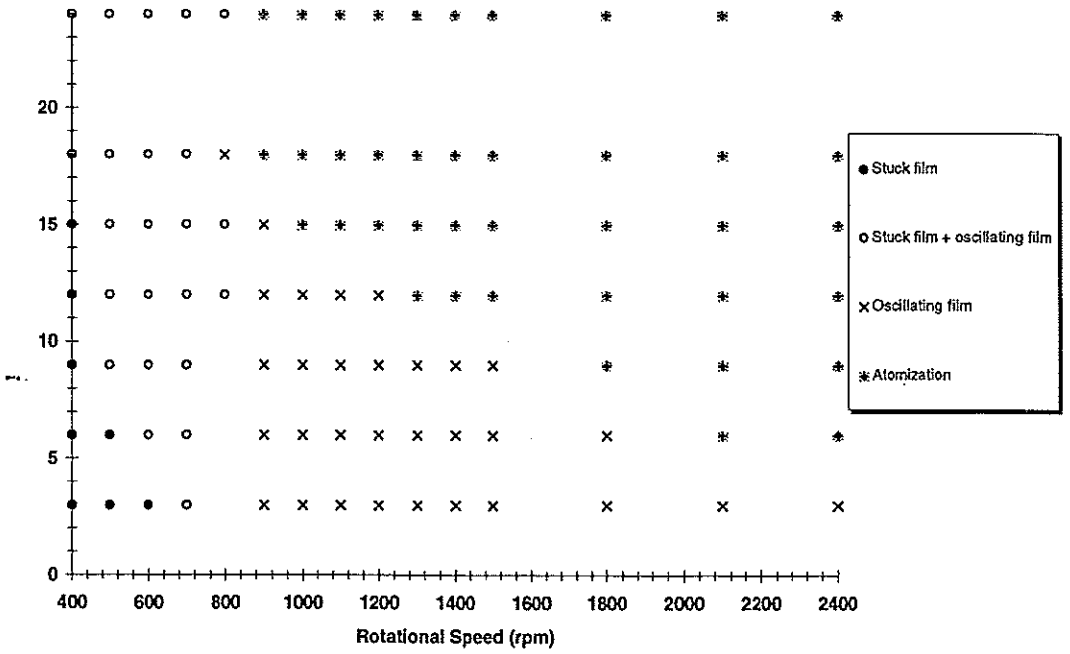

Figure 3. Flow chart – system heptane / methanol in descending mode

THE MODEL

The overall setup is schematized in Figure 4. The CPC column consists in two parts with different volumes: the off-column volume and the chromatographic column volume occupied by the mobile and the stationary phases.

The axial dispersion due to the mobile phase flowing in the off-column volume is first estimated. The column is bypassed with a ZDV union (Upchurch, ZDV = Zero Dead Volume) between the inlet and the outlet tubes.

The corresponding convection-diffusion equation for the mobile phase plug flow with axial dispersion model in each volume is :

$$U\frac{\partial C}{\partial z}+\frac{\partial C}{\partial t}=D_{ax}\frac{\partial^2 C}{\partial z^2}$$

where C is the solute concentration, U the linear velocity (m/s), D_{ax} the axial dispersion coefficient, z the axial coordinate. The corresponding transfer function in the Laplace domain is:

$$G(s)=e^{\frac{Pe}{2}-\frac{Pe}{2}\cdot\sqrt{1+\frac{4.\tilde{t}_s.s}{Pe}}}$$ with the Péclet number, $Pe=\frac{U.L}{D_{ax}}$,

and the mean residence time, $\bar{t}_s = \frac{L}{U} = \frac{Vm}{Q} = \frac{\varepsilon_m . Vc}{Q}$

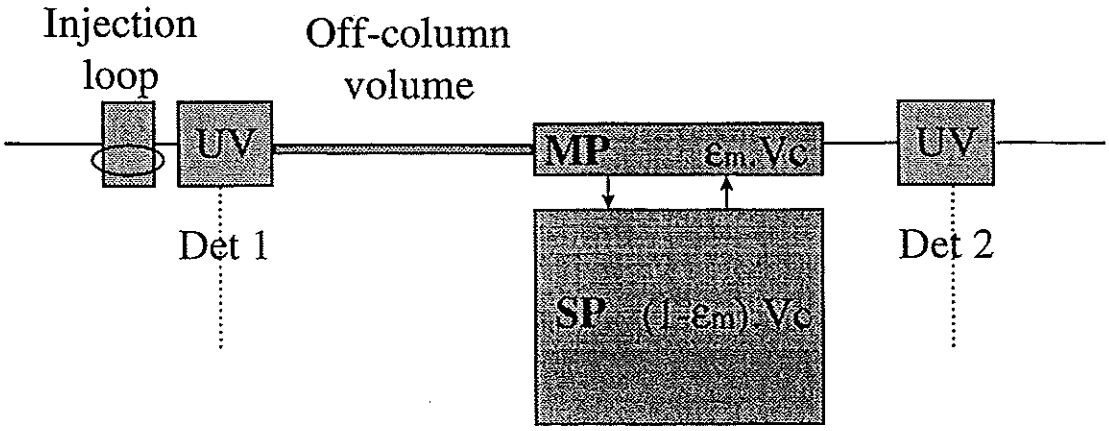

Figure 4. The column and the different volumes
(Vc: the column volume, ε_m = Vm/Vc: the mobile phase fraction)

A computer program has been developed: the experimental curves are first normalized and then converted in Fourier series. Owing to the transfer function, the theoretical outlet curve is calculated and the model parameters ($\bar{t}_s$ and Pe) are fitted, using the Rosenbrook algorithm, in order to minimize the difference between theoretical and experimental curves. Details on the method can be found in [8].

PHASES RATIO

1.Off-column volume
Methanol rich phase (LP) is pumped at flow rates ranged from 3 up to 24 ml/min through the off-column volume. The mean residence time of the solute and so the off-column volume, Vo, are calculated. Vo is equal to:

Vo = 3.11 ml ± 5%

2.Chromatographic column
The column has a 16.1 ml volume. It is preliminary filled with the stationary phase, the rotor is driven at the desired rotational speed, and then the mobile phase is pumped at a given flow rate. The resulting equilibrium of the two phases in each cell gives the minimum mobile phase volume available at this operating conditions. There are two methods to measure this volume: a direct measurement of the displaced stationary phase volume at the outlet of the column, and a calculation through the mean residence time in the mobile phase. The two methods are in good agreement, showing that there is no dead volume in the mobile phase. The mobile phase fraction, ε_m, seems to be a linear function of the flow rate at a given rotational speed, whereas it decreases with the acceleration field, reaching a limit value (Figure 5). When Q leads to 0, the ε_m value gives the minimum of mobile phase ratio available in the instrument ε_{mo}, when there is no mobile phase in the cells [4].

ε_{mo}=0.20 ± 5%. 20% of the mobile phase volume does not participate in the separation step.

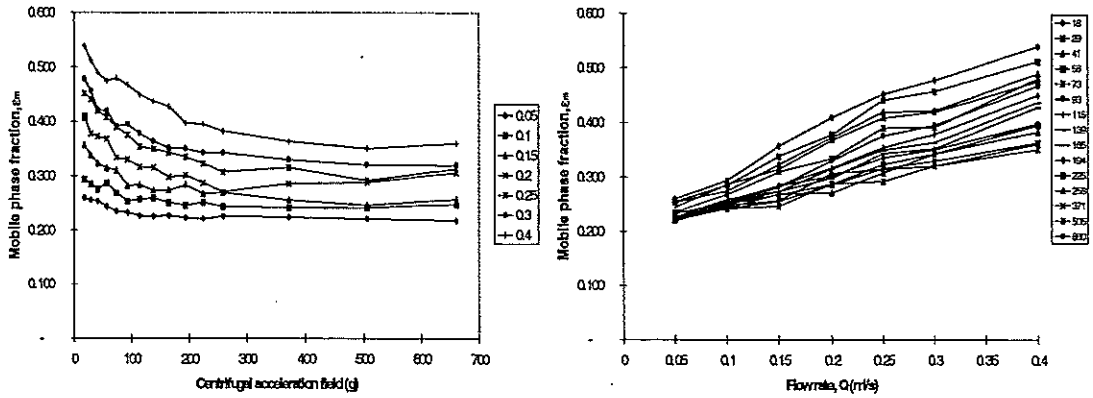

Figure 5. Mobile phase fraction as a function of the centrifugal acceleration field (on the left) and the flow rate (on the right)

AXIAL DISPERSION

1. Off-column axial dispersion

The off-column volume (3.1 ml) is equivalent to a 382 cm length 0.04 in. ID peek™ tube. The corresponding Reynolds number varies from 70 to 600, and it is typical of a laminar flow. In Figure 6, the axial dispersion coefficient is plotted vs. the linear velocity U.

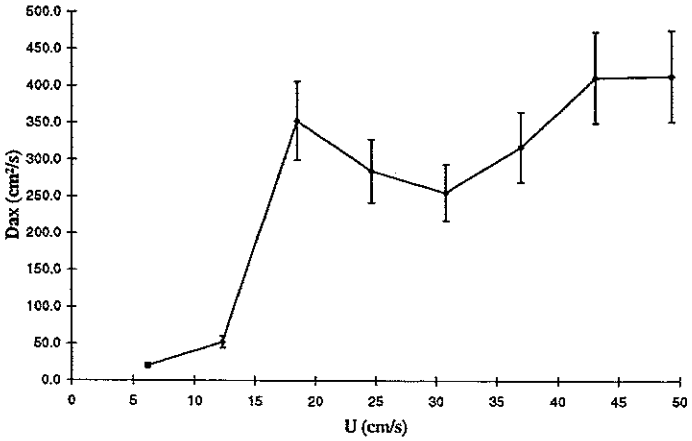

Figure 6. The axial dispersion coefficient (cm²/s), as a function of the linear velocity (cm/s) in the off-column volume

In established laminar flow in straight pipes, D_{ax} is proportional to U^2 [9]. When U is greater than 18 cm/s, the law is not verify any more, and D_{ax} reaches a limit value (around 400 cm²/s). The bends, valves and joints create disturbances and diminish the laminar character of the flow in the off-column setup. This values of D_{ax} are used into the following calculation of the column dispersion.

2.Mobile phase dispersion

The mobile phase dispersion coefficients are presented on Figure 7. The values of these coefficients are 100 times lower than those obtained for the off-column volume. There is no apparent influence of the mobile phase fraction value. Inside the column, straight ducts are very short, there is no sufficient length between two cells to have an established laminar flow. However D_{ax} decreases as the centrifugal field grows up to 93 g. This value corresponds to the transition between stuck film and atomization. Then the axial dispersion coefficient is very small and constant (3-6 ml/min), or negligible (Q≥9 ml/min). In all cases, the mobile phase flow behavior is close to a plug flow one.

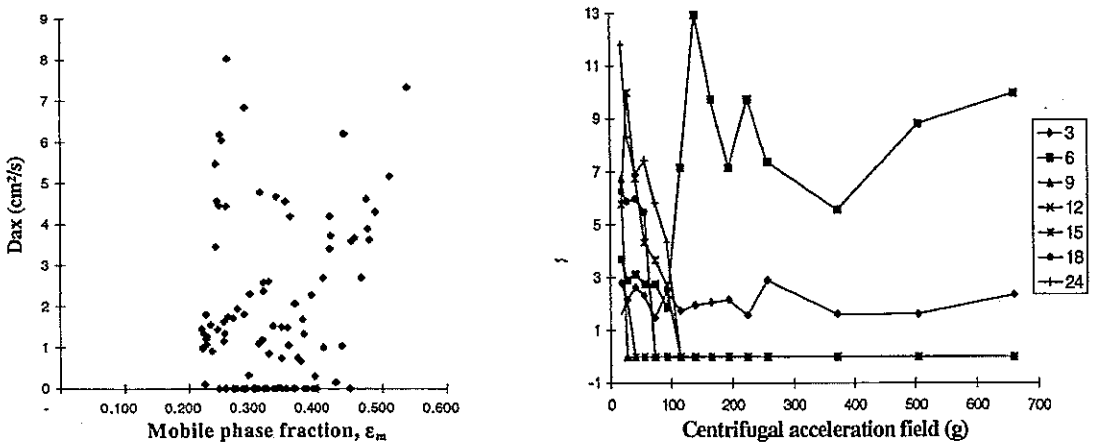

Figure 7. D_{ax} as a function of the mobile phase fraction and the centrifugal acceleration field.

Van Buel and al. [2] found the same result in different apparatus derived from the Sanki Eng. Ltd. (Japan) CPC-LLN model.

Off-column fittings are an important source of band broadening. Both diameter and length of tubing have to be diminished. The CPC column design characterized by tortuous ducts, sudden enlargements and contractions provides a plug flow mobile phase for this low viscous phases system.

REFERENCES

[1] Villermaux J., Schweich D., Sardin M., *Preparative and Production Scale Chromatography*, Ganetsos G., Barker P.E. (Eds), Marcel Dekker, Inc., 701 (1992)

[2] van Buel M.J., van der Wielen L.A.M., Luyben K.Ch.A.M., AIChE J., 43 (1997), 693

[3] Scott R.P.W., Kucera P., J. Chromatogr., 119 (1976), 467

[4] Foucault A.P., Camacho Frias E., Bordier C.G., Le Goffic F., J. of Liq. Chromatogr., 17 (1994), 1

[5] Marchal L., Foucault A., Patissier G., Rosant J.M., Legrand J., J. Chromatogr. A, 869 (2000), 339

[6] Foucault A.P., Marchal L., Rosant J.M., Farias Neto S., Legrand J., Durand P., Pittsburgh Conference, New Orleans, Abstract 878 (1998)

[7] van Buel M.J., van Halsema F.E.D., van der Wielen L.A.M., Luyben K.Ch.A.M., AIChE J., 44 (1998), 1356

[8] Lengentilhomme P., Brujes L., Legrand J., Chem. Eng J., 67 (1997), 83

[9] Sir Taylor G., Proc. Roy. Soc. A, 219 (1953), 186

INCORPORATION OF TRACER TEST INFORMATION INTO THE CONTROL LOOP DESIGN OF A CONTINUOUS FLOW PROCESS

A. J. Niemi[1], K. Zenger[2], P.Viitanen[3]

[1,2]Helsinki University of Technology, Control Engineering Laboratory, P.O.Box 5400, FIN-02015 HUT, FINLAND
[3]Indmeas Oy, Tekniikantie 21 C, 02150 Espoo, FINLAND. Present affiliation: Tellabs Oy, Sinimäentie 6, 02630 Espoo, FINLAND

Abstract. An industrial mixer cascade with three successive compartments was modeled by means of a tracer test. The frequency response of the process was determined by using analytical models and by calculating the Fourier transformation of the residence time distribution (RTD) data numerically. Based on the frequency response a compensator was designed to control the output concentration of the process. The performance of the closed loop system was tested by simulation.

INTRODUCTION

The operation of continuous flow production processes is controlled by automatic measurement and regulation devices. The smoothness of operation and quality of product depend on the level of process control, and the design of a proper control requires that the dynamic model of the process is known to a sufficient detail in a numerical or analytical form.

The unit impulse response model of the process is an appropriate starting point of the control design. For mass transfer processes, such a model is equal to the residence time distribution function which can be determined by a tracer. For the design of control loops, analytical models can be fitted and used. Frequency domain models are used which can be derived from analog models, but can also be obtained directly from the numerical tracer test data, by means of the Fourier transformation [1]. After a process model of the latter type is available, one from a number of control design methods can be used to obtain the corresponding control structure and to tune the control parameters [2].

Starting from the tracer data obtained at a test of an industrial process vessel, the design of its feedback control is described in the following. Both the design based on traditional stability and control quality criteria, and the use of a more advanced, robust control approach are discussed.

THE PROCESS AND THE TRACER TEST

1. The tested vessel and the process

Subject of the tracer test was an industrial mixer consisting of three successive compartments separated from each other by perforated plates (Fig. 1). Such mixers

are used in the chemical wood pulping industry for causticizing, i.e. for recovering of sodium hydroxide, NaOH, by reaction of sodium carbonate, Na_2CO_3, with originally particulate lime, $CaO/Ca(OH)_2$. Because this reaction is very slow, a maximal conversion of the reactants requires their long residence in the reactor which determines the size of the vessel and the preferable form of the RTD. An industrial causticizing plant consists usually of a series of three such vessels of three compartments each. Feed of the reactants is controlled in dependence of the composition of the outlet flow. The present study relates to the testing and control of a single (the first) vessel only. Its volume was 228 m^3 and the throughput 172 m^3/h at the time of the test. The volumes of the compartments were almost equal.

2. Tracer and measuring equipment

About 10 mCi of ^{82}Br as KBr-solution was used as tracer. The tracer was introduced to the process input by pouring the solution (about 5 l) instantly .

2 inch NaI(Tl)-scintillation detectors were used to monitor tracer concentration both at the inlet and the outlet of the reactor. The detection points were physically quite near to each other beside the reactor wall. Thus, a very precise collimation and heavy lead shielding of the detectors had to be used. The results indicated that both detectors were still subject to changing background effected by the tracer remaining in the reactor.

3. Measurements

Two separate measurements were made. The measurement of tracer concentration until background level was ensured by long test times 5 h and 10 h. Results from separate tests were identical within the limits of measurement uncertainty.

The volume of the reactor was calculated using manually measured reactor dimensions and liquid level. The flowmeter measuring the process flow rate was calibrated with a separate transit time measurement using radioactive tracer as well.

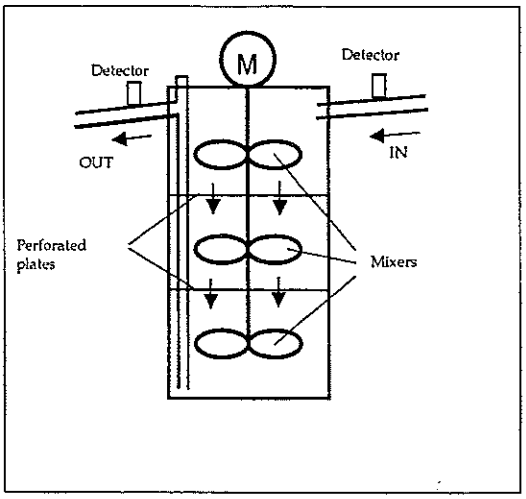

Figure 1. Schematic drawing of the studied reactor. Note, that physically the inlet and outlet lines were beside each other.

DATA PREPARATION

1. Data preparation

Routine data preparation included observing constant background and radioactive decay as well as filtering the data for presentation purposes. In addition to these a changing background was encountered at the present measurement.

The changing background was estimated by the tracer concentration measured by the detector at the inlet of the reactor. A reasonable time after the injection the tracer seen by this detector consisted only of constant background and the tracer in the reactor. Investigation of this changing background proved that the background had an exponentially decaying and a constant component. This pointed out clearly that the tracer effecting the changing background was the one residing in the uppermost compartment of the reactor. The time constant of the background was also equal to the theoretical one for one compartment.

2. Preliminary modeling

The structure of the reactor suggests the simple model of three identical ideal mixers in series. This was used as the first approximation and a somewhat satisfactory model was achieved. However, the lack of modeling of backmixing was clearly indicated.

A backmixing model was fitted using two specialised tracer software packages. Backmixing component fitting to the measured data was 50 %. As a first guess this value is considerably high and suggests that the reactor performance could be improved by decreasing the cross-sectional area of perforation (Fig. 2).

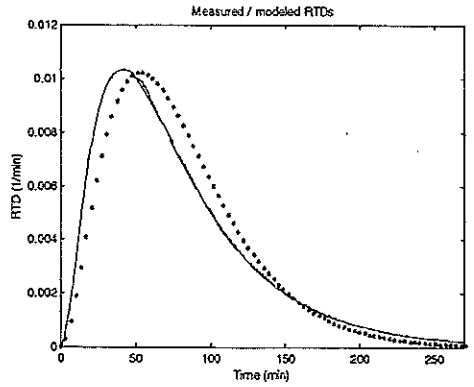

Figure 2. Measured RTD (solid); RTD of a three mixers in series (dotted); RTD of three mixers with recycling (dashed).

MODELING IN TIME AND FREQUENCY DOMAINS

1. Frequency response

The frequency response of the system can be obtained by taking the Fourier transformation of the unit impulse response (or residence time distribution). If the RTD is available only as a time series, the Fourier transformation can be approximated by

$$G(j\omega) = \int_0^\infty g(t)e^{-j\omega t}dt \approx h\sum_{n=1}^{N} g[(n-1)h]e^{-j\cdot 2\pi\frac{(k-1)(n-1)}{N}} \tag{1}$$

in which g is the RTD given by N samples, h is the time interval between the samples and the frequency scale is determined by

$$\omega = \frac{2\pi(k-1)}{Nh}, \quad k = 1,2,\ldots,N \tag{2}$$

In the current example case the RTD consisted of 270 points, and the time interval between the points was one minute.

2. Analytical models

The traditional technique of modeling has been to fit a process model to the numerical data obtained by measurements. Usually, a suitable process configuration consisting of perfect mixers, plug flow vessels and bypassing or recirculation is first chosen, whereafter the parameters are optimized in order to get the best fit when compared to the measured RTD. As mentioned earlier, in the current example a series of three perfect mixers with or without recycling might be good candidates for the model. The differential equations of the two models are

$$\begin{cases} \mu_1\dfrac{dc_1}{dt} = -c_1 + c_0 \\ \mu_2\dfrac{dc_2}{dt} = c_1 - c_2 \\ \mu_3\dfrac{dc_3}{dt} = c_2 - c_3 \end{cases} \qquad \begin{cases} \mu_1\dfrac{dc_1}{dt} = -(1+b)c_1 + bc_2 + c_0 \\ \mu_2\dfrac{dc_2}{dt} = (1+b)c_1 - (1+2b)c_2 + bc_3 \\ \mu_3\dfrac{dc_3}{dt} = (1+b)c_2 - (1+b)c_3 \end{cases} \tag{3}$$

where $c_i, i = 1,2,3$ are the concentrations in the vessels, $\mu_i = V_i / Q_i$ and b is the recycling ratio. The best fit of the latter model when compared to the measured RTD was obtained by b = 0.5. The physical parameters in both models are V_i = 76m^3, Q_i = 2.9m^3/min, i = 1,2,3 The transfer functions from input to output concentrations can be calculated from (3)

$$G_1(s) = \frac{5.366\cdot 10^{-5}}{s^3 + 0.1132s^2 + 0.004268s + 5.366\cdot 10^{-5}} \tag{4}$$

$$G_2(s) = \frac{12.07\cdot 10^{-5}}{s^3 + 0.1886s^2 + 0.009604s + 12.07\cdot 10^{-5}} \tag{5}$$

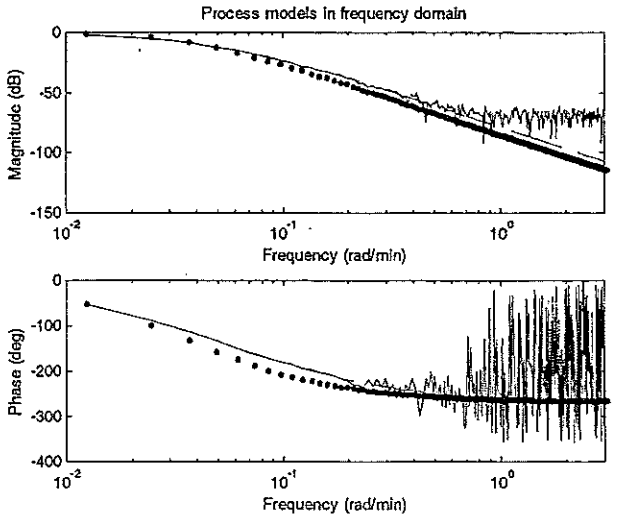

Figure 3. Frequency responses given by the equations (4)-(5), and the response obtained by taking the Fourier transformation of the data.

The obtained frequency responses are presented in Fig. 3. At lower frequencies the curves obtained by the model of three mixers with recycling and the curve obtained by calculating the numerical Fourier transformation of the measured data coincide very well, whereas the model of three perfect mixers gives lower amplitude values. However, when approaching the Nyquist frequency $\pi / h \approx 3.14$ rad/min the numerical response deteriorates clearly. This is because the numerical determination of the frequency response is known to be prone to disturbances especially if the measured data is corrupted by noise. The numerical frequency response can well be used as a basis of control design up to the frequency 1rad / min.

CONTROLLER DESIGN

1. Control configuration

In Fig. 4 a "two-degree-of-freedom" controller configuration is presented [3].

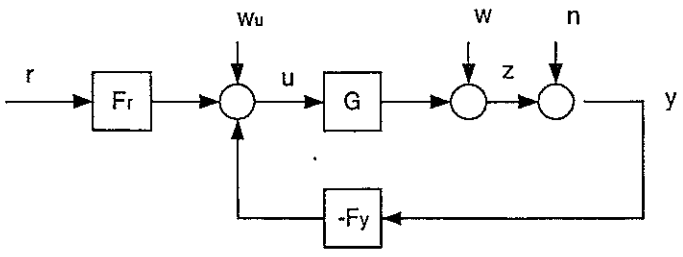

Figure 4. 2-DOF control configuration. G is the plant model; F_r and F_y are compensators; r, u, z, y are the reference, control, output, and measured output signals, respectively; w_u, w, and n are disturbance signals.

The control literature uses the *loop transfer function*

$$L = GF_y \tag{6}$$

as the basis of e.g. stability issues and loop shaping design procedures in classical control analysis and synthesis.

Consider the case with $F_r = F_y$ and $e = r\text{-}z$. Based on the diagram it is straightforward to write the following equations (in Laplace domain)

$$\begin{aligned} z &= Tr + Sw - Tn + GSw_u \\ e &= r - z = Sr - Sw + Tn - GSw_u \\ u &= SF_y r - SF_y (w+n) + Sw_u \end{aligned} \tag{7}$$

in which the *sensitivity* and *complementary sensitivity functions* are

$$S = (1+GF_y)^{-1} \tag{8}$$

$$T = (1+GF_y)^{-1} GF_y \tag{9}$$

2. Control design

The specifications for the control performance can be stated by using information obtained from the preceding equations [3]. The magnitude of the closed loop transfer function $G_c = T$ has to be close to 1 for the controlled variable to follow the reference signal. The sensitivity function S has to be small so that disturbances or modeling errors do not essentially affect the performance. The complementary sensitivity function T should be small to minimize the effects of measurement noise. To keep the control signal as small as possible, the transfer functions SF_y and S should not be too large.

Note that the above demands contain fundamental conflicts; e.g. from (8) and (9) it follows that at each frequency

$$S + T = 1 \tag{10}$$

so that both functions can not be "small" at the same time. Fortunately, the system and measurement disturbances usually occur at different frequency ranges so that it is a good idea to design the controller so that S is small at low frequencies and grows at higher frequencies, while T decreases.

Loop shaping techniques were used to design a lead-lag type of compensator for the process [4]. The transfer function of the compensator is

$$F_y = F_r = G_{cm} \frac{(1+s/w_z)(1+w_l/s)}{1+s/w_p} \tag{11}$$

which proves equivalent to the the classical proportional-integral-derivative (*PID*) controller (with a lag term in the derivative part) [5]

$$u = K\left(1+\frac{1}{sT_i}+\frac{sT_d}{1+(T_d/N)s}\right)(r-y) \tag{12}$$

with the parameters

$$\begin{aligned} K &= G_{cm}\left(1+w_l/w_z - w_l/w_p\right) \\ T_i &= 1/w_l + 1/w_z - 1/w_p \\ T_d &= w_p/(w_z w_p + w_l w_p - w_z w_l) \\ N &= w_p^2/(w_z w_p + w_l w_p - w_z w_l) - 1 \end{aligned} \tag{13}$$

By the loop-shaping design procedure the tuning values in equation (11) were obtained as $G_{cm} = 1$, $w_z = 0.05$, $w_l = 0.05$ and $w_p = 1$. Correspondingly, $K = 1.95$, $T_i = 39$ min, $T_d = 9.26$ min and $N = 9.26$ in equation (12).

The frequency responses and simulation results are shown in Figs. 5 and 6. The closed loop performance is good and loop and sensitivity functions have a shape needed for a robust control design.

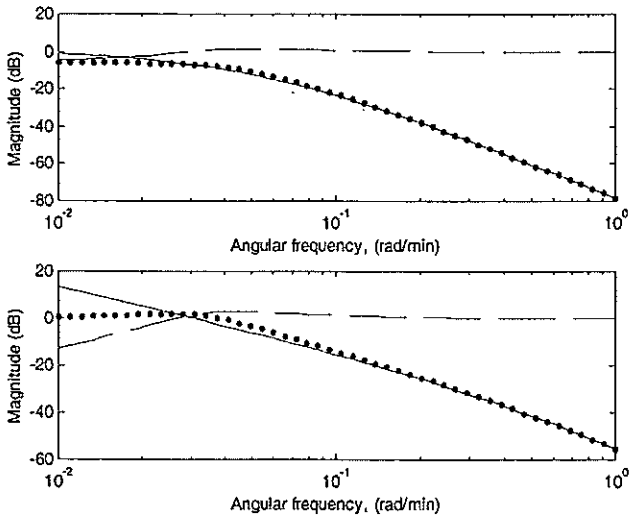

Figure 5. Loop transfer function (solid), sensitivity function (dashed), complementary sensitivity function (dotted). Up: uncompensated system. Down: compensated system.

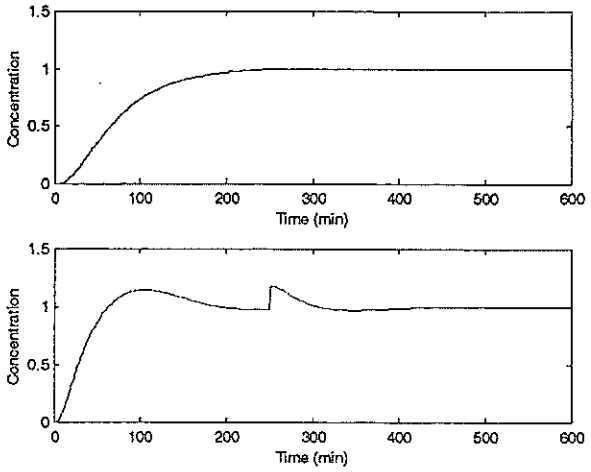

Figure 6. Up: Step response of the open loop system. Down: Closed loop response. At time $t = 0$ a unit step has been introduced through the reference signal; at time $t = 250$ a step disturbance of magnitude 0.2 has been introduced at the output of the process.

CONCLUSIONS

The tracer response shows that a part of the feed passes fast to the outlet, which affects the steady-state yield of the reactor. The by-pass is not properly reproduced by the tanks-in-series model and not fully by the backmixing model either.

A feedback compensator was designed based on the frequency response model of the process. The sensitivity and complementary sensitivity functions were designed to obtain a closed loop system with robust performance. The operation of the closed loop was tested by simulation, and was found good.

The method of using measured RTD data in order to obtain a frequency response model of the process was in this example case found adequate. However, more problematic cases may be met, because the numerical Fourier transformation oscillates, if the measured RTD is noisy.

REFERENCES

[1] Männistö, H., Niemi, A., On the Dynamics of a Cellulose Bleaching Plant. In: *Radioisotope Tracers in Industry and Geophysics*, IAEA, Vienna (1967), pp. 371-384.

[2] Niemi, A. J. (contributor), The Use of Tracer Data for Process Control. In: *Guidebook on Radioisotope Tracers in Industry*, IAEA, Vienna (1990), pp. 192-200.

[3] Glad, T., Ljung, L., *Control Theory, Multivariable and Nonlinear Methods*, Taylor & Francis (2000).

[4] Skogestad, S., Postlethwaite, I., *Multivariable Feedback Control, Analysis and Design*, John Wiley & Sons Ltd. (1996).

[5] Åström, K., Hägglund, T., *PID Controllers: Theory, Design, and Tuning*. Instrument Society of America (1995).

CORRECTING THE RESULTS OF RADIOACTIVE TRACER EXPERIMENTS FOR THE EFFECTS OF THE DETECTION CHAIN

Ph. Berne[1], V. Blet[2]

[1] DTEN/SAT, CEA/Grenoble - 17 rue des Martyrs - 38054 Grenoble Cedex 9 - France
[2] LETI/DTS, CEA/Grenoble - 17 rue des Martyrs - 38054 Grenoble Cedex 9 - France

Abstract. This paper presents several results on the effect of the nuclear detection chain on the output of tracer experiments with gamma-emitting tracers. Simple modelling for that effect is proposed. The assessment of that effect is attempted. Rigorous correction is found to be impossible in the general case. Two types of corrections are outlined. Both make use of a deconvolution procedure. One is valid for purely convective flow and requires that detector response to an infinitely flat tracer disk be known. The other one can be applied in the case of the « two measurements » method, and is shown to be valid for axial dispersed plug flow in straight pipes.

INTRODUCTION

Gamma-emitting radioisotopes are widely appreciated as tracers, for their through-the-wall measurement capability. One drawback is however the « blurring effect » due to the radioactive detection chain. This effect can easily be illustrated by the following experiment: a point γ source is made to move at constant velocity inside a pipe fitted with a shielded γ-detecting probe. This configuration is quite close to the ideal impulse tracer injection in a purely convective flow. Response from the probe should therefore be a very sharp Dirac-like signal (count rate zero except when the source is right in front of the probe). The actual response looks much more like a flattened peak, as illustrated on Figure 1 (response width is about 30 cm, while detector diameter is no more than 5 cm).

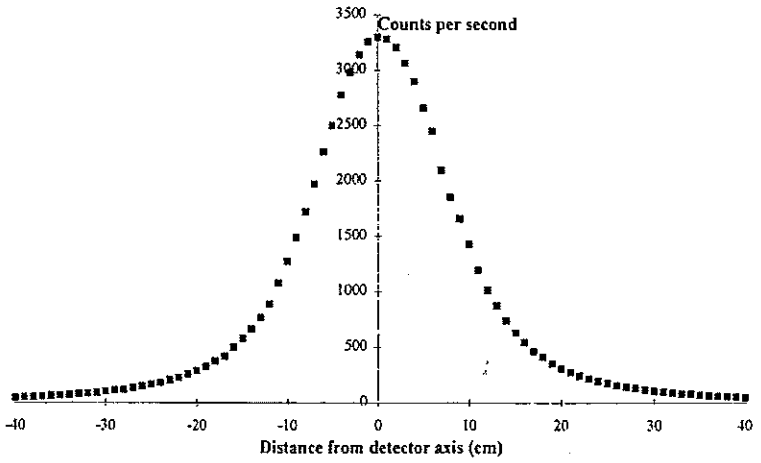

Figure 1. Typical detector response for moving point source experiment [1]

The reason for that problem is that γ photons are able to reach the detector in many indirect ways, through its walls or through the shielding or even by multiple redirections. The present work addresses the problem of correcting the signal from γ detection probes for this effect, or in other words of extracting the pristine Dirac signal from the blurred peak. It is however limited to a *uniform radial tracer concentration* profile inside a cylindrical pipe, an assumption which is valid in porous media column experiments or in turbulent flow in long pipes for example.

MODELLING COUNT RATES

Let us first assume that a point source of a particular radioisotope with activity A is located at some point (x,y,z) inside the pipe. This source gives rise to count rate $\dot{n}$ (in counts per second) from the detector. Because radioactive detection is essentially a linear process, it is possible to unambiguously define for that specific radioisotope function $T(x,y,z)$ as:

$$T(x,y,z) = \frac{\dot{n}}{A} \tag{1}$$

Let us now suppose the point source is taken away and that some amount of tracer is dispersed inside the tube. Volumic tracer activity field (in Bq/m^3 for example) inside the tube is now $a(x,y,z,t)$. Activity within elementary volume dV will be equal to $a.dV$, causing elementary count rate $d\dot{n}$:

$$d\dot{n} = T(x,y,z)a(x,y,z,t)dV \tag{2}$$

Total instantaneous detector count rate will therefore be:

$$\dot{n} = \int_V T(x,y,z)a(x,y,z,t)dV \tag{3}$$

where V is the detection volume, i.e. the volume inside which function T is not zero.

If the uniform radial concentration profile assumption is true, function $a(x,y,z,t)$ reduces to $a(z,t)$ (assuming that direction z is the axis of the tube). In that case, equation (3) can be rearranged as:

$$\dot{n} = \int_{-L}^{L} T_s(z)a(z,t)dz \tag{4}$$

where $T_s(z)$ is defined as:

$$T_s(z) = \iint_S T(x,y,z)dx.dy \tag{5}$$

and S is the cross section of the tube and L the « detection length », that is to say the distance from the detector beyond which T_s is zero. Function T_s can be interpreted as the response of the detector to an infinitely flat disk of tracer moving inside the tube, as a function of the position of the disk (more or less a surface-source version of the function on Figure 1). In a few cases (for example experiment in a small column), direct measurement can be attempted. Otherwise, Monte-Carlo simulations are a reliable method for accessing this function. As a confidence-building example,

Figure 2 compares the experimental results from Figure 1 with a Monte-Carlo simulation with computer code Ecrin [2].

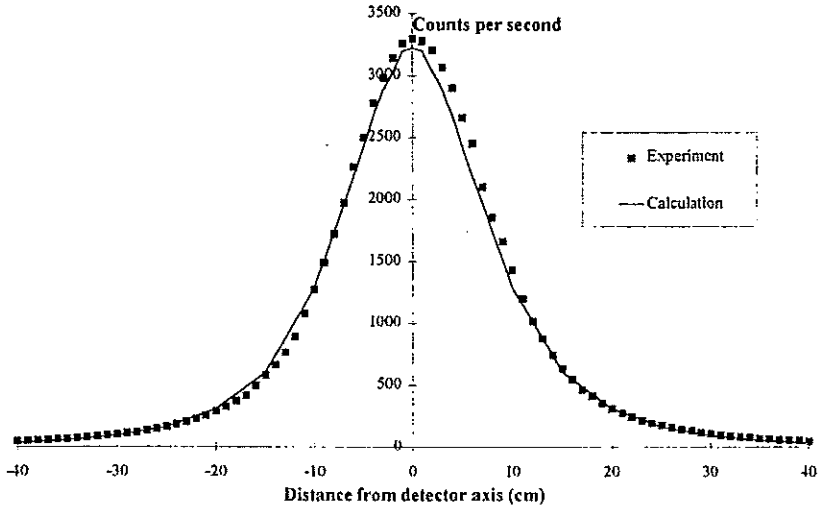

Figure 2. Comparison of experimental results with Monte-Carlo simulation [1]

Equation (4) can be used in two ways. The first one consists in computing $\dot{n}(t)$ when both $T_s(z)$ and $a(z,t)$ are known. This can easily be done with standard techniques for function integration. In this way, it is possible to assess the influence of the detection chain for a given activity history. An example is given in next section. The other one corresponds to the calculation of $a(z,t)$ when $\dot{n}(t)$ and $T_s(z)$ are known. It amounts to correcting measured count rates to find the original activity history. An attempt will be made at treating this much more difficult problem in the following sections.

ESTIMATING THE INFLUENCE OF THE DETECTION CHAIN

As an example, the following case is treated here: $a(z,t)$ is assumed to follow the classical axial dispersed plug (ADP) flow model [3], while $T_s(z)$ is modelled as a Gaussian function:

$$a(z,t) = \frac{A}{\sqrt{2\pi}\sigma(t)} \exp\left(-\frac{(z-ut)^2}{2\sigma(t)}\right) \tag{6}$$

$$T_s(z) = \frac{K}{\sqrt{2\pi}\sigma_D} \exp\left(-\frac{(z-z_D)^2}{2\sigma_D^2}\right) \tag{7}$$

where A is injected activity per unit surface, u fluid velocity (m/s), $\sigma(t) = \sqrt{2Dt}$ the spatial standard deviation (in metres) of the tracer wave at time t (D is the dispersion coefficient, m^2/s). K is a proportionality factor (in $cps.m^3/Bq$), σ_D the

spatial standard deviation of T_s (in metres) and z_D the position of the detector. Tracer injection is made at t=0 and z=0.

In that case, equation (4) can be integrated analytically:

$$\dot{n}(t) = \frac{AK}{\sqrt{2\pi\left(\sigma^2(t)+\sigma_D^2\right)}} \exp\left(-\frac{(z-ut)^2}{2\left(\sigma^2(t)+\sigma_D^2\right)}\right) \tag{8}$$

Introducing Péclet number $Pe=uz_d/D$, ratio $r = \sigma_D / z_D$ and dimensionless time $\theta = ut / z_D$ allows to transform this equation into:

$$\dot{n}(t) \propto \frac{1}{\sqrt{2\pi\left(\frac{2\theta}{Pe}+r^2\right)}} \exp\left(-\frac{(1-\theta)^2}{2\left(\frac{2\theta}{Pe}+r^2\right)}\right) \tag{9}$$

This equation is illustrated on Figure 3, which compares the actual activity history $a(z_D,t)$ and the instantaneous count rate from the detector, for r=0.2 and Pe=5 or 100. In spite of the relatively large value of r, little effect is visible at low Péclet number. At large Péclet number however, the detection chain induces a marked deformation of the recorded signal.

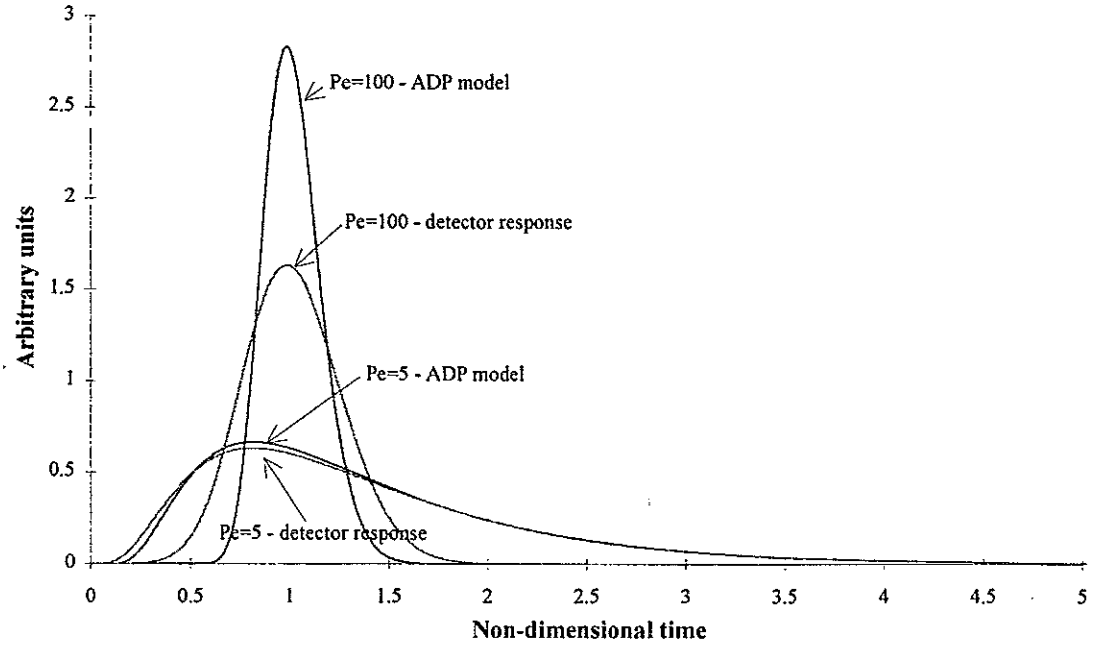

Figure 3. Comparison of actual activity history and detector response

The problem that we are facing now is solving equation (4) for $a(z_D,t)$, i.e. the activity history in front of the detector. We believe this problem has no general solution. The reason is that measured count rate $\dot{n}(t)$ explicitly depends on activity history at all points within the detection length. This means that there is no univocal relationship between $\dot{n}(t)$ and $a(z_D,t)$ and that the problem can only be solved within certain approximations or assumptions.

1. « Convective » approximation

Since the difficulty lies in the dependence of $\dot{n}(t)$ on all the points within the measurement volume, it should be possible to solve it by making an assumption on the relationship between activity histories at $z=z_D$ and at the other points. The simplest possible assumption is that the tracer wave travels at constant velocity u without any deformation. This amounts to supposing that tracer flow is purely convective, or in other words that dispersion is zero (or Péclet number is infinite, in the framework of the ADP model). In that case:

$$a(z,t) = a\left(z_D, t - \frac{z - z_D}{u}\right) \tag{10}$$

After some manipulation, equation (4) can be rearranged into:

$$\dot{n}(t) = u \int_{-L_D}^{L_D} T_s(u\xi)\, a(z_D, t-\xi)\, d\xi \tag{11}$$

which is the time convolution of functions $T_s(ut)$ and $a(z_D,t)$. Solving this equation for $a(z_D,t)$ amounts to deconvolution of $\dot{n}(t)$ by $uT_s(ut)$ - a possibly tricky but manageable affair.

From equation (11), it is possible to compute the (time) variance of measured count rate, $\sigma_{\dot{n}}^2$:

$$\sigma_{\dot{n}}^2 = \sigma_{a(z_D,t)}^2 + \frac{\sigma_D^2}{u^2} \tag{12}$$

where $\sigma_{a(z_D,t)}^2$ is the variance of function $a(z_D,t)$ and σ_D is defined as in the previous section (spatial standard deviation of T_s in metres). This equation seems to indicate that the effect of the detection chain is more important at low velocities. In fact, $\sigma_{a(z_D,t)}^2$ is quite often also a function of velocity for given injection conditions. In the case of ADP flow for example, $\sigma_{a(z_D,t)}^2$ is approximately proportional to u^{-2}, which means that the relative contribution of both terms in equation (12) will not depend on velocity.

The main hypothesis for this method is that dispersive effects should be negligible. It seems, however, that this condition should not be taken too strictly. This point is illustrated by Figure 4, which compares the exact count rate predicted by equation (9) with the approximate count rate from equation (11), in the case of ADP tracer flow and Gaussian detector response, for a Péclet number of 5. In spite of that rather low value, differences are found to be rather small « most of the time » (however, the convolution equation unrealistically predicts non-zero count rate *before* the tracer is actually injected).

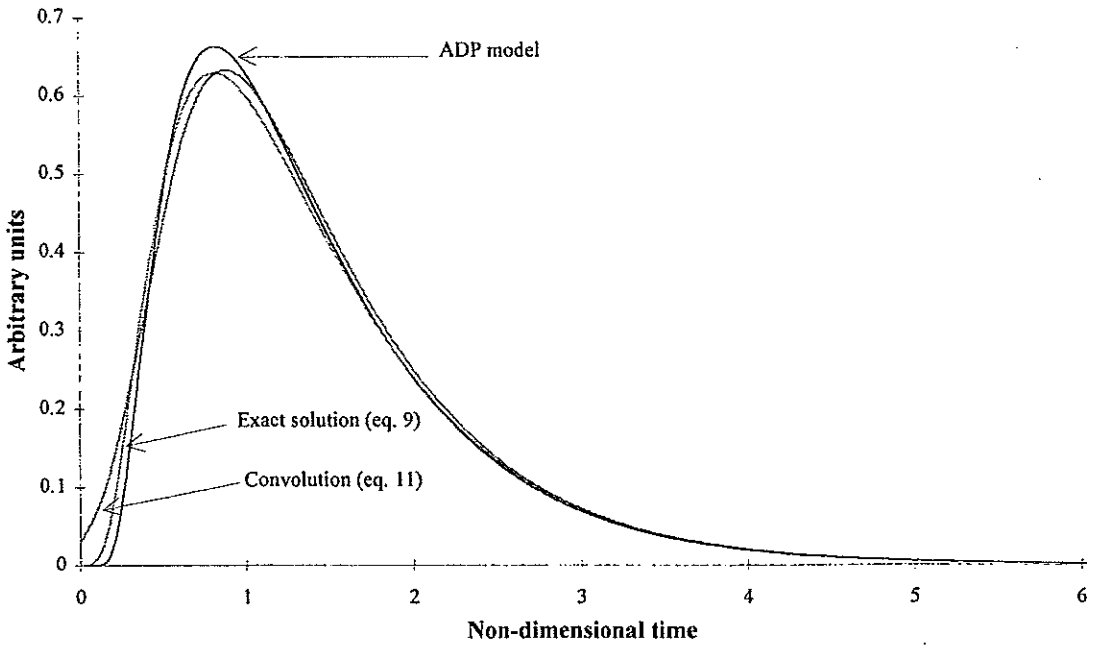

Figure 4. Comparison of exact solution (9) and convolution (11)

2. The case of the « two measurements » method

A popular method for radioactive tracer experiments (for example for flow rate measurement) consists in positioning two detectors alongside the pipe under investigation, at distances z_1 and z_2 from the injection point taken as the z origin. This configuration is illustrated on Figure 5.

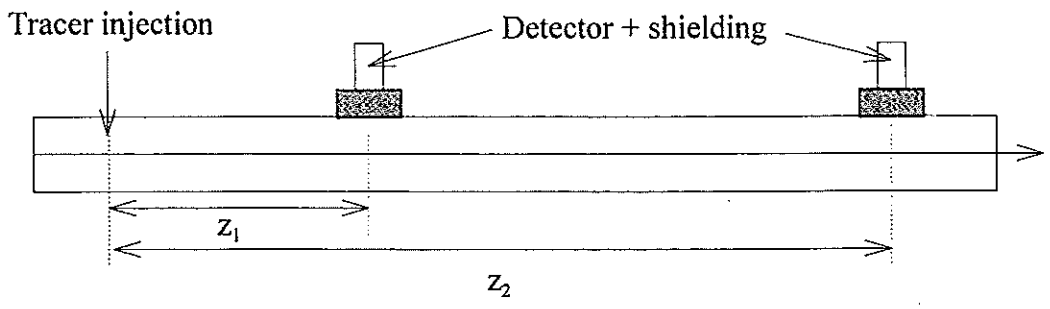

Figure 5. « Two measurements » method

Assuming detection configurations (type of detector, shielding, pipe thickness and so forth) are identical at points z_1 and z_2, the same $T_s(z)$ function applies for both detectors with a z_2-z_1 translation only.

It is generally possible to define a « transfer function », $f(z,z',t)$, that relates $a(z,t)$ and $a(z',t)$ in the following way:

$$a(z',t) = a(z,t) \otimes f(z,z',t) \tag{13}$$

where $\otimes$ denotes the time convolution product (z' should obviously be downstream z). To be verified, equation (13) implies (i) that tracer activity is conserved and (ii) that the time variance of $a(z,t)$ should increase with z, which is usually the case in pipe flow experiments. If $z=z_1$ and $z'=z_2$, $f(z,z',t)$ is the activity transfer function between detectors 1 and 2, which is indeed the information that is expected from a « two measurements » experiment.

In some cases, function $f(z,z',t)$ depends on z'-z only:

$$f(z,z',t) = f(0,z'-z,t) \tag{14}$$

Equation (14) is verified in several popular models for tracer transport (axial dispersed plug flow with open conditions at both boundaries or perfects mixers in cascade for example; on the other hand, strictly speaking, it is not verified with the ADP model with no-dispersion boundary conditions). Equation (14) also implies that:

$$f(0,z+z',t) = f(0,z,t) \otimes f(0,z',t) \tag{15}$$

Equation (4) indicates that count number by detector i should be equal to:

$$\dot{n}_i = \int_{-L}^{L} T_{is}(z) a(z,t) dz \tag{16}$$

Provided detection conditions are identical and condition (14) is verified, equation (16) can be manipulated to give the following relation:

$$\dot{n}_2(t) = \dot{n}_1(t) \otimes f(z,z',t) \tag{17}$$

which means that deconvolution of $\dot{n}_2(t)$ by $\dot{n}_1(t)$ will yield the transfer function between detectors 2 and 1. This was already observed in reference [1], but we give here formal proof (though with some restrictions) of this fact.

So far we have been dealing with *instantaneous* count rates, while in real-life experiments only *cumulated* count rates can be accessed. In many cases, counting time is short enough to make the difference immaterial. However, in our opinion further modelling effort should allow to extend our conclusions to cumulated count rates, with the extra bonus that proper deconvolution of signals should also correct the blurring effect due to time integration of counts.

CONCLUSIONS

We summarize here the results that have been obtained on the correction for detection chain response:

- The relationship between detector count rate and instantaneous volumic activity field in a pipe has been established. It involves a response function that can be obtained from standard Monte-Carlo computer codes. If the activity field is uniform in all cross sections, this relationship simplifies into a one-dimensional form, the parameters of which can also be accessed by Monte-Carlo simulations.
- The analytical expression of count rate as a function of time has been established, in the case when tracer transport can be described by the popular axial dispersed plug flow model and detector response can be modelled as a Gaussian function. This expression allows to assess the deformation due to detector response.
- If tracer transport can be considered as purely convective (i.e. without dispersion effects) a simple deconvolution procedure allows to correct count rates for detector response.
- With the « two measurements » configuration involving two identical detectors alongside a pipe, deconvolution of the signal from the downstream detector by the signal from the upstream one yields, under certain conditions, the true transfer function between the detectors.

REFERENCES

[1].Blet, V., Berne, Ph., Tola, F., Vitart, X., Chaussy, C., *Recent developments in radioactive tracers methodology,* Applied Radiation and Isotopes, 51 (1999), 615-624.

[2] Tola, F., *Ecrin, code Monte-Carlo de simulation de la réponse d'un détecteur à un mélange de traceurs radioactifs uniformément distribués dans une conduite cylindrique,* Internal report CEA/DTA/DAMRI/SAR/96-111/T40 (1996).

[3] Villermaux, J., *Génie de la réaction chimique,* Ed. Tech & Doc Lavoisier, Paris (1982).

APPLICATION OF THE POSSIBILITY THEORY TO THE AUTOMATIC GENERATION OF COMPARTMENT MODELS

S. Claudel, C. Fonteix, J.-P. Leclerc

Chemical Engineering Science Laboratory, 1, rue Grandville 54001 Nancy, FRANCE

Abstract. Residence Time Distribution (RTD) measurements can be interpreted and simulated using compartment models which consist in interconnection of elementary modules e.g. plug flow reactor or perfect mixing cell. However, the choice of the appropriate model may be a troublesome task when the considered reactor is of a complex geometry. The present investigation was aimed at developing a new algorithm for the automatic generation of compartment models based both on RTD curves and physical description of the studied processes. We used for this purpose the possibility theory developed by Zadeh [4] which consists in affecting weighing coefficients on the possible occurrence of a given event. This method has been never used in chemical engineering but was successfully tested in human sciences, as by Sandri [3] for investigations of associative human memories. Compilation of existing work allowed the selection of nearly forty models, which makes it possible to describe the major industrial situations. Then, a list of rules on the RTD curves and processes characteristics could be deduced. Weighing coefficients for possibility degree and necessity degree have been introduced to link the rules to the models. The so-called "fusion" procedure consisting of the compilation of all rules, leads to selecting the most appropriate model. The method was successfully tested on numerous examples taken from the relevant literature, in particular on a commercial scale CFB boiler and on a screw-loop reactor.

INTRODUCTION

Generally two main techniques are used to recover hydrodynamic information, an analytic one: the Computational Fluid Dynamics (CFD) based on the numerical resolution of Navier-Stockes' equations and a systemic method: the Residence Time Distribution (RTD) based on tracer experiment interpretation. CFD gives an accurate description of the flow pattern. Although it is a powerful method, it requires a long calculation time to simulate quite simple systems. RTD remains an interesting method to derive simple hydrodynamic model for complex industrial systems.

Complex geometry induces a more complex flow behavior and requires an adapted corresponding model. Although a simple model can be sufficient for representing correctly the RTD, it is not perfect enough to represent the real flow and to give physical information concerning this flow. Therefore, a very good knowledge of the geometry of the reactor and the operating conditions is necessary to establish a model as representative as possible of the real flow, and to permit to draw useful information for future experiments (better operating conditions, realistic simulations,...).

Recently, Laquerbe [1] developed a software based on a genetic algorithm to generate compartment models from RTD experimental data. Calculations are started from an infinity of possible models, before progressive screening. The approach based only on mathematical fitting of the experimental RTD

curve may result in models without physical meaning. Physical aspects taken from the process itself lead to a knowledge which cannot be generated by mathematical treatment alone. The present investigation presents a new algorithm for the automatic generation of "compartment models" based both on RTD curves and physical description of the studied processes.

Every compartment model is composed of two parts, a structural part, which takes into account the architecture of the model, and a parametric part, which contains all the intrinsic parameters of the elementary reactors. Our idea is based on the possibility to determine the structure of the model using qualitative information about both RTD curve and characteristics of the studied process without any fitting of the parameters. This last step will be solved later using existing software, which allows optimization of the parameters [2]. Thus, there will not be any interference between the determination of the structure and the choice of the parameters. For example, if the curve presents a pure delay compared to the injection, structural determination should detect the presence of a plug flow reactor without determination of the corresponding delay time.

A detailed review of more than 120 publications dealing with RTD measurements shows that around 40 different compartment models (typical models are given table 1) allows to cover the major industrial situations. Using the symbolism introduced above, the models defined in the articles have to the maximum 5 building blocks and 3 branches in parallel.

Table 1: Examples of chosen models

NUMBER OF MODEL	MODEL
0	"JOKER" All alternatives are possible
5	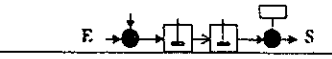
16	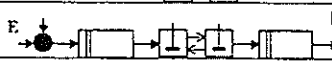
26	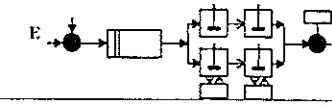
39	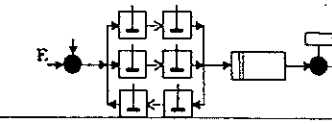

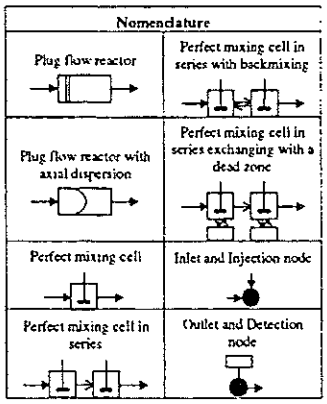

Strong relationships between curves and processes characteristics and structure of the model have been determined. For example:

- A tail of the RTD curve indicates a probable dead volume
- The presence of more than 3 peaks induces probable recirculation
- A jet effect at the inlet indicates a probable presence of a plug flow
- Etc...

We have selected the Possibility Logic, which allows a proper determination of the model of the studied processes using the collected data about RTD and the process and these relationships [7]. Moreover, this method presents the following advantages:

- Friendly user interface to facilitate utilization by a non expert,
- The algorithm is flexible enough to allow addition of new models and/or relationships,
- The algorithm is able to separate clearly the selected models,

- The algorithm is able to interpret vague answers of the user (may be, for example).

DESCRIPTION OF THE USED METHOD

The possibility Theory was developed by Zadeh [4] in 1978 and expanded by Dubois and Prade [5][6]. Possibility Logic is a new form of information theory which is related to but independent of both fuzzy sets (from fuzzy logic) and probability theory [4][6]. We combine advantages of the fuzzy expert system principle and the fuzzy control principle in one system which can differentiate at maximum the models. Then this theory corresponds, a priori, to the min-max version of the fuzzy logic, that means the intersection is modeled by the min-operator and the union is modeled by the max-operator.

Indeed, the main idea of the fuzzy expert system is to use a collection of fuzzy membership functions and rules, instead of Boolean logic. The communication on the expert system side as well as on the user side in the language of expert or user seems to be the most appropriate.

The basic idea in fuzzy control is to incorporate human knowledge of the process operator in the controller architecture. A control program uses a list of linguistic rules of the control strategy of the operator (experience, intuition, heuristics and facts). Indeed, a human controller use qualitative rather quantitative terms to describe the decisions concerning certain processes control as in batch chemical reactors.

This utilization of the possibility logic regroups the two aspects of fuzzy logic, and thus this system uses two values, the possibility degree comes from fuzzy expert system which eliminates uncertainty, the necessity degree comes from fuzzy control which adds certainty. To be evolutive, we will use implications like in the fuzzy expert system not with sequential rules, but with simultaneous rules.

This system includes an interface user/machine through initial input data and final output results. Moreover, the user can provide vague answers to the questions because the system is designed to manage thus (for example, an answer could be "I do not know", "a little" or "yes at a certain percentage" instead of just "yes" or "no"). Indeed, the system must be equipped with inference tools to manage this type of answers. Because of two values, possibility and necessity, the differentiation between the models is maximum.

We will point out here just the principal properties and proposals which we used from this theory [7].

If Π is a possibility degree and N a necessity degree, the following properties give the relations between possibility and necessity for an event A :

$$\Pi_A < 1 \Rightarrow N_A = 0 \quad (1)$$

$$N_A > 0 \Rightarrow \Pi_A = 1 \quad (2)$$

$$N_A \leq \Pi_A \quad (3)$$

where Π_A and N_A are, respectively, the possibility degree and the necessity degree of event A.

From (1) and (2), either A is not completely possible and then it is not at all necessary, or A is at least a little necessary and then it should be completely possible. Property (3) with (1) and (2) implies some eventualities:

1- $N_A = 1$ and $\Pi_A = 1$: it is sure that A is verified,

2- $N_A < 1$ and $\Pi_A = 1$: it is possible that A is verified and A is more necessary verified than $\overline{A}$,

3- $N_A = 0$ and $\Pi_A = 1$: both A and $\overline{A}$ are possible but not necessary at all. (ignorance)

4- $N_A = 0$ and $\Pi_A < 1$: it is possible that A is verified and $\overline{A}$ is more necessary verified than A ,

5- $N_A = 0$ and $\Pi_A = 0$: it is sure that $\overline{A}$ is verified.

Where $A \cap \overline{A} = \emptyset$ and $A \cup \overline{A} = E$

We note that possibility theory and probability theory are very similar, because issued from the same theory, but fundamental differences exist between them. Dubois and Prade [6] underline the fact that the Probability theory dones't permit to represent the difference between two states of knowledge distinguished only by a difference of confidence in available information.

$$N_A \leq P_A \leq \Pi_A \tag{4}$$

where P_A is the probability of event A .

To follow this theory, our system should verify the propriety, below, in all circumstances:

$$\text{Max}(\Pi(y), 1 - N(y)) = 1 \qquad \forall y \in Y \tag{5}$$

In addition, if there are several alternatives y , we should have:

$$\text{Inf}_{(y \in Y)} \Pi(y) = \text{Inf}_{(y \in Y)} (1 - N(y)) \tag{6}$$

where Y contains all possible alternatives y .

The standard premise (A) is characterized by the proposal A which must be theoretically true if the rule is applicable. If it is not that indicates that the proposal A is false. A rule is written $A \rightarrow B$ (A implicates B). The premise A is one we should have, in theory, to obtain the conclusion B . In practice, it is rare that A is completely carried out. Thus, if the reality is A', the corresponding conclusion will be B'. It remains the question how to evaluate B' starting from A' on one hand, and from A and B on the other hand. This is possible with an inference calculation.

The principle of an inference calculation is based on the intersection-projection which respect to equations (5) and (6). In addition, this intersection-projection principle is conservative and doesn't produce any skew. Thus the norms of Zadeh are suitable.

Then, the inference calculation of each rule r is given by:

$$\Pi_{B'}(y,r) = \mathrm{Max}[\Pi_B(y,r), 1 - N_{A'}(1,r)] \quad (7)$$

$$N_{B'}(y,r) = \mathrm{Min}[N_B(y,r), N_{A'}(1,r)] \quad (8)$$

Thus only $N_{A'}(1,r)$, the degree of truth of the premise, should be determined by the questionnaire.

The conclusion of each rule is a set of values $\Pi(y,r)$ and $N(y,r)$ where r is the n° of the rule and y a number of the model. Attention, if there is n-1 model candidates, the number of alternatives is n, the n^{th} corresponding with all possible models others that the n-1 first.

From $\Pi(y,r)$ and $N(y,r)$ it is necessary to deduce some $\Pi_F(y)$ et $N_F(y)$, for all rules, an aggregation of the data by fusion of data.

The inference calculation gives the equations (7) and (8), and from these, we define the fusion calculation, for all the rules r, as following:

$$\Pi_F(y) = \frac{\mathrm{Max}[\mathrm{Inf}_{(y)}\Pi_{B'}(y,r), \alpha \mathrm{Inf}_{(y)}(1 - N_{B'}(y,r))]}{\mathrm{Max}[\mathrm{Inf}_{(y)}\Pi_{B'}(y,r), \mathrm{Inf}_{(y)}(1 - N_{B'}(y,r))]} \quad (9)$$

$$N_F(y) = 1 - \frac{\mathrm{Max}[\mathrm{Inf}_{(y)}(1 - N_{B'}(y,r)), \beta \mathrm{Inf}_{(y)}\Pi_{B'}(y,r)]}{\mathrm{Max}[\mathrm{Inf}_{(y)}\Pi_{B'}(y,r), \mathrm{Inf}_{(y)}(1 - N_{B'}(y,r))]} \quad (10)$$

where α et β are constants defined by a specific method.

With this fusion method, we are able to select the most probably and physically representative model because it gives possibility and necessity degrees for each y^{th} model.

For each model, we should attribute 2 coefficients (Π and N) for each fact based on an expert knowledge, our knowledge, our collaborations, our research in articles and on D.T.S. software. The difficulty of this technique is a big number of coefficients (around 2000), we have to introduce in the system. Indeed, 48 facts for each of the 40 models + one "joker" model which represents all the other possible alternatives. Thus, we can summarize all steps as follows. With a questionnaire, the user "selects", by an interface, which facts are true, partially true or false. This permits the user to give an answer even if he is not sure of the answer, the user's answer is modulated. Then, the inference tools calculate the answers of the activated real rules (as, we saw above, it is $N_{A'}(1,r)$). Finally the fusion engine aggregates all the data and finds a list of models from the most probable and physically representative model to the less one.

EXAMPLES OF APPLICATION

From the literature, typical simple examples have been used to test this method. Some facts and their opposites are "asked" from the user, because

each of the two opposite facts brings some diverse information. Sometimes a fact is interesting, while its opposite is not, so this last fact is not included in the user form. Then, the system uses the inference tools for the sliced answers to find a conclusion for the activated rules. Thus, the fusion engine aggregates these conclusions to find a list of models from the most probable and physically representative to the less one. Table 2 shows the experimental set-up and the proposed models by the authors and obtained by our algorithm.

Table 2: Comparison of the models of the examples

Scheme of the process	Model proposed by the authors	Model proposed with our system
Screw-loop reactor 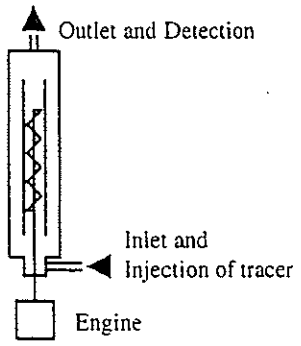	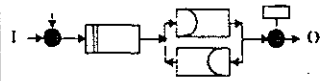	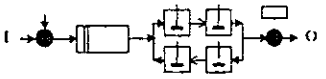
CFB boiler 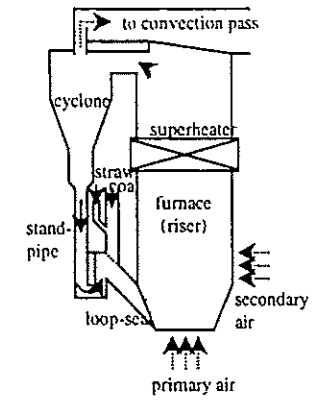	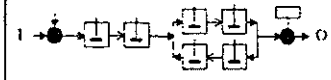	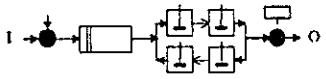

Screw-loop reactor [8]

A screw-loop reactor is used for processing high viscosity fluids in case of an increase of viscosity during the process. This reactor is divided in three segments, a riser, a downcomer and a pre-mixing zone, which is near the inlet. Tracer experiments were conducted using either a viscous compound in water and detected by temperature measurements or a dye tracer detected by optic measurements. The authors considered separately the segments for the modeling, then they found a three-elementary-block model. A plug-flow, which represent the pre-mixing zone, in series with a two-parallel-branch block where one branch is in recirculation and represents the downcomer.

With our system, we have converted the information given by curve and process into facts, as shown in table 3 for the main activated facts.

Table 3: Example of activation of facts in a screw-loop

Information from curve and process	Corresponding activated facts
"recycling through riser and downcomer"	Presence of a recirculation loop
Entrance and pre-mixing	Presence of a jet effect
There are distinct parts divided by walls	Presence of walls which separate clearly the process in several parts
Saw 1 peak on the curve	Presence of 1 peak on the curve
Saw a long tail	Presence of a tail
Saw curve is asymmetric	Curve is not symmetric

The algorithm tries by this analysis to reproduce the expert reasoning. For example: First, injection and detection of tracer are studied respectively at the inlet and at the outlet of the installation, then there is a jet effect because of the pre-mixing zone, finally we can suppose the presence of a plug-flow reactor as first elementary block and not at last block. Then, all conclusions of the activated facts are aggregated to find a physically representative model (see table2). These models are very similar and this difference is only due to the non-presence of this model in our list because the two models are equivalent.

Commercial scale Circulating Fluidized Bed (CFB) boiler [9]

A CFB boiler is use for combustion of coal and other solid fuels, due to its fuel flexibility and low emission levels of SO_2 and NO_x. Tracer experiments were conducted using a radioactive tracer ^{56}Mn to determine a hydrodynamic model. The authors proposed, as model of the CFB, a cascade of perfectly mixing cells in series with recirculation.

Table 4: Example of activation of facts in CFB

Information from curve and process	Corresponding activated facts
Scheme of process	Agitation by fluid recirculation
Good shape of agitation	No stagnant zone
Scheme of process and "particle recirculating rate"	Presence of a recirculation loop
Saw 2 peaks on the curve	Presence of 2 peaks on the curve
Saw a long tail	Presence of a tail
Saw curve is asymmetric	Curve is not symmetric

The information issued from the curve and the process permit us to activate the corresponding facts in order to find a representative model after the fusion procedure, as shown in table 4. The difference between the 2 models is due to the fact that the model found by the authors doesn't exist in our list of models. However, the number of tanks in the first cascade is relatively high (more than 20), then the two models are equivalent.

CONCLUSIONS AND PERSPECTIVES

This paper presented an algorithm, which is able to generate a physically representative model based not only on curve analysis, but also on information about the process. From a complete bibliographic research and knowledge of experts we have found some rules governing the modeling. The possibility theory, introduced by Zadeh presents the advantages to be able to differentiate at maximum between the models by using two variables: possibility, which eliminates uncertainty, and necessity, which adds certainty. This technique is evolutive because of the utilization of simultaneous rules. The result is found by the fusion technique, which aggregates all conclusions of the activated rules at the same time, so to add a new rule, the user needs just to insert this rule in the program, and it is similar to add a new model. Then the result is given in the form of a list from the most probable and physically representative model to the less one. We have proved that a system of automatic generation of models, which are physically representative, is feasible. For the future, it is necessary to realize the validation by optimization of the coefficients. Then, it will be interesting to go on the development of this method by adding new rules and new models.

REFERENCES

[1] Laquerbe, C., Laborde, J.C., Floquet, P., Pibouleau, L., Domenech, S., *Identification of parametric models based on RTD theory. Application to safety studies in ventilated nuclear enclosures.*, Computers chem. Engng, 22 (1998), S347-S353

[2] Leclerc, J.P., Claudel, S., Lintz, H.G., Potier, O., Antoine, B., *Theoretical interpretation of Residence Time Distribution measurements in indutrial processes. Oil and gas technology*, Revue de l'IFP, 55 (2000), 159-169

[3] Sandri, S., Bittencourt, G., *Possibilistic semantic nets*, Proccedings of the 5th Int. Conf. IPMU, Paris, 2 (1994), 838-843

[4] Zadeh, L.A., *Fuzzy sets as a basis for a theory of possibility*, Fuzzy Sets and Systems, 1 (1978), 3-28

[5] Dubois, D., Prade, H., *Théorie des possibilités : applications à la représentation des connaissance en informatique.*, Editions Masson (1985)

[6] Dubois, D., Prade, H., Possibility Theory, Plenum Press, New York (1988)

[7] Claudel, S., Fonteix, C., Leclerc, J.P., Lintz, H.G., *Application of the Possibility theory to the modeling of flow in complex processes*, submitted to 6th World Congress of Chemical Engineering, 23-27 September 2001.

[8] Lin, W., Weinell, C.E., Hansen, P.F.B., Dam-Johansen K., *Hydrodynamics of a commercial scale CFB boiler-study with radioactive tracer particles*, Chemical Engineering Science, 54 (1999), 5495-5506

[9] Kersting, C., Prüss, J., Warnecke, H.J., *Residence time distribution of a screw-loop reactor: experiments and modeling*, Chemical Engineering Science, 50 (1995), 299-308

FITTING DATA WHEN NO PHYSICAL MODEL IS AVAILABLE

Costa, C. B., Baccaglini, V. R., Spogis, N., Guirardello, R. and J. R. Nunhez*
Universidade Estadual de Campinas - UNICAMP, Faculdade de Engenharia Química,
Departamento de Processos Químicos, 13083-970, Campinas, São Paulo, Brazil

Abstract. This paper presents an extension of the Modified Spline Technique (MST) formulation for data fitting named power spline. This method is based on a technique which couples the maximum likelyhood principle to the spline method which makes it suitable to fit data when no physical model is available. Two new techniques were implemented to the former method which are: (1) the location of intervals are not restricted to the experimental points anymore and (2) the method guarantees no inflection points for curves strictly concave up or down.

INTRODUCTION

Cubic splines have been widely used for data fitting. This method works reasonably well for a well behaved set of points, but it gives unrealistic inflection points when the experimental data shows some experimental error. To overcome this inconvenience, Klaus and Van Ness [1] developed a new technique named Extended Spline Fit Technique (EST), which combines the Least Squares principle to the Cubic Spline Method. This method much improves the data fitting because the intervals for the cubic splines are no longer necessarily chosen as the distance of every two consecutive data points, nor are the values of the dependent variable fixed at its experimental value. The intervals can and should have more than two points and the best spline cubic curve for the interval is determined using least squares. Nunhez *et al.* [2,3] developed a new technique entitled the Modified Spline Technique (MST) which combines the Maximum Likelihood Principle to the Cubic Spline Method and extends the previously mentioned method. Since it allows for uncertainties for both the dependent and independent variables, the MST has been shown to be superior for data fitting when compared to the EST.

Tamir [5] and Taitel and Tamir [4] developed a variation of the EST known as Sectionwise Fitting (SF), which is the EST technique with the possibility of locating the intervals at points other than the experimental ones. The technique improves data smoothing for it allows the location of interval boundaries to be arbitrary, so infinite choices for the intervals can be made. Another very important aspect developed by Taitel and Tamir [4] is the capability of imposing that curves strictly concave, or convex, have their concavity respected. It is particularly important for systems where inflections would show inconsistent physical behavior, such as inflection points in vapor pressure against mixture composition curves. When there is a maximum, or minimum in these systems, it means the mixture is azeotropic and any inflection point would indicate the presence of an azeotropic point. If the oscillation is spurious due to the fitting procedure, an azeotropic point which does not exist would appear. Therefore it is necessary to guarantee the model representation respect the physical restriction.

THEORETICAL DEVELOPMENT

The Cubic Spline Method consists of the determination of a set of piecewise cubic functions which are continuous at their interval boundaries. The intervals are defined at every two consecutive points. The continuity requirement is imposed by a set of constraints that forces the first derivative of two consecutive cubic spline functions to be equal at their common boundary point. This is achieved by a set of constraints [3].

The Extended and Modified Spline Techniques allow a number of points to lie on each interval, and the best cubic spline is determined by the Least Squares criterion for the EST and the maximum likelihood principle for the MST. In this case, the EST becomes a particular case of the MST.

The application of the maximum likelihood principle to all experimental data is equivalent to minimizing the objective function S given by:

$$S = \frac{1}{2}\sum_{i=1}^{N} [W_{X_i}(X_i - x_i)^2 + W_{Y_i}(Y_i - y_i)^2] \ , \qquad (1)$$

where the weights are :

$$W_{X_i} = \frac{1}{\sigma_{X_i}^2} \ ; W_{Y_i} = \frac{1}{\sigma_{Y_i}^2},$$

X_i and Y_i = experimental data,

x_i and y_i = fitted value, and

σ_{X_i} and σ_{Y_i} = standard deviation.

The fitted values (x_i, y_i), i=1,2, ..., N, are subject to the following set of constraints:

$$F_i = y_i - f_k(x_i) = 0 \qquad x_{(k)} \le x_i \le x_{(k+1)} \qquad (2)$$

K=1, 2, ..., K

where $f_k(x_i)$ is the spline cubic function for the k^{th} interval.

$$f_k(x_i) = \frac{C_{k+1} - C_k}{6L_{k+1}}(x_i - x_{(k)}) + \frac{C_k}{2}(x_i - x_{(k)}) + \frac{A_{k+1} - A_k}{L_{k+1}} - \frac{C_{k+1} + 2C_k}{6}L_{k+1}(x_i - x_{(k)}) + A_k \qquad (3)$$

k=1, 2, ..., K+1

where $A_k = f_k(x_{(k)})$ and $C_k = f_k''(x_{(k)})$

(4)

It is at this point the first extension to the MST is introduced. The intervals can now take any value for $x_{(k)}$, and they do not necessarily need to be restricted to the values of the experimental points anymore. The only requirement is that the intervals contain at least three points so as to have a minimization for the selection of the best cubic spline following (1) (Figure 1). The choice of the intervals is still a matter of experience of the user, even though some guiding rules have already been noticed. Nunhez *et al.* [2] have pointed out that the best fits have been obtained for intervals of three points or a maximum of four. This is still true, but the extension of the MST allows a wider choice of interval boundaries. The power spline software suggests a choice of intervals but an experienced user would easily find an interval selection that would produce a best fit (lesser value for the objective function S).

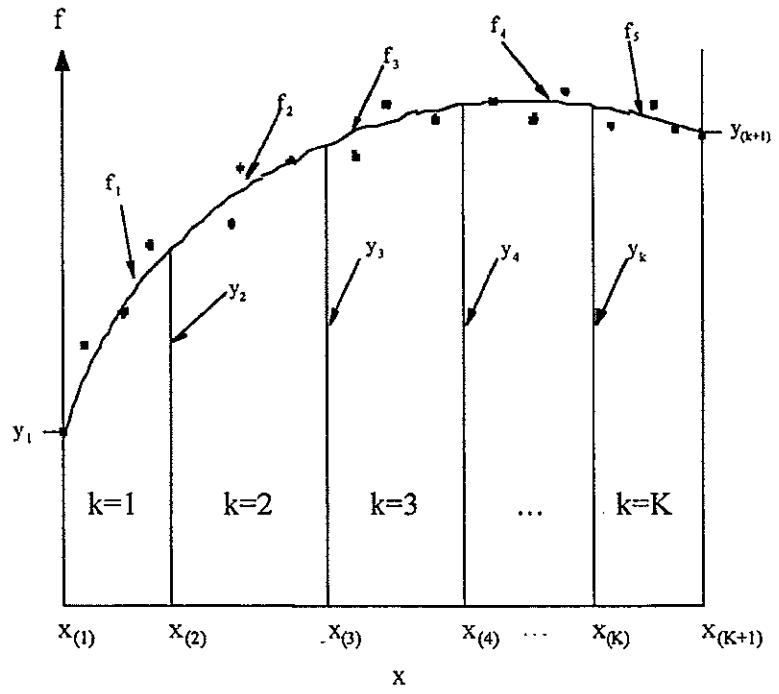

Figure 1 - Selection of the interval boundaries.

The functions are continuous, and the following set of conditions is required at the interval boundaries:

$$f'_{k-1}(x_{(k)}) = f'_k(x_{(k)}) \tag{5}$$

The following set of constraints is derived from (5):

$$\phi_k = \frac{L_k}{6} C_{k-1} + \frac{L_k + L_{k+1}}{3} C_k + \frac{L_{k+1}}{6} C_{k+1} - \frac{A_{k-1}}{I} + \frac{1}{I} + \frac{1}{I} A_k - \frac{A_{k+1}}{I} = 0 \tag{6}$$

k=2, ...,K

The minimization of (1) with constraints (2) and (5) requires the use of Lagrange Multipliers. More details for the minimization can be found in Nunhez *et al* [2].

The second modification to the method is the imposing of an additional constraint which forces strictly concave or convex curves to maintain their concavity. It is achieved by the imposing of a constraint to the second derivative of the spline curves. For these curves, the second derivative does not change sign, because the splines are third degree polynomials, so when any change in sign for the second derivative arises in any fit, it is then replaced by zero and the system is calculated again until all values of the second derivative have the same sign.

RESULTS AND DISCUSSION

One example has been selected from the literature to investigate the potential of the new method. The power spline has been applied to the boiling temperature against composition of the mixture tetrahydrofuran-water at atmospheric pressure, which has an azeotropic point. The data has been extracted from Hirata [6]. As already shown by Taitel and Tamir [4], this set of data is very hard to be fit and the use of polynomials is totally unsuitable since it indicates the presence of spurious inflection points which physically

would mean azeotropic points that the system do not exhibit. The normal modified spline fit is not able to fit this curve properly because there are many oscillations in the data points. Table 1 shows the results if there is no restriction to the concavity of the curve and Table 2 gives the parameters for this fit. Since the curve is concave up, the second derivative of the curve should be positive because the spline functions are a set of third degree polynomials. The first derivative change sign in the composition ranging from 0.25 to 0.82. There are three changes in sign that would indicate that there are three azeotropic points, which is not true. Even though the fit is good as far as deviations are concerned, it is physically wrong due to mathematical, rather than physical conditions. This limitation is easily handled by imposing the additional constraint to the second derivative, generating a fit free from inflection points. Table 3 shows the fit and Table 4 gives the parameters for this fit. Figure 1 shows the quality of the curve fitting.

Table 1 – Boiling temperature for the tetrahydrofuran-water system without imposing any restriction to the second derivative.

Data point	Mixture fraction	Standard deviation	Fitted fraction	Absolute deviation	Temperature Celsius	Standard deviation	Fitted Temperature	Absolute deviation	First derivative	Second derivative
* 1	0	0	0	0	100.0	0	100.00	0	-2332.1	110800
2	.02	0.01	.0185	.0155	73.00	0.01	73.000	0.000207	-748.24	60897.
* 3	.04	0.01	.0401	-.000053	66.50	0.01	66.500	-0.000083	-63.902	2458.0
4	.06	0.01	.0615	-.001462	65.59	0.01	65.596	-0.005794	-25.226	1155.2
* 5	.08	0.01	.0772	.002729	65.32	0.01	65.301	0.018730	-14.568	193.08
6	.10	0.01	.1038	-.003753	64.94	0.01	64.977	-0.036906	-10.168	139.20
* 7	.15	0.01	.1465	.003476	64.70	0.01	64.643	0.057211	-6.076	52.163
8	.20	0.01	.2021	-.002094	64.32	0.01	64.383	-0.062758	-3.336	46.441
* 9	.25	0.01	.2497	.000314	64.30	0.01	64.275	0.025266	-1.242	41.541
10	.30	0.01	.3000	-.000184	64.27	0.01	64.252	0.017666	0.104	11.967
* 11	.35	0.01	.3500	-.000003	64.25	0.01	64.260	-0.010261	-0.317	-17.404
12	.40	0.01	.4001	-.000072	64.23	0.01	64.240	-0.010379	-0.69218	-8.9800
* 13	.45	0.01	.4500	.000017	64.20	0.01	64.198	0.001867	-0.93083	-0.5829
14	.50	0.01	.4998	.000162	64.16	0.01	64.147	0.013293	-1.2183	-10.951
* 15	.55	0.01	.5502	-.000145	64.06	0.01	64.067	-0.007144	-2.0324	-21.413
16	.60	0.01	.6002	-.000154	63.94	0.01	63.946	-0.005725	-2.6837	-4.633
* 17	.65	0.01	.6498	.000162	63.82	0.01	63.814	0.006471	-2.4997	12.039
18	.70	0.01	.7000	-.000029	63.70	0.01	63.701	-0.001432	-2.0030	7.7536
* 19	.75	0.01	.7500	.000013	63.61	0.01	63.609	0.000734	-1.7222	3.4881
20	.80	0.01	.8000	-.000013	63.54	0.01	63.542	-0.001886	-0.68356	38.036
* 21	.82	0.01	.8200	.000014	63.53	0.01	63.537	-0.006737	0.21387	51.830
22	.84	0.01	.8403	-.000265	63.57	0.01	63.557	0.012636	0.0980	133.99
* 23	.86	0.01	.8604	-.000426	63.64	0.01	63.632	0.007575	5.6227	215.67
24	.88	0.01	.8779	.002093	63.73	0.01	63.756	-0.025946	0.0675	64.045
* 25	.90	0.01	.9017	-.001683	63.97	0.01	63.946	0.023572	0.1387	-142.17
26	.92	0.01	.9190	.000966	64.05	0.01	64.063	-0.013442	0.1872	147.76
* 27	.94	0.01	.9408	-.000839	64.29	0.01	64.284	0.005837	14.382	512.13
28	.96	0.01	.9591	.000847	64.61	0.01	64.614	-0.004112	20.596	166.54
* 29	.98	0.01	.9808	-.000755	65.07	0.01	65.066	0.003816	19.791	-241.09
30	.99	0.01	.9875	.002486	65.39	0.01	65.392	-0.002345	106.00	25746
* 31	1.0	0	1	0	69.97	0	69.970	0	727.16	73753

The asterisk (*) shows that the point is an interval boundary.

Table 2 – Interpolation parameters for the fit in Table 1

k	Ak	Ck

4	64.64774	70.46671
5	64.37746	.0000000
6	64.24033	.0000000
7	64.10321	.0000000
8	63.96438	.0000000
9	63.82366	.0000000
10	63.68350	.0000000
11	63.58666	.0000000
12	63.60436	268.9836
13	63.93424	.0000000
14	64.30124	118.5804
15	65.06639	648.5101
16	69.97000	71452.53

Figure 1 - Boiling temperature of the mixture tetrahydrofuran – water at 760 mmHg

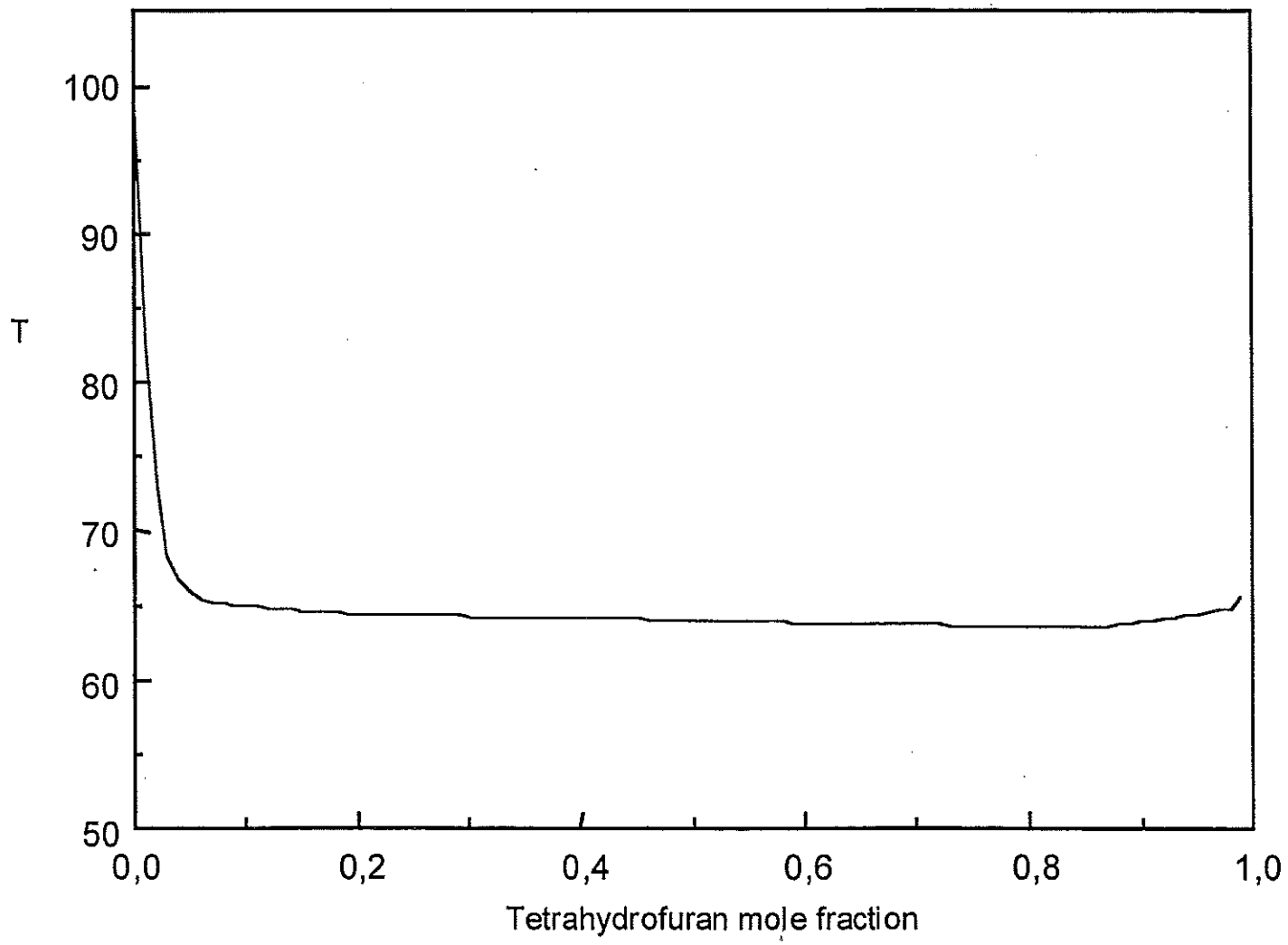

CONCLUDING REMARKS

1	100.0000	110804.0
2	66.50008	2458.000
3	65.30127	193.0797
4	64.64279	52.16273
5	64.27473	41.54095
6	64.26026	-17.40358
7	64.19813	-.5829297
8	64.06714	-21.41314
9	63.81353	12.03878
10	63.60927	3.488122
11	63.53674	51.82952
12	63.63242	215.6666
13	63.94643	-142.1750
14	64.28416	512.1254
15	65.06618	-241.0904
16	69.97000	73752.51

Table 3 – Boiling temperature for the tetrahydrofuran-water system without imposing restriction for the second derivative.

Data point	Mixture fraction	Standard deviation	Fitted fraction	Absolute deviation	Temperature Celsius	Standard deviation	Fitted Temperature	Absolute deviation	First derivative	Second derivative
* 1	0	0	0	0	100.0	0	100.00	0	-2338.8	111390
2	0.002	0.001	0.0183	0.00162	73.00	0.01	73.000	0.00021	-750.87	61287
* 3	0.004	0.001	0.0400	-0.00004	66.50	0.01	66.500	-0.00007	-62.374	2318.8
4	0.006	0.001	0.0617	-0.00171	65.59	0.01	65.597	-0.00675	-25.413	1091.8
* 5	0.008	0.001	0.0771	0.00292	65.32	0.01	65.301	0.01906	-15.320	221.99
6	0.100	0.001	0.1032	-0.00315	64.94	0.01	64.971	-0.03065	-10.266	165.79
* 7	0.150	0.001	0.1474	0.00264	64.70	0.01	64.648	0.05226	-5.042	70.467
8	0.200	0.001	0.2030	-0.00297	64.32	0.01	64.457	-0.13683	-2.174	32.682
* 9	0.250	0.001	0.2511	-0.00108	64.30	0.01	64.377	-0.07746	-1.388	0
10	0.300	0.001	0.3005	-0.00054	64.27	0.01	64.309	-0.03880	-1.388	0
* 11	0.350	0.001	0.3499	0.00013	64.25	0.01	64.240	0.09665	-1.388	0
12	0.400	0.001	0.3992	0.00081	64.23	0.01	64.172	0.05814	-1.388	0
* 13	0.450	0.001	0.4487	0.00134	64.20	0.01	64.103	0.09679	-1.388	0
14	0.500	0.001	0.4983	0.00174	64.16	0.01	64.034	0.12564	-1.388	0
* 15	0.550	0.001	0.5487	0.00133	64.06	0.01	63.964	0.09562	-1.388	0
16	0.600	0.001	0.5994	0.00638	63.94	0.01	63.894	0.04598	-1.388	0
* 17	0.650	0.001	0.6501	-0.00508	63.82	0.01	63.824	-0.00366	-1.388	0
18	0.700	0.001	0.7007	-0.00740	63.70	0.01	63.753	-0.05330	-1.388	0
* 19	0.750	0.001	0.7510	-0.00102	63.61	0.01	63.684	-0.07350	-1.388	0
20	0.800	0.001	0.8010	-0.00103	63.54	0.01	63.614	-0.70409	-1.388	0
* 21	0.820	0.001	0.8208	-0.00787	63.53	0.01	63.587	-0.05666	-1.388	0
22	0.840	0.001	0.8400	0.00004	63.57	0.01	63.568	0.00219	-0.168	127.06
* 23	0.860	0.001	0.8615	-0.00145	63.64	0.01	63.604	0.03564	4.082	268.98
24	0.880	0.001	0.8805	-0.00051	63.73	0.01	63.724	0.00638	8.046	147.00
* 25	0.900	0.001	0.9035	-0.00348	63.97	0.01	63.934	0.03576	9.734	0
26	0.920	0.001	0.9176	0.00237	64.05	0.01	64.074	-0.02355	10.071	47.675
* 27	0.940	0.001	0.9387	0.00133	64.29	0.01	64.301	-0.01125	11.820	118.58
28	0.960	0.001	0.9604	-0.00041	64.61	0.01	64.608	0.00236	17.355	390.64
* 29	0.980	0.001	0.9810	-0.00101	65.07	0.01	65.066	0.00361	28.060	648.51
30	0.990	0.001	0.9871	0.00287	65.39	0.01	65.393	-0.00281	101.88	23474.
* 31	1.000	0	1	0	69.97	0	69.970	0	712.53	71453.

The asterisk (*) shows that the point is an interval boundary.

Table 2 – Interpolation parameters for the fit in Table 3

k	Ak	Ck
1	100.0000	111385.5
2	66.50007	2318.831
3	65.30094	221.9858

A new fitting method, namely power spline has been presented and is suitable to be used when there is no physical model to represent the data. The method is very flexible and have an additional fitting capability which allows physical phenomena that generate data curves strictly concave up or concave down to be properly fit by imposing a restriction to the second derivative of the function, as shown in the example.

A computer software has been generated from the method and is in its first version. It can be freely obtained from www.feq.unicamp.br/~nunhez.

NOTATION

A_k	Cubic spline interpolation parameter
C_k	Cubic spline interpolation parameter
$f_k(x)$	Cubic spline function
$f_k'(x)$	First derivative of the cubic spline function
$f_k''(x)$	Second derivative of the cubic spline function
F_i	Constraint equation at i^{th} point
K	Number of interval boundaries
L_k	Interval of the k^{th} cubic spline function
N	Number of experimental points
S	Objective function for the maximum likelihood principle
X_i	Experimental value for the independent variable for the i^{th} point
x_i	Fitted value for the independent variable for the i^{th} point
Y_i	Experimental value for the dependent variable for the i^{th} point
y_i	Fitted value for the dependent variable for the i^{th} point
W_{X_i}, W_{Y_i}	Weights with respect to x_i and y_i, respectively

Greek letters

σ_{x_i}	Standard deviation for x at i
σ_{y_i}	Standard deviation for y at i
ϕ_k	Continuity equation for the k^{th} interval

REFERENCES

[1] Klaus, R. L. and Van Ness, H. C., 1967, An Extension of the Spline Fit Techinique and applications to thermodynamic data. *AIChE Jl* **13**, pp 1132.

[2] Nunhez, J. R., Mori, M. and D'Ávila, S. G., 1993, Fitting thermodynamic data using the Modified Spline Technique. *Computers Chem. Engng* **17**, pp 1091.

[3] Nunhez, J. R., 1990, Método Spline Modificado. MS thesis, UNICAMP - Universidade Estadual de Campinas.

[4] Taitel, Y., and Tamir A., 1983, Avoiding Unwarranted Inflection Points in Fitting of Data. *AIChE Jl* **29**, 153.

[5] Tamir, A., 1981, Azeotropes prediction by "Sectionwise Fitting". *Chem. Engng Sci.* **36**, 37-46. Pergamon Press, Oxford.

[6] Hirata, M. , Ohe, S. and Nagahama, K. Computer Aided Data Book of Vapor-Liquid Equilibria, Kodansha Ltd, Elsevier Scientific Publishing Co, 1975.

B - Industrial application

B B1 - GEOLOGY, HYDREOLOGY AND OIL FIELD APPLICATIONS

REACTIVE TRACING METHODS IN NATURAL POROUS MEDIA

M. Sardin[1] and M.O. Simonnot[1,2]

[1] Laboratoire des Sciences du Génie Chimique – CNRS – Groupe ENSIC (INPL), 1 rue Grandville, BP 451, 54001 Nancy, France
[2] EEIGM -INPL, 6 rue B. Lepage, 54000 Nancy

Abstract. : Reactive tracers are solutes, which allow one to in-situ determine site-specific parameters governing pollutant transport. Preliminary laboratory experiments allowed one to determine the type of interactions, which control the retention of pollutant in a given porous medium, and the interaction-specific parameters associated. But, generally, the poor representativity of laboratory soil samples does not permit to determine the site specific-parameters due to the heterogeneity of the natural porous media and to the structure of the flow at the field scale. The effective site-specific parameters are obtained using reactive tracer, presenting the same type of reactivity as the pollutant but being not toxic and less strongly retained. The method is illustrated by some examples from our own results and literature.

INTRODUCTION

The dynamics of pollutants in soils and ground waters is a widely open topic because of the complexity of the systems. Modeling for detailed risk assessment or evaluation of the efficiency of a remediation technique needs to have an accurate image of motion and interactions of pollutants. Computer codes coupling flow and geochemistry now allow us to simulate the transport of interactive solutes in a given geometry. But they have to be fed with realistic data, which are generally obtained by laboratory measurement on samples extracted from polluted soils or aquifers. These techniques present some disadvantages. At first, they require numerous samples of materials from contaminated soils or aquifers. Then, the analytical procedure is very time-consuming and difficult to perform in representative conditions. At last, the results are only point values and in heterogeneous media the spatial distribution mapping needs to use stochastic techniques. Also, the difficulty to have a good representation of natural porous media is not only in the nature of involved materials or types of pollutant, but also in the complex structure of the percolated media. The research works aimed at describing the soil or aquifer structure in details and modelling the porous media through stochastic approaches are more and more operating. But, it exists a large domain for the development of tracing techniques. A substance transported with ground water as a tracer interacting with certain sites of an active surface of the explored medium causes a typical deformation of the breakthrough curves (BTCs), which is a signature of the studied interactions. These techniques give an integral information on the structure and reactivity of the porous media with only few measurements and can be used to validate the detailed approaches. It so becomes possible to associate the fundamental knowledge obtained in laboratory and the operating parameters involved in the transport models at a large scale. The aim of this paper is to review the different methods, which have been or can be used for determining the global site-specific parameters, characterising available (or effective) adsorption surface area or cation

exchange capacity, mass transfer parameters, organic matter fraction, etc., in addition to flow parameters.

PRINCIPLE OF THE METHOD

The motion of a pollutant in natural porous media is controlled by a typical interaction or a set of interactions. The associated parameters to physico-chemical interactions can be classified into two categories [1]. The first one includes the specific interactions parameters: they are representative of thermodynamic equilibria, *i.e.* the equilibrium constant or a distribution coefficient often deduced from the mass action law. The second one includes the "site-specific" interaction parameters, which give the capacity of the studied medium for a given pollutant, *i.e.* the amount of active sites of the stationary phase in contact with the mobile fluid.

In front of the complexity of pollutants, soils and sub-soils, a classification of physico-chemical interactions is essential to develop a founded and consistent approach. An example is given by the computer code IMPACT [2], which proposes a classification presented in Table 1. In this code, conversely to the detailed chemical approach, the species are distinguished according to their mobility instead of the phase in which they are located (liquid, gas or solid). For instance, a species present in the diffuse double layer is viewed as a stationary species even if it is located in the water and not at the solid surface. This is an important difference, which is often responsible for a lack of understanding between chemists and transport modellers.

Table 1 : Typology of interactions in the IMPACT computer code

Type of reactions	Specific-site parameters
Homogeneous reactions	
• in the mobile phase: reactions in solution e.g. oxidation, acid dissociation	
• in the stationary phase: surface ionisation, site dissociation.	Ionisable site capacity
Heterogeneous reactions	
• between gas and liquid: Henry's law	Liquid/gas ratio
• between liquid and liquid: water/organic matter partition	Organic carbon fraction
• between fluids and solids:	
• without solid alteration: ion exchange, adsorption, surface complexation	Exchange capacity, specific site concentration, iron oxide content.
• with solid alteration: dissolution/precipitation	Mineral content.

As a simple example, the motion of a pollutant is often compared to the one of water through the retardation factor R, which is the ratio between the two apparent mean velocities of water and pollutant, u_w and u_p or their mean retention times, t_0 and t_r, respectively. For a pollutant interacting with a porous medium according to a linear adsorption law, we write:

$$\mathrm{R} = \frac{u_w}{u_p} = \frac{t_r}{t_0} = 1 + \frac{M}{V_p} K_d \qquad (1)$$

M is the mass of solid explored by the flow and V_p the pore volume accessible to water given in coherent units. K_d is conventionally measured by standard methods in

batch reactors, and it is assumed for scale-up, that the total mass of porous media at the field scale is active and is involved in the interaction process. Unfortunately, that is rarely verified and the ratio M over V_p is not known *in-situ*.

The principle of the method can be summarised as follows. Let us assume that the interaction mechanism between a given pollutant and a natural soil sample has been determined by preliminary laboratory studies and that the retention process depends on one type of soil component or even on one type of surface reaction site. Owing to spatial variability, or water saturation of soil, the concentration of reactive site measured under laboratory conditions is generally different from the one observed under field conditions. The direct measurement with the pollutant at the field scale is replaced by a suitable species, which may be used to measure the effective reactivity of the medium at the field scale. Selecting a reactive tracer consists in finding a solute for which the interaction mechanisms involve the same sites as the pollutant, no toxic and presenting weaker interaction with the porous media in order to perform *in situ* experiment in a reasonable time. Mechanism elucidation and reactive tracer selection typically pertain to laboratory experiments. Field experiments with reactive tracer are interpreted to recover the site-specific parameter. Finally, a computer model can be fed with the site- and interaction-specific parameters to predict pollutant transport. This method is illustrated below by some examples from our own experience or from the literature. They will focuse on the choice of reactive tracers.

EXAMPLES OF REACTIVE TRACER USE

1. Partitioning tracers

1.1 Organic matter fraction, f_{oc}

The works of Karickhoff et al. [3] followed by the ones of Schwarzenbach and Westall [4] have shown that the transport of non-polar organic contaminants was essentially controlled by the organic matter content of soil or aquifer. In a large domain of solubility of the pollutant in water, the soil partition coefficient of this kind of pollutant is constant and can be deduced from the well-known "Karickhoff's law". It is assumed that the soil partition coefficient K_d is proportional to the organic carbon fraction of soil, f_{oc}, and to the partition coefficient with organic carbon, K_{oc}. This coefficient can be calculated from the tabulated data of the partition coefficient of the pollutant between water and octanol, K_{ow}.

$$K_d = f_{oc} K_{oc} \; with \; \log K_{oc} = 1.00 \log K_{ow} - 0.21 \qquad (2)$$

The organic carbon content appears as a site-specific parameter to deduce the dynamics of organic compounds in soil. For instance, column experiments (figure 1) performed on a natural soil containing 2% organic carbon [5-6] have shown that the BTCs of three Polycyclic Aromatic Hydrocarbons have the same type of behaviour on this type of soil. The distribution coefficients deduced from the mean residence time (table 2) are very close of those calculated from eq. (2). Moreover, the BTCs are superimposed upon normalisation of the time axis by the mean retention time, t_r, given at constant flow rate by:

$$\frac{t_r}{t_0} = R = 1 + \frac{M}{V_p} K_d = 1 + \frac{M f_{oc}}{V_p} K_{oc} \quad (3)$$

We remark in figure 1 that dispersion appears to be higher than the one of the water tracer, indicating that the interaction has a consequence not only on the retention volume, but also on the dispersivity.

Table 2: Measured and calculated K_d from Karickhoff law's(eq.(2))

PAH	Octanol/water partition coefficient (Log K_{ow})	Measured K_d ($L.kg^{-1}$)	Calculated K_d ($l.kg^{-1}$)	Solubility in water at 20°C (mg/L)
Toluene	2.69	n.d.	4	518
Naphtalene	3.37	15	19	31
Fluorene	4.18	119	123	1.9
Phenanthrene	4.57	290	298	1.1

But the main fact is that the position and the dispersion can be directly deduced from one experiment with a single reactive tracer, the similar molecules having the same transport properties.

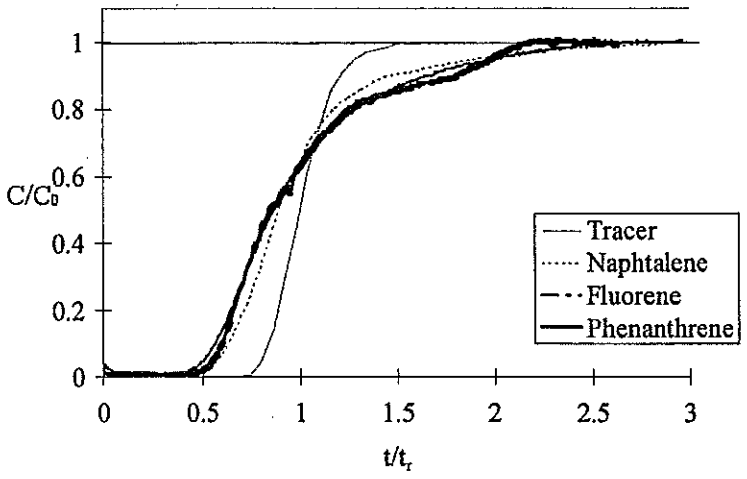

Figure 1: BTCs of different PAHs (Naphtalene, Fluorene, Phenanthrene at 80 % of their solubility in water) showing their identical behaviour in an organic sandy soil column from Netherlands(Clays, 4 %, foc, 2 %)[4].

Thus, to evaluate the motion of PAHs in an organic soil, the reactive tracer has to be a biodegradable simple aromatic compound soluble in water with a low K_{ow} e.g. toluene (see Table 2).

1.2. Residual non aqueous phase liquid saturation

The estimation of spatially variable residual non-aqueous phase liquid (NAPL) saturations in heterogeneous porous media can be solved by using a tracer test technique. A number of authors [7-8] have shown that breakthrough curves of partitioning tracers at extraction wells can be used to obtain an accurate measurement of the average saturation and total volume of NAPL present in the

volume of an aquifer swept by the tracers. The comparison between the temporal moments of partitioning and non-partitioning tracer BTCs is used to deduce areas of high residual NAPL saturation. Recently, James *et al.* [9] have developed this method to estimate the residual NAPLsaturation in a non uniform flow field. The main tracers used were alcohol as isopropanol or butanol.

1.3. Soil-water content

The method proposed by Nelson *et al.* [10] to determine the soil-water content is based on the use of a tracer test with non-partitioning and partitioning tracers introduced into the system in the gas phase. Partitioning tracers dissolve into the water, which retards their gas-phase transport relative to that of the non-partitioning tracers. Retardation of the partitioning tracers is a function of the amount of water present. The performance of this new method has only been tested in laboratory and in a large weighing lysimeter. Soil-water contents estimated from the tracer tests were reasonably close to the values obtained using gravimetric and time domain reflectometry measurements.

The retardation for gas phase transport of a tracer retained by the aqueous, phase, sorbed or retained at the gas-water interface is given by:

$$R = 1 + \frac{\theta_w}{\theta_a K_H} + \frac{\rho_b K_{Dsat}}{\theta_a K_H} + \frac{K_{IA} A_{IA}}{\theta_a} \tag{4}$$

where θ_w is the volumetric water content, θ_a is the air-filled porosity, K_H is the Henry's law constant, K_{Dsat} is the sorption coefficient, ρ_b is the dry soil bulk density, K_{IA} is the adsorption coefficient between the gas phase and the gas-water interface, and A_{IA} is the specific surface area. When sorption and interfacial accumulation of the partitioning tracer are negligible, R is given by the two first terms:

$$R = 1 + \frac{\theta_w}{\theta_a K_H} = 1 + \frac{\theta_w}{(\varepsilon - \theta_w) K_H} \tag{5}$$

where ε is the total porosity. From eq.(5) it is obvious that a gas-phase tracer experiment conducted with partitioning and non partitioning tracers can provide a measurement of θ_w, if K_H is known.

The tracer selection depends on the following criteria: low toxicity, low cost, low background levels, no biodegradation or other transformation at the time-scale of the experiment, no sorption onto porous media, low detection levels and eventually an appropriate K_H value. A tracer with a suitable K_H would yield a retardation factor large enough to be measurable with some level of certainty but small enough in order that the test duration remains practical. For instance Nelson *et al.* [10] used methane as a water tracer and dibromodifluoromethane as a reactive tracer. Toluene could have been chosen, but knowing that toluene is sorbed by the soil organic matter, the soil organic matter content must be known.

1.4. Water/organic matter exchange interface

To evaluate the transfer between water and organic matter, which can either be naturally occurring or coming from a massive pollution (e. g. coal tar), it is necessary to know not only the volume of organic matter, but also the exchange

surface area in contact with the leaching water. In fact, the evaluation of a leaching process is determined by thermodynamic properties of pollutant and by the kinetics of mass transfer. For instance, the characteristic time of a process limited by internal diffusion in an aggregate of organic matter is:

$$t_d = \frac{\alpha.\mu_F.V_a^2}{D_e.S_a^2} \tag{6}$$

where α is the aggregate capacity, μ_F a shape factor, D_e the effective diffusion coefficient in the matrix, V_a and S_a the aggregate volume and external surface. The $l=V_a/S_a$ ratio, the aggregate characteristic length, is not easy to evaluate *in-situ*.

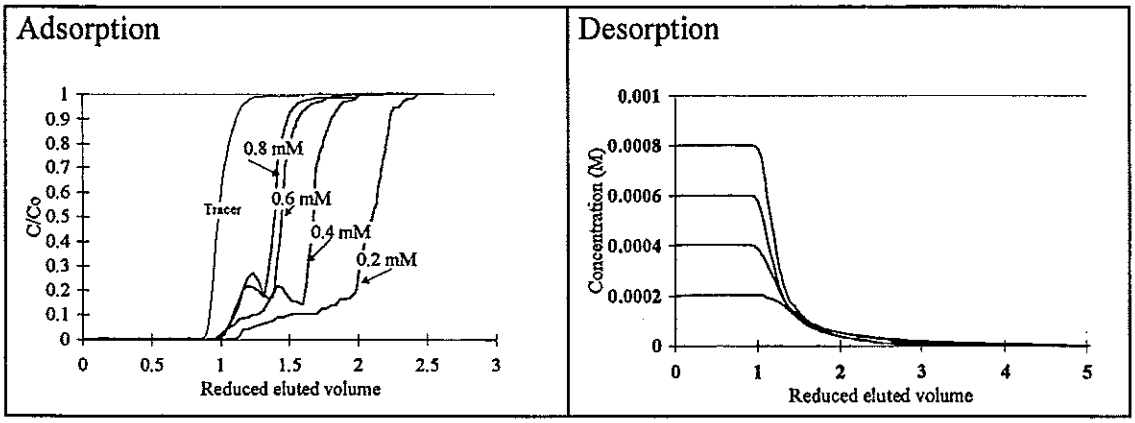

figure 2 : Example of BTCs of a hydrophilic surfactant through a soil column impregnated with a heavy hydrocarbon. The adsorption desorption process is non linear and can be simulated by a Langmuir type interaction. The surface area (1.7 m^2/g) is deduced from the one of the surfactant molecule (35Å) and the maximal adsorbed concentration [5].

The use of interface tracers can appear as a solution to evaluate the exchange surface area. A hydrophilic surfactant, as sodium octylbenzensulfonate, is an attractive solution [5]. This well-known molecule has been used as a test molecule in the development of techniques of enhanced oil recovery by surfactant flooding [11]. Its interest is to have a high Critical Micellar Concentration (0.012 $Mol.L^{-1}$) and to saturate the water/organic interface at low concentration (10^{-3} $Mol.L^{-1}$). This molecule was tested to evaluate the repartition of saturated hydrocarbon in sandy soil column. The surface area (1,7 m^2/g) obtained by adsorption measurement is very close to the one expected from the surface properties of the soil column indicating a homogeneous repartition of the hydrocarbon [5]. This method is a complement of the methods measuring the residual saturation of non aqueous liquid in soil and allows one to evaluate the characteristic size of organic aggregates.

2. Site-specific tracers

2.1 Cation exchange capacity

Another important parameter in soil is the cationic exchange capacity (CEC). Jauzein et al. [2] have proposed, in the frame of a new concept, the relay substance method, for predicting the transport of inorganic pollutants in soil, to use the cation lithium to evaluate the effective CEC in field conditions. The method is illustrated by the prediction of caesium transport at the field scale.

Caesium is viewed as a radionuclide pollutant. It is strongly retained by the soil, whereas lithium has a small affinity. By laboratory experiments it was shown that the caesium cation explored the same sites as the lithium cation. Thus, the properties of cation exchange of ceasium and lithium with the divalent cations of the soil water have been quantitatively determined: exchange capacity and selectivity coefficients. Then, the effective exchange capacity under field conditions was obtained using lithium as a relay substance. The field experiments, using iodide as a water tracer, lead to show that iodide and lithium BTCs were superimposed upon normalisation of the time axis by the mean residence time. This behaviour is typical of linearly interacting solutes. By linearisation of the classical equation of cation exchange, the effective CEC could be deduced from the retardation factor of lithium with respect to iodide. The prediction of caesium transport was then made possible. At this occasion, the authors put to light the important role played by the conditions of dilution by field water if the interaction of the pollutant with soil was non linear. The concept of "dilution earliness" was used to predict limiting situations of dilution and the corresponding BTCs. It was even suggested that non linearly interacting solute could be used as relay substances to get information on dilution along the transport process.

2.1. Iron oxide/hydroxide content

The role of ferric iron in soil is very important from two points of view. At first, it plays an important role as an electron acceptor in biochemical processes. Certain pollutants like BTEX can be degraded in anoxic aquifers via microbial activated redox reactions. At last, it is one of the main supports of reaction sites for surface complexation processes of heavy metals with soil surface. The *in-situ* measurement of iron oxide content is very important to evaluate the retention of heavy metals by a soil. The idea developed by Mayer et al.[12] is to use a reactive tracer specific to the iron oxide/hydroxide interaction but not very strongly adsorbed. This one can be found among oxy anions, which present a characteristic sequence of high to low sorption from HPO_4^{2-}>MoO_4^{2-}>SO_4^{2-}. This adsorption is non-linear in a large concentration range and can be modelled with a pH-dependent Langmuir isotherm. The maximum capacity at a given pH is constant and delivers the iron content. Unfortunately, a lot of other factors (sorption on other oxides or organic material) may disturb the method. This measurement has to be coupled with other evaluations as the organic matter fraction.

CONCLUSIONS

The different tracing methods and reactive tracers described above give a large panel of methods to evaluate the distribution of a pollutant in a natural porous media or to quantitatively evaluate its transport properties at the field scale. A few experiments have been performed to validate this approach which gives excellent tools to calibrate transport models. Recently, Davis *et al.* [13] have published a very large experiments at Cap Cod site, Massachusetts (USA) using a multispecies reactive transport experiment to evaluate the evolution of the polluted aquifer. The results provide a chemically complex data set that can be used in the testing of reactive transport models. In the frame of the French project named "Centre d'Etude des Friches Industrielles" in Lorraine, we propose to develop a similar experimentation adapted to organic pollutants, especially PAH, which are persistent chemicals contaminating the sites of old metallurgic and gas plants.

REFERENCES

[1] Jauzein M., André C., Margrita R., Sardin M., Schweich D., The relay substance method: a new concept for predicting pollutant transport in soils. in Proceedings of Geoval-90, may 14-17, 1990, Stockholm-Sweden, Ed. OCDE, Paris 1991.

[2] Jauzein M., André C., Margrita R., Sardin M., Schweich D., A flexible computer code for modelling transport in porous media: IMPACT, Geoderma special issue, 44, 2-3 (1989), 93-113.

[3] Karickhoff S.W., Brown D.S., Scott V., Sorption of hydrophobic pollutants on natural sediments, Water Res. 13, (1979) 241-248.

[4] Schwarzenbach R.P., Westall J., Transport of non polar organic compounds from surface to groundwater, Environ. Sci. Technol. 15 (1081) 1360-1367.

[5] Appert-Collin J.C, Contribution à l'analyse des risques liés au transport d'HAP dans les milieux poreux naturels, Thèse de l'INPL, nov. 15, 1999, Nancy.

[6] Appert-Collin J.C., Dridi-Dahouadi S., Simonnot M.O., Sardin M. Nonlinear sorption of Naphtalene and Phenanthrene in natural porous media : column experiments. Physics and Chemistry of the Earth, (1999).

[7] Annable M.D., Rao P.S.C., Hatfield K., Graham W.D., Wood A.L., and Enfield C.G., Partitioning tracers for measuring residual NAPL: Field-scale test results, J. Environ. Eng. 124 (6) (1998), 198-503.

[8] Jin M., Delshad M. , Dwarakanath V., McKinney D.C., Pope G.A., Sepehrnoori K., Tilburg C., Jackson R.E., Partitioning tracer test for detection, estimation, and remediation performance assessment of subsurface nonaqueous liquids, Water Resour. Res. 31 (1995), 1201-1211.

[9] James A.I., Graham W.D., Hatfield K., Rao P.S.C., Annable M. D., Estimation of spatially variable residual non aqueous phase liquid saturation in non uniform flow fields using partitioning tracer data, Water Resour. Res. 36 (2000) 999-1012.

[10] Nelson N.T., M.L. Brusseau, T.D. Carlson, M.S. Costanza, M.H. Young, G.R. Johnson, P.J. Wieranga, A gas-phase partitioning tracer method for the in situ measurement of soil-water content, Water Resour. Res., 35 (1999) 3699-3707.

[11] Sardin C., Maunier C., Dridi S., Simonnot M.O., Transient transport of surfactant in a calcareous and clayey sand, Physics and Chemistry of the Earth, Vol. 23, N°2(1998) 221-227.

[12] Mayer M., Irmler S., Dahmke A, Development of a reactive tracer for iron oxide/hydroxide quantification in sediments, Proceedings of the ESF conference (1997).

[13] Davis J.A., D.B. Kent, J.A. Coston, K.M. Hess, J.L. Joye, Multispecies reactive tracer test in an aquifer with spatially variable chemical conditions, Water Resour. Res., 36 (2000), 119-134.

INTERWELL TRACER TECHNOLOGY IN OIL RESERVOIRS: STATE-OF-THE-ART

T. Bjørnstad[1,2], Ø. Dugstad[1], C. Galdiga[1] and J. Sagen[1]

[1] Institute for Energy Technology, P.O.Box 40, N-2027 Kjeller, Norway
[2] Institute of Chemistry, University of Oslo, P.O.Box 1033, N-0131 Oslo, Norway

Abstract. This article describes very briefly the present status of interwell tracer technology for reservoir evaluation purposes. Firstly, laboratory tracer development and quality assurance methods are outlined. These consist of experiments on thermal, chemical and microbial stability, static sorption, phase partitioning and dynamic flooding properties. Secondly, the best available tracer analysis methods are mentioned. These include gamma spectrometry and liquid scintillation counting for radioactive tracers and HPLC and GC/MS for non-radioactive tracer compounds. Detection limits for non-radioactive gas tracers are < 10^{-13} l/l while non-radioactive water tracers may be detected in the ppt-region. Thirdly, a new simulator development is described. The tracer simulation module is coupled to a modern commercial reservoir simulator. It contains features to reduce numerical dispersion of the tracer pulse. Lastly, results are shown from the North Sea Snorre field from the use of the new non-radioactive tracers.

INTRODUCTION

Tracers have been used to measure fluid flow in oil reservoirs for decades. A summary of the use before 1990, from the perspective of tracer behavior, is provided in [1]. There are some quoted success stories and some reports where the authors claim that the experiments have been failures. Some failure conclusions may be right and some questionable. In the first case tracers have been used without sufficient knowledge of their behavior under actual reservoir conditions, and they may have been subject to degradation. In the latter case non-show of tracers have wrongly been interpreted as being synonymous to non-performance.

In the latter years the value and importance of tracer examinations have been broadly recognized, and there is a growing demand for such examinations on a global basis. In the North Sea tracer examinations have become an integrated part in reservoir monitoring and management. This is largely due to an extensive development of the technology as such over the last decade. Better understanding of the behavior of traditional tracers has been obtained and a suite of new tracers has been developed. This development has improved the reliability of field tests. In the following a brief outline of this development will be given along with the current status and outlook.

TRACER DEVELOPMENT AND QUALITY ASSURANCE

1. Thermal and chemical stability

Thermal stability of water tracers is examined in batch experiments (aerobic or anaerobic) where aliquots of tracer mixtures in reservoir fluids are exposed to different temperatures for different time periods. Tritiated water, HTO, is always added in a known amount to act as a standard reference water tracer. Other parameters may be ionic composition and pH.

Samples are analysed with respect to remaining original tracer concentration. Radioactive tracers are detected by gamma-spectrometry or liquid scintillation

counting (LSC), and the chemical tracers are commonly analysed by HPLC or GC techniques.

2. Microbial stability

Microbial stability of water tracers shows up in the tests described above by a substantial degree of degradation at temperatures below 70 °C while the tracer survivability may be better at higher temperatures.

3. Sorption characteristics

The tracer compounds are contacted with crushed reservoir-like rock dispersed in formation water. Convenient substrates are sandstones and chalk representing main reservoir rock types and kaolin representing clays. HTO is added for standardization. Further experimental parameters are temperature and time.

4. Phase partitioning

Phase distribution (in water, oil gas) of tracer candidates is examined in phase equilibration tests. Different methods are in use. In the batch method the phase mixing and separation takes place in a mixing apparatus where samples can be extracted from each phase for analysis of tracer concentration as a function of time and temperature. Experiments run until obtained equilibrium.

In the dynamic procedure a small-volume tracer pulse is forced through a porous medium (preferably ≈ 1-dimentional) with known oil saturation at moderate linear flow rate (25-250 cm/d) together with the standard reference tracer, which is HTO and CH_3T for water and gas tracers, respectively. Difference in transportation time between reference and tracer candidate is used to calculate the partition coefficient, or K-value, of the tracer candidate. Parameters are temperature and fluid compositions (including pH) and pressure (when applicable).

5. Dynamic flooding properties

Finally, the tracers are examined in core-flooding experiments. Different types of equipment are available. It is common to use cores of consolidated reservoir or reservoir-like rock (i.e. sandstones and/or carbonate material). Core dimensions

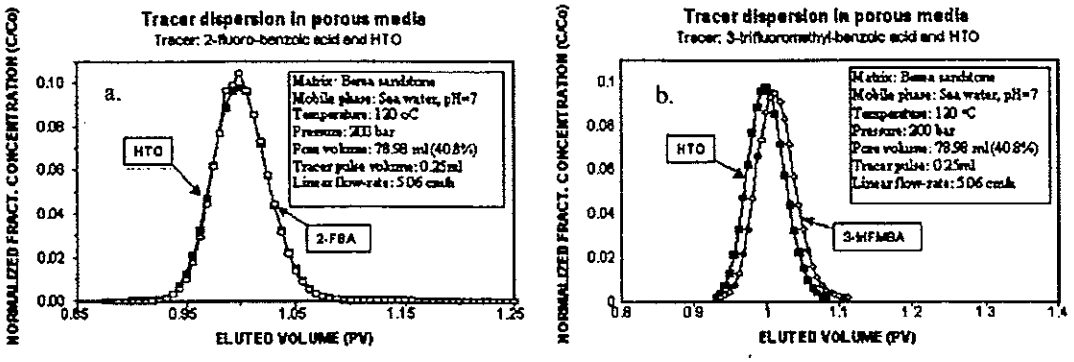

Figure 1. Examples of tracer dispersion curves of 2-fluorobenzoic acid (a) and 3-trifluoromethyl-benzoic acid (b) compared to tritiated water from flooding experiments in sandstone. Parameters are given in the figure insets.

normally range from dxl=2.8x7.7 cm (=1.5x3 inch) to dxl=5.1x51.2 cm (=2x20 inch). Other equipment is based on the use of crushed rock material filled into a chromatographic column of varying dimensions.

The tracer and a reference (HTO or CH_3T) are injected together as a pulse into the core. The production profiles of the tracer candidate and the reference may be directly compared. Examples of dispersion curves are given in Figure 1.

CURRENT WATER AND GAS TRACERS

1. Water tracers

A number of "traditional" radioactive and non-radioactive water tracers have been re-examined along the lines described above, and search for new possible tracer

Table 1. Examples of examined compounds

Comp.	Label	Comp.	Label	Comp.	Label.
I^-	$^{125,131}I$	$Ni(CN)_4^{2-}$	^{63}Ni	Na^+	^{22}Na
Br^-	^{82}Br	$Co(CN)_6^{3-}$	$^{56,57,58\,60}Co$,	ALAL	T, ^{14}C
Cl^-	^{36}Cl	$Co(CN)_5(^*CN)^{3-}$	^{14}C	ARAL	T, ^{14}C
SCN^-	^{35}S, ^{14}C	$Ag(CN)_2^-$	^{110}Ag	ALA	T, ^{14}C
CN^-	^{14}C	$Au(CN)_4^-$	^{195}Au	ALFA	-
SO_4^{2-}	^{35}S	$Fe(CN)_6^{3-}$	$^{55,59}Fe$	PCBA	-
CO_3^{2-}	^{14}C	$IrCl_6^{2-}$	^{192}Ir	PFBA	-

ALAL= aliphatic alcohols, ARAL= aromatic alcohols, ALA= light aliphatic acids, ALFA= aliphatic fluorinated acids, PCBA= poly-carboxylic benzoic acids, PFBA= poly-fluorinated benzoic acids

compounds are continuously ongoing. Possibility for ultra-low detection limits is required. Hence, especially, the fluorinated aromatic acids have attracted attention because of their success in tracing of groundwater. Table 1 gives a flavour of the types of compounds, which have been under examinations.

Table 2. Presently qualified water tracers

Non-radioactive	Radiolabelled
Inorganic molecules: D_2O, SCN^-, $Co(CN)_6^{3-}$	Organic molecules: CH_2TOH, $^{14}CH_3OH$ $CH_3{}^{14}CHOHCH_3$, $CH_3CTOHCH_3$
Three mono-fluoro benzoic acids: 2-FBA, 3-FBA, 4-FBA	
Six di-fluoro benzoic acids: 2,3-DFBA, 2,4-DFBA, 2,5-DFBA, 2,6-DFBA, 3,4-DFBA, 3,5-DFBA	Inorganic molecules: HTO, $^{22}Na^+$, $^{125}I^-$, ($^{131}I^-$), ($^{82}Br^-$), $^{36}Cl^-$, $^{35}SCN^-$, $S^{14}CN^-$, ($^{35}SO_4^{2-}$), $^{56}Co(CN)_6^{3-}$, $^{57}Co(CN)_6^{3-}$, $^{58}Co(CN)_6^{3-}$, $^{60}Co(CN)_6^{3-}$ $Co(CN)_5(^{14}CN)^{3-}$
Six tri-fluoro benzoic acids: 2,3,4-TFBA, 2,3,5-TFBA, 3,4,5-TFBA,2,4,6-FBA, 2,3,6-TFBA, 3,4,6-TFBA	
Two four-fluoro benzoic acids: 2,3,4,5-FFBA, 2,3,5,6-FFBA	

A comprehensive amount of information has been generated about the reservoir behaviour of these compounds. Some pass through the eye of the needle in good shape while others show instability of one or the other kind. This excludes them from reservoir use, at least under certain reservoir conditions. Such information resulted in the following Table 2 of presently qualified reservoir water tracers.

Note that conditions (stability, cost/availability, detection limit, toxicity) are associated to each of the tracer compounds in Table 2 for their safe and reliable use in oil reservoirs. Some information can be found in [2] and [3], but most of the data is not yet published otherwise than in private confidential research reports.

2. Gas tracers

Traditional gas tracers are radiolabelled (mainly tritiated) light hydrocarbon gases methane, ethane, propane and butane. In addition, ^{85}Kr has been occasionally used. In 1985 IFE started development of a new series of gas tracers, - the perfluorinated light cyclic "hydro"-carbons. After an intensive laboratory phase they were qualified in subsequent field experiments in the beginning of the nineties [4,5]. Currently available gas tracers are listed in Table 3.

Table 3. Presently qualified gas tracers

Radioactive				
CH_3T, $^{14}CH_4$, CH_3CH_2T, $^{14}CH_3CH_3$, $CH_3CH_2CH_2T$, $^{14}CH_3CH_2CH_3$, $CH_3CH_2CH_2CH_2T$, $^{14}CH_3CH_2CH_2CH_3$, ($^{14}CO_2$), ^{85}Kr, ^{127}Xe, ^{133}Xe				
Non-radioactive				
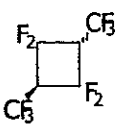 PDMCB	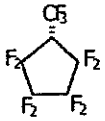 PMCP	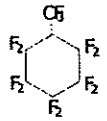 PMCH	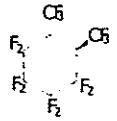 1,2-PDMCH	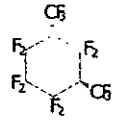 1,3-PDMCH
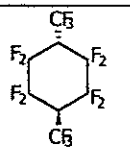 1,4-PDMCH	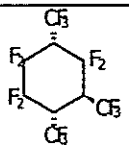 1,3,4-PTMCH	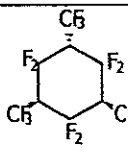 1,3,5-PTMCH	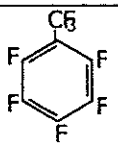 PFT	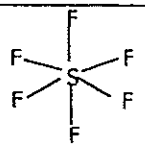 SF_6

If one can compromise somewhat on detection limit, there are several other applicable compounds, which can be used as reservoir gas tracers.

TRACER ANALYSIS

1. Radioactive tracers

Radioactive tracers are analysed by gamma spectrometry or with liquid scintillation (LSC) methods. Often, a sample purification, a pre-concentration procedure or even a chemical separation procedure is needed before counting, see for instance [6]. Detection limits for water tracers vary from 0.005Bq/l for $S^{14}CN^-$ and similar compounds, which may be enriched into a small liquid volume compatible with the scintillator cocktail, via 0.02 Bq/l for direct gamma spectrometry to 1.5 Bq/l for

HTO. Detection limit for organic gas tracers analysed with a combination of combustion (12 L gas at STP conditions) and LSC are approximately 0.0025 Bq/l.

2. Non-radioactive tracers

2.1. Inorganic anion water tracers

Non-radioactive $Co(CN)_6^{3-}$ is analysed by a combination of tracer separation with ion exchange methods, neutron activation of the enriched sample and gamma spectrometry. Other ions, for instance SCN^-, are analysed with a combination of chemical enrichment techniques and HPLC.

2.2. Fluorinated aromatic acid water tracers

HPLC with diode array detector enables analysis in the microgram/litre range [7].

However the application of fluorinated benzoic acids in petroleum reservoirs with large well distances makes even more sensitive techniques desirable. Gas chromatography in combination with mass spectrometry detection and confident identification (GC/MS), even at ultra trace concentrations, is possible.

Today, the recommended analytical procedure involves the following steps: Filtration of 250 ml water sample with a lipophilic filter and acidify to approx. pH≈ 2. Tracer compounds, now in protonized form, is separated in solid phase extraction (SPE) with a C-18 column. The tracer is then eluted with a few ml of organic solvent and evaporated to a smaller volume. Thus, pre-concentration factors > 1000 can be achieved. Addition of pentafluorobenzyl bromide transforms the fluorinated benzoic acids into their corresponding more volatile esters suitable for GC. Electron impact ionisation (EI-mode) or negative ion chemical ioniziation (NICI-mode) are used with the MS. These methods allow a sensitivity and unambiguous tracer identification at sub-microgram/litre concentrations (ppt-level) [8,9].

2.3. Perfluorinated organic gas tracers

Gas chromatography in combination with electron capture detection (ECD) is the widely used technique for PFC analysis in reservoir gas matrices. However, recently a new analytical method with superior sensitivity and confident tracer identification at trace levels was introduced. This method is based on GC/MS in combination thermal desorption of so-called CATS (capillary absorption tube samplers). CATS are used to selectively extract tracer compounds from natural gas by sorption in a substrate. The operation is carried out at the production facility. Thus, gas tracer samples may now be shipped in ordinary mail because there is no need for pressurized cylinders. Detection limits < 10^{-13} l/l are obtained [10].

SIMULATOR DEVELOPMENT

1. Stream-tube model

Several stages in tracer modeling have been performed at IFE. Based on the polymer flow solutions [11], 1-dimensional analytical solutions for incompressible tracer flow were deduced [12]. The model was generalized to two dimensions by using the concept of a stream-tube model [13].

2. IFE ITRC tracer simulator

Since 1992 a tracer module coupled to an existing commercial simulator has been developed. The goal was to integrate the tracer module with both semi-compositional, compositional and black oil simulators.

As is the case for the host reservoir simulator, the tracer module is based on a finite volume formulation on general types of grid such as corner point geometry and radial grids. One of the advantages of the tracer module lies in the "modular" concept, which allows the tracer equations to be solved separately from the rest of the reservoir flow equations. This implies that the solving of several tracer transport equations (multi-tracer) will be fast compared to defining ordinary chemical components in the host simulator. Another advantage of the tracer module is that special numerical techniques may be applied when solving the tracer equations. First of all, the tracer module selects its own optimal time-step, which may be a lot smaller than the time-step of the host simulator, thus gaining numerical accuracy. Both explicit and implicit integration methods are available. Another important numerical feature is that a flux limiting (TVD) numerical scheme is applied when integrating the transport equations [14]. A van Leer limiter [15], a spatially third order limiter, and the Fromm limiter, are used. In addition to this, the tracer module performs the tracer calculation on a separate grid, which may be a lot finer than the grid applied in the host simulator. In combination with the TVD numerical scheme this gives a good numerical performance, reducing the numerical dispersion of narrow tracer slugs.

Recently, a full tensor formulation of anisotropic dispersivity for general faulted corner point geometry grids, has been implemented using multi-flux methods developed by the host simulator company [16]. The tracer velocities on the separate refined tracer grid are estimated either by interpolation of the flow rates of the host simulator, or by solving the Laplacian equation including a compressibility and well source term. On rectangular grid an analytical solution is used [17], which is expressed in terms of a fast convergent series. On corner point geometry grids a numerical solution is used.

In addition to the numerical features of the tracer module, separate grid properties related to the tracer components may be given on the tracer refined grid. Such refined physical parameters can be used in the simulation process to gain improved knowledge about a specific reservoir.

FIELD APPLICATION

1. Water tracing

The Snorre field is a giant oil reservoir (sandstone) in the Norwegian sector of the North Sea. Injection water and gas have been monitored with tracers [18]. Figure 2a shows the 4-fluoro benzoic acid (4-FBA) production curve together with the production curve of SCN^-, HTO, and $S^{14}CN^-$.

2. Non-radioactive gas tracers

Gas tracer data are shown in Figure 2b. Note that PMCH is produced without any significant increase in GOR. The corresponding gas injected in well P-25 is going

into solution and does not move as free gas. However, the three gas tracers, which are injected in well P-28 in different periods of the WAG program, are all produced

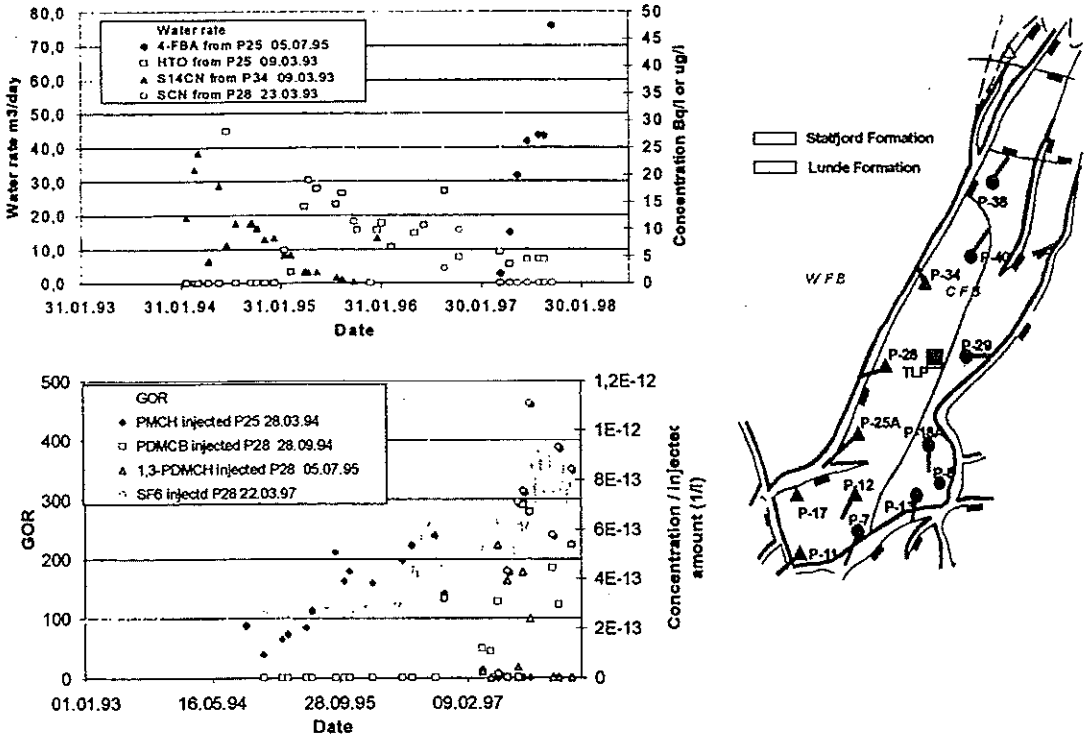

Fig. 2 a and b. Water (a) and gas (b) tracer data collected in well P-29 in Snorre.

simultaneously as the GOR in the well increases. These tracers are mainly moving in the gas phase. The interpretation made is that the gas from the different injection periods are mixed in a gas cap. When this gas cap has grown large enough break-through occurs, and all tracers are produced more or less at the same time.

This type of interpretation can be carried out without any advanced simulation. It is important, in a systematic way, to integrate the data obtained from the geological model, primary production data, 4D-seicmic data (if available) and tracer data. To enable such integrated interpretation including tracers, one needs to collect a sufficient number of data points over the tracer production curve. Too often it is seen that interpretation is difficult due to limitation in tracer data.

CONCLUSION AND OUTLOOK

A number of new non-radioactive tracer compounds for injection water and injection gas in oil reservoirs have been developed during the last 10 years and qualified in full-field experiments. The gas tracers are mainly light perfluorinated cyclic "hydro"-carbons, while the water tracers are mainly polyfluorinated aromatic acids. Detection limits in the ppt-region are obtained with GC/MS-techniques for the water tracers while the gas tracers may be analysed in 10^{-13} L/L range with a combination of CATS technology and GC/NICI-MS. An advanced state-of-the-art tracer simulator has been developed and coupled to a commercial full-field reservoir simulator (CMG software).

Tracer development is continuing, and several new molecular classes ranging from small deuterated compounds to heavy DNA-fragments are showing promising preliminary results both with respect to performance and detectability. Tracer modelling is continuing also including inverse methods.

REFERENCES

[1] Bjørnstad, T., *Selection of tracers for oil and gas reservoir evaluation*, Research Report IFE/KR/E-91/009, 1991, 43pp.

[2] Bjørnstad, T., *Recent and current oil field tracer development for interwell application,* in T. Bjørnstad & G. Pope (eds.): Proceedings from the 2nd Tracer Workshop, University of Texas at Austin, Nov. 14-15, 1994, published as Research Report IFE/KR/E-95/002, 1995, p.101-112.

[3] Bjørnstad, T., *New development in tracer technology for reservoir description,* Research Report IFE/KR/E-98/006, 1998, 24 pp.

[4] Dugstad, Ø., Bjørnstad, T. and Hundere, I.A., *Measurement of gas tracer retention under simulated reservoir conditions,* J. Petrol. Sci. Eng. 10(1993), 17-21.

[5] Ljosland, E., Dugstad, Ø., Bjørnstad, T. and Hundere, I.A., *Perfluorocarbon tracer study at the Gullfaks field in the North Sea,* J. Petrol. Sci. Eng. 10(1993), 27-38.

[6] Bjørnstad, T., Brendsdal, E., Michelsen, O.B. and Rogde, S.A., *Analysis of radiolabelled thiocyanate tracer in oil field brines,* Nucl. Instr. Meth. in Phys. Res. A299(1990), 629-633.

[7] Galdiga, C. and Greibrokk, T., *Trace analysis of fluorinated aromatic carboxylic acids in aqueous reservoir fluids by HPLC,* J. Liq. Chrom. & Rel. Technol. 21(1998), 855-868.

[8] Galdiga, C. and Greibrokk, T., *Ultra-trace determination of fluorinated aromatic carboxylic acids in aqueous reservoir fluids using solid-phase extraction in combination with gas chromatography mass spectrometry,* J. Chromatogr. A793(1998), 297-306.

[9] Galdiga, C. and Greibrokk, T., *Ultra-trace determination of fluorinated aromatic carboxylic acids in aqueous reservoir fluids by solid phase extraction in combination with negative ion chemical ionisation mass spectrometry after derivatization with pentafluorobenzyl bromide,* Fresenius J. Anal. Chem. 361(1998), 797-802.

[10] Galdiga, C. and Greibrokk, T., *Ultra-trace detection of perfluorocarbon tracers in reservoir gases by adsorption/thermal desorption in combination with NICI-GC/MS,* Fresenius J. Anal. Chem. 367(2000), 43-50.

[11] Johansen T., Winther R., *The solution of the Riemann problem for a hHyperbolic system of conservation laws modelling polymer flooding*, SIAM J. Math. Anal., 19(1988), 541-566.

[12] Johansen T., Antonsen B., Sagen J., Hidle S., *A theory of multicomponent chromatography for tracers in two phase flow*, Proceedings from The Fifth European Symposium on Improved Oil Recovery, Budapest, April 1989.

[13] Martin J.C., Wegner R.E., Numerical Solution of Multiphase, *Two-dimensional incompressible flow using stream-tube relationships*, Soc. Pet. Eng. J., Oct. (1979), 313-323.

[14] Blunt M., Rubin B., *Implicit Flux Limiting Schemes for petroleum reservoir simulation, Eur. Conf. Math. Oil Rec.,* (1990) 131-138.

[15] Rubin B., Blunt M., *Higher order implicit Flux Limiting Schemes for black oil simulation,* Technical Paper SPE- 21222, 1991.

[16] Sammon P. H., *Calculation of convective and dispersive flows for complex corner point grids,* Technical Paper SPE-62929, 2000.

[17] Sagen J., Cvetkovic B., Brendsdal E., Halvorsen G., You Y.L., Bjørnstad T., *Reservoir chemical-thermal simulation with tracers,* Technical Paper SPE-36921, 1996.

[18] Dugstad, Ø., Aurdal, T., Galdiga, C., Hundere, I. and Torgersen, H.J., *Application of tracers to monitor fluid flow in the Snorre field: A field study,* Technical Paper SPE-56427.

APPLICATION OF "BIPI" TESTS EMPLOYING NATURAL AND ARTIFICIAL TRACERS IN WATERFLOODED OIL FIELDS OF THE NEUQUINA BASIN (ARGENTINE)

C. Somaruga[1], C. Gazzera[2] and C. Wouterlood[2]

[1]Engineering Department. Comahue University. Buenos Aires 1400, (8300) Neuquén. Argentina.
[2]Petrolera Perez Companc SA. Area Entre Lomas. CC 306 - Q8300BGC. Neuquén. Argentina.

Abstract. A methodology to determine the origin and distribution of bottomwater in an oil producing well influenced by several injectors in waterflooding projects is presented. This methodology is complementary of interwell tracer tests and salinity records analysis and was denominated BIPI (brief interruptions of producing-injecting wells) test. It requires the closing of a well (injector or producer) during a short time and its later re-opening. The original flow pattern in the surroundings of the tested producing well is affected while the well is closed. So the water coming from a dominant injector can move forward invading areas of a layer that have been previously occupied by other waters. Once the well is re-opened, if there is a tracer concentration contrast between the waters, a concentration change is registered.
The concentration change was measured and also its recurrence in waters produced during interwell tracer tests and during waterfloodings that are employing different injection water from the formation one. Also it was determined the original flow distribution in the surrounding of the producing well by means of a simple balance of tracer mass.
It is presented and analyze here the results from tests that were performed in an oil field of the Neuquina Basin. They allowed to visualizing the current condition of the bottomwater flow as well as to make predictions on future performance.

INTRODUCTION

The petroleum extraction process is performed in several consecutive stages, ordinarily denominated primary, secondary and tertiary recovery. The primary happens when the oil is surgent or is extracted by pumping. The secondary require the injection of water in certain wells (injectors) forcing the displacement of the petroleum toward the rest of the wells (producers) (Figs.1 and 2). The tertiary recovery constitutes a variant of the secondary that consists on the combined action of the water and other agents as polymers and/or surfactants intensificating the laundry action and displacement of the remainder petroleum.

When one of these methods loses efficiency is indispensable to reconsider it or to attempt other techniques more sophisticated and expensive. To guarantee the effectiveness of a restate or of a new production technique it is essential to have reliable information about the actual state of the reservoir. For example during the petroleum displacement by injected water, it is frequent to find hydraulic shortcuts among wells communicated through high permeability channels. This retards the petroleum displacement in areas of lower permeability. The identification of this problem, allows its correction, through the modification of the injection pattern (for example, by the conversion of the two wells into injectors). In other occasions the shortcuts correction is achieved injecting polymers. In order to detect and evaluate these unbalances in the water injection, the reservoir engineers analyze the information coming from interference tests, interwell tracer tests and historical records (water fraction and salinity). The last two, allow to explore the distribution of water injection, with the following limitations. In this work we try to improve their predictive capabilities by means of the application of the proposed methodology.

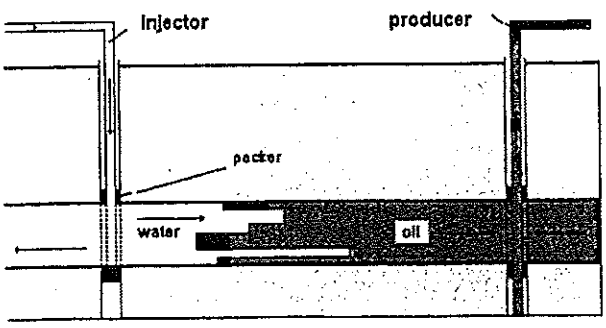

Figures 1. Displacement of petroleum by water.

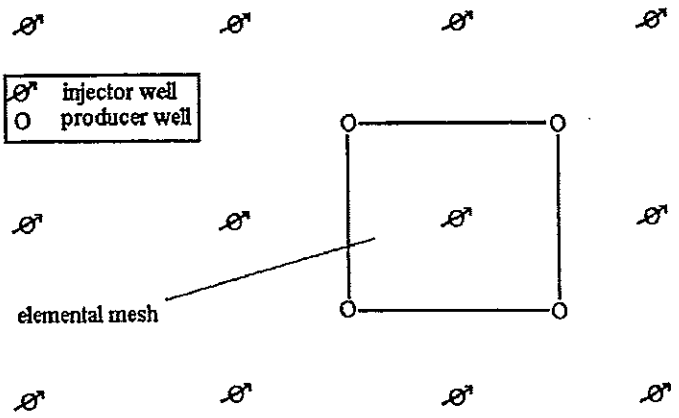

Figure 2. Usual disposition of injectors and producers

1. Interwell tracer tests

The interwell tracer tests constitute undoubtedly the more effective diagnose tool due to its easiness to study the injected water distribution and the evaluation of the reservoir parameters, yielding good sensibility at heterogeneity[1,2,3]. An interwell tracer test requires the injection of an easily identifiable and generally soluble substance in the injection water. Transported together with the water towards the producing wells, also connected hydraulically with the injector, will allow drawing tracer concentration records.

The limitation of these tests resides in that frequently does not recover the whole injected tracer mass, so it is impossible to discriminate among the internal and external contributions of the mesh. In conventional interwell tracer tests each producing well can receive water from different injector wells that eventually can be external to the analyzed mesh (Fig.3).

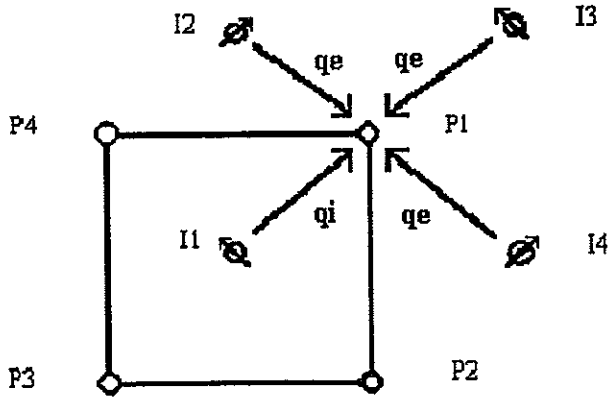

Figure 3. Water contributions to the producing well P1 from inside (I1) and outside (I2, I3, I4) injectors

If the total tracer mass injected in the well I1 (A_t) is recovered at a given time, it indicates that there is no water pushing oil inside the mesh. In this case, the distribution of injected water can be determined by direct proportionality from the amount of tracer recovered in each producer well. Neglecting irreversible diffusion effects, the mass of tracer recovered in a producer well P (A_{rp}) is

$$A_{rp} = \int_0^t q_p \, C \, dt \qquad (1)$$

where q_p is the flow of water produced by the well, C the tracer concentration and t the time of the test. The water flow rate coming from the injector of the mesh (q_{pi}) will be

$$q_{pi} = \frac{A_{rp}}{A_f} \cdot q_I \tag{2}$$

where q_I is the injector flow rate. Finally the water flow rate in the well " P " from the exterior of the mesh (q_{pe}) is

$$q_{pe} = q_p - q_{pi} \tag{3}$$

Unfortunately in most cases it is observed that only a fraction of the tracer mass injected appears in the producing wells at reasonable times[2,3,4]. The rest can be travelling very slowly in other layers toward the producing wells or other sectors. Therefore, a partial tracer recovery can underestimate the water flow contributed by the injector of the mesh (Eq.2) and overestimate the external water flow (Eq.3). Therefore the streamlines of the layers will not be correctly definite, leading to wrong simulation and interpretation. If were possible to prolong the test indefinitely it could be very probable that a fraction of the flow supposedly contributing from outside of the mesh would result in a contribution of the main injector of the mesh.

The methodology proposed in this work procure to determine the fraction of internal and external flows, without the necessity of waiting for the unlikely total tracer recovery. Also it procures to identify each external injector contribution.

2. Salinity analysis

The analysis of salinity records has been and is being a very usual practice among the reservoir engineers, allowing the evolution control of secondary recovery projects characterized by the present saline contrast among the injection water (of salinity Sal_i) and formation water (of salinity Sal_f). The arrival of injection water, generally less saline that of formation water, reduces the salinity of the water in a producing well in proportional form to the contributed flow rate (Fig.4), resulting a salinity value "Sal". A saline mass balance in the producing well leads to the equation:

$$q_{1A} = \frac{Sal_f - Sal}{Sal_f - Sal_i} \; q \tag{4}$$

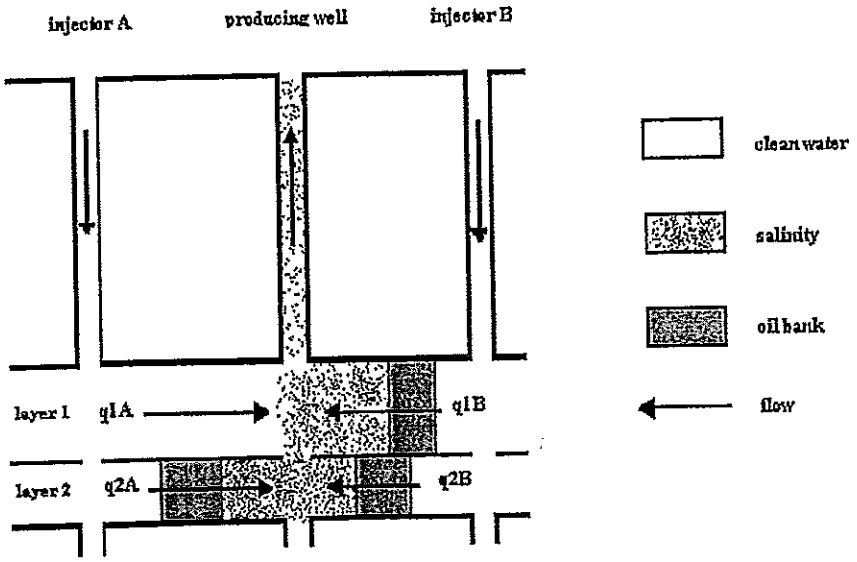

Figures 4. Clean water arrival at the producer.

The Eq.4 allows to determine the injection water contribution to the producing well but it doesn't allow to know if that contribution is originated in one or several injectors, also it does not allow to identify which is which of those injectors and evaluate its particular contributions. The proposed methodology tries to give answer to these queries.

BRIEF INTERRUPTIONS PRODUCTION-INJECTION (BIPI) TEST

1. Objectives and methodology

The aim is to evaluate the water flow coming from a particular injector in the surroundings of a producing well that has had breaktrougth of injection water and that is being influenced by two or more injectors. To achieve this we perturb the flow by shuting-in the well and evaluating the modifications observed in the tracer and/or salinity records.

2. Case A: Shut-in of producing wells

The proposed methodology requires in this first variant, the shut-in of the producing well at time t_s and its later re-opening at t_r. The original water flow pattern in the surroundings of the well will be affected while the producing well remains closed. The closed time (t_r-t_s) should be brief so that the distortion is not prolonged in excess, but the sufficiently long as to cause a representative perturbation.

2.1. Salinity records evolution

It is expected that after the shut-in of the producer, the contribution of injection water from the dominant injector go ahead in the layer invading sectors that have been occupied by formation water before (Fig.5a).

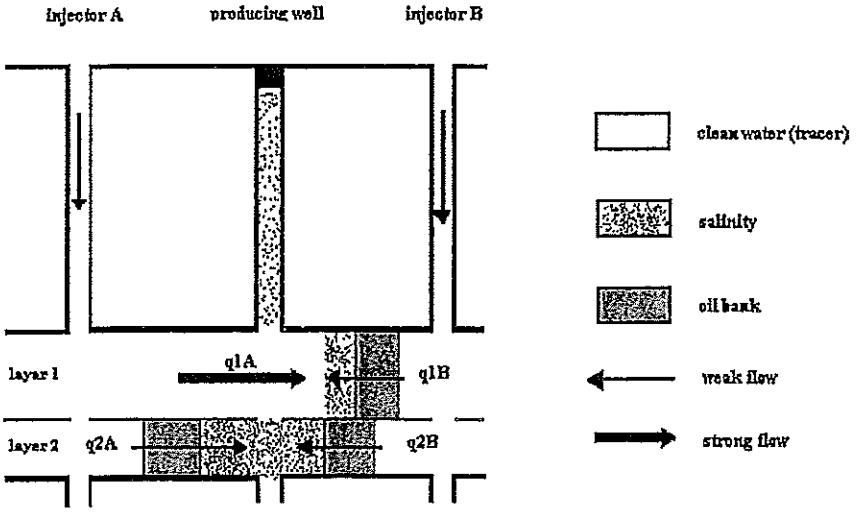

Figures 5a. Flow pattern after the shut-in of the producing well.

Once the producing well is reopening a salinity reduction should be recorded, because the sector (of the layer 1) influenced by the injector B, has been already invaded by injection water coming from the injector A (Fig.5b). The measure of the salinity change allows evaluate the injector B contribution that goes through the layer 1, in opposed direction. Denominating Sal_i to the salinity of the injection water and Sal_f to the formation water, we can write the salinity previous to the shut-in (Sal) as:

$$Sal = \frac{q_{1A} Sal_i + q_{1B} Sal_f + q_2 Sal_f}{q} \qquad (5a)$$

being:

$$q = q_{1A} + q_{1B} + q_2 \tag{5b}$$

Once the shut-in time of the producing well is completed and reopened, there will be a final salinity (Sal'):

$$Sal' = \frac{q_{1A}Sal_i + q_{1B}Sal_i + q_2 Sal_f}{q} \tag{5c}$$

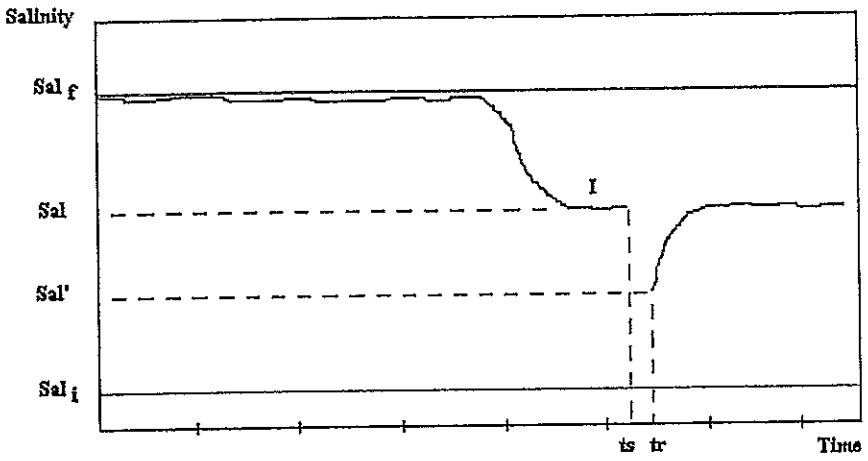

Figure 5b. Hypothetical salinity record evolution for the case of Fig.5a.

The resolution of the Eqs. 5a, 5b and 5c will allow to evaluate each contribution of the injectors A and B that go toward the producer, through the layer 1. If there are others injectors that contribute with formation water, through the layer 1, their contribution would be part of q_{1B}.

2.2. Tracer records evolution

The analysis of tracer records perturbed by the shut-in of the producing well, presents two variants, because the tracer can arrive to the well from a dominant injector or from one not dominant. If it arrives from a dominant injector, for example the injector A of Fig.5a, once carried out the shut-in and later reopening of the producing well, an increase of tracer concentration should be observed, resulting the value:

$$C' = \left(1 + \frac{q_{1B}}{q_{1A}}\right) C \tag{6}$$

where C is the concentration previous to the shut-in, and C' is the concentration later to be reopened the producing well. As in the case of salinity analysis, the Eq.6 determine if in the layer with breaktrougth of injection water there are contributions coming from other external injector.

However if the tracer arrives from a non-dominant injector, the situation is more complex. The shut-in of the producing well can facilitate the water without tracer coming from a dominant injector, generate a clean area around the producing well. After that, the original flow pattern is reestablished by opening the producer. In consequence the clean area will be recorded as a concentration valley. Later, an edge will appear, indicating the arrival of the tracer front that had been left back during the previous stage (Fig.6). The analysis of occurrence times for the mentioned events (well shut-in, re-opening and tracer edge detection) can give information about the original flow distribution, but is not clear how to make it in a quantitative way.

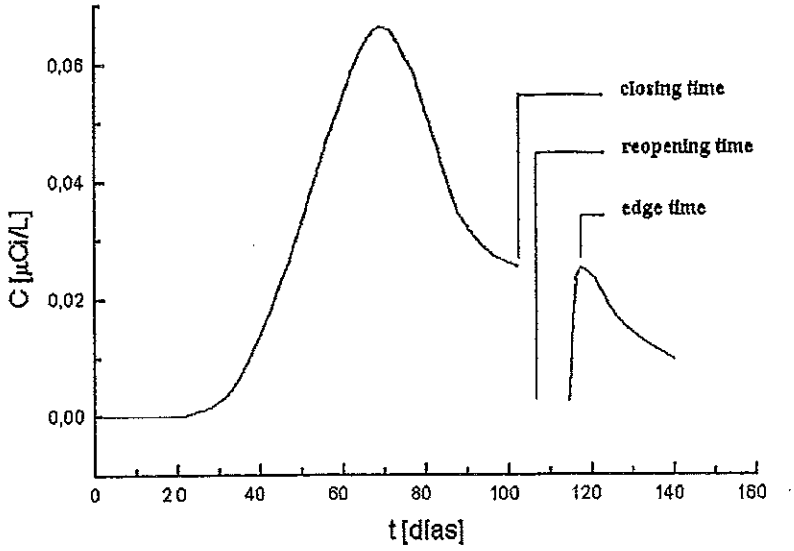

Figure 6. Hypothetical concentration curves for tracer in "setback" case.

3. Case B: Shut-in of injecting wells.

With exemption of the last case presented, the analysis of the perturbation that take place by the shut-in and re-opening of the producing wells would allow to evaluate the water contribution from two injectors through a layer, but it could not be identified who is responsible of each contribution. With the aim of covering this lack it intended to analyze the perturbations generated by the shut-in of injectors.

3.1 Salinity records evolution

Two variants can arise depending on closing an injector that forces the arrival of injection water or closing an injector that forces the arrival of formation water in the tested producer.

Case I: shut-in of an injector that forces the arrival of injection water in the producer. In relation to the case of Fig.4, the shut-in of the injector A can allow the advance of the formation water (forced by the injector B) on the sector occupied by injection water before. Meanwhile, the salinity should increase up to a saturation value (Fig.7) reaching it when the formation water finishes its invasion in the sector. Finally, the reopening of the injector A should reestablish the original salinity, after a certain time. Because of the salinity has reached the formation water value, it will not be possible to evaluate in this case the flow q_{IB}.

Case II: shut-in of injector that forces the arrival of formation water at the producer. If the closed injector is the one that contribute with formation water (injector B in Fig.4), a salinity reduction should be recorded, reaching a stable value Sal' similar to that of Eq.5c. The original salinity will be reestablished after its reopening (Fig.8). Besides, in this case, the Eqs. 5a, 5b and 5c allows the evaluation of the flow rate q_{IB}.

3.2. Tracer records evolution

The tracer records analysis is simpler than that of salinity because the injectors that are sought to be close are contributing with water without tracer. Therefore their clausure will cause salinity concentration increase proportional to the water flow that are contributing to the producer (Fig.9). For the case of Fig.4, considering tracer arrival from the injector A through the layer 1, and shut-in of injector B, the balance of tracer mass in the producing well lead again to Ec.6.

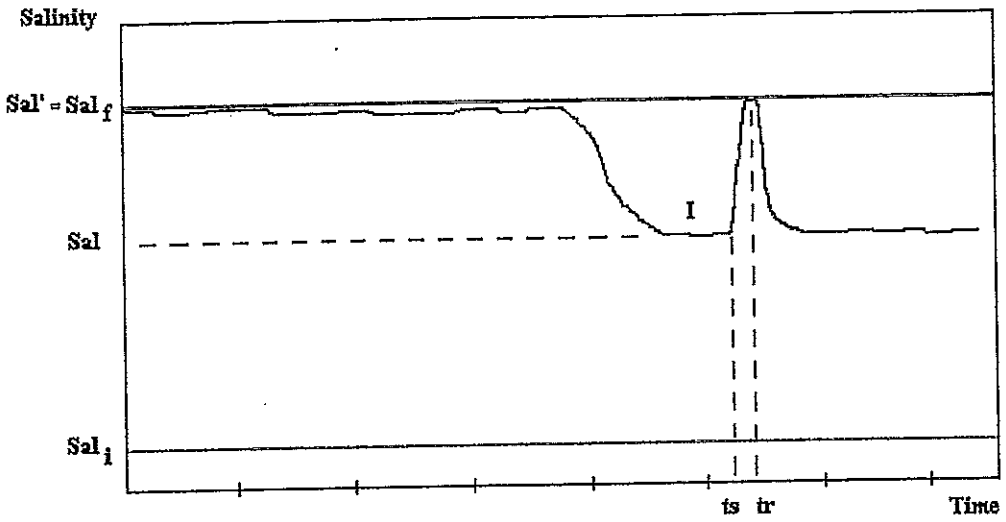

Figures 7. Hypothetical salinity record perturbation caused by the shut-in and reopening of an injector that force the arrival of injection water at the producer

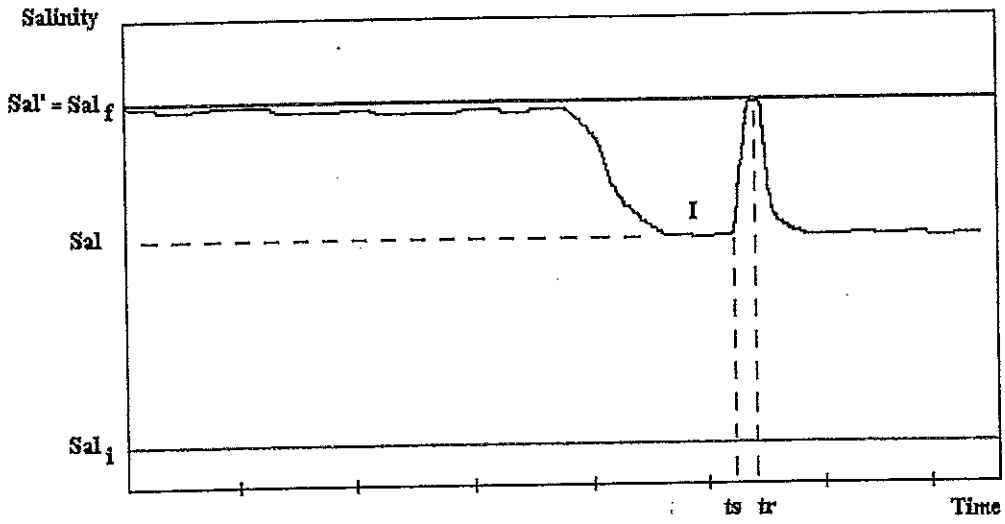

Figures 8. Hypothetical salinity record perturbation caused by the shut-in and reopening of an injector that forces the arrival of formation water at the producer.

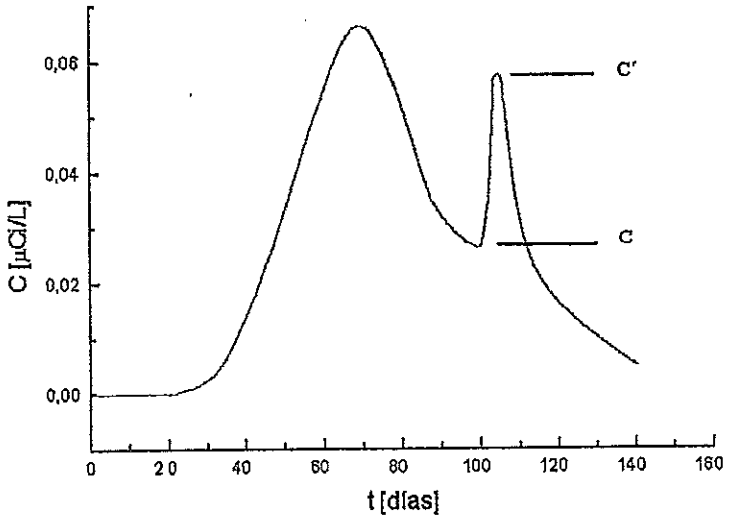

Figures 9. Hypothetical tracer concentration record perturbed by the shut-in of an injector that contributes water without tracer.

3.3. Optimal shut-in time

Special attention should be paid after the injector shut-in, to check that a stable value of salinity (Sal') or tracer concentration (C') was reached. This would guarantee that a new flow pattern was established in the surroundings of the producing well. Obviously the optimal shut-in time will depend on the distance among the wells as well as on parameters of the rock (permeability, layer thickness, porosity) and of the fluids (viscosity, compressibility).

3.4. Several injectors

If several injectors contribute with water without tracer (or water formation) to a producer, in the same layer where the injector that was previously closed is contributing, it can be invaded the surroundings of the producer with water without tracer or water formation (Fig.10). Indeed, the shut-in of the injector B could facilitate the advance of the tracer on its influence area, but it would be also possible an advance of clean water coming from the injector C. Consequently the associated concentration jump $\Delta C_B = C_B' - C_B$ will be smaller than to the corresponding to the complete tracer invasion in the area influenced by injector B. The later shut-in of the injector C would generate another pick of height $\Delta C_C = C_C' - C_C$. In this situation it can be considered that the water contribution of each injector it is proportional to the concentration jump that causes their shut-in:

$$\frac{q_{1B}}{q_{1B}+q_{1C}} \approx \frac{\Delta C_B}{\Delta C_B + \Delta C_C} \tag{7}$$

$$\frac{q_{1C}}{q_{1B}+q_{1C}} \approx \frac{\Delta C_C}{\Delta C_B + \Delta C_C} \tag{8}$$

with

$$\frac{q_{1B}+q_{1C}}{q_{1t}} = \frac{\Delta C_B + \Delta C_C}{C_m} \tag{9}$$

where

$$C_m = \frac{C_B + C_C}{2} \tag{10}$$

is the averaged initial concentration for the shut-in of injectors B and C.

Once calculated q_{IA} by integration of the tracer record concentration (Eqs.1 and 2), or starting from the salinity, by application of Eq. 4, the later resolution of the Eqs. 7, 8 and 9 would allow to evaluate the flows q_{IB} and q_{IC}.

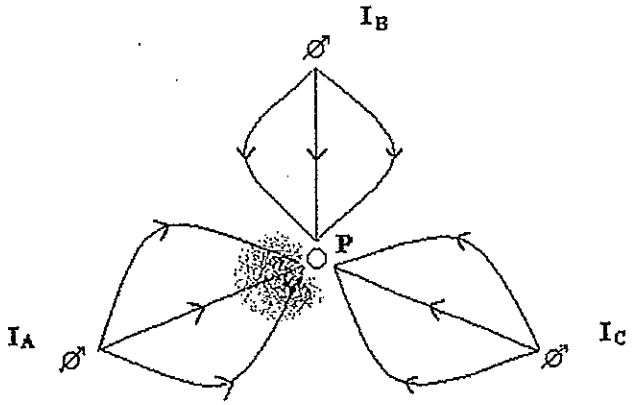

Figure 10. Several injectors contributing water through a same layer to a producer.

FIELD TEST

1. Description

A field test was carried out in a mesh of a secondary recovery project that is developing in Charco Bayo Field (Fig.11) in the Neuquina Basin (Argentine). The aim is to study the behavior of the salinity and tracer records comparatively, when the flow is perturbed by the shut-in of wells. 370 GBq (10 Ci) of Tritium has been injected (like tritiaded water) in impulsive form, in the well I88. The corresponding water injection rate is 100 m^3/día with salinity (Sal_I) 1.2 gr/L. The salinity of the formation water (Sal_F) is 96.7 gr/L.

Tritium has been detected particularly in the producer P46, distant 600 meters to injector I88. The well P46 produces 30 m^3/día of water with salinity (Sal) of 40 gr/L (aprox.). The continuous contribution of Tritium from the injector I88 toward this well, has motivated that its election, due to is possible to calculate, in precise way, the water flow rate derived toward it, by integration of the tracer concentration record (Eqs.1 and 2). Also was supposed that the fault is a seal that disconnect the injector I42.

2. Salinity records analysis

The proposed methodology supposes in a first stage the analysis of the salinity records perturbed by shut-ins and/or reductions of injection flow rates, that occurred in the previous year to the Tritium injection. The purpose is to check the influence of the injectors on the producer P46. In a second stage it will be analyzed the salinity records perturbed by the shut-in of the producing well P46 in order to evaluate the injector's contributions quantitatively. It is important to mention that the interpretations have been based on the analysis of historical records resulting from monthly samplings. Therefore certain estimations by interpolation and extrapolation were required.

2.1. Shut-in of injection wells

During the year previous to the tracer injection, some modifications took place in the injected flow rate in injectors I88 and I48. Specifically an abrupt increase of salinity was detected in the water produced by the well P46 after a reduction in the water flow rate of injector I88 (Fig.12). Salinity changes were not detected as a consequence of modifications in the injection flow rate of well I48.

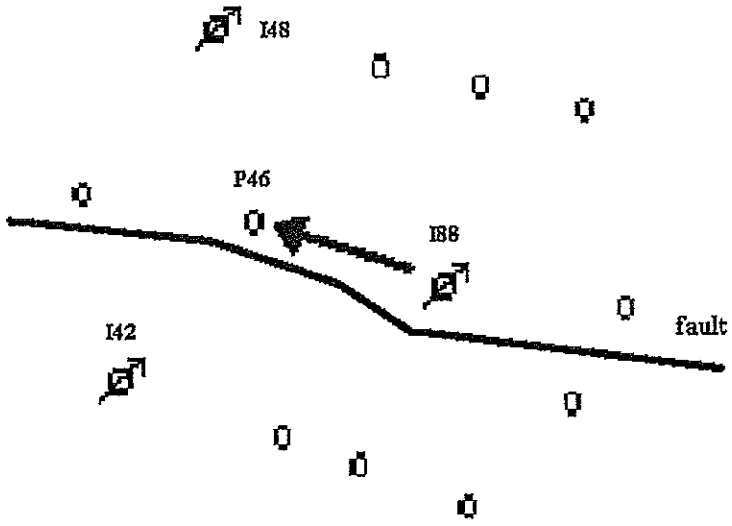

Figure 11. Sector where the field test was developed.

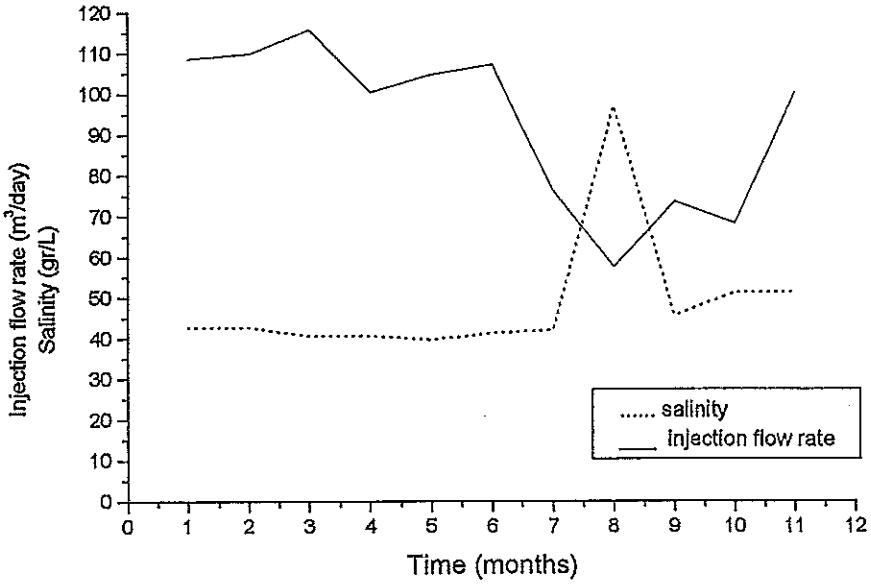

Figures 12. Perturbations of injection water flow rate in well I88 and salinity response in well P46.

These results suggest a substantial contribution of injection water from injector I88. Evidently the reduced injection of well I88 facilitated the invasion of formation water, presumably pushed by the injector I_{48} toward the producer P46.

Nevertheless is important to highlight the apparent existence of a threshold in the injection flow rate of well I88. In reference to Fig.12, only values inferior to the threshold (located between 75 and 55 m^3/day), would allow the

invasion of formation water from other injector. This fact prevents the utilization of Eqs. 7, 8 and 9 for evaluation of injection flow rates.

2.2. Shut-in of producing well

A significant salinity reduction was detected later of the shut-in and reopening of producer P46 (Fig.13). The initial salinity value of 45.8 gr/L decreased to 2.15 gr/L (extrapolated). The application of Eqs. 5a, 5b and 5c allowed the operator to determine the existence of one or several contributing layers with:

- q_{1A} = 15.97 m^3/day of injection water from an injector.
- q_{1B} = 13.73 m^3/day of formation water pushed by another injector.
- $q_{2A} = q_{2B}$ = 0 m^3/day of water from layers without breakthrough of injection water.

From the analysis performed in 2.1 is clear that

$q_{1A} = q_{88}$ = 15.97 m^3/d. and $q_{1B} = q_{48}$ = 13.73 m^3/d.

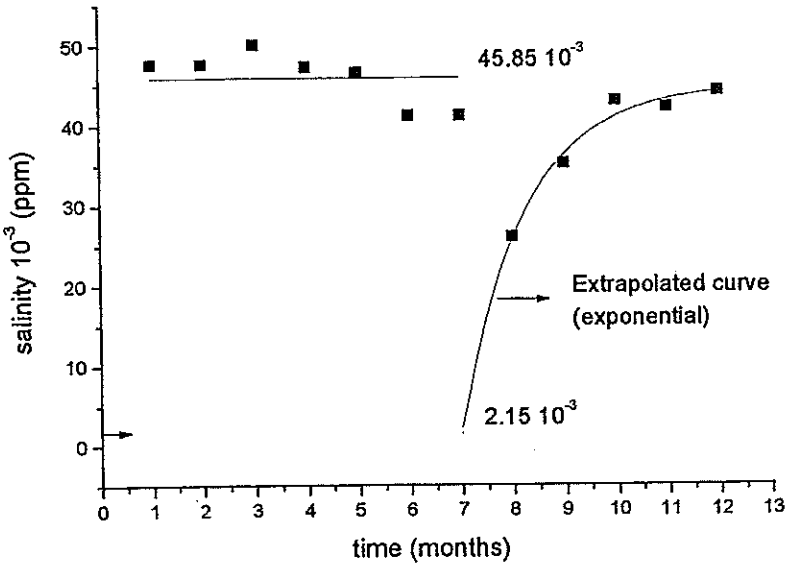

Figures 13. Perturbation of salinity record of well P46 caused by its shut-in and reopening.

3. Tracer record analysis

3.1. Shut-in of the producing well

The experimental tracer record obtained in the well P46 is shown in Fig.14. The well P46 was closed at day 601 when the tracer concentration was 0.043 uCi/L. Three days later the well was reopened, registering 0.081 uCi/L. Thus, from Eq.6:

$$\frac{C'}{C} = \frac{q_{88} + q_{48}}{q_{88}} = 1.893 \qquad (11)$$

The valued of q_{88} obtained by integration of the tracer concentration record of Fig.14 was q_{88} = 12.14 m^3/day, thus the estimation of the total flow rate is

$$q_{88} + q_{48} = 1.893 \times 12.14 \text{ m}^3/\text{day} = 22.98 \text{ m}^3/\text{day}$$

The continuous tracer production in well P46 announces that the water flow rate q_{88} obtained by tracer record integration, will increase respect to the calculated at the day 1436.

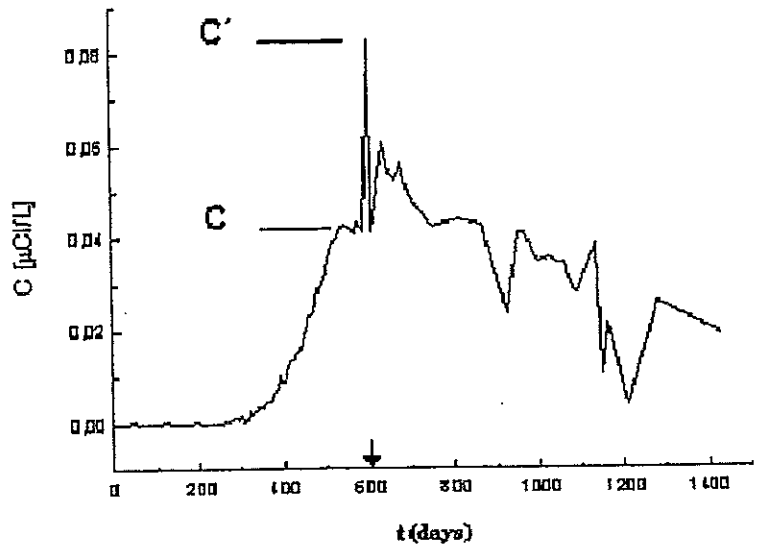

Figure 14. Tracer concentration record in producer well P46.

4. Discussion

From this results we can conclude that:

· The analysis of salinity records of the well P46 perturbed by shut-in of injectors, indicates that the dominant injector is the I88. Nevertheless the apparent lack of linearity between Δq and ΔC disables the utilization of Eqs. 7, 8 and 9 for injector flow rate evaluations.
· The analysis of salinity records of the well P46 perturbed by its own shut-in indicates that the well I88 is contributing 15.97 m^3/d. The rest (13.73 m^3/d) can come from the I48.
· By integration of Tritium concentration record has been determinated at this time, that injector I88 is contributing 12.14 m^3/d, although this value can be increased with a bigger recovery tracer.
· The analysis of tracer concentration record of the producing well P46 perturbed by it own shut-in, indicate that approximately 53% of the produced water comes from the injector I88 (15.90 m^3/d), in agree with the value obtained from salinity analysis.
· It is expected that the difference among the value obtained by integration of tracer concentration records and that obtained from the analysis of the records perturbation caused by its shut-in (equivalent at 3.76 m^3/d) will decrease while it's continue recording tracer.
· From the point of view of the oilfield productivity, the results indicate that the sector swept by the injector I88 has been totally flooded, coming formation water from injector I48 or other external to the mesh. This suggests the possibility of future arrivals of petroleum banks from this sector.

CONCLUSIONS

· The field results obtained from the analysis of salinity records agree with those obtained by the analysis of tracer record.
· This would enable the use of the proposed methodology, like a tool to deepen the knowledge about the origin and distribution of the water at a producing well, whenever is possible to differentiate via salinity or artificial tracers. It is particularly important in the case of salinity analysis because their control and record is a current

practice among the reservoirs engineers, to which can be easily added the analysis of salinity records perturbed by shut-in of wells.

· In the case of interwell tracer tests the proposed methodology is able to evaluate water flow rates from injector wells, without necessity of awaiting the unlikely total recovery of the tracer mass injected. This contributes to a correct definition of streamlines and better simulation and interpretation of the tests.

· Nevertheless the results, it is indispensable the realization of other tests with strictly controlled shut-ins of injectors and producers. Also it should be carried out dense samplings of the produced water, trying to cover the whole interval of time. It would avoid it the necessity of estimate for interpolation and extrapolation.

REFERENCES

1.Abbaszadeh-Dehghani M. and Brigham W. Tracer Testing for Reservoirs Description". Journal of Petroleum Technology, N°5, 519-527 (1987).

2. Hutchins, R. and Dovan, H. Aqueous Tracers for Oilfield Applications". SPE paper 21049 (1991).

3. Lichtenberger G. J. Field Applications of Interwell Tracers for Reservoir Characterization of Enhanced Oil Recovery Pilot Áreas". SPE paper 21652 (1991).

4. Somaruga C. and Crapiste, G. "New G. Methodology in Conventional Interwell Tracer for Evaluation of Secondary Recovery Process". SPE paper 68889 (2000).

MEASUREMENT OF INFILTRATION VELOCITY WITH FLUORESCENT TRACERS: IMPROVED METHODOLOGY

Ph. Berne[1], V. Blet[2], P. Burghoffer[1], O. Gerbaux[1], D. Getto[1]

[1] DTEN/SAT, CEA/Grenoble - 17 rue des Martyrs - 38054 Grenoble Cedex 9 - France
[2] LETI/DTS, CEA/Grenoble - 17 rue des Martyrs - 38054 Grenoble Cedex 9 - France

Abstract. This paper presents several improvements in a classical tracer-decay method for the measurement of underground water infiltration velocity. From a practical point of view, evidence is gathered of perturbation due to temperature dependence of fluorescent tracer properties; a correction is proposed. From a theoretical point of view, the mathematical behaviour of a previously derived model is explored and an improved adjustment procedure is defined.

INTRODUCTION

A standard method for measuring infiltration velocity of underground water in an aquifer is the following: a certain portion of height of a screened well is isolated and some amount of tracer is injected into that portion. Due to fresh water inflow from the aquifer, tracer concentration will decrease. The rate of that decrease bears « some relation » with the desired quantity, i.e. infiltration velocity. Fluorescent tracers are commonly used for that kind of measurement (Figure 1).

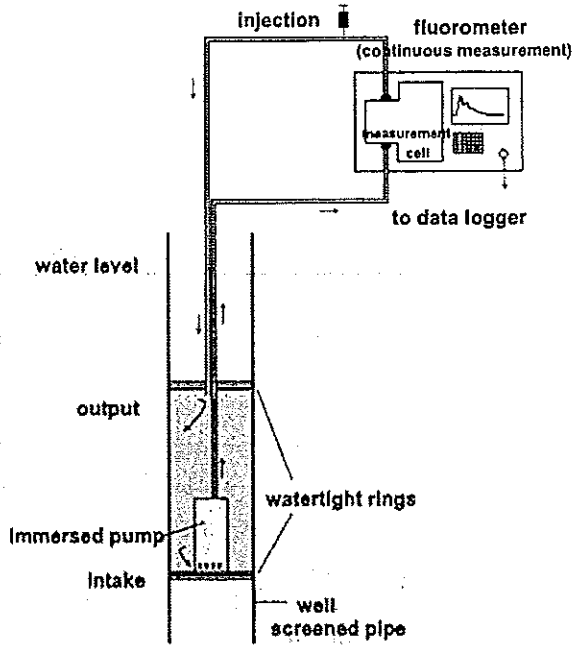

Figure 1. Classical set-up for infiltration velocity measurement

Using classical fluorometers, it is generally not possible to measure tracer concentration directly inside the well: water has to be pumped out, taken to the measuring device and injected back into the piezometer through a recirculation loop.

This procedure has two main drawbacks:

- if the flow rate from the aquifer is low and the pumping rate high, temperature of water in the loop will increase markedly because of energy dissipation due to friction in the piping. A rise in temperature is known to modify the properties of fluorescent tracers and therefore perturb measurement;
- the relationship between flow rate from the aquifer and tracer concentration history is not a simple one. Among other things, water recycling creates oscillations in tracer concentrations (see example on Figure 2) that are difficult to analyse.

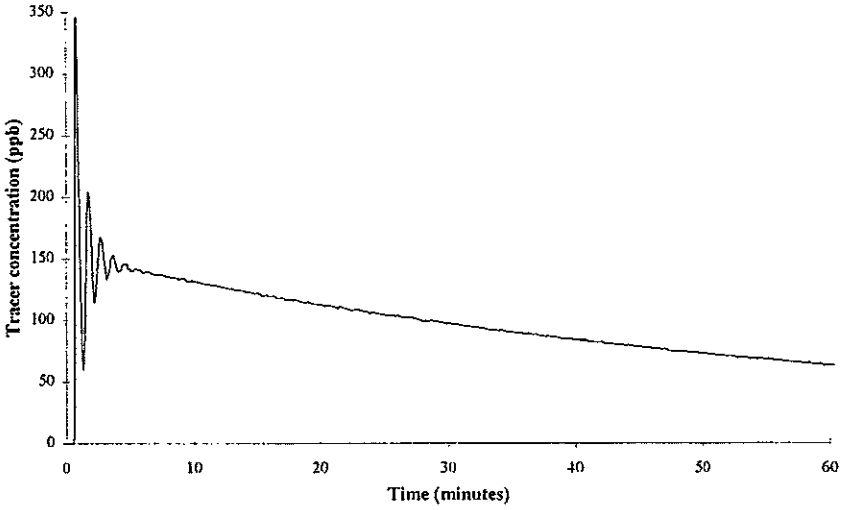

Figure 2. Typical output from water infiltration measurement

First point has been studied by means of a small scale mock-up in which aquifer discharge can be simulated. With respect to the second point, a conceptual model and the associated software were previously devised [1] for interpretation of tracer concentration curves. In the present work, mathematical behaviour of this model is further explored and a new interpretation procedure is presented.

EXPERIMENTAL

The mock-up consists in a Plexiglas tube, 51 mm in diameter and 0.5 m in length, closed by watertight caps at both ends, in which an immersed pump is placed. A series of 12 holes on the side of the tube are connected to a peristaltic pump, simulating the flow through the aquifer. Simulated aquifer flow rate Q_a can be varied in the range 0.005 to 0.16 l/min, recirculation flow rate Q_p is set at 0.9 or 1.7 l/min. The volume of the recirculation loop is estimated at 1.26 l. Tracer is rhodamine WT.

A series of tests were made with different values for Q_a and Q_p, including Q_a=0. The latter experiment showed an actual decrease of measured tracer concentration even though there was no fresh water inflow, while temperature was steadily increasing as measured in the fluorometer cell (Figure 3). The problem was obviously linked with modification of the fluorescent properties of Rhodamine as a function of temperature.

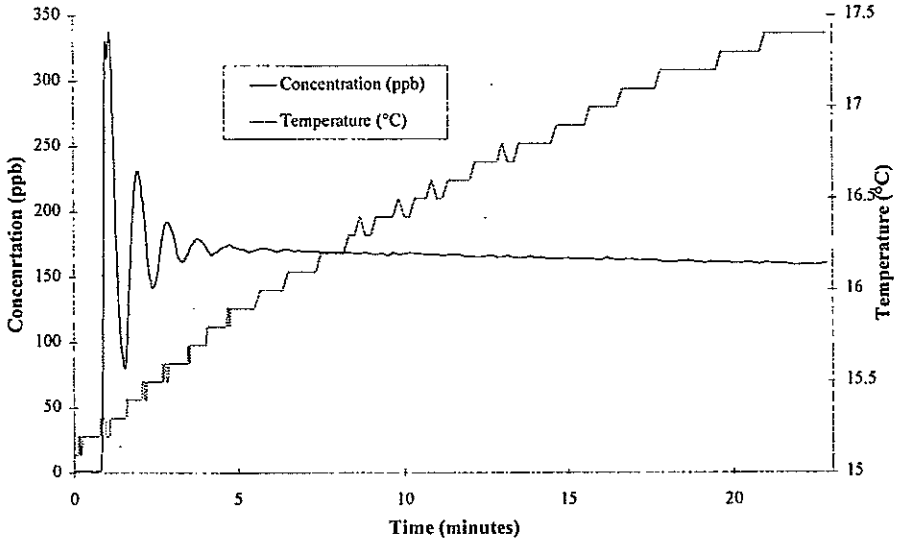

Figure 3. Concentration and temperature histories with Q_a=0

Some correction for water temperature was clearly needed. To achieve that, a small test bench was built, allowing controlled-temperature flow of water into the fluorometer, in the range 5 to 30 °C, with a concentration level of 5 to 500 ppb. Results from this experiment allowed to fit a correlation in the form:

$$F(T) = F(T_r)\exp\left(-n\left(T - T_r\right)\right) \qquad (1)$$

where $F(T)$ is the fluorescence reading at temperature T and T_r a reference temperature taken as 20 °C. Equation (1) allowed to correct the tracer restitution curves, even though in the case of Figure 3 it was not sufficient to set a constant concentration level at the end of the experiment. Small leaks in the watertight caps were found responsible for that problem and accordingly corrected.

MODELLING

1. Conceptual model

In reference [1] a model was already proposed for interpretation of tracer concentration curves. This model is based on the assumption that main flow within the measurement volume (i.e. in the section of tube between the watertight caps) can be represented as monodimensional axial dispersed plug flow, perturbed by discharge from the aquifer. For the sake of simplicity, the Mixing cells in Cascade (MC) model [2] has been chosen to represent this axial dispersed plug flow. This kind of modelling was strongly suggested by visual observation of tracer movement

inside the above-mentioned mock-up. The external loop including the fluorimeter is modelled as a series of two pure plug flows. This conceptual model is illustrated on Figure 4.

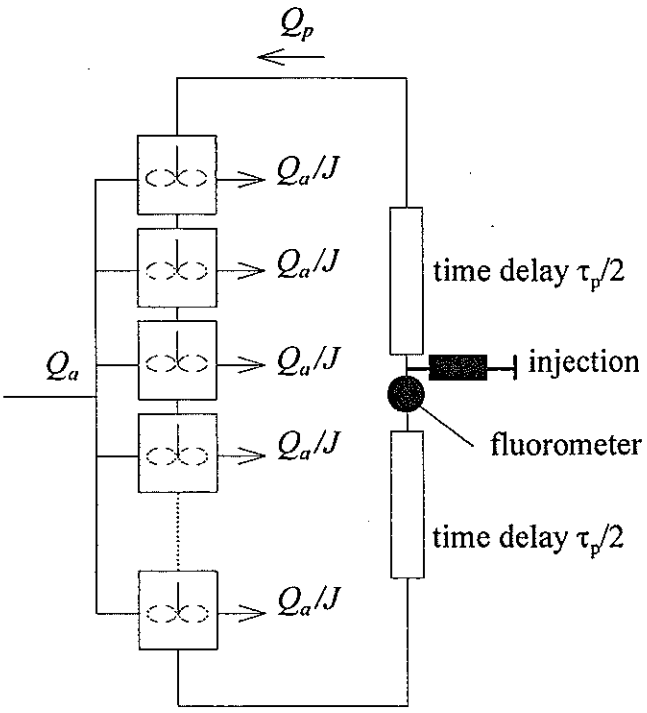

Figure 4. Conceptual model for measurement system

Model parameters are the following:

- volume of measurement cell V_f
- volume of external piping V_p
- number of mixing cells J
- flow rate from the aquifer Q_a
- pump flow rate Q_p
- injected mass of tracer m.

2. Direct solution

Tracer balance equations can be written for each measurement cell:

$$\frac{\tau_f}{J}\frac{dc_i}{dt} = c_{i-1} - \left(1+\frac{\beta}{J}\right)c_i \qquad (2)$$

where c_i is tracer concentration (e.g. tracer mass per unit volume); parameters β and τ_f are defined as:

$$\beta = \frac{Q_a}{Q_p}, \tau_f = \frac{V_f}{Q_p} \qquad (3a, b)$$

Equation (2) can readily be translated into the Laplace domain:

$$\frac{\bar{c}_i}{\bar{c}_{i-1}} = \frac{1}{1+\frac{\beta}{J}+\frac{\tau_f s}{J}} \qquad (4)$$

where $\overline{c}$ is the Laplace transform of c, and s denotes the Laplace variable. At this stage, one can consider that the tracer wave is cycling an infinite number of times within the system, and solve the set of balance equations for each cycle. An analytical solution in the time domain was proposed in [1]:

$$c_f = \frac{m}{Q_p \tau_g} \sum_{n=1}^{\infty} \frac{\alpha^{Jn}}{(Jn-1)!} \left(\frac{t - n\tau_p}{\tau_g} \right)^{Jn-1} \exp\left(-\frac{t - n\tau_p}{\tau_g} \right) H\left(t - n\tau_p\right) \qquad (5)$$

where H is the Heavyside step function and parameters α and τ_g are defined as:

$$\alpha = \frac{Q_p}{Q_p + Q_a / J}, \tau_g = \frac{V_f}{JQ_p + Q_a} \qquad (6a, b)$$

Solution (5) can be seen as a series of overlapping peaks of decreasing amplitude, as illustrated by the example in Figure 5 (m=1, Q_p=1, J=2, β=0.1 - τ_f=0.01 and τ_p=0.02 in non-dimensional time units):

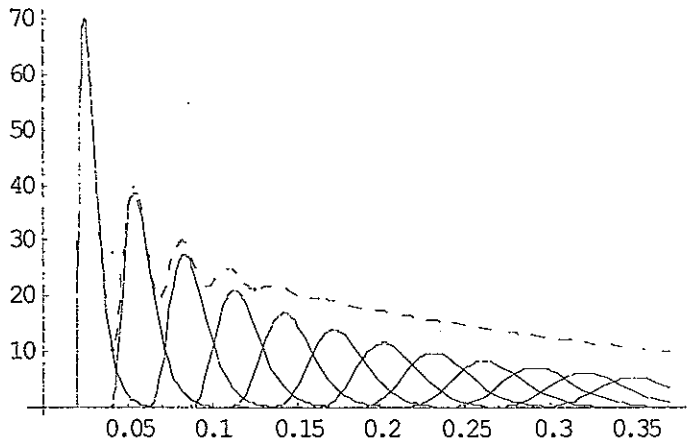

Figure 5. Representation of equation (5) (solid lines: individual peaks - dashed line: c_f)

The position of the maximum of peak number i, t_i, is easily calculated from equation (5). It is found that first peak maximum is situated at:

$$t_1 = (J-1)\tau_g + \tau_p \qquad (7)$$

and that the interval between two consecutive maxima is a constant:

$$t_i - t_{i-1} = J\tau_g + \tau_p \qquad (8)$$

t_1 is found to be always smaller than $\tau_f + \tau_p$. The interval between two peaks is also smaller than $\tau_f + \tau_p$, though (with J larger than 1 and β significantly smaller than 1, which is usually the case) approximately equal to that quantity. In summary, our model predicts that peak maxima should be separated by an equal time interval, and that first maximum should appear after that time interval at the latest. This remark bears some consequences on the analysis of real tracer history curves, since it is not unusual that the succession of measured peaks does not respect this constraint.

3. Solution in the Laplace domain

An alternative approach is to use equation (4) to write a balance equation at some point in the model (for example at the inlet of the series of mixing cells). Solving the resulting equation for $\bar{c}_f$ provides the following relation:

$$\bar{c}_f = \frac{m}{Q_p} \frac{\exp\left(-\tau_p s\right)}{\left(1+\frac{\beta}{J}+\frac{\tau_f s}{J}\right)^J - \exp\left(-\tau_p s\right)} \tag{9}$$

From this equation, zero and first order statistical moments for $\bar{c}_f$ can readily be calculated:

$$\mu_0 = \frac{m}{Q_p} \frac{1}{\left(1+\frac{\beta}{J}\right)^J - 1} \tag{10}$$

$$\mu_1 = \frac{\left(\beta + J\right)^{J-1}\left(\beta\tau_p + J\left(\tau_f + \tau_p\right)\right)}{\left(\left(\beta + J\right)^J - J^J\right)} \tag{11}$$

It is recalled that μ_0 is the area of the $c_f(t)$ curve, while μ_1 is the mean age of tracer as recorded by the fluorometer. When β is small, μ_0 reduces to $m/Q_p\beta$. In the case when m and Q_p are known, the latter relation allows direct calculation of parameter β and flow rate from the aquifer Q_a.

Another easily accessible information from equation (9) is the long term behaviour of function $c_f(t)$. Classical Laplace transform theory indicates that $c_f(t)$ can be expressed as a sum of exponentials:

$$c_f(t) = \sum a_i \exp\left(s_i t\right) \tag{12}$$

where s_i's are the poles of $\bar{c}_f$, i.e. the s values for which $\bar{c}_f$ is singular, or the solutions of:

$$\left(1+\frac{\beta}{J}+\frac{\tau_f s}{J}\right)^J = \exp\left(-\tau_p s\right) \tag{13}$$

It is possible to show that equation (13) has a single real root s_0 in the interval $\left[-\frac{J+\beta}{\tau_f}, 0\right]$ and that this root has the smallest possible modulus. The $\exp\left(s_0 t\right)$ term will therefore become dominant in $c_f(t)$ when time tends to infinity. Straightforward (though tedious) manipulation of the Laplace transform shows that, in the long run, $c_f(t)$ can indeed be approximated with the following function:

$$c_f(t) \approx \frac{m}{Q_p} \frac{\exp\left(-s_0 t\right)}{\tau_p + \tau_f \exp\left(\frac{s_0 \tau_p}{J}\right)} \tag{14}$$

In situ tracer experiments very generally exhibit this decaying exponential behaviour at large values of time, which tends to confirm the validity of our model.

Lastly, equation (9) can easily be reverted to the time domain by the use of some adequate numerical method (for example Fast Fourier Transform - FFT - as suggested in [2]). This method is found to be very effective and much less prone to error than direct computation of equation (5).

INTERPRETATION PROCEDURE

A procedure for interpretation of tracer curves was presented in [1]. It consisted in optimisation of certain parameters in equation (5) (β, τ_f, τ_p, ratio m/Q_p and to some extent J). Using the results established in the previous section, we propose two alternative methods for interpretation of the tracer curves.

1. Using the exponential part of the concentration history

As mentioned above, most tracer concentration curves actually have an exponential tail. Calculating time constant θ of this tail provides an estimate of $s_0 = -1/\theta$, the root of equation (13) with the smallest possible modulus. Provided J, τ_f and τ_p are known, equation (13) can then be solved for β. Such is not the case in general (J for example is usually not known). However, provided θ is large compared with $\tau_f + \tau_p$, the following equivalence can be proved:

$$\beta \approx \frac{\tau_f + \tau_p}{\theta} \tag{15}$$

This equation is a very simple means for estimating β. If for some reason $\tau_f + \tau_p$ is not known, it can be approximated as the time period between two successive tracer peaks (as shown in the previous chapter). Flow rate Q_a can then be calculated as βQ_p, which requires that Q_p be known - a simple enough measurement.

This method has been applied to our mock-up experiments. Results are shown by the following graph comparing measured and actual values of flow rate Q_a:

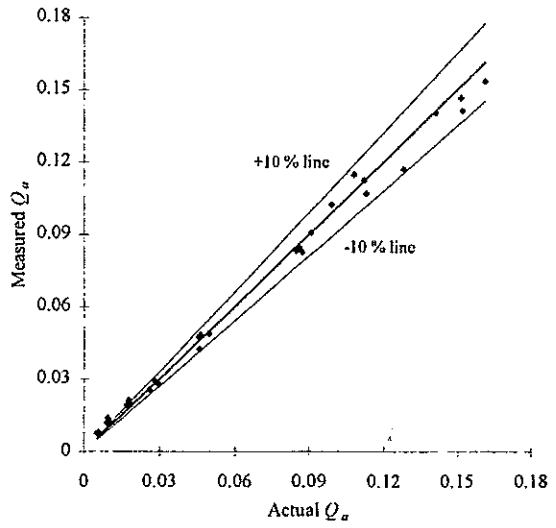

Figure 6. Comparison of actual and measured values for Q_a

Agreement is found to be better than 10 % except for the lowest flow rates. This method proves therefore proves quite effective. Its only limitation is that θ should be large compared with $\tau_f + \tau_p$.

2. Global parameter adjustment

Lastly, an optimisation routine (based on the Levenberg-Marquardt algorithm, [3]) has been built using numerical inversion of equation (9) by FFT. This routine allows optimisation of parameters τ_f, τ_p, J, β and m/Q_p against experimental data. An extra degree of freedom, delay time τ_r, has been added in the case the succession of measured peaks does not respect equations (7) and (8) (such a case does happen in real experiments and may be related to non-monodimensional flow of tracer in the intial stages). This correction simply amounts to multiplying the Laplace transform in equation (9) by $\exp(-\tau_r s)$. It should be verified a posteriori that τ_r is small compared with the other time constants.

Figure 7 illustrates the application of this routine to one of our mock-up experiments. Excellent fit is obtained. The optimised value of parameter β is 0.12, which results in aquifer flowrate Q_a=0.106 l/min, a fairly good estimation since the actual value of Q_a was set at 0.113 l/min.

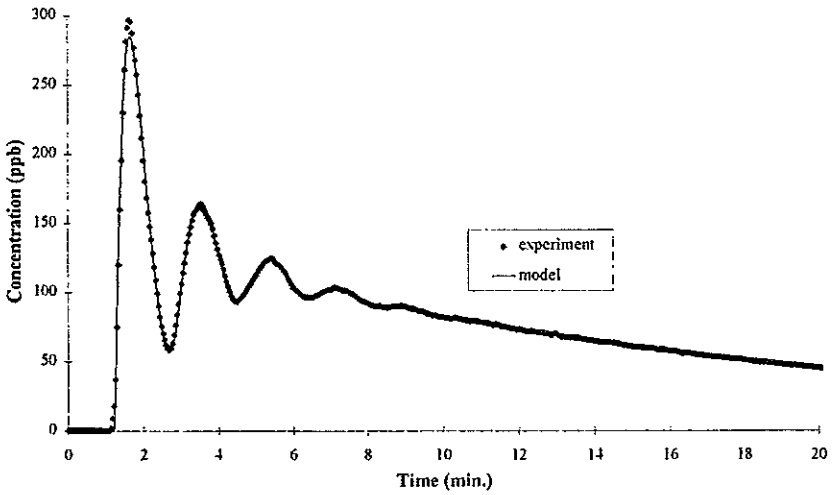

Figure 7. Model adjustment against experimental data

REFERENCES

[1] Courtois, N., Burghoffer, P., Gerbaux-François, O., Getto, D., Measurement of groundwater flow by the dilution method using dye tracing under natural hydraulic gradient conditions, in *Tracers and Modelling in Hydrogeology*, IAHS Publ. N° 262 (2000), 219-224.

[2] Villermaux, J., *Génie de la réaction chimique*, Ed. Tech & Doc Lavoisier, Paris (1982).

[3] Press, W.H., Teukolsky, S.A., Vetterling, W.T., Flannery, B.P., *Numerical recipes in Fortran*, Cambridge University Press, Cambridge (1992).

ENHANCED OIL PRODUCTION BY MASSIVE GAS INJECTION STUDIED WITH RADIOTRACER TECHNIQUE

A. Haugan[1],B. Cvetkovic[1], T. Bjørnstad[1,2], J. Müller[1] and Ø. Dugstad[1]

[1]Institute for Energy Technology, P.O. Box 40, N-2027 Kjeller, Norway
[2]Institute of Chemistry, University of Oslo, P.O.Box 1033, N-0315 Oslo, Norway

Abstract. Water injection is recognised as one of the most effective methods for secondary oil production. With time, the production rate decreases and finally reaches a level where further water injection cannot be economically justified. One has reached the practical state of residual oil saturation to water injection.

At this stage, additional oil may be recovered by gas injection. Various mechanisms are involved. The most important are gravitational drainage, oil evaporation and oil swelling. The injection gas may be lean natural gas (mainly methane and ethane), nitrogen or carbon dioxide. Various gases have different effects.

The objective of the work presented in this article was to establish an experimental set-up that can be used to study enhanced oil production by massive gas injection with radiotracer technique, and to provide data that will be used for simulation.

The present article describes a basic experiment where oil from non-fractured rock is produced into a fracture due to methane gas injection through the fracture. The experiment was made possible by means of radiotracer technology.

INTRODUCTION

Water injection is recognised as one of the most effective methods for secondary oil production. With time, the production rate decreases and finally reaches a level where further water injection cannot be economically justified. One has reached the practical state of residual oil saturation to water injection.

At this stage, additional oil may be recovered by gas injection. Various mechanisms are involved. The most important are gravitational drainage, oil evaporation and oil swelling. The injection gas may be lean natural gas (mainly methane and ethane), nitrogen or carbon dioxide. Various gases have different effects.

The objective of the work presented in this article was to establish an experimental set-up that can be used to study enhanced oil production by massive gas injection with radiotracer technique, and to provide data that will be used for simulation.

The present article describes a basic experiment where oil from non-fractured rock is produced into a fracture due to gas injection through the fracture. The experiment was made possible by means of radiotracer technology.

A core of chalk, coated on all sides except at one end, was used to represent the non-fractured rock. The uncoated end represented the fracture. The core was saturated with oil (pentane) that again was saturated with methane at 38.5 °C and 100 bars. The pentane was mixed with a gamma-emitting tracer (^{131}I-benzene). The methane inside the core was labelled with tritium, which is a soft beta-emitter. The uncoated end of the core was then continuously swept by dry non-labelled methane gas. The methane produced from the core was continuously measured by a beta-

counter, while the produced pentane was sampled and measured by weight. The distribution of the gamma-emitting tracer along the core was measured by a gamma-scanner. The experiment lasted for 19 days.

Similar experiments have been performed before [1,2]. However, these experiments were performed without tracers. With the use of tracers one can obtain additional information about the mechanisms involved in oil production by gas injection into a fractured reservoir. The gas tracer made it possible to continuously measure the exchange of methane between that original in the core and the methane that was injected into the fracture. The ^{131}I-benzene tracer made it possible to see whether the oil production was due to evaporation to the gas phase or due to convective movement of the fluid into the fracture.

EXPERIMENTAL SET-UP

A sketch of the experimental set-up is shown in Figure 1. It shows a coated chalk core from the Paris Basin, with a simulated fracture at one end, placed inside a titanium flow-cell. The dimensions of the square chalk core is 3.2 × 3.2 × 36 cm, and its porosity is 30 %. The dimensions of the fracture is 2.8 × 2.8 × 0.2 cm. The flow-cell is filled with water surrounding the core at a pressure, which always is 5-10 bars higher than the pressure inside the core to avoid leakage from the core. Outside the confining water, there is a layer where water from a heat-bath circulates to keep the temperature inside the core at a constant level (not shown on the sketch). A piston cylinder and an HPLC pump were used to fill the core with the labelled pentane-methane mixture before the experiment. Another piston cylinder and HPLC pump are used to pump unlabeled methane through the fracture during the experiment. A backpressure regulator (BPR) is used to regulate the pressure inside the core. A separator is used to separate the produced liquid and gas by cooling. The produced gas is then sent through a flow beta-counter to measure the amount of tritiated methane produced from the core. A gamma-scanner measures the profile of the gamma-emitting tracer inside the core.

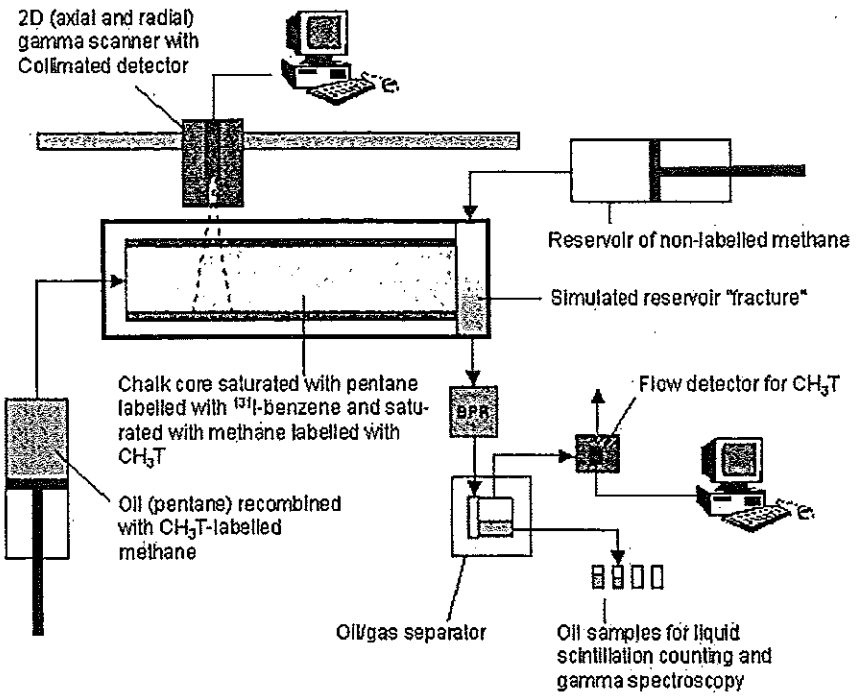

Figure 1. Sketch of the experimental set-up.

MEASUREMENTS

^{131}I-benzene was used as the oil tracer. It is a gamma-emitting tracer (E_γ = 364 keV), and its concentration profile along the core can be measured by the gamma-scanner. Due to much lower vapour pressure than pentane (see Table 1), this tracer is supposed to follow the convective movement of the pentane in the core. It can be used to measure the concentration profile of the pentane at the beginning of the experiment and to investigate if the oil recovery is due to evaporation or not.

A beta-emitting tracer is needed to monitor the production of methane gas from the core. Tritiated methane ($E_{\beta max}$ = 18 keV) was used for this purpose.

At the beginning of the experiment, the chalk core was filled with a binary liquid mixture of pentane (mixed with ^{131}I-benzene) and tritiated methane gas at 38.5 °C and 100 bars. The pentane was saturated with methane. Thus, the liquid density was 519 kg/m^3 and the mole fraction of pentane in the liquid phase was 56.9 %, according to the CMG software Winprop [3]. The amount of pentane and methane inside the core was then 0.677 moles and 0.513 moles, respectively.

The unmarked methane gas was injected into the fracture at a flow-rate of 4.0 ml/h. The start of the experiment was defined at the point of time when the beta-counter started to detect tritiated methane gas. The experiment was stopped after almost 19 days.

It was mentioned in the introduction that the main production mechanisms in gas injection are gravitational drainage, oil evaporation (into the gas phase) and oil swelling into conductive fractures. Due to the experimental set-up, gravitational drainage will not contribute to the oil production. Further, since the pentane is saturated with methane, oil swelling will not contribute to the oil production either. Therefore, it was assumed that oil evaporation to the gas phase would be the main mechanism for oil production in this experiment.

Table 1. Vapour pressure for I-benzene and pentane at different temperatures. The vapour pressures are given in kPa, and are taken from CRC Handbook of Chemistry and Physics, 77th edition, 1996-1997.

	−76.6 °C	−53 °C	−18 °C	25 °C	37 °C	50 °C
I-benzene				0.133		0.632
Pentane	0.13	1.0	10.0	68.3	104.07	159

1. Distribution of ^{131}I along the core

Due to low activity of ^{131}I inside the core, a large collimator opening was used to obtain a reasonable count-rate by the gamma-scanner. It had a circular opening with diameter of 6 cm and a depth of 4 cm. The resolution of the gamma-scans is therefore not optimal.

One gamma-scan was performed each day during the experiment. Four of them are shown in Figure 2, where background and decay corrections have been performed. Position 0 is the location of the fracture, and the core is located between 0 and 36 cm. The gamma-scans indicate activity even outside the core. This is not real, but a consequence of the resolution.

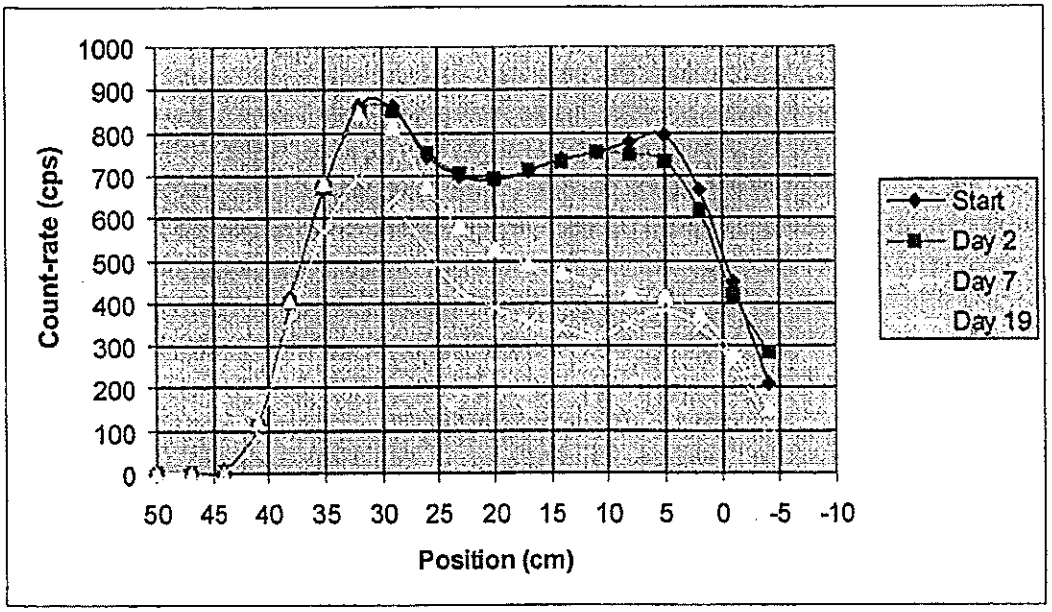

Figure 2. Gamma-scans showing the distribution of ^{131}I along the core. The location of the fracture end is at position 0, and the location of the closed end is at position 36 cm.

The start profile was taken just before the methane flooding through the fracture started. The distribution of ^{131}I was not homogeneous, but contained a peak at both ends of the core. The reason for this is either that the core was not completely saturated, or that the ^{131}I-benzene was not completely mixed with the pentane.

The profile at day 2 was similar with the only difference that the peak at the fracture end was reduced. At least a part of this reduction is due to emptying the fracture. At day 7 the activity has been reduced considerably at the fracture side of the core, but not at the closed end of the core where the activity is unchanged. At day 19 the activity has been reduced even at the closed end of the core.

2. Pressure difference

The pressure difference between the fraction and the closed end was measured during the experiment. The result is shown in Figure 3. The highest pressure was recorded in the fracture. This measurement indicates the capillary pressure between

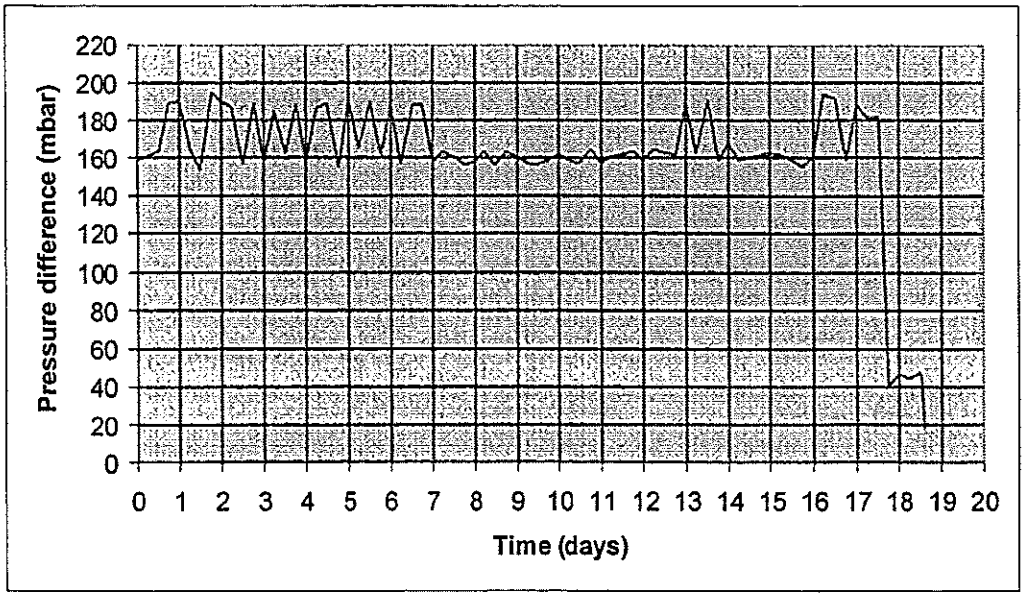

Figure 3. Pressure difference across the core. The pressure was higher in the fracture than at the closed end.

the gas and oil as long as the closed end is completely saturated with oil. This pressure fluctuated between 160 and 190 mbars the first 17 days, then it suddenly dropped to zero. This is the time when the injection gas reaches the closed end of the core.

3. Methane, pentane and ^{131}I-benzene recovery

Prior to the experiment, tritiated methane gas with the same radioactive concentration as the gas initially inside the chalk core was directed through the beta-counter. This count-rate was used to calibrate the beta-counter.

The beta count-rate was continuously measured during the whole experiment, and used to calculate the methane recovery. The quotient obtained when dividing the count-rate by the calibration count-rate, i.e. when only tritiated methane was passing

the beta-counter, equals the fraction of tritiated methane of the total amount of methane passing the beta-counter. Knowing the flow-rate, the amount of produced tritiated methane can be calculated by integrating the count-rate curve. Further, knowing the original amount of tritiated methane inside the core, the recovered methane can be calculated. The result is shown in Figure 4.

The produced pentane was weighted after it was separated from the methane gas by cooling. Knowing the total amount of pentane inside the core at the start of the experiment, the recovered pentane was calculated. The result is shown in Figure 4.

The produced ^{131}I-benzene was estimated by integrating the distribution curves given in Figure 2, and the result is given in Figure 4.

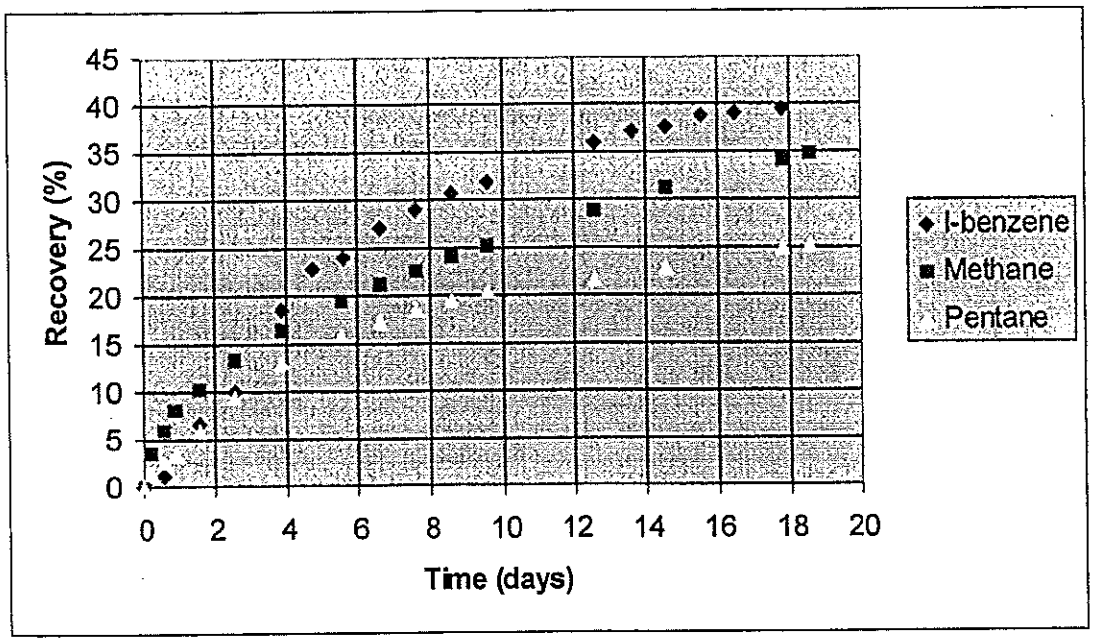

Figure 4. Recovered methane, pentane and ^{131}I-benzene from the chalk core.

DISCUSSION

The recovery curves in Figure 4 show that the recovery of ^{131}I-benzene is more effective than the recoveries of pentane and methane. This indicates that the main production mechanism is convective movement of the fluid into the fracture. The pentane evaporates, and the methane diffuses into the gas phase, and is therefore produced at a slower rate than the ^{131}I-benzene. The recovery of methane is faster than the recovery of pentane due to slower transfer from the liquid to the gas phase and/or due to larger diffusion coefficient in the gas phase.

These results are very surprising, and should be confirmed by other experiments. The cooler in the gas/oil separator did not keep the temperature as low as anticipated by the experimental design. Most of the time the temperature was between −70°C and −50°C, but temperatures as high as −20°C was measured for short periods of time (see Figure 5). The vapour pressures for pentane at these temperatures are

given in Table 1. Some of the pentane did therefore follow the methane flow through the beta-counter. Thus, the obtained results underestimate the pentane recovery.

If it is assumed that the methane gas leaving the separator is saturated with pentane, the amount of pentane leaving the separator can be calculated from the ideal gas law $n = PVR^{-1}T^{-1}$, where n is the number of moles, P is the vapour pressure, V is the gas volume passing through the separator, R is the gas constant, and T is the absolute temperature. The results for three relevant temperatures are given in Table 2. Thus, with this assumption and a stable temperature of −76.6 °C, the lost pentane would be 2.1 % of the total amount inside the core at the beginning of the experiment. If the temperature had been stable at −53 °C, the lost pentane would be 15 % of the total amount. If the temperature had been stable at −18 °C, all the produced pentane would have been lost.

However, the large ^{131}I-benzene recovery shows that the oil production is not only due to oil evaporation into the gas phase.

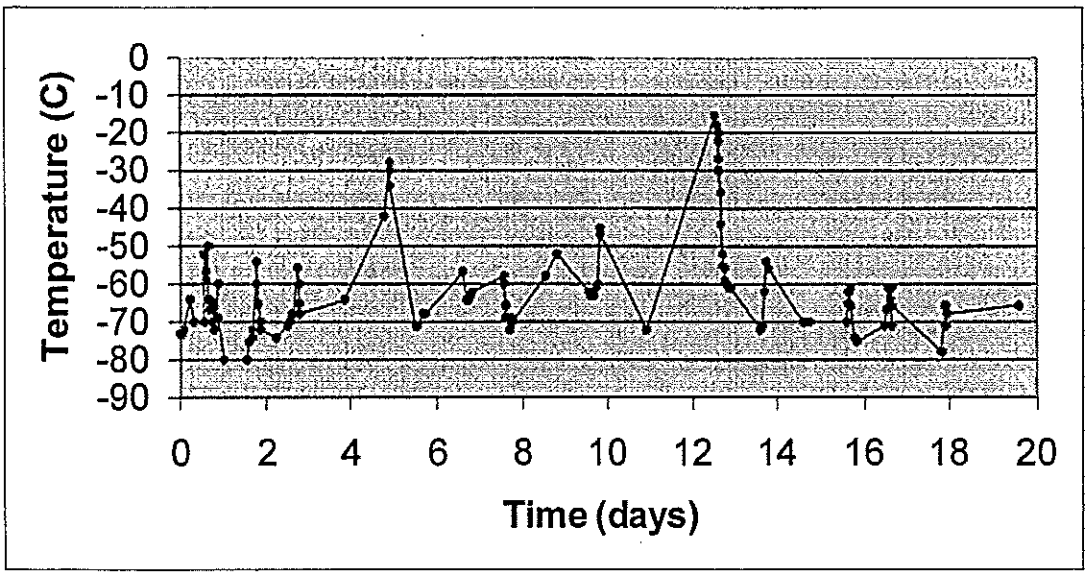

Figure 5. The temperature inside the separator during the experiment.

Table 2. Amount of pentane, given in mole, leaving the separator if it is assumed that the methane gas leaving the separator is saturated with pentane.

−76.6 °C	−53 °C	−18 °C
0.0145	0.0997	0.860

CONCLUSIONS

The performance of a new analytical method for the ultra trace determination of perfluorocarbon tracers has been described. The new method is superior in terms of sensitivity and tracer identification. In addition, the use of adsorption tubes enables automated analyses and non-restricted gas sample shipment with express services or ordinary mail. Hence, analytical results, e.g. from Overseas Samples, can be reported in very short terms.

REFERENCES

[1] Lovelock, J.E., Ferber, G.J., Atmos. Environ. 16 (1982), 1467
[2] Lagomarsino, R.J., Raymond, J., Latner, N. J., Chromatogr. 595 (1992), 359
[3] Draxle, R.R., Dietz, R., Lagomarsino, R.J., Start, G., Atmos. Environ. 25A (1991), 2815
[4] Dietz, R., Spandau, D.J., Senum, G.I., D`Ottavio, T.W., Goodrich, R.W., 50th Anniversary 1938/1988: Division of Analytical Chemistry newsletter (1988)
[5] Upstillgoddard, R.C., Watson, A.J., Liddicoat, M., Anal. Chim. Acta 249 (1991), 555
[6] Menzies, K.T., Pong, C.M., Randel, M.A., 80th Annual Meet. of the Air Pollution Control Assoc. NY (1997)
[7].Kleven, R., Høvring, O., Opdahl, S.T, Bjørnstad, T., Dugstad, Ø., Hundere, I.A., Technical Paper SPE-35651, Calgary (1996)
[8] Dugstad, Ø., Aurdal, T., Galdiga, C., Hundere, I., Torgersen, H.J.T., Technical Paper SPE-56427 Houston (1999)
[9] Ljosland, E., Dugstad, Ø., Bjørnstad, T., Hundere, I.A., J. Pet. Sci. Eng. 10 (1993), 27
[10] O`Mahony, T.K.P., Cox, A.P., Roberts, D.J., J. Chromatogr. 637 (1993), 1
[11] Galdiga, C.U., Greibrokk,T., Chromatographia 46 (1997), 440
[12] Lagomarshino, R.J., J. Chromatogr. Sc. 34 (1996), 405
[13] Senum, G.I., Cote, E.A., Dòttavio, T.W., Dietz, R.N., Brookhaven National Laboratory Report BNL-42769 (1989)
[14] Dougherty, R.C., Dalton, J., Biros, F.J., Org. Mass Spectrom. 6 (1972), 1171
[15] Oehme, M., Fresenius J. Anal. Chem. 350 (1994), 544
[16] Begley, P., Foulger, B., Simmonds, P., J. Chromatogr. 445 (1988), 119
[17] de Bortoli, M., Pecchio, E., J.High Resolut. Chromatogr. & Chromatogr. Commun. 8 (1985), 422
[18] Ghaoui, L., Dessai, E., Wentworth, W.E., Weisner, S., Zlatkis, A., Chen, E.C.M., Chromatographia 20 (1985), 75
[19] Dietz, R.N., Goodrich, R.W., Cote, E.A., Wieser, R.W., Brookhaven National Laboratory Report BNL-33846 (1986)
[20] Galdiga, C.U., Greibrokk, T., Fresenius J. Anal. Chem. 367 (2000), 43

B B2 - CIVIL ENGINEERING, MINERAL ENGINEERING AND METALLURGY

SUSPENDED SEDIMENT BEHAVIOR IN IRRIGATION CANALS OF PAKISTAN. STUDY WITH RADIOACTIVABLE AND FLUORESCENT TRACERS

A. Vabre[1] and P. Brisset[1]

[1] CEA – DAMRI, Saclay, France

Abstract. This paper presents a measurement campaign using tracer techniques. A tracer is a material easy to identify which, once introduced in a population of physical phases to trace, has the same chemical or hydrodynamical behavior than one of them.
On the selected irrigation system (Jamrao), a clear tendency to the sediment deposition has been identified during the past functioning. Based on these observations, a measurement campaign using tracers has been elaborated. This technique has been chosen because of its sensitivity, indeed the sediment deposition phenomena are very slow ones. In most of the cases the observation durations have to be in the magnitude of years or even decades to obtain significant evolutions. Whereas using tracer techniques, even very small depositions of materials can be qualified and especially quantified.
In order to explain the observed deposition during the measurement campaign, a topographic and hydraulic component is added. Indeed, the sediment transport phenomena are mainly explained by the liquid flow behavior.

INTRODUCTION

This measurement campaign is included in a research program that deals with dynamic sedimentology on irrigation canal systems, with an exclusive application on Pakistani ones. This is a common project between IMFT[1], CEA[2], IIMI-Pakistan[3], Cemagref[4] and ISRIP[5]. It has started in 1995 and in 1997 two PhD programs have been initiated. The project aims at studying the sedimentary phenomena in irrigation canal systems using two different and complementary approaches. A first one, called mechanistic, lies on a deterministic explanation of the sedimentary phenomena on linear reaches of the canals of the system. A second one, called global, lies on global description and explanation of the sedimentary phenomena on the whole irrigation system. The two approaches work with different scales of time and space for the sedimentary phenomena. The typical values for the time and space steps for the mechanistic approach are 7 days and 100 m while they are 10 years and 10 km for the global approach.

The present measurement campaign is linked to the global approach, the detailed objectives and methodology are presented in a technical report [18].

[1] Institut de Mécanique des Fluides de Toulouse, France
[2] CEA :Commissariat à l'Energie Atomique, France
[3] International Water Management Institute, Pakistan
[4] La recherche pour l'ingénierie de l'agriculture et de l'environnement, France
[5] International Sedimentation Research Institute of Pakistan, Pakistan

Two methods are successively employed in order to represent and explain globally the sedimentary phenomena in the irrigation canal system:

- ✓ Topographic surveys, during long periods of time in the magnitude of decades to observe significant variations of the topographic parameters.
- ✓ Tracer techniques, during short periods of time in the magnitude of months are sufficient to observe relevant informations.

The first method is implemented on the existing data set of the case study during the past period of functioning between 1932 and 1982, so during a period of 50 years. The second is implemented on the single tracer measurement campaign of 1998 that has lasted 4 months, presented in this paper.

The hydraulic and sedimentologic parameters, for both the measurement techniques, have to be recorded in the same time as well, in order to explain the observed variations of either the topographic parameters or the tracer ones. The used values are the average measurement during the studied period.

MEASUREMENT METHOD

1 Case study

A case study of irrigation canal system (Jamrao) has been chosen in the Sindh province of Pakistan. A data collection on the past functioning of the system has allowed to observe a clear tendency to the sediment deposition. In the upstream reaches, the sand deposition thickness is more than 3.0 m for a water depth of 2.6 m. The range of variation of the parameters in the whole system is presented in the Table 1 below.

Table 1. Range of variation of the parameters in the system

Parameters	Definition	Minimum values	Maximum values
Q (m^3/s)	discharge	6.60	112.67
V (m/s)	water velocity	0.42	1.22
R_H (m)	hydraulic radius	1.16	2.74
J (m/m)	energy slope	$8.00\ 10^{-5}$	$1.96\ 10^{-4}$
d_{50} (μm)	median size of the particules	80	188

2 Determination of the measurement stations

The chosen case study of irrigation system (Jamrao), as all irrigation systems, is composed of a typology of canal from upstream to downstream in the system. Only the main canal and distributaries are taken into account in the following study while the full description considers three levels of canals.

Because of there large sizes, a set of three parameters has been developed in order to separate the canal in homogeneous reaches [13,14,15]. The first parameter

warranties stable conditions for the water flow in the considered reach [19]. The second parameters specifies to the reach to have a sufficient length to allow the deposition of a particle that enters in it [8]. Then, the third parameter imposes to the reach length to remain below than 95 % of the length concerned by the deposition (L_{max}), this length being defined according to a non-equilibrium law of sediment transport [5].

The final locations of the measurement stations are then determined to represent an average deposition in the reach, so at $L_{moy}=0.15\ L_{max}$ from the head of the reach. An elementary area of investigation represents each measurement location, then the measurements are extrapolated to the whole reach.

The set of parameters to determine homogeneous reaches has been applied on the data of the irrigation canal system case study. That has allowed to determine 21 homogeneous reaches in the system, and so 21 associated measurement stations. A number of 13 measurement stations has been added in order to represent the smaller canals of the system (distributaries).

3 Tracers of the sands

According to the observed trends of global deposition in the chosen irrigation canal system (Jamrao), a measurement campaign using tracer techniques is implemented to observe and explain those phenomena. The tracers represent the solid materials that get deposit in the system, and the measurement campaign aims at showing the spatial distribution of the deposition in the system. The tracers are injected at the head of the system, and then, during a given period of time, the tracer deposition at the measurement stations is sampled and measured.

In order to explain the observed masses of tracers at the measurement stations, all the topographic, hydraulic and sedimentologic parameters are recorded as well during the campaign. An ISRIP team has been employed to carry out this work. This team has also been very useful for the solid samplings (that contain the tracers) in the system during the whole campaign.

The tracing particles are chosen of two different natures. The size distribution of both of them is the same as the natural particles of the system.

First of all, radioactivable tracer are used, they are inert materials (not radioactives), usually glasses that contain intrinsically and irreversibly a doping element (easy to radioactivate) in its stable isotopic state. This technique is under development in CEA and has been tested during the present measurement campaign. In our case, the irrigation canal system being natural and in real size, the tracer dilution is very high. Because of the set of natural elements present naturally in the case study, the only doping element that could be used is iridium. It is anyway an element that is commonly present at a very low rate in environment [2] and that presents very good features for the measurement by neutron activation analysis [9].

Then, fluorescent tracers are used. They are natural sands painted with a red fluorescent paint that is excited under an ultraviolet light.

Those tracing particles are then injected punctually [16,4] at the head of the system and sampled in natural sand samples at the measurement stations of the system. The tracers are then dosed within the samples.

4 Field measurements

The field measurement consist in collecting:

- ✓ Cross section and the water level: R_H (hydraulic radius)
- ✓ Water surface slope: J (energy gradient)
- ✓ Average velocity and the water discharge: V et Q (velocity and discharge)
- ✓ Suspended sediment samples: C (concentration)
- ✓ Bed of the canal sediment samples: d_{50} (median diameter)

The duration of the field program has been 12 weeks, with a complete rotation within the site in 2 weeks, so 6 data sets have been collected.

5 Analysis of the solid samples

5.1 Size ditribution

The sediment samples of the canal bed, after sampling, were dried and a measure of the distribution size has been carried out in the ISRIP laboratory. The total number of samples were 204, i.e. 34 measurement stations times 6 samplings.

5.2 Fluorescent tracers

A specific instrumentation throw numerical imaging has been developed for the measurement of the fluorescent tracers. The main idea is to obtain quantitative results with this method that is usually employed for qualitative measuremnt. This instrumentation has been developed within a MSc training period [6] and the analysis carried out in a CEA laboratory.

The method consists in carrying out a mapping of a sample (20 g) with a high resolution CCD camera. Then, the tracer grains are located on the images and their sizes measured. In our case, a resolution of $14\ \mu m$ per pixel has been achieved with images of 739 times 575 pixels. For each sample, 2592 images are recorded and treated and about 10 grains detected.

5.3 Radioactivable tracers

The analysis method for the radioactive tracers is the neutron activation analysis. It consists in activating the doping element under a high neutron flux. The element, that has become radioactive, is then measured through gamma spectrometry.

The technological choice for the irradiation has been a nuclear reactor for which the flux of thermal neutrons, that are the most efficient for the activation, is very high. Indeed, the use of neutron sources was not possible because of the high dilution of tracers in the samples of the present campaign and the limited neutron flux of such sources [10].

A duration of one hour of irradiation is fixed as a maximum with a sample of about 50 g. Indeed, the elements that are present naturally in the samples also become radioactive after irradiation and make the sample very active, and then difficult to manipulate. It is anyway necessary to cool the sample after irradiation to allow the gamma spectrometry measurement.

All the neutron activation analysis have been carried out in a Pakistani nuclear center because of an easier logistic in transporting the samples and an intention to develop a collaboration with this center.

MEASUREMENT RESULTS

6 Topographic and hydraulic measurements

The topographic and hydraulic data sets are synthesized through the sediment transport capacity η [3,7,11,17]. A wide range in the values of η is observed. It is because the irrigation canal system is observed in its whole, with an associated range of hydraulic flow conditions that is very wide. That point is crucial in our study in which a wide range of deposition trends is also observed. That increases the quality of the statistics on the data. A hypothesis to use average values for the hydraulic flow conditions has been done for the work. A moderate value of 15 % in the standard variations of η is observed that confirms this hypothesis.

7 Tracer measurements

The neutron activation analysis has been carried out in Pakistan and high inconsistencies were observed on the data sets, so two corrective measures were taken. First, a technique as accurate as possible has been developed for the fluorescent tracers measurements, see the section 5.2. And second, a correction technique of the radioactivable tracers results is proposed and is based on calibration samples.

The neutron activation analysis has been carried out on 300 samples, divided in 204 field samples, 46 duplication samples and 50 calibration ones. On the duplication samples, an average relative error of 40 % is observed. The correction technique of the radioactivable tracers results lies on a set of calibration samples that has been mixed within the field samples. The measurement method that has been used for those samples is the same as the field ones. On the calibration samples, the average and standard deviation have been calculated and deviant values were eliminated in order to minimize the standard variation of the data set [12,1]. The measured values of the tracer content in the samples are never nil and this even if the actual value in the sample is nil, the minimum content is *70 ng*. Also, the measured results always over estimate the actual tracer content with a factor of *18* . The measured results are then corrected according to these remarks because of the pragmatic feature of the study. Then, another correction on the data set has been done where deviant values were eliminated in order to minimize the standard variation under the principle presented above. The final date set is presented on the figures below. The measurement of the fluorescent tracer content has been carried out on 204 field samples.

The results are presented on the figures 1 and 2, respectively for the large canals and the small one. On the figure 1, the results are presented for the 21 station points determined with the homogeneous reaches set of parameters, they are: Ji, Di, Si and Wi. On the figure 2, the results are presented for the 13 station points chosen among the small canals, they are: SD, RA, BI, PA, MA, DO, BA, LA and Sai.

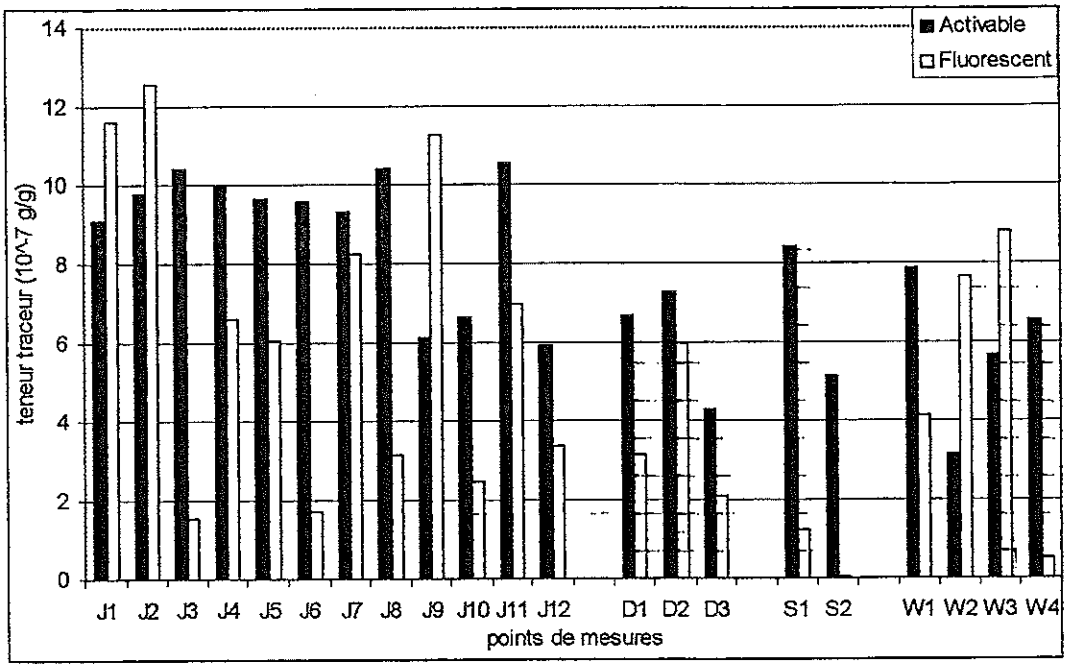

Figure 1.Tracer content in the wide dimension canals

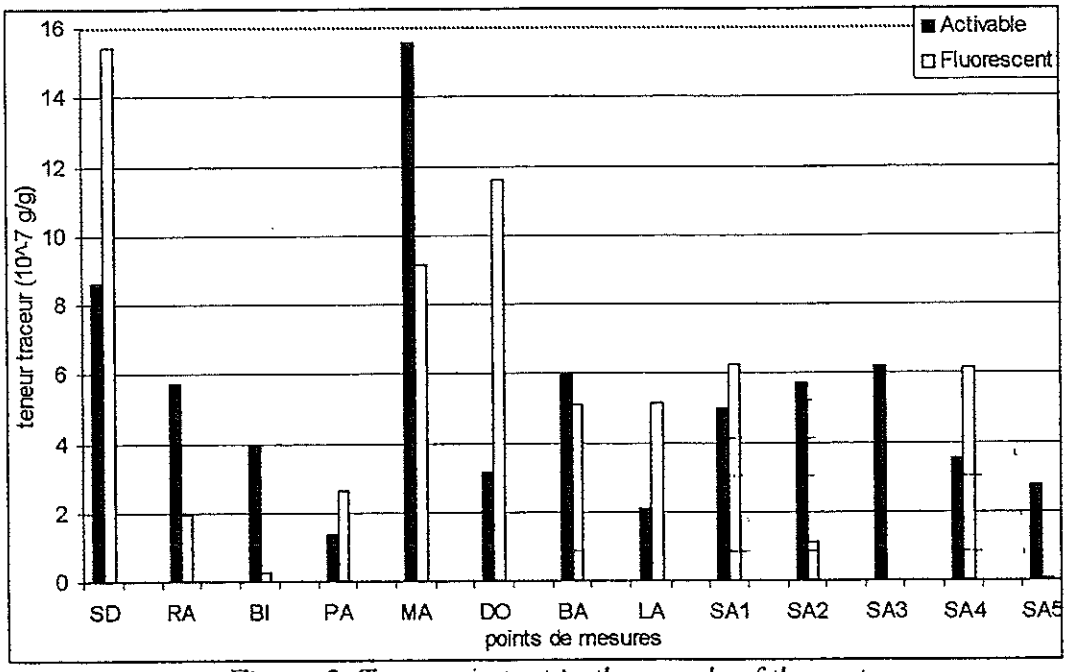

Figure 2. Tracer content in the canals of the system

In the large canals of the system, the comparison between the results of the two tracing methods are very good. It's mainly because, for this type of canals, the distribution size of the particle is high. Then the tracing particle size is high as well and the measured masses of tracer in the samples are high, so with low measurement errors. This is not the case for the small canals of the system for which some measurements present very low values for the masses of tracers, or even have distribution sizes of the particles also very low, and then induce very high measurement errors.

The comparison in between the two methods is globally quite good. Indeed, the global observed trends for the deposition are compatible. Nevertheless, wide differences are observed for certain canals of the system, and especially for the smallest ones. The results obtained with the radioactivable tracers are always preferred because they are more reliable. Indeed, the labeling technique in the mass for such tracers presents a definitive character. This is not the case for the fluorescent tracers, for which the paint at the upper layer of the grains can be eroded during the transport. This phenomenon has been observed in two cases. First, for the samples taken in the measurement stations far from the injection point, so very upstream. And second, for the samples taken a long time after the injection, so at the end of the campaign. For both these cases, the results in radioactive tracers were significant while nil results were measured for the fluorescent tracers.

Anyway, the advantage in using the fluorescent tracers is to dispose of contradictory informations when the correction technique of the radioactivable tracers was used and deviant values were eliminated. Another advantage of the fluorescent tracers is that they were seen by eye directly in the samples during the field program and allows to monitor the campaign.

CONCLUSION

A pragmatic (global) approach has been chosen in this work for the study of sedimentary phenomena. The data set collected during the measurement campaign is minimum and sufficient, both for the experiment duration and the spatial resolution. This choice is linked to the kind of approach chosen for the study and it seems that the results are very satisfactory for both the representation of the phenomena and the calibration of theoretical laws (not presented in the paper).

The obtained measurement errors are the same order of magnitude compared to any study in the field of hydraulic and sediment transport. Also, the goal of the study being to implement an irrigation management approach of the sediment transport phenomena, again an error below 50 % is very much sufficient.

Such measurements of the global deposition trends in an irrigation canal system would never have been possible without tracer techniques. Indeed, in order to obtain significant variations on the deposition phenomena, the topographic parameters have

to be observed during decades while with the tracer techniques, only a 4 months measurement campaign has allowed to obtain relevant informations.

Finally, the measurement method with radioactivable tracers is under development in CEA, the present field experiment is a pilot one. The results are very much encouraging and it is possible to apply the technique on other applications in order to observe similar physical phenomena than the ones of the present study, i.e. the deposition of solid materials.

REFERENCES

[1] AFNOR. *Guide pour l'expression de l'incertitude de mesure.* Norme Française NF ENV 13005. Indice de classement X 07-020, (1999) 105 p

[2] Alvarez, L.W., Alvarez, W., Asaro, F. & Michel, H.V. *Extraterrestrial cause for the cretaceous-tertiary extinction. Experimental results and theoretical interpretation.* Journal Science, Volume 208, Number 4448, (1980) 1095-1108

[3] Bagnold, R.. *An approach to the sediment transport from general physics.* Geological Survey Professional Paper 422-1, United States Government Printing Office, Washington Edition, (1966) 37 p.

[4] Brisset, P.. *L'application des radioéléments en sédimentologie.* Note Technique CEA, DAMRI/SAR/S/NT/ 94-410, (1994) 28 p

[5] Daubert, A. & Lebreton, J.C. *Etude expérimentale et sur modèle mathématique de quelques aspects des processus d'érosion des lits alluvionnaires en régime permanent et non permanent.* Twelfth Congress of the International Association for Hydraulic Research. Affouillements locaux du lit à l'aval des ouvrages hydrauliques, Vol. 3, (1967) 26-37

[6] Doublier, A. & Vabre, A. *Mesure de la teneur en traceur fluorescent dans des échantillons de sable pour des applications sédimentaires.* Note Technique CEA, DAMRI/SAR/S/NT/99-413, (1999) 60 p

[7] Engelund, F.A. & Hansen, E. A monograph on sediment transport in alluvial streams. Teknisk Forlag, Skelbaekgade, Copenhagen V, Denmark, Technical University of Denmark Edition, (1967) 64 p

[8] Hazen, A. *On sedimentation.* Transactions of the American Society of Civil Engineers (ASCE), 53(980), (1904) 235-244

[9] Huet, C. *Etude bibliographique pour le choix d'un traceur activable.* Note Technique CEA, DAMRI/SAR/S/NT/98-41, (1998) 35 p

[10] Huet, C. *Détermination expérimentale de la limite de détection de différentes terres rares.* Note Technique CEA, DAMRI/SAR/S/NT/98-416, (1998) 33 p

[11] Le Guennec, B. *Transport solide et morphologie fluviale.* Polycopié de cours. Institut National Polytechnique de Toulouse. Ecole Nationale Supérieure d'Electrotechnique, d'Electronique, d'Informatique et d'Hydraulique de Toulouse, (1994) 102 p

[12] Neuilly, M. *Modélisation et estimation des erreurs de mesure.* Commission d'Etablissement des Méthodes d'Analyses du Commissariat à l'Energie Atomique. Technique et Documentation – Lavoisier, (1993) 644 p

[13] Ramez, P. *Méthodologie de lissage de la géométrie d'un cours d'eau. Approche Globale par Tronçon.* Document non publié. Division Hydrologie-Hydraulique. Cemagref Lyon, (1996) 9 p

[14] Renault, D. & Godaliyadda, G.G.A. *Generic typology for irrigation systems operation.* Research Report 29. International Water Management Institute (IWMI), Sri Lanka, (1999) 22 p

[15] Rosgen, D. *Applied river morphology.* Edition Widland Hydrology. Pagosa Springs, Colorado, (1996) 369 p

[16] Tola, F. *The use of radioactive tracers in dynamic sedimentology. Part I : Methodology. Part II : Analysis of results.* Note Technique CEA-N-2261, (1982) 42 p

[17] Vabre, A. & Le Guennec, B. *Identification of sediment deposition laws on an irrigation canal system in Pakistan.* Working Paper WP 2000-03, Cemagref Montpellier (1999) 15 p

[18] Vabre, A. *Campagne de mesures au moyen de traceurs de juin à novembre 1998 sur Jamrao Canal System. Objectifs et méthode.* Rapport CEA, DAMRI/SAR/S/RAP/98-104/V17, (1998) 16 p

[19] Yang, C.T. *Unit stream power and sediment transport.* Journal of the Hydraulics Division. Proceedings of the American Society of Civil Engineers (ASCE), Vol. HY 10, (1972) 1805-1825

Tracing of surface treatment reactors

R.Nicolle*, F.Kop*, J.Muller*, Z.Zermout** (Usinor)

*IRSID Voie romaine 57283 Maizières lès Metz France **CED 60100 Montataire France

Abstract. Gas and liquid flow between the various compartments of surface treatment reactors have strong influences on the control of the reactant composition and temperature and consequently on the performance of the reactor.
Two industrial examples are presented:

- tracing of a multi bath continuous pickling reactors to determine the amount of back mixing and its consequences on productivity
- Tracing of multi-compartment annealing reactors to evaluate the gas exchanges between compartments.

Mathematical modelling (CFD or RTD) describes the observed behaviours.

1. Introduction

Many reactors, in iron and steel making as well as in surface treatments have been investigated using tracers[1]; most of them are counter-current reactors. The high advancement rates that are to be achieved, the high quality standards of our products, most often require that the product which leaves the reactor has its last contact with a fresh and pure reactant, otherwise it could be polluted by reaction products or by-products that would lower its properties. Furthermore, counter-current reactors have high utilisation rates of the reactants, which also minimise the quantity of by-products, and therefore contribute to the environment protection.

However, in our continuous processes, the steel strip, which travels in counter-current with the fluid phase - either a liquid or a gas - may drag large amounts of reactants in the opposite direction with the main fluid flow. This creates fluid back mixing that may impair the proper operation of these reactors.

This paper presents some cases that have been investigated using tracers.

2. Back mixing – a frequently encountered situation

The back mixing flow induced by the strip movement is roughly described, in 2D laminar conditions, by the classical parabolic law depending on β (fig. 1)

$$\beta = -\frac{\rho_N}{\rho}\frac{Q_N}{h_f L_f V_b}$$

V_b is the strip travelling velocity,
Q_N is the net gas flow rate under normal (STP) temperature and pressure conditions,
ρ_N is the specific mass of the gas under normal conditions,
ρ is the gas specific mass (temperature T); h_f is height, L_f is the width of the furnace.

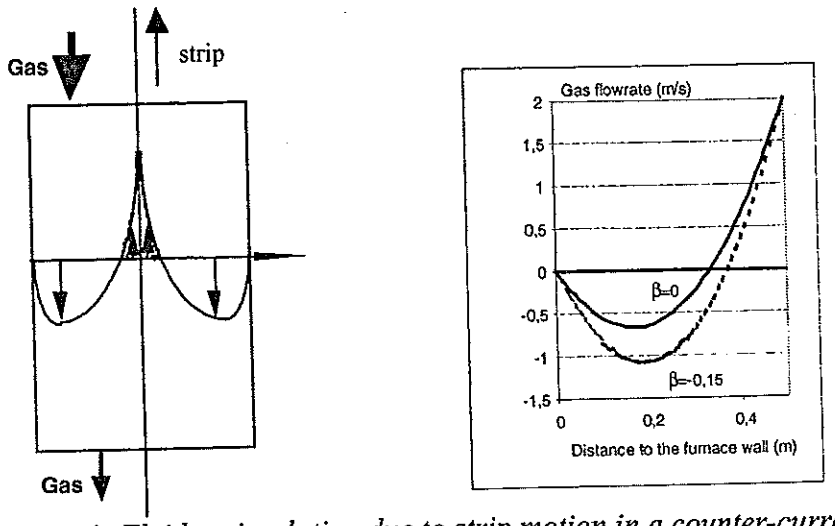

Figure 1: Fluid recirculation due to strip motion in a counter-current reactor

The amount of back mixing depends obviously on the gas flow rate, on the strip speed and on the transversal dimensions of the reactor. However, our recent work, as well as published data[2], suggests that this phenomenon has to be described in 3D as the recirculation loop is most often located at the strip edges.

3. Liquid isothermal reactors: evaluation of back mixing flow rates

3.1. The pickling reactor

The pickling line for carbon steel strips is constituted with three to five connected tanks with a total length of the order of 75 to 150m, through which the steel strip travels at a rate of 2 to 6m/s (each tank has a volume of about 100m^3). Fresh acid is injected into the last bath at a flow rate Q of 5 to 8 m^3/h. The acid concentration Ci decreases from the initial concentration in the injection bath down to the final concentration in the used bath as a consequence of the pickling reaction.

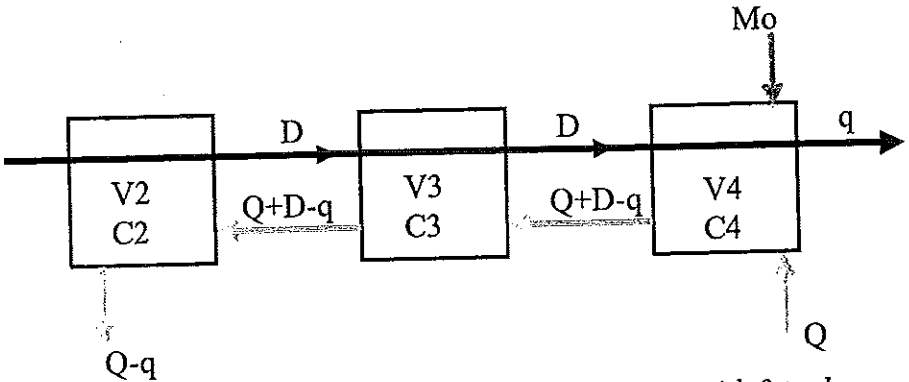

Figure 2: Schematic presentation of a pickling reactor with 3 tanks

The main flow sheet of this process is presented on figure 2. A flow D is dragged by the strip between each tank, and despite efficient wiping rolls at the exit of the last tank, the steel strip drags a small flow of acid q into the rinsing stage. In

the opposite direction, a volume Q of fresh acid is injected into the last tank, which flows through all the tanks; an upstream tank exchanges a volume Q+D-q with its downstream neighbour. The amount of used bath that leaves the first tank is Q-q.

3.2. Evaluation of the back mixing flow rate from tracing experiments

Tracing has been carried out by injection of a Dirac impulse into the last acid tank together with the fresh acid (more specifically through the inhibitor injection tube). Bath samples have been taken regularly from each tank for analysing the evolution of the tracing element. As may be seen on figure 4, the tracer concentration decreases almost exponentially in the last tank, where tracer injection has been carried out, suggesting that each pickling tank may considered as a well mixed reactor. Indeed, the large velocity of the strip favours bath mixing.

The tracer concentration in the other tanks shows a maximum as a function of time suggesting that these reactors may be mixed reactors in series as well.

In consequence, the following model has been built for describing the dynamic behaviour of the various tanks. The equations correspond to the flow diagram and the variables presented on figure 2.

$$V\frac{dC_4}{dt} = Dirac(t).Mo - (Q+D+q).C_4 + D.C_3$$

$$V\frac{dC_3}{dt} = (Q+D).C_4 - (Q+2D).C_3 + D.C_2$$

$$V\frac{dC_2}{dt} = (Q+D).C_3 - (Q+D).C_2$$

Values of the Laplace transformation have been calculated by the trapezium method. Curves have been adjusted in Laplace space and fitted to the theoretical equations; the equation system describing the dynamic behaviour of the acid tanks has been solved literally, giving the following formula. Each curve of Laplace transformation has been fitted by its equation, where D is the only adjustable parameter.

$$\frac{1}{C_4} = \frac{V^3.s^3 + (3.Q.V^2 + q.V^2 + 4.D.V^2).s^2 + (3.Q^2.V + 3.D^2.V + 6.Q.V.D + 2.Q.V.q + 3.D.V.q).s + (2.Q^2.D + Q.D^2 + Q^3 + 2.Q.q.D + q.D^2 + Q^2.q)}{Mo.(V^2.s^2 + (3DV + 2QV)s + (2.Q.D + D^2 + Q^2)}$$

$$\frac{1}{C_3} = \frac{V^3.s^3 + (3.Q.V^2 + q.V^2 + 4.D.V^2).s^2 + (3.Q^2.V + 3.D^2.V + 6.Q.V.D + 2.Q.V.q + 3.D.V.q).s + (2.Q^2.D + Q.D^2 + Q^3 + 2.Q.q.D + q.D^2 + Q^2.q}{Mo.((QV + DV)s + 2.Q.D + D^2 + Q^2)}$$

$$\frac{1}{C_2} = \frac{V^3.s^3 + (3.Q.V^2 + q.V^2 + 4.D.V^2).s^2 + (3.Q^2.V + 3.D^2.V + 6.Q.V.D + 2.Q.V.q + 3.D.V.q).s + (2.Q^2.D + Q.D^2 + Q^3 + 2.Q.q.D + q.D^2 + Q^2.q}{Mo.(Q^2 + 2.Q.D + D^2)}$$

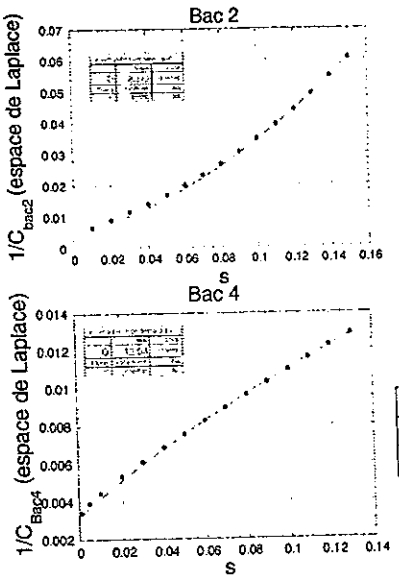

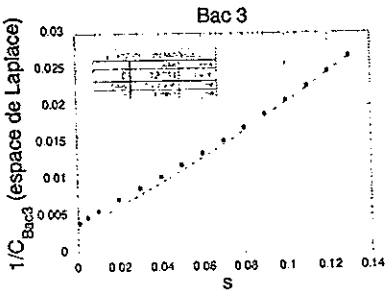

	Bac 4	Bac 3	Bac 2
D : m3/h	12,04	12,21	12,14
R : corrélation	0,9993	0,996	0,9991

Figure 3: Laplace transformation of the concentration curves in the 3 tanks

Figure 3 shows the fair adjustment of each curve; the calculated values for the back mixing flow between tanks is about 12,1m^3/h for the three tanks (± 1%).

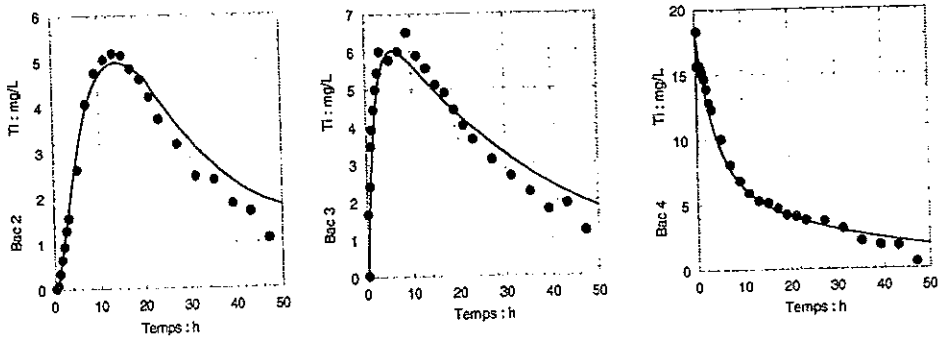

Figure 4: Tracer concentration in the 3 tanks: real vs. model

3.3 Reaction kinetics, another way of calculating the back mixing flow

The back mixing flow rate D may be calculated by another method. Each bath composition (acid Y_i) varies through the action of two phenomena:

- the chemical pickling reaction in each bath ΔX_i; the kinetics law is already known from laboratory experiments and is proportional to the acid concentration Y_i

$$\Delta X_i = k.S.\ \Delta t.Y_i.(X_{i-1} + a).(X_i + a) = (X_{i-1}-X_i)$$

- The back mixing flow from the less concentrated acid tank into the upstream tanks more concentrated in acid.

The acid concentration into each of the three acid tanks is given by the three following equations:

$$0 = Q.Yo-(Q+D).Y_3-\Delta X_3.\rho+D.Y_2$$

$$0 = (Q+D).Y_3-(Q+2D).Y_2-\Delta X_2.\rho+D.Y_1$$

$$0 = (Q+D).Y_2-(Q+D).Y_1-\Delta X_1.\rho$$

Solution of these three equations gives the back mixing flow rate D and the kinetics constant for the pickling reaction k. The value for D: D=11,5m^3/h, solution of these equations is indeed very close to the value determined by tracing 12,1 m^3/h.

4. Gas non-isothermal reactors: the annealing reactor

4.1. The annealing reactor

Annealing furnaces are large volume reactors (1000 to 4000m^3) devoted to steel recrystallisation. The incoming steel strip is first heated up to temperatures of 700°C to 900°C, then cooled down using gas jets. The annealing gas, a N_2-H_2 mixture, flows through the furnace with a flow rate of the order of hundreds of m^3/h whereas the cooling jet flow rates, recycled through heat exchangers and blowers are of the order of tens of thousands m^3/h. A wall with an opening through which the sheet travels separates the holding and cooling zones of the annealing furnace.

Gas flow between those two zones results from two main processes:

-The blowers suction from the cooling zone and the gas carried along with the travelling sheet, which both create a gas flow in the direction of the strip movement

-The net gas flow that is counter current with the strip movement, as the gas flows from the cooling zone to the preheating furnace.

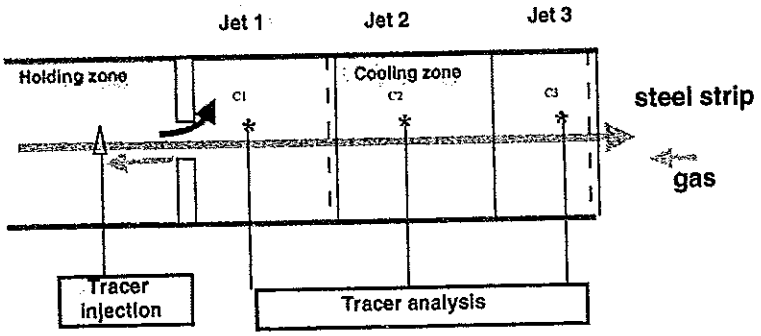

Figure 5: Schematic presentation of an annealing reactor

In order to quantify the value of the gas exchanges between the various sections of the annealing furnace, He tracer has been injected as a Dirac impulsion into the holding zone and a simultaneous helium analysis has been carried out in the 3 cooling zones.

4.2. Evaluation of the back mixing flow rate from tracing experiments (RTD)

From these tracing curves, gas flow through the line may be modelled using RTD simulation. The balance under dynamic conditions results from the transfer function of a series of interconnected elementary reactors such as those shown on figure 6; the same jet section had to be separated into two reactors that are situated on the top and on the bottom of the strip for a better fit of the RTD curves using four adjustment parameters (α and Qi) for the 3 curves:

$$\frac{dC_1}{dt} = \frac{1}{V_1}[Q_1 C_0 + (Q_2+Q)C_2 + \alpha(Q_1+Q_2+Q)C'_1 - (1+\alpha)(Q_1+Q_2+Q)C_1] \quad (1)$$

$$\frac{dC'_1}{dt} = \frac{\alpha}{V_2}(Q_1+Q_2+Q)(C_1 - C'_1) \quad (2).$$

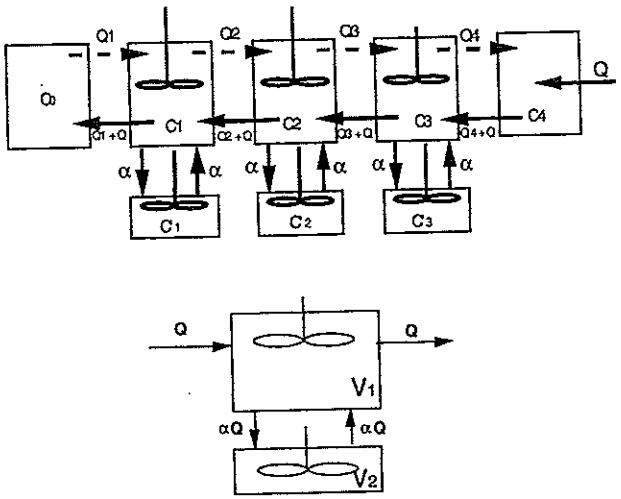

Figure 6: Description of the cooling section as a series of unit operations

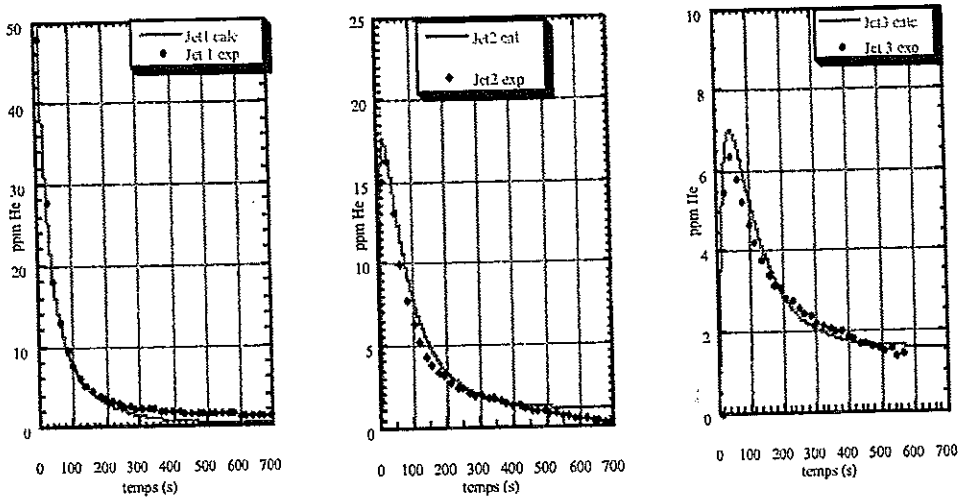

Figure 7: Tracer analysis in the various cooling sections (real vs. model)

The resulting mathematical model gives the comparison between measured and model shown on figure 7. The values of the flows between sections are Q1= 935 m^3N/h, Q2=Q3=360m^3N/h and Q4= 350m^3N/h.

4.3. Evaluation of the exchange flow rates from steady state mass balances

Gas exchanges between the various sections of an annealing furnace may also be calculated from the gas compositions in the various sections. Under steady state conditions, the concentration of a tracer element contained in the gas phase may be interpreted using the following simple model.

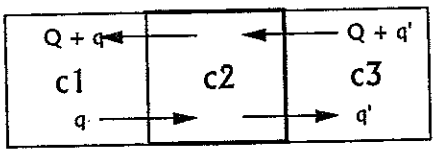

$$q = (Q + q').\frac{(C_2 - C_3)}{(C_1 - C_2)}$$

Figure 8: A simple model for interpreting gas exchanges in steady state

The results obtained by such a method, although variating from one test to the other, are of the same order as the calculated data from gas tracing experiments (figure 9).

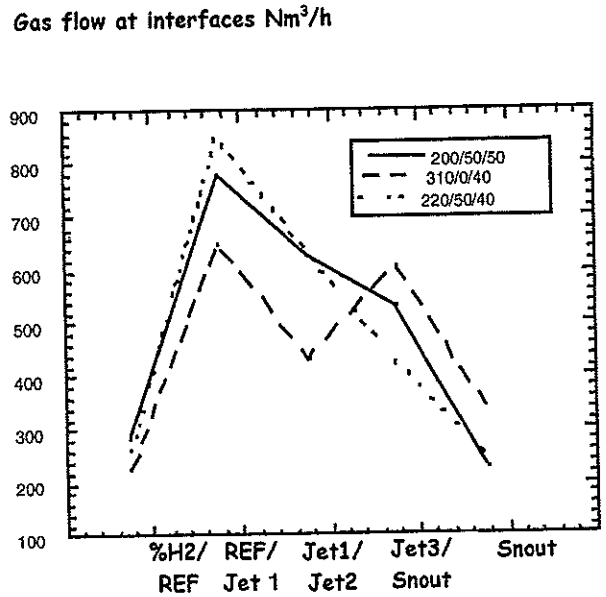

Figure 9: Evaluation of the gas flow between sections from mass balances

4.4. CFD modelling: a tool for designing improved reactor geometry

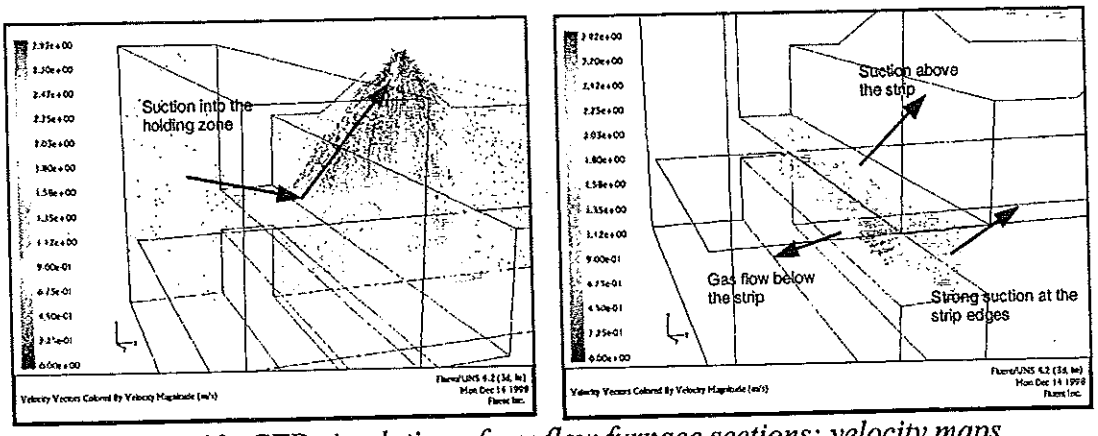

Figure 10: CFD simulation of gas flow furnace sections: velocity maps

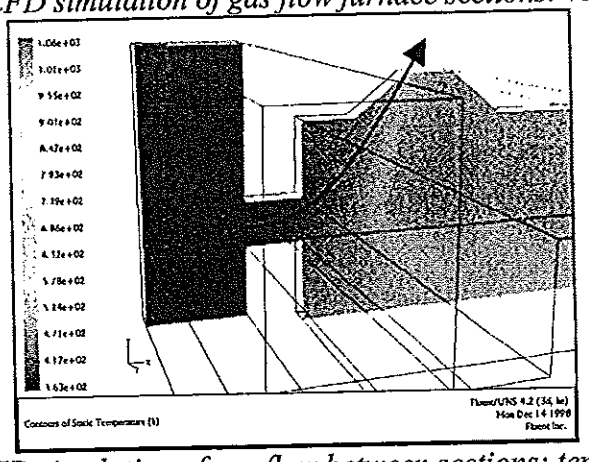

Figure 11: CFD simulation of gas flow between sections: temperature map

A CFD model of this zone of the furnace has been developed; it shows that large gas volumes are sucked from the warm holding zone into the cooling zone thus leading to undesired heat tranfers which reduce the production capacity of the line. These figures show that gas is preferentially sucked at the edges and the bottom face of the strip suggesting ways, that have been further simulated, to reduce it.

5. Conclusions

In counter flow reactors, fluids may be dragged backwards into the "upper" stages of the process lines, thus leading to unfavourable consequences on the process and product quality. Tracing methods applied to surface treatments may quantify these fluxes and help in the design of more convenient reactor geometry.

Acknowledgement

We wish to thank ECSC for partial funding & S.Fiorelli for the gas tracer work

References

1. R.Nicolle, JM.Steiler, M.Wanin Traçages dans la Sidérurgie La Revue de Métallurgie CIT Jan. 2000 61-71

2. SD.Sciffer, GM.Evans, JA.Lucas CFD Modelling in a continuous strip coating line 2nd International conference on CFD Australia 6-8th December 1999

MODELING OF THE COPPER ORE CONCENTRATION PROCESSES BASED ON THE EXPERIMENTAL RTD FUNCTIONS

Z. Stęgowski

Faculty of Physics & Nuclear Techniques, University of Mining & Metallurgy, 30-059 Krakow, Poland.

Abstract. Radiotracer experiments, in copper ore industrial process, are same efficient method for kinetics parameters and flow rate determination. The experimental Residence Time Distribute (RTD) functions obtained from these measuring allow to describe the theoretical models of the elementary processes and to calculate same real values of these model parameters. This paper presents the experimental RTD functions obtained in Polish Copper Industry during last several years. Presented data include the following devices: ball mill, spiral classifier, hydrocyclon and filter. Based on these data the mathematical models for each single operation will be present too. For mathematical modelling the commercial software DTS has been used.

INTRODUCTION

The Copper Industry is one of the largest company in Poland. This industry includes mining, concentration and foundry processes. Thirty millions tons of copper ore are processing per year. In the concentration process the copper ore which includes about 1%-2% of copper are benefiting for concentration material which includes 20% of copper. The concentration process includes three steps: comminution, benefication and dewatering process. For optimisation and the automatisation of this process the knowledge of the proper accurate flow parameters of each operation (milling, classification, flotation etc.) is necessary. One of the more efficient methods applied to investigations of industrial flow processes is the radiotracer method. In Polish Copper Industry this method has been used from more than 20 years [4]. At present, as electronics, computers, data storage and data analysis software developing, this method is mach powerful than at the start.

The main goal of this paper it is presentation the experimental Residence Time Distribution (RTD) functions for examples devices like, ball mill, spiral classifier, hydrocyclon and filter and, based on these data, the mathematical models description for each operation. For mathematical modelling the commercial software DTS has been used

RADIOTRACER METHOD

Radiotracer method provides the means for behavior determination of the selected material in a flow system. The idea of radiotracer method consists in injection of radioactive tracer to the input of the system and analysis of gamma-radiation intensity distribution (system response) at the output [5]. The possibility of achieving high activity of the tracer per mass unit together with high efficiency of gamma-rays detection allow injection of a small quantity of the tracer in comparison to the flowing material. Thanks to this, the injection does not disturb the process's

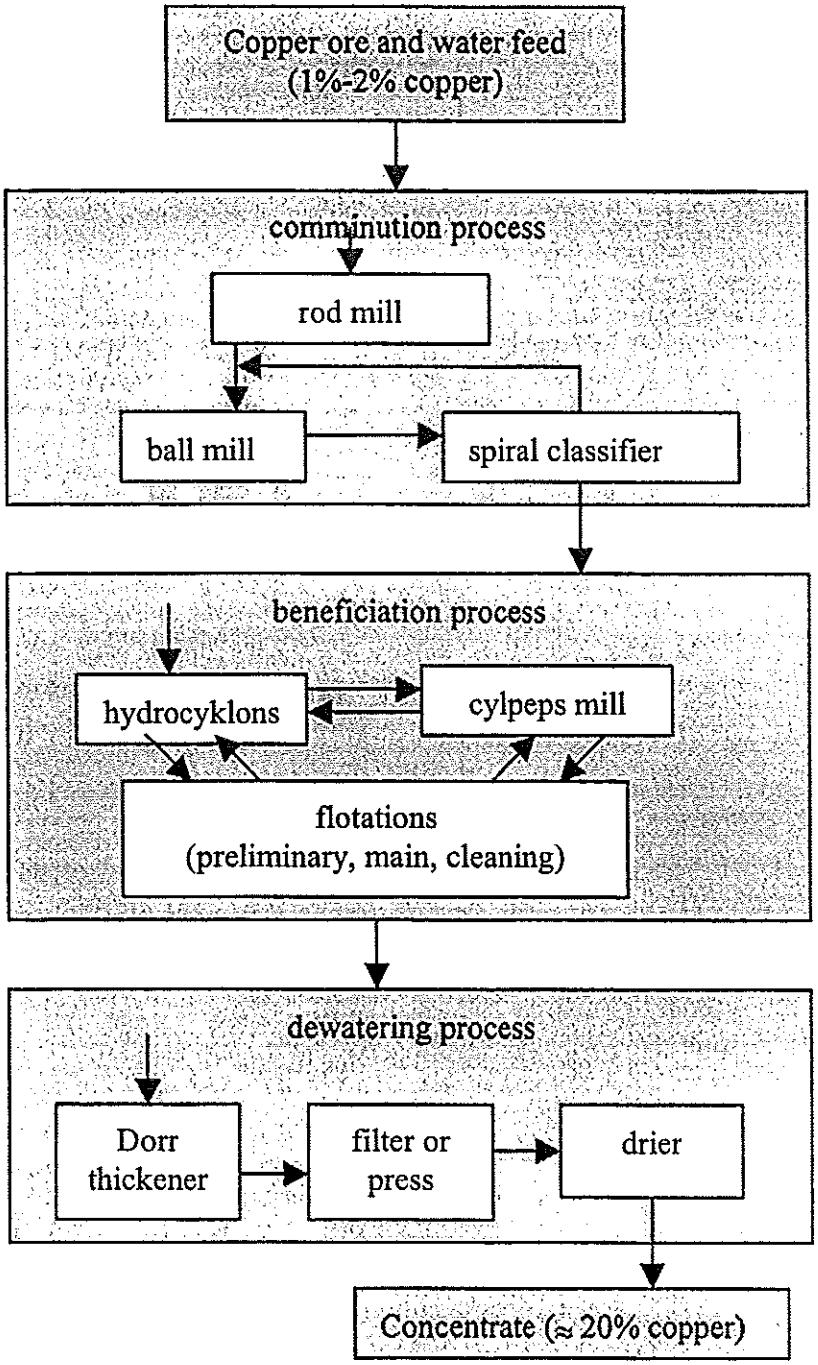

Figure 1. General schema of a copper ore concentration process

kinetics. The properly selected radiotracer, which is naturally associated with the traced population in a flow process, provides information on the main population. The method does not influence the process's conditions since detectors placed outside the flow, measure the intensity of gamma rays from the radiotracer. In industry condition, like copper ore concentration process, the radiotracer method is only one which allows property easy and practically on-line, to describe the real kinetic flow parameters. For copper ore concentration we can to use the separate radiotracer for water, solid ore grains or different grains size. For system with the recirculation loop the radiotracer method allows not only to describe the recirculations kinetics but also to obtain the recirculation flow value.

The radiotracer emitting γ-radiation is injected (as a pulse function) to the system by inlet. The scintillation probe, placed on system's outlet, is detecting the gamma radiation as a time function. The counting rate is directly proportional to the concentration of the radiotracer in the flowing stream where the probe placed. When the impulse tracer injection is done that measured function is RTD.

Natural copper in ore contains the two stable isotopes ^{63}Cu and ^{65}Cu. Due to the thermal neutron activation in a nuclear reactor the radioactive isotope ^{64}Cu is obtain from isotope ^{63}Cu. This isotope is perfect tracer for copper ore processing studying. The half-life of ^{64}Cu is 12.7 hours and its mainly emits a positron which immediately annihilates with electron and two gamma rays having energy 510 keV are emitted.

DTS SOFTWARE

The experimental radiotracer's data, depends from the application, need the proper analysis. One of the advanced software it is the DTS package for flow process modelling [2]. This is object oriented programming software working in Windows Systems. The software can simulate the response to an input of any complex network. Eight different elementary reactors can be chosen which based on perfect mixer and dispersion models [3]. The parameters can be optimising by comparison of experimental data with the response of the model. Processes with multiple inlets or outlets can be modelled by convolution and optimisation procedures. Local measurements may be validated through the possibility to simulate the local response within the model and to optimise the corresponding parameters. This use of the well-known elementary "bricks" permits us to work directly in the Laplace domain where we know, in particular, that the convolution product is transformed into a simple product of the functions.

Three basic models and their parameters are presented in table 1. These models have been used for copper ore concentration processes modelling for experiments presented in this paper.

Table 1. DTS single models used for presented data analysis in this paper.

model's name	model's symbol	parameters
Plug flow	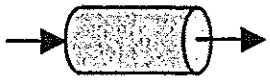	T - flow time
Perfect mixers in series	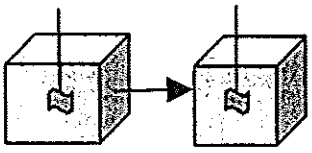	τ - total mean residence time I - number of perfect mixers
Perfect mixers in series with exchange zones	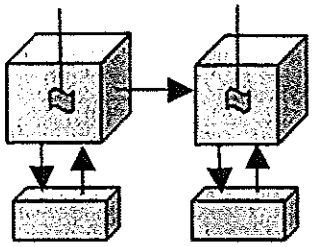	τ - mean residence time for mixers I - number of perfect mixers τ_m - mean residence time for exchange zones K - ratio between exchange zones volume and mixers volume

MILLING AND CLASSIFIER PROCESS

Drum mills are oftener used for grinding in ore processing. Ball mill is one of drum mills where the iron balls are the grinding medium. Rotating drum lifts the balls for same height from which the balls settle down and collide with another bolls. The copper ore with water flow along the drum mill and the ore particles are grinding trough the collided balls. The reduced size small grains flow out of the mill with the top water surface.

Spiral classifier is used directly after boll mill grinding. The main goal of this process is separated the biggest grains, that not enough grinding, and inserts them again to the boll mill. This process based on speed sedimentation difference between grains on different size. Bigger grain come down on the bottom and moving out to the underflow by the rotating spiral worm. The smaller grains flow out to the overflow with the top water surface.

In this paper is presented the grinding system where the material from the mill's outlet flowing to the spiral classifier and material from classifier's underflow flowing back to the mill. The material from classifiers overflows flowing out to a beneficiation process. Figure 2 shows this system with applied models for mill and classifier. The radiotracer investigation was made by injection of the cooper's radiotracer to the inlet of the mill (as a pulse function). The scintillation probes were

placed in mill's outlet and classifier's overflow. The experimental data from these probes and fitted models are showed in figures 3 and 4. The parameters obtained for the models are presented in table 2.

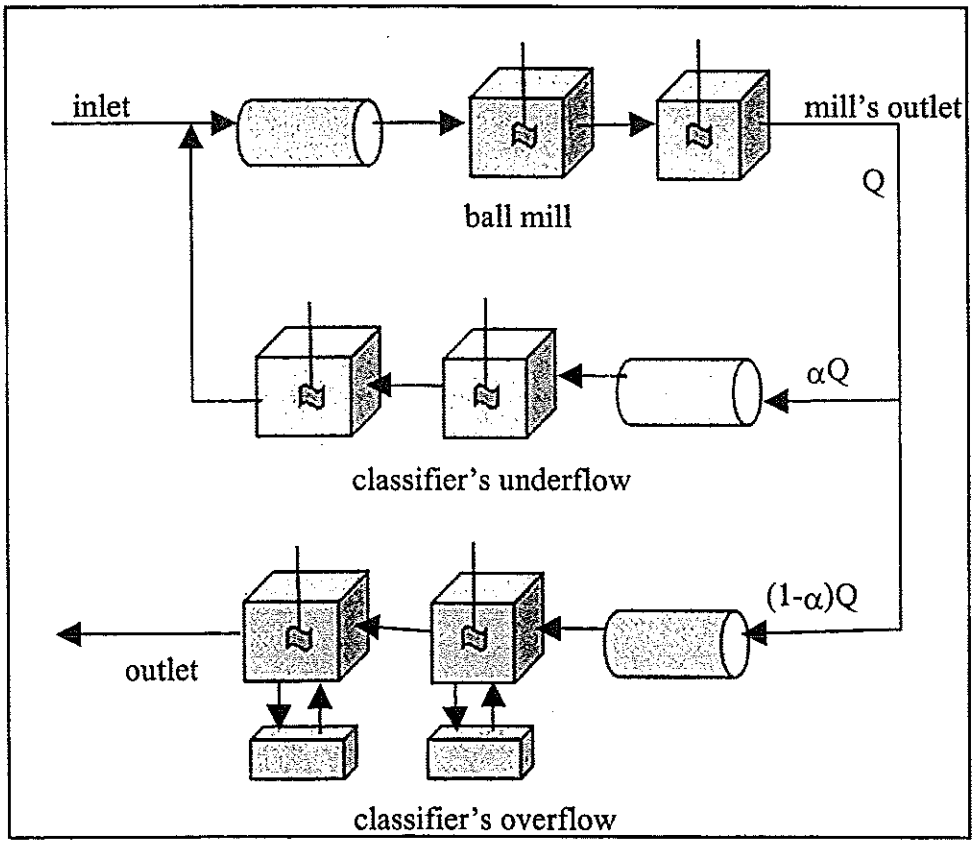

Figure 2 Model for ball mill and spiral classifier

where: Q – flow rate in the mill,
α - the part of Q flowing through classifier's underflow.

Table 2. Obtained parameters for ball mill and spiral classifier

	T [min]	τ [min]	I	τ_m [min]	K	α [%]
Ball mill	0.30	2.9	5.5	-	-	-
classifier's underflow	0.27	3.7	2.0	-	-	78
classifier's overflow	0.04	0.8	2.4	0.53	2.1	-

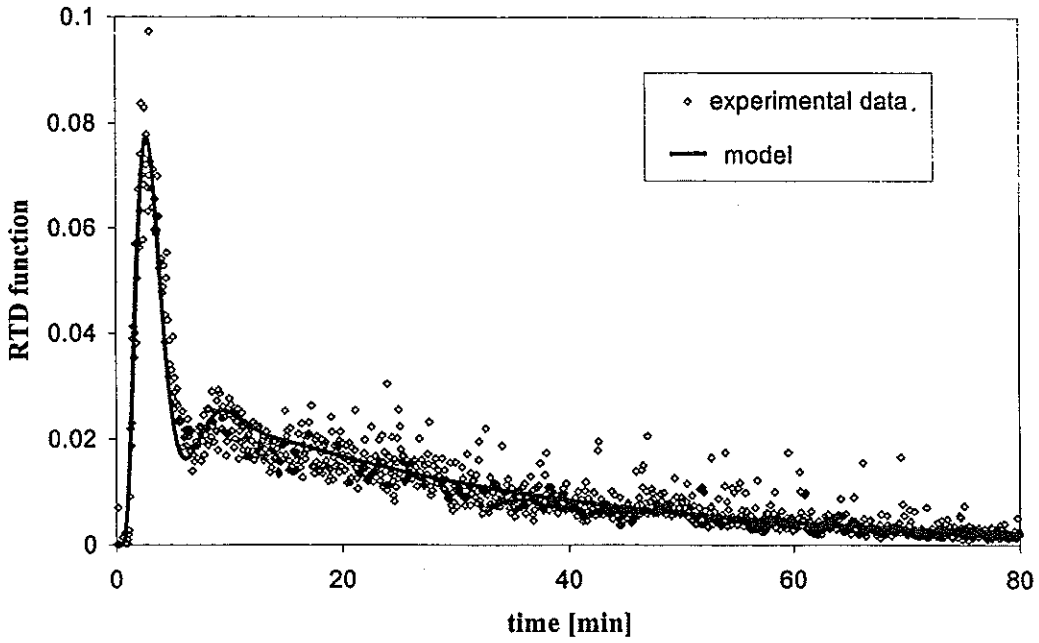

Figure 3: Experimental data and model fitted in outlet of the ball mill.

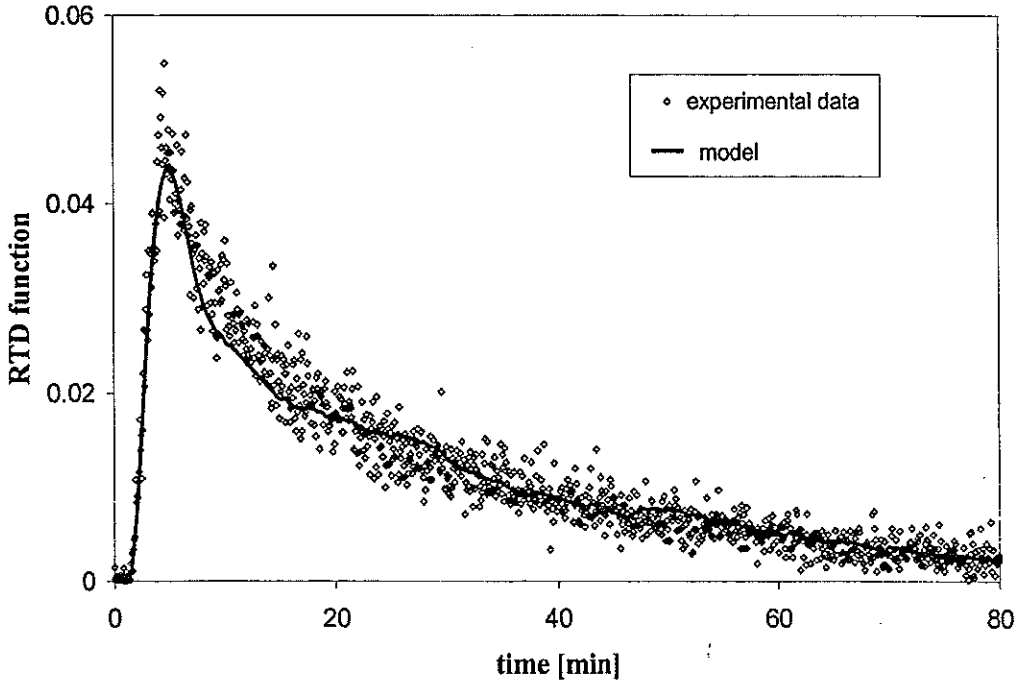

Figure 4: Experimental and model fitted in outlet of the classifier's overflow .

HYDROCYCLONE

Hydrocyclone is a device where the grain material classification proceeds in the field of the centrifugal force action. The centrifugal forces generated by flowing liquid on spiral trajectory in motionless vessel. This spiral flowing is generated by tangential enter the suspended solids with proper velocity. The physical difference of the grains, size and specific gravity affords possibilities to separate the grains in hydrocyclone. Inside the hydrocyclone the two backward rotated streams formatted. One rotates close the hydrocyclone wall flows down with bigger and heavy grains to underflow. Second rotates inside flows up with small and lightweight grains to overflow. The hydrocyclone separate much smaller grain than the spiral classifier.

The radiotracer experiment was made for hydrocyclone worked inside the beneficiation process. In this case was not possible to make the pules injection of the radiotracer and the scintillation probes were placed in tree places: hydocyclone's inlet, underflow's outlet and overflow's outlet. Figure 5 shows the hydrocyclone's model. The experimental data from these probes and fitted model are showed in figures 6 and 7. The parameters obtained for the hydrocyclone's model are presented in table 2.

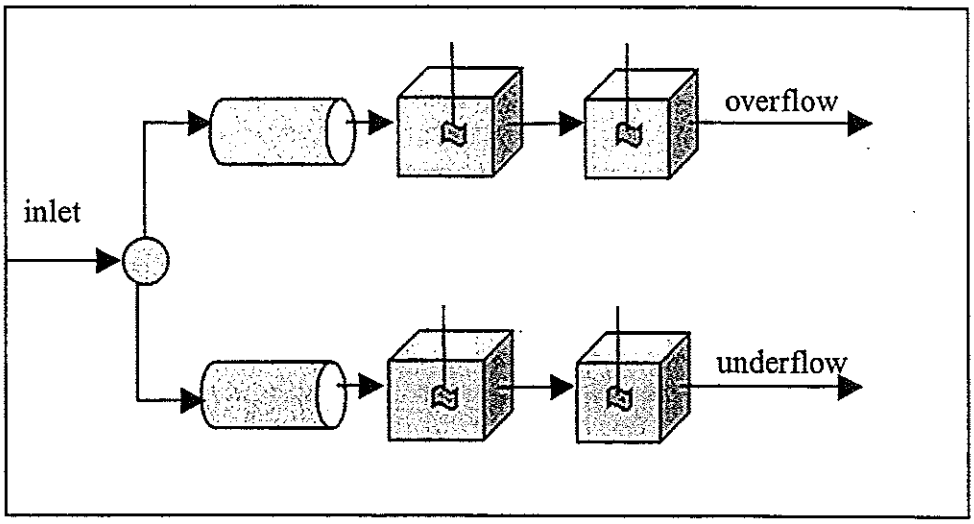

Figure 5. Model for hydrocyclone

Table 4. Obtained parameters hydrocyclone's model

	T [s]	τ [s]	I
overflow	0.26	3.2	2.5
underflow	0.72	2.7	1.0

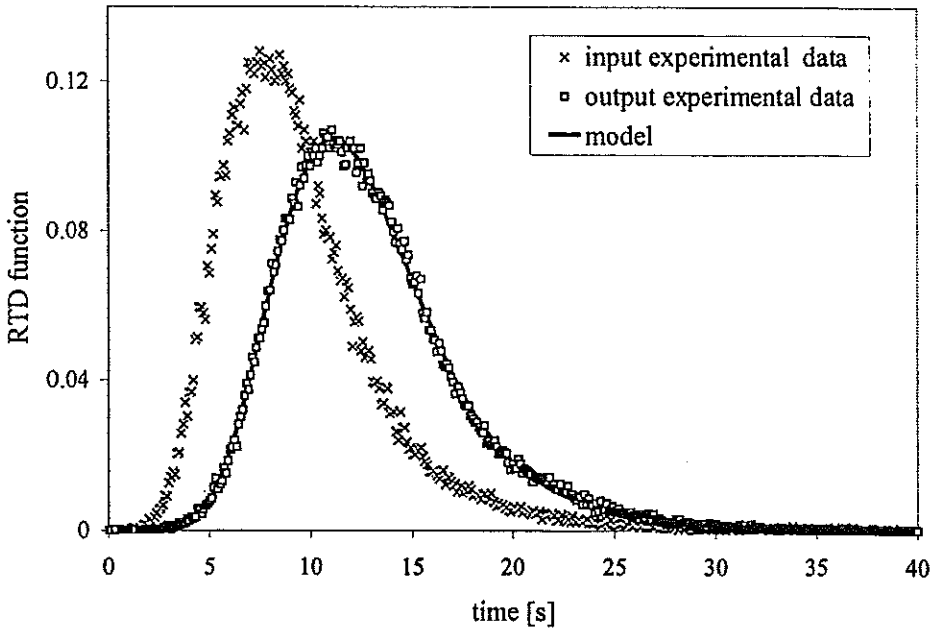

Figure 6: Experimental data for input and overflow of hyrocyclone and model fitted by convolution method .

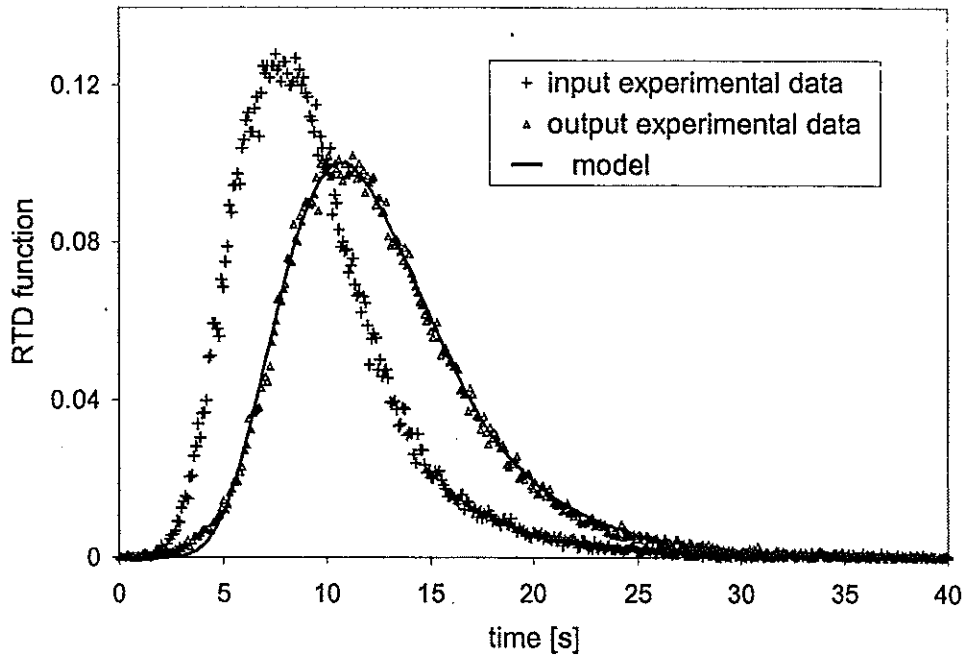

Figure 7: Experimental data for input and underflow of hydrocyclone and model fitted by convolution method .

FILTER

Filter is a device working in the copper ore dewatering process. Filter's feed it is material from Dorr thickener, which include about 80% water. After filtration the material, include about 20% water, is passed to the drier. Filter is a vessel filled by water and solid mater. Special rotate membranes are sink for half in the vessel. Under pressure system the solid mater deposits on the membranes which rotate under surface and solid meter is removed outside of the filter.

In radiotracer experiment injection of the cooper's radiotracer was made to the inlet of the filter (as a pulse function). The scintillation probe was placed in filter's outlet of the solid mater. Figure 8 shows the filter's model. The experimental data from these probe and fitted model are showed in figures 9. The parameters obtained for the filter's model are presented in table 2.

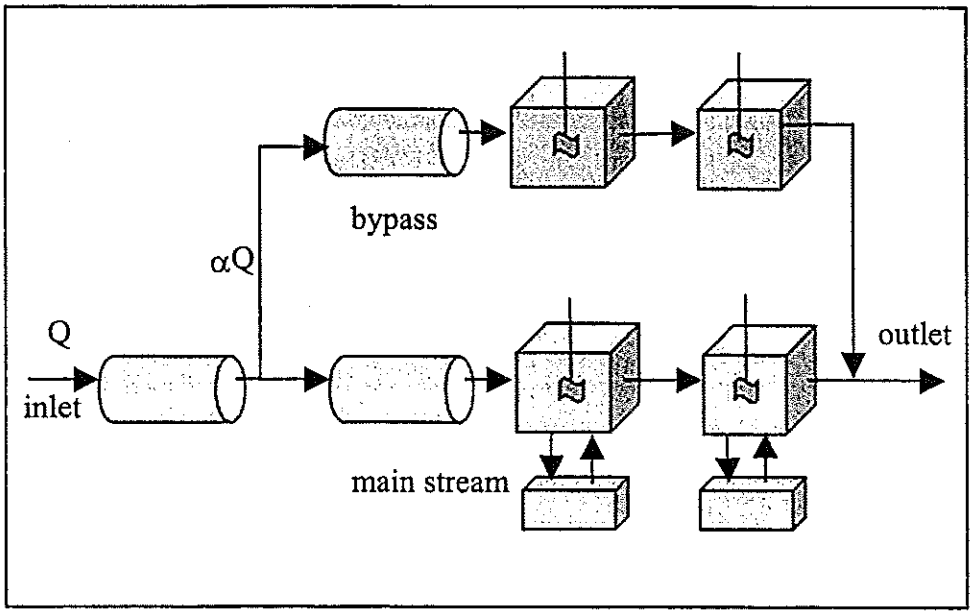

Figure 8. Model for filter

where: Q – flow rate in the filterl,
α - the part of Q flowing through bypass.

Table 4. Obtained parameters filter's model

	T [min]	τ [min]	τ_m [min]	K	I	α
inlet	1.0	-	-	-	-	-
bypass	0.4	2.1	-	-	4	9 %
main stream	3.4	8.3	12.5	1.8	3	-

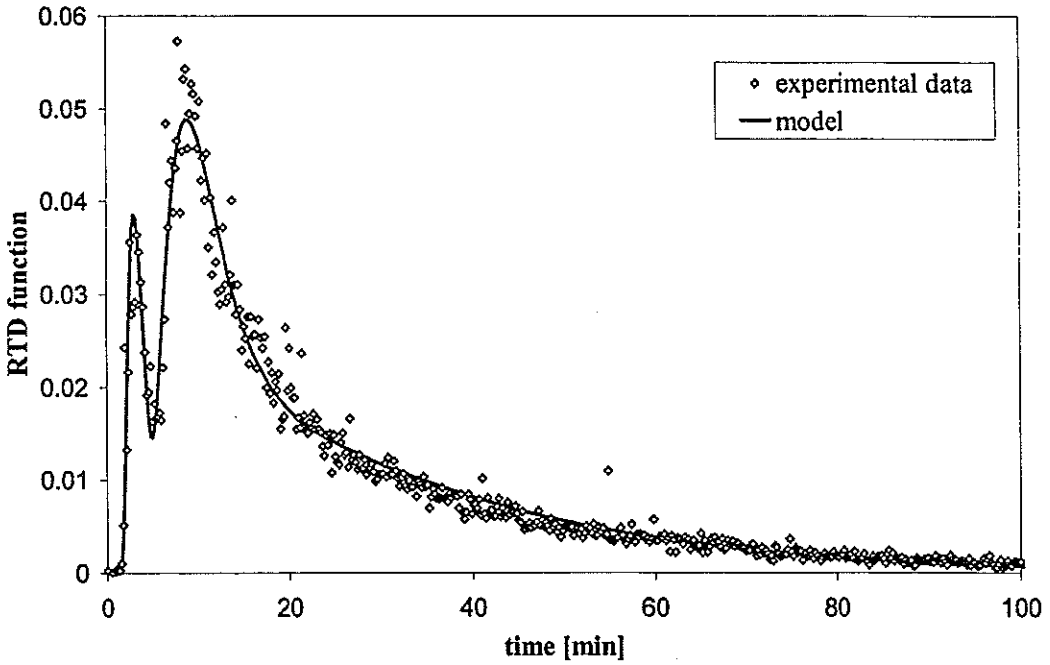

Figure 9: Experimental data and model fitted for filter .

CONCLUTION

The radiotracer investigation and proper modern software, like DTS, it is a very powerful instruments for copper ore concentration processes analysis. This allows to obtain proper models for each process end to determine their parameters. It is very helpful for whole process optimisation and automatisation.

REFERENCES

[1] Danckverts P. V., *Continuous flow systems, Distribution of Residence Times*, Chemical Engineering Science (1953), 2, 1, 1-13.

[2] Leclerc J-P., Detrez C., Bernard A. and Schweich D. *DTS un logiciel d'aide à l'élaboration de modèles d'écoulement dans les réacteurs,* Revue de l'Institut Français du Pétrole, (1995), 50, 5, 641-656.

[3] Levenspiel O. Chemical Reaction Engineering, 3 ed., John Wiley & Sons, New York (1999),.

[4] Petryka L., Furman L.,Przewlocki K., Stegowski Z., *Radioisotope Investigation of Copper Ore Dressing Processes*, Nuclear Geophysics (1993),, vol. 7 no. 2, pp. 313.

[5] Przewlocki K., Petryka L., Stegowski Z. *Radiotracer Identification of the Copper Ore Benefication Process*, Isotopenpraxis (1990),, vol. 26, n°9, pp. 439-444.

[6] Stegowski Z., *Accuracy of Residence Time Distribution Function Parameters*, Nuclear Geophysics (1993), vol. 7 no. 2, P. 335.

MEASUREMENT OF SLIP VELOCITY DURING HYDROTRANSPORT THROUGH VERTICAL PIPES

L. Petryka[1], R. Keblowski[1], X. Gao[2], Kushartono[3], R. Murzyn[1]

[1]University of Mining & Metallurgy, Al. Mickiewicza 30, 30-059 Krakow, Poland
[2]China Institute of Atomic Energy, P.O.275(104) Beijing 102413, China
[3]Centre for Research and Development of Isotopes and Radiation Technology, Jl. Cinere Ps. Jumat PO. Box 7002 JKSKL, Jakarta 12070, Indonesia

Abstract. A different velocity of complex flow's components influent on energy and pressure losses in any two phase flow. However in hydrotransport, the value of slip velocity results from differences of specific gravity of components and solid fraction's concentration in mixture, but is also modifying by parameters characteristic for particular flow. Some of them as shape of stones, content of impurities modifying liquid viscosity, and the smooth of pipes internal surface, are hard to measure and difficult to describe. More accurate is direct measurement of slip velocity by radioisotopes. The paper describes such measurements in vertical pipes, where due to application of sealed radioactive sources and tracers, as well as two statistical methods of data processing, accurate values of slip velocity were obtained. Separate labeling of different solids and liquid, as well as applying eight scintillation probes, allow observation of velocity along almost 7 m of $\phi = 6"$ pipe.

In the presented measurements, due to application of cross-correlation and Fourier Transform for data analysis, error of transportation delay was keep below 1%, independently from observed fluctuations of flow. It may be anticipate that proposed methods of measurement and data processing would be apply in great number of different flow industrial processes.

INTRODUCTION

Industry which often applying a hydrotransport looking for reduction of energy lost, wear of pipes and increase of the transport efficiency. This task may be obtained by construction of laboratory rigs and application of radioisotope methods for flow examination both in small and full scale.

UMM research activity suggests that multiphase flow should be analyze by combination of radiotracer and γ transmission measurements [1 – 4]. Such approach gives opportunity to derive advantages of the both methods. For example, it is hard to distinguish movement of flow's components by photon beam transmission only. On the other hand, only limited part of stream may be labeled by radioisotopes but typical industrial flow is hard to keep stable during repeating measurements.

Optimization of manganese pebbles' undersea exploitation, gives opportunity for describing the new methods of flow examination by radiotracers and sealed radioactive sources. The paper presents results of such experiments.

TWO PHASE FLOW EXAMINATION

The simplified schema of experimental installation with half number of applied probes may be seen in Fig. 1. During the experiment, on pipe ϕ 150 mm, eight measuring probes were placed. Four of them consists of the scintillation detector and ^{242}Am in special collimators. The rest of probes were used for radiotracer measurements only. Electronically controlled pump forced flow of water with velocity up to 5.0 m/s in the greater loop. The smaller one feeding the stream by stones of diameter

varying from 5 up to 35. During experiments, volumetric concentration of solid phase was kept in range from 10% to 20%. The beginning measurements were based on sealed radioactive sources only. Comparison of results obtained from signals recorded by the four γ absorption sets, reveals sufficient precision of transportation delay determination for slip velocity observation.

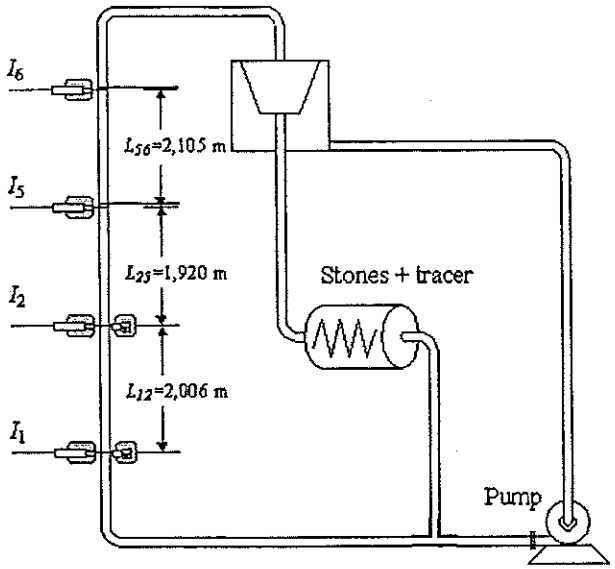

Figure. 1. Schema of hydraulic installation at Agriculture University in Wroclaw

In the following series, γ transmission measurements were supplied by radio-tracers. In those experiments, the isotope of ^{82}Br was applied as tracer for the both, liquid and solid fractions, because the tracer in insoluble Hg_2Br_2 was placed inside stones and protected by an epoxy glue. Distinguish of signals representing solid or liquid fraction based on differences in dispersion of recorded γ radiation intensity. Due to sampling time equal to 1 ms, accurate information when the labeled stone or water appear in a particular cross section of the pipe was recorded. Stones do not follow, however the straight path in the stream and measurement of average velocity of sufficiently great number of solid particles was necessary. In this experiment it was achieved due to many recirculations of labeled stones in close loop, but steady conditions of flow was essential for that method. Example of results obtained in experiment Wro17 are presented in Fig. 2 and following one up to Fig. 4.
Different heights of peaks are effect of the labeled stone distance from a detector, and local density of mixture in that area. Moreover, it is a result of value and orientation of labeled particle velocity in that particular moment. The area marked with rectangle, one may observe increased in Fig. 3.

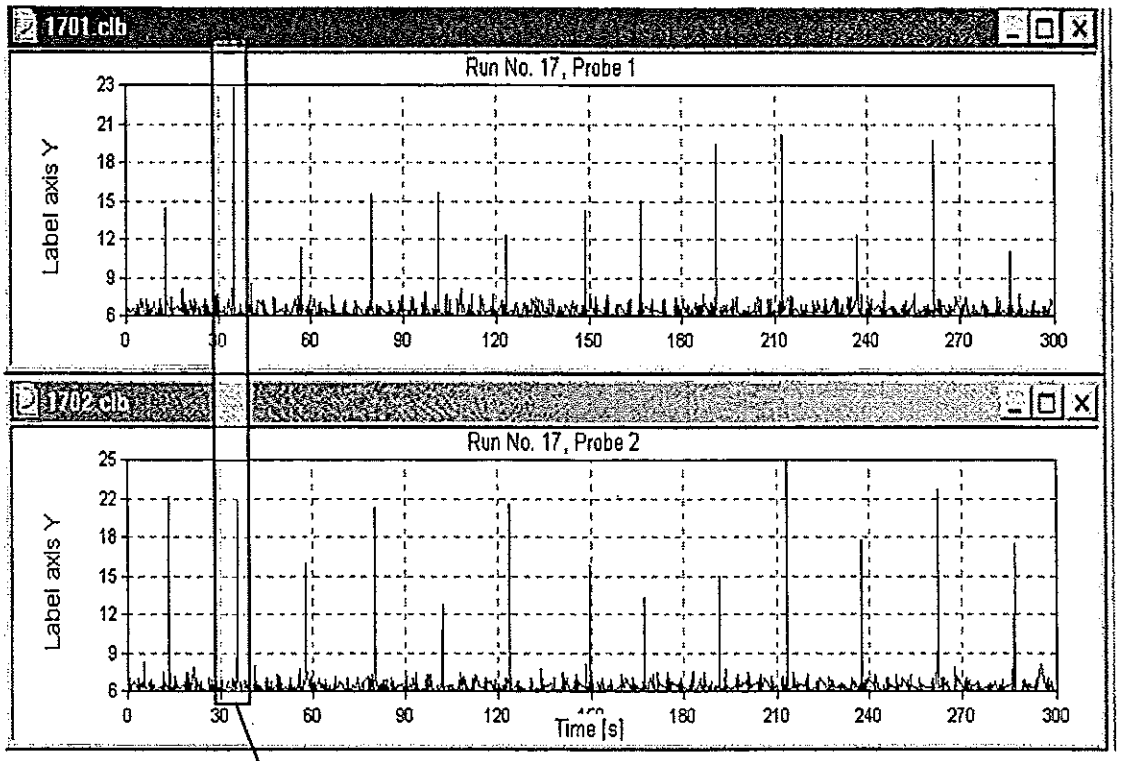

Figure. 2. Count rates recorded by the last two probes in measurement Wro17

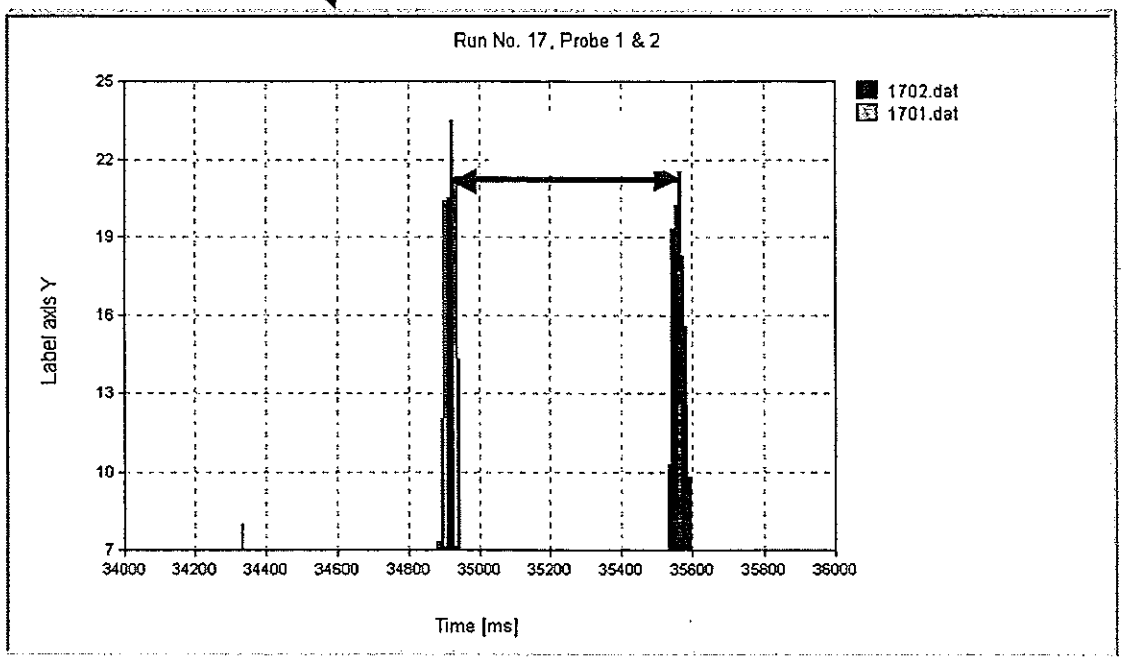

Figure. 3. Determination of single stone transportation delay in measurement Wro17

From this figure one can read transportation delay of stone equal to 643 ms, what at distances between probes 2006 mm, gives speed 3.120 m/s.
Analysis of several circulations of labeled stones through measuring - section settled between probes 1 and 2 shows Fig. 4. It is easy to notice that the most probable delay is equal to 643 ms, what gives average velocity of labeled stones on 3.120 m/s.

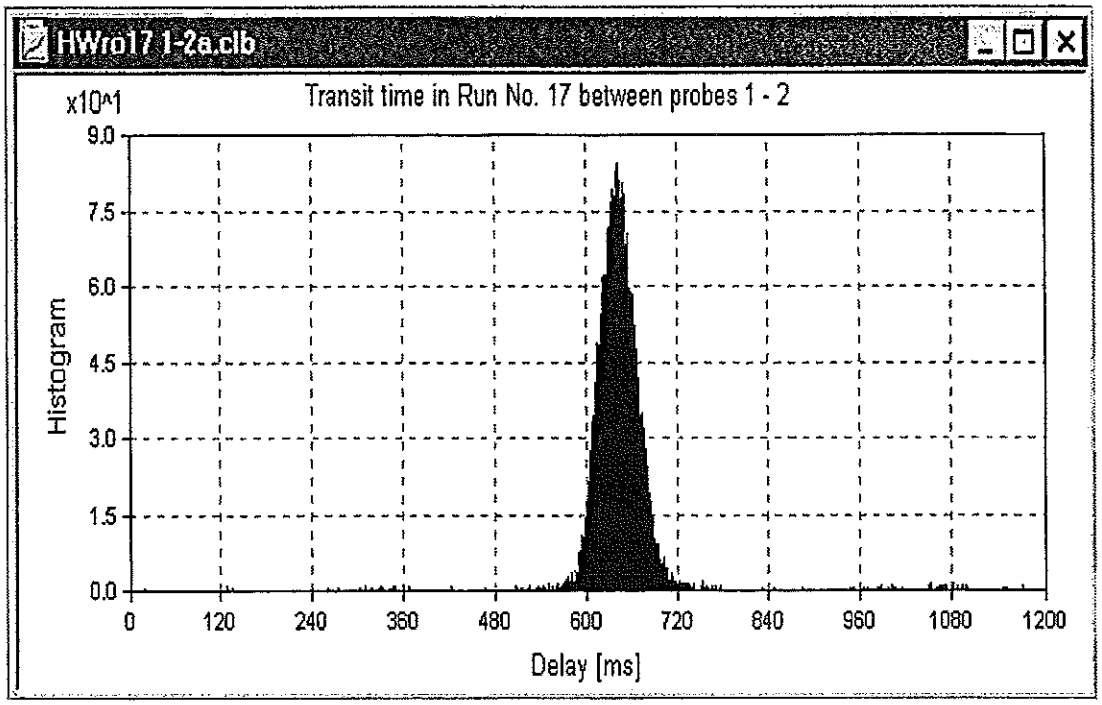

Figure 4. Histogram representing RTD of great stones (ϕ = 30 mm) in pipe section between probes 5 and 6 (Wro17)

In similar way the RTD of labeled fraction in vertical pipe were observe due to signals obtain from applied probes.

Table 1. Transportation delays in experiment Wro17

Delay [ms]					
$t_{d1,2}$	$t_{d2,5}$	$t_{d5,6}$	$t_{d1,5}$	$t_{d2,6}$	$t_{d1,6}$
643	605	660	1242	1261	1893

Table 2. Precision of experiment Wro17

Delay [ms]			Error [%]
$t_{d1,2} + t_{d2,5}$	$t_{d1,5}$	Difference	
1248	1242	6	0.5
$t_{d2,5} + t_{d5,6}$	$t_{d2,6}$		
1265	1261	4	0.3
$\Sigma t_{d1,2,5,6}$	$t_{d1,6}$		
1908	1893	15	0.8

Comparison of transportation delay values derived from signals delivered by probes shown in Fig. 1, gives possibility to evaluation measurement's precision. Errors presented in the last column of Table 2 are result of mostly fluctuations of stones path in stream then measurement errors.

In experiment Wro17, radioisotope was used for labeling the greatest class of stones (ϕ = 30 mm). In Table 3 is easy to observe increasing velocity of stones in vertical column.

Table 3. Velocity of great stones (ϕ = 30 mm) in experiment Wro17

$v_{1,2}$	$v_{2,5}$	$v_{5,6}$	Mean	Std	
m/s	m/s	m/s	m/s	m/s	%
3.12	3.17	3.19	3.16	0.03	0.9

Detailed analysis of recorded data reveals, however, how hard is reduction of fluctuations of hydromixture density and velocity of flow in industry. That limits applicability of long lasting repetition of radiotracer measurements. In consequence, in the following experiments, the sealed sources and radiotracers were applied simultaneously. Single probes, without sealed sources, gives signals describing concentration of tracers. The γ transmission sets, recorded the both, radiation emitted by tracer and sealed source. Example of such results, recorded by the first two probes in experiment Wro28 is presented in Fig. 5. It is easy to recognize that during record of γ radiation intensity, emitted by sealed americium source, small stone (ϕ = 5 mm), with ^{82}Br inside was injected.

Due to advanced software for data processing, separation of signals representing radiotracer concentration from those describing absorption of γ radiation, was obtained. Application of that idea to slip velocity evaluation of the labeled fraction presents Fig. 6. The solid fraction of total hydromixture in measurement Wro28, consists of particles which diameter varies from 5 to 35 mm (KWro28 1-2abs1.dat). RTD representing that flow was compared with similar distribution obtained from signals representing the smallest particles (ϕ = 5 mm).

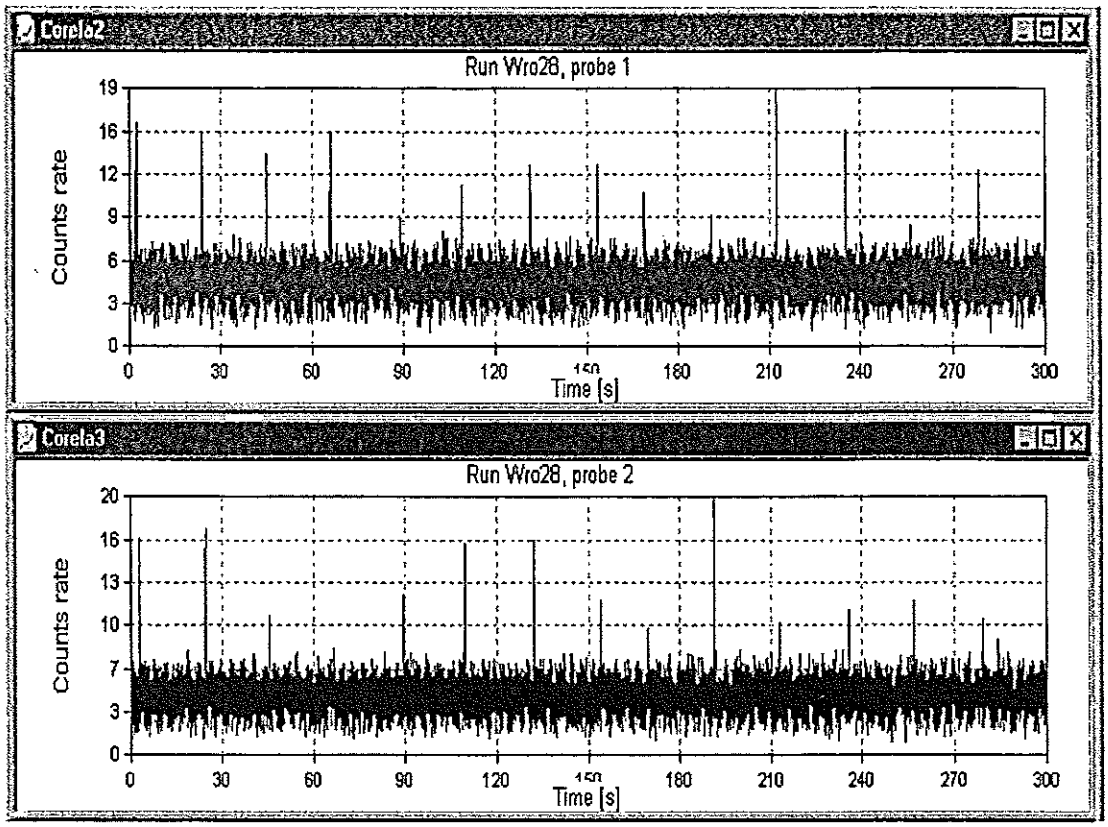

Fig. 5. Count rates recorded by the first two probes in measurement 28

The above data allow determination of transportation delay distribution by cross correlation analysis, separately for radiation emitted by tracer and γ radiation beam emitted by americium source. Results are presented in Fig.6. The mean transportation delay of total mixture (broad distribution) is equal to 565 ms, but delay of small number of labeled stones (narrow distribution) is equal 578 ms. This figures gives mean velocity of stream equal to 3.55 and 3.47 m/s as velocity of small stones.

In the same way analysis of all particle's transportation was analyzed when velocity of water varying from 2.0 m/s up to 5.0 m/s. During series of experiment, feeding of solid fraction in flow was hard to keep stable. In result, variations of density forcing fluctuations of slip velocity were observed. Figure 7 presents slip velocity of manganite pebbles in vertical pipe in relation to water velocity. Significant dispersion of obtained data results from density and shape of solid particles variation. That phenomena will be in detail study in the new experiments planned for this year.

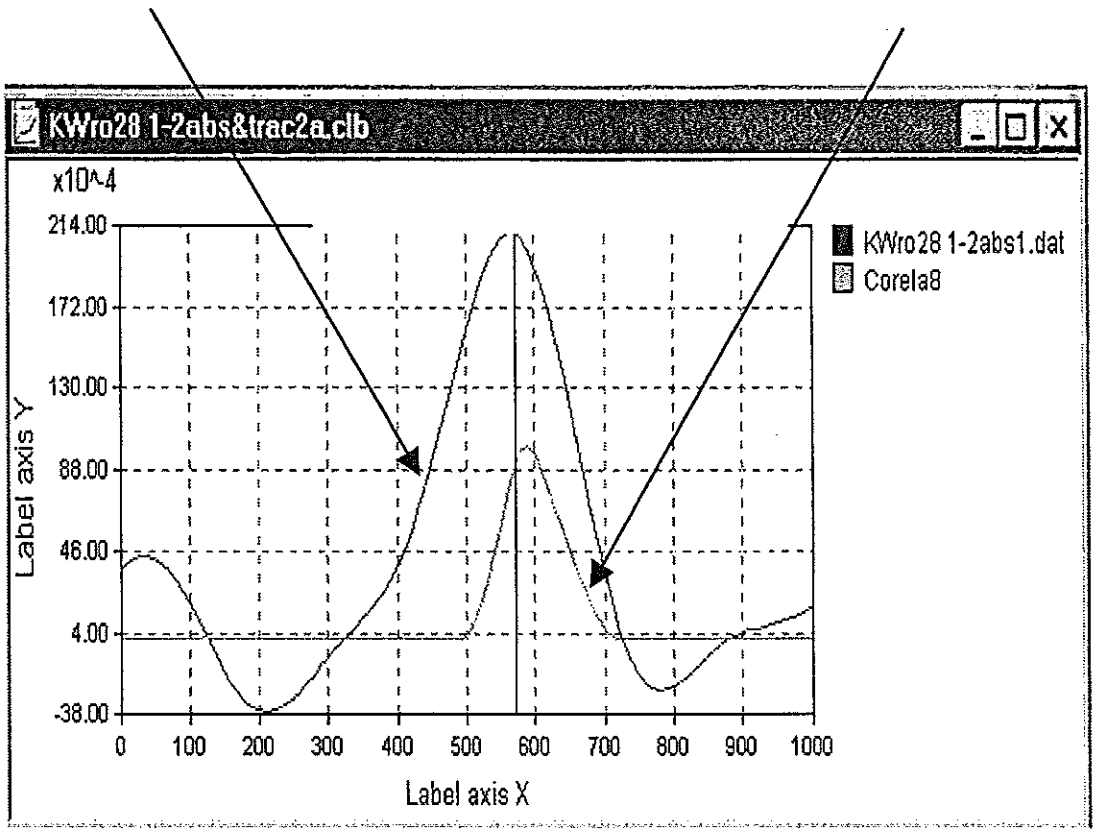

Figure 6. Cross – correlation distributions obtained in experiment Wro28

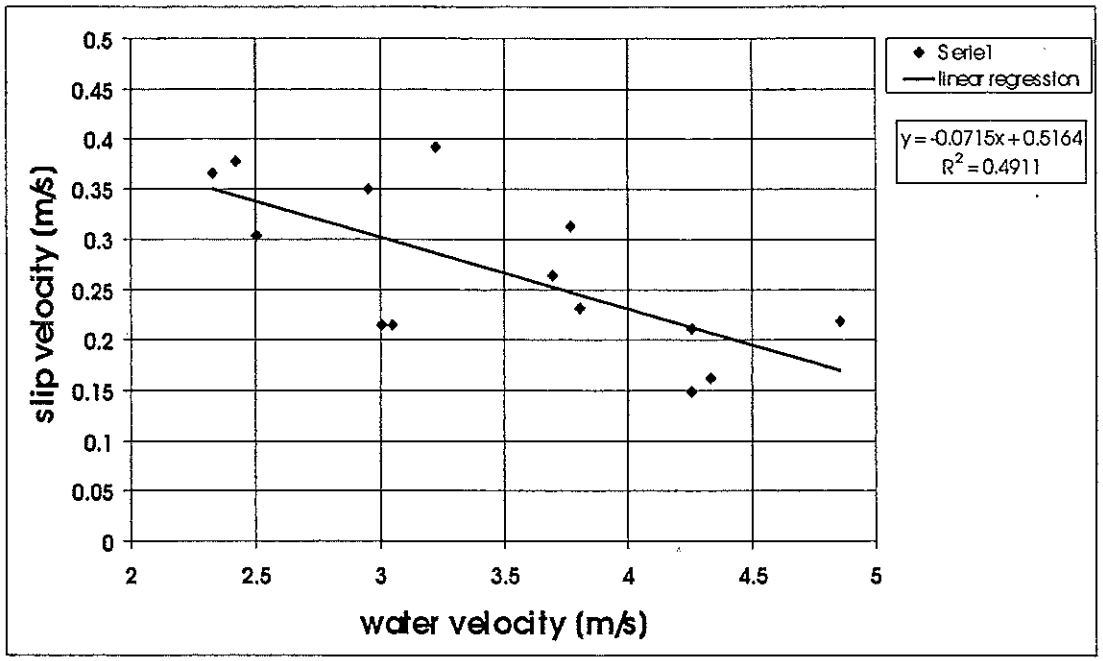

Figure 7. Slip velocity variation of manite pebbles

CONCLUSIONS

Presented results illustrating how simultaneous application of sealed radioactive sources and tracers may help in two phase flow analysis. In the proposed method continuous examination of stream density by γ beam was complemented by repetition of radiotracer measurements. Use of four probes for each of those methods gives possibility of checking accuracy of obtained results. Short sampling time and high efficiency of scintillation probes facilitates proper conduction of experiments. In consequence error of velocity measuring was kept below 1%. Also application of cross correlation analysis helps in proper processing of great number of data and delivers proper values of velocity.

In consequence the proposed measurements may be applied in examination of complex industrial two phase flows.

REFERENCES

[1] Przewlocki, K., Furman, L., Petryka, L., Stegowski, Z., Kaminski, J., *Measurements of slip velocities in the vertical pipes of sand-stone-water slurries,* J. Hydrol. Hydromech, 44, No 1, (1996) 3 – 11,

[2] Petryka, L., Oszajec, J., *The cross-correlation method of solid particle velocity measurements in industry,* Nuclear Geophysics vol. 7, No 2, (1993) 323 – 333,

[3] Petryka, L., Keblowski, R., *Precise velocity measurements in two-phase flow by means of sealed radioactive sources,* Report no. 9326 for International Atomic Energy Agency, (1999) 1 – 28,

[4] Max, J., (1972) "methodes et techniques du traitment du signal et application aux mesures physiques", Vol 1, Pricipes et apparellage de traitement en temps reel. Paris

B B3 - CHEMICAL ENGINEERING

PROBING OF MULTIPHASE OPAQUE FLOWS BY RADIOACTIVE TECHNIQUES

M.P. Dudukovic[1] and B.A. Toseland[2]

[1]Chemical Reaction Engineering Laboratory, Campus Box 1198, Washington University, St. Louis, MO 63130-4899, USA
[2]Air Products and Chemicals, Allentown, PA, 18195, USA

EXTENDED ABSTRACT. Multiphase flows are frequently encountered in numerous and diverse industries such as chemical, petroleum and petrochemical processing, food production, manufacture of specialty chemicals, pharmaceuticals and materials, extraction and refining of metals, biotechnology. Examples are gas-solid flows (bubbling and churn-turbulent fluidized beds, dense risers, pneumatic conveying, etc.), liquid-solid flows (fluidized beds, risers, conveying of solids), gas-liquid-solid flows (slurries in agitated tanks, bubble columns, three phase fluidized beds). These systems are frequently operated in churn turbulent flow conditions and contain a large volume fraction of the dispersed phase, which makes them opaque and inaccessible to probing with optical techniques, such as PID, LDV, LDA etc,, that are usually employed in fluid dynamics. Yet the need for measurement of fluid dynamic quantities such as phase holdup and phase velocity distributions is acute since predictive techniques or models for such multiphase flows, with highly concentrated dispersed phase at churn-turbulent flow conditions, are not readily available. Two relatively recent reviews [1,2] pointed out that among the available noninvasive techniques for tomographic and velocimetry measurements in multiphase flows those based on the use of radioactive materials seem very promising.

In this presentation only gamma ray based tomography, velocimetry and tracer techniques are discussed with the focus on the recent work accomplished in our Chemical Reaction Engineering Laboratory (CREL). At CREL we have developed, designed, constructed and operated our own gamma ray based third generation computer tomography CT scanner [3,4]. The 100 mCi encapsulated Cs137 source is rotated 360° around the cylindrical vessel (column) being scanned together with the fan beam of collimated sodium iodine detectors facing the source. Spatial resolution better than 5 mm and a density resolution better than 0.04 g/cm^3 are achieved with the original scanner. The CT unit is used to obtain gas holdup profiles in bubble columns at high pressure and high superficial gas velocity as well as solids holdup profiles in risers. The improvement in the scanner allowing resolutions of 1mm and its use in detecting holdup profiles in packed beds and stirred tanks are also discussed.

The Computer Aided Radioactive Particle Tracking (CARPT) technique, introduced by Lin et al [5], has been further developed in CREL as a powerful tool for evaluation of the velocity field in opaque multiphase systems [6,7,8,9]. In CARPT one monitors the motion of a single gamma ray emitting particle (Sc46 is used in CREL) by an array of scintillation detectors located strategically all around the column. For monitoring liquid motion in bubble columns a neutrally bouyant tracer particle is used (a composite of polypropylene, air and scandium). For monitoring the motion of solids in fluidized beds, risers and stirred tanks, the tracer particle of the size and density representative of the solids in the system is prepared and used. New experimental results regarding ensemble averaged liquid and solids motion in bubble columns and liquid-solid risers, respectively, are presented together with the evaluation of backmixing parameters. The wealth of information regarding turbulent stresses, eddy diffusivities, velocity auto-correlations and cross-correlations, residence time distributions, mixing etc. is outlined. The use and utility of CARPT-CT in validation of CFD models is also described.

CARPT-CT techniques allow probing of multiphase systems in laboratory and pilot plant scale, and the data is mainly used for validation of CFD models and for the development of phenomenological, physically based,

models for the observed flow patterns. An example of such a phenomenological model for bubble column reactors is reviewed [10]. In operating pilot plants or commercial reactors there are some possibilities for CT implementation but the chances of conducting CARPT experiments are at present more remote. However, gamma ray densitometry and pressure drop measurements can provide information regarding the gas holdup profile in bubble columns which then could be used in a phenomenological model to predict liquid recirculation [10,11]. Radioactive tracer studies using gas and liquid tracers provide the information on overall mixing in the column which can be successfully interpreted with the developed phenomenological model. Examples of our bubble column work at LaPorte, Texas are presented.

In summary, techniques based on the use of radioactive isotopes are capable of providing a wealth of information about opaque multiphase flows. Modern techniques like CT and CARPT provide not only time averaged holdup and velocity patterns in the system but also reveal the detailed description of flow structures and large scale turbulence. Classical tracer impulse response studies provide an insight into the overall flow patterns in the system and are useful in testing the phenomenological and CFD models.

ACKNOWLEDGEMENT

Both authors would like to acknowledge the support of the US Department of Energy (DOE-FC-PC 95051) which made the CARPT-CT and tracer work possible. M.D. is also grateful for the support of industrial sponsors of CREL.
This presentation summarizes the work of many people whose contributions we gratefully acknowledge. They are N. Devanathan, Y. Yang, S. Degaleesan, J. Chen, A. Kemoun, B. Saennes, N. Rados, B.C. Ong, M. Al-Dahhan, P. Gupta and others.

REFERENCES

[1] Chaouki, J., Larachi,, F. and Dudukovic, M.P. (eds), "*Non-Invasive Monitoring of Multiphase Flows*", Elsevier, Amsterdam (1997)
[2] Chaouki, J., Larachi, F. and Dudukovic, M.P., "*Non-Invasive Tomographic and Velocimetric Monitoring of Multiphase Flows*", Ind. & Eng. Chem. Research, 36(11) (1997), 4476-4503
[3] Kumar, S.B, Moslemian, D., and Dudukovic, M.P., "*A Gamma Ray Tomographic Scanner for Imaging Void Fraction Distribution in Bubble Columns*", Flow. Meas. Instr., Vol. 6(1) (1995), 61-73
[4] Kumar, S.B. and Dudukovic, M.P., "*Computer Assisted Gamma and X-ray Tomography: Applications to Multiphase Flow Systems*", Ch. 2, 47-103 in (1) above
[5] Lin, J.S., Chen, M.M. and Chao, B.T., "*A Novel Radioactive Particle Tracking Facility for Measurement of Solids Motion in Gas Fluidized Beds*", AIChE Journal, 31 (1985), 465-473
[6] Devanathan, N., Moslemian, D. and Dudukovic, M.P., "*Flow Mapping in Bubble Columns Using CARPT*", Chem. Engg. Sci., 45 (1990), 2285-2291
[7] Degaleesan, S., "*Fluid Dynamic Measurements and Modeling of Liquid Mixing in Bubble Columns*", D.Sc. Thesis, Washington University, St. Louis (1997)
[8] Larachi, F., Chaouki, J., Kennedy, G. and Dudukovic, M.P., "*Radioactive Particle Tracking in Multiphase Reactors: Principles and Applications*", Ch. 11, 335-406 in (1), (1997)
[9] Roy, S., "*Quantification of Two Phase Flows in Liquid-Solid Risers*", D.Sc., Thesis, Washington University, St. Louis (2000)
[10] Degaleesan, S., Dudukovic, M.P., Toseland, B.A. and Bhatt, B.L., "*A Two Compartment Convective Diffusion Model for Slurry Bubble Column Reactors*", Ind. & Eng. Chem. Research, 36(11) (1997), 4670-4680
[11] Gupta, P., Ong, B.C., Al-Dahhan, M., Dudukovic, M.P. and Toseland, B.A., "*Hydrodynamics of Churn Turbulent Bubble Columns: Gas-Liquid Recirculation and Mechanistic Modeling*", Catalysis Today, 2253 (2000), 1-17

RESEARCH AND DEVELOPMENT IN RADIOTRACER METHODOLOGY AND TECHNOLOGY

J. Thereska

International Atomic Energy Agency, Vienna, Austria

Abstract. An IAEA Coordinated Research Project (CRP) has promoted further the radiotracer technology, in particular has validated the residence time distribution (RTD) function in investigating many chemical engineering reactors, such as grinding mill and flotation cell, incinerator, crystallizer, trickle bed reactor and waste water treatment units.

INTRODUCTION

A Coordinated Research Project (CRP) on "Radiotracer technology for engineering unit operation studies" was undertaken by the International Atomic Energy Agency (IAEA) during 1998-2000 period. The main objective was to further develop and refine radiotracer methodology and promote new applications.

The basic radiotracer methodology consists in accurate formulation of the Residence Time Distribution (RTD) and its utilization for system analysis. This is almost a well-established methodology with universal applications, the trend of which is standardization and simplification through customizing in software and hardware and making it more safe, cost-effective and competitive.

Relevant target areas for radiotracer applications are defined. Though the technology is applicable across a broad industrial spectrum, the petroleum and petrochemical industries, mineral processing and waste-water treatment sectors are identified as the most appropriate target beneficiaries of radiotracer applications: these industries are widespread internationally and are of considerable economic and environmental importance.

RTD SOFTWARE

There were two RTD software's packages validated under the CRP, which can be considered as available standards in routine tracer work:

- The Progepi RTD software produced by the Laboratory of Chemical Engineering Sciences, Nancy, France. The Progepi RTD software is intended for researchers and engineers to simulate the outlet of flow compartment models to an injection of tracer. It allows the user to simulate the response to any input of any complex network of elementary interconnected basic flow patterns.

- The CTU RTD software prepared by the Department of Process Engineering of the Czech Technical University of Prague, Czech Republic. The last version was completed under the IAEA support.

In general, both software are useful for evaluation and processing of tracer experiments. The Progepi software has a modern front/end (Windows) and is more user friendly than the CTU one (MS DOS based).

RTD VALIDATION IN CASE STUDIES

Following didactic RTD case studies have been selected:
Study of laboratory scale continuous ore grinding mill;
Heavy metal release in a pilot scale municipal solid waste incinerator;
Massecuite fluid flow in sugar crystallization process;
Liquid flow in trickle bed reactors;
Liquid flow in leaching tanks.

1. Study of laboratory scale continuous ore grinding mill

Radiotracer tests were conducted in a laboratory scale continuous mill. Water tracer was ^{137m}Ba. The fine particles tend to behave very much like water. The difference in behavior of fine grains to larger size fractions was quite considerable. Tracer experiments have shown a classification effect: relative mean residence time of fine particles decreased as water was added to the process. This interesting indication means that increasing the amount of water in the process (decreasing slurry density) tends to improve the grinding result. This is quite opposite to industrial practice where high slurry densities are used.

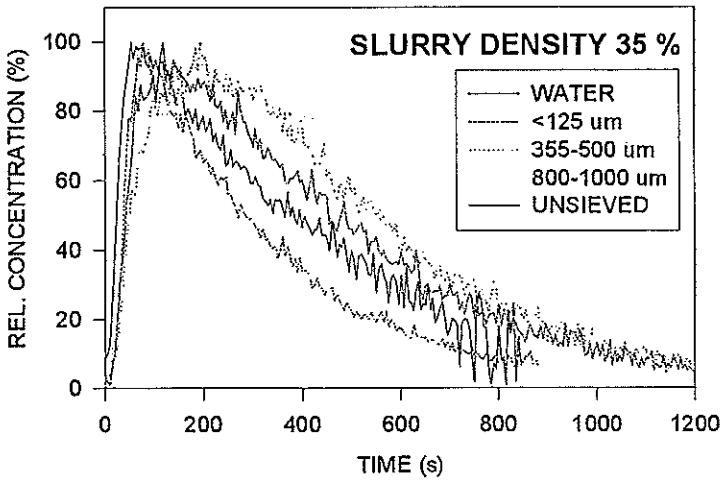

Fig. 1.: Experimental RTDs for Nickel ore

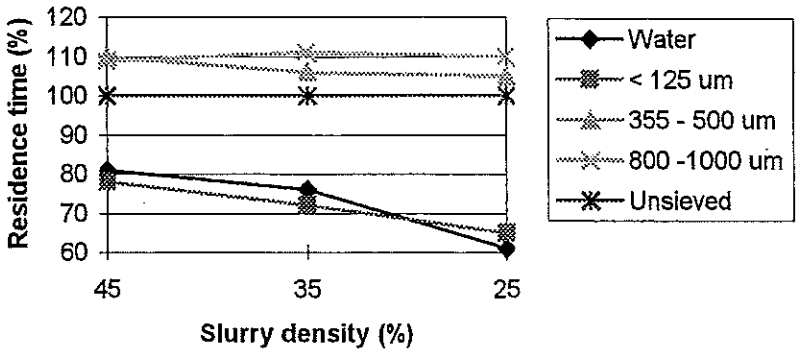

Fig. 2. Mean residence times of sieved fractions compared to the unsieved ore.

2. Heavy metal release in a pilot plant scale municipal solid waste incinerator

Heavy metal release in solid waste incinerator is an important problem in waste management. Zinc and copper are today two of the important heavy metals which cause environmental problems in the bottom ash. Both have quite different physico-chemical properties. Under the prevailing conditions zinc is a volatile and copper is a more or less non-volatile heavy metal.

200 mCi of ^{64}Cu and of ^{69m}Zn were used in each test. In addition, 200 mCi of $^{113m}In_2O_3$ was injected to determine the solid phase RTD within the incinerator. Alongside the grate the In-113m radiation was measured at six different detector positions. The RTD of material inside the grate was needed to localize the position of evaporation process into the grate.

Figure 3 reveals the differences between the evaporation behavior of copper and zinc inside the incinerator.

The slight evaporation of copper occurs gradually alongside the whole grate. 3 - 5 % of copper evaporated confirms the hypothesis that even under chemically favorable conditions no substantial copper evaporation occurs.

The intensive evaporation of zinc takes place very fast in a special narrow area inside the grate. The place of the intensive evaporation depends on the operating conditions, but always is located at high temperature part of the grate, where the reducing conditions are more evident. The zinc evaporation can reach up to 100%.

The radiotracer tests in the pilot plant confirmed the hypotheses that reducing conditions in connection with high temperatures enhance the evaporation of zinc. Copper, as non-volatile heavy metal is not evaporated significantly from the furnace bed as expected.

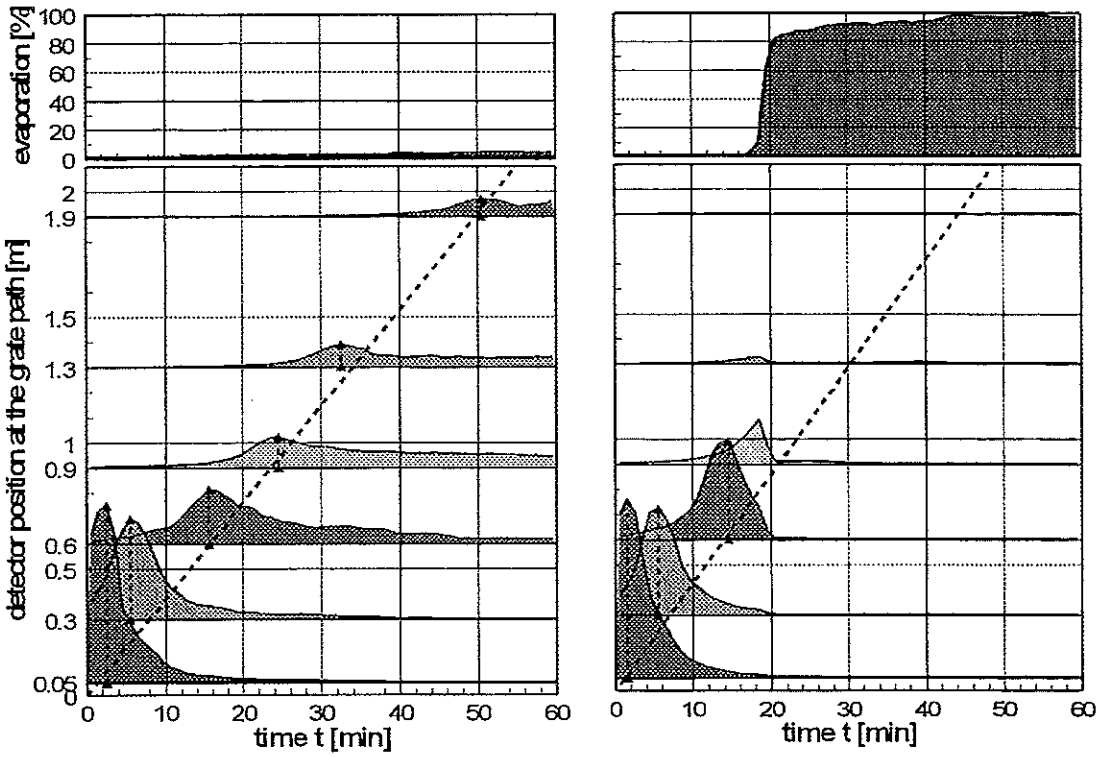

Fig. 3. Copper and zinc RTD inside the grate and in the absorber

3. Massecuite fluid flow in sugar crystallization process

The role of exhaustion low-grade crystallizer in a sugar factory is to reduce loss of sucrose in separated molasses that exit the process. Several types of crystallizers have been designed, each of them operating under specific conditions.

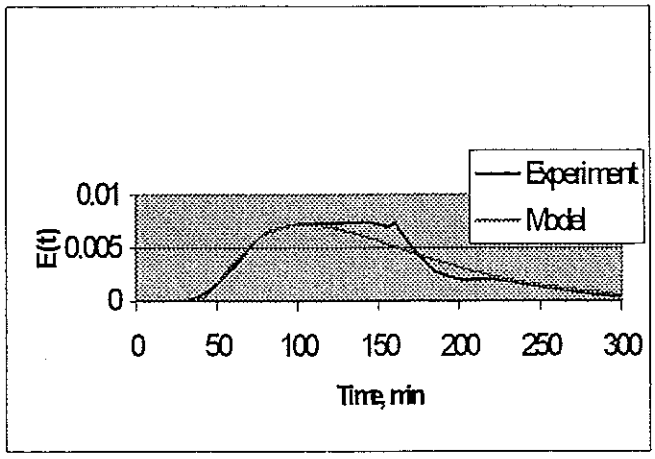

Fig. 4. RTD of Crystallizer and its model

Radiotracer tests using Tc-99m were performed. The fitting of experimental curve with RTD model was satisfactory (Fig.4). The model consists of an initial plug flow reactor (which reflects the inlet of the pumped massecuite) followed by two parallel paths (flows), one represents a plug flow reactor connected to a perfect mixing cell in series with backmixing and the other shows a plug flow reactor connected directly to the exit.

4. Liquid flow in trickle bed reactor

Trickle bed reactor (TBR) is a reactor in which a liquid and a gas phase flow concurrently downwards through a fixed bed of catalyst particles while the reaction takes place.

The trickle bed reactors are designed to behave as a plug flow reactors. However, some axial intermixing is always inevitable. The simple axial dispersion model is suitable to describe hydrodynamics of packed bed systems having no stagnant regions and nonporous packing. The model fails to describe the long tail present in experimental RTD curves. The long tails may carry useful information about the process.

To describe the RTD curves with long tail, Villermaux and Van Swaaij (1969) proposed the Axial Dispersion-Plug Flow with Exchange (ADPE) Model (exchange between dynamic and stagnant regions).

The model contains four parameters: the residence time τ, the dynamic fraction of liquid φ, the number of transfer units N, and the Peclet number Pe. It is clear that this model reduces to axial dispersion model for N=0.

The moments of the distribution function for C_1 at the exit of the reactor can be calculated directly by Laplace transform. The non-dimensional mean residence time and variance are calculated as:

$$M_1 = 1 + \frac{1}{Pe}$$

$$\sigma^2 = \frac{2}{Pe} + \frac{3}{Pe^2} + \frac{2(1-\varphi)^2}{N}\left(\frac{1}{Pe} + 1\right)$$

The above-described ADPE model was used to simulate RTD data obtained in trickle bed reactor (Fig. 5).

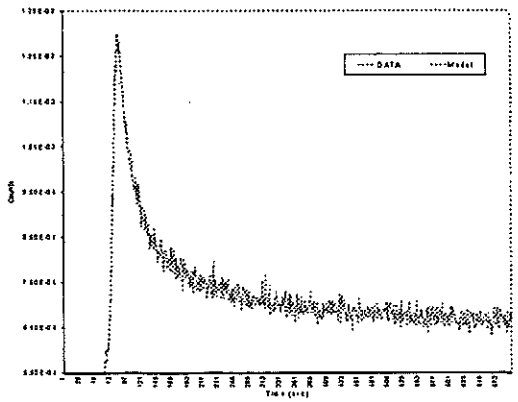

Fig. 5. Model simulation curves for a trickle bad reactor

5. Radiotracer investigation of wastewater treatment plant

In the frame of the CRP, tracer investigations have been conducted in a number of wastewater plants, in Islamabad (Pakistan), Plock (Poland), Havana (Cuba) and Nancy (France).

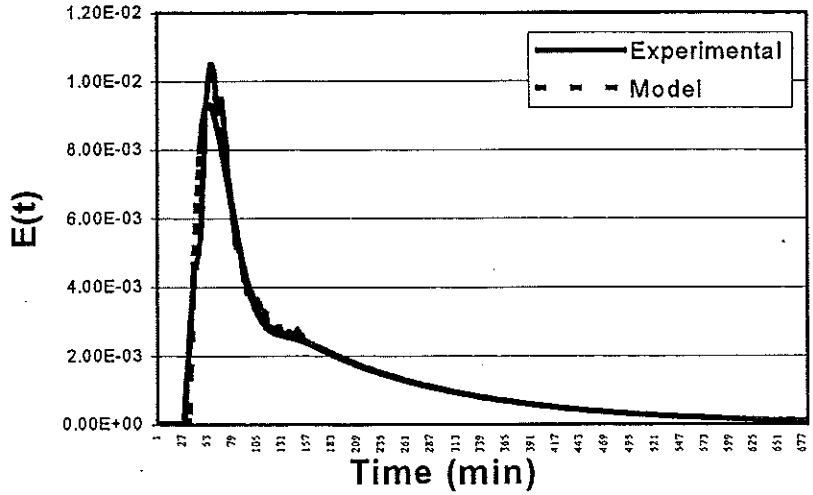

Fig. 6. Typical tracer output from settling tank

Typical RTD of water phase in settling tank (Fig.6) shows that the model is composed of a main stream going from the inlet to the outlet with a recirculation on the bottom of the tank.

Due to high gas flow rate, tracer experiments conducted in aeration tank have shown that water and sludge have generally similar flow behavior. The fluid flow can be modeled either by perfect mixing cells in series or by perfect mixing cells in series with back mixing (fig.7). The number of mixing cells is a function of both gas and water flowrates but also of the geometrical configuration.

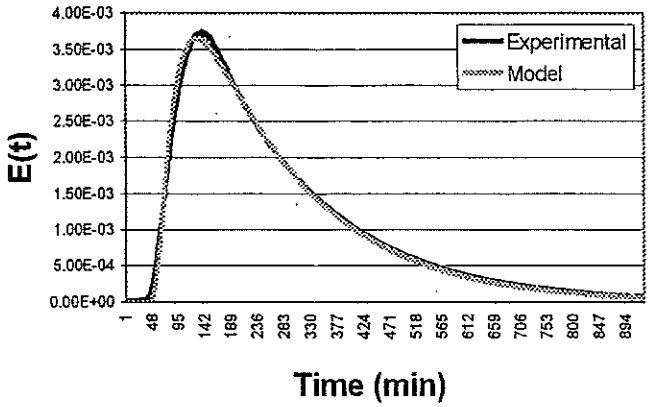

Fig.7. Typical tracer output for aeration tank.

The following figure, as an example, shows the experimental RTD curve and its model for a clarifier.

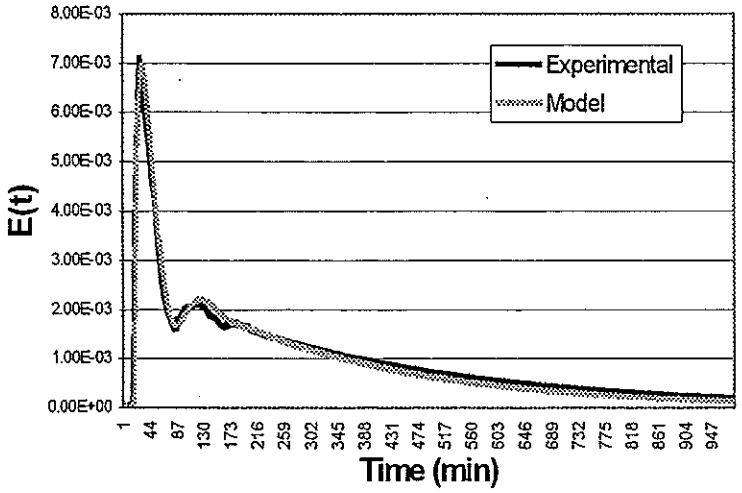

Fig. 8. Experimental RTD curve and its model for a clarifier

The model is reproduced in the following figure:

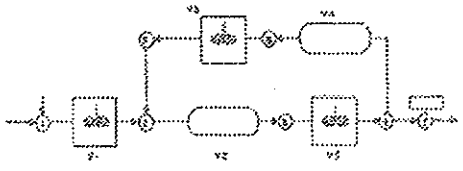

Fig.9. V1, V3, V5 represent perfect mixing, whereas V2, V4 are plug flow modules

6. RTD application for analyzing gold slurry leaching tanks

Pongkor Gold Mine in Indonesia was planned to process 182 500 tons of free gold oxide ore per year with a total recovery of 95% for gold and 60 % for silver. The overall flow rate through leaching tanks was 65 m3/h in average with fluctuations going from 55 to 75 m3/h .

The main objectives of the radiotracer investigation were:
- to measure slurry retention time of tank 1 (volume 1000 m3) and tanks 7 and 8 (volume 290 m3), as the most important tanks in leaching process,
- to obtain information on mixing and to measure or locate possible malfunctions inside these processing tanks.

Potassium bromide KBr-82 liquid radiotracer was injected. The experimental curve obtained in tank 1 is presented below (Fig.10).

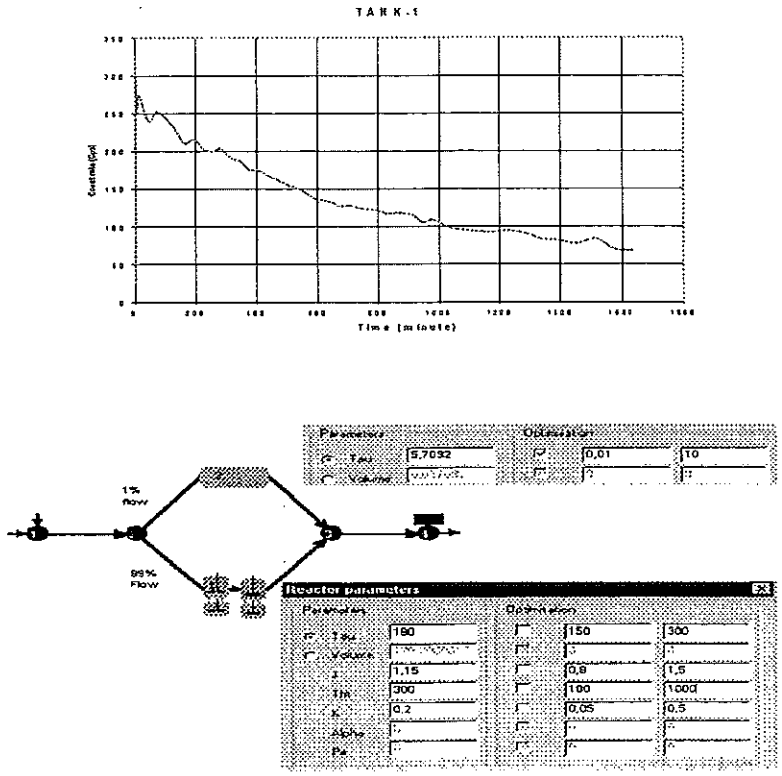

Fig.10. The experimental curve and model at the output of tank 1

The main exponential curve represents the main flow of slurry inside the tanks and shows a perfect mixing process. Model of perfect mixer + exchange with stagnant zone + surface flow fits well. In tank 1 the mixing is perfect in 87 % of the total volume, in tank 7 in only 72 %, and in tank 8 in 75 % of the total volume. In tanks 7 and 8 nearly 25-28% of total volume is almost dead.

The higher peak at the beginning of the curve, just a few minutes after the radiotracer was injected, show the by-pass or short-circuit. This surface flow is more evident in tank 1, where from modeling it was estimated to 3-5 percent of total flow rate, while in tank 7 it was 1-2%.

QUALITY CONTROL AND STANDARDIZATION IN TRACER WORK

Quality control of industrial tracer services is an important aspect of tracer technology nowadays. It has to be expected that the issue of quality assurance, certification and accreditation will become of increasing importance for tracer groups in the near future, as they provide and sell services to customers. In Finland, flow measurements have obtained accreditation. In France, CEA works to obtain the ISO 9001 accreditation.

Standardization of methods and procedures within tracer applications is so far limited to the 25-year old ISO standards for flow measurements. The CRP has envisaged that specific activities such as leak detection, thin layer activation, mercury inventory and formulation of RTD function for troubleshooting can be suitable for standardization. Modeling and interpretation of results, however, seem beyond the scope of standardization. To prepare an ISO standard takes great efforts, and a clearly expressed need from the end-users is required to justify said effort. The issue of standardization of tracer studies should be further assessed by the Agency. It is time to think about establishment of an International Tracer Society, similar to NDT society.

COST-BENEFIT ANALYSIS

It is generally accepted that the benefits resulting from radiotracer applications exceed the cost of equipment and studies at least several folds. Based on a retrospective analysis of the data, it was found that the average cost-benefit ratio has been about 1:20 in many routine troubleshooting applications. However, in some instances remarkable benefits were derived, as for example, 1:4500 for leak detection in the petroleum industry.

There are few short-term investments, which will give a return of this magnitude. The cost effectiveness of radiotracer applications should be widely promulgated to encourage industrialists to take full advantage of the technology.

TRENDS IN TRACER TECHNOLOGY RESEARCH AND DEVELOPMENT

1. Integration of RTD tracing with CFD simulation for industrial process visualization and optimization

At present, two methods are used for investigation of industrial complex processes, radiotracer residence time distribution (RTD) experimental technique (systemic analysis), and computer fluid dynamics (CFD) simulation. The numerical simulation

of complex systems through Computational Fluid Dynamics (CFD) methods is a new approach more powerful for process visualization.

The real time experimental RTD tracing is simple and reliable; it provides various important hydrodynamic parameters but it is impossible to localize and visualize flow pattern inside the systems. The CFD is a fine and predictive analysis, which provides nice spatial pictures of the insight of a process, such as flow patterns and velocity map. Due to lack of physical experimental data the CFD calculation provides qualitative results only, especially in systems with strong interaction of hydrodynamics with physico-chemical reactions. This is the reason why CFD models have to be verified and validated by experimental tracer RTD results.

The RTD-CFD interaction is both sides. The CFD can be used also to complement the information obtained from the RTD systemic approach. CFD provides data that can quantify RTD systemic model, which means the CFD model, can "degenerate" into more quantitative RTD systemic analysis, providing more comprehensive results for chemical engineers. In fact, these two approaches, experimental and numerical, are complementary to each other. The RTD systemic approach detects and characterizes main features of the flow (mixing and recirculations) while CFD enables to locate them. The trend is to combine experimental and numerical approaches in order to obtain reliable quantitative results for industrial complex processes.

2. Radiometric techniques for multiphase flow determination

Accurate measurement of flow in multi-phase systems (e.g. liquid-solid, solid-gas or gas/water/oil) is of great interest in many industrial processes, especially in oil, coal and mining industries, mineral ore processing, chemical and petrochemical plants, and long distance fluid transportation pipelines.

The radiotracer technique based on injection of radiotracer into the system provides accurate results mainly in mono-phase flows. Radiotracer technique is used mostly for calibration of flow meters than for continuous flow rate measurements. Gamma-ray transmission technique, known as gamma ray cross correlation technique, seems attractive for on-line flow rate measurement, in particular in multiphase flows. A possible new CRP on "Radiometric Techniques for Multiphase Flow Determination" would be relevant in this respect.

3.Radiotracer imaging techniques for industrial process visualization

New development is expected in introducing new radiotracers 2D and 3D imaging techniques for localization and visualization of flow patterns in multiphase systems.

Among the various techniques, the Single Photon Emission Computed Tomography (SPECT) method shows some promise. 2D imaging with a gamma-camera is also an attractive device at the laboratory scale. Single particle tracking technique has been developing, in particular to investigate fluidized bed reactors.

The emission tomography is the last step in research and development in radiotracer methodology. The real time imaging techniques for flow pattern visualization inside vessels are important for detecting troubleshooting of gas, liquid or solid phases. This trend is quite similar to nuclear medicine imaging.

The emission tomography provide two-dimensional maps of the count rates which, when properly interpreted, yield the radiotracer instantaneous concentration field. Coupled with single radioactive particle tracking, which yields the velocity field, the above techniques complement each other and provide unique means for quantification of multiphase opaque flow fields which cannot be accomplished by any other means. A potential CRP could be initiated to validate radiotracer-imaging techniques for visualization of fluid patterns inside structures for industrial process design and optimization.

ACKNOWLEDGMENTS

We wish to thank experts from Argentina, China P.R., Cuba, Czech Republic, Denmark, Finland, France, Germany, India, Norway, Pakistan and Poland for their contribution to the IAEA Coordinated Research Project (CRP).

REFERENCES

[1] Guidebook on Radioisotope Tracers in Industry Technical Reports Series No.316, IAEA, Vienna (1990).
[2] Hintikka VV, Kalapudas RP & Viitanen PI. (1999) Effect of Rheology of Grinding Efficiency in the Laboratory Scale Continuous Classifying Mill. Mineral Processing and Extractive Metallurgy Review, Vol 20. Numbers 1-3. pp. 133-154.
[3]. Niemi, A.J., Thereska, J., Plasari, E., Kacaj, M. Tracer studies of flotation in the laboratory and in mineral processing plant. Nuclear Geophysics, Vol. 7, No.2, pp. 305-311, 1993
[4] Leclerc J.P., Claudel S., Lintz H.G., Potier O. and Antoine B. "Theoretical Interpretation of Residence-Time Distribution Measurements in Industrial Processes", Oil & Gas Science and Technology – Rev. IFP, Vol. 55, No.2, pp.159-169 (2000)
[5] Sevel T., Pedersen N.H., Genders S. "Tracing of Oil, Gas, and Water in the Oil and Gas Industry", 7th ECNDT Conference, 26-29 May (1998)
[6] Zitny, R., Thyn, J. Residence Time Distribution Software Analysis, User's Manual, IAEA Computer Manual Series, Vienna (1996).
[7] Thyn J.Zitny R., J.Kluson, T.Cechak; Analysis and diagnostics of industrial processes by radiotracers and radioisotope sealed sources, CVUT, Prague, 2000
[8] Chmielewski A.G., Palige J. Radiotracer investigations of industrial wastewater equalizer-clarifiers, Nukleonika, Vol. 43, No. 2, 1998, p 185-194.
[9] Plasari, E., Thereska, J., Leclerc, J.P., Villermaux, J. Tracer experiments and residence-time distributions in the analysis of industrial units: case studies. Nukleonika, Vol. 44 No. 1 p.39-58, 1999, Poland.

DETERMINATION OF ORIFICE GAS FLOW IN A MODEL INTERCONNECTED GAS-SOLID FLUIDISED-BEDS SYSTEM USING ^{81m}Kr AS RADIOTRACER

Z. I. Kolar[1], C. S. Stellema[1,2], M. N. Boers[1,2], R. Dekkers[3], A. W. Gerritsen[2], C. M. van den Bleek[2]

[1] Department of Radiochemistry, Interfaculty Reactor Institute, Delft University of Technology, Mekelweg 15, 2629 JB Delft, THE NETHERLANDS
[2] Chemical Reactor Engineering Section, Department DelftChemTech, Faculty of Applied Sciences, Delft University of Technology, Julianalaan 136, 2628 BL Delft, THE NETHERLANDS
[3] Amersham Cygne, Den Dolech 2, 5612 Eindhoven, THE NETHERLANDS

Abstract. Short-lived ^{81m}Kr (half-life 13.3 s) obtained from a commercial ^{81}Rb/^{81m}Kr generator was used as the radiotracer for air in four-scintillation detectors aided measurements of air flow through an orifice connecting two gas-solid fluidised-beds of a four-bed interconnected fluidised-beds laboratory scale model system. By applying different aeration rates to the beds the solids were kept circulating through the system (passing two orifices and two overflow weirs). The aim of the study was the determination of the rate of the (undesirable) airflow through the orifice. It appeared that although the net flow was unidirectional it was actually a resultant of two substantial but oppositely directed flows of air in each of the orifices.

INTRODUCTION

1. Interconnected fluidised-beds

Many chemical processes require a steady circulation of solids between different reaction vessels. Particularly in the petroleum industry, the development of catalytic cracking represented the first practical use of solids circulation systems. In such systems the high conveying velocity in pipelines between vessels often results in excessive mechanical damage (attrition) of solids.

Attempts to circumvent this problem led to design of interconnected fluidised-beds reactors or systems in the early eighties [1-2]. These reactors consist of a number of fluidised-beds often interconnected via submerged orifices and overflow weirs. By applying different aeration rates to the beds the solids are kept circulating through the system, flowing from downcomers to risers via orifices and from risers to downcomers over the weirs and so on.

Since the advent of the interconnected fluidised-beds the mechanisms or driving forces underlying the auto-circulation of solids in systems consisting of two or more separate but mutually connected fluidised beds has been a widely studied topic [1-3]. Research and development of such systems to be used for continuous handling and chemical processing of solids is also one of the research areas of the Delft University of Technology. One of the possible applications of the interconnected fluidised-beds systems is for the gas-solid acceptation/regeneration processes such as coal combustion combined with SO_2 absorption followed by regeneration of the absorber; all this within one interconnected-beds system. These studies dealt with

transport and mixing of solids and to lesser extent of gas in laboratory scale two- or four-bed systems [4-7].

One of the few ways of non-invasive probing of solids transport in gas-solid fluidised beds is by means of radiotracers i.e. solid particles labelled with a gamma rays emitting radionuclide. Such a particle can conveniently be monitored by means of external detectors of gamma radiation. The thus obtained data may provide information on the radiotracer whereabouts, information which eventually should lead to the elucidation of the mechanisms governing solids transport in (interconnected) fluidised beds. This approach has been used extensively in some of our studies of solids behaviour in an interconnected fluidised-beds system [8-11].

Circulation of solids and gas-solid contacting is the main purpose of interconnected fluidised-beds. Operational conditions are set to control the solids flow. A side effect is the gas flow through the orifices connecting downcomers to risers. This gas flow has two consequences. First it may result in a gas flow difference under and above the orifice, leading to other bed behaviour then expected from the set fluidisation velocity. The second consequence concerns the possible and even undesirable chemical reactions of fluidisation gas with contents of the adjacent beds. For the first reason only the net transoreficial gas flow is important, but for the second reason the bi-directional gas flows seems to be even more important.

The utility of the radiotracer method is not restricted to the investigation of solids behaviour only; it is equally applicable for studies of gas behaviour in gas-solids fluidised-beds. This paper describes the design and use of a non-invasive, radioactive gas-based radiotracer technique for measurements of aforementioned orifice gas flows in a laboratory-scale, four-bed, interconnected fluidised-beds system. All experiments were carried out with beds of fluidised glass particles.

2. Radiotracer and nucleonics

The radiotracer-aided measurements of transoreficial airflow were preceded by measurements in which helium was used as the tracer for air [5]. Disadvantages of this method are the possible disturbance of the beds by the measurement set-up, the large feed fractions of helium needed, low density of helium compared to air, diffusion effects and large number of concentration profile measurements required to determine gas flow at one set of conditions. The measurement of the net orifice gas flow was reproducible with an imprecision of less than 4%. However, systematic errors can be present.

A proper tracer should fulfil the basic requirements for an ideal tracer, namely that it has to be identical with the tracee in all its relevant physical and chemical properties and be applicable in a non-invasive way. To be feasible for air transport studies in a cold air fluidised bed of glass particles, the tracer for air (= tracee) should approximate its diffusion coefficient in air as closely as possible. Obviously an ideal tracer for air will be a gas species of air having diffusion coefficient value in air matching that of air in air. At T = 289.15 K the diffusion coefficient of air in air, is $D_{air,air}$ = 0.18 cm^2/s [12-13]. The analogous value for helium in air, is $D_{He,air}$ = 0.63 cm^2/s, thus with respect to its diffusivity in air helium is not an ideal tracer for air. Air components argon and krypton have diffusion-coefficients values matching air in air values better than helium, namely 0.18 and 0.14 cm^2/s, respectively.

Non-invasive measurements of gas transport in interconnected fluidised-beds systems can most conveniently be carried out by using high specific activity (Bq/mol) radiotracers, labelled with gamma rays emitting radionuclides and one or more external gamma ray detectors. Other aspects, such as the half-life of the radionuclides, energy of the emitted radiation, photon abundance, practical availability, radiation health regulations and protection measures were also considered. This led to the choice of ^{81m}Kr as the most adequate and practically suitable radiotracer for our measurements.

^{81m}Kr is a short-lived radionuclide decaying with a half-life of 13.1 s to ^{81}Kr (half-life = 2.1×10^5 year) [14]. It emits Kr X-rays, 190.3 keV gamma ray of high abundance (0.66 photons per disintegration) and internal conversion electrons of 176 and 188 keV [14]. The radionuclide ^{81m}Kr is a decay product of ^{81}Rb (half-life = 4.58 hour = 16.5 ks) [14]; a radionuclide usually obtained by proton irradiation of ^{82}Kr.

A common way of obtaining considerable quantities of ^{81m}Kr is from ^{81}Rb/^{81m}Kr generators currently commercially available [15] and widely used for delivering ^{81m}Kr to patients undergoing pulmonary ventilation studies. The rate of formation of ^{81m}Kr in such a generator is about 53 kBq/s per MBq of ^{81}Rb actually present in the generator. Most of the thus formed ^{81m}Kr can be eluted from the generator by passing air through it (for example 0.05 litre/s) and will provide a continuos flow of radiotracer directly feed to the fluidisation air.

As the ^{81}Rb/^{81m}Kr generators usually contain considerable amounts of both radionuclides being sources of ionising radiation, measures have to be taken in order to reduce the radiation intensity level around both the generator and experimental set-up including the piping connecting generator and the set-up. However, the emission of radiation from commercial generators is usually reduced to acceptable levels by shielding them with tungsten and lead. The ^{81m}Kr containing air leaving the experimental set-up should carefully be collected and led to either a buffer vessel where it can completely decay or to atmosphere through a stack.

Shielding of different parts of experimental set-up and the detectors – mostly scintillation ones - can easily be achieved by leaden plates or foils. The half-thickness of lead for absorption of 190.3 keV gamma rays of ^{81m}Kr is 0.51 mm [16]. However, interaction of 190.3 keV gamma rays with lead results in the emission of Pb X-rays, predominantly K X-rays (five) with energies ranging from 72.8 to 87.3 keV [14]. As a fraction of these X-ray photons may reach the detectors the monitoring of 190,3 keV gamma rays has to be based on the measurement in an energy window of less then 100 keV centred on 190 keV.

EXPERIMENTAL

1. Experimental set-up

All experiments were carried out in a system (shown in Figure 1) consisting of four, 10-mm thick-Perspex made, regular prism-shaped compartments with a 0.1 m × 0.1 m square base and a total high of 1.05 m (internal dimensions). Each prism or compartment was attached to two other compartments forming a rectangular whole. The compartments 2 & 3 and 4 & 1 (see Figure 1) were interconnected with centrally placed, horizontal, cylindrical orifices with a diameter of 0.03 m and

lengths of 0.02 m with their centre 0.1 m above air distribution plate. The other two pairs of compartments, namely 1 & 2 and 3 & 4 were provided with 0.39 m high overflow openings with 0.1 m wide, sharp-edge weirs at 0.3 m above the mentioned plate. The common open spaces above the fluidised beds in compartments 1 & 2 and 3 & 4 are usually referred to as freeboards. The 0.003 m thick air distribution plate, made of porous bronze was located at about 0.06 m above the bottom of each of the compartments. The four spaces between the bottoms and the plates, the so-called "wind boxes", were filled with glass marbles in order to obtain an as even air distribution as possible.

The fluidised-beds system was filled with 14 kg spheroid glass particles with an average diameter of 680 μm, density of 2650 kg/m^3 and a minimum fluidisation (superficial) velocity, U_{mf} = 0.36 m/s. Fluidisation air of about 289 K was led from the flow controllers into the four separate wind boxes i.e. compartments.

^{81m}Kr was obtained from ^{81}Rb/^{81m}Kr generators - produced by Amersham Cygne, Eindhoven, The Netherlands [14] - each containing about 600 MBq ^{81}Rb. Each generator was sufficient for a day of experimentation. One of the beds of the interconnected fluidised-beds system was continuously fed via its window box and the distributor plate with ^{81m}Kr containing air. This is made up by mixing generator elution air (0.05 l/s) with the main air stream. Note that U_{mf} = 0.36 m/s corresponds to 3.6 l/s air. Other beds are also fed with air but with no radiotracer in it.

About 0.4 m above the weirs, at the end of the freeboards, begins the gas i.e. air-^{81m}Kr mixing section consisting of four waved metal sheet based static mixer elements per compartment The purpose of gas mixing is to ensure that the gas entering the visual field of the external radiation detectors is spatially homogenous with respect to the radiotracer concentration in it. Only then will the intensity of radiation impinging a detector be directly proportional to the radiotracer concentration in its visual field just above the mixing section.

Four 3"× 3" NaI(Tl) scintillation detectors each aiming at the upper part of a compartment from a distance of 0.1 m. The radiation was collimated by 0.006 m thick leaden plates to create an 0.1 m high visual field between the mixing section and the top of a compartment (see Figure 1). The detectors were rolled twice in a 0.003 m thick leaden sheet to prevent the detection of radiation not coming from the visual field. Moreover, at mixer and detector height the compartments were lined with 0.003 m thick lead sheets in order to prevent a detector detecting radiation from another compartment then the closest one. Each detector was coupled to a preamplifier, amplifier-single channel analyser (Canberra AMP/TSCA 2015 A). A PC-mounted card with an adjustable dwell time acquired the pulses from the single channel analysers. A multichannel analyser (Trackor Northern TN 7200) was applied for checking the gamma ray spectra to be used for estimation of 190.3 keV (net) photopeak fraction in results obtained by single channel counting with an energy window of 165 to 225 keV.

The ^{81m}Kr containing air leaving the experimental set-up was mixed with a high flow rate air stream and then released to atmosphere through a 60 m high stack.

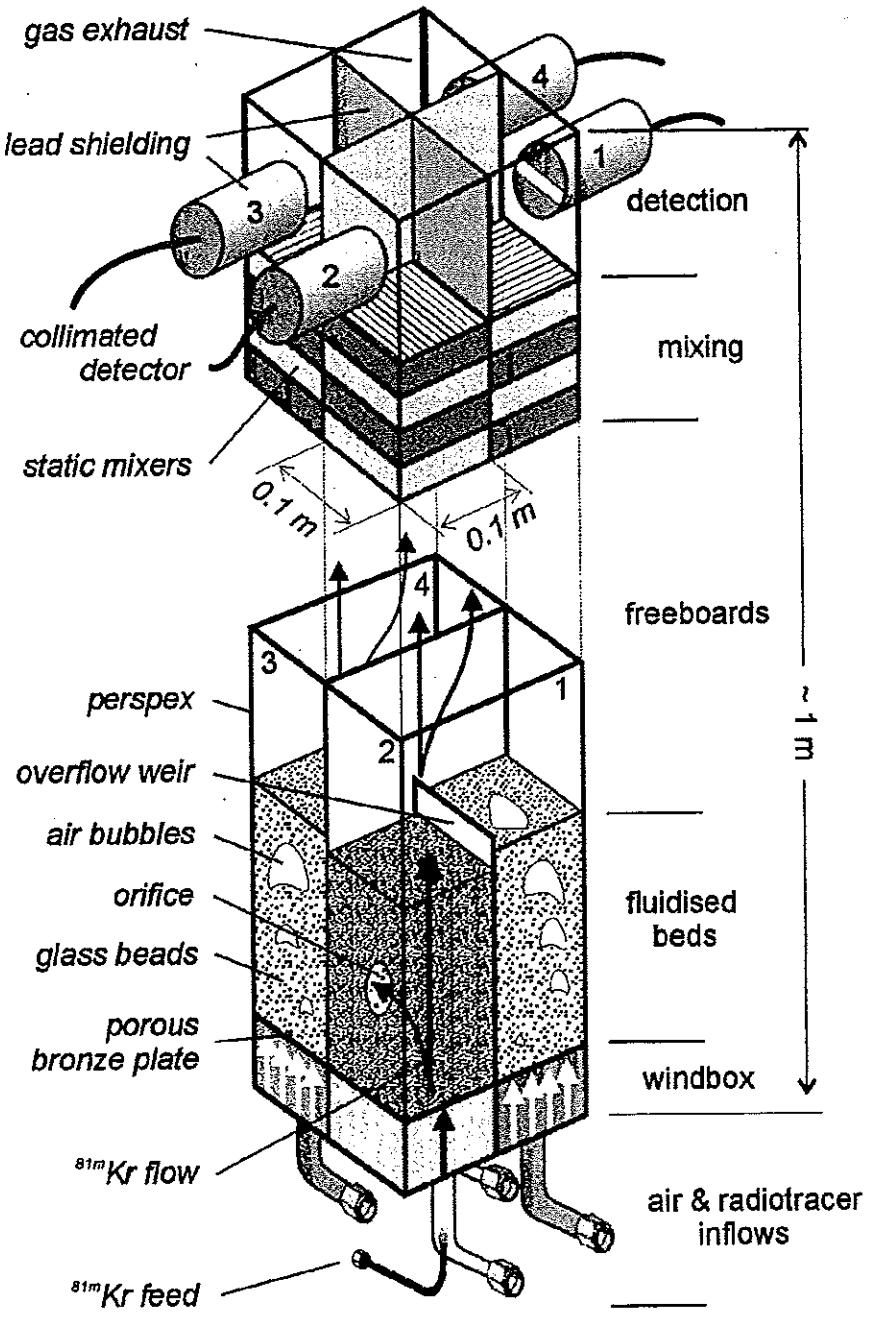

Figure 1. A schematic sketch of the experimental set-up. The black arrows indicate the radiotracer flow.

2. Measurement and calculation

The measurements are performed by continuos flow of radiotracer containing air in compartment 2 and detecting the fraction of supplied radiotracer leaving each compartment. Pairs of diagonal positioned compartments were operated at an equal gas velocity, providing identical flows in both orifices. The experiments were performed in such a way that a series of measurements starts with the downcomers at the riser fluidisation velocity. After a measurements of 100 seconds (dwell time

set to 1 s), the downcomers fluidisation gas velocity was decreased and another measurement could be started after the interconnected fluidised-bed system come to equilibrium. Every series ends at a downcomers gas velocity of 0.7 U_{mf}.

Detectors 3 and 4 are the detectors of compartment 3 and 4, respectively. Compartment 3 is connected to the radiotracer entry compartment, compartment 2, by an orifice. Compartment 4 is connected to compartment 3 by a freeboard. The gas, which has traversed the orifice, leaves the set-up through compartment 3 and 4. Therefore the orifice gas flow, OGF, can be calculated by equation:

$$OGF = \Phi_2 \, (R_{p,3} + R_{p,4}/(R_{p,1} + R_{p,2} + R_{p,3} + R_{p,4})$$

Φ_2 (l/s or kg/s) is the total gas flow through the radiotracer entry compartment. The processed count rates $R_{p,1}$, through $R_{p,4}$ (1/s) are obtained by multiplying the single channel count rates R_1 through R_4, pertaining to the energy window of 165 to 225 keV, by a factor $f_p = R_{photopeak}/R_{window}$. This factor was calculated from spectra obtained under experimental conditions including conditions as set for actual experiments. Note that the detector efficiency for 190.3 keV gamma rays of ^{81m}Kr was the same for all the detectors and that because of the short residence times no decay correction has been made for the possible differences in passage time due to the spread of radiotracer over more than one compartment.

If the entry compartment, compartment 2, acts as downcomer, above equation signifies the orifice gas flow from downcomer to riser, $OGF_{D\rightarrow R}$. To determine the net orifice gas flow one has to subtract $OGF_{R\rightarrow D}$ from it. The latter is determined by operating the radiotracer entry compartment as riser and the adjacent compartment as downcomer.

RESULTS AND DISCUSSION

Only a small selection of the large amount of experimental results and their evaluation can be presented here. The accent will be put on the typical results illustrating the utility of the applied methodology. For more information the reader is referred to [11].

Figure 2 shows the results pertaining to the bi-directional transport of gas through the orifices, namely the flow from a downcomer to riser, $OGF_{D\rightarrow R}$, and vice versa, $OGM_{R\rightarrow D}$, as a function of the dimensionless aeration rate and riser aeration, $U_R = 2\ U_{mf}$. The last points in Figure 2, at $U_D/U_{mf} = 2$, denote the exchange of gas between two equally fluidised beds. The net OGF i.e. ($OGF_{D\rightarrow R}$ - $OGF_{R\rightarrow D}$), is zero. In fact, these points describe the lateral gas dispersion in a regular fluidised bed if the orifice has no limiting influence.

Figure 3 shows the net OGF (%) relative to the total downcomer gas flow, i.e.$100(OGF_{D\rightarrow R} - OGF_{R\rightarrow D})/\Phi_D$ where $\Phi_D = \Phi_2$, given as a function of the dimensionless downcomer fluidisation rate U_D/U_{mf}. The figure is based on the OGF data used in Figure 2.

An interesting feature to be discussed is that at zero pressure drop over the orifice (see [14], $U_D/U_{mf} \approx 0.72$) the net orifice gas flow, OGF, is above zero. This effect may be attributed to gas-solids drag, namely there is a positive solids flow due to the

particle pressure in the downcomer [5]. The fact that there is orifice gas flow in both directions, also when the net OGF flow is zero, may pose problems to the operation of an industrial interconnected fluidised-beds system.

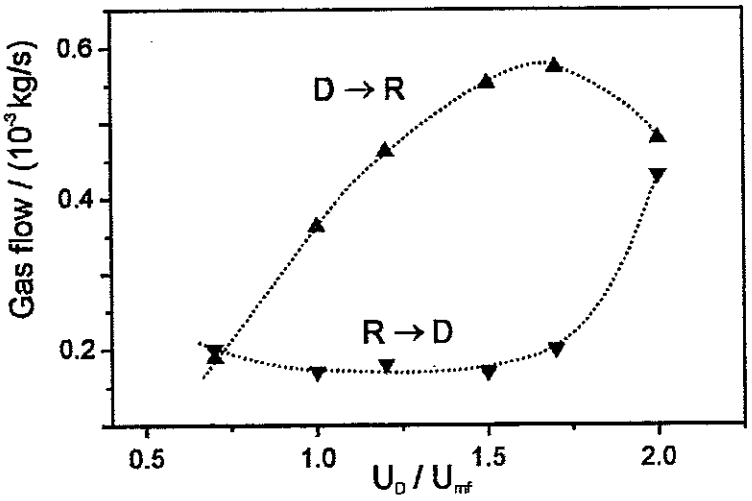

Figure 2. $OGF_{D\to R}$ and $OGF_{R\to D}$ (0.001kg/s) versus dimensionless fluidisation rate U_D/U_{mf} Orifice diameter = 0.03 m, total solids mass = 14 kg and U_R = 2 U_{mf}.

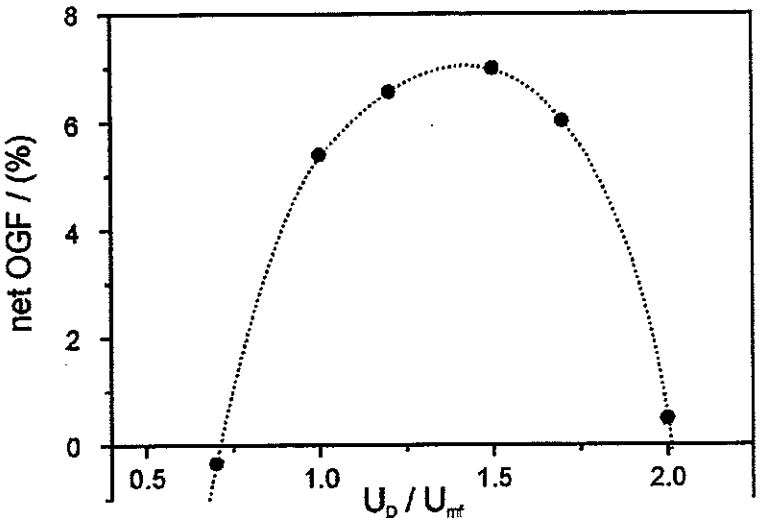

Figure 3. Net orifice gas flow, OGF, as % of the gas flow at the bottom of the downcomer as a function of the dimensionless fluidisation rate, U_D/U_{mf}. Orifice diameter = 0.030 m, total system mass = 14 kg and U_R = 2 U_{mf}.

CONCLUSION

A novel, radiotracer gas method has been developed and successfully used to determine the bi-directional gas flows and the net gas flow through an orifice connecting two air-solids aerated fluidised beds making part of a interconnected fluidised-beds system. By varying different process parameters, such as aeration

rates, solids circulation rate, solids mass, orifice diameters and measure the influence of these parameters upon the behaviour of individual beds as well as the interconnected fluidised-beds system one should be able acquire a better insight in the mechanisms underlying the transport of both solid and gas phase in these systems.

Acknowledgements. The authors are indebted to W. den Hollander for technical assistance and to him and Ms. T.G. Verburg for helping with manuscript preparation.

REFERENCES

[1] Kurimoto, M., Ogata, H., Koya, T., Furusawa, T., Kunii, D., *Circulation system of fluidized solids within a single vessel,* in: Proceedings of the 2nd World Congress of Chemical Engineering, Montreal, 3 (1981), 23-26.

[2] Kuramoto, M., Furusawa, T., Kunii, D., *Development of a New System for Circulating Fluidized Particles within a single vessel,* Powder Technology, 44 (1985), 77-

[3] Fox, D., Molodtsof, Y., Large, J. F., *Control Mechanisms of Fluidized Solids Circulation Between Adjacent Vessels,* AIChE Journal, 35 (12) (1989), 1933-1941.

[4] Korbee, R., Schouten, J. C., van den Bleek, C. M., *Modelling interconnected fluidized bed systems,* AIChE Symp. Series 87 (281) (1991), 70-77.

[5] Korbee, R., Snip, O. C., Schouten, J. C., van den Bleek, C. M., *Rate of solids and gas transfer via an orifice between partially and completely fluidized beds,* Chem. Eng. Sci., 49 (1994), 5819-5832.

[6] Korbee, R., *Regenerative Desulfurization in an Interconnected Fluidized Bed System,* Doctoral Dissertation, Delft University of Technology (Delft, November 20, 1995), Delft, 1995, pp. 224, ISBN 90-5651-017-7.

[7] Snip, O. C., *The Interconnected Fluidized Bed reactor for gas/solids regenerative processes,* Doctoral Dissertation, Delft University of Technology (Delft, May 20, 1997), Delft University Press, Delft, 19997, pp. 222, ISBN 90-407-1451-7, NUGI 813.

[8] Stellema, C. S., Kolar, Z. I., de Goeij, J. J. M., Schouten, J. C., van den Bleek, C. M., *Solids Residence Time Distribution in Interconnected Fluidized Beds,* AIChE, Symp. Series, Vol. 93 (317) (1997), 40-45

[9] Abellon, R. D., Kolar, Z. I., den Hollander, W., de Goeij, J. J. M., Schouten, J. C. , van den Bleek, C. M. , *A single radiotracer particle method for the determination of solids circulation rate in interconnected fluidized beds,* Powder Technology, 92 (1997), 53-60

[10] Stellema, C. S., Mudde, R. F., Kolar, Z. I., de Goeij, J. J. M., Gerritsen, A. W., van den Bleek, C. M., *Single particle tracking in interconnected flluidized beds,* in: Proceedings of the Ninth Engineering Foundation Conference on Fluidization (Durango, Colorado, U.S.A., May 17-22, 1998), Eds. Lian-Shih Fan, Knowlton, T. M., Ed. Engineering Foundation, New York, U.S.A., 1998 (ISBN: 0-939204)

[11] Stellema, C. S., *Radiotracers for Gas/Solids Flows in (Interconnected) Fluidized Beds,* Doctoral Dissertation, Delft University of Technology, (Delft, February 2, 1999), Delft University Press, Delft, The Netherlands, 1999, 153 pp., ISBN 90-407-1808-3/CIP

[12] Perry, R.H., Green, D.W., Maloney, J.O., *Perry's Chemical Engineers' Handbook,* Ed. McGraw-Hill, Inc., New York, St. Louis, San Francisco etc., (1984), p. 3-285. ISBN 0-07-Y66482-X.

[13] Lide, D.R., *CRC Handbook of Chemistry and Physics,* 73rd edition, Ed. CRC Press, Boca Raton, Ann Arbor, London, Tokyo, (1992-1993), p. 14-11. ISBN-8-8493-0473-3.

[14] Lederer, C.M., Shirley, V.S., (Eds.), *Table of Isotopes,* 7th edition, Ed. John Wile & Sons, Inc., New York, Chichester, Brisbane, Toronto, 1978, ISBN 0-471-04179-3 and 0-471-04180-7 pbk.

[15] Anonymous, *$^{81}Rb/^{81m}Kr$-krypton generator,* Amersham Cygne, Eindhoven, 1999.

[16] Hubbell, J.H., Seltzer, S.M., *Tables of X-Ray Mass Attenuation Coefficients and Mass Energy-Absorption Coefficients 1 keV to 20 MeV for Elements Z = 1 to 92 and 48 Additional Substances of Dosimetric Interest,* NISTIR 5632, Ed. U.S. Department of Commerce, National Institute of Standards and Technology (NIST), Gaithersburg, MD, U.S.A., 1995.

A NEW TECHNIQUE FOR THE DETERMINATION OF CONTACT TIME DISTRIBUTION (CTD) FROM TRACERS EXPERIMENTS IN HETEROGENEOUS REACTORS

M. Magos Rivera, M. Tayakout-Fayolle, C. Jallut

LAGEP (Laboratoire d'Automatique et de Génie des Procédés), UMR CNRS 5007, Université Claude Bernard et ESCPE-Lyon, 43, bd du 11 novembre 1918, 69622 Villeurbanne Cedex, France, jallut@lagep.univ-lyon1.fr

Abstract. The concept of Residence Time Distribution (RTD) has been widely used in the case of homogeneous isothermal reactors [1]. For an isothermal heterogeneous reactor like a catalytic fixed-bed one for example, the chemical reaction occurs only within the pores of the catalyst pellets. The reactor is then made of an inactive zone (the mobile fluid phase) and an active zone (the pores within the pellets or stationary phase). The residence time distribution within this active zone has been defined by Shinnar and co-workers [2] as the Contact Time Distribution (CTD). In this paper, we propose an algorithm to calculate the CTD. We illustrate the method by using simulated data. To apply the technique, one has to perform two tracers experiments. A first tracer must be used to measure the RTD in the whole system (the distribution of the time spent in the mobile and the stationary phase). A second tracer must be used to measure the RTD in the mobile phase. The mobile phase RTD can be measured for example by using a non-porous solid instead of the porous one.

INTRODUCTION: THE CONCEPTS OF CONTACT TIME DISTRIBUTION

The concept of Residence Time Distribution is very classical for homogeneous isothermal reactors [1,3-5]. The basic idea is to use a Lagrangian representation of the steady - state flow through a reactor by the means of a Residence Time Distribution $g(t_s)$. A reactant can be consumed during all the time spent in the reactor and in the case of a first order reaction, the fraction of unconverted reactant at the outlet of the reactor $\overline{X}$ is given by:

$$\overline{X} = \int_0^\infty e^{-kt_s} g(t_s) dt_s = \hat{g}(k) \tag{1}$$

$\hat{g}(s)$ is the Laplace transform of $g(t_s)$, k (s^{-1}) the first order chemical reaction rate constant. For reactions the rate of which are non linear with respect to the concentrations, upper and lower bounds for $\overline{X}$ can be calculated by considering the degree of micromixing in the reactor [5,6].

In the case of an isothermal heterogeneous reactor like a fixed-bed or fluidized-bed catalytic reactor, one is interested in defining a contact time t_c and its distribution $\Psi(t_c)$ so that a relation similar to (1) holds to calculate $\overline{X}$:

$$\overline{X} = \int_0^\infty e^{-kt_c} \Psi(t_c) dt_c = \hat{\Psi}(k) \tag{2}$$

Within the context of gas fluidized-bed catalytic reactors modeling, Nauman and Collinge have proposed a concept of Contact Time Distribution [7]. As a matter of fact, if one considers a first order chemical reaction that occurs at the surface of catalyst pellets, application of relation (1) by using the gas phase RTD leads to yields greater than those measured. The reason is that the contact between the gas and the solid surface does not exist in a continuous way because of bypassing effects, particularly due to bubble formations. Nauman and co-workers have given a method for the CTD measurement by using adsorbable tracers [8] and they have applied these concepts to pilot plant reactors [9-11].

Within the framework of fixed-beds catalytic reactors modeling, Shinnar and co-workers [2,4,12] have defined a concept of CTD by considering that the reactor is the combination of a chemically active zone and a chemically inactive one [13-16]. A residence time distribution characterises each of these zones. The work presented here is related to the concept of Contact Time Distribution as defined by Shinnar and co-workers.

STOCHASTIC BASIS OF THE CTD CONCEPT

The following material is taken from reference [2]. The total time t_s spent by a tracer element in the reactor is the sum of two elapsed times:

- the time spent in the stationary phase t_c (the pores of the support);
- the time spent in the mobile phase $t_f = t_s - t_c$, t_s being the total time spent in the reactor (figure 1).

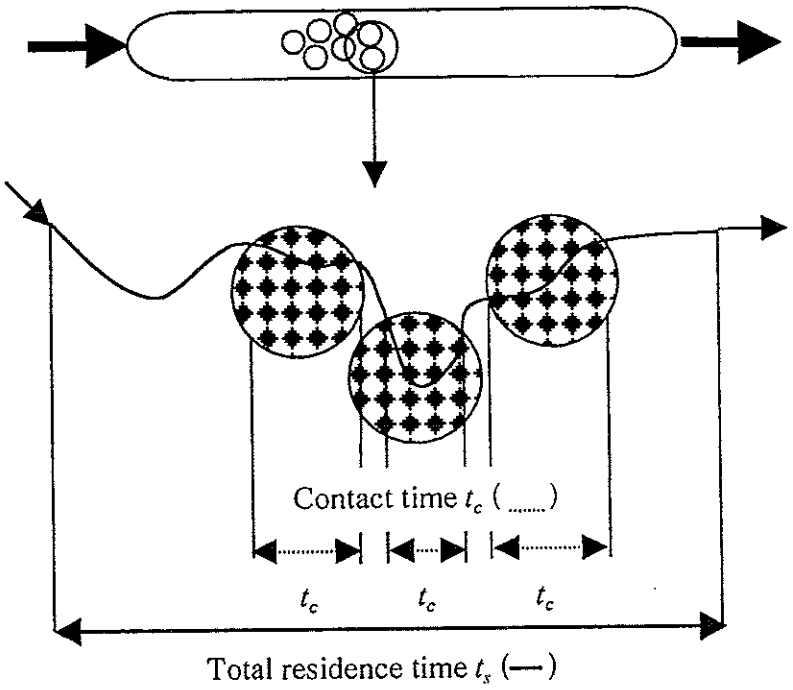

Figure 1. Illustration of the concepts of total and fluid residence times as well as contact time

Let us define the functions:

- $g(t_s)$: the residence time distribution in the whole system or the probability density for t_s;
- $f(t_f)$: the residence time distribution in the mobile phase or the probability density for t_f;
- $\Psi(t_c)$: the residence time distribution in the stationary phase or Contact Time Distribution, the probability density for t_c;
- $\chi(t_c / t_f)$: the conditional probability for the contact time t_c, assuming the time spent in the mobile phase t_f.

It is clear from basical results in probability theory that the following relations hold:

$$\psi(t_c) = \int_0^{\infty} f(t_f)\chi(t_c / t_f)dt_f \tag{3}$$

$$g(t_s) = \int_0^{t_s} f(t_f)\chi\left((t_s - t_f)/t_f\right)dt_f \tag{4}$$

Let us now consider two non-overlapping stretches of times t_{f1} and t_{f2} spent in the mobile phase and the associated times, respectively t_{c1} and t_{c2}, spent in the stationary phase. If one can assume that the two events (t_{c1} assuming t_{f1}) and (t_{c2} assuming t_{f2}) are independent, then the following relation holds:

$$\chi\left(t_c /(t_{f1} + t_{f2})\right) = \int_0^{t_c} \chi(t / t_{f1})\chi\left((t_c - t)/t_{f2}\right)dt \tag{5}$$

or in the Laplace domain:

$$\hat{\chi}\left(s /(t_{f1} + t_{f2})\right) = \hat{\chi}(s / t_{f1})\hat{\chi}(s / t_{f2}) \tag{6}$$

Only a function of the form $\hat{\chi}(s) = e^{-t_f \varrho(s)}$ can satisfy the condition (6) so that the following results hold from equations (3) and (4):

$$\hat{\Psi}(s) = \hat{f}(\varrho(s)) \tag{7}$$

$$\hat{g}(s) = \hat{f}(s + \varrho(s)) \tag{8}$$

where $\hat{f}(s)$ is the Laplace transform of $f(t_f)$, $\hat{g}(s)$ is the Laplace transform of $g(t_s)$, $\hat{\Psi}(s)$ is the Laplace transform of $\Psi(t_c)$. $\varrho(s)$ depends on the mass transfer between the mobile and stationary phase as well as the mass transfer within the stationary phase.

If a first order chemical reaction occurs in the stationary phase, $\Psi(t_c)$ in relation (2) is clearly defined as following:

$$\overline{X} = \int_0^{\infty} e^{-kt_c}\Psi(t_c)dt_c = \hat{f}(\varrho(k)) = \hat{\Psi}(k) \tag{9}$$

Villermaux has also given this result within the framework of chromatographic reactor modeling [17,18]. In order to demonstrate the result, he used the model of an infinity of elementary plug flows in parallel.

DETERMINATION OF $\Psi(t_c)$ FROM TRACERS EXPERIMENTS

One can propose at least two methods for the determination of $\Psi(t_c)$.

1. Estimation of the parameters of a model

Within the framework of the modeling of a fixed-bed liquid phase polymerization reactor [19,20], we used a tracer visiting the mobile and the stationary phase leading to the measurement of $g(t_s)$. The model that we used for the system is based on the following assumptions:

- the fluid flow is equivalent to a plug flow with axial dispersion;
- the transport of the tracer within the pellets is represented by the Fick law;
- a mass transfer coefficient allows to express the tracer flux between the fluid and the pellets external surface.

According to these assumptions, one can derive the Laplace transform of $g(t_s)$:

$$\hat{g}\left(s+\varrho(s)\right) = \frac{4p(s)e^{\frac{Pe}{2}(1-p(s))}}{\left(1+p(s)\right)^2 - \left(1-p(s)\right)^2 e^{-Pep(s)}} \tag{10}$$

$$p(s) = \left(1+\frac{4D_{Ax}}{u^2}\left(s+\varrho(s)\right)\right)^{\frac{1}{2}} \tag{11}$$

$$\varrho(s) = \frac{\frac{D_{eff}a}{\varepsilon_b R}}{\frac{D_{eff}}{k_f R} + \left(\Phi(s)\coth\left(\Phi(s)\right) - 1\right)^{-1}} \quad \text{with } \Phi(s) = \sqrt{\frac{sR^2\varepsilon_p}{D_{eff}}} \tag{12}$$

with: a the interfacial area (m^{-1}), D_{Ax} and D_{eff} ($m^2.s^{-1}$) respectively the axial dispersion coefficient and the apparent diffusion coefficient within the pellets, k_f ($m.s^{-1}$) the mass transfer coefficient between mobile and stationary phases, L (m) the bed length, R (m) the pellets radius, u ($m.s^{-1}$) the fluid velocity, ε_b and ε_p respectively the bed and pellets porosity and $Pe = \frac{uL}{D_{Ax}}$ the Peclet number. By performing a time domain fitting, we obtained the time constants or non-dimensional groups contained in equations (10) to (12). By using a numerical procedure to invert the Laplace transform $\hat{g}\left(\varrho(s)\right)$ (see equation (10)), (DINLAP of the IMSL package), we finally obtained $\Psi(t_c)$ [21].

2. Direct calculation of $\Psi(t_c)$

2.1. Principle

In order to avoid a reference to a model, we propose here a method to calculate $\Psi(t_c)$ provided that one perform two tracers experiments:

- a first tracer has to be used to measure the RTD in the whole system $g(t_s)$;
- a second tracer has to be used to measure the RTD in the mobile phase $f(t_f)$ (the mobile phase RTD can be measured for example by using a non-porous solid instead of the porous one).

To calculate $\Psi(t_c)$, we must use the equation (3). Then, it is necessary to build a family of conditional probability functions $\chi(t_c/t_f)$ from equations (4) and (5). Such a construction is performed numerically by considering the numerical approximations of the integrals (3), (4) and (5).

2.2. Numerical technique

For the sake of simplicity, let us suppose that the sampling period is equal to 1. The functions $f(t_f)$, $g(t_s)$, $\Psi(t_c)$ and $\chi(t_f/t_c)$ are then respectively approximated by the following vectors $(f_0 \ . \ . \ . \ f_M)^T$, $(g_0 \ . \ . \ . \ g_N)^T$, $(\psi_0 \ . \ . \ . \ \psi_N)^T$ and $(\chi_{0/i} \ . \ . \ . \ \chi_{N/i})^T$, $i = 0..M$. Then, equation (3) can be approximated by the following equation:

$$\psi_k = \sum_{i=0}^{N} f_i \chi_{k/i} \tag{13}$$

It is clear that $\chi_{0/0} = 1$ and $\chi_{k/0} = 0$, $k = 1..N$. As a matter of fact, given the fact that the sojourn time in the fluid is 0, the probability that the sojourn time in the solid is greater then 0 is 0. Furthermore, we have also the following properties: $\chi_{i/j} = 0$ if $i + j > N$ and $\chi_{i/j} \neq 0$ if $i + j \leq N$. The probability of having the total residence time t_s is supposed to fall to 0 after the rank N. As for equations (4) and (5), they are respectively approximated by:

$$g_k = \sum_{i=0}^{k} f_i \chi_{(k-i)/i}, \ k = 0..N \tag{14}$$

$$\chi_{k/(m+n)} = \sum_{i=0}^{k} \chi_{i/m} \chi_{(k-i)/n}, \ k = 0..N \tag{15}$$

From equation (15), one can see that if the conditional probability $\chi_{k/1}$, $k = 1..N$, is known, on can build any other conditional probability function. For example, $\chi_{k/2} = \sum_{i=0}^{k} \chi_{i/1} \chi_{(k-i)/1}$, $\chi_{k/3} = \sum_{i=0}^{k} \chi_{i/2} \chi_{(k-i)/1}$ and so on. The problem

is then reduced to calculate $\chi_{k/1}$, $k = 1..N$ so that equation (14) is satisfied. As probability density functions, $\chi(t_c / t_f)$ have also to satisfy the classical condition $\int_0^\infty \chi(t_c/t_f)dt_c = 1$ so that $\sum_{i=0}^{N} \chi_{i/k} = 1,\ k = 1..M$.

According to the above mentioned properties, the equations (14) can be expressed by using matrices as follows:

$$\begin{pmatrix} g_0 \\ g_1 \\ \cdot \\ \cdot \\ \cdot \\ g_k \\ \cdot \\ g_N \end{pmatrix} = \begin{pmatrix} 1 & 0 & 0 & \cdot & \cdot & \cdot & 0 \\ 0 & \chi_{0/1} & 0 & 0 & \cdot & \cdot & 0 \\ 0 & \chi_{1/1} & \chi_{0/2} & 0 & \cdot & \cdot & 0 \\ 0 & \chi_{2/1} & \chi_{1/2} & \cdot & \cdot & \cdot & 0 \\ & & & & & & \chi_{0/M} \\ \cdot & \cdot & \chi_{2/2} & \cdot & \cdot & \cdot & \cdot \\ & & & & & & \cdot \\ \cdot & \cdot & \cdot & \cdot & \cdot & \cdot & \chi_{(N-M)/M} \\ \cdot & \cdot & \chi_{(N-2)/2} & \cdot & \cdot & \cdot & 0 \\ 0 & \chi_{(N-1)/1} & 0 & \cdot & \cdot & \cdot & 0 \\ 0 & 0 & 0 & \cdot & \cdot & \cdot & 0 \end{pmatrix} \begin{pmatrix} f_0 \\ f_1 \\ \cdot \\ \cdot \\ f_i \\ \cdot \\ f_M \end{pmatrix} \qquad (16)$$

2.3. Simulation example

We have used the model described by the equations (10) to (12) and the DINLAP routine of the IMSL package to simulate the residence time distributions $g(t_s)$, $f(t_f)$ and $\Psi(t_c)$ according to equations (7) and (8).

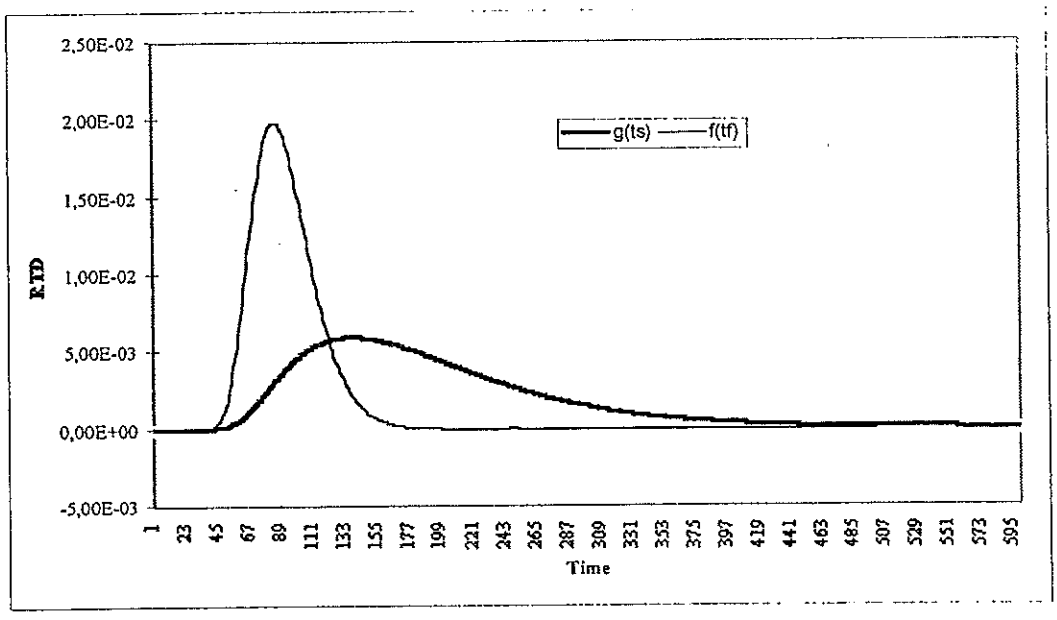

Figure 2. Simulated residence time distributions $g(t_s)$ and $f(t_f)$

One can see on the figure 2 an example of simulated signals $g(t_s)$, $f(t_f)$ with $Pe=36.1$, $\frac{D_{Ax}}{u^2}=14.8$ s, $\frac{D_{eff}{}^a}{\varepsilon_b R}=1.26\ 10^{-2}\ s^{-1}$, $\frac{D_{eff}}{k_f R}=8.4\ 10^{-2}$, $\frac{R^2\varepsilon_p}{D_{eff}}=250.6$ s.

The first estimation of $\chi_{k/1}$, $k=1..N$ is simply $(1\quad 0\quad 0\quad .\quad 0)^T$. The next ones are obtained by progressively spreading $\chi_{k/1}$, $k=1..N$ so as to shorten the distance between $g(t_s)$ and the estimated or reconstructed signal $\tilde{g}(t_s)$.

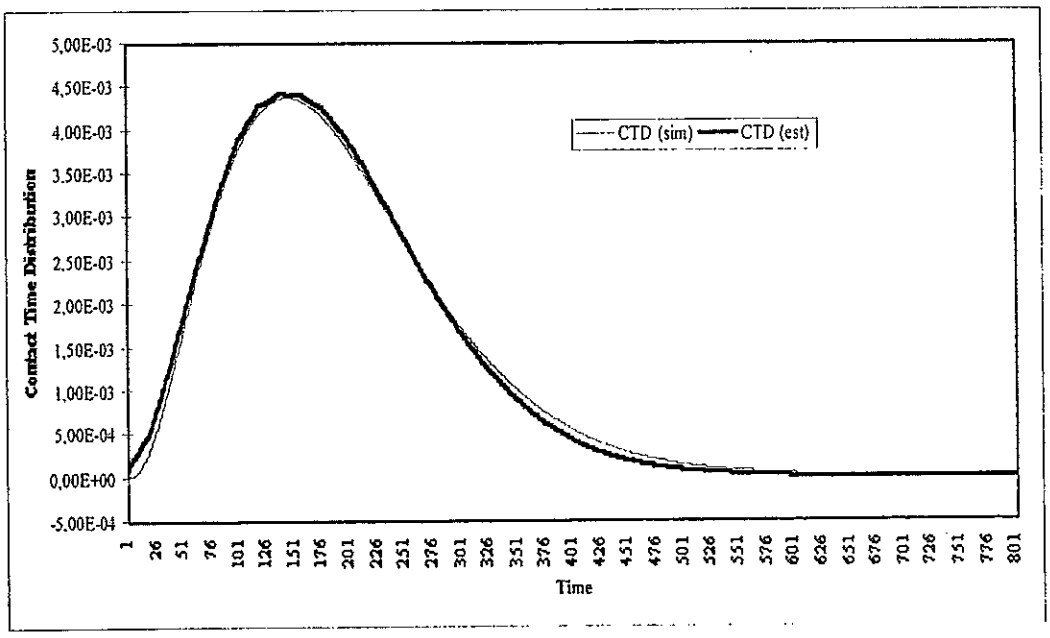

Figure 3. Comparison between the simulated contact time distribution $\Psi(t_c)$ and the reconstructed one $\psi(t_c)$

As it can be seen on figure 3, our method allows to extract a good approximation of $\Psi(t_c)$ from $g(t_s)$ and $f(t_f)$.

CONCLUSION

By using simulated values for the two tracers experiments, we have shown that it is possible to extract the CTD in a fixed bed reactor without using a model of the system. We plan to apply our technique to experimental data.

Acknowledgement: M. Magos Rivera tanks CONACYT and UAM for supporting his work.

REFERENCES

[1] Danckwerts P.V., *Continuous flow systems. Distribution of residence times*, Chem. Engng. Sci., 2(1953), 1-15

[2] Shinnar R., Naor P., Katz S., *Interpretation and evaluation of multiple tracer experiments*, Chem. Engng. Sci, 27(1972), 1627-1642

[3] Nauman E. B., *Residence time distribution and micromixing*, Chem. Engng. Comm., 8(1981), 53-131

[4] Shinnar R., *Use of Residence and Contact Time Distributions in reactor design*, Chemical Industries, 26(1986), 63-149

[5] Villermaux J., *Génie de la réaction chimique. Conception et fonctionnement des réacteurs*, Lavoisier, Technique et documentation, Paris (1995)

[6] Zwietering Th. N., *The degree of mixing in continuous flow systems*, Chem. Engng. Sci., 11(1959), 1-13

[7] Nauman E. B., Collinge C. N., *The theory of contact time distributions in gas fluidized beds*, Chem. Engng. Sci., 23(1968), 1309 - 1316

[8] Nauman E. B., Collinge C. N., *Measurement of contact time distributions in gas fluidized beds*, Chem. Engng. Sci., 23(1968), 1317 - 1326

[9] Collinge C. N., Doheim M. A., *Mixing and performance in heterogeneous chemical reactors*, Trans. IChemE, 56(1978), 69-72

[10] Doheim M. A., Collinge C. N., *Contact time distribution in fluidized - bed reactors. Part I : Measurements at room and higher temperatures and Part II : Application of mathematical models and parameter estimation*, The Chemical Engineering Journal(1980), 19, 39-56

[11] Pustelnik P., Nauman E. B., *Contact time distributions in a large fluidized bed*, AIChE J., 37(1991), 1589-1592

[12] Silverstein J., Shinnar R., *Design of fixed bed catalytic microreactors*, Ind .Engng. Chem., Process Des. Dev., 14(1975), 127-137

[13] Krambeck F. J., Katz S., Shinnar R., *A stochastic model for fluidized beds*, Chem. Engng.Sci. 24(1969), 1497-1511

[14] Raghuraman J., Varma Y. B. G., *A stochastic model for residence time and contact time distributions of the gas in multistage fluidised beds* , Chem. Engng. Sci. 29(1974), 697-703

[15] Gibilaro L. G., *Residence time distributions in regions of continuous flow systems*, Chem. Engng Sci., 34(1979), 697-702

[16] Aris R., *Residence time in several environments* , in: Recent advances in the engineering analysis of chemically reacting systems, Doraiswamy L. K. (Eds.), Wiley and Sons, 38-49 (1984)

[17] Villermaux J., *Deformation of chromatographic peaks under the influence of mass transfer phenomena*, J. Chrom. Sci., 12(1974), 822-830

[18] Villermaux J., The chromatographic reactor, in: Percolation Processes, Theory and Applications, NATO ASI (1978)

[19] Jacquier V., Jolimaitre E., d'Onofrio A., Hamaide T., Tayakout-Fayolle M., Jallut C., *Catalyse hétérogène de polymérisation anionique coordinée par ouverture de cycles oxygénés : mise en oeuvre et modélisation des transferts de matière dans un procédé à lit fixe*, Entropie, n° 212-213(1998), 87-98

[20] Jacquier-Gonod V., *Polymérisation anionique coordinée par ouverture de cycles oxygénés : du procédé discontinu au procédé continu sur colonne réactive*, PhD thesis, Claude Bernard University, Lyon, France(1998)

[21] M. Tayakout-Fayolle, C. Jallut, Modélisation d'un réacteur catalytique à lit fixe à l'aide du concept de distribution des temps de contact. Application à la polymérisation anionique coordinée par ouverture de cycles oxygénés, Colloque Génie des Procédés Chimiques, Physiques et Biotechnologiques, Toulouse, 26-27 Novembre 1998

INFLUENCE OF THE RESIDENCE TIME DISTRIBUTION KNOWLEDGE ON GAS-LIQUID MASS TRANSFER COEFFICIENT ESTIMATION.

M. Forissier[1], M. Mitrovic[1], I. Pitault[1], D. Ronze[2]

[1]Laboratoire de Génie des Procédés Catalytiques, UMR CNRS-CPE 2214,ESCPE Lyon, 43 bd du 11 Novembre, 69616 Villeurbanne Cedex, France
[1]Université Claude Bernard, Lyon I, IUT A, Département Génie Chimique, 43 bd du 11 Novembre, 69622 Villeurbanne Cedex, France

Abstract. Measurements of the gas-liquid mass transfer coefficient, k_La_L, have been performed in a three-phase gas-liquid-solid reactor (Robinson-Mahoney reactor). The estimation of k_La_L depends on the gas and liquid model dispersion. A misestimating of those two parameters leads to erroneous values of k_La_L. In our experiments, we attempted to determine k_La_L for oxygen absorption in water taking into account the phase dispersion. Our results indicate that simultaneous analysis of liquid and gas are necessary in order to obtain reliable values.

1. Introduction

Three-phase gas-liquid-solid systems have been widely used for hydrotreating reactions. Determination of the intrinsic reaction kinetics is a crucial step in the overall process knowledge and development. Choosing the better laboratory reactor for kinetics studies remains a complex task. One should ensure that the measured data are only controlled by chemical kinetics and not hidden by purely physical processes as mass transfer. The Mahoney-Robinson reactor has been elaborated in order to offer an optimal contact between gas-liquid and liquid-solid [1]. It consists in a multiple-impeller configuration with a stationary catalytic basket. This reactor seems to present some advantages in kinetic studies [2 – 4], but the limits of the chemical control are still unknown.

In order to clarify the overall limits of this laboratory investigation reactor, we have to explore the gas-liquid and liquid-solid mass transfer ; this paper deals only with the former : gas-liquid mass transfer coefficient (k_La_L) measurements. To obtain reliable k_La_L values, Nocentini et al. [5] and Linek et al. [6] showed the influence of gas dispersion on mass transfer coefficient in a multiple-impeller configuration. This influence is to be clarified in a Mahoney-Robinson reactor, because of hydrodynamics modification due to the presence of the catalytic basket.

Oxygen absorption is often used to determinate k_La_L. This standard dynamic method is based on step change of oxygen concentration in inlet gas [7], and allows to keep a constant gas hold-up during the experiment [6, 8] ; its drawback is the necessity to characterise the gas dispersion in order to estimate the gas-liquid coefficient. In some studies gas dispersion is neglected [9, 10] ; however this strategy can lead to erroneous values of k_La_L [6, 8, 11] which can be avoided by determining the gas behaviour via a residence time distribution (RTD). Low soluble gas is used, such as nitrogen or helium : in this case, the mass transfer during the RTD measurement is neglected [8, 12 – 15]. A variant of the dynamic method is

proposed to eliminate the gas dispersion effect, the start-up dynamic method : aeration is started into deoxygenated liquid without gas hold-up [16]. The gas hold-up is formed during the experiment and does not correspond to a steady state. This technique is not suitable for k_La_L measurement, as far as the time to reach a steady state gas hold-up is comparable with the k_La_L experiment time.

For the k_La_L measurements, the standard dynamic method (oxygen absorption in water) was selected. We have measured at first the dissolved oxygen concentration and the gas hold-up. A first estimation of k_La_L is obtained postulating a model for the gas dispersion. Secondly, a RTD study of the gas phase is realised in order to check the gas dispersion, and eventually to correct the model proposed previously for the gas dispersion. Finally, mass transfer coefficient and gas dispersion are determined analysing simultaneously gas and liquid phases.

2. Experimental

2.1. Reactor (figure 1)

Our reactor is adapted from the Robinson-Mahoney reactor [1]: a transparent (PMMA) tank contains a fixed annular catalytic basket. Its inner diameter and its height are respectively 0.08 m and 0.22 m. A rotating shaft with blades creates a flow through the basket to the reactor wall and induces an upward and a downward stream. The multi-impeller configuration is constituted by two four pitched blades impellers surrounding one six flat blades impeller. To prevent vortexing, the catalytic basket is fitted out with four baffles inside and outside the basket and it is filled with stainless steel cylinders (2 mm diameter, 6 mm length) in order to simulate the catalyst. The basket screen is 0.7 mm diameter wire with a screen opening of 0.7 mm. The reactor is closed on liquid and opened on gas. The gas inlet and outlet are located respectively at the bottom and at the top of the vessel.

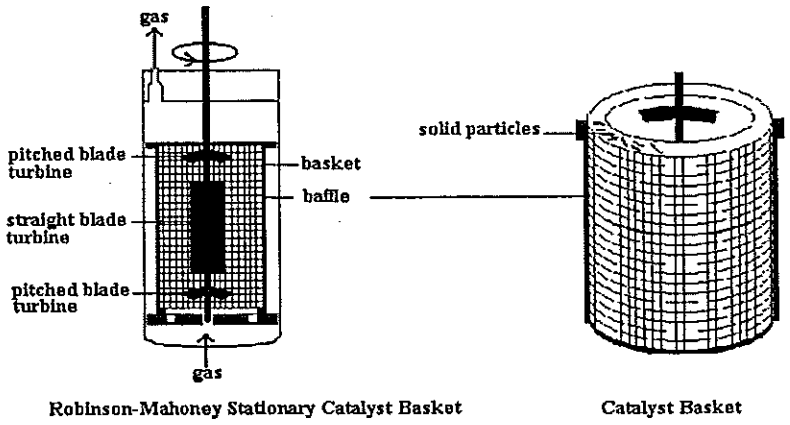

Figure 1 : Robinson-Mahoney stationary catalyst basket and reactor.

2.2. Gas analysis

To analyse gas composition, two methods are used : a catharometer detector (TCD) for binary systems (He/N_2) and a mass spectrometer (Gaslab 300 from VG GAS) for ternary systems ($He/N_2/O_2$).

2.3. Liquid analysis

In this work, only dissolved oxygen in liquid (distilled water) is measured by an oxymeter electrode (WTW GmbH, OXI 323).

2.4. Methods

All experiments are performed at room temperature and atmospheric pressure. Gas flow varies between 1 and 5 $mL.s^{-1}$ and agitation speed between 500 and 1750 rpm.

In order to study the influence of the liquid viscosity, additions of glycerol in water are realised. They allow variations of viscosity without any effect on the superficial tension ; the properties are given in the table 1.

Table 1. Properties of mixtures (water + glycerol) at 298 K [17].

Mixtures	Viscosity (mPa.s)	Superficial tension ($mN.m^{-1}$)
Water	1	72.0
Water + 10% wt glycerol	1.3	70.5
Water + 20% wt glycerol	1.7	69.5

To estimate the gas hold-up, ε_G, the reactor is first fully filled with liquid. Then, the agitation speed is started. After agitation speed stabilisation, the gas is introduced and ejects some liquid from the reactor : this ejected volume gives an estimation of gas hold-up.

Tracing experiments are carried out on two ways, depending whether the tracer is more or less soluble in distilled water.

In the first case (little soluble tracer), permanent gas (vector) is helium and tracer is nitrogen. The reactor is initially flowed by helium in order to remove nitrogen from aqueous phase. Nitrogen is then introduced through a 4-way valve and analysed in the gas phase at the outlet of the reactor using TCD detector. Liquid phase has not been analysed.

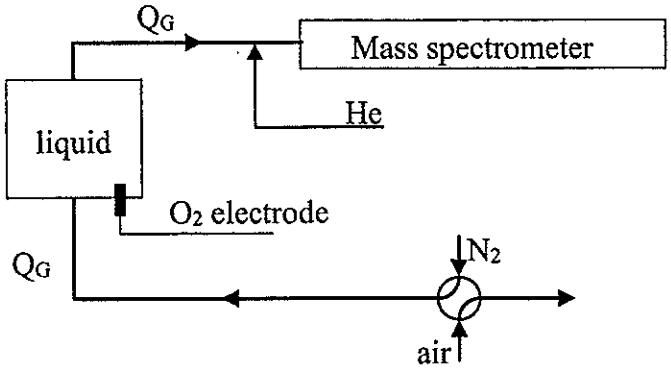

Figure 2 : Set-up for simultaneous gas and liquid analysis experiments.

When using a more soluble tracer, permanent gas (vector) is nitrogen and tracer is oxygen from air. The reactor is initially flowed by nitrogen in order to

deoxygenate the aqueous phase. Air is then introduced through a 4-way valve ; the gas phase is analysed at the outlet of the reactor using a mass spectrometer ; a constant helium flowrate is added at the inlet of mass spectrometer to monitor the flowrate leaving the reactor. Oxygen in the liquid phase is simultaneously analysed with the oxymeter (figure 2).

3. Results

3.1. Liquid phase analysis

Mass transfer coefficients in gas-liquid system are classically estimated through dynamic oxygenation, explicitly or implicitly assuming gas and liquid are perfectly mixed.

Mixing time measurement by conductivity tracer method indicates that this time represents 2 to 5 % of the absorption time and allows to consider that the liquid phase is perfectly mixed. If perfect gas mixing assumption is considered, mass balances for oxygen in gas and liquid are written as follows :

$$\text{Liquid :} \quad \frac{dC_L}{dt} = k_L a_L \left(\frac{C_G}{m} - C_L\right)$$

$$\text{Gas :} \quad Q\,C_{Go} = Q\,C_G + \varepsilon_G V_R \frac{dC_G}{dt} + k_L a_L\,(1-\varepsilon_G)\,V_R \left(\frac{C_G}{m} - C_L\right) \qquad (1)$$

C_L and C_G are the oxygen concentrations in liquid and gas phases, Q is the gas flow and C_{G0} is the tracer concentration in the inlet gas, m is the equilibrium constant and V_R is the volume accessible to the fluid.

The experimental gas hold-up, $\varepsilon_G = \frac{V_G}{V_G + V_L}$, varies from 2 to 8 % in our conditions.

Solving system (1) for given $k_L a_L$ value, using Laplace transform, leads to calculated $C_L(t)$. Then $k_L a_L$ is fitted to minimise the sum of square differences between calculated and experimental liquid phase concentrations.

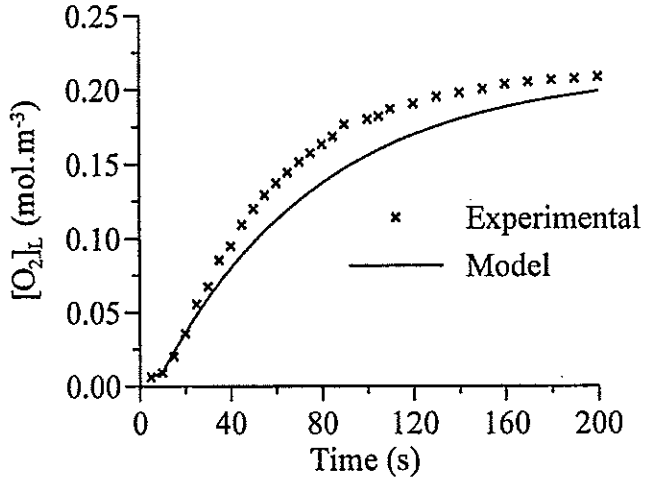

Figure 3 : Oxygen analysis in aqueous glycerol solution of 20%, with a gas flow of 1mL.s^{-1}, 1750 rpm

In most of our experimental conditions, significant differences appear between calculated and experimental concentrations (figure 3). If calculations are run fitting both parameters k_La_L and ε_G, calculated and experimental concentrations are in better agreement, but calculated values of gas hold-up are far (about 30%) from the experimental ones. Then the model proposed for the gas phase should be improved, using a non-transferable tracer (N_2) to characterise the gas flow.

3.2. Gas phase analysis

Nitrogen concentration curves in the outlet flow are given on the figure 4. The shapes of the curves are approximately the same. Nevertheless, at 500 and 1000 rpm, uncontrolled variations appear on the curves (figure 4).

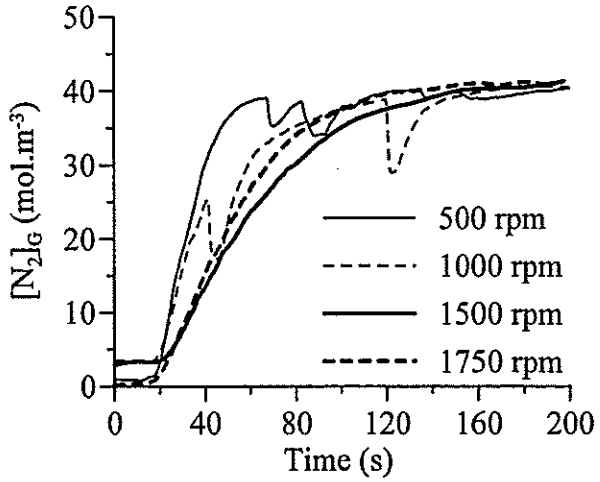

Figure 4 : Profiles of N_2 concentration for several agitation speeds.

These variations are linked to an observed dead volume that is evacuated from time to time from the reactor. When gas is introduced in the reactor, we observe formation of a pseudo-stationary volume of gas under the cover. The bubbles issued from the basket rise up close to this volume and either coalesce with it or are expulsed from the reactor : the coalescence appears to be scarce but the volume of the gas is growing up slowly, until it reaches the outlet ; this moment corresponds to the observed variation in the experimental curves.

Considering the tracer as non-transferable, the integration of experimental curves gives directly the value of the accessible gas volume and therefore the value of the gas hold-up. Unfortunately, these calculated values are higher (about 20%) than the experimental ones. This difference is due to gas solubility. Joseph and Shah [18] in the case of bubble columns, and Rovero et al. [19] for an agitated tank indicate that, to neglect the gas solubility induces large errors on RTD studies even for low soluble gas as helium in water.

Thus, the system (1) should also be applied for N_2 tracing. To fit both gas hold-up and mass transfer coefficient leads to ε_G values comparable with experimental values, but leads to k_La_L values about 10^{-10} s^{-1} which seem very low. This result can't only be attributed to the low tracer solubility, but can also be interpreted as a consequence of the previous observation concerning a pseudo-stationary gas

volume. This part of gas volume is actually less involved in gas dispersion and due to its low specific area, its contribution to the mass gas-liquid transfer can be neglected.

In conclusion, the gas dispersion model described by the system (1) is inadequate. In order to clear up the transfer phenomena, we have to develop a simultaneous gas and liquid phase analysis method.

3.3. Gas and liquid phase analysis

In this part, nitrogen and air flow rates are 1 $mL.s^{-1}$ and helium flow rate (figure 2) is 0.5 $mL.s^{-1}$. As helium concentration in the gas phase is constant (figure 5), outlet gas flow is stable, although at 500 and 1000 rpm, some variations in oxygen and nitrogen concentrations can be observed as previously.

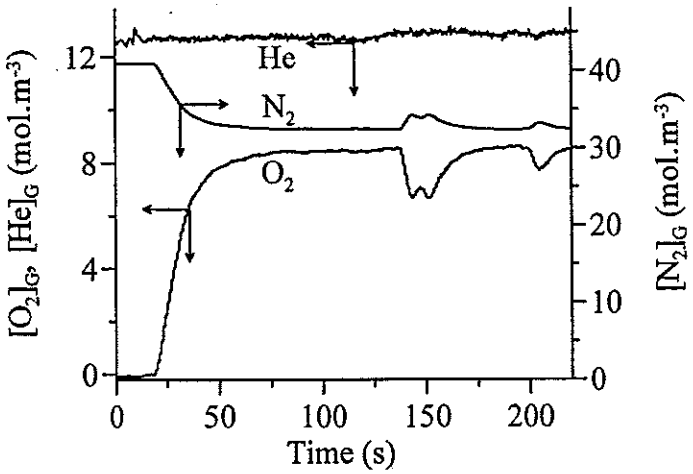

Figure 5 : Analysis of the gas phase at 500 rpm.

To take into account the observed dead volume of gas, several models (figure 6) have been tested to describe oxygen concentration in both phases. The parameters obtained by fitting those models lead to a general structure represented by the model type D. The gas is split in two parts: volume V_1 that transfers to the liquid, and dead volume V_2, that doesn't participate in mass transfer.

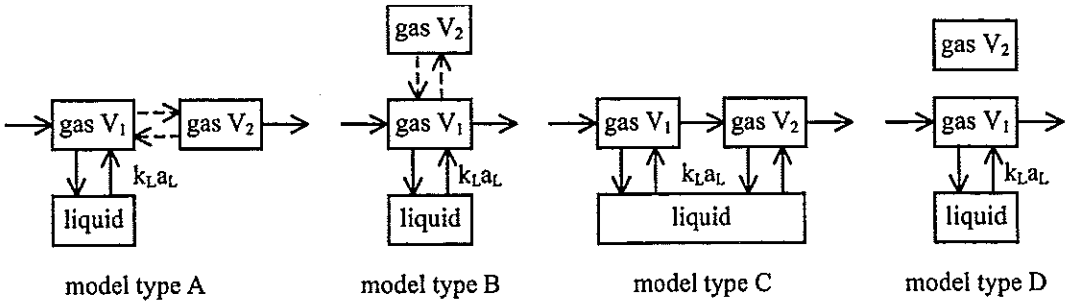

Figure 6 : Models

To determine k_La_L values, V_1 volume and k_La_L parameters are optimised. This optimised volume is smaller than the measured gas volume V_G ; the difference is

attributed to the dead volume V_2. For instance, at 1500 rpm and 1mL.s^{-1} in pure water (figure 7), the following values are obtained :

$k_La_L = 0.05\ s^{-1}$ $\quad V_1 = 20\ mL$ $\quad \frac{V_2}{V_G} = 46\ \%$

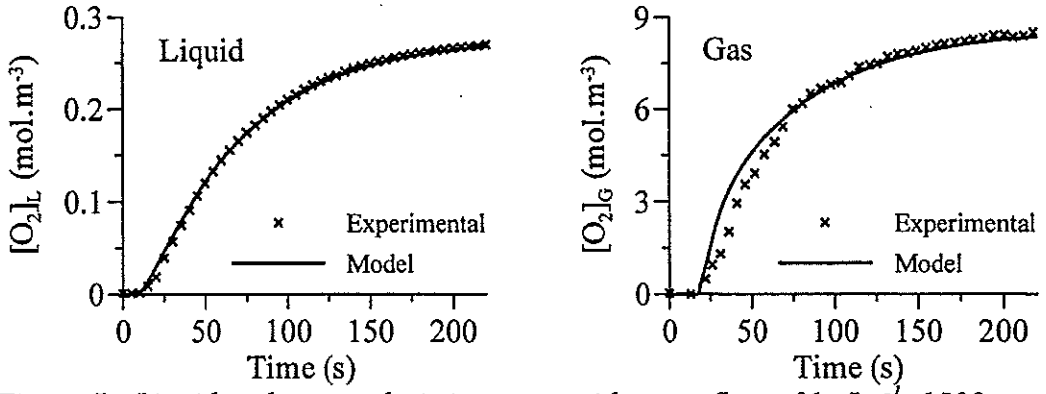

Figure 7 : Liquid and gas analysis in water, with a gas flow of 1mL.s^{-1}, 1500 rpm.

The ratio (dead volume to total gas volume) is relatively high and can't be neglected. Moreover, it decreases with increasing agitation speed and gas flow rate, and increases with increasing surface tension. Nevertheless, the dependence between k_La_L and V_1 estimations is to be considered too. A covariance matrix built up from experimental and calculated values, allows to estimate the covariance factor between k_La_L and V_1 and the parameters' precision. The covariance factors are around 0.8 at 500 rpm, 0.9 at 1000 rpm and 1 at 1500 rpm and 1750 rpm; then k_La_L and V_1 values are highly linked. The mean precision of k_La_L and V_1 is about 20-30 % except for some cases (for high agitation speeds : 1500 and 1750 rpm) where the calculated precision are not significant.

4. Conclusions

Tracer experiments in gas-liquid systems have often been analysed with underlying assumption of perfectly mixed gas and liquid phases, allowing to determine the mass transfer parameter using only the liquid phase analysis. This simplification can lead to misunderstanding the involved phenomena. Therefore the simultaneous gas and liquid analysis used here allows to estimate the gas-liquid mass transfer coefficient for oxygen absorption in water, without an *a priori* assumption of the gas flow pattern. Values of k_La_L were estimated with a mean precision of 20 %, despite the strong dependence between k_La_L and gas volume.

Acknowledgements. We acknowledge the Institut Français du Pétrole which supports this work, and specially Pierre Galtier.

[1] Mahoney J.A., Nato, Advanced Study Institute Serie, Serie E, 51 (1981), 487-513.
[2] Schweitzer J-M., Modélisation cinétique des réactions catalytiques d'hydrocraquage par la théorie des événements constitutifs, PhD, Lyon (1998).
[3] Trasobares S., Callejas M.A., Benito A.M.and Martinez M.T., Industrial and Engineering Chemical Research, 37 (1998), 11-17.

[4] Vanrysselberghe V. and Froment G.F., Industrial and Engineering Chemical Research, 35 (1996), 3311-3318.
[5] Nocentini M., Pinelli D. and Mageli F., Industrial and Engineering Chemical Research, 37 (1998), 1528-1535.
[6] Linek V., Moucha T. and Sinkule J., Chemical Engineering Science, 51 (1996), 3203-3212.
[7] Dang N.P.D., Karrer D.A. and Dunn, I.J., Biotechnology and Bioengineering, 19 (1977), 853-865.
[8] Chapman C.M., Gibilaro L.G. and Nienow A.W., Chemical Engineering Science, 37 (1982), 891-896.
[9] Albal R.S., Shah Y.T. and Schumpe A., Chemical Engineering Journal ,27 (1983), 61-80.
[10] Essen V.J., Chemical Processing, 62 (1999), 47-52.
[11] Linek V. and Sinkule J, Transactions of the Institution of Chemical Engineers, 69 (1991), 308-312.
[12] Benadda B., Ismaili S. and Otterbein M., Chemical Engineering Technology, 20 (1997), 192-198.
[13] Gal-Or B. and Resnick W., Industrial and Engineering Process and Design Development, 5 (1966), 15-19.
[14] Hanhart J., Kramers H. and Westerterp K.R., Chemical Engineering Science, 18 (1963), 503-509.
[15] Thijert M.P.G., Oyevaar M.H., Kuper W.J. and Westerterp K.R., Chemical Engineering Science, 47 (1992), 3339-3346.
[16] Brehm A., Oguz H. and Kisakürek B., 5th European Conference on Mixing, Würzburg, Allemagne, 10-12 June (1985).
[17] Timmermans J., *The physico-chemical constants of binary systems in concentrated solutions, vol. 4 : systems with inorganic + organic or inorganic compounds*, Interscience Ltd, London, 1960.
[18] Joseph S. and Shah Y., Canadian Journal of Chemical Engineering, 64 (1986), 380-386.
[19] Rovero R., S. Sicardi S., Baldi G., Osella M. and Conti R., Chemical Engineering Science, 36 (1987), 161-167.

HYDRODYNAMICS AND MASS TRANSFER IN A MECHANICALLY AGITATED HIGH PRESSURE REACTOR

N. M. Lima Filho[1], E. B. M. Medeiros[1], D. Ronze[2] e A. Zoulalian[2]

[1] University Federal of Pernambuco – Department of Chemical Engineering - Recife, PE, Brazil
[2]University Nancy 1, Faculty of Sciences, 54506 Vandoeuvre lès Nancy, FRANCE

Abstract : Performances of three-phase catalytic reactors (good selectivity, high hold-up rates, long catalyst life-time, etc) depend on several factors. The reactor we propose to study was mechanically agitated, closed for the liquid and solid phases and open for the gas-phase. It is known that the determination of certain features related to hydrodynamics and mass transfer is a classical task; however, few measurements were done at reactor pressures higher than atmospheric up to now. Therefore, we propose to accomplish these measurements not only at atmospheric pressure but also at higher pressures, to study their influences the on these features.

INTRODUCTION

The complex, heterogeneous nature of the mechanically agitated reactors makes necessary the deep knowledge of its operation features in the design and extrapolation of these types of reactor. The hydrodynamic and mass transfer characteristics are very important. Hydrodynamic studies such as Residence Time Distribution (RTD) of the gas phase were accomplished through the injection of a poorly water-soluble tracer (nitrogen in helium). The studies of the gas-liquid mass transfer parameters in the reactor were accomplished with the same methodology, using now a more water-soluble tracer (carbon dioxide). The measurements of the volumetric mass transfer coefficient k_La in perfectly mixed reactors are numerous, and there are also the reactor geometric parameters and physic-chemical properties of the fluid, but the authors study mainly the influence of: the agitation velocity and the gas-phase volumetric rate or the gas-phase superficial velocity. At pressures higher than atmospheric pressure, its effect on k_La, k_L and a are confirmed by many authors. ALBAL *et al* [1] studied the effect of the pressure between 1.38 and 9.65MPa on k_L in a mechanically agitated tank with stationary gas phase. SRIDHAR and POTTER [2] concluded that the effect of the pressure on the gas-liquid interfacial area was negligible at pressures about 1Mpa, and that k_L doesn't depend on the pressure, even when a turbulence promoter was added (glass balls with 75μ in diameter). LEDAKOWICZ *et al* [3] accomplished studies used by ALBAL *et al* [1], with pressures between 0.1 and 6MPa, and had the same conclusions. CHANG [4] measured the volumetric mass transfer coefficient between 0.1 and 5MPa in a autoclave with stationary gas phase. They verified that, depending on the nature of the gas, increasing hydrogen, nitrogen or methane pressure, k_La rises, decreases or keep constant depending on the agitation velocity. This modification is explained by the change of a and of k_L as a function the pressure. They concluded that k_La doesn't depend on pressure, though they didn't verify the topography of the gas-liquid interface at the work conditions. Other studies of this type relative to the agitated tanks and bubble columns were published by OYEVAAR and WESTERTEP [5] and CHANG [4]. With the exception of CHANG [4], the authors verified the effect of the pressure on

k_L and a, related to changes in the fluid properties. But effects are generally negligible, and k_L doesn't depend on pressure.

EXPERIMENTAL APPARATUS

In our experiments, we used the experimental equipment shown in figure 1. The reactor is a stainless steel tank mechanically agitated, with total volume of 1.5 liters and with an inside diameter of 108mm. It has an agitator moved by an electromagnetic device, with rotation velocity regulated between 200 and 2000 rpm, a gas distributor and a temperature controller with type k thermocouples (chromium-aluminum).

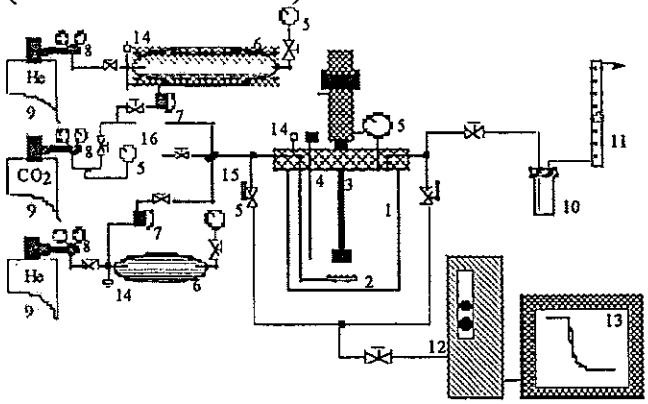

Figure 1. Experimental assembly used in the measurement of DTR and k_La.

1. Reactor; 2. Gas distributor; 3.Agitation system; 4.Thermocouples; 5.Manometers; 6. Gas reservoir; 7 and 8. Pressure regulator; 9.Cylinders; 10.Gas-liquid separator; 11. Rotameter; 12. Detector; 13. Computer; 14.Safety valves; 15. Four-ways valves; 16. Gas mixer.

The apparatus also includes three gas cylinders, one of them contain N_2 or CO_2 and the two others containing He, each one having a pressure regulating reservoir where their pressure were controlled by two calibrated pressure collectors; a four-ways valve allowing the introduction of the gas into the reactor, either a mixture of helium and tracer or pure helium; before the four-ways valve are two inox, 1/8 inch valves, that allows the regulation of the main flow, and a third valve at the exit of the reactor, allowing pressure and flow regulation. The data acquisition is accomplished by a microcomputer having an Analog Devices RTI-800 interface. The electric sign produced by the thermal conductivity detector is turned discrete in regular time intervals.

MODELLING AND PRESENTATION OF THE TRANSFER MEASUREMENTS

The method adopted was the dynamic method of physical absorption of the gas solute soluble in the liquid phase. From the results obtained for both the tracers, we obtained the characteristics of the gas-liquid transfer of the transferred solute. This technique is applied to three-phase reactors allowing the analysis of the mass transfer characteristics and also the solute diffusion transport in the bulk of the porous solid particles contained in the reactor, (NIIYAMA and SMITH, [6], BURGHART and SMITH, [7]. In the case of a experimental device, the reactor was fed with helium, with a stimulus of tracer (CO_2) at the reactor inlet. From the experimental data we can assess the

characteristics of the gas-liquid transfer. From the analysis of the experiments the flow model is the one considered sketched in Figure 2.

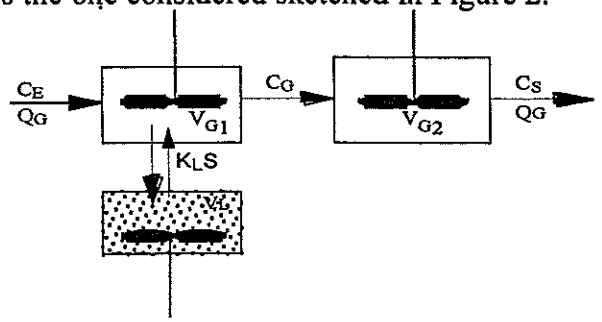

Figure 2. Reactor model for the mass transfer dynamic experiences

The gas volumes V_{G1}, V_{G2}, and the liquid volume V_L are supposed to be homogeneous. The sum $V_{G1} + V_{G2}$ represents the volume of the mechanically agitated reactor, V_{G2} is the volume of the gas above the liquid level. C_E, C_G and C_S are, respectively, the tracer concentrations at the inlet, at the exit of the biphasic zone and at the exit of the reactor. The tracer mass balances in the three zones are written respectively:

$$V_{G1}\frac{dC_G}{dt} = K_LS\left[\frac{C_G}{H} - C_L\right] + Q_G\left[C_E - C_G\right] \quad (1)$$

$$V_L\frac{dC_L}{dt} = K_LS\left[\frac{C_G}{H} - C_L\right] \quad (2)$$

$$V_{G2}\frac{dC_S}{dt} = Q_G\left[C_G - C_S\right] \quad (3)$$

In these equations, K_LS represents the overall gas-liquid mass transfer coefficient for the transferred coefficient. The balance equations may be solved in the Laplace transformer domain. This way, we obtain the transfer function of the global system:

$$G^*(s) = \frac{K_La + s}{\left[\tau_1\tau_2 s^2 + \left(\tau_2 K_La + \frac{K_La}{H}\frac{V_L}{Q_G} + 1\right)s + K_La\right]\left[1+\tau_2 s\right]} \quad (4)$$

Where :

$$\tau_1 = \frac{V_{G1}}{Q_G} \quad ; \quad \tau_2 = \frac{V_{G2}}{Q_G} \quad ; \quad K_La = \frac{K_LS}{V_L} \quad (5)$$

We remember that for a tracer who was not absorbed, the transfer function is written:

$$G(s) = \frac{1}{(1+\tau_1 s)(1+\tau_2 s)} \quad (6)$$

G(s) is nothing more than the Laplace transformer of the gas phase RTD that was formerly measurements using as a tracer a non-absorbed gas (nitrogen). We emphasize that these measures allow us to determine the τ_1 and τ_2 parameters. To estimate H and K_La, we used the 1st order momentum (μ_1) and the variance (σ), from the transfer functions $G^*(s)$ and G(s).

We have respectively:

$$\mu_1^* = \frac{1}{H}\left(\frac{V_L}{Q_G}\right) + \tau_1 + \tau_2 \quad (7)$$

$$\mu_1 = \tau_1 + \tau_2 \tag{8}$$

$$\sigma^{*2} = \frac{1}{H^2}\left(\frac{V_L}{Q_G}\right)^2 + \frac{2}{K_L a}\frac{1}{H}\left(\frac{V_L}{Q_G}\right) + \tau_1^2 + \tau_2^2 \tag{9}$$

$$\sigma^2 = \tau_1^2 + \tau_2^2 \tag{10}$$

The precedent relations allow us to obtain the Henry constant of the transferred solute"H" and the overall volumetric transfer coefficient K_La by the relations:

$$H = \frac{1}{\mu_1^* - \mu_1}\frac{V_L}{Q_G} \tag{11}$$

$$K_L a = \frac{2(\mu_1^* - \mu_1)}{(\sigma^{*2} - \sigma^2) - (\mu_1^* - \mu_1)^2} \tag{12}$$

RESULTS AND DISCUSSION

The variables calculated are the gas residence time τ in the reactor, the fraction α and the gas volume present in the gas-liquid emulsion, the gas hold-up ε_G and the volume of the gas above the liquid V_{GC}.

The gas hold-up variations in function of the feed flow Q_G and the agitator velocity are presented in the Figures 3 and 4. The effect of the agitator velocity is clearly more important than that of the gas flow.

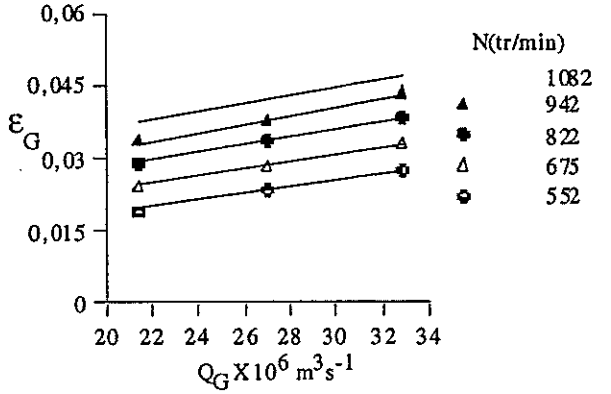

Figure 3 - Variation of ε_G as function of Q_G

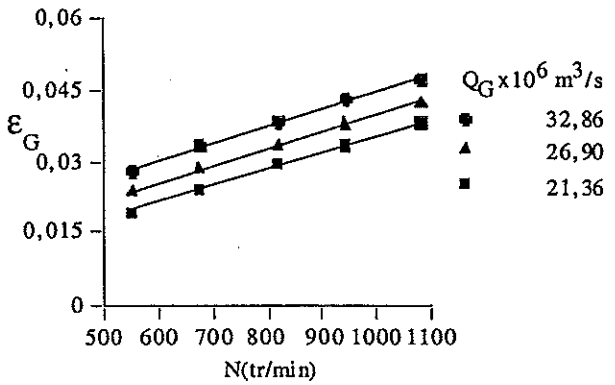

Figure 4 - Variation of ε_G as function of N

The experimental values of the gas hold-up were compared with the values obtained from the correlation proposed by SMITH [8] for mechanically agitated reactors:

$$\varepsilon_G = 0{,}1\,(d_A/D)^{1{,}25}\,(Re\,.\,Fr\,.\,N_A)^{0{,}35} \qquad (13)$$

The Figure 5 shows that our experimental values are close to the values obtained by the correlation, with a difference of 15%.

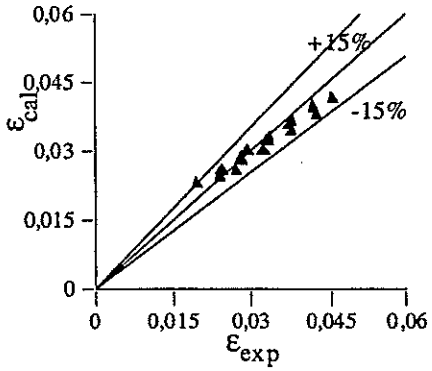

Figure 5. Comparison of the experimental values and the values calculated by Smith's correlation [8]

The RTD measurements were carried out at atmospheric pressure, as well as at total pressures varying from 1 to 40 bars. For constant gas flow we evaluated the effect of the pressure on the gas hold-up and concluded its independence relative to the total pressure for two different agitation velocities (Figure 6). Definitively, the gas hold-up depends on the gas flow and on the agitation velocity but not on the total pressure, in the range of the tested pressures.

The overall volumetric transfer coefficient K_LS was measured at atmospheric pressure as a function of the gas flow and of the agitation velocity. K_LS shows a sensible rise with the agitation velocity (Figure 7) and a little rise with the gas-phase volumetric flow (Figure 8). This behavior is similar to the one obtained by MAHFUD [9] in a mechanically agitated gas-liquid reactor which has almost the same volume as ours, and using the same tracer (CO_2).

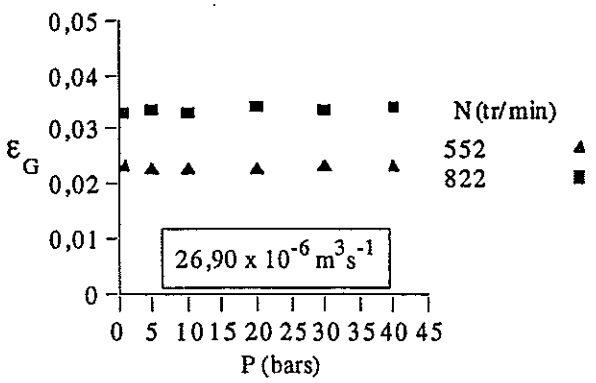

Figure 6. Variation of ε_G in function of the total pressure (constant Q_G and N)

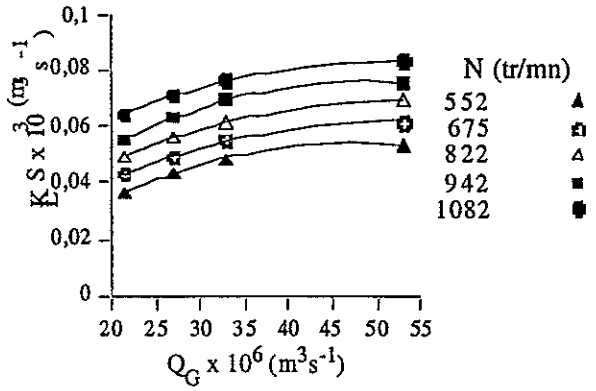

Figure 7. Influence of the gas flow on K_LS for transferred CO_2

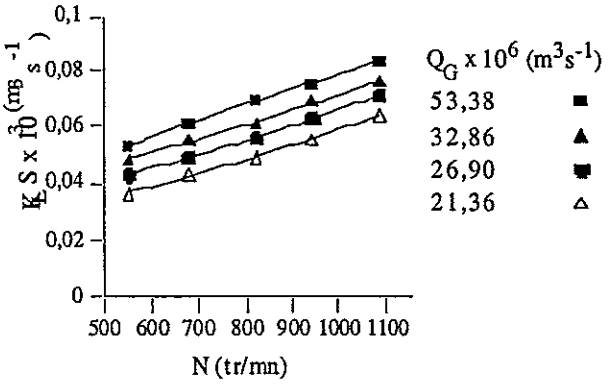

Figure 8. Influence of the agitation velocity on K_LS for transferred CO_2

The Figure 9 shows that our experimental values are close to the values obtained by the MAHFUD [9], correlation with a difference of 15%. This correlation is:

$$K_L S = 8{,}85 \times 10^{-3} N^{0{,}6} \overset{0}{Q}\overset{}{21}_G \qquad (14)$$

The characteristics of the gas-liquid transfer in the mechanically agitated reactor have the same magnitude as in the reactor employed by MAHFUD [9]. These values are relatively small when compared with others found in the literature. The agitator which was used, the propeller type, is probably less efficient than a Rushton turbine.

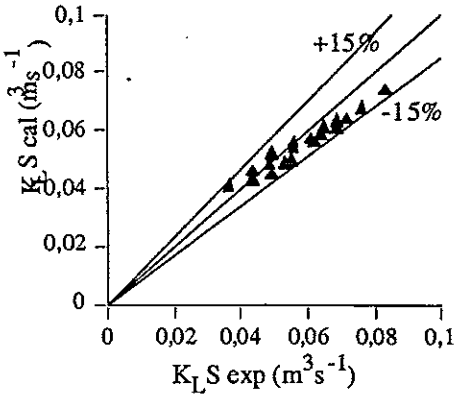

Figure 9. Interpretation of the experimental results obtained by the correlation of MAHFUD [9]

The liquid volume, the temperature, the agitation velocity and the normal volumetric gas flow were fixed (respectively V_L = 1.2 x 10^{-3} m^3 , T=25°C, N=552 rpm, Q_G=53.38x10^{-6} m^3/s TPN) and we determined $K_L S$ for different values of total pressure. In the studied range (Figure 10) we didn't observe any variation in the overall mass transfer coefficient. This result is similar to the one obtained by ALBAL et al. [1].

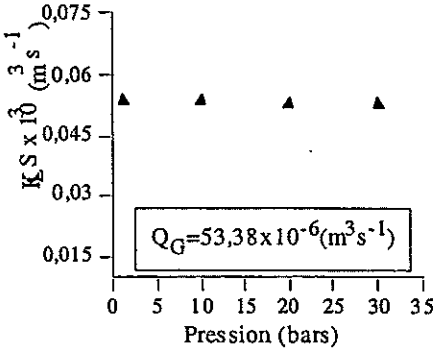

Figure 10. Evolution of $K_L S$ in function of the pressure for the absorption of CO_2

CONCLUSIONS

The RTD measurements in the gas phase allowed us to assume that the macro-mixture of the gas phase inside the reactor is perfectly mixed and that the gas hold-up is independent of the total pressure of the system between 1 and 40 bars. The influence of the agitation velocity is clearly much more remarkable than that of the gas flow. When we fixed these parameters we noted that the gas hold-up and the volumetric mass transfer coefficient did not depend on the total pressure. So, if we admit that the specific area of the gas bubbles depends on pressure, we are led to a contrary variation of the overall mass transfer coefficient as a function of the total pressure inside the reactor. The overall mass transfer coefficient is such that: $1/K_L = 1/k_L + 1/HK_G$, where K_G diminishes in function of pressure, if the solute diffusivity in the gas phase decreases with the pressure. If we admit that k_L and H are independent of the pressure, we have that $1/K_L$ raises as a function of pressure. It means that K_L

decreases in function of pressure and this diminution is compensated by the increase in the interfacial area that corresponds to a decrease of the bubbles size in the size in the bulk of liquid as a function of the total applied pressure.

NOMENCLATURE

a	gas-liquid interfacial area	m^2/m^3
C_E	tracer concentration at the inlet	mol/L
C_G	tracer concentration at the exit of the biphase zone	mol/L
C_S	tracer concentration at the exit of the reactor	mol/L
D	inside diameter of the reactor	m
RTD	residence time distribution	
d_A	diameter of the agitator base,	m
d_B	average diameter of the gas bubbles	m
$G(s)$	transfer function of the material system	
K_L	mass transfer coefficient at the liquid side	m/s
K_G	mass transfer coefficient at the gas side	m/s
K_La	volumetric transfer coefficient	s^{-1}
K_LS	overall gas-liquid transfer coefficient	m^3/s
V_{G+L}	volume of the gas-liquid emulsion	m^3
V_{GC}	volume of the gas above the liquid	m^3
τ_1	residence time in the gaseous emulsion	s
τ_2	residence time in the gas above the liquid	s
μ_1	first order momentum of the non-absorbed gas	
μ_2	second order momentum of the non-absorbed gas	
μ_1^*	first order momentum of the absorbed gas	
σ^2	variance of the non-absorbed gas distribution	
σ^{*2}	variance of the absorbed gas distribution	
σ_L	superficial tension of the liquid	N/m

N	agitator velocity	tr/min
P	pressure	bar
Q_G	gas volumetric flow	m^3/s
t	reaction time	s
T	temperature	K
V_G	gas volume	m^3
V_L	liquid volume	m^3
Re	Reynolds number	
Fr	Froude number	
N_A	aeration number	
H	Henry constant	
α	volume fraction	
ε_G	gas hold-up	
θ	reduced time	
τ	residence time	s
μ	dynamic viscosity	Pa.s
ρ	volumetric mass	kg/m^3

Index

G	gaseous
L	liquid
x	inlet
y	outlet
G+L	gas-liquid

REFERENCES

[1] ALBAL, R. S., SHAH, Y. T., SCHUMPE, A. e CARR, N. L., "Mass transfer in multiphase agitated contactors", The Chemical Engineering Journal, **27**, 61-80 (1983).

[2] SRIDHAR, T. et POTTER, O. E., "Interfacial areas in gas-liquid stirred vessels", Chemical Engineering Science, **35**, 683-95 (1980).

[3] LEDAKOWICZ, S., BREHM, A. et OGUZ, H., "Effect of Suspended Inert Solid Particles on Gas-Liquid Mass Transfer in Mechanically Agitated Contactors", Hungarian Journal of Industrial Chemistry Veszprém, **13**, 487-501 (1985).

[4] CHANG, M. Y., "Mass transfer characteristics of gases in liquids and slurries at elevated pressures and temperatures in agitated reactors". Thèse de Ph.D., Université de Pittsburgh, Pennsylvanie, Etats Unis (1990).

[5] OYEVAAR, M. H. et WESTERTERP, R., "Mass transfer phenomena and hydrodynamics in agitated gas-liquid reactors and bubble columns at elevated pressures: State of the art" Chem. Eng. Process., **25**, 85-98 (1989).

[6] NIIYAMA, H. et SMITH, J. M., "Adsorption rates of oxygen in aqueous slurries of activated carbon", AIChE Journal, **2**, No 4, 592-596 (1977).

[7] BURGHARDT, A. e SMITH, J. M., "Dynamic response of a single catalyst pellet", Chem. Eng. Sci., **34**, 267-273 (1979).

[8] SMITH, J. L., Proc. 7th Europ. Congress on Mixing, Eds Bruxelmane M. and Froment G. Ed. Royal Flemish Society of Engineers, Brugge, 18-20, 233-241 (1991).

[9] MAHFUD, "Etude de la réduction du dioxyde d'azote d'un effuent gazeux dans un réacteur gaz-liquide mécaniquement agité", Thèse de Doctorat INPL (1994), Nancy, France.

MODELING AN ELECTROCHEMICAL REACTOR BY USE OF RESIDENCE TIME DISTRIBUTION

H. Chifflet[1], C. Eysseric[1], J.P. Caire[2]

[1] Centre d'Etudes de la vallée du Rhône, DRCP / SE2A / LGCI
CEA Marcoule, BP 71, 30207, Bagnols sur Cèze (France)
[2] LEPMI - ENSEEG - INPG -UMR 5631- 1130, rue de la Piscine - BP 75 –
38402 Saint Martin d'Hères Cedex (France)

Abstract. Gas evolving at electrodes leads to complex fluid mechanics in any industrial electrolyzer. Residence time distribution (RTD) and tracer methodology can be applied in this respect with some modifications due to the acceleration of electrolyte in presence of gas bubbles. This paper presents an application of RTD for the design of a new two-phase flow electrolyzer devoted to the separation of radioactive products.

INTRODUCTION

The selective separation of americium in a nitric acid flow including other chemical compounds is studied within the framework of the 1991 BATAILLE's bill. The continuous electrolyzer of interest uses electrogenerated mediators. It is designed to be integrated into the SESAME process[1] which aims at using the properties of americium in its oxidized state Am(VI), the separation of which is possible with a common solvent extraction process. For many years, batch electrolyzers devoted to oxidation mediators, and specially Ag(II) generation, have been developed [2-4]. In the case of SESAME process, the development of a continuous process electrochemical reactor appears to be particularly interesting because of the continuous functioning mode of the liquid-liquid extraction operations which follow the electro-oxidation one. The direct experiments in presence of americium are limited because of the difficulty of experiments using radioactive solutions. So global numerical modeling of the electrolyzer behavior was developed in parallel with experiments [5]. Modeling makes the understanding, the simulation of electrolyzer and the process design possible. However, at first it requires the knowledge of the hydrodynamics of the reactor, leading to an intensive use of the RTD methodology.

This paper focuses on the tracer methodology used for the study of fluid flow behavior in presence or in absence of electrogenerated bubbles in two small scale electrolyzers named ELSA06 and ELSA20 (a 3X scale replicate of ELSA06).

MEASURES AND EXPERIMENTAL APPARATUS

Figure 1 presents a horizontal cross section sketch of the cylindrical electrochemical reactor ELSA. A porous diaphragm separates the cathode and anode compartments. In this respect, RTD measurements consider only the anode compartment located in the external concentric space.

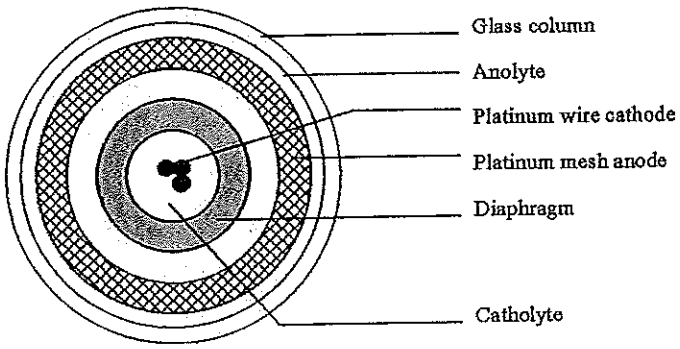

Figure 1. Horizontal cross section of ELSA electrolyzer

The electrolyte flow was a very conductive 1M nitric acid solution. Representative anolyte flows of the typical process are small since they range from 5 to 30 $ml.min^{-1}$. Such a very conducting medium complicated the choice of a tracer compatible with the functioning of the electrolyzer. $KMn0_4$ appeared as a tracer well suited in such an electrolyte. It was chosen for it is not involved in the electrochemical process and presents good stability properties in so aggressive a medium. A spectrophotometer was used for the detection of the $KMnO_4$ tracer. A desorber was placed at the electrolyzer output to get rid of O_2 bubbles generated at the anode susceptible to generate an important noise on the signal given by the spectrophotometer. The nitric vapors appearing at cathode in presence of current were supposed to be completely absorbed in an irreversible way. The experiments in presence of electrogenerated bubbles were made with a 3 A intensity in the case of ELSA20 and 0.9 A intensity for ELSA06.

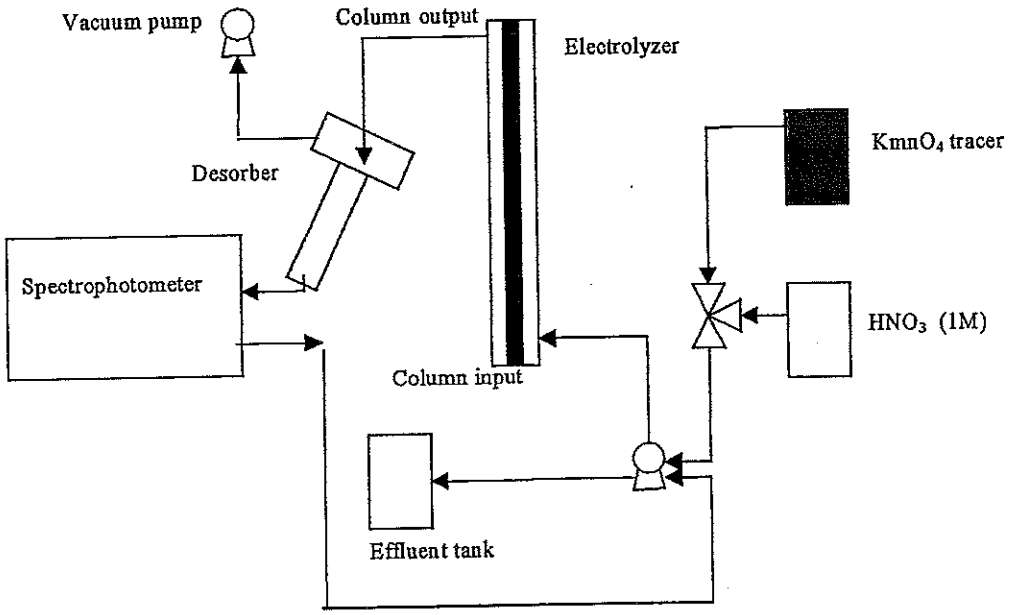

Figure 2. Experimental apparatus

Reproducibility of measurements was the first major aim. The flow rates of interest range from 4.25 to 24.5 ml.mn^{-1}. Dirac peaks appeared to perturb such small flows, then step tracer injection was systematically preferred. The tracer injection was produced by use of a common three-way chromatography valve. Since the spectrophotometer signal was noisy, a gliding mean over five successive measures was systematically performed. A numerical normalization was achieved at the end of each measurement to obtain the proper concentration step. The signal reproducibility of two successive experiments was evaluated by use of a statistical variation coefficient (VC) defined as :

$$VC = \frac{\sqrt{\frac{\sum \left(x_i^{exp_1} - x_i^{exp_2}\right)^2}{N}}}{x_{exp}} 100 \qquad (1)$$

For experiments without any current, the VC's were always lesser than 2%. This value was then used as a fit criterion for all the study. All the results were processed using the DTS code [6].

HYDRODYNAMIC MODEL

Four successive models of growing complexity were tested to fit the experiments. Figure 3 presents the last model consisting of two parallel branches including a series of continuous stirred reactors (CSTR) with or without fluid exchange. It will be noted that analog models are encountered in literature dealing with hydrodynamic behavior of electrochemical reactors [7, 8].

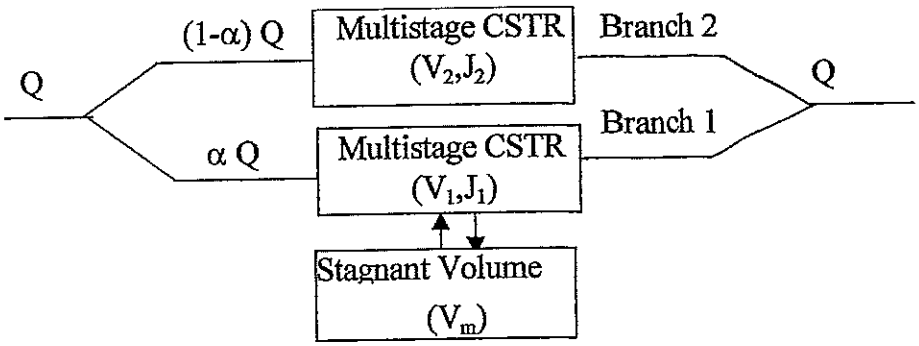

Figure 3. Equivalent model of ELSA reactor used in this work

RESULTS

Figure 4 presents the respective tracer output signals obtained for tubing alone, and for the column in presence and in absence of current. The first curve of figure 4 led

to a 7 ml correction of volume corresponding to the tubing. This correction was systematically applied for each trial.
It must be pointed out that, in such a bubble column, the liquid flow is accelerated by the gas bubbles evolving at electrode. Then the mean residence time measured reflects in fact the global two-phase flow one. The accessible liquid volume deduced from RTD curves is in good agreement with the one calculated after the estimation of the gas retention profile.

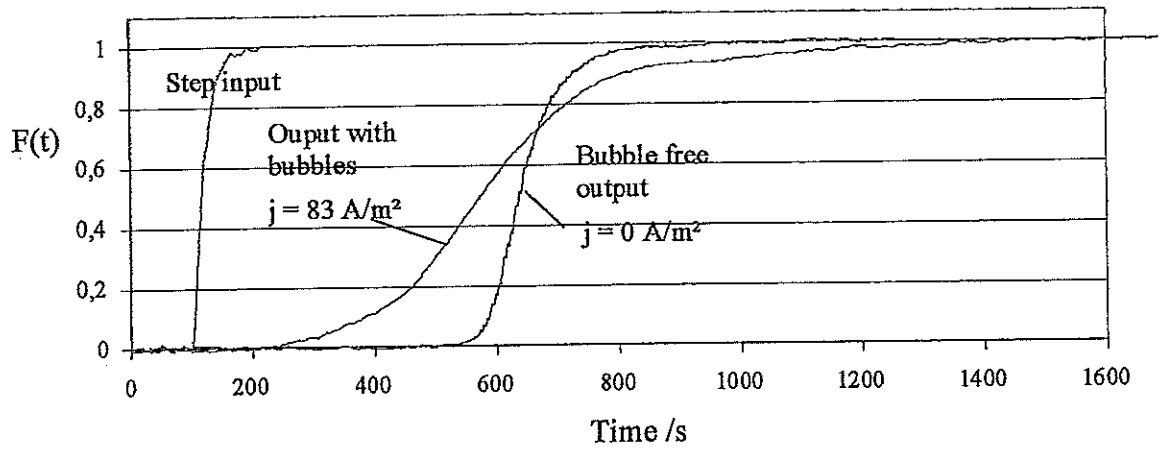

Figure 4. Responses to a step injection obtained for ELSA20 for 20 ml.min^{-1} liquid flow rate

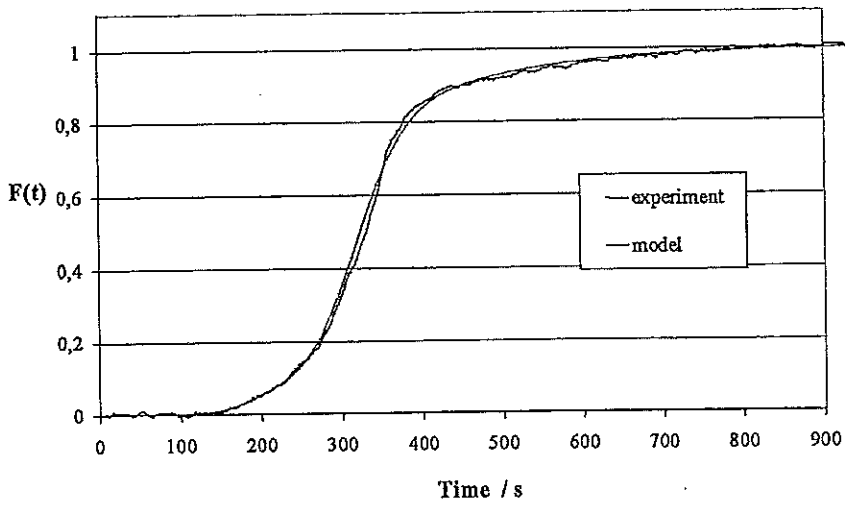

Figure 5. Comparison of experiments and model

Figure 5 presents a typical fit obtained with the model of figure 3. The fit was obtained for J_1=4, J_2 = 30, t_m = 100 s, V_1 = 25 ml, V_2 = 40 ml, V_m = 2,5 ml and a 0,4 value for α. The fit criterion measured by a 1.8 % CV was good. Moreover, all

these values appeared acceptable from a physical point of view, and seemed in perfect agreement with the geometry of the electrochemical reactor.

INTERPRETATION OF RESULTS

The first branch of figure 3 is made of a series of J_1 CSTRs of volume V_1 linked to a volume V_m. This branch is necessary to describe both the foot and the queue of the signal. The volumes V_m represent 9% of the global volume of this branch for small liquid flow and disappear for the largest flows. The second branch made of a series of J_2 simple CSTRs of volume V_2 mostly influences the central part of the signal. A V.C. lesser than 2% proves the capability of the hydrodynamic model.

Typical fits obtained for ELSA20 from the model are summarized in Figure 6. This figure shows that the model has given a pretty good representation of experimental curves since the V.C. remains lesser than 2% for the four liquid flows of interest.

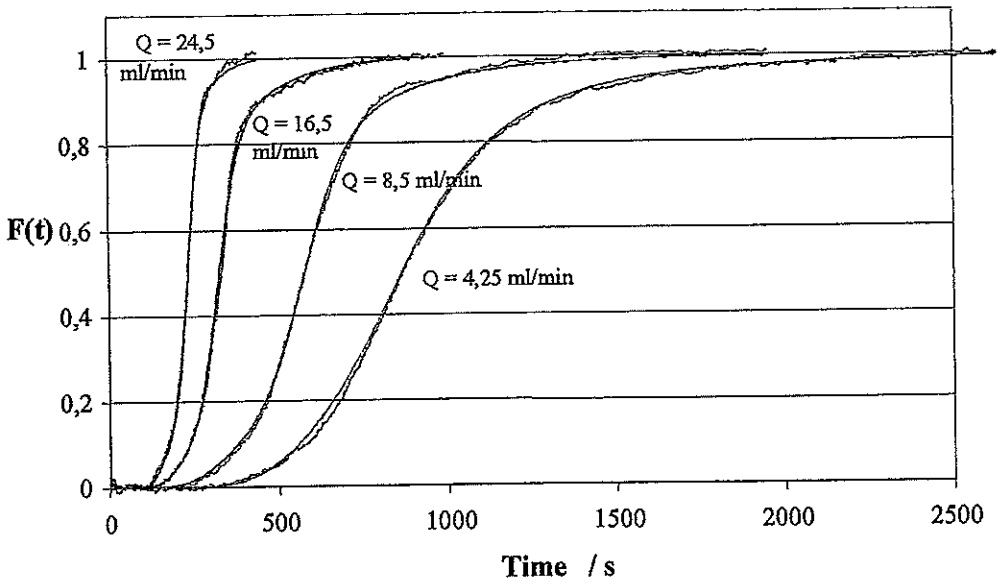

Figure 6. RTD experimental curves and model for ELSA20 (3A intensity)

For ELSA20 and ELSA06, it appears that the parameter α decreases when the electrolyte flow increases. Then the corresponding flow in the second branch is more important for growing flows. The evolution with liquid flow rate of the relative sum of volumes V_1 and V_2 is presented in figure 7.

A second observation concerns the number of CSTRs in the two respective branches J_1 and J_2. The hydrodynamics of the second branch is very close to the behavior of a true plug flow reactor and J2 is much larger than J1. Then, for both reactors the sum of volumes V_2 increases with the electrolyte flow, but the effect is of particular importance for the smaller reactor, ELSA06.

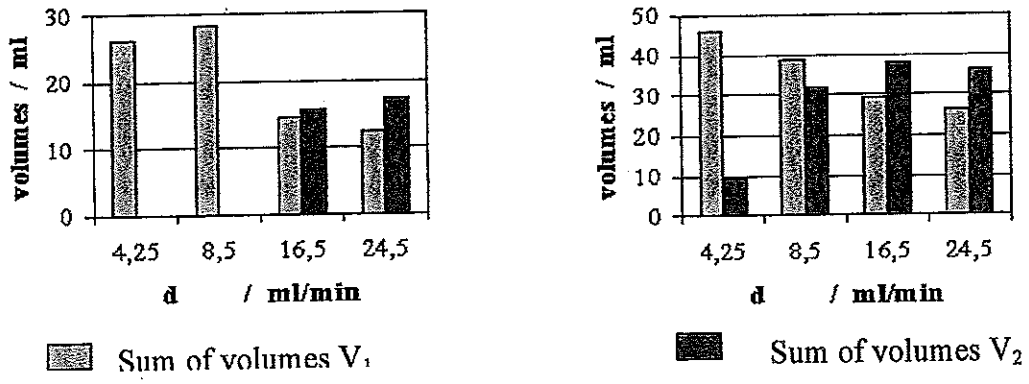

Figure 7. Evolution of volumes V1 and V2 for ELSA06 and ELSA20

For small flows, the model is equivalent to a simple series of CSTRs with exchange of mass characterized by a mean number of reactors J_m defined by:

$$J_m = \alpha J_1 + (1-\alpha) J_2 \qquad (2)$$

Figure 8 presents the evolution of Jm, the mean number of CSTRs, obtained for both ELSA reactors in function of the liquid flow rate.

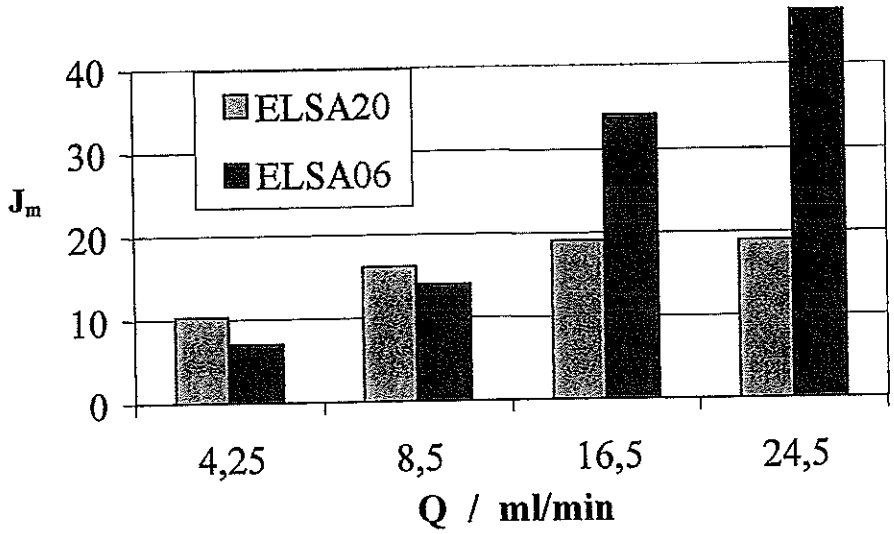

Figure 8. Evolution of the mean CSTRs number J_m as a function of flow rate for ELSA06 and ELSA20

In correlation, we observe on figure 7 that the exchange volume V_m decreases when the electrolyte flow grows up and disappears when the flow rate is larger than 16.5 $ml.min^{-1}$. This is probably due to the presence of adhering bubbles on the mesh

electrode that can be seen through the glass wall of the reactor. Effectively, both the bubbles and this effect disappear at larger flow rates [9].

DISCUSSION OF THE PHYSICAL MODEL

At low flow rates, the equivalent model is reduced to the first branch. When the flow rate increases, particularly in the case of ELSA06, a larger proportion of the flow is concerned by the plug flow part of the model. The first branch behaves like a perfect CSTR and J_1 is lesser than 10. This branch was associated to be the part of liquid flowing in the mesh of anodes where the turbulence is due both to the grid and the numerous small oxygen bubbles.

The dead volumes can also be associated with this zone since they decrease when the flow increases. This effect can be explained by the bubbles which are trapped on the mesh and detach at high flow rate.

The other branch of figure 3 is then assimilated to the free area situated between the diaphragm and the glass column. In such a clear area, it is obvious that a plug flow regime can easily develop.

The following figure represents both repartition and evolution of the equivalent surfaces associated with the flows of each branch in a cross section of the column reactor perpendicular to the symmetry axis. It shows the respective evolution of each branch of the model when the flow increases. At small liquid flow rates, only the first branch of model appears. The second branch corresponding to the plug flow part of reactor becomes increasingly effective when the flow rate increases.

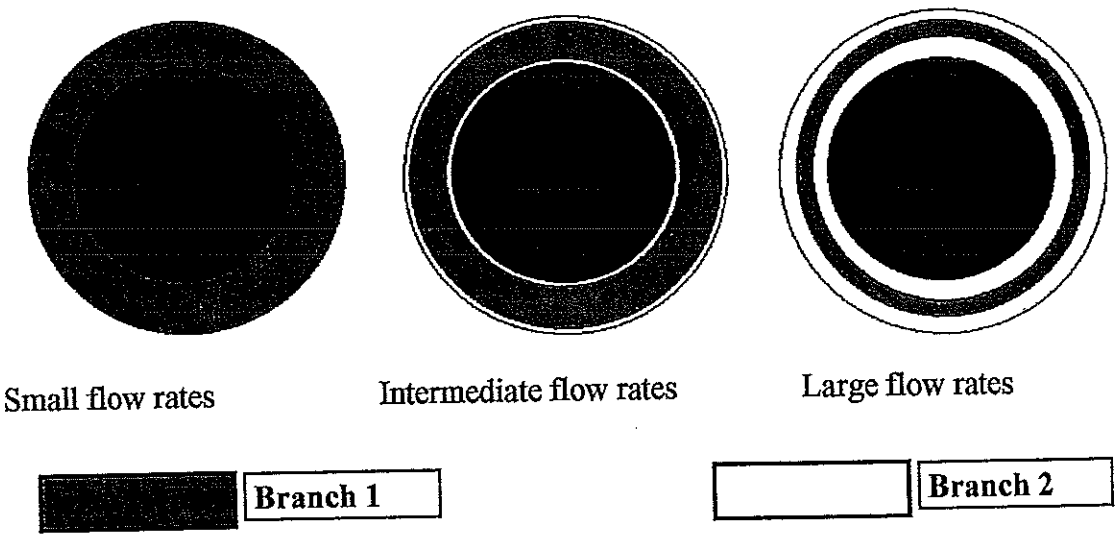

Figure 9. Evolution of the areas associated to the two branches of model in a cross section of the column reactor

CONCLUSIONS

The model has exhibited the problems related to the acceleration of the two-phase flow anolyte. These problems were solved by a simple correction applied on the mean computed residence time. RTD evidenced the effect of the bubbly fluid flow, particularly in the volume of the mesh electrode. The RTD curves are well fitted by the model for both the pilot reactors. It gave a satisfying and comprehensive description of the two-phase flow in each reactor in the whole fluid velocity domain of interest. It was also used successfully for a further coupling with electrochemical and chemical equations in a more general numerical model.

References

[1] Adnet, J.M, Donnet, L., Faure, N., Bros, P.,Brossard, Ph., Josso, F., The development of the SESAME process, Proceedings of the 5th International information exchange meeting on actinide and fission product partitioning and transmutation, Mol, Belgique, 25-27 Nov, 1998

[2] Bourges, J., Madic, C., Koehly, G., Lecomte, M., Dissolution du bioxyde de plutonium en milieu nitrique par l'argent(II) électrogénéré, J. Less Comm. Metals, 122 (1986) 303-311

[3] Moutiney, M.H. and al., Electrogenerated Ag(II) for recovery of PuO2 from wastes, ENC'94, European Nuclear Conference, Nice, France, 2-6 october, 1994

[4] Chiba, Z., Mediated electrochemical oxidation of mixed wastes, Lawrence Livermore Laboratory Report, UCRL-JC-112669, 1993

[5] Chartier, D., Donnet, L., Adnet, J.M., Electrochemical oxidation of Am(III) with lacunary heteropolyanions and silver nitrate, Radiochimica Acta, 83, (3), 129-134, 1999

[6] DTS™, Notice d'emploi du logiciel de simulation D.T.S. version 2.1, Progepi, Nancy, France (1990)

[7] Gonzalez-Garcia, J., Montiel, V., Aldaz, A., Hydrodynamic Behavior of a Filter-Press Electrochemical Reactor with Carbon Felt as a Three-Dimensional Electrode, Ind. Eng. Res., 37, 4501-4511, 1998

[8] Gonzalez-Garcia, J. and al., Characterization of an Electrochemical Pilot-Plant Filter-Press Reactor by Hydrodynamic and Mass Transport Studies, J. Ind. Eng. Res., 39, 1132-1142, 2000

[9] Eigeldinger, J., Vogt, H., The bubble coverage of gas-evolving electrodes in a flowing electrolyte, Electrochemica Acta, 45 (2000) 4449-4456

RADIOISOTOPE TRACER STUDY IN A PILOT-SCALE TRICKLE BED REACTOR

H.J. Pant[1], A.S. Pendharkar[1], J.S. Prasad[2], R.N. Maiti[2], R. Chawla[2], R.N. Lahri[2], D. Ram Babu[2] and Ph. Berne[3]

[1]Isotope Applications Divisions, Bhabha Atomic Research Centre, Mumbai 400 085 (India)
[2] Engineers India Limited, Gurgaon, Haryana (India)
[3] DTEN/SAT – CEA/Grenoble, 17 rue des Martyrs 38054 Grenoble cedex - France

Abstract. Trickle bed reactor (TBR) is a reactor in which a liquid and a gas phase flow cocurrently downwards through a fixed bed of catalyst particles while the reaction takes place. The trickle bed reactors find a number of applications in petroleum refining, chemical, petro-chemical and bio-chemical processes due to their suitability for hydroprocessing operations.The knowledge of radial distribution, mean residence time (MRT), liquid holdup and degree of axial mixing is a basic requirement to evaluate the reactor performance of a TBR, its optimal size, the physical and chemical interactions and the pumping requirements. Measurement and analysis of residence time distribution (RTD) of liquid phase facilitate the determination of these parameters. This paper describes the measurement of RTD of liquid phase in a pilot-scale trickle bed reactor operating at high pressure. Kerosene and nitrogen were used as liquid and gas phase, respectively. Porous alumina catalyst particles were used as packing. Bromine-82 as para-dibromo benzene was used as a tracer to measure RTD of organic liquid phase. The RTD of kerosene was measured as a function of liquid and gas flow rates and pressure. The axial dispersion model with exchange between active and dead zones was proposed and used to simulate the measured RTD data and model parameters i.e mean residence time (τ), Peclet Number (Pe), dynamic fraction of the liquid (ϕ) and the number of transfer units (N) were obtained. The results of the simulations indicated intermediate degree of axial mixing of liquid phase. The RTD predicted by the axial dispersion model with exchange between active and dead zones fits well to the experimentally measured RTD data and thus is a suitable model to describe the dynamics of the liquid phase in TBRs filled with porous catalyst particles.

INTRODUCTION

A trickle bed reactor (TBR) is a reactor in which a liquid and a gas phase flow cocurrently downwards through a fixed bed of catalyst particles while the reaction takes place. In certain cases, the two phases also flow cocurrently upwards. The cocurrent upward flow operation provides better radial and axial mixing than the downward flow operation, thus facilitating better heat transfer between the liquid and solid phases. This is highly useful in exothermic reactions where heat is required to be removed continuously from the reactor. However, due to higher axial mixing in the upward flow operation, the degree of conversion, a crucial factor in the operation of a reactor, is very low. Therefore, cocurrent downward flow operation is preferred because of lower axial mixing, better mechanical stability and less flooding, thus facilitating processing of higher flow rates and increased reactor capacity.

In the last few years, the TBRs have been studied extensively by chemical engineers due to their suitability for many operations in petroleum refining, chemical, petro-chemical and bio-chemical processes. The major processes carried out in TBRs are hydrotreating, hydrocracking, hydrodesulfurization,

hydrodenitrogenation, hydrodewaxing, hydrodemetallisation and hydrofinishing. In effluent treatment plants, the TBRs are used for removal of organic matter from wastewater streams by aerobic bacterial action. The potential applications, advantages and disadvantages of the TBRs have been reviewed in an article [1].

The knowledge of hydrodynamics of liquid phase in a TBR is of paramount importance to evaluate its performance and predict its behaviour. One of the simple and commonly used approaches to study the hydrodynamics of a reactor is to measure the residence time distribution (RTD) of process fluid and to determine the hydrodynamic parameters such as mean residence time, liquid holdup, degree of dispersion and evaluate the radial distribution of the fluid from the measured RTD curves. Radioisotope tracer techniques are widely used to measure the RTD of process fluid in industrial process systems [2]. This paper describes measurement of RTD of liquid phase using radiotracer technique and simulation of RTD curve using a mathematical model.

EXPERIMENTAL

The schematic diagram of the experimental setup is shown in Fig. 1. The TBR consists of a stainless steel column, 6 inches in diameter, filled with alumina catalyst particles cylindrical extrudates shape. Bed porosity is 0.47. A wire mesh is mounted at the bottom of the reactor to support the packing. A liquid distributor is mounted at the top of the packing. Nitrogen (viscosity: 0.017 Cp at 40 ^{0}C) and kerosene (density: 786 kg/m^3, viscosity: 2.4 Cp at 40 ^{0}C) were used as gas and liquid phase respectively and flowed cocurrently downwards through the column. The kerosene stored in a tank of 2.5 m^3 capacity was continuously pumped into the column from the top through the distributor mounted about 0.2 m above the packing. The nitrogen was continuously introduced into the column from the top from a compressor after passing through a surge tank. After passing through the packed bed, the liquid and gas phases were separated in a gas-liquid separator at the bottom of the reactor. Two precisely calibrated rotameters were used to measure the liquid (Q_l) and gas flow rates (Q_g). The nitrogen was released into the atmosphere and the kerosene contaminated with radiotracer was stored in a separate tank at the bottom of the reactor. The experiments were carried out at ambient and elevated temperature. The experimental conditions are listed in Table 1.

A series of radiotracer experiments was carried out to measure RTD of liquid phase. Bromine-82 (half-life: 36 h and gamma energies: 0.55, 0.62, 0.70, 1.48 Mev) as paradibromobenzene was used as a tracer for liquid phase. The experiments were carried out at different combinations of liquid and gas flow rates and about 18 MBq (0.5 mCi) activity was used in each experiment. The tracer was instantaneously injected into the inlet liquid feedline using a specially designed injection system. The tracer was injected after steady state flow condition was achieved. The movement of tracer was monitored at the inlet and outlet of the column using collimated NaI(Tl) scintillation detectors separated by a distance of 2.09 m. In order to investigate the radial distribution/maldistribution of liquid phase at the outlet of the reactor, three detectors mounted at an interval of 90^0 angle were used. All the detectors were calibrated to have the same efficiency and connected to a

five-channel data acquisition system (DAS), which was set to record 1000 data points at an interval of two seconds and connected to a laptop computer.

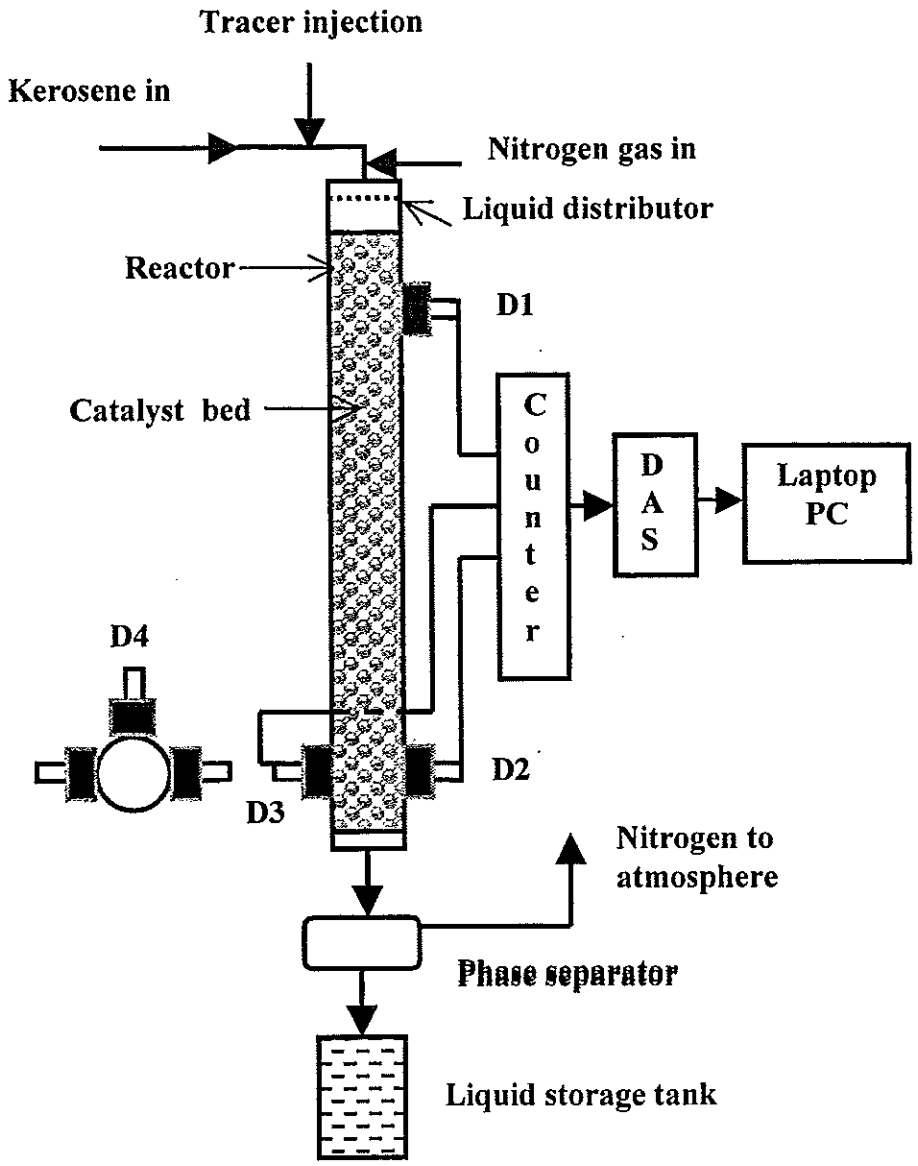

Figure 1. Schematic diagram of the experimental setup.

DATA ANALYSIS AND RESULTS

The measured data were corrected for background and background rise and normalised so that the area under the curves is unity. The normalised RTD were analysed for radial distribution and simulated using a suitable mathematical model.

Radial distribution, in addition to axial dispersion, is another parameter, which determines the efficiency and product quality in industrial packed bed systems. It is of practical significance in reactors with large diameters. An attempt was made to investigate the radial distribution of liquid phase through the packed bed. The tracer concentration curves recorded by the three detectors at the outlet were superimposed on each another and compared. The visual inspection of the normalised output tracer distribution curves indicated minor degree of radial maldistribution or channeling in some of the runs as could be seen from Fig. 2

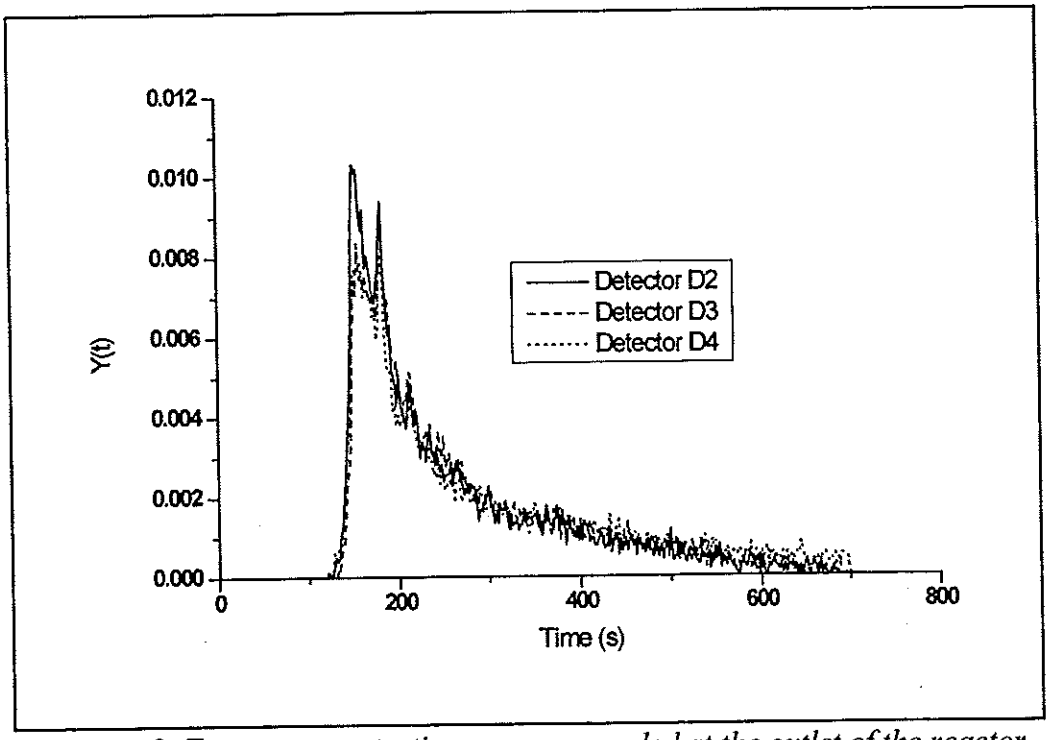

Figure 2. Tracer concentration curves recorded at the outlet of the reactor by the three detectors (P=6 kg/cm^2, Q_g=1.09 x10^{-3} m^3/s, Q_l=10.0 x 10^{-5} m^3/s)

The residence time distribution curves recorded at the outlet of the reactor have a long tail and thus could not be simulated using the simple axial dispersion model [2]. The long tail present in the RTD curve, E(t), may be due to (i) exchange between dynamic and stagnant fluid (ii) exchange between the liquid flow and the porous catalyst particles (iii) the effective diffusion coefficient of the tracer in the particles and (iv) the axial dispersion coefficient of the liquid phase. To describe the RTD curves with long tail measured in packed beds, Villermaux and Van Swaaij [3] proposed a model known as Piston with Dispersion and Exchange (PDE) model. The model is based on the following considerations:

The liquid flow through the packed bed is divided into two parts i.e. a dynamic part consisting of fluid through the bed as plug flow with axial dispersion and a stagnant part consisting of perfectly mixed, isolated stagnant zones exchanging mass with the dynamic part. All mass transfer and diffusion resistances are lumped in a mass transfer coefficient. The mass balance equations describing the model and analytical solution of the model for an impulse injection of tracer are described in

details in references [3,4]. The model has four parameters i.e. mean residence time (τ) dynamic fraction of liquid volume (ϕ), number of transfer units (N) and Peclet number (Pe). The impulse response of the model is calculated in the Laplace domain and translated into the time domain by Fourier transform method. The response of the model, $Y_m(t)$, to a pulse input, X(t), is obtained by convoluting the input signal, X(t), with the impulse response of the model, E(t), and is given as:

$$Y_m(t) = \int_0^\infty X(t-T)E(T)dT \tag{1}$$

The model-simulated curve, $Y_m(t)$, is fitted to the experimental curve, Y(t), and the optimised values of the model parameters corresponding to the best fit are calculated. The quality of the fitting is judged by calculating the value of root mean square error function and is defined as:

$$RMS = \left[\frac{1}{n}\left\{\sum (Y(t) - Y_m(t)\right\}^2\right]^{0.5} = Minimum \tag{2}$$

Least square curve-fitting technique based on Levenberg-Marquardt algorithm was used to obtain the bet fit and corresponding optimised model parameters [4,5]. A computer routine was developed and used to simulate the experimentally obtained RTD curves. The three curves recorded at the outlet of the reactor were simulated independently and values of model parameters were obtained. A representative plot showing the comparison of experimentally measured and model simulated RTD curves is shown in Fig. 3. The mean values of model parameters (τ, ϕ, N and Pe) estimated from model simulation are given in Table 1. The mean residence time (τ) obtained from the model simulation was used to estimate the total fractional liquid holdup using the following relation:

$$H_T = \frac{\tau\, Q_L}{V_R} \tag{3}$$

where H_T: fractional liquid holdup, Q_L: volumeteric liquid flowrate (m^3/s), V_R: effective reactor volume (m^3).

DISCUSSION

It is observed that the PDE model fits very well to the experimental curves. However a large variation in values of model parameters has been observed. This variation may be because of a number of reasons such as inaccurate measurement of tail section of the RTD curve and its truncation, model itself, sensitivity of the model parameters to the variation in model parameters, radial maldistribution of liquid phase and fluctuations in operating conditions during experiments etc. No quantitative analysis of the sensitivity of the error function to the variations in the values of the model parameters has been carried out in the present work. However, the error analysis carried out by Yang *et al.* [4] and Stegeman *et al.* [5] indicated that RMS error is a weak function of Peclet number (Pe) and number of transfer units (N). The values obtained for these parameters are not very precise and represent only order of magnitude. The error function is much more sensitive to the values of mean residence time (τ) and dynamic fraction of

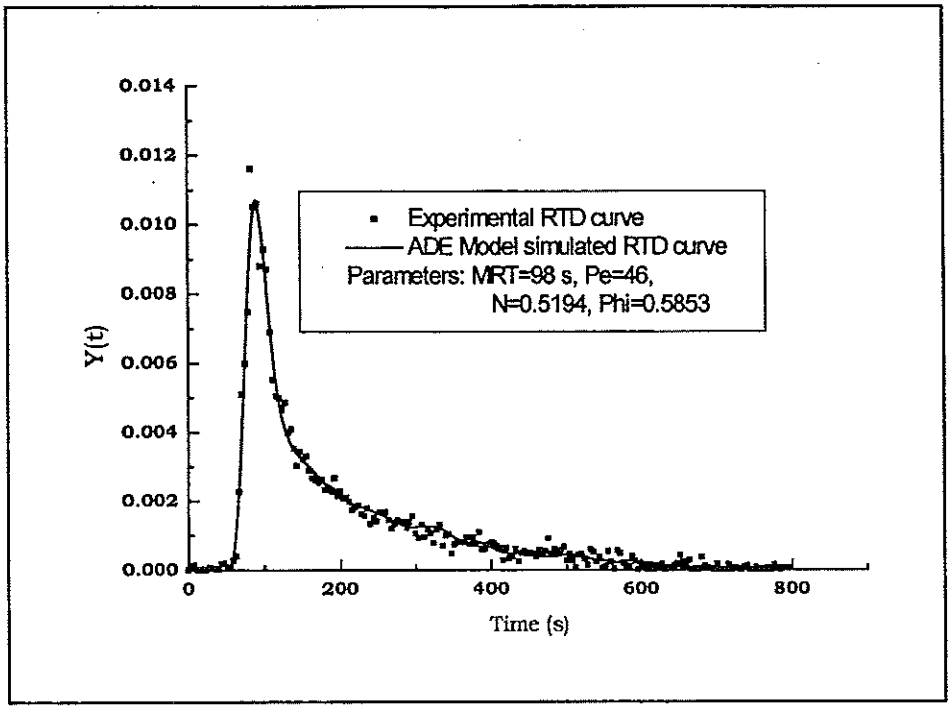

Figure 3. Comparison of experimental and model simulated RTD curve ($P=6$ kg/cm^2, $Q_g=1.92 \times 10^{-3}$ m^3/s, $Q_l=13.33\ 10^{-5}$ m^3/s)

Table 1. Results of model simulation

Sr. No	P (kg/cm^2)	$Q_g \times 10^{-3}$ (m^3/s)	$Q_l \times 10^{-5}$ (m^3/s)	τ (s)	Pe	N	ϕ	H_T
1.	1	0	10.00	146	44	0.962	0.565	0.395
2.	6	1.09	3.33	279	45	0.896	0.653	0.252
3.	6	1.09	6.67	211	47	0.680	0.547	0.381
4.	6	1.09	10.00	172	48	0.831	0.478	0.466
5.	6	1.09	13.33	126	43	0.459	0.513	0.455
6.	6	1.92	3.33	430	22	0.787	0.385	0.384
7.	6	1.92	6.67	311	35	0.904	0.340	0.561
8.	6	1.92	10.00	166	61	0.848	0.456	0.449
9.	6	1.92	13.33	98	46	0.519	0.585	0.354
10.	10	0.652	3.33	380	45	0.550	0.486	0.343
11.	10	0.652	6.67	330	62	1.00	0.362	0.595
12.	10	0.652	10.00	255	67	0.948	0.352	0.690
13.	10	0.652	13.33	139	68	0.880	0.472	0.502
14.	1	0.652	13.33	115	77	0.641	0.571	0.415
15.	10	1.154	3.33	347	48	1.270	0.523	0.397
16.	10	1.154	6.67	225	67	1.150	0.442	0.406
17.	10	1.154	10.00	149	65	0.792	0.540	0.403
18.	10	1.154	13.33	110	52	0.565	0.526	0.397

liquid volume (ϕ) and thus the precision of determination of τ and ϕ is expected to be much better than Pe and N. Considering the above facts, it could be stated that the individual parameters are determined within 10-20% accuracy. Therefore no definite trends in model parameters with respect to varying liquid flow, gas flow and pressure have been observed.

The variation of τ with respect to varying liquid flow rate, gas flow rate and pressure are shown in Fig. 4. From the results it could be stated that, the mean residence time (τ) decreases with increasing liquid flow rate. However, no clear trends in τ with varying gas flow rate and pressure has been observed. At a constant pressure and liquid flow rate, no definite trend has been observed with varying gas flow rates. At a constant liquid flow and pressure (10 kg/cm^2), it is observed that values of τ are lower at higher gas flow rate however, at a pressure (6 kg/cm^2) τ is higher at higher gas flow rate. This does not seem to be logical and needs to be confirmed by repeating the experiments.

The Peclet number (Pe) increases non-linearly with varying liquid flow rates initially, but tends to decrease or become constant after a particular liquid flow rate. This may be due to intensified mass transfer between dynamic and stagnant liquid zones at higher flow rates. At a constant liquid and gas flow Pe increases with increasing pressure. However, no definite trend in Pe is observed with varying gas flow rate.

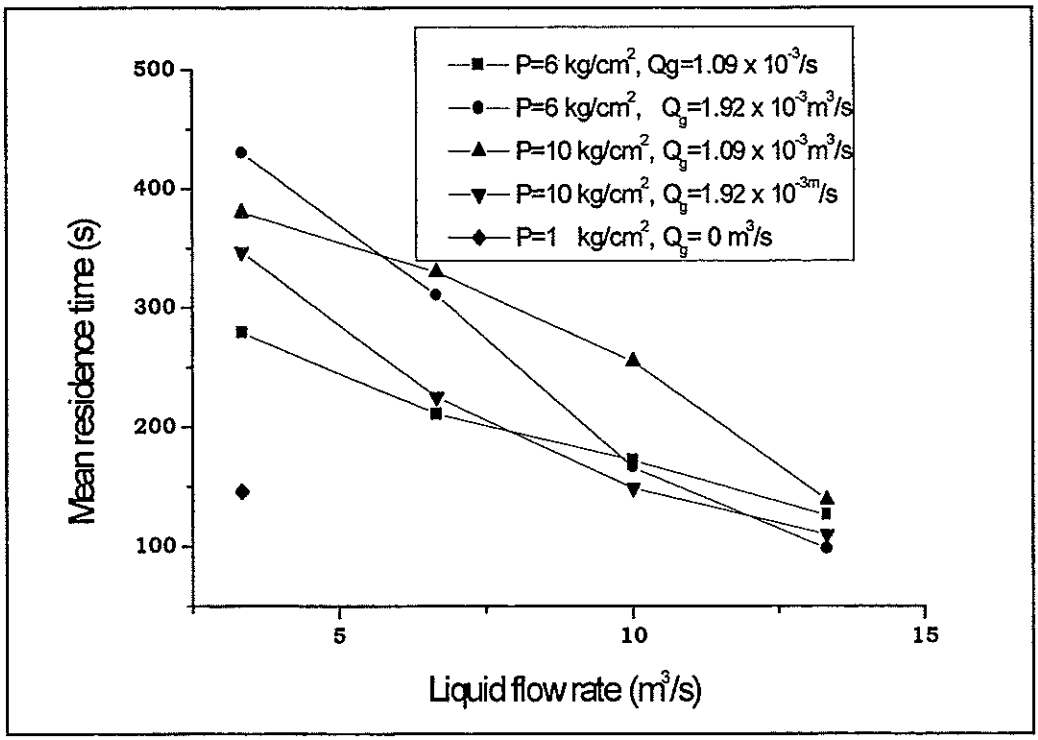

Figure 4. Variation of mean residence time with liquid and gas flow rates and pressure.

No definite and clear trend in N has been observed with varying gas flow, liquid flow and pressure. The dynamic fraction of the liquid volume (ϕ) appears to be increasing with increasing liquid flow rate and decreasing with increasing gas flow. At a constant liquid and gas flow, ϕ is lower at higher pressure. The total fractional liquid holdup (H_T) increases with increasing liquid flow and appears to be independent of gas flow. At a constant liquid and gas flow, H_T is higher at higher pressure.

CONCLUSIONS

The residence time distribution of liquid phase in a cocurrently operated TBR has been measured. The experimentally measured RTD of liquid phase in cocurrently operating TBRs can be described by Piston with Dispersion and Exchange Model (PDEM) proposed by Villermaux and van Swaaij. The model fits very well to the experimental curves, but the values of the best-fit parameters may not be unique. The four model parameters can be adapted to give a good fit with a large scatter in individual parameter values.

No significant radial maldistribution of liquid phase was observed in the reactor. The mean residence time of liquid phase is decreasing function of liquid flow rate. The values of Peclet number obtained from model simulation at different operating conditions indicate that the reactor behaves as a plug flow system with significant degree of mass transfer between dynamic and stagnant liquid zones.

Radiotracer technique in conjunction with model simulation techniques provides an excellent means to investigate the hydrodynamics of liquid phase in pilot scale trickle bed reactor operating at ambient temperature and high pressure.

REFERENCES

[1] Saroha, Anil K., Nigam, K. D. P., *Trickle bed reactors*, Reviews in Chemical Engineering, 12 (1996), 207-347.

[2] International Atomic Energy Agency, *Guidebook on Radiotracers in Industry*, Technical Report Series No. 316, IAEA, Vienna, Austria. (1990), 374.

[3] Villermaux, J., Van Swaaij, W.P.M., *Modèle représentatif de la distribution des temps de séjour dans un réacteur semi-infini à dispersion axiale avec zones stagnantes*, Chem. Eng. Sci., 24 (1969), 1097-1111.

[4] Yang, X..L., Euzen, J.P., Wild, G., *Residence time distribution of the liquid phase in gas-liquid fixed-bed reactors with porous particles*, Chem. Eng. Sci., 45 (1990), 3311-3317.

[5] Stegeman, D., Edwin, F., van Rooijen, Kamperman, A.A., Weijer, S., Westerterp, K.R., *Residence time of liquid phase in a cocurrent gas-liquid trickle bed reactor*, Ind. Eng. Chem. Res., 35 (1996), 378-385.

SIMPLE TRACING METHOD USED TO CHARACTERISE A PACKING EFFECT ON HYDRODYNAMIC OF BUBBLE COLUMNS

S. Moustiri, G. Hébrard and M. Roustan

Laboratoire d'Ingénierie des Procédés de l'Environnement (LIPE, EA 833)
135 Avenue de Rangueil. Dpt GPI-INSA-31077 Toulouse cedex 4 France.

Abstract. The purpose of the present work is to study the effect of a stainless steel packing on the hydrodynamic of two bubble columns of different diameter (15 and 20 cm) operating with co-current up-flow of gas and liquid.
A non steady state salt tracing method is used to characterise the axial liquid mixing with and without packing into the bubble columns. The obtained results show that the axial liquid mixing is affected by the presence of this packing, tending toward the plug flow.

INTRODUCTION

Bubble columns find widespread application in the industrial processes such absorption, catalytic slurry reactions, bioreactions, coal liquefaction and wastewater treatment. Some of these processes depend strongly on the hydrodynamic of the reactors and are more efficiency when the liquid flow is plug. In this study we have succeeded to decrease the liquid mixing using specific packing.

MATERIALS AND METHODS

The columns used are respectively 0.15 and 0.20 m in diameter and 4.25, 4.50 m height. The liquid is tap water at laboratory temperature and the gas used for all experiments is compressed air. Two gas spargers, a perforated plate and a flexible membrane discs, which covered the whole cross section of the column, were used. The sparger characteristics and their connection with the columns are described in table 1.

Table 1. Gas sparger characteristics.

Gas spargers	Square pitch arrangement (mm)	Orifice diameter (mm)	Holes (per cm^2)	Thickness (mm)
Membrane	5	(initial 0.5)	4	2.5
Perforated plate	5	2.5	4	20

Experiments were performed at superficial gas velocities ranging from 0.52 to 5.5 cm/s and at superficial liquid velocities from 0.62 to 2.16 cm/s. The Residence Time Distribution (RTD) curve of the liquid phase was determined by the classical method of tracer. An addition of a shot tracer (NaCl, 100g.l^{-1}) is realised at the bottom of the bubble column, into the liquid inlet, while the time variation of tracer concentration probe (Tacussel XE 100) connected to a conductimeter and to a computer is used to follow this time variation. The response curve obtained

represents the Residence Time Distribution (RTD).

The selected model was the axial dispersion model characterised by the Peclet number (Pe) and the axial liquid dispersion coefficient (Ezl). Assuming the previous operating condition described, the reactor can be considered as closed to the dispersion. The Peclet number is then calculated using the variance σ^2 of the curve RTD in the following equation:

$$\sigma^2 = 2/Pe - (2/Pe).(1-e^{-Pe}) \quad (1)$$

The axial liquid dispersion coefficient (Ezl) can be deduced from Peclet number value:

$$Ezl = U_l H_c / Pe \quad (2)$$

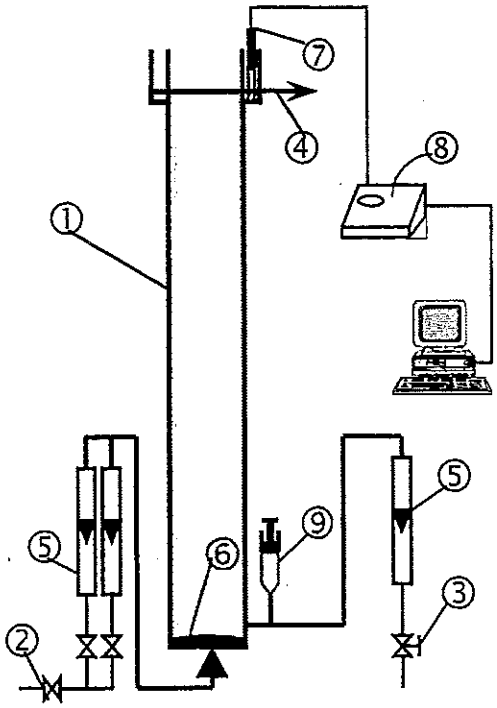

Figure 1. Experimental plant. 1: column, 2: gas inlet, 3: liquid inlet, 4: liquid outlet, 5: rotameter, 6: sparger, 7: conductivity cell, 8: conductimeter, 9: tracer injection.

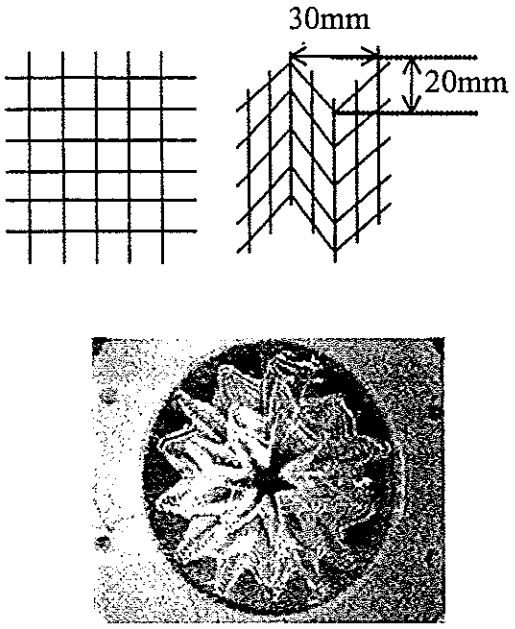

Figure 2. Packing device (grid welded used).

The packing used is made of stainless steel in shape of grid welded of 12.5 mm of coasts; the diameter of yarn constituting the grid is of 0.63 mm. The grid welded is then waved as shown in Figure 2, and it is folded as to fill entirely the bubble columns volume.

EXPERIMENTAL RESULTS

1. Improvement of tracer quantity injected

Residence Time Distribution (RTD) curve was used to characterise liquid flow. In the first time an experimental study has been realised to determine the quantity of salt which must be injected in the liquid inlet. In fact, to be detected, tracer quantity must be enough to have some conductivity value. In the other hand, the tracer quantity injected must not be elevated, so as to keep it in the linearity field between concentration and conductivity.

Figure 3 presents the quantity of salt effect on RTD curve and μ/τ value. The curve corresponding to the more important salt quantity injected has a long tail. Some salt has not been perfectly mixed with the liquid, and has remained in the bottom of column. We can notice on Figure 3 that the injected salt quantity has influenced the μ/τ value. In fact, depending on salt concentration obtained, the linearity field between concentration and conductivity cannot be applied.

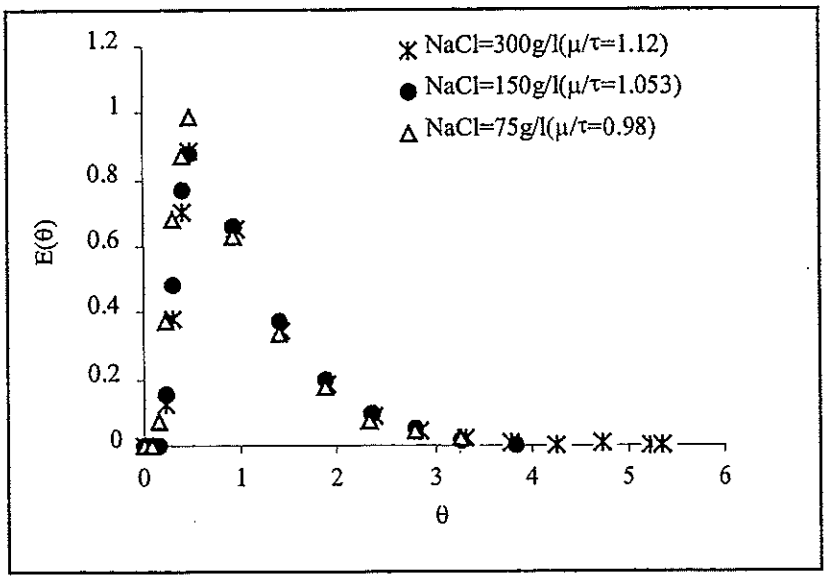

Figure 3. Effect of [NaCl] on RTD curve and μ/τ value

According to Villermaux [1], if there is no stagnant zone, the passage time $\tau=V_R/Q_l$ is equal to the mean residence time μ. The demonstration of this condition is as following:

By definition we have: $V_R/Q_l = \tau$, $dV_R/dQ_l = \mu$, $dQ_l/Q_l = E(t)dt$ and $\int E(t)dt = 1$.
So we can write: $dV_R/Q_l = \mu\, E(t)dt \Rightarrow V_R/Q_l = \mu \int E(t)dt = \mu \Rightarrow \mu = \tau$.
In this study, for each case the condition $0{,}95 \leq \mu/\tau \leq 1{,}05$ has been tested.

The salt quantity influences more or less the RTD curve depending on operating conditions. At high superficial liquid velocity, its effect is less important, because elements tracer are easily transported by liquid recirculations which avoids salt settling at the bottom of the column.

Several experiences have been achieved in order to determine the ideal concentration. To be able to work with the same quantity of salt, we chose to use the

concentration for which we didn't have a disruption in results at low superficial liquid velocity. The quantity of salt injected solution is then, as the final concentration in salt (C_0), in the range of 30 to 70 mg/l. Therefore, whatever the operating conditions, we chose to inject 40 ml of a solution of 100 g/l of NaCl.

2. Axial Liquid dispersion

The liquid phase shows an intermediate behaviour between plug flow and perfectly mixed flow depending on the gas and liquid velocities, column diameter and gas sparger used. Liquid mixing is a result of various contributing mechanisms. These include global convective recirculation of the liquid phase [2], turbulent diffusion due to the eddies generated by the rising bubbles [3], and molecular diffusion, which compared to the other factors is negligible.

1.1. Axial liquid dispersion without packing

In Figure 4 we present different RTD curves obtained at different operating conditions. These curves show the effect of superficial gas and liquid velocities on liquid mixing.

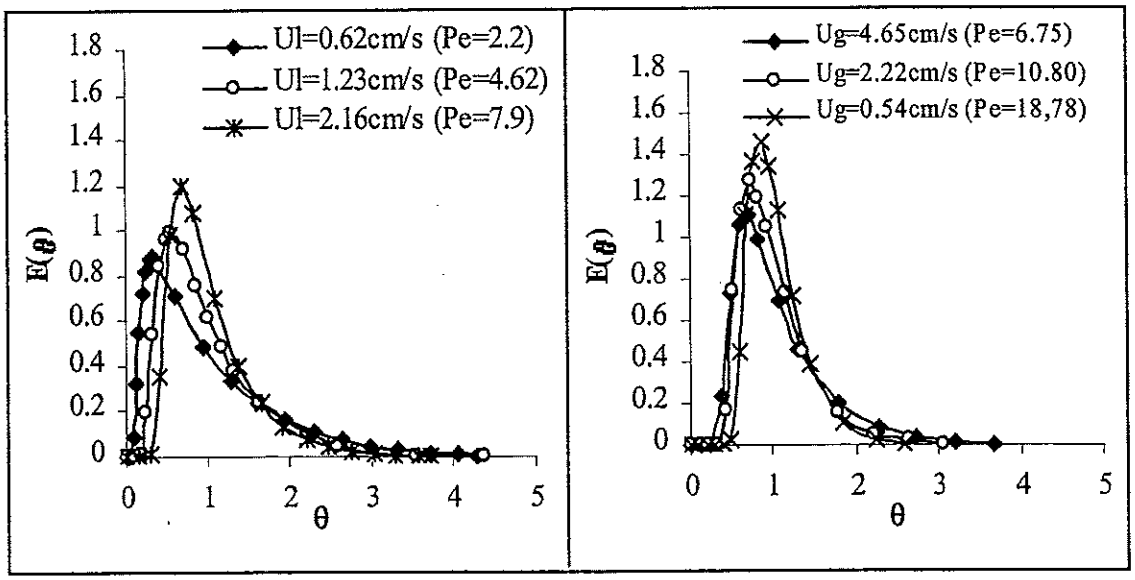

$U_g = 4.65$ cm/s $U_l = 1.85$ cm/s

Figure 4. Effect of superficial gas and liquid velocities on liquid mixing; column I, membrane sparger

At constant U_l, if U_g increases Peclet number decreases indicating that the flow gets agitated. Ityokumbul [4] assumed that the liquid mixing is considered to be caused by the motion of gas bubbles in the liquid. According to the visual observations, at low gas velocity, bubbles are small (3 mm), and rise uniformly without creating perturbations on liquid flow. In this case liquid circulation is absent, indicating an increased residence time of the fluid elements. On the other hand, at higher gas velocity, large fast-rising bubbles appear which disrupt the system contents, resulting an increase in the liquid dispersion.

For a given U_g, the Peclet number increases with increasing liquid velocity

which means that the liquid flow tends toward the plug flow. When U_l increases, liquid element velocities increase, their residence time in the reactor decreases and hence the Peclet number increases.

Table 2. some examples of Peclet number versus superficial gas and liquid velocities obtained with a membrane sparger without packing

U_l (cm/s)	U_g (cm/s)	Pe	
		Dc=15 cm	Dc=20 cm
0.62	0.54	8.7	4.4
	2.22	6.4	3.2
	5.67	1.8	1.5
1.23	0.54	13.2	6.3
	2.22	8.9	4.2
	5.67	2.5	1.9
1.86	0.54	18.8	6.4
	2.22	9.8	6.6
	5.67	3.7	3.3

As seen from Table 2, Peclet number obtained with D_c = 20 cm approximately reduces to half of its corresponding value for D_c = 15 cm under some operating conditions, indicating a pronounced effect of column diameter at lower values of U_g. However, the effect seems to be less for the higher U_g and U_l.

According to Field and Davidson [5], Whalley and Davidson [6] and Towell and Ackerman [7], the liquid mixing increases with column diameter, therefore the Peclet number decreases with D_c. This is due to the formation and increasing size of gross liquid circulation cells with column diameter, leading to greater axial mixing.

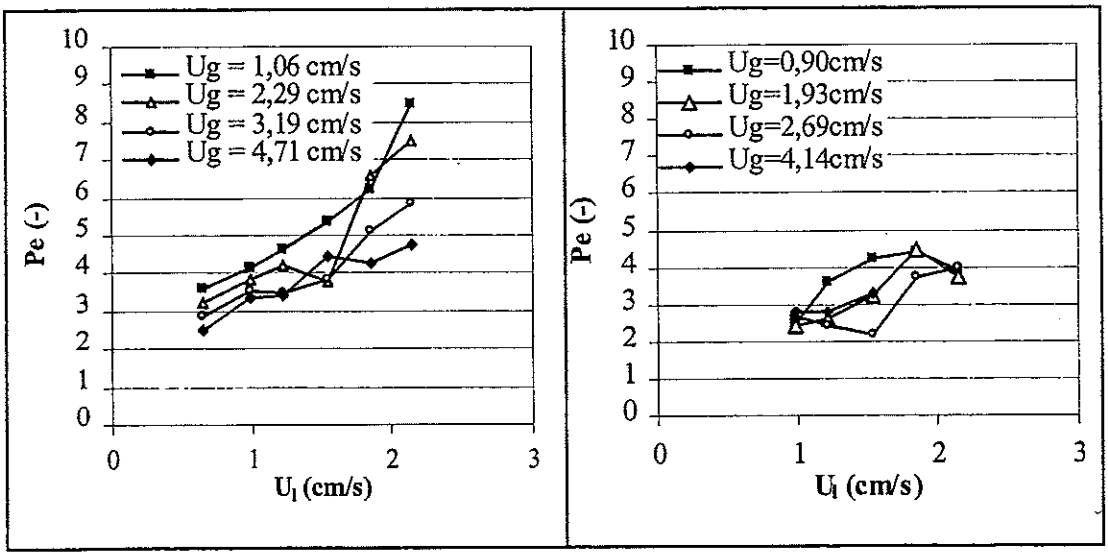

Membrane ***Perforated plate***

Figure 5. Peclet number versus superficial gas and liquid velocities

Figure 5 shows Peclet number evolution with superficial gas and liquid velocities. These results were obtained using a membrane and a perforated plate and show type of gas sparger effect on liquid mixing.

We can note that Peclet number is less important with the perforated plate. It does mean that the liquid is more agitated. In fact, the perforated plate provides relatively large bubbles which create liquid circulations and therefore liquid mixing.

1.2. Axial liquid dispersion with packing

In Table 3 we present some examples of Peclet number obtained on both columns equipped with a membrane as gas sparger in the presence of the packing.

Table 3. some examples of Peclet number versus superficial gas and liquid velocity obtained with a membrane sparger in presence of packing

U_l (cm/s)	U_g (cm/s)	Pe	
		Dc=15 cm	Dc=20 cm
0.62	0.54	18.6	3.38
	2.22	21.1	5.1
	5.67	11.9	4.3
1.23	0.54	28.3	3.9
	2.22	28.5	7.6
	5.67	27.7	6.9
1.86	0.54	22.0	3.3
	2.22	42.7	8.7
	5.67	44.9	11.6

In accordance with the results obtained without packing, liquid mixing is more important on large bubble column and increases with superficial liquid velocity. We expect that the packing creates local agitation in bubble column and therefore the liquid should be more agitated. Actually, this type of packing canalises bubbles movement, which reduces liquid mixing. In fact, since there is a fraction of liquid transported by the bubbles wakes, the presence of this packing makes that liquid element leave the reactor after having passed practically the same time which reduces the liquid recirculation. Since number and size bubble increase with U_g, liquid mixing becomes less important at height superficial gas velocity and Peclet number increases with U_g.

The results obtained with the membrane and the perforated plate show that gas sparger don't affect the liquid mixing. In the ranges of superficial gas and liquid velocities Peclet number obtained with the perforated plate varies from 2 to 12 and with the membrane Peclet number changes from 3 to 14. In accordance with the visual observations, the nozzles of the perforated plate generate bubbles of large size which are split in to small bubbles once arrived at the packing level. For this fact, the gas sparger does not affect liquid mixing.

1.3. Comparison between the two systems results

If we compare the whole of the results, we note that the Peclet number is more

important with the packing indicating that the liquid tends toward a plug flow. In Figure 6 we present an example of RTD curve obtained with and without packing and we note that the shape of the RTD curve with the packing is relatively narrow indicating that the time residence of different liquid elements are near one of the other. This result affirms the previous assumption about the liquid recirculations which are reduced in the presence of this type of packing.

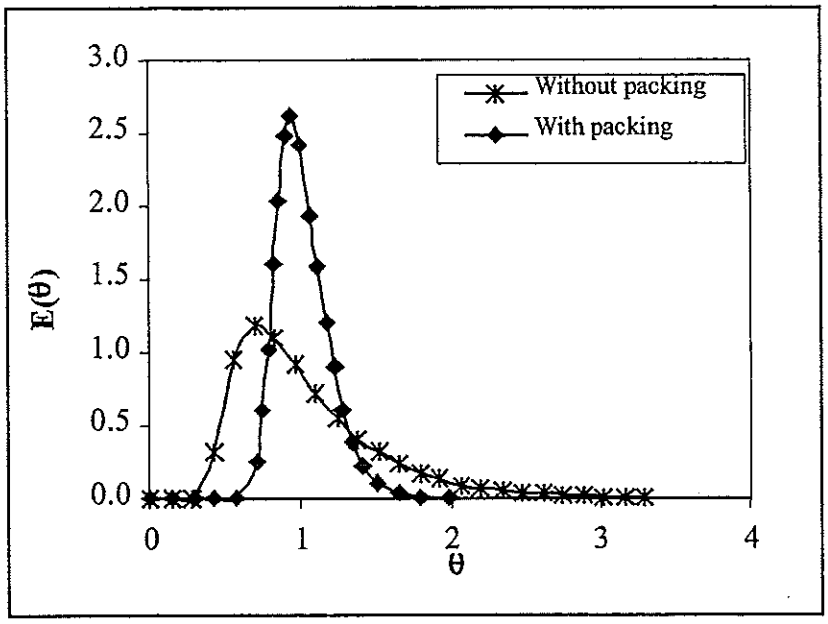

Figure 6. example of "Residence Time Distribution" curve with and without packing $D_c = 15$ *cm,* $U_g = 4.63$ *cm/s,* $U_l = 2.16$ *cm/s*

CONCLUSION

A classical method of tracer has been used to determine the effect of stainless steel packing on liquid mixing of bubble columns. Two columns of different diameter and tow types of gas sparger were used. The following conclusions can be drawn from this work:

Initially a preliminary survey has been done to determine the salt quantity optimal, which we must injected into the column. The final concentration must be in the linearity field between the concentration and the conductivity, and enough to be detected.

The application of this method permitted us to characterise the liquid hydrodynamic with and without packing.

Generally, Peclet number with the packing is greater than that without packing. With the packing, the Peclet number is more important because it canalises bubbles ascension, and the liquid flow becomes plug. The packing effect is more noticed in column I (D_c=15 cm).

Hence in order to control the hydrodynamic of bubble columns, the present packing can be introduced. It can improves the efficiency of a first order reaction by decreasing the liquid mixing.

NOMENCLATURE

D_c = column diameter, (L)
$E(\theta)$ = Residence Time Distribution function versus reduced time, (-)
Ezl = liquid axial dispersion, (L^2T^{-1})
H_c = column height, (L)
Q_l = liquid debit, (L^3T^{-1})
U_g = superficial gas velocity, (LT^{-1})
U_l = superficial liquid velocity, (LT^{-1})
V_R = reactor volume, (L^3)

Dimensionless numbers
Pe = Peclet number, $(U_l H_c/(1-\varepsilon_g)Ezl)$

Greek symbols
μ = mean residence time, (T)
θ = reduced time, (-)
σ^2 = variance of distribution, (-)
τ = passage time, (T)

REFERENCES

[1] J. Villermaux, Génie de la réaction chimique, *Lavoisier, Paris (1993).*
[2] N. Devanathan, D. Moslemian and M.P. Dudukoviċ, Flow mapping in bubble columns using CARPT, *Chem. Eng. Sci., 45 (1990) 2285.*
[3] L.S. Fan and K. Tsuchiya, Bubble wake dynamics in liquids and liquid-solid suspensions, *Butterworth-Heinemann, Boston (1990).*
[4] M.T. Ityokumbul, N. Kosaric and W. Bulani, Gas hold-up and liquid mixing at low and intermediate gas velocities. I. Air-Water system. *Chem. Eng. J. 53 (1992) 167-172.*
[5] R.W. Field and J.F. Davidson, Axial dispersion in bubble columns, *Trans. IChemE. 58 (1980) 228-235.*
[6] P.B. Whalley and J.F. Davidson, Liquid circulation in bubble columns, *Proc of the symposium on multiphase flow systems, Symp ser, No. 38.J.5, Ichem, London (1974) 1-5.*
[7] G.D. Towell and G.H. Ackerman, Axial Mixing of Liquid and Gas in Large Bubble Reactors, *Proc of Fifth European/Second International symposium (1972).*

SALT TRACER USE IN LOOP MULTIPHASE REACTORS

A. Couvert[1], S. Simon[2], D. Bastoul[2], M. Roustan[2], P. Chatellier[3]

[1] CNGE – ENSCR, avenue du Général Leclerc, 35700 Rennes - Beaulieu
[2] INSA - LIPE – Dpt. Génie des Procédés Industriels, 135 avenue de Rangueil, 31077 Toulouse Cedex 4
[3] Suez-Lyonnaise des Eaux - CIRSEE, 38 avenue du Président WILSON, 78230 Le Pecq

Abstract. The aim of this study was to describe the use of a salt tracer method in loop reactors such as air-lift reactors (ALR) and oxidation ditches (OD). The first part concerned the method, its advantages (rapid to implement, reliable, and providing information whatever the number of phases in the reactor) and its limitations. The second part dealt with the application of this method in the two loop reactors. I was shown that the liquid velocity and the mixing parameters (circulation and mixing time, Peclet number and axial dispersion coefficient) could be correctly estimated owing to the Voncken model.

INTRODUCTION

The characterisation of multiphase bioreactors' performances requires the knowledge of the hydrodynamics of these systems, that is the knowledge of several typical parameters. In this way, the liquid velocity V_l, the mixing time t_m, the Peclet number Pe and the axial dispersion coefficient E_{ZL} have to be measured or calculated. Numerous methods exist to get values of these parameters. One method consists in introducing an object which density is the same as the liquid density (like a ping-pong ball filled with water), and timing its route in the reactor. It is an intrusive and approximate, but rapid and cheap method to have an idea of the liquid velocity. In the same family, a radioactive particle can be used as a tracer. It is an extremely precise method to measure the liquid velocity, but not easy to implement and very expensive. Another methods are based on the following of a physical change of the liquid in time. It can be the pH, if an acid or basic solution is injected in the liquid, the colour, if a coloured product is introduced in a transparent reactor, the temperature, by cooling of an anemometric probe, or the conductivity if the tracer used is a salt. There are also non intrusive latest techniques which allow to obtain more information on the local liquid velocity : PIV (Particle Image Velocimetry), method which is still expensive and can only be employed in one-phase flow or two-phase flow with small quantity of gas, or the Ultrasonic Velocimetry. The objective of this study is to describe the salt tracer method, and to implement it in two types of loop reactors. The mixing parameters will be calculated from the Voncken method.

MATERIAL AND METHODS

1. Plants

1.1. Air-lift reactor (ALR)

An air-lift reactor is a loop plant in which the liquid recirculates as a result of the difference in the mean density of the fluid between the riser (aerated part) and the downcomer. As a consequence, they do not need liquid pumping like stirred tanks, and the shear stress is mild throughout the reactor compared to a bubble column.

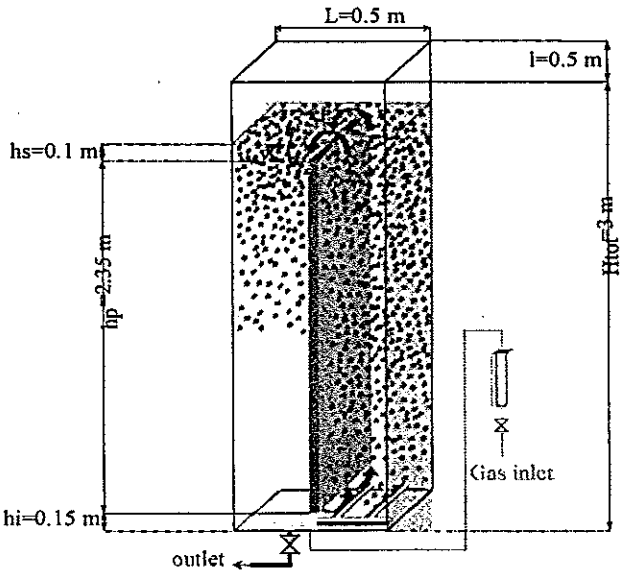

Figure 1. Air-lift reactor

A schematic diagram of the experimental apparatus is shown in the figure 1. The experimental conditions were as given in the table 1. The gas sparger is composed with 2 tubular plastic membranes, located at 5 cm from the bottom of the vessel, but only in one of the two parts of the reactor, the riser. Liquid and gas used are water and air. The main operating parameter is U_{gr}, superficial gas velocity, equal to the ratio of the gas flow rate in the riser Q_{gr} and the riser section area A_r.

Table 1. Air-lift reactor characteristics

Geometric parameters	Dimensions
Reactor height : H_{tot} (m)	3
Reactor depth : L (m)	0.5
Reactor width : l (m)	0.5
Reactor cross section area : A (m^2)	0.25
Internal baffle height : h_p (m)	2.35
Up-flow cross section area : A_r (m^2)	0.125
Down-flow cross section area : A_d (m^2)	0.125
Height below internal baffle : h_i (m)	0.15
Height above internal baffle : h_s (m)	0.1
Non aerated water level : h_l (m)	2.6
Liquid volume (m^3)	0.65

1.2. Oxidation ditch (OD)

The pilot plant has a small-scale oblong geometry (1 m^3 of volume) with outer and inner flow guide. The straight section is 2 m long and the radius of outer flow guide is 0.5 m. This configuration allows to consider the oxidation ditch as an horizontal loop reactor. The liquid velocity is induced by axial immersed impellers. These ones are recommended for their ability in pumping and creating a good circulation of the liquid phase. Two types of impellers were used in the pilot plant : typical marine

propellers (MP of 0.144 m and 0.1 m diameters) and an A310 Lightnin (0.15 m diameter). The main operating parameter is the rotation speed of impeller N.

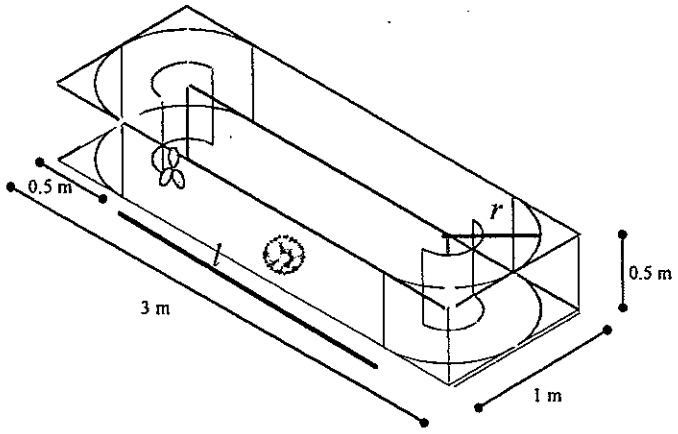

Figure 2. Schema of the Oxidation Ditch

2. Tracer method

The principle consists in :

- injecting a known quantity of NaCl (about 0.1 kg) in a strong mixing area of the reactor (at the top of the downcomer in the ALR, at the impeller in the OD),
- storing the resistance (linked to the conductivity, and then to the salt concentration) of the liquid phase owing to a conductimetric probe type Tacussel XE 100 connected to a conductimetre type Tacussel CD 6N and a PC (see figure 3).

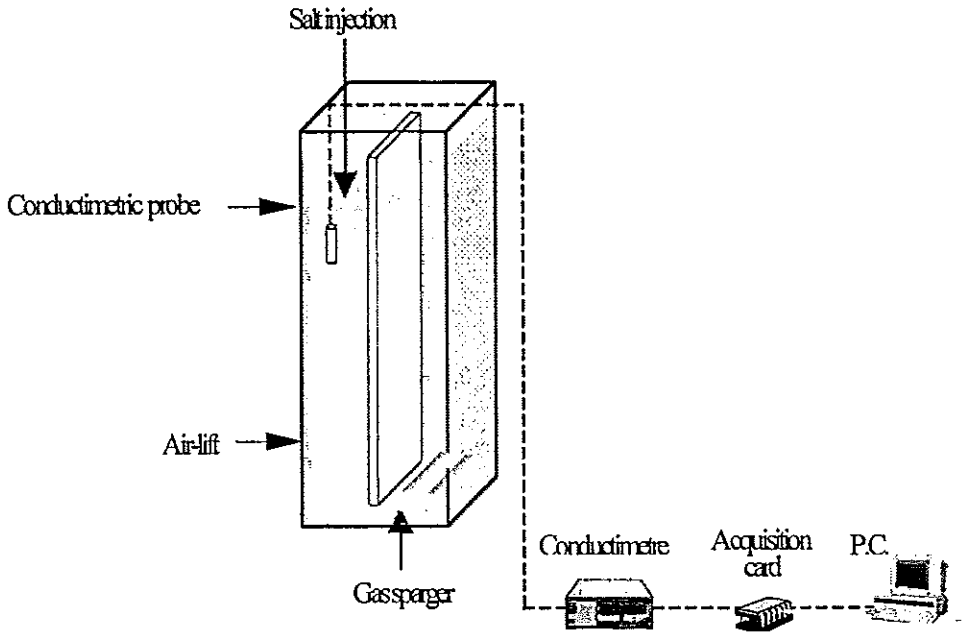

Figure 3. Experimental set-up of the salt tracer method

The signal obtained within this kind of reactor, which are loop reactors, is an absorbed sinusoïde (see figure 4). The mayor inconvenient of this method is that the introduction of a salt can modify the physico-chemical properties of the liquid phase, and then the hydrodynamics of the reactor. Moreover, it is not always possible to inject a salt in the liquid to implement the method (in the industry for example, the plants can not be stopped to proceed to this type of experiments).

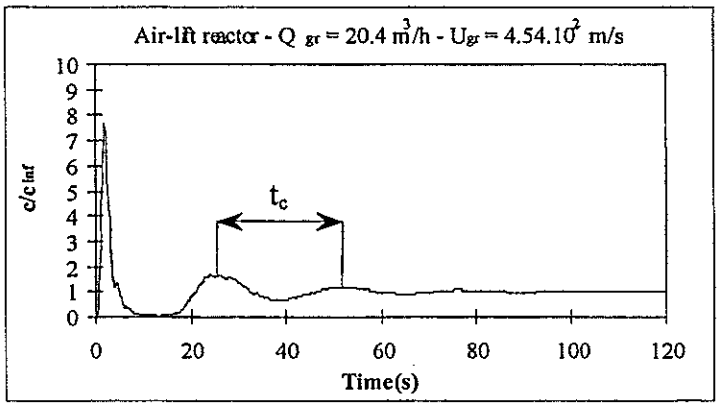

Figure 4. Example of response curve obtained with the salt tracer method

Several types of information can be obtained from this curve :

- an estimation of the mean circulation time t_c, corresponding to the time between two peaks or two valleys;
- the value of the mixing time t_m, time after which the salt concentration reaches x% of the final value, that is time for which the salt concentration is x% homogeneous or (1-x%) heterogeneous (x was chosen equal to 98 for the air-lift reactor);
- the liquid velocity V_l, calculated from the ratio of the tracer route L (estimated) and the circulation time t_c (eq. 1 & 2 or 3):

$$V_l = \frac{L_{loop\ reactor}}{t_c} \tag{1}$$

$$L_{air\ lift} = 2.(h_p+h_i+h_s)+2.(L/2) \tag{2}$$

$$L_{oxidation\ ditch} = 2.l+2.(\pi\, r) \tag{3}$$

- the Peclet number Pe, and the axial dispersion coefficient E_{ZL} adjusted owing to the experimental curve to the Voncken's model [8] (eq. 4 and 5).

$$\frac{c(t)}{c_{inf}} = \left(\frac{Pe}{4\partial\theta}\right)^{0,5} \times \sum_{j=0} exp\left(-\frac{Pe}{4\grave{e}}(j-\grave{e})^2\right) \tag{4}$$

$$Pe = \frac{L.V_l}{E_{ZL}} \tag{5}$$

c is the salt concentration at time t, c_{inf} is the homogeneous salt concentration (x=100%), L is the length of a loop circulation, θ is the dimensionless time (t/t_c).

The superposition of the experimental curve and the Voncken model is done by adjusting both Pe and t_c. The difference between the two curves is quantified by the following criterion (eq. 6) :

$$E = \frac{\sqrt{\sum_{i=1}^{N} (y_{exp} - y_{théo})^2}}{N-1} \tag{6}$$

RESULTS AND DISCUSSION

1. Air-lift reactor

The figures 5 to 9 show the parameters obtained owing to the tracer method in the air-lift reactor.

The time necessary to the liquid to do a loop in the reactor t_c decreases from 45 s to 25 s when the superficial gas velocity U_{gr} (or the gas flow rate) increases from 0 to 0.015 m/s, which is called critical superficial gas velocity $U_{gr_{crit}}$(see figure 5).

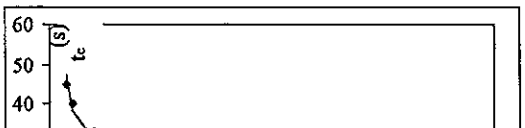

Figure 5. Circulation time

Beyond this value, t_c is constant whatever U_{gr}. Petrovic et al. [6] observed the same tendency in a draft-tube air-lift reactor. As a consequence, the circulation time can be correlated by :

$$\frac{t_c}{t_{c\,min}} = \frac{U_{gr}}{U_{gr} + k} \tag{6}$$

with $t_{cmin} = 24.9$ s and $k = -4.10^{-5}$ m/s.

Several authors have put in evidence the increasing liquid velocity versus $U_{gr}^{0.33}$ or $U_{gr}^{0.4}$ (Bello et al. [1], Gravilescu et al. [3]). For low values of U_{gr}, the results obtained are the same for us. Nevertheless, the figure 6 shows that for $U_{gr} > U_{gr_{crit}}$, V_l reaches a plateau value of about 0.24 m/s. And so, the liquid velocity can be correlated by the equation 7.

$$\frac{V_l}{V_{lmax}} = \frac{U_{gr}}{k + U_{gr}} \tag{7}$$

with $V_{lmax} = 0.24$ m/s and $k = 1.96.10^{-3}$ m/s.

Moreover, some liquid velocity measurements have been done in the low part of the downcomer, using the P.I.V. method (part of the reactor in one-phase flow), and the comparison of the results obtained using the salt as a tracer and the P.I.V. data shows that the tracer method is reliable (see figure 7).

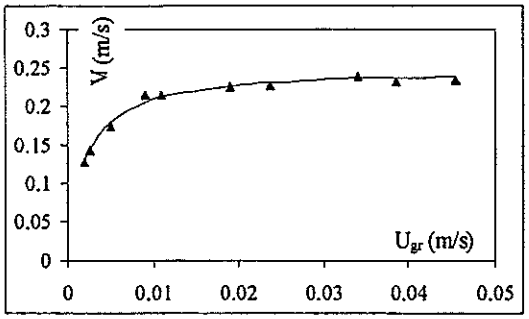

Figure 6. Circulation liquid velocity

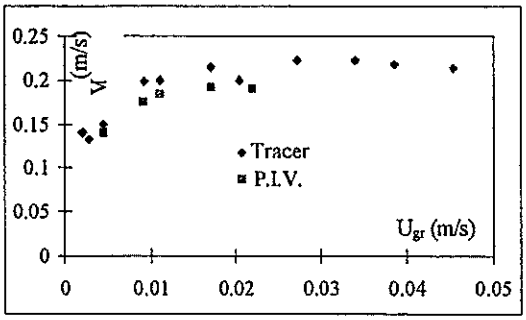

Figure 7. Comparison Tracer/PIV

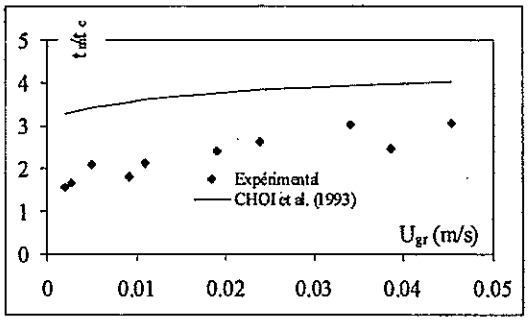

Figure 8. Mixing and circulation times ratio

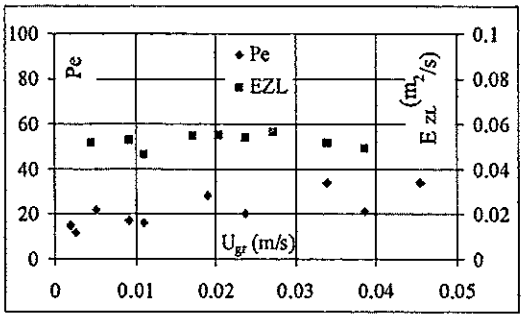

Figure 9. Peclet number and axial dispersion coefficient

As the mixing time t_m is a data dependent on the geometrical characteristics of a reactor, it has been chosen to describe the evolution of the ratio t_m/t_c. The figure 8 gives evidence that the ratios obtained by Choi et al. [2] are lower than the ones calculated for our reactor, that is to say that our reactor is better mixed. This can be explained by the fact that Choi et al. studied an external-loop reactor, which

behaviour can be assimilated to a plug-flow more than a perfectly mixed reactor. Moreover, the values found for our reactor are similar to those reported by Roustan et al. [7] for mechanically agitated reactors ($t_m/t_c \approx 2.3$ for x = 98%).

The figure 9 shows that neither the Peclet number Pe nor the axial dispersion coefficient E_{ZL} are influenced by the superficial gas velocity. Pe varies between 15 and 35 (most of the values are in the range [20 – 30]), and E_{ZL} between 0.04 and 0.06 m^2/s. These data reveal that our ALR is a well-mixed reactor; indeed, Merchuk et al. [4] found values of 0.01 to 0.04 m^2/s in the same range of gas flow rate.

2. Oxidation ditch

The figure 10 reports the experimental velocity U_c versus impeller speed (N) for the MP impeller (0.1 m and 0.144 m diameters). The velocity increases linearly with N. The values of the slope are 0.016 for MP 0.1 m and 0.027 for MP 0.144 m, and are constant for each impeller, but depend on the impeller's diameter. Meziane et al. [5] have put in evidence the increasing liquid velocity versus rotation speed :

$$U_C = b\,N \tag{8}$$

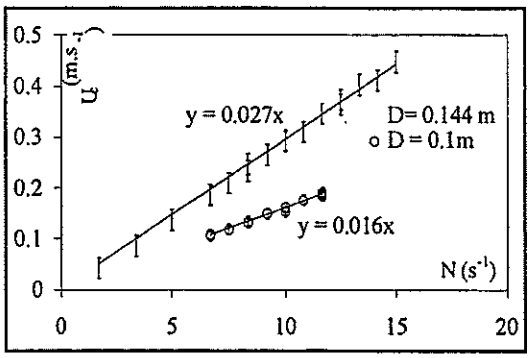

Figure 10 : Mean circulation velocity for marine propellers

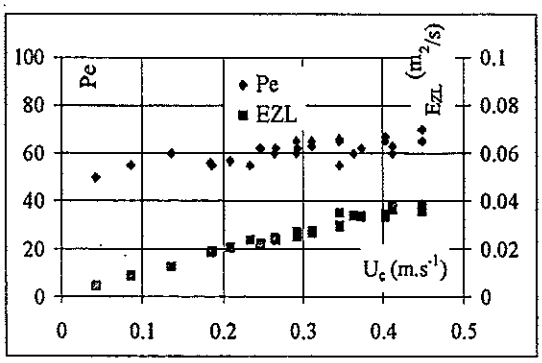

Figure 11 : Peclet number and axial dispersion coefficient

The figure 11 shows the variations of the Peclet number Pe and the axial dispersion coefficient E_{ZL} versus mean circulation velocity U_c. Pe varies between 40 and 60, and E_{ZL} between 0.01 and 0.04 m^2/s. In spite of highly dispersed results, it would be preferable to use high numbers and diameters of impellers. At last, experiments have been carried out in two-phase flow.

The salt tracer method can also be used to validate the numerical approach. An example of experimental results is given on the figure 12. The numerical method fits the experimental data with a good precision. The turbulence was described by the classical k-ε model. The boundary conditions used at the wall were obtained from the classical logarithmic law model. At the outlet of the impeller, they were likened to the boundary conditions of a jet (eq. 9 & 10) :

$$k = 0.003\,U_p^2 \tag{9}$$

$$\varepsilon = \frac{6k^{3/2}}{D} \qquad (10)$$

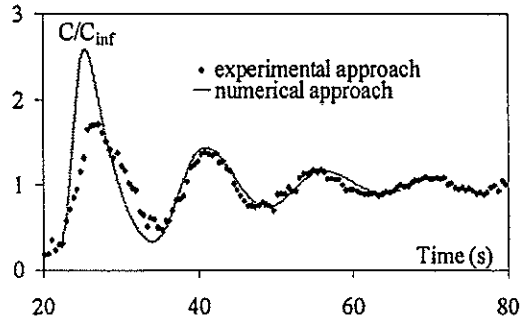

Figure 12 : Comparison of experimental and numerical response curve with the salt tracer method in oxidation ditch

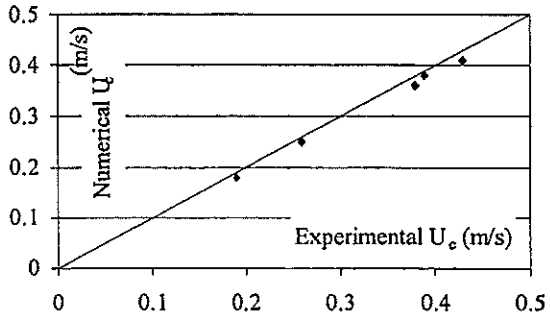

Figure 13 : Comparison of experimental and numerical velocity in oxidation ditch

The modelling consists of imposing a constant velocity for U_p in order to keep the pumping flow rate Q_p constant. The figure 13 reports the numerical velocity versus the experimental velocity in the oxidation ditch. Good agreement is obtained (within 5% of error). The numerical modelling, validated by salt tracer method, allows the circulation velocity and the axial dispersion coefficient to be deduced in very complex geometry as loop reactor.

CONCLUSION

As a conclusion, it has been shown that the salt tracer method and the Voncken's model leads to good global results. Moreover, it can be used in two- or three-phase flow, without any modification in the implementation, and providing results of the same quality and reliability. The use of this method in an air-lift reactor and an oxidation ditch have permitted to measure or calculate the liquid velocity, the circulation and mixing times, the Peclet number, the axial dispersion coefficient. Moreover, recent technologies like P.I.V. or numerical tools have been validated by this method. Easy to implement, it will often be chosen to have a first idea about the circulation and mixing parameters.

REFERENCES

[1] Bello R.A., Robinson C.W., Moo-Young M., *Can. J. Chem. Eng.*, 62 (1984), 573-577.
[2] Choi K.H., Lee W.K., *J. Chem. Tech. Biotechnol.*, 56 (1993), 51-58.
[3] Gravilescu M., Tudose R.Z., *Bioprocess Eng.*, 14 (1995), 33-39.
[4] Merchuk J.C., Contreras A., Garcia F., Molina E., *Chem. Eng. Sci.*, 53(4) (1998), 709-719.
[5] Meziane A., PhD Thesis n°182, INSA Toulouse (France) (1988).
[6] Petrovic D.L.J., Posarac D., Dudukovic A., *Chem. Eng. Sci.*, 45(9) (1990), 2967-2970.
[7] Roustan M., Bruxelmane M., *Techniques de l'Ingénieur*, A10 (1983), 5910-6.
[8] Voncken R.M., Proefschrift ter verkrijging van de graad van doctor in de technische wetenschappen, Technische Hogeschool te Delft, (1966).

CARBON DIOXIDE DYNAMIC ANALYSIS IN γ-Al_2O_3 FIXED BED

Moraes, J. E. F. , Lucena, S. & Abreu, C. A. M.

Laboratório de Processos Catalíticos, Federal University of Pernambuco, 50.740-521 Recife, PE, Brazil

Abstract. An heterogeneous model formulated for description of gas-solid fixed bed continuous processes was evaluated through dynamic analysis of gas-solid contact. The hydrodynamic effects, mass transfer and interaction fluid-solid were taken into account.The distribution (RTD) dynamic technique was employed by estimating the first and second order moments and it was possible to determine the parameters in the model. These parameters, which describe the dynamic profile of carbon dioxide, were then optimized through the deconvolution of the transfer function of the system. Experiments were carried out under isothermal conditions (313K, 348K, 383K) and atmospheric pressure. The fluid phase was composed of carbon dioxide diluted in argon and the solid phase was composed of alumina pellets(γ-Al_2O_3, dp=2.00mm). Carbon dioxide concentration dynamic profiles were obtained after imposition of negative steps to the tracer (carbon dioxide) concentration at the input of the system. For the model it was estimated: the axial dispersion coefficient, which ranged from E_z=31.19$cm^2.s^{-1}$ to 68.35$cm^2.s^{-1}$; the external mass transfer cofficient k_f = 36.05 to 78.95 $cm.s^{-1}$; the effective intraparticle diffusivity D_{eff} = 0.00646 $cm^2.s^{-1}$ to 0.00733 cm^3s^{-1}; the adsorption kinetic constants k_{ad} = 3.40 $s^{-1}$to 32.05 s^{-1}; and the adsorption equilibrium constant K_A = 28.33 to 32.42 .These values can be used to predict the dynamic concentration profiles of in a catalytic process(methanol synthesis, methane reforming,....) where catalysts similar to γ-Al_2O_3 are employed .

Keywords: **Fixed bed, mass transfer, axial dispersion, adsorption..**

INTRODUCTION

The process of mass transfer of a component in a catalytic bed from the bulk of the external fluid into the solid, based on the mechanism of steps in series, may be quantified as relations established between the contents of the component at each level of the system. This is possible when relations at one level are applied and relations are established at an immediately lower level. The quantification of the mass transfer effects in these gas-solid fixed bed process was made possible by experimental techniques, in some cases, which could be linked to theoretical models (Dogu and Smith, 1975; Arnost and Schneider, 1994; Schneider and Valus, 1985; Ruthven and Shah, 1977; Van Deemter et al., 1956). In the present work the dynamic negative-step method was used with carbon dioxide diluted in argon as the tracer. The results for γ-Al_2O_3 packing were analyzed taking into account hydodynamic effects, mass transfer and interaction fluid-solid.

DYNAMIC OF GAS-SOLID PROCESS

An heterogeneous model(HPAD) was formulated for description of gas-solid fixed bed continous processes through dynamic analysis of gas-solid contact. The hydrodynamic effects, mass transfer and interaction fluid-solid were taken into account. The fluid phase was composed of carbon dioxide as tracer diluted in argon and the solid phase was alumina porous pellets.

The application of a mass balance for the tracer component in the interstitial fluid yields :

$$E_z \frac{\partial^2 C}{\partial z^2} - u\frac{\partial C}{\partial z} - \frac{3(1-\varepsilon)}{\varepsilon R} No = \frac{\partial C}{\partial t} \qquad (1)$$

where C is concentration of the tracer, E_z is the axial dispersion coefficient, u is the interstitial velocity of the fluid phase, and R and ε are the particle radii and the bed porosity, respectively.

The mass transfer in the external surface of the particle is given by :

$$No = D_c\left(\frac{\partial C_i}{\partial r}\right)_R = k_f\left[C - (C_i)_R\right] \qquad (2)$$

where D_e and k_f are the effectif diffusion and the mass transfer coefficients, respectively.

The diffusion of the fluid component in the pores of the solid can be represented by :

$$\frac{D_c}{\beta}\frac{\partial^2 C_i}{\partial r^2} + \frac{2}{r}\frac{\partial C_i}{\partial r} - N_i = \frac{\partial C_i}{\partial t} \qquad (3)$$

Assuming a linear kinetics of adsorption for CO_2 in γ-Al_2O_3 the molar flux of the tracer from the intraparticle fluid to the internal surface is expressed by :

$$N_i = k_a\overline{\partial C_i} - \frac{n_a}{K_A} = \frac{\partial n_a}{\partial t} \qquad (4)$$

where k_a is the adsorption kinetics constant, n_a is the concentration of the adsorbed tracer and K_A is the equilibrium adsorption constant.

For the tracer at the outlet of the fixed bed the transfer function $H(s)=C_S(s)/C_E(s)$ is obtained by combining equations 1,2, 3 and 4 and is given by :

$$H(s) = \exp - L\frac{u}{2E_z}\sqrt{1 + \frac{4E_z}{u^2}W(s)} - 1 \qquad (5)$$

where L is the length of the alumina bed and W(s) is a function expressed by :

$$W(s) = \frac{3(1-\varepsilon)}{\dfrac{\varepsilon R^2}{D_c}} 1 - \frac{\dfrac{k_f R}{D_c}}{Ao(s) + \dfrac{k_f R}{D_c}} + s \qquad (6)$$

where:
$$Ao(s) = R\left(\frac{\beta k(s)}{D_c}\right)^{1/2} \coth R\left(\frac{\beta k(s)}{D_c}\right)^{1/2} - 1 \quad (7)$$

$$k(s) = s + \left[(k_a)^{-1} + (sK_A)^{-1}\right]^{-1} \quad (8)$$

EXPERIMENTAL METHODS AND PARAMETER ESTIMATION

In the mass transfer processes and gas-solid contact, porous γ-alumina (Rhône Poulenc, GCO-70) was used. Continuous samplings of the mobile phase (Ar) in contact with 34.5g of the solid bed were made through a thermal conductivity detector with an AD/DA detector/microcomputer interface. The methodologies applied to estimate the flow, the mass transfer and the gas-solid interaction parameters for both CO_2-Ar/γ-Al_2O_3 systems were:

- the treatment of the negative-step curves at the entrance and outlet of the bed; the identification of the base lines and the adjustment of the lower curve by an exponential;
- the residence time distribution (RTD) determination and method of the moments applied to the normalized curves; the comparison of the experimental methods with the expression obtained from the transfer function H(s) (5), developed for γ-Al_2O_3 ;
- the evaluation of the model parameters considered as initialization values when obtained by linearization; the optimization of the concentration values calculated by the models in the real domain and then compared with the experimental data .

RESULTS AND DISCUSSION

From the operations with the CO_2-Ar gas phase and γ-Al_2O_3 solid system in a flow range of 25.10 $cm^3\ s^{-1}$ to 41.15 $cm^3\ s^{-1}$, at 1 atm and at temperatures of 40°C, 75°C and 110°C, changes in concentration in the gas flow at the entrance and outlet of the fixed bed were obtained. The suppression of CO_2 in the argon feed stream in the fixed bed resulted in normalized negative-step curves for the two systems. The values of the parameters k_a and K_A were obtained from the moments of the RTD curves and H(s) for the system and were used in the initialization of H(s) optimization in the time domain(Box, 1965). This procedure introduces modifications in the values of the initialized parameters, reducing to a minimum the differences between the concentrations calculated in the model and those measured by the RTD experiment. The concentrations at the outlet of the bed were calculated by

$$C_s^T(t) = TF^{-1}\left[H(s)C_E(s)\right] \quad (9)$$

where TF^{-1} is the fast Fourier inverse .

The parameters E_z, k_f and D_e, used to start the optimization procedure, were estimated by the equations (11) and (12) (Ruthven,1984) and (13) (Bird,1960):

$$E_z = \frac{1}{\tau} D_m + Ru \tag{10}$$

$$k_f = \frac{ShD_m}{2R} \tag{11}$$

$$D_e = (\beta / \tau)\left(D_m^{-1} + D_k^{-1}\right)^1 \tag{12}$$

Figure 1 shows a typical experimental RTD curve obtained for the tracer at the outlet of the alumina bed .

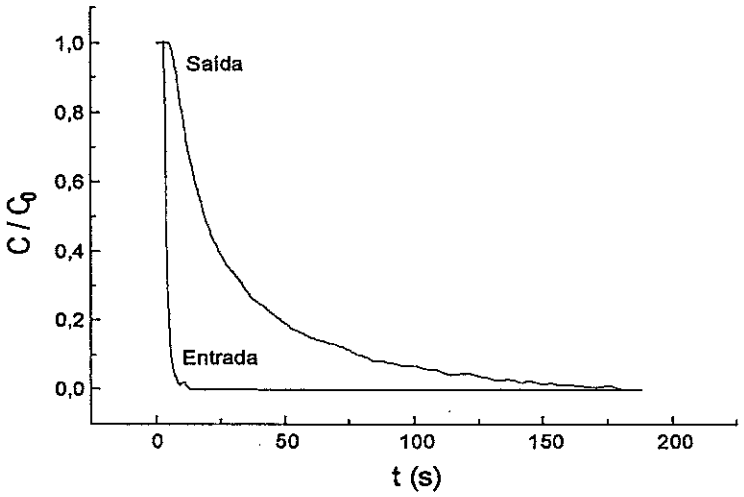

Figure 1. Experimental Dynamic Profiles of CO_2; P =1 atm; Fixed Bed γ-Al_2O_3; 25,34 $cm^3.s^{-1}$; T = 75°C

With the initial values of the parameters applied to expression of $C_S^T(t)$, by the inversion and optimization methodologies, one has access to the optimized final values of the parameters. The results obtained are given in Table 1.

Table 1. Gas-solid optimized parameters

T (°C)	t_0 (s)	k_f (cm.s^{-1})	E_z (cm^2.s^{-1})	k_a (s^{-1})	K_A	D_C x10^3 (cm^2.s^{-1})	FO x 10^3
	0.59	36.05	67.01	28.11			0.66
	0.50	36.40	66.71	27.73			0.64
40	0.44	36.67	68.35	28.64	32.42	6.46	0.86
	0.40	38.92	67.98	32.05			0.64
	0.38	38.95	68.35	29.46			1.05
	0.69	51.67	45.08	8.57			1.03
	0.59	52.63	46.36	8.45			1.45
75	0.53	53.47	47.03	8.56	30.32	6.91	1.21
	0.47	55.85	47.18	8.53			1.05
	0.39	58.43	47.98	8.59			1.16
	0.70	76.67	31.19	3.46			1.08
110	0.59	78.92	32.78	3.70	28.35	7.33	1.20
	0.49	78.95	33.95	3.4			1.39

Figure 2 shows a experimental RTD of CO_2 at 75°C obtained at the outlet of the alumina bed compared with the values of the HPAD model .

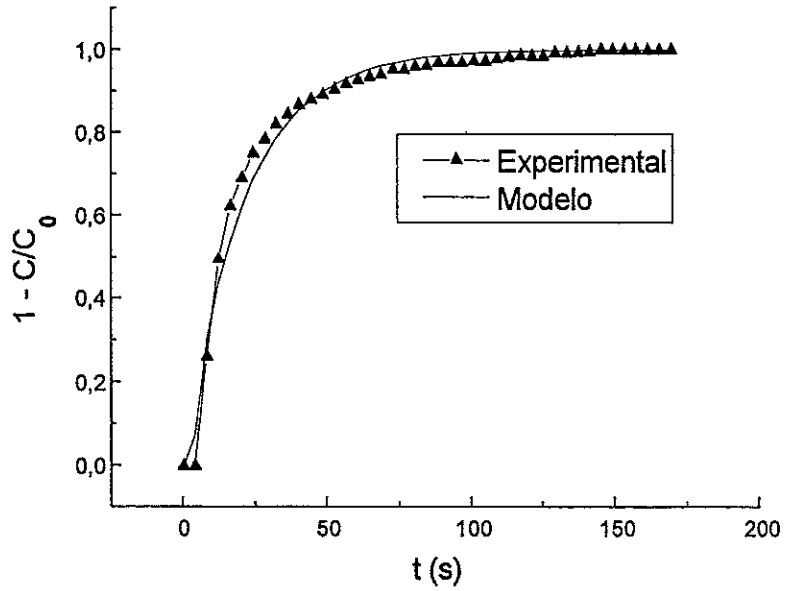

Figure 2. Simulation of the RTD for CO_2 tracer at 75 °C; P =1 atm ;
Fixed bed γ-Al_2O_3

CONCLUSIONS

An heterogeneous plug flow with axial dispersion (HPAD) was formulated for description of a gas-solid fixed bed continuous process. Carbon dioxide concentration dynamic profiles in γ-Al_2O_3 fixed bed were obtained after imposition of negative steps of concentration to the tracer at the input of the system. For the HPAD model it was estimated: the axial dispersion coefficient, which ranged from E_z=31.19$cm^2.s^{-1}$ to 68.35$cm^2.s^{-1}$; the external mass transfer cofficient k_f=36.05 to 78.95 $cm.s^{-1}$; the effective intraparticular difusivities D_{eff}= 0.00646 $cm^2.s^{-1}$ to 0.00733 cm^3s^{-1}; the adsorption kinetic constants k_{ad} = 3.40 $s^{-1}$to 32.05 s^{-1}; and the adsorption equilibrium constant K_A = 28.33 to 32.42 .

REFERENCES

Arnost, D. and Schneider, P., Effective Diffusivities from Dynamic Diffusion Cell: The General Moment Analysis, *Chem. Eng. Sci.*, 49 (3), 393 (1994).

Box, P., A New Method of Constrained Optimization and a Comparison with Other Methods, *Computer Journal*, 8, 42-52 (1965).

Dogu, G. and Smith, J. M., A Dynamic Method for Catalyst Diffusivities, *A.I.Ch.E. Journal*, 21 (1), 58 (1975).

Schneider, P. and Valus, J., Transport Parameters of Porous Catalyst via Chromatography with a Single Pellet-String Column , *Chem. Eng. Sci.*, 40 (8), 1457 (1985).

Ruthven, D. M. and Shah, D. B., Measurements of Zeolithic Diffusivities and Equilibrium Isotherms by Chromatography, *A.I.Ch.E. Journal*, 23, 4 (1977).

Van Deemter, J. J., Zuiderweg, F. J. and Klinkenberg, A., A Longitudinal Diffusion and Resistance to Mass Transfer as Causes of non-Ideality in Chromatography, *Chem. Eng. Sci.*, 5, 271 (1956).

RADIO-TRACER STUDIES OF AN EBULLATED BED REACTOR

S. Kressmann[1], J.M. Schweitzer[1], F. Roche[2]

[1]IFP, Centre d'Études et de Développement Industriel "René Navarre", B.P. 3, 69390 Vernaison, FRANCE
[2]ESCPE LYON, B.P. 2077, 69616 Villeurbanne Cedex, FRANCE

Abstract. Residua from heavy crude oils can be upgraded through various existing processes. Among these processes, the catalytic hydroconversion ebullated-bed process (H-Oil) has the unique feature of deeply converting heavy feedstocks with high impurity contents while operating with a long cycle time. This is accomplished through daily on-line catalyst replacement of a small portion of the catalyst bed. The ebullated-bed reactor includes an internal recirculation of the reactor liquid to ebullate the catalyst bed.

The paper will present background information on the H-Oil Process and discuss some of the recent improvements that have been developed for this technology. A residence time distribution study was conducted using a radiotracer on a new laboratory bench unit of this process. This experiment quantified the reactor hydrodynamics and the liquid hold-up. These parameters are critical to insure a safe extrapolation of the pilot plant results.

INTRODUCTION

The ebullated-bed technology utilizes a three-phase reactor (liquid, vapor, and catalyst). It is most applicable for exothermic reactions and for feedstocks which are difficult to process in a fixed-bed or plug flow reactor due to high levels of contaminates (see 1). The first application of this reactor technology was for vacuum residue hydroprocessing, using the H-Oil Process. This process accounts for 50 per cent of this market due to its unique flexibility to handle a wide variety of heavy crude oils while producing clean fuel oil and transportation fuels. The H-Oil Process is now licensed by IFP NA (2, 3, 4 and 6). The improvement of this process and the technology are an important challenge for the treatment of heavy crude oils. H-Oil industrial licensees require a quick response to their problems or to require improvements due to new regulations or changes in the selectivity of the process. One of the important technical methods for responding to these demands is the chemical engineering studies and all the procedures of scale up/down associated with the design of facilities such as the cold mockup and bench unit. These tools and methods need to be simple but close to the industrial operating conditions.

A residence time distribution study that was conducted using a radiotracer in a bench unit representative of the industrial unit. The objective of this experiment is to set a methodology to better understand the hydrodynamics of this process and subsequently develop a reactor model for the bench unit. This can be combined with a kinetic model to aid in process scale-up.

BACKGROUND ON THE H-OIL PROCESS

Typical operating conditions for the H-Oil Process are shown in Table 1. It is a high

pressure, high temperature process. The operating pressure is relatively high to insure a sufficient reactor outlet hydrogen partial pressure, resulting in good hydrogenation and stable operation.

Table 1 : H-Oil Process Operating Conditions

Temperature, °C	410-440
Total pressure, bar	100-200
Catalyst Space Velocity, h –1	0.25-1.5
Catalyst Replacement Rate (CRR), kg/ton Feed	0.3-2.5
Single Train Throughput, bpsd (Demonstrated)	Up to 34 000

A schematic of the ebullated-bed reactor is shown in Figure 1. It is a fluidized-bed three-phase system with an excellent continuous mixing of liquid and catalyst particles. The inherent advantages of a good back-mixed bed are excellent temperature control and since bed plugging and channeling are eliminated, low and constant pressure drops over several years of continuous operation. Therefore, ebullated-bed reactors have the unique characteristic of stirred reactor type operation with a fluidized catalyst. This results in the ability to handle exothermic reactions, solids containing feedstocks and a flexible operation while changing feedstocks or operating objectives.

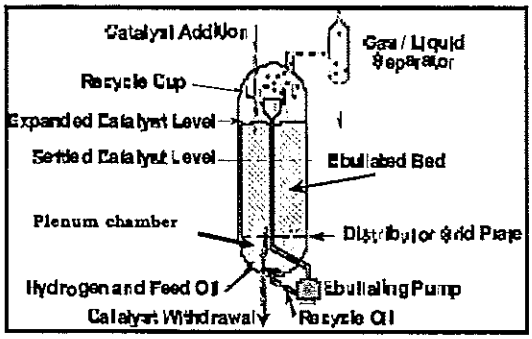

Figure 1: Schematic representation of H-Oil Reactor

The catalyst used for the ebullated-bed is typically a 0.8-mm diameter extrudate with nickel-molybdenum active metals. The catalyst used is held in a fluidized state through the upward lift of liquid reactants (feed oil plus recycle) and gas (hydrogen feed and recycle) which enter in the reactor plenum and are distributed across the bed through a distributor and grid plate. The height of the ebullated catalyst bed is controlled by the rate of liquid recycle flow. This liquid rate is adjusted by varying the speed of the ebullating pump (i.e., a canned centrifugal pump) which controls the flow of ebullating liquid obtained from the internal vapor/liquid separator inside the reactor.

RTD STUDY

1. Objectives

For the development of ebullated bed process, a new bench unit has been constructed and commissioned. This unit operates at commercial operating conditions (temperature and pressure) and closely simulates the commercial yields and product qualities. The qualification of the reactor is an essential point of the methodology of scale-up of data obtained on this bench unit to the commercial unit. The RTD tool has been used for the characterization of the reactor model of the H-Oil Process on the bench unit with the objective to set correctly the scale-up procedure. The reactor model has a great importance for the calculation of performances and namely the conversion of the residue (i.e. perfect stirred reactor, perfect plug flow or series of continuous tank). The results of this RTD study can then be compared to a CSTR. Also the conversion of heavy product is kinetic enhanced if the liquid hold-up at the operating conditions is maximized in the reactor. Therefore the objective is to trace the liquid phase and estimate the liquid hold-up repartition in the reactor versus different operating conditions such as the recycle flow of liquid and the feed hydrogen flow.

2. Experimental

Argon 41 was selected using many criteria: interaction with catalyst, detection, solubility in liquid phase, etc. The injection of this radiotracer was performed in the hydrogen make-up line which is mixed with the feed coming from discharge feed pump. Figure 2 shows a schematic representation of the bench unit in the RTD configuration. A first detector was positioned on the line going to the reactor to measure the inlet pulse. Several detectors were located along the length of the reactor for the estimation of liquid hold-up in the reactor. The last detectors were intended to evaluate the flow at the reactor outlet and in the recycle (ebullating) line.

The configuration of the bench unit is equivalent to the commercial unit. A recycle cup is installed in the reactor to separate liquid and gas before the suction of the recycle pump. The liquid coming from the discharge pump is re-injected at the reactor bottom for the ebullation of the bed.

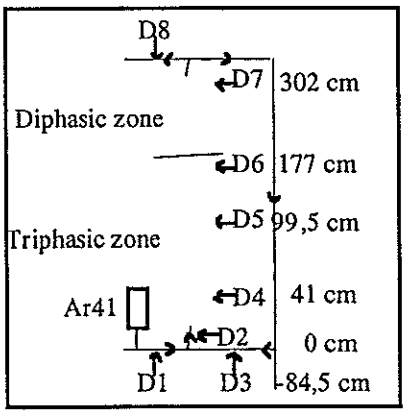

Figure 2 : typical detectors configuration

3. Methodology of Radiotracer study of the ebullated-bed reactor

Argon is injected as one-shot tracer input. The detector D1 will measure the form of the tracer peak at the inlet. The linear velocity between two detectors is determined using the ratio of the distance between two detectors and the mean residence time difference between the two detectors.

The knowledge of the mean linear velocity leads to the value of the liquid hold-up in this portion of the reactor by dividing this value by the superficial liquid velocity:

$$\varepsilon_l = \frac{V_{sl}}{V_l} \tag{1}$$

ε_l is the liquid hold-up, V_{sl} the Superficial liquid velocity, V_l the linear liquid velocity

4. Results on the liquid hold-up

Figure 3a shows that the liquid hold-up increases slightly along the reactor axis for a given set of operating conditions and a fixed recycle flow of liquid. This observation confirms the fact that the solid density is higher at the bottom of the reactor and decreases along the reactor axis. At the top of the reactor there is no catalyst and the reactor hydrodynamic is closer to a bubble column, therefore the liquid hold-up is
maximum.

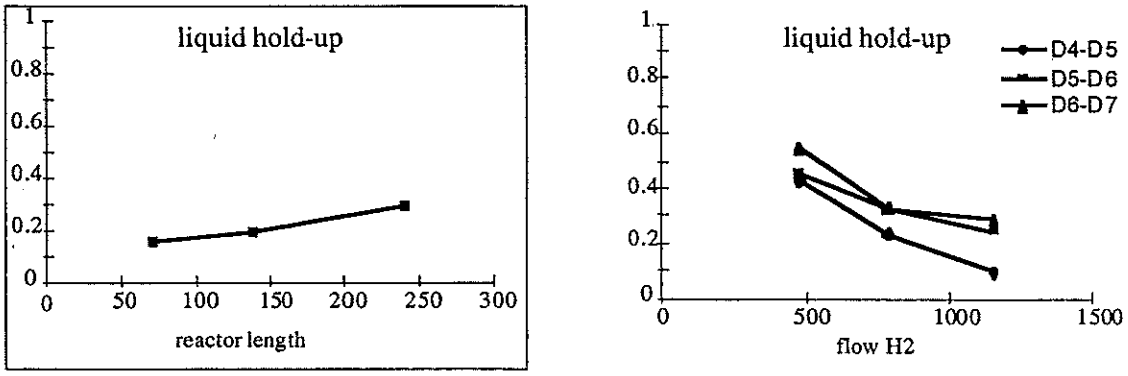

Figure 3a and 3b : Evolution of liquid hold-up versus operating conditions

Figure 3b shows the evolution of the liquid hold-up in the reactor versus the hydrogen flowrate. The liquid hold-up decreases when the hydrogen flowrate increases. This phenomenon shows the impact of hydrogen flow on the performance of the reactor. This parameter has to be optimized to minimize excess gas hold-up and to maximize the conversion. The lower limit of this hydrogen flowrate is a function of the minimum hydrogen partial pressure required at the reactor outlet.

Figure 4 shows the response of four detectors (D1, D4, D6 and D8) to a pulse of Argon41 for a selected operating condition. The detector D1 shows the inlet pulse, the form here was quite similar to a triangle with a significant tail. The shape of the inlet signal has been be taken into account for the outlet signal modelling. The first

peak recorded by detector D4 indicates the progression of the pulse along the reactor. The second and third peaks were due to the Argon re-injected via the recycle line. This point confirms the presence of Argon in the liquid phase. These multiple peaks are typical signals coming from a recirculating system. The decrease of the intensity of the successive peaks is due to the loss of the tracer at the outlet of the reactor as we are in open system and we lose the vapour produced for each conversion per pass in the reactor.

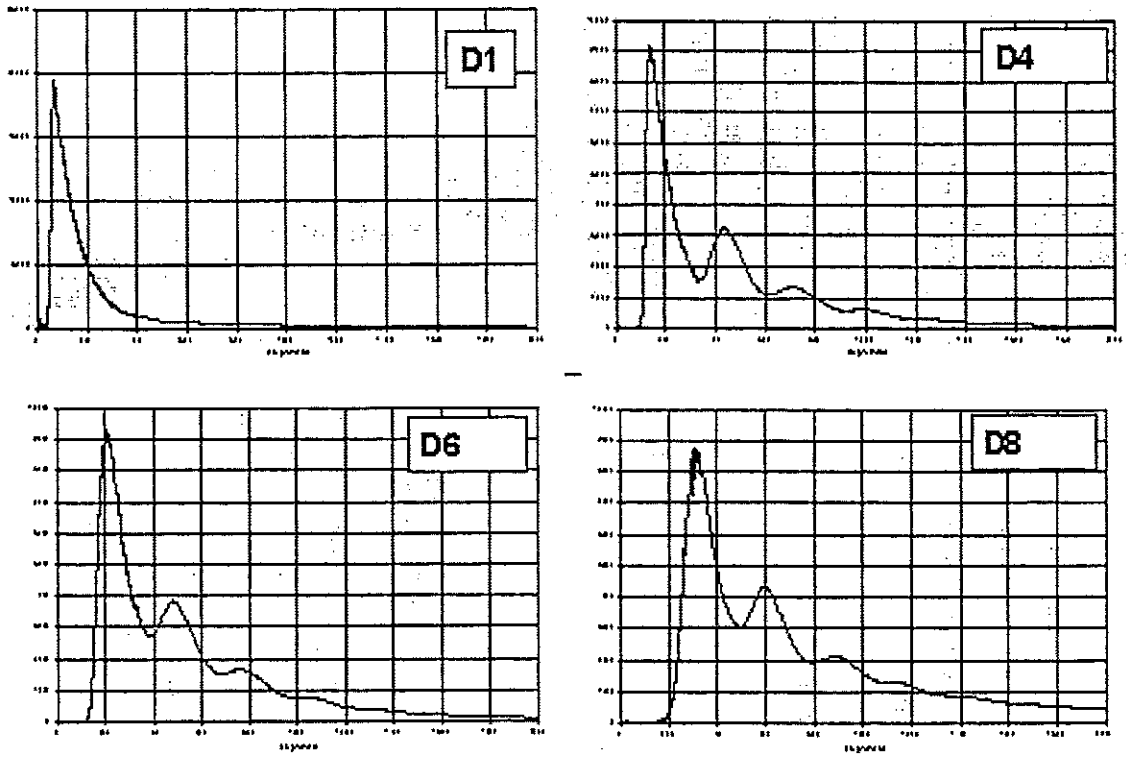

Figure 4: Typical response curves obtained after one-shot tracer

5. Modelling of Results

This recirculated system can be represented as an association of a dispersed plug flow model for the reactor itself and a perfect plug flow for the recycle line. We have modelled the bench reactor using these assumptions and the equations used are described below. The first equation for the dispersed plug flow model takes an axial dispersion coefficient (D_{ax}) into account in the conventional plug flow equation. After simplification of these equations, the Peclet number, which is the ratio of convective term under dispersion coefficient, is the only unknown parameter which is determined by adjusting the model with our RTD results.

$$D_{ax}\cdot\frac{\partial^2 C}{\partial z^2}-u\frac{\partial C}{\partial z}=\frac{\partial C}{\partial t} \quad\Leftrightarrow\quad \frac{1}{Pe}\leftrightarrow\frac{\partial^2 C}{\partial Z^2}-\frac{\partial C}{\partial Z}=\tau\cdot\frac{\partial C}{\partial t} \qquad \text{reactor} \qquad (2)$$

$$-u\frac{\partial C}{\partial z}=\frac{\partial C}{\partial t} \quad\Leftrightarrow\quad -\frac{\partial C}{\partial Z}=\tau\frac{\partial C}{\partial t} \qquad \text{recycle line} \qquad (3)$$

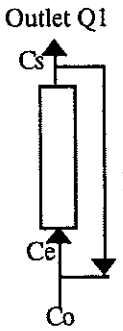

$$Z = \frac{z}{L} \qquad \tau = \frac{L}{u} \qquad Pe = \frac{u.l}{D} \tag{4}$$

$$r = \frac{Q_2}{Q_1} \qquad Ce = \frac{1}{1+r} Co + \frac{r}{1+r} Cs \tag{5}$$

Figures 5a and 5b show the results for D5 detector at a low and a medium recycle flow rate (respectively 6.8 L/hr and 20 L/hr). In the first case, a Peclet of approximately 13 was estimated after adjustment of the model to the data. In the second one, the estimated Peclet value is 50. The Peclet number was determined based on the first peak representation. We have also plotted the exponential decay of an ideal stirred tank using the same residence time and made the superposition with our recirculating system. We can conclude that the response of our bench reactor is intermediate between a perfect CSTR and a perfect plug flow reactor.

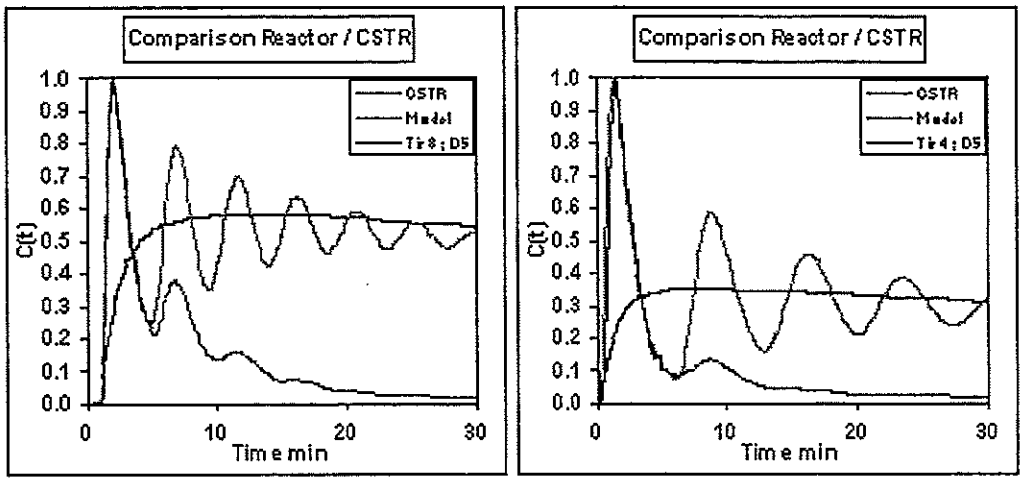

Figure 5a and 5b : Modelling curve compare to experimental and perfect CSTR reactor

The second peak and others peaks are not correctly represented by our model. In order to correct this point, we assume that during the separation of gas/liquid we have lost the Argon in gas phase due to low recycle flow rate in the reactor. The calculated quantity of Argon in the gas phase to fit correctly the experience varies between 55 % v/v (gas phase, 20 L/hr) and 80 % v/v (gas phase, 6.8 L/hr) according to the experiment. Using those molar fractions, the modified model responses are presented in Figure 6a and 6b and shows a very good agreement between the experimental results and the model. The dispersed plug flow model, which integrates gas/liquid separation for the prediction of argon in the recycle line, gives a perfect representation of the experimental curves.

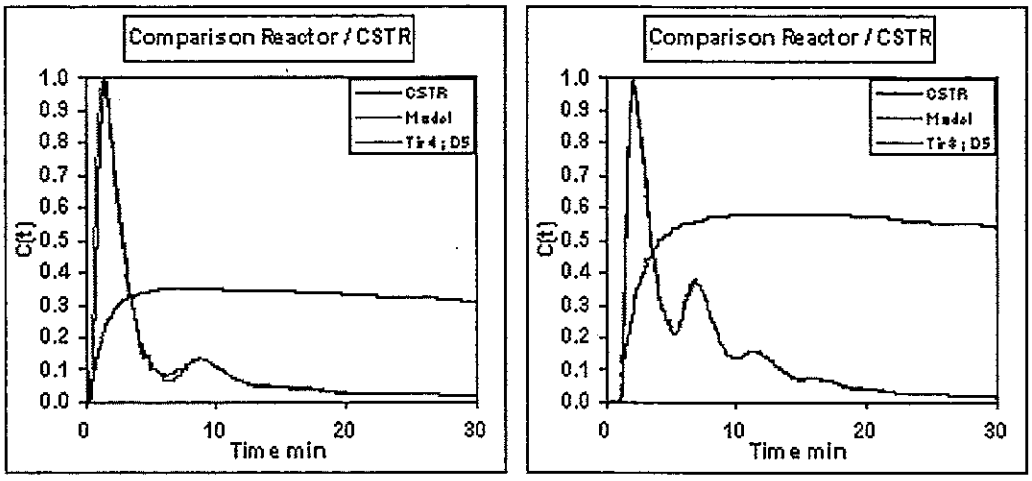

Figure 6a and 6b : Integration of the vaporisation of Argon in the model reactor

The 16 fitted trials permitted to establish a correlation connecting the Peclet number with significant operating parameters of the reactor such as the superficial gas and liquid velocities and the gas and liquid hold-up.

For example, in catalyst zone, this correlation is :

$$Pe = 894.1 \leftarrow Vsl - 18.9 \leftarrow Vsg + 101.6 \leftarrow \varepsilon l - 152.5 \leftarrow \varepsilon g - 29.2 \qquad (6)$$

Vsg is the superficial gas velocity, Vsl the superficial liquid velocity, ε_l the liquid hold-up, ε_g the gas hold-up

Several conclusions can be reached. The Peclet number increases when the recycle flow rate increases too. The reactor tends to be a perfect plug flow reactor model. On the contrary, the Peclet number decreases when the hydrogen flow rate increases. The reactor then tends to be a perfect continuous stirred reactor model.

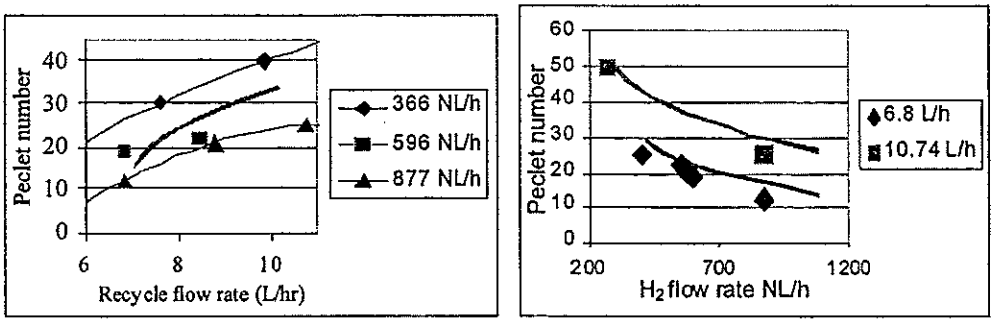

Figure 7 and 8 : Peclet number evolution with recycle flow rate and hydrogen flow rate

CONCLUSIONS

The radiotracer study is a useful method to determine the liquid hold-up inside an ebullated-bed reactor at different operating conditions. This knowledge enables one to characterise the hydrodynamic behaviour of the ebullated bed reactor and to compare the system (reactor and recycle line) with a continuous stirred tank reactor. The tests show that the bench unit catalytic zone is equivalent to dispersed plug flow reactor associated to a Peclet number between 10 and 50 and which depends of the operating parameter (Vsl, Vsg).

The knowledge of the bench unit hydrodynamics is useful to support the comparison of pilot plant data with industrial data and to scale-up pilot plant results.The scale-up of the process can be achieved through pilot plant operation and process modeling. It is very important to ensure the scale-up procedure and to characterize the pilot plant operation. The RTD Study discussed in this paper was useful to address those points.

ACKNOWLEDGEMENTS

The RTD work was conducted with the support of CEA (Commissariat à l'Energie Atomique) for performing the experiments using radioactive Argon 41 tracer. The authors acknowledge MM V. Blet and X. Vittar for fruitful discussions and the work done during the tracing campaign.

REFERENCES

[1] Morel F., Kressmann S., Harlé V., Kasztelan S., *Processes and Catalysts for Hydrocracking of Heavy Oil and Residues*, Stud Surf. Sci. Catal., 106, (1997), 1.

[2] Colyar, J.J. and Wisdom, L.I. (1994), *Second Generation Ebullated-Bed Technology*, JPI Petroleum Refining Conference, Tokyo, Japan.

[3] Colyar, J.J. and Wisdom, L.I., (1997), *The H-Oil Process: A Worldwide Leader in Vacuum Residue Processing*, 1997 National Petroleum Refiners Association Annual Meeting, San Antonio, TX.

[4] Colyar, J.J. and Wisdom, L.I. (1992), *Upgrading Vacuum Residue from Mexican Crudes for Petroleos Mexicanos Hydrodesulfurization Residue Complex Miguel Hidalgo Refinery*, Japan Petroleum Institute, Tokyo, Japan.

[5]. Levenspiel O., *Chemical Reaction Engineering*, 2nd Edition, John Wiley, New York, 1972.

[6]. S. Kressmann, J. J. Colyar, E. Peer, A. Billon, F. Morel, *H-Oil Process Based Heavy Crudes Refining Schemes*, 7th Unitar Conference on Heavy Crude and tar Sands, Beijing, China, October 27-30, 1998, pp 857-866.

TRACER RESPONSE RTD-MEASUREMENTS IN SPIRAL-WOUND RO-MEMBRANES

D. Van Gauwbergen[1], E. Neyens[1] and J. Baeyens[1]

[1]K.U.Leuven, Department of Chemical Engineering, de Croylaan 46, 3001 Heverlee, BELGIUM

Abtract. Reverse osmosis (RO) finds increasing applications as separation technique in chemical, agro-industrial and environmental technology. To model the process,the separation efficiency is expressed in terms of mass transfer with material balances, pressure drop through the module and mass transfer coefficients as dominant parameters. Important underlying factors are the geometry of the module and the hydrodynamic flow regime since mass transfer and pressure drop are a function of these factors. The determination of the concentrate channel flow regime can be carried out through the measurement of the residence time distribution (RTD).

Our research has been mainly focussed on commonly used spiral wound modules although some RTD-experiments have also been performed using plate-and-frame modules [1]. RTD measurements resulting from a step change in tracer concentration were made for various experimental layouts i.e. (i) a short Millipore spiral wound membrane module of diameter 0.045 m and length 0.305 m and (ii) a long Desal spiral-wound membrane module of diameter 0.0975 m and length 1.017 m.

The 'mesh step' model relates the flow conditions in the spacer filled concentrate channel to the boundary layer thickness. This boundary layer is assumed to develop in a saw-tooth fashion between successive mixings as a result of the presence of the net-type turbulence promoter. The RTD-function can be expressed in terms of the boundary layer thickness (δ) or its ratio to the half channel width (δ/h) which can assume two extreme values i.e. zero, corresponding to plug flow and one, corresponding to laminar flow. Experimental results define δ/h and stress the importance and relevance of the mesh-step approach in describing concentration polarisation phenomena in spiral wound modules.

Keywords. concentrate channel, residence time distribution (RTD), concentration polarisation, pressure drop, mesh step approach

INTRODUCTION

Net-type turbulence promotors (spacers) are commonly used in spiral-wound membrane modules to enhance the fluid mixing, and increase the associated transfer phenomena. The concentrate (feed) section of the module plays the key role. The presence of the spacer alters the geometry of the concentrate channel and determines the hydrodynamics to a large extent. Appropriate definitions of the characteristic dimension of the channel and of the associated Reynolds number are needed in the determination of e.g. the pressure drop or mass transfer coefficient. The geometry of the module and derived Reynolds number are detailed in [2] and summarised hereafter.

To assess the effect of the spacers on the overall hydrodynamic flow regime in the concentrate channels, the measurement of the residence time distribution (RTD) was used in our research. The present paper describes (i) RTD-measurements as resulting from a step change in tracer concentration and (ii) the RTD-response curves and their relation with the regime of channel flow.

GEOMETRIC CHARACTERISTICS

The hydrodynamics in a spiral wound module are influenced by the overall geometry of the channel, as well as by the presence of the spacer material. The characteristics of the spacer leafs are of major importance. The concentrate spacer keeps the two membrane sides of the high pressure envelope at a distance of 0.5 to 1.0 mm.

The characteristic dimension of the spacer-filled channel is the hydraulic diameter, d_h, which can be related to geometrical data [channel thickness d(m) and width B (m); overall voidage fraction ε; the volume occupied by the spacer V_{SP}; the total (empty) channel volume V_t and the specific surface area of the spacer a_{SP}] [2]. Table 1 summarises the characteristic geometric data of the concentrate spacers used in our experimental set ups for RTD-measurements.

Table 1. Geometric data for different concentrate spacers

	d_{SP} [mm]	d_F [mm]	l_m [mm]	ε [-]	a_{SP} [mm^{-1}]	d_h [mm]
Lab scale experiments						
RO25 Millipore	0.80	0.400	2.6	0.88	10.0	0.95
Desal 11 AG-4040	0.66	0.340	2.4	0.89	11.8	0.81

The normal feed rate for 4040 spiral wound (spacer filled) modules in industrial applications varies between 700 and 3600 l/h, corresponding to a velocity between 0.06 and 0.3 m/s. RTD-experiments are therefore carried out with all experimental set ups for this range of velocities. Introducing the d_h-values in the expression for the Reynolds number yields values between approximately 35 and 400. For open channels these low values of Re would indicate that the flow is laminar. Due to the presence of the turbulence promoters, no such conclusion should be made for the concentrate channels.

RTD IN CONCENTRATE CHANNELS

1. Experimental procedure

RTD-experiments using a step injection of a KCl-tracer solution are performed with an experimental set up containing a spiral wound membrane as shown in Fig. 1, at varying feed rate. Details of the techniques as applied to the spiral-wound modules are described elsewhere [2].

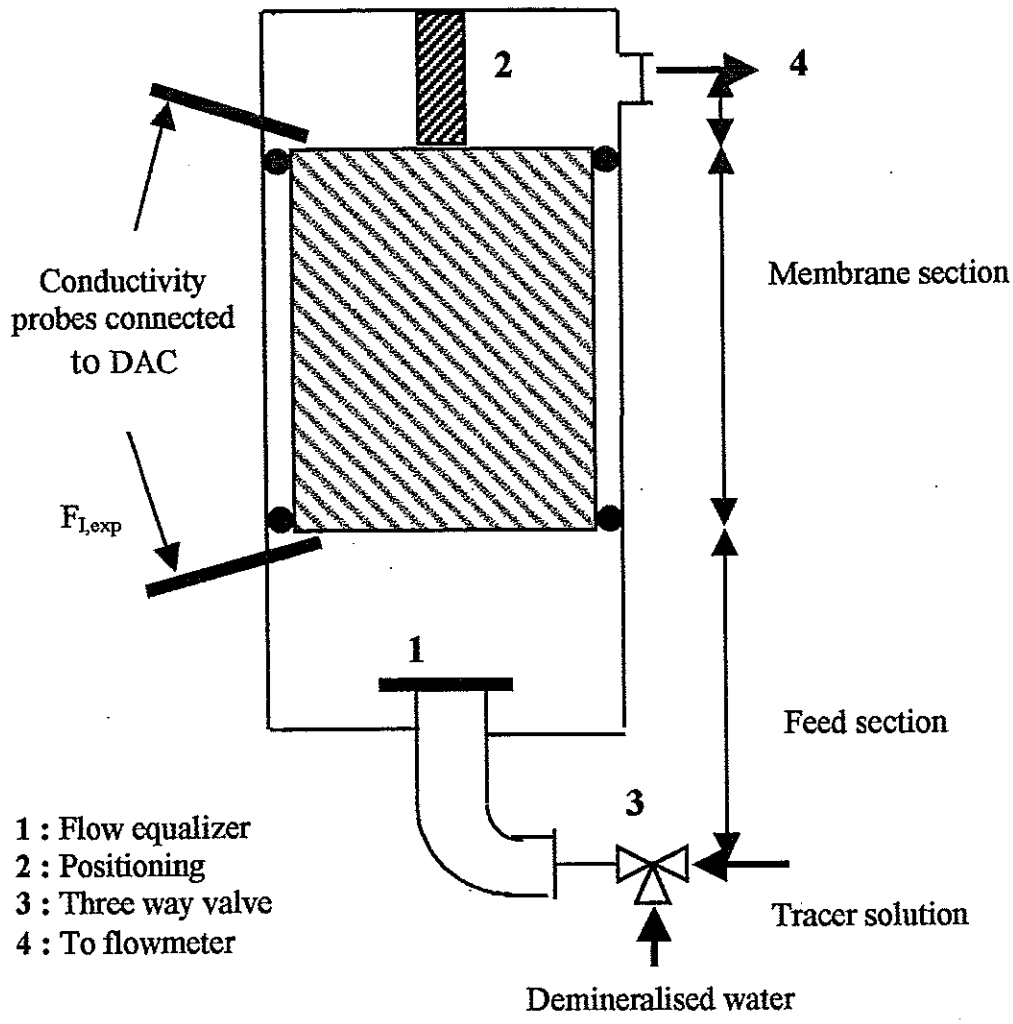

Figure 1. Experimental set up

To avoid preferential flow patterns in the concentrate channel, the set up is provided with an inlet zone and a flow equaliser, to obtain a fully developed flow profile before the flow enters the spiral wound element. To eliminate the effect of this zone on the RTD of the spiral wound membrane element, the principle of convolution needs to be applied because the entry time exceeds 3% of the mean residence time [3].Conductivity probes are located just underneath and above the spiral wound membrane cell. The evolution of the conductivity is registered with the Data Acquisition Card (DAC), time zero corresponding to the step injection.

The membrane module used in the small scale experiments is the 2514 RO25 (Millipore) membrane element, whereas a 4040 Desal 11AG membrane module is used in the large scale set up. Details concerning the spacer material are summarised in Table1. For all experimental set ups the flow of demineralised water and tracer solution are metered by a rotameter located downstream of the membrane module.

2. Illustration of results and data treatment

The measured response curve to a step function is the F(t)-curve, obtained from tracer concentrations :

$$F(t)=\frac{C(t)-C(0)}{C_\infty-C(0)} = \frac{[\text{conductivity at time t}] - [\text{conductivity at time 0}]}{[\text{conductivity at infinite time}] - [\text{conductivity at time 0}]} \quad (1)$$

An illustration of the transformed results for the Desal 11AG experimental set up is given in Fig. 2 which also illustrates the repeatability of the experiments

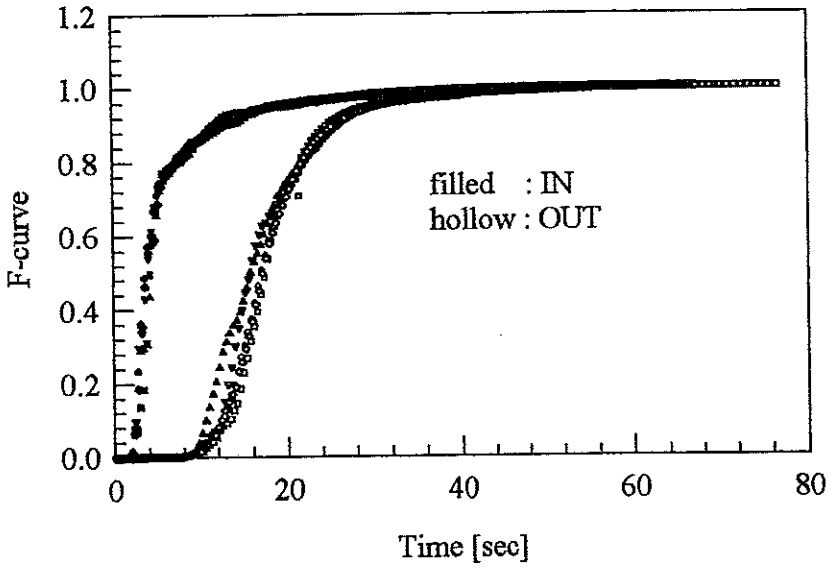

Figure 2. Illustration of the transformed F-curve of experimental data Desal 11AG (341.8 l/h)

The average residence time of the fluid in the membrane module, τ_{exp}, is an important characteristic. For a linear system, this average residence time can be obtained as the difference of the means of the outlet and inlet signals [4]:

$$\tau_{exp} = \left[\int_0^1 t\cdot dF(t)\right]_{out} - \left[\int_0^1 t\cdot dF(t)\right]_{in} = \left[\sum_{i=1}^{N-1}\{F(t_{i+1})-F(t_i)\}\frac{\{t_{i+1}+t_i\}}{2}\right]_{out} - \left[\sum_{i=1}^{M-1}\{F(t_{i+1})-F(t_i)\}\frac{\{t_{i+1}+t_i\}}{2}\right]_{in} \quad (2)$$

This experimentally determined residence time can be compared with the theoretical residence time τ_c as follows :

$$\tau_c = \frac{\text{free volume of concentrate channel}(m^3)}{\text{flow rate}(m^3/s)} \quad (3)$$

with a free volume as determined by immersion experiments [5].

Due to the experimental set-up with measurement of response curves over two systems connected in series, the convolution principle should be applied [4]. If $F_I(t)$ is the experimentally determined F-curve at the entrance of the membrane module, $F_L(t)$ the experimental F(t)-curve at the exit of the module and $E_m(t)$ the theoretical E-curve over the concentrate channel, then the convolution principle fixes the F*(t)-curve by convolution of F_I and E_m or $F^* = F_I * E_m$. Through the convolution principle of $F_I(t)$ and $E_{M,theo}(t)$ the resulting F*(t)-curve should correspond with the measured F_L-curve provided the model parameters are accurately selected to represent the flow regime.

3. Average residence time

The average experimental residence time τ_{exp} is calculated starting from the inlet and outlet response curves with Eq.2 and the results are illustrated in Fig. 3 together with the 'theoretical' residence time τ_c for the spiral wound modules as a function of Re. This figure illustrates that the experimental average residence time of the concentrate channel is smaller than the theoretical residence time. This indicates that at lower flow rates a dead volume is present in the spiral wound module, which disappears at higher flow rates. From visualisation experiments with a plexiglass flat sheet set up, it was seen that air bubbles are entrapped in the mesh of the spacer causing dead zones and that these air bubbles are flushed out at higher flow rates.

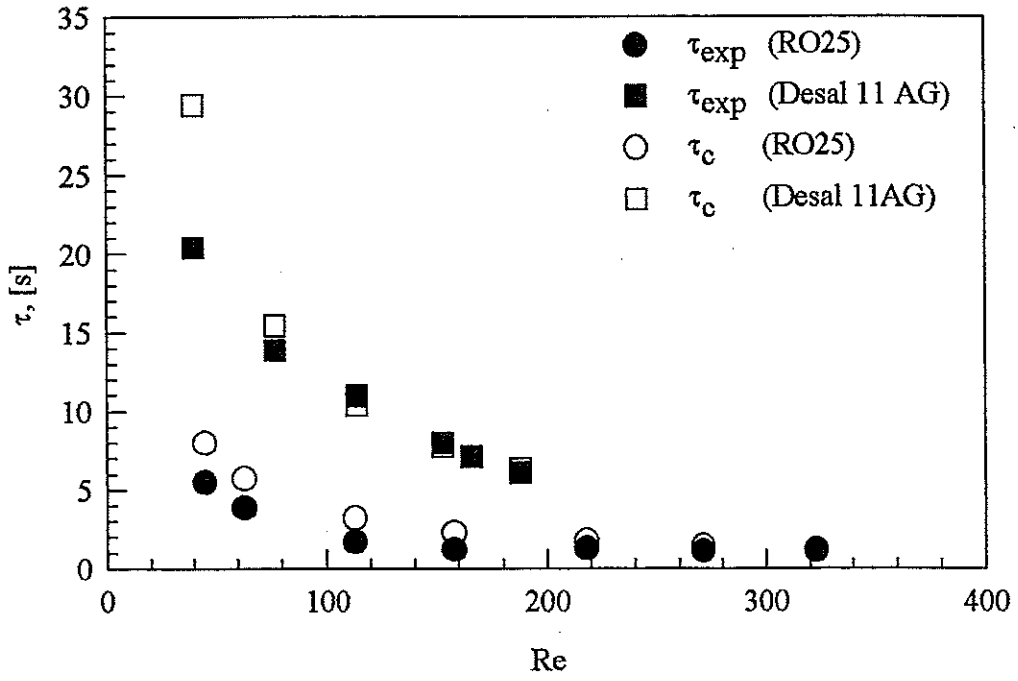

Figure 3. Experimental and theoretical residence time as a function of Re for spacer filled channels

FLOW MODELLING

1. Theoretical background and hydraulic principles

The concentration of solute at the membrane surface can be calculated from the film theory as follows [6] :

$$\frac{C_M - C_P}{C_F - C_P} = \exp\left(\frac{J_v}{k}\right) \tag{4}$$

where k is the solute mass transfer coefficient.

The polarisation phenomena are a function of the flow and concentration at the concentrate side, and will be less pronounced provided a more turbulent flow is reached. This is achieved by inserting a spacer in the feed channel and by operating at a tangential velocity as high as possible without causing a high pressure drop. Several literature correlations are available to predict the transfer coefficient and its associated Sherwood number as a function of Re and Sc number. The expression developed by the mesh step model [7] is

$$k = 0.753 \cdot \left(\frac{u}{n}\right)^{0.5} Sc^{0.33} \sqrt{\frac{K}{(2-K)M}} \cdot D \tag{5}$$

The Re-dependency of the pressure drop in the concentrate channel can be computed from manufacturer specifications if available, or from theoretically

derived or semi-empirical equations. Friction factors are commonly used to describe the relationship between the pressure loss and the flow rate through channels or Re-number :

$$f=\frac{dh}{L}\cdot\frac{\Delta P}{\frac{\rho v^2}{2}}=\frac{k_f}{\mathrm{Re}^n} \tag{6}$$

with d_h = hydraulic diameter, L = length of section with pressure drop ΔP, v = velocity valid for the specific correlation, k_f = constant and Re = Re-number based on d_h and v.

An exponent n equal to 1 corresponds to laminar flow and the exponent is approximately 0.25 for fully developed turbulent flow [8]. Various literature correlations can be found to describe the pressure loss. Hickey et al. [8] found an exponent of 0.493 from experiments with spacers which differed significantly in thickness, porosity and strand density. Shock et al. [9] investigated mostly RO feed spacers and proposed a correlation with exponent 0.3. Da Costa et al. [10] have concentrated their research on UF feed spacers and concluded that the behaviour displayed by all spacers is clearly equivalent to the turbulent flow regime with $n \approx 0.25$.

2. Mesh step model

Different approaches are available to describe the flow motion of liquids through a system. A first approach is based on the 'mesh-step' model which is frequently used to determine the polarisation and mass transfer characteristics of the membrane module. A second approach is the result of the structural resemblance of the spacer filled concentrate channel with e.g. packed beds and since the flow in the concentrate channel will not differ largely from plug flow , two relevant models can be considered [4,11], i.e. either the plug flow with dispersion model (PFDM) or the probabilistic time delay model (PTDM). These more complex models are assessed elsewhere for both spiral wound and plate-and-frame modules [1,12].

Net-type turbulence promoters (spacers) are commonly used in spiral wound membrane modules to enhance the fluid mixing, and increase the associated transfer phenomena. The flow over such nets is characterised by the shedding of vortices at the discrete threads of the net, and these vortices, eventually decaying to a highly irregular, nearly turbulent flow, cause convective mixing.

The mesh step model, introduced by Winograd et al. [7] accounts for the presence of the spacer and defines an average constant boundary layer thickness near the membrane leafs. This thickness depends not only on the spacer geometry but also on the flow conditions.

In the unobstructed case, the process occurring is the development of a boundary layer in a developed laminar flow. With the net present, velocity (and concentration) undergo a sudden partial mixing at the spacer thread, the effect of which is such that after the mixing the velocity and concentration profile are a given fraction of the

thickness before mixing. After this elementary mixing process, the boundary layer again develops for a length of one mesh step, at the end of which mixing is repeated and so on. The boundary layer hence develops in a saw-tooth fashion with a constant average thickness after a considerable length. The velocity profile under these circumstances is axi-symmetric and is presented in Fig. 4. Preference is given to a quadratic function to describe the velocity profile. The use of a hyperbolic function would increase the accuracy of the prediction, but its mathematical transformation into E(t)-curves is more complicated. For the flow lengths under consideration, the boundary layer thickness, δ, will always be smaller than the channel half thickness, h.

$$v(y)0<y<\delta=v_\infty\cdot\left[2\cdot\left(\frac{y}{\delta}\right)-\left(\frac{y}{\delta}\right)^2\right] \qquad (7)$$

$$\delta<y<h=v_\infty$$

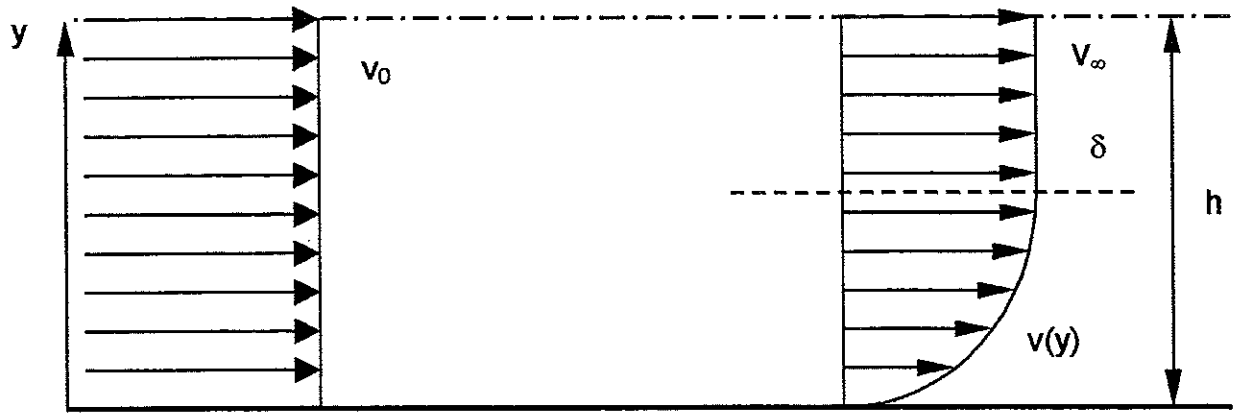

Velocity profile

Figure 4. Velocity profile with the 'mesh step' model

From the law of conservation of mass, v_∞ can be calculated as a function of v_0 :

$$v_0\cdot h=\int_0^\delta v(y)\cdot dy+\int_\delta^h v_\infty(y)\cdot dy \qquad (8)$$

$$v_\infty=\frac{v_0}{1-\delta/(8\cdot h)}$$

The residence time distribution $E_m(t)$ is a result of the velocity profile in the concentrate channel of the spiral wound module Em(y) is therefore defines as follows for $0<y<\delta$:

$$E_m(y)\cdot dy = \text{fraction in slit between y and y + dy}$$

$$= v_\infty \cdot \left[2\cdot\left(\frac{y}{\delta}\right) - \left(\frac{y}{\delta}\right)^2\right] \frac{W\cdot dy}{v_0 \cdot W \cdot h} \qquad (9)$$

Because the residence time distribution $E_m(t)$ is expressed in function of time t, the relationship between y and t must be derived :

$$t = \frac{L}{v(y)} = \frac{\tau\cdot(1-\delta/3h)}{\left[2\cdot\left(\frac{y}{\delta}\right) - \left(\frac{y}{\delta}\right)^2\right]} \qquad (10)$$

$$dy = \frac{\tau/t^2\,(1-\delta/3h)}{(2/\delta - 2/\delta^2)} \qquad (11)$$

Finally this leads to the expression :

$$E_m(t) = \frac{3}{2}(1-\delta/3h)\cdot\delta/3h\cdot\frac{\tau^2/t^3\cdot dt}{\sqrt{1-\tau/t\cdot(1-\delta/3h)}} \qquad t/\tau > \quad 1-\delta/3h \qquad (12)$$

In case of $\delta<y<h$ the velocity profile is represented by plug flow with constant velocity v_∞. The corresponding residence time distribution is

$$E_m(t) = 0 \qquad t/\tau < \quad 1-\delta/3h \qquad (13)$$

$$= \delta(t) \text{ with area} = \frac{1-\delta/h}{1-\delta/3h} \qquad t/\tau = \quad 1-\delta/3h \qquad (14)$$

The δ/h ratio in these model equations characterises the flow regime with two extremes corresponding to respectively plug flow (δ/h = 0) and fully developed laminar flow (δ/h = 1). Real flow patterns in the spacer filled channel can be either of both extremes or can be a combination of both.

RESULTS AND DISCUSSION

Fig. 5 illustrates the fitting results for experiments with the large scale spiral wound set up (DESAL 11 AG 4040) using both extreme values of δ/h i.e. 0 and 1. The fitting results at varying feed flow rate give an indication that the plug flow regime is not fully established at low operating velocities, but describes the hydrodynamics reasonably well at higher flow rates.

As stated in the 'mesh step' model of Winograd et al. [7] the ratio of the concentration (δ_c)and velocity (δ) boundary layer thickness is only a function of the Sc-number and may be considered a constant for a certain feed solution, and δ_c/h is

proportional to $Re^{-1/2}$. The fitted results of δ/h with respect to $Re^{-1/2}$ as presented in Fig. 6, are therefore indicative that the 'mesh-step' model of Winograd et al. [7] is suitable to describe the concentration polarisation phenomena in spiral wound modules.

Based on the RTD experimental results, it is acceptable to assume that the hydrodynamics of the spiral wound module are of plug flow, turbulent nature. Hence preference is given to the correlation of Shock et al. [9] to describe the pressure loss because their research focussed on RO feed spacers and because the exponent n = 0.3 is in good agreement with the turbulent flow regime.

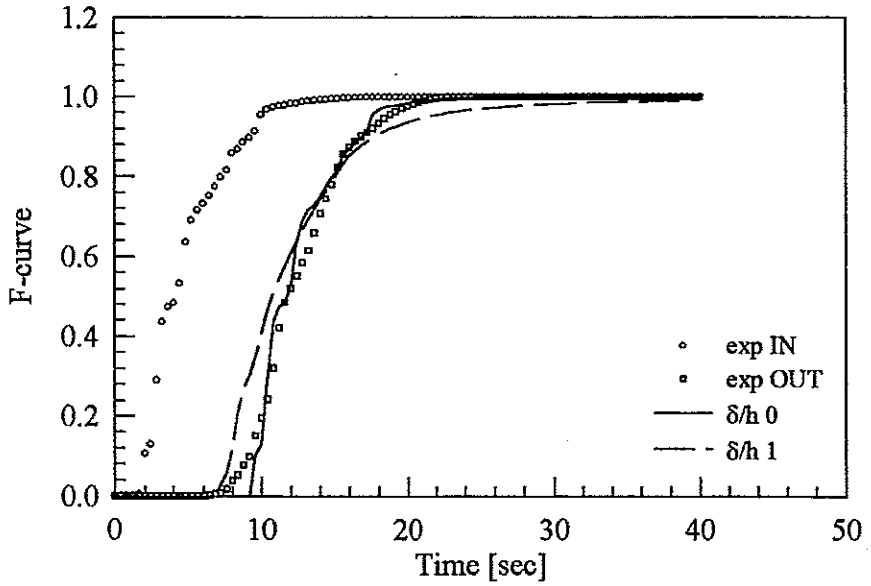

Figure 5. Fitting results with mesh step model (DESAL 2118 l/h

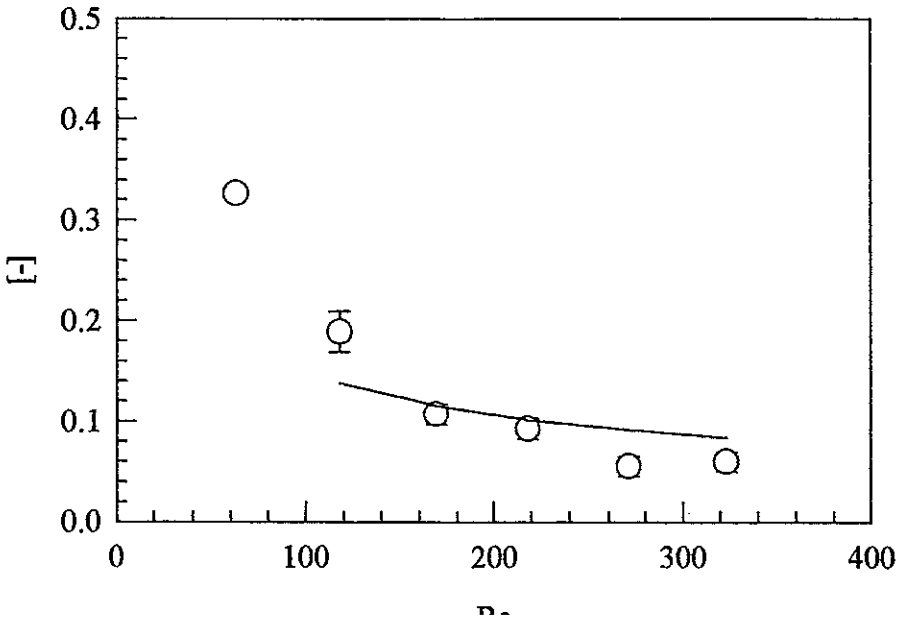

Figure 6. Effect of operating flow rate (RO25)

CONCLUSIONS

RTD experiments using a step injection of KCl-solution are performed to determine the flow regime in the concentrate channel of a spiral wound module. The mesh-step model initially introduced to describe the mass transfer coefficient in concentration polarisation phenomena is adapted to interpret the RTD experimental results. Through a least square analysis the parameter δ/h (= ratio of the average constant boundary layer thickness over the half channel thickness) is determined. Based on the RTD results it is acceptable to assume that the hydrodynamics of the spiral wound module is of plug flow, turbulent nature. Therefore preference is given to the correlation of Shock et al. [9] to describe the pressure loss in the concentrate channel of the spiral wound module. At higher flow rates at which industrial membrane modules are normally operated to avoid excessive concentration polarisation, δ/h is linearly dependent on $Re^{-0.5}$, indicating that the mesh-step model of Winograd et al. [7] is suitable to describe the concentration polarisation phenomena in spiral wound modules

REFERENCES

[1] Van Gauwbergen D., Jamar S., Baeyens J, *Macroscopic flow conditions in plate-and-frame membrane elements*, Filtration and Separation, 37 (2000), 125-132

[2] Van Gauwbergen D., Baeyens J, *Macroscopic fluid flow conditions in spiral-wound membrane elements*, Desalination, 110 (1997), 287-299

[3] Roetzel W., Balzereit F., Rev. Gen. Therm., 36 (1997), 635-648

[4] Westerterp K.R., van Swaaij W.P.M. and Beenackers A.A.C.M., *Chemical reaction design and operation*, 2nd edition, John Wiley & Sons, 1984

[5] Van Gauwbergen D., Baeyens J., *Assessment of the design parameters for wastewater treatment by reverse osmosis*, Wat. Sc. Techn., 40 (1999), 269-276

[6] Rautenbach R. and Albrecht R., *Membrane processes*, 2nd edition, 1989, John Wiley & Sons

[7] Winograd Y., Solan A. and Toren M., *Mass transfer in narrow channels in the presence of turbulence promotors*, Desalination, 13 (1973),171-186

[8] Hickey P.J., Gooding C.H., in:R. Bakish (Ed.), *Friction loss in spiral-wound membrane modules*, Proc. 6th Int. Conf. on Pervaporation Processes in the Chemical Industry, Bakish Materials Corp., Englewood, NJ, (1992), 153-169

[9] Shock G., Miquel A, *Mass transfer and pressure losses in spiral-wound modules*,Desalination, 64 (1987), 339-352

[10] Da Costa A.R., Fane A.G. and Wiley D.E., *Spacer characterization and pressure drop modelling in spacer filled channels for ultrafiltration*, J. Memb. Sc., 87 (1994), 79-98

[11] Buffham B.A., Gibilaro L.G. and Rathor M.N., AIChE Journal, 16 (1970), 218-223

[12] Van Gauwbergen D., Baeyens J., Proc. Int. Spec. Conf. Memb. Techn. in Env. Management, Tokyo, 1999, 202-210

B B4 - ENVIRONMENT

INVESTIGATION OF HEAVY METAL EVAPORATION DURING THERMAL TREATMENT ON A FORWARD-ACTING GRATE WITH THE HELP OF RADIOTRACERS

T. Jentsch[1], M. Beckmann[2], M. Davidovic[3], S. Biollaz[4]

[1]Fraunhofer-IZFP-EADQ, Krügerstraße 22, 01326 Dresden, GERMANY
[2]Bauhaus-Universität Weimar, Coudraystraße 13, 99423 Weimar, GERMANY
[3]CUTEC-Institut GmbH, Leibnizstraße 21 + 23, 38678 Clausthal-Zellerfeld, GERMANY
[4]Paul-Scherrer-Institut, 5232 Villigen, SWITZERLAND

Abstract. This paper deals with the introduction of short-lived radioactive isotopes of selected heavy metals in order to detect the location, time, and amount evaporated during the combustion of municipal waste in a pilot plant-scale forward-acting grate system. During this process, ^{69m}Zn (13.8 h half-life) and ^{64}Cu (12.7 h half-life) proved relatively good representatives of isotope species. Since the isotopes used are gamma-emitters, all measured data could be collected without direct contact and sampling-free. The determination of the evaporation location took place using 11 NaI(Tl)-scintillation detectors positioned along the forward-acting grate; the acquisition of the evaporation rate data ensued with the help of a detector located within an absorber positioned to wash the flue gas flow.

INTRODUCTION AND OBJECTIVE

The possibilities for the optimization of the process control of the so-called classical combustion of residual waste in grate systems have not yet been completely explored [1]. The objectives of the optimization include a further reduction in the amount of flue gas and the pollutant load, an increase in the total efficiency, as well as the improvement of the ash quality. This paper places particular emphasis on the improvement of the ash quality. The goal is to produce an ash which can be implemented in the construction industry through the application of primary measures, in other words through the process control itself. A prerequisite for this is the maintenance or reduction of the eluate and solid concentration of inorganic salts and heavy metals below the limiting values. The process conditions (in particular temperature, gas atmosphere, residence time) are adjusted so that these pollutants are either evaporated and are therefore not present in the ash or are strongly mineral-bound in such a manner that they are no longer available. Results concerning the behavior of heavy metals and salts are already available from experiments done on the laboratory scale [2, 3, 4]. These results originate from experiments using small charges (several g to kg) and in batch operation. In order to be able to transfer this knowledge into the praxis and for the optimization, the next step must be to determine the location and amount of heavy metal evaporation under realistic conditions, in other words in a continuously-operated pilot plant.

A determination of the heavy metal content is usually carried out through the sampling of the total flue gas flow and the corresponding analysis. A detection directly at the location of evaporation using conventional sampling and analysis is, due to the harsh conditions in the combustion chamber, particularly difficult and can not be carried out on-line with respect to the analysis. In addition, a very complex measurement network is necessary for an investigation over the complete firing bed surface.

The radiotracer method provides the possibility to follow the behavior, location and concentration of a certain heavy metal species on-line during the entire combustion process in a technical waste treatment plant. The following quantities can be determined with the help of this method, using the combustion process in a grate system on the pilot plant-scale as example:

- the location of the heavy metal evaporation,
- the time course of the heavy metal evaporation as well as
- the amount of heavy metal evaporated.

APPROACH AND CHOICE OF TRACER

The solution to this objective lies in the introduction of the radioactive isotope of a certain heavy metal which occurs in the input waste mass flow of a combustion plant. The isotope must be a short-lived gamma emitter. Radiation detectors located along the sides of the combustion chamber register the time course of the tracer concentration in the waste mass flow at different positions. They make a determination of the location of the marked heavy metal species during the entire residence time in the solid bed possible. The heavy metals evaporated during the combustion process and carried out of the combustion chamber with the flue gas are caught to a certain degree by the absorber. A radiation detector in this absorber registers the temporal concentration course of the heavy metal tracer evaporated. Since the collection of measured values by all detectors is started simultaneous with the introduction of the tracer (DIRAC-impulse), concentration changes in the time course of the measured signal at the absorber detector in the range of the combustion chamber can be assigned and the heavy metal evaporation can then be localized in the solid bed. The quantification of the amount of heavy metal evaporated is made possible through a calibration of the absorber detector signal.

The investigations were carried out in a pilot plant-scale forward-acting grate at the Clausthaler Umwelttechnik Institut GmbH (CUTEC) in Clausthal-Zellerfeld. The plant consists of the following components:

- grate
- combustion chamber
- heat exchanger and
- flue gas purifier

as shown in Fig. 1 in a technical flowchart which includes the measurement and testing methods. The plant has a thermal capacity of 0.4 MW making a transfer of the results obtained to the industrial scale possible.

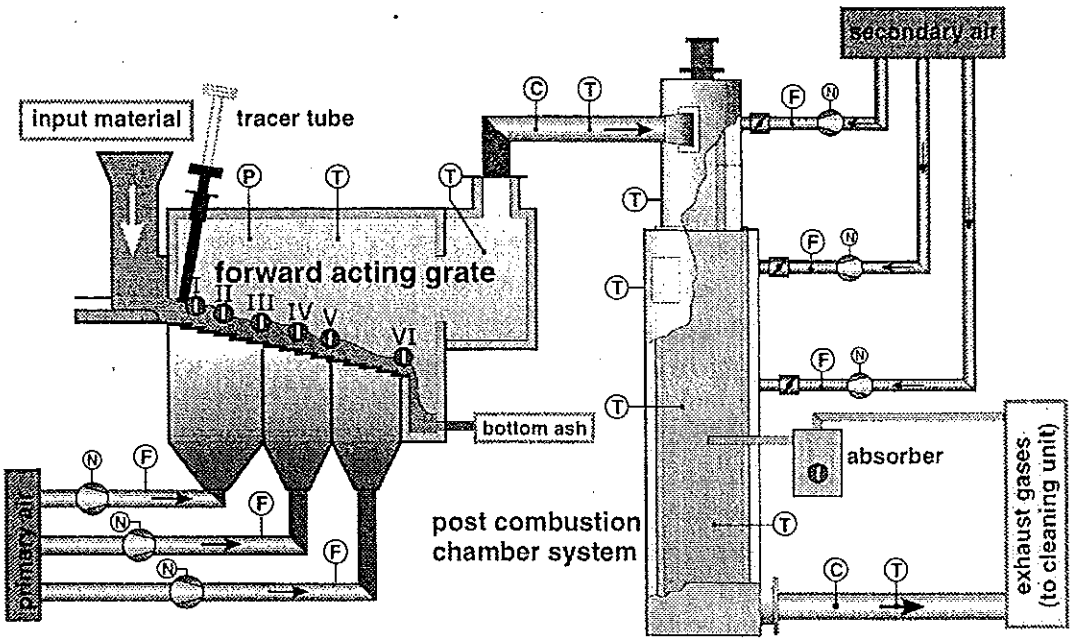

Figure 1. Technical flowchart of the forward-acting grate plant including measurement and testing methods; @ radiation detector, C concentration measurement, F flowmeter, N speed control, P pressure indicator, T temperature sensor

The detection and quantification of the amount of heavy metal evaporated proceeds through gas washing in a special absorber with a liquid absorbent in which the evaporated heavy metals are completely and evenly distributed within a very short time period. In order to limit the expenditure, a partial gas flow of ca. 1 vol.-% of the total gas flow was withdrawn and directed through a special glass gas washer in the by-pass as shown in Fig. 2.

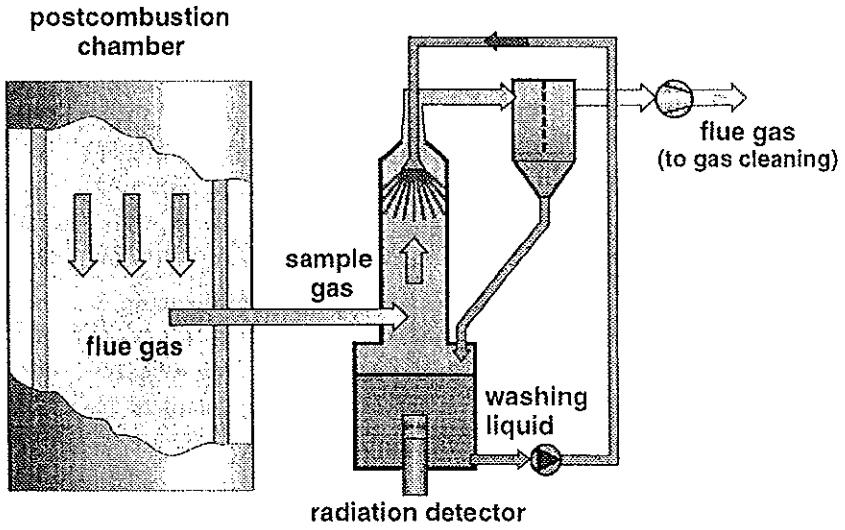

Figure 2. Scheme of the absorber for the washing of the partial gas flow and quantification of the amount of heavy metal tracer evaporated

A 0.1 M solution of nitric acid served as washing liquid and lead to a nearly complete absorption of the heavy metals out of the partial flue gas flow. The contents of the absorber were circulated continuously in order to intensify the mass transfer, for a short-term and even distribution of the elutriated heavy metals in particular. A 1.5"-NaI(Tl)-scintillation detector located in the center of the absorber bottom container registered the time course of the relative tracer concentration in the washing liquid, which corresponds to the time course of the heavy metal evaporation in the furnace.

Of the many elements of interest to choose from, copper and zinc were selected for the investigations in the pilot plant. Copper is representative of the nearly nonvolatile elements and zinc of a species which can be easily evaporated under certain conditions.

In the literature, the use of radioactive isotopes of copper and zinc are usually mentioned in connection with the investigation of the ore beneficiation processes [5-8]. For this purpose, samples of the input material of the respective process to be examined were activated in a experimental reactor. The isotopes, resulting from the activation with thermal neutrons, ^{64}Cu with a half-life of 12.7 h and ^{65}Zn with a half-life of 244 days served as radioactive tracers. Other radioactive isotopes can also be formed depending upon the purity of the input material, i.e. ^{56}Mn in the case of activation of copper minerals.

The applications described in [5-8] deal with relatively homogenous input materials for the ores to be labeled. Since waste however is a particularly heterogeneous material, the procedure described in [5-8] is not a suitable solution for the problem presented here. In this case a mixture – also including long-lived isotopes – representative of the elements present in the input material would result and the measuring signal could not be clearly assigned to the heavy metals to be investigated. Therefore, an extremely pure input material of each heavy metal must be used for the activation.

The elements chosen for this investigation, copper and zinc, have radioactive isotopes whose nuclear physical parameters fulfill the above-mentioned requirements of tracer characteristics: ^{64}Cu and ^{69m}Zn. The isotope ^{64}Cu arises through the neutron capture by the isotope ^{63}Cu, has a half-life of 12.7 h, and is detectable without direct contact and sampling-free through the apparatus and container walls due to the gamma radiation from positron annihilation. It can be generated through the activation of highly purified copper in the experimental reactor. The isotope ^{66}Cu, formed by the activation of the metal in its natural composition from the ^{65}Cu isotope, has a half-life of only 5 min and is at the time of the tracer injection (after several hours) no longer detectable.

The ^{69m}Zn isotope can also be produced through neutron capture by ^{68}Zn in the experimental reactor. With a half-life of 13.8 h and an emission of gamma radiation during the isomeric transition to the ground state with an energy of 439 keV, it demonstrates comparable tracer characteristics to ^{64}Cu. However, the long-lived ^{65}Zn isotope (244 day half-life) is also formed in the natural mixture of isotopes, which includes the ^{64}Zn isotope, during the activation of even an ultrapure sample of natural zinc. Therefore, a pure quantity of ^{68}Zn is necessary for the generation of ^{69m}Zn.

ACTIVITY ESTIMATION AND GENERATION

The activity necessary for the measurement is primarily determined through the concentration measurement of the heavy metal species in the flue gas absorber. The effective activity of the tracer was fixed at 1850 MBq (50 mCi) with respect to the determination of even very low concentration changes in the flue gas. The Monte-Carlo simulation [9] for the estimation of the measuring effect at the absorber detector and the calculation with a method presented in [10] for the measuring effect of the detectors positioned along the grate support the choice of these values.

The formation of the radioactive isotopes ^{64}Cu and ^{69m}Zn takes place through the reaction of thermal neutrons with the nucleus of the stable starting isotope ^{63}Cu or ^{68}Zn. The specific activity of the tracer needed for the solution of the given problem can only be achieved in an experimental reactor with high neutron flux. The irradiation was carried out in the experimental reactor BER II with a potential neutron flux of up to $2 \cdot 10^{14}$ $cm^{-2}s^{-1}$ at the Hahn-Meitner-Institut in Berlin. Table 1 summarizes the conditions for the neutron activation of the zinc and copper samples.

Table 1. Conditions for the neutron activation of the zinc and copper sample

Starting isotope	Target isotope	Sample mass in mg	Sample application	Neutron flux in cm^{-2} s^{-1}	Irradiation time in h	Activity at the end of irradiation in MBq [11]
^{63}Cu	^{64}Cu	40	labeling	$2\ 10^{14}$	1.5	19 000
^{63}Cu	^{64}Cu	0.4	calibration	$2\ 10^{14}$	1.5	190
^{68}Zn	^{69m}Zn	75	labeling	$2\ 10^{14}$	16	7 250
^{68}Zn	^{69m}Zn	0.75	calibration	$2\ 10^{14}$	16	72.5

The values listed in the last column of Table 1 were calculated with the help of data for the saturation activity given in [11]. The values for the activity at the end of irradiation, which are to a certain degree clearly above the 1850 MBq fixed initial activity, are necessary to compensate for the decay between the end of irradiation and the time at which the isotope is introduced to the system. In spite of similar half-lives, the activity of the copper isotope must be about three time greater than that of the zinc isotope, since the emission probability per nuclear transformation for the effective radiation emitted by the copper isotope due to positron annihilation is only 37%.

Copper granulate with a purity of 99.8% and a grain size between 0.2 and 0.6 mm was used to produce ^{64}Cu. For the generation of ^{69m}Zn, metal ^{68}Zn flakes with an average edge length of ca. one millimeter and an enrichment factor of 98.3% were used. As indicated by the sample irradiation, any traces of impurities did not lead to relevant, or from the point of view of radiation protection risky, generation of undesired isotopes.

MEASUREMENTS

Eleven slotted collimated, shielded, and water-cooled 1"-NaI(Tl)-scintillation radiation detectors were positioned on the exterior walls of the forward-acting grate in order to determine the location of the heavy metal evaporation. Ten detectors were mounted in pairs on opposite sides at the height of the solid bed next to the forward-acting grate. The sites between two primary air supply zones, and their centers, were chosen as the preferred positions for the detectors (Fig. 1). The first detector was positioned directly behind the tracer input site and served for the quality control of the DIRAC-impulse-shaped tracer addition in particular. The shielding and collimating of the detectors made a oriented acquisition of the radiation from the respective apparatus section of interest possible. This was carried out using multipurpose, modularly set-up cylindrical blocks consisting of ten 1 cm thick metal plates made of a tungsten alloy. The 4 cm high and 1 cm wide collimate slot plates, of which two were positioned per block, were oriented in such a way that the smallest possible area of the forward-acting grate could be registered by the detector. An additional, however unshielded, 1.5"-NaI(Tl)-scintillation radiation detector was positioned in the hollow in the bottom of the absorber to wash the partial flue gas flow, which was withdrawn continuously using a lance through a hole drilled in the wall of the post-combustion chamber (Fig. 2).

A model fuel, consisting of 60 ma-% wood, 30 ma-% lava, and 10 ma-% RDF (**r**efuse **d**erived **f**uel), was used for the investigations. The pilot plant was operated steady-state with a fuel mass flow of 60 kg/h.

The heavy metal content of the residual waste shows a great range of variation depending upon the type of waste and its composition. This range spans ca. 60 to 2100 mg/kg for copper and 50 to 6500 mg/kg for zinc [i.e. 12, 13]. The activated metal samples were pressed into RDF-pellets for the examinations described here, so that the average copper content amounted to 800 mg/kg and 1500 mg/kg for zinc.

The addition of the labeled fuel onto the forward-acting grate was carried out using a special input adapter directly on the solid bed at the beginning of the grate. With a continuous fuel mass flow of 60 kg/h and an average fuel residence time of ca. 1 h on the forward-acting grate, a good approximation of a DIRAC-shaped input impulse can be assumed for a short-term addition of 50 g labeled material in the form of RDF-pellets.

EVALUATION AND RESULTS

The signals from all of the detectors are conveyed over a special conductor to a PC-supported acquisition system. This system allows for the parallel connection of up to 16 radiation detectors; the minimal adjustable measuring interval applicable for all detectors is 100 milliseconds. The reading of the connected detector counters takes place between two measuring time intervals within a time period of less than one millisecond. The storage capacity of over 65,000 measured values per counter channel allows for an adequate measurement registration duration per experiment. A width of 32 bits for each counter channel prevents a counter overflow. The time courses of the counting rates registered by each detector, proportional to the tracer

concentration under steady-state conditions, are represented in real time on the monitor, making a convenient observation of the tracer transport possible.

Measuring intervals with a duration of five seconds were selected for the measurements in the forward-acting grate. The countrate-time courses for the detectors used were presented as results for each experiment. The subsequent processing of the measured values was performed after subtracting the background radiation caused by the natural environment and carrying out a half-life correction for the corresponding nuclide.

From the *time course* of the measured signal from the detector in the absorber for the washing of the partial flue gas flow, the time point and duration at which the heavy metal tracer evaporation takes place can be seen. Since the measurements for all detectors begin simultaneously, the evaporation location in the furnace can be determined with adequate precision through the countrate-time course along the forward-acting grate.

The *amount* of heavy metal evaporated per unit time can be determined after appropriate calibration of the test set-up through the measured values collected at the detector in the absorber. The zinc and copper ampoules, referred to in Table I for the calibration, containing a hundredth of the amount necessary for the labeling served this purpose. Possible mistakes through varying radiation conditions could therewith be prevented. After dissolving the content of an irradiated ampoule for the calibration in a given amount of concentrated nitric acid, a defined volume corresponding to a known copper or zinc content was added at intervals of a few minutes to the uncontaminated liquid in the absorber and the accompanying measured signal registered. The conditions prevailing in the grate system during the experiment were also realized during the calibration procedure.

1. Results of the copper evaporation experiment

Fig. 3 shows the results of one of the two experiments carried out in the forward-acting grate combustion plant with activated copper granulate added to the process in the above-describe manner in the form of RDF-pellets. In both experiments, carried out with overstoichiometric (altogether oxidizing) conditions, a copper evaporation of 3 or 5% could be established. As can be seen in the upper diagram in Fig. 3, the evaporation takes place continuously during the entire tracer residence time on the grate. From the shape of the residence time distribution curves for the different detector positions along the grate, no significant change can be seen at any time that would imply an increased evaporation in a particular zone in the plant. The asymmetric course of the residence time distribution is distinctive, which clearly leads to differences between median and modal values, in other words between average and most probable residence times. The cause of this residence time behavior, untypical for a forward-acting grate, is most likely the spherical form of the copper granulate used. A portion of the granulate is probably oriented on the moving grate plates in such a way that these particles repeatedly end up under the fixed grate plates, are not forced forward, and are therefore strongly delayed as they pass through the grate system. In spite of these phenomena, a good linear connection between transport path and residence time can be determined by observing the most likely residence time (modal value of the distribution), as shown by the dashed line in Fig. 3.

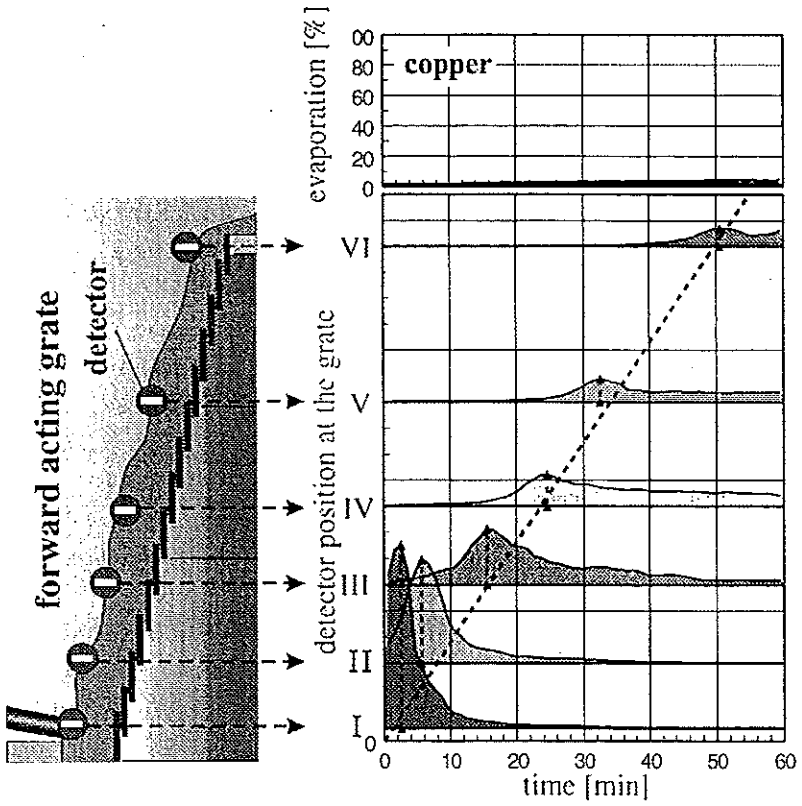

Figure 3. Results of a copper evaporation experiment

2. Results of the zinc evaporation experiment

Experiments with labeled zinc were carried out under three different operating conditions where the oxygen partial pressure (under/overstoichiometric) and the combustion temperature were varied. The combustion temperature was influenced through the variation of the moisture content in the input material whereas the oxygen partial pressure was regulated through change of the volumetric flow rate of the primary combustion air supply. As measurements of the oxygen content in the material bed have shown, reducing conditions prevail in the front section of the grate during overstoichiometric as well as understoichiometric operating modes. Reducing conditions and high temperatures are prerequisites for considerable zinc evaporation. The measurements with activated zinc have confirmed this statement. With understoichiometric as well as overstoichiometric conditions, a zinc evaporation could be observed, which takes within a time period of a few minutes in a narrowly restricted section of the grate place in each case, in the section in which the local reducing conditions prevail.

Fig. 4 shows the results of an experiment which was carried out with moist input material under altogether reducing conditions. In the upper diagram in Fig. 4, the rapid evaporation, which is characterized by a steep increase in the zinc concentration in the absorber liquid within a time period of ca. 3 minutes, can be clearly seen. In this time period, more than 80% of the added tracer amount is evaporated. The evaporation begins ca. 18 minutes after the addition of the labeled RDF-pellets to the process. At this time, the main portion of the activated zinc has

passed through the detector pair III (Fig. 1) and is then located in the grate section above the second primary air supply zone directly in front of detector pair IV.

In this example, the evaporation can be followed very well using the residence time distribution measured along the forward-acting grate. If a nearly unchanged residence time distribution is registered at the position of the detector pair III, then the expected concentration maximum at the position of the detector pair IV will not be reached. At the end of the grate (detector pair IV), no signal is registered by the detectors.

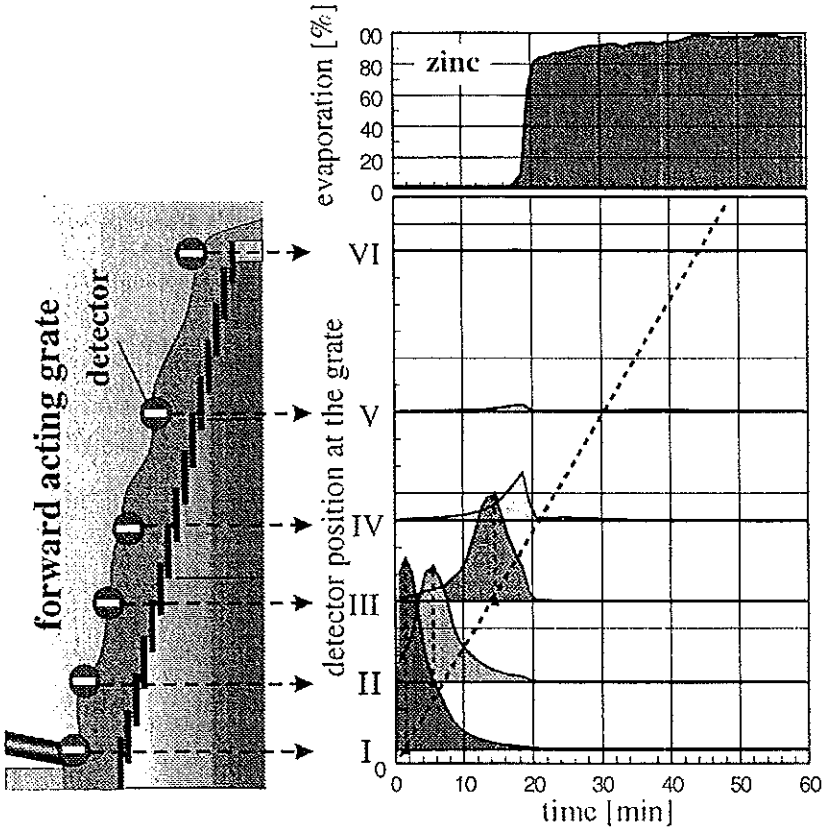

Figure 4. Results of a zinc evaporation experiment

CONCLUSIONS

With the investigations described in this paper, it could be shown that the radiotracer method is very suitable to simultaneously quantify and localize the heavy metal evaporation in the process of thermal waste treatment. Using this method, it is possible to follow the actual path of selected heavy metals, which is either not possible with other measuring techniques or only with considerable (sampling and analytical) expenditure. The knowledge gained here contributes significantly toward a better understanding of the impact of an aimed manipulation of process conditions during the combustion and gasification of waste with respect to a controlled evaporation of heavy metals. In addition, the radiotracer method offers solution possibilities for other problems in which the determination of the heavy metal pathways play a role.

Thanks. The cooperation of many people was necessary in order to successfully carry out the measurements. The authors therefore thank the colleagues at the Hahn-Meitner-Institut Berlin for supplying the tracer, in particular Dr. Alber, Dr. Buchert, and Mr. Gatschke. For the support during the tracer experiments, the authors would also like to thank Dr. Bätz and Dr. Zeuner from the TU Dresden as well as Mr. Schuler from the PSI. We also thank Mr. Marti and Dr. Ludwig from the PSI for their assistance with the design and construction of the tracer absorber.

The project was financially supported through the Schweizerischen Nationalfonds (Swiss national fund), whom the authors would also like to thank.

REFERENCES

[1] Scholz, R., Beckmann, M., Schulenburg, F., *Abfallbehandlung in thermischen Verfahren*, Teubner-Reihe Umwelt. B.G. Teubner GmbH, Stuttgart, Leipzig, Wiesbaden (2001), ISBN 3-519-00402-X
[2] Laboruntersuchungen SM PSI ---- SERGE
[3] Vehlow, J., *Reststoffbehandlung- Schadstoffsenke Thermische Abfallbehandlung*, FDBR- Symposium „Die Thermische Abfallverwertung der Zukunft", Rostock, 23. Februar 1996
[4] Hunsinger, H., Merz, A., *Beeinflussung der Schlackequalität bei der Rostverbrennung von Hausmüll*, GVC- Symposium Abfallwirtschaft Herausforderung und Chance. Würzburg, 17-19. Oktober 1994
[5] Petryka, L., Przewlocki, K., *Optimization of Copper Ore Concentration Processing by Means of Radioactive Tracers*, Isotopenpraxis 25(1989)4, 139-143
[6] Przewlocki, K., Petryka, L., Stegowski, Z., *Radiotracer Investigation of the Copper Ore Concentration Process*, Isotopenpraxis 26(1990)9, 439-444
[7] Michalik, J.St., Palige J., Bazaniak, Z., *Radiotracer Investigations of the Shaft Processes in Polish Zinc and Lead Metallurgy, Part. I. Investigation of Charge Materials Movement*, Isotopenpraxis 26(1990)5, 210-215
[8] Michalik, J.St., Palige J., Bazaniak, Z., *Radiotracer Investigations of the Shaft Processes in Polish Zinc and Lead Metallurgy, Part. II. Investigation of the Chemical Behaviour of Zinc*, Isotopenpraxis 26(1990)5, 216-221
[9] Henniger, J., *AMOS – ein multivalent nutzbares Programmsystem zur Berechnung von Strahlungstransportproblemen. In: Strahlenschutz: Physik und Meßtechnik*, Band 1, 26. Jahrestagung des Fachverbandes für Strahlenschutz e.V., Karlsruhe, 24.-26. Mai 1994, Verlag TÜV Rheinland
[10] Zeuner, A., *Beiträge zur Prozeßanalyse und Prozeßkontrolle mit offenen Radionukliden*, Dissertation B, Technische Universität Dresden (1990)
[11] Erdtmann, G., *Neutron Activation Tables*, Kernchemie in Einzeldarstellungen, Volume 6. Verlag Chemie, Weinheim, New York (1976)
[12] Reimann, D.O., Hämmerli, H., *Verbrennungstechnik für Abfälle in Theorie und Praxis*, Schriftenreihe Umweltschutz, Bamberg (1995)
[13] Hämmerli, H., *Grundlagen zur Berechnung von Müllfeuerungen. In: Müllverbrennung und Rauchgasreinigung*, Thommé-Kozmiensky, K.J. (Hrsg.), E. Freitag-Verlag, Berlin (1983)
[14] Bätz, H., *MEAS II – Beschreibung und technische Dokumentation*, Handbuch zum Meßwerterfassungssystem, Dresden (1994)

BACTERIAL TRANSPORT IN UNSATURATED FLOW THROUGH SAND FILTER

Bertrand Sélas*, Abdel Lakel*, Yves Andres**,
Pierre Le Cloirec**

*Centre Scientifique et Technique du Bâtiment, département C.A.P.E., division Gestion des Pollutions et Epuration, 11 rue Henri Picherit, BP 82341,44323 NANTES cedex 03, France
Phone: (33)2 40 37 20 79 Fax : (33)2 40 37 20 40 e-mail: selas@cstb.fr, lakel@cstb.fr

** Ecole des Mines de Nantes, Département Systèmes Energétiques et Environnement, 4 rue A. Kastler, B.P. 20722, 44307 Nantes cedex 03, France.
Phone: (33)2 51 85 82 52 Fax : (33)2 51 85 82 99 e-mail: yves.andres@emn.fr, pierre.le-cloirec@emn.fr

Abstract. In onsite wastewater treatment plants, effluents are pretreated by septic tank and treated by soil infiltration or sand filtration systems, with unsaturated conditions. This process can remove efficiently carbon, nitrogen and suspended solids. But for microbial pollution, the treatment efficiency and reliability are very variable and depends on the hydrodynamic behavior and filtering media characteristics. Contamination of superficial water and groundwater due to pathogenic viruses and pathogenic bacteria is responsible for many diseases and outbreaks and represents a risk for human health.

The objective of this work is to define and to describe by models the behavior of microorganisms in unsaturated filtering media. Hydrodynamic characteristics are one of the most important parameter involved in microorganisms removal. The residence time distribution method (RTD) was used to characterize the hydrodynamic. Experiments were carried out on column of different length (30 and 50 cm) packed with sand. Flow rate of 90 $cm.d^{-1}$ with a pulse periodic flow, was used. The influence of chemical composition of the injected solution on the treatment efficiency for a given load has also been studied with:

- ionic strength (presence of Ca^{2+} and Mg^{2+}),
- organic matter (acetate ion: major organic component in septic effluent)
- sterile raw water.

In a first time, the RTD have been studied with using a conservative tracer (KI), to determine the main hydrodynamics parameters, applying the tanks-in-series with mass exchange model.

In a second time, the RTD with bacterial tracers (*E.coli*) in the four solutions was applied, in aim to define microbial behavior in filtering media, including adsorption and filtration phenomena. This work allowed to determine retardation factors according to the hydraulic loads and chemical composition.

1. Introduction

Contamination of superficial water and groundwater due to pathogenic virus (rotavirus, calcivirus, Norwalk virus, astrovirus, etc) and pathogenic bacteria (streptococcus, salmonella, enterococcus, etc) is not a recent problem. It is responsible for many diseases and outbreaks that represent a risk for human health. But nowadays, this trouble gained a considerable attention due to public health concerns [1, 2, 3]. Indeed, the lack or inefficiencies of barriers to stop the transport of pathogenic germ makes the consumer of contaminated water run unacceptable risks. Because the ground water contamination is a main problem for public health [4, 5, 6], it has focused the attention of most researchers in transport mechanisms of bacteria and virus in the ground. Three mechanisms can occur in retention of bacteria: filtration, adhesion that included sorption and development of a biofilm, and mortality [7, 8, 9, 10].

In onsite wastewater treatment plants, effluents are pretreated by septic tank and treated by soil infiltration or sand filtration systems, with unsaturated conditions. These systems can remove efficiently carbon, nitrogen (like ammonia oxidized in nitrate) and suspended solids [11]. But for microbial pollution, the treatment efficiency and reliability are very variable and depends on the hydrodynamic behavior (unsteady flow rate) and filtering media characteristics (porosity, moisture...).

The objective of this work is to define and to describe by models the transport of microorganisms in unsaturated filtering media.

MATERIALS AND METHODS

1. Chemicals

Physiological solution consisted of 9 g NaCl L^{-1} in distilled water. Nutrient Broth at 20 g l^{-1} (BIOKAR) for the enrichment of cells, and Tergitol 7 agar with triphenyltetrazolium for analyse (*E.coli* strain appears brown with a yellow halo) were used.

2. Bacterial strains

A single bacterial strain was used in this study: *Escherishia coli* (ATCC 11775). Bacteria were cultivated on nutrient broth in 1 L erlenmeyer flasks on a rotary shaker at 100 rpm and 37 °C. Cells were harvested in the early stationary phase by centrifugation for 10 min at 4500 rpm. After washing the cells twice with 20 mL of physiological solution, they were resuspended in a small volume of physiological solution and stored on refrigerator (5±3 °C) for 24 hours.

Cell surface charges were characterized by measuring the pH of point of zero charge [12]. Briefly, cells in suspension in $NaNO_3$ 0.1 mol.L^{-1} were titrated with NaOH 10^{-1} mol.L^{-1} and HNO_3 10^{-1} mol.L^{-1} under N_2 atmosphere using a Metrohm Titrimeter, Herizau, Switzerland. The same method was used for the sand.

The cell sizes were measured with Malvern MasterSizer S, Malvern, England in liquid phase. The mean diameter value was 1.06 µm [D(v,0.1) = 0.67 µm; D(v,0.9) = 1.66 µm].

3. Set-up and experiments

Quartz sand was used as filtering media. The specific area A_s of quartz sand was calculated after sieving [11].

Cylindrical PVC column, with an internal diameter of 8 cm, and different lengths (10, 30, 50, 70 and 90 cm) was carried out. All column parameters and characteristics are listed in table 1. To achieve a constant packing density, the column was filled with dry sand (5 hours at 180 °C), and hydraulic compaction was applied with sterile distilled water to reach a bulk density of 1.59 g cm^{-3}. The column was later drained and imbibed again overnight with experimental solutions for 3 pores volume. The mediums were supplied to the column via a single, centrally placed tube [13]. Effluent fractions were collected with a CF-1 Spectrum collector, and KI was analyzed with a multimeter Métrix MX 562 (millivoltmeter function)

equipped with a iodine specific electrode (ORION, 9453BN) and a reference electrode (Ag/AgCl).

For tracing set-up, 5 column lengths for the conservative tracer experiments were used. Solution was supplied to the top of the filtering media at a periodic flux (50 seconds ON, 140 second OFF), using a different rate pump (31.77, 10 and 5.55 mL min^{-1}). When steady state was obtained, a short pulse of tracer was injected. The fraction at the end of the column was collected at defined step time.

In the case of bacterial transport, we operated with two column lengths (30 and 50 cm). Solution was supplied to the soil surface at a periodic flux (50/140 seconds ON/OFF), using a constant rate pump (10 mL min^{-1}).

4. Physic characterization of filtering media

For a good reliability of the experiments, filtering media was well characterized by various approaches. The results are summarized in table 1. The porosity ε of the filtering media was determined as proposed by Mohammedi, 1998 [11].

Table 1 : Column parameters

Parameters of the column experiments	
Parameter	Value
Column diameter	8 cm
Sand grain effective diameter	0.55 mm
Sand grain uniformity coefficient	1.89
Specific area	6450 m^{-1}
Measured surface area of sand (BET)	0.5 $m^2 g^{-1}$
Relative density	2.61
Bulk density	1.59 g cm^{-3}
Porosity	0.41
pHpzc (Ca + Mg 10^{-3} $mol.L^{-1}$)	7.5
pHpzc	5.85
Cation Exchange Capacity	$2.4*10^{-5}$ $mol.g^{-1}$

In the first set of experiments, we used KI injection pulses for understanding the hydraulic parameters after establishing the steady state. In the second set of experiments, we used a stock of *E. coli* in different solutions:
[A] isotonic water (NaCl 9 $g.L^{-1}$); [**B**] isotonic water (NaCl 9 $g.L^{-1}$) + $CaCl_2$ (10^{-3} $mol.L^{-1}$) + $MgCl_2$ (10^{-3} $mol.L^{-1}$); [**C**] isotonic water (NaCl 9 $g.L^{-1}$) + sodium acetate(500 $mg.L^{-1}$); [**D**] decanted and sterilized raw water.

Hydrodynamic approach was separated in two steps. Firstly, the retained and drained water volume were measured. The sum of this two volume represents the total volume involved in the filtering media. Then, the travel time tp (total volume Vt divided by flow rate Q) was determined. Furthermore, residence time distribution (RTD) was calculated [14] after realized experiments using a KI solution.

Secondly, the RTD was fitting using software (DTSPRO 4.2) developed by PROGEPI. The scheme retained for our experiences is the perfect mixing cells in

series exchanging with a dead zone. The different parameters used for this model are presented in Figure 1.

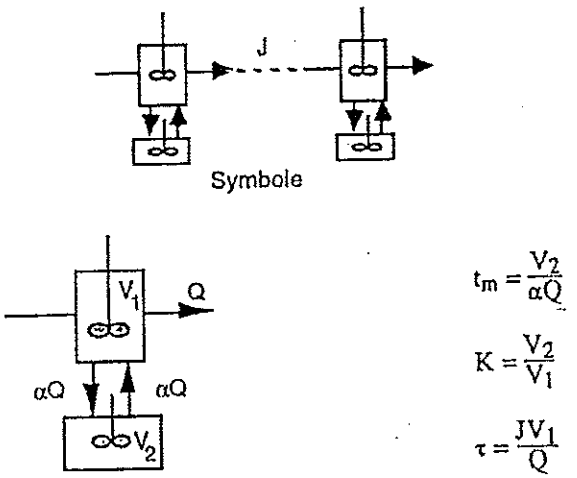

Figure 1: Parameters taking place in the perfect mixing cells in series exchanging with a dead zone model (J, number of cells in series; V_1, volume of dynamic phase; V_2, volume of stagnant phase; αQ, flow exchange between V_1 and V_2)

RESULTS

1. Hydrodynamic

1.1. KI tracing

The first step was to evaluate the mean residence time for a conservative tracer in a range of hydraulic loads and length of column. The typical tracing curve is represented in *Figure 2*. With this residence time distribution (RTD) curve, a mean residence time (ts) is calculated. The results of ts are presented in *Figure 4*.

1.2. Bacterial tracing

A typical bacterial-tracing curve is presented in *Figure 3*. From this curve the breakthrough times for a bacterial concentration ratio of 10^{-5} were extract. The results are summarized in *Table 2* for 30 and 50 cm column length. The KI values are given for comparison. It can be noted that the shape of curves presented in figures 2 and 3 are different in relation with the injection method (pulse for KI and step for bacteria).

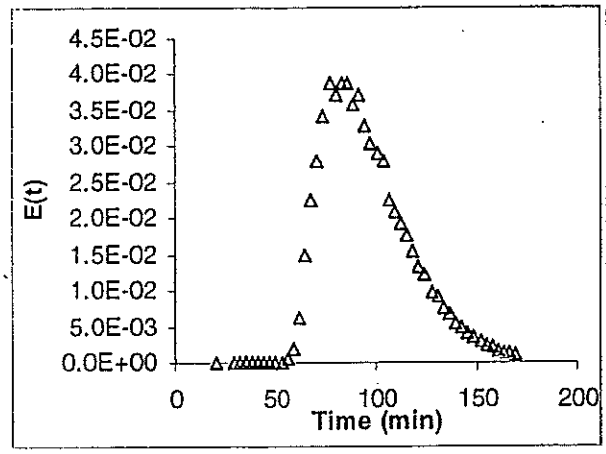

Figure 2: RTD for KI in a 50 cm long column, at 90 cm.d^{-1}

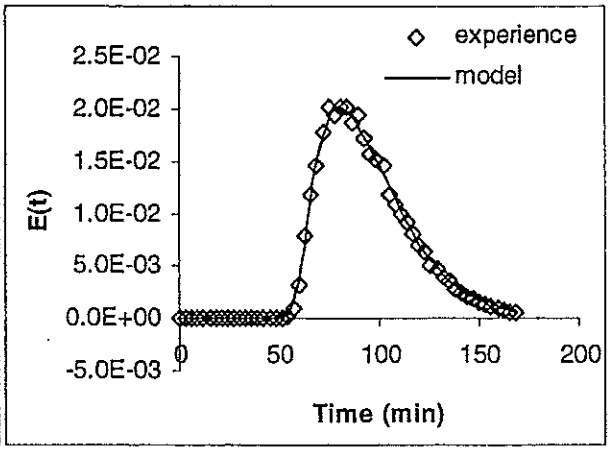

Figure 4: Variation of mean residence time versus hydraulic load and column length

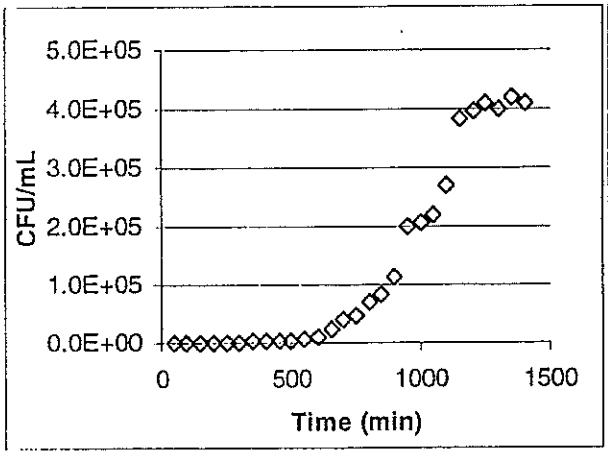

Figure 3 : RTD for a bacterial step input signal, in a 30 cm long column, at 90cm.d^{-1}, NaCl solution.

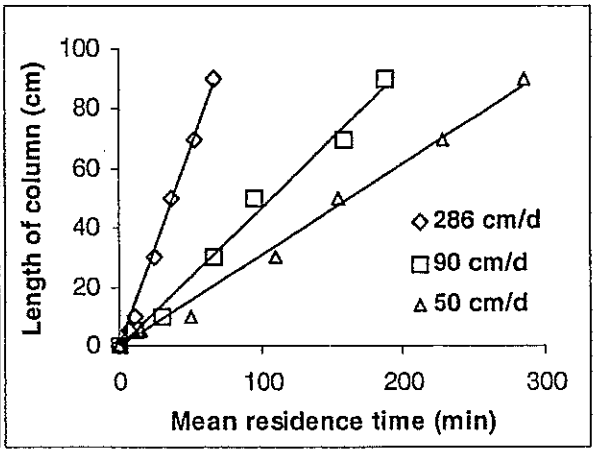

Figure 5: Fit of a tracer breakthrough curve (50 cm, 90 cm/d) for τ =68, tm =9, J =120 and K=0.38

The breakthrough time gives only an information on the bacterial exit. On an other hand, (ts) calculation, allows to know the behaviour of bacteria in the filtering media. This latter value is important for the reduction of pathogen germs in individual onsite wastewater system. Moreover, the adhesion and the predation evolution are similar to the ts evolution. For our results the mean residence time (ts) is calculated according to [17]. The results of this calculus are given in table 3.

Table 2: Comparison of different breakthrough times of bacteria and KI, at 90 cm/d

Media	Column length	
	30 cm	50 cm
	Breakthrough time (C/Co > 10^{-3})	
NaCl 9 $g.L^{-1}$	250	1065
Ca^{2+} + Mg^{2+} 10^{-3} $mol.L^{-1}$	50	525
Acetate 500 $mg.L^{-1}$	75	300
Sterile raw water	45	75
KI	30	50

Table 3: Comparison of different mean residence times (ts) for bacteria and KI, at 90 $cm.d^{-1}$

Media	Column length	
	30 cm	50 cm
NaCl 9 $g.L^{-1}$	961	2328
Ca^{2+} + Mg^{2+} 10^{-3} $mol.L^{-1}$	818	1250
Acetate 500 $mg.L^{-1}$	779	1037
Sterile raw water	432	333
KI	67	96

2. Modeling

The DTSPRO software was used for fitting the obtained curves. Applying the tank in series model with matter exchange, we obtained J, τ, K, and t_m (see figure 1). Examples of these parameters are given in Table 4 for 1 hydraulic loads and 2 column lengths.

Table 4: Parameters for DTSPro model, 90 $cm.d^{-1}$ hydraulic load

	τ	V	J	t_m	K	Tsmod
30 cm KI	63	198.3	15	8.00	0.02	64
50 cm KI	68	214	120	9.00	0.38	94
30 cm bacteria NaCl	530	1664	50	0.06	0.9	1007
50 cm bacteria NaCl	1250	3925	300	0.1	0.95	2437

DISCUSSION

The filtering media play an important role in residence time distribution, and also in bacterial reduction [15]. The quartz sand used is characteristic of individual on-site wastewater system. The results of hydrodynamic tracing show a linear response for each couple length versus hydraulic load. This is consistent with other previous published results [11]. A relation between mean retention time, length of column and hydraulic load was found (Figure 4). The corresponding equation is:

$$ts = \alpha.h.u^{-\beta} \qquad (1)$$

where ts is the mean retention time (min), h is the column length (cm), u is the hydraulic load (cm/min) and α, β are empirical constants. For the sand used, $\alpha = 0.3$ and $\beta = 0.7$, like in [11]. Nevertheless, this author works only with 90 cm column. So we have extrapolated the relation to different lengths of column and found a good agreement between the various fit. It can be noted that this empirical relation is available for length superior to 10 cm.

For bacterial tracing, there is an important interaction concerning bacteria and sand, depending on effluent composition: a neutral effluent (NaCl 0.9 $g.L^{-1}$) leads to an important retardation of the breakthrough time of *E.coli* (*Table 2*). Moreover, solutions containing Ca^{2+} and Mg^{2+} at 10^{-3} $mol.L^{-1}$, or dissolved organic matter (DOM) (sodium acetate at 500 $mg.L^{-1}$) reduce the mean retention time of bacteria (*Table 3*). Generally it can be proposed the following sequence for the breakthrough time and ts values:

$$NaCl > Ca^{2+} + Mg^{2+} > \text{acetate} > \text{sterile raw water}$$

A hypothesis for this phenomenon is that interactions between bacteria and sand are due to physico-chemical sorption. More the bacteria were retained (great breakthrough time), more they were sorbed to the sand (high ts). Jonhson and Logan, (1996) [16], show that presence of Ca^{2+} and Mg^{2+} enhances adsorption of bacteria, using a pure quartz, with a pHpzc near 2. In our experiments, taking into account of the sand pHpzc value of 7.5 and bacterial pHpzc near 6, it can be postulated that with calcium and magnesium ions, charge repulsion occurs. Effectively, the ions present in solution can be adsorbed by the bacterial surfaces and reverse the global cell wall charge. There are fewer interactions between sand and bacteria, and bacteria are less retained than for NaCl experiments. It have to note that the presence of cations (Ca^{2+}, Mg^{2+}) may bridged bacteria, and thus filtration can take place.

For the experiments with acetate, there is a competition for adsorption sites, for the reason that this molecule and bacteria as similarly charged [15]. Then, bacteria are released from the column. Harvey et al., (1989) [9] noticed that bacteria are fixed when DOM concentration is at low level.

For sterile raw water, bacteria have the same comportment than for cations and acetate experiments, but with a shorter mean retention time. The two phenomena described for acetate and cations are involved in the transport of bacteria by septic effluent. Acetate represents 70 % of the dissolved organic matter in a septic effluent and cations like Ca^{2+} and Mg^{2+} take place in this solution.

In terms of model, each curve of DTS was fitting with the DTSPRO V4.2 software. It was postulated that the perfect mixing cells in series exchanging with a dead zone (Figure 1) was the more efficient in our case. We take into account four parameters, τ, J, t_m, K. K represents the ratio dynamic volume under stagnant volume. Globally, K increases with decreasing of hydraulic load. For the other parameters, we found an increase of value with an increase of column length (data not shown).

Finally, this approach leads us to calculate a modeled value of ts (note tsmod) with the following equation:

$$ts\,\mathrm{mod} = \tau(K+1) \qquad (2)$$

The tsmod values determined in the case of KI tracing curve obtained for 30 and 50 cm at 90 $cm.d^{-1}$ are respectively 64 and 94 minutes. For bacterial tracing with NaCl (30 and 50 cm at 90 $cm.d^{-1}$) tsmod values are respectively 1007 and 2437 min. Less than 5 % of variation between experimental ts (Table 3) and tsmod (Table 4) was found.

CONCLUSION

The use of KI in tracer experiments allows to a better understanding and hydrodynamic characterization of unsaturated conditions developed in individual onsite wastewater systems. The experimental and modeling methods are in good agreement. In a second part of this work, the bacterial transport was successfully experimented with the same methodology.

In further studies, experiments with a biofilm in the filtering media will be performed. Another development of this research is the behavior of viruses in such process.

BIBLIOGRAPHIE

[1] Bajolet O., Chippaux-Hyppolite C., *Les rotavirus et autres virus de diarrhées*, Bull. Soc. Path. Ex., 91, 5-5 bis, (1998), 432-437

[2] Van Asperen I. A., Medema G., Borgdorff M. W., Sprenger M. JW., Havelaar A. H., *Risk of gastroenteritis among triathletes in relation to faecal pollution of fresh water*, Int. Jour. Of Epidemiology, 27, (1998), 309-315

[3] Fleisher J. M., Kay D., Wyer M. D., Godfree A. F., *Estimates of the severity of illnesses associated with bathing in marine recreational waters contaminated with domestic sewage*, International Journal of Epidemiology, 27, 1998, 722-726

[4] Craun F. G., *A summary of waterborne illness transmitted through contaminated groundwater*, Journal of Environmental Health, 48, 3, (1985),122-127

[5] Yates M.V., Yates, S. R., *Modeling microbial fate in the subsurface environment*, CRC Critical Reviews in Environmental Control, 17, 4, (1988), 307-344

[6] Yates M. V., *Septic tank density and ground-water contamination*, Ground Water, 23, 5, (1995), 586-591

[7] Corapcioglu M. Y., Haridas A., *Transport and fate of microorganisms in porous media: a theoretical investigation*, Journal of Hydrology, 72, (1984), 149-169

[8] Corapcioglu M. Y., Haridas A., *Microbial transport in soils and groundwater: a numerical model*, Advances Water Resources, 8, December, (1985), 188-200

[9] Harvey R. W., George L. H., Smith R. L., LeBlanc D. R., *Transport of microspheres and indigenous bacteria through a sandy aquifer: results of natural- and forced-gradient tracer experiments*, Environmental Science and Technology, 23, 1, (1989), 51-56

[10]Harvey R. W., Garabadian S. P., *Use of colloid filtration theory in modeling movement of bacteria through a contaminated sandy aquifer*, Environmental Science and Technology, 25, 1, (1991), 178-185

[11]Mohammedi M., *Etude de matériaux de garnissage en vue d'une réduction géométrique des filtres biologiques dans le cadre de l'assainissement autonome*, Thèse 3 ème cycle, Université de Limoges, (1998)

[12]Sposito G., *On points of zero charge*, Environmental Science and Technology, 32, 19, (1998), 2815-2819

[13]Bond W. J., Wierenga P. J., *Immobile water during solute transport in unsaturated sand columns*, Water Resources research, 26, 10, (1990), 2475-2481

[14]Villermaux J., *Génie de la réaction chimique*, Tec & Doc , Lavoisier, (1993), Levenspiel O., *Chemical reaction engineering*, John Wiley & Sons, (1972)

[15]Weber-Schirk M. L., Dick R. I., *Physical-chemical mechanisms in slow sand filters*, JAWWA, 89, 1, (1997), 87-100

[16]Johnson W., Logan B. E., *Enhanced transport of bacteria in porous media by sediment-phase and aqueous-phase natural organic matter*, Water Research, 30, 4, (1996), 923-931

[17]Levenspiel O., *Chemical reaction engineering*, John Wiley & Sons, (1972)

HYDRODYNAMIC BEHAVIOUR OF GAS AND LIQUID FLOWS IN A GAS/LIQUID COLUMN – APPLICATIONS TO DEODORIZATION OF WASTE GASES

P. Humeau[1], J.N. Baléo[1], P. Pré[1], F. Raynaud[2], J. Bourcier[2], P. Le Cloirec[1]

[1]Ecole des Mines de Nantes, GEPEA, B.P. 20722, 44307 Nantes cedex 03, France
[2]VERITE S.A., Parc d'activité Vendée Sud Loire, 85600 Boufféré, France

Abstract. The knowledge of hydrodynamic behaviour of a gas-liquid column is of great interest as the transfer efficiencies are influenced by the flow patterns. An experimental study was carried out in an absorber working countercurrently in order to evaluate the dependence of gas and washing solution flow patterns on operating conditions (gas and water loads, packing materials). The flow of each phase was characterized using hydrodynamic parameters from residence time distribution methodology. A dispersion model represents the gas flow. It results that the dispersion factor should not be neglected in such systems. A tanks-in-series with mass exchange model is used to characterize the liquid flow. This kind of model enables the determination of the liquid volume which really participates in the transfer process. The results allow the best designing of the gas-liquid column for a suitable deodorization rate to be predicted.

INTRODUCTION

Biological processes used for air treatment as biofiltration or bioscrubbing are an interesting alternative when gas is characterized by high flow but low compound concentrations [1]. However, such processes are seldom used industrially because design and operating conditions are not well established, leading to expensive installations.

The aim of the work is to develop and optimise a bioscrubber for specific air treatment applications (wastewater treatment plant, food-processing industries...). So it is necessary to evaluate the dependence of gas and washing solution flow patterns in a countercurrent gas/liquid column on operating conditions (gas and water loads, packing materials), which have an important impact on mass transfer of quite soluble odorous compounds as ammonia or hydrogen sulfide [2,3].

A study of residence time distribution (RTD) of each phase was carried out to get the hydrodynamic parameters (mean residence time, dispersion). These hydrodynamic parameters allow the association of the treatment rate with the behaviour of the absorber to be defined [5].

The study presented in this paper is first relative to the determination method of RTD curves and to the representation mode of the flows. The influence of operating conditions on hydrodynamic parameters of each phase is considered and discussed. Then, the operating conditions leading to the optimal deodorization rate are defined and explained, according to the flow patterns of gas and liquid in the transfer column. This approach allows the bioscrubber design to be optimised in accordance with the effluent characteristics.

MATERIALS AND METHODS

1. Material

The experimental set-up is composed of a Plexiglas absorber, with inner diameter 0.192 m and height 3.42 m, working countercurrently (Figure 1). Two successive contact modes could be distinguished: a gas-liquid contact in an empty column over 1 m, where the liquid phase was sprayed from a spray nozzle (Lechler 460 523 17), and a gas-liquid contact in a packed column, where characteristics as packing material and porous bed height could be modified.

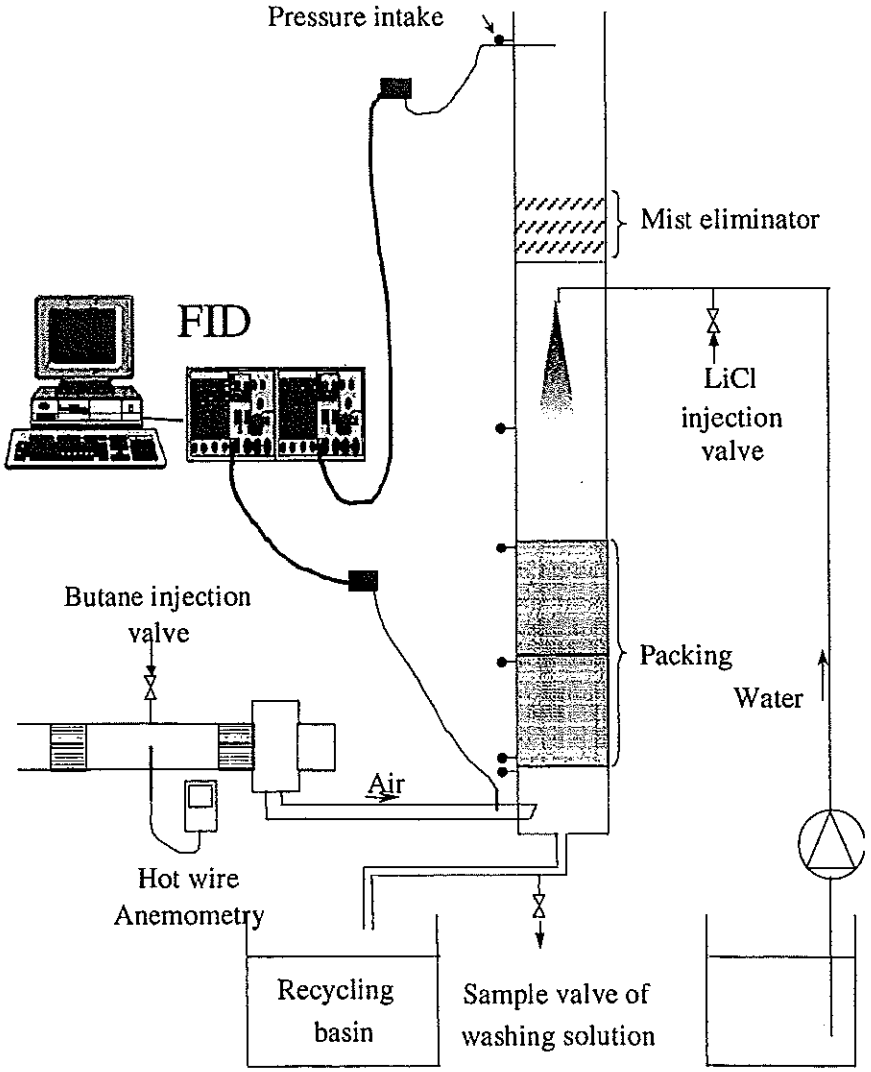

Figure 1. Experimental set-up used for flow pattern study

Gas loads ranged from 0.083 to 0.997 $kg.m^{-2}.s^{-1}$, and four liquid loads were studied: 0.400, 0.492, 0.560 and 0.690 $kg.m^{-2}.s^{-1}$. Three packings were used: 10 mm ceramic Raschig rings, 16 mm polypropylene (PP) Pall rings and 45 mm × 18 mm PP Spiralpac (tellerettes). The packing characteristics (specific surface area, bed voidage and tortuosity and capacity of water retention) are reported in Table 1.

Table 1. Packing characteristics

Packing	Raschig rings	Pall rings	Tellerettes
Specific surface area a_g	508 $m^2.m^{-3}$	329 $m^2.m^{-3}$	141 $m^2.m^{-3}$
Bed voidage ε	0.61	0.91	0.93
Tortuosity τ	1.27	1.05	1.04
Static liquid holdup per volume of packed bed	31.6 $mL.L^{-1}$	3.9 $mL.L^{-1}$	1.8 $mL.L^{-1}$

2. Methods

2.1. Liquid holdup determination

The knowledge of liquid holdup in a gas-liquid column is of great interest to determine the space time and to characterize the retention volume of liquid. From this evaluation, the optimum operating conditions and design of the bioscrubber could be defined. The total holdup h_t is considered as the sum of the static holdup h_s and the operating holdup h_o. The operating holdup depends on liquid and gas loads. From steady-state conditions, the two flows were stopped simultaneously. The amount of liquid collected after 15 min of drainage corresponds to h_o [6].

2.2. RTD curves

The study of residence time distributions of each phase in the column was performed with a pulse injection of a tracer at the reactor inlet and by recording the concentration-time of tracer living the vessel [7].

The tracer retained was butane C_4H_{10} for air flow. The injection came from a cylinder of butane gas (2000 ppm ± 2%), flowing at 8460 $mL.min^{-1}$ during 2 s (flowmeter AALBORG N044-40, sapphire float). This method allows the measurements to be repeatable with constant butane injection quantities (1.36 mg of C_4H_{10}). Butane was detected continuously at the inlet and outlet with a Flame Ionization Detector FID (Cambustion HFR 400 FFID).

The tracer retained for liquid flow was lithium chloride. The beginning of the experiment was the injection of 1 mL of LiCl 0.1 M. Liquid was sampled 1 s every 3 s at the outlet of the column. Lithium ions were measured with an atomic absorption spectrophotometer (Perkin-Elmer 2280).

RESULTS – DISCUSSION

1. Gas flow

The dispersion model was used for the representation of gas flow. The mean residence time $\bar{t}$ and the Peclet number (Pe) were calculated following the method of statistical moments from the RTD curves. The solution of the dispersion model could be obtained from equations 1 to 3 under steady-state conditions with the corresponding set of boundary conditions of closed-open vessel.

$$\bar{t} = \left[\int_0^\infty t_s . E(t_s) . dt_s\right]_{out} - \left[\int_0^\infty t_s . E(t_s) . dt_s\right]_{in} \qquad (1)$$

$$1+\frac{2}{Pe}+\frac{1}{Pe^2} = \frac{\bar{t}^2}{\sigma^2}.\left(\frac{2}{Pe}+\frac{3}{Pe^2}\right) \quad (2)$$

$$\sigma^2=\left[\int_0^t (t_s-\bar{t})^2.E(t_s).dt_s\right]_{out}-\left[\int_0^t (t_s-\bar{t})^2.E(t_s).dt_s\right]_{in} \quad (3)$$

The results of mean residence time $\bar{t}$ and dispersion coefficient D for different operating conditions are reported in Table 2.

Table 2. Mean residence time $\bar{t}$ and dispersion coefficient D in the gas-liquid column according to operating conditions

U_G	Liquid flow rate	Spray column (no packing)		Raschig rings		Pall rings		Tellerettes	
($m.s^{-1}$)	($kg.m^{-2}.s^{-1}$)	$\bar{t}$ (s)	D ($m^2.s^{-1}$)	$\bar{t}$ (s)	D ($m^2.s^{-1}$)	$\bar{t}$ (s)	D ($m^2.s^{-1}$)	$\bar{t}$ (s)	D ($m^2.s^{-1}$)
0.07	0	-	-	65.0	1.4×10^{-3}	102.5	8.4×10^{-3}	43.9	2×10^{-3}
	0.400	29.0	1.8×10^{-3}	52.5	6.5×10^{-3}	48.6	8.7×10^{-3}	48.0	5.1×10^{-3}
	0.492	45.2	51.4×10^{-3}	71.3	6.6×10^{-3}	45.9	8.5×10^{-3}	46.8	9.3×10^{-3}
	0.560	39.6	20.0×10^{-3}	87.3	13.4×10^{-3}	50.1	10.8×10^{-3}	45.1	6.5×10^{-3}
	0.690	39.7	37.8×10^{-3}	185.0	7.1×10^{-3}	44.9	9.1×10^{-3}	46.2	7.1×10^{-3}
0.204	0	13.4	5.6×10^{-3}	19.0	1.4×10^{-3}	16.5	2.9×10^{-3}	13.5	3×10^{-3}
	0.400	14.4	31.6×10^{-3}	21.0	6.5×10^{-3}	14.4	22.7×10^{-3}	14.9	14.3×10^{-3}
	0.492	14.9	42.0×10^{-3}	21.2	6.6×10^{-3}	15.0	20.4×10^{-3}	15.0	23.0×10^{-3}
	0.560	-	-	19.2	13.4×10^{-3}	14.0	25.0×10^{-3}	13.5	6.8×10^{-3}
	0.690	14.0	23.6×10^{-3}	22.6	7.1×10^{-3}	14.5	17.8×10^{-3}	13.9	20×10^{-3}
0.476	0	-	-	8.7	1.4×10^{-3}	-	-	6.5	5.6×10^{-3}
	0.400	-	-	9.3	6.5×10^{-3}	-	-	6.4	32.5×10^{-3}
	0.492	-	-	9.3	6.6×10^{-3}	-	-	7.1	70.4×10^{-3}
	0.560	-	-	10.2	13.4×10^{-3}	-	-	6.7	72.4×10^{-3}
	0.690	-	-	9.0	7.1×10^{-3}	-	-	6.6	15×10^{-3}

The mean residence time of air seems to be influenced by the gas velocity and the packing. The observed variations for a given gas velocity according to water load can be considered as negligible, except for the mean residence time variations for low gas velocity in the column packed with Raschig rings. The mean residence time decreases when the gas velocity increases. Moreover, lower is the bed voidage, greater is the $\bar{t}$ value, as is shown by values obtained with Raschig rings and the two other packings (Figure 2).

The D values increases with the gas velocity. The results reveal that the dispersion cannot be neglected in a two-phase (spray column) and three-phase system, as the Peclet number varies from 17 (U_G = 0.07 $m.s^{-1}$, column packed with Raschig rings) to 140 (U_G = 0.68 $m.s^{-1}$, column packed with Tellerettes) for a liquid load of 0.560 $kg.m^{-2}.s^{-1}$. The kind of packing does not have a significant influence on the dispersion factor. In return, the water load has an important impact on this parameter. A relation (equation 4) was established by Laddha *et al.* [2], from experiments in a spray column (diameter: 5 cm), to predict the dispersion parameter.

$$\frac{U_G.\bar{d}_g}{D}.\left(\frac{U_L}{U_G}\right)^{0.5} = 0.014.\exp\left[0.0005.\left(\frac{d_o.u_o.\rho_G}{\mu_G}\right)\right] \quad (4)$$

with

$$\bar{d}_g = 0.4852.\left(\frac{u_o^{\,2}}{2.d_o.g}\right)^{-0.0665}.\left[\frac{10.764.\sigma}{(\rho_L-\rho_G).g}\right]^{0.5} \qquad (5)$$

The dispersion is expressed according to the characteristics of continuous phase, as superficial velocity U_G ($m.s^{-1}$), viscosity μ_G ($kg.m^{-1}.s^{-1}$), density ρ_G ($kg.m^{-3}$) and the characteristics of dispersed phase, as superficial velocity U_L ($m.s^{-1}$), density ρ_L ($kg.m^{-3}$) and superficial tension σ ($N.m^{-1}$). Moreover, the mean diameter of droplets $\bar{d}_g$ (m) is estimated with relation (5) according to nozzle characteristics (velocity u_o and orifice diameter d_o).

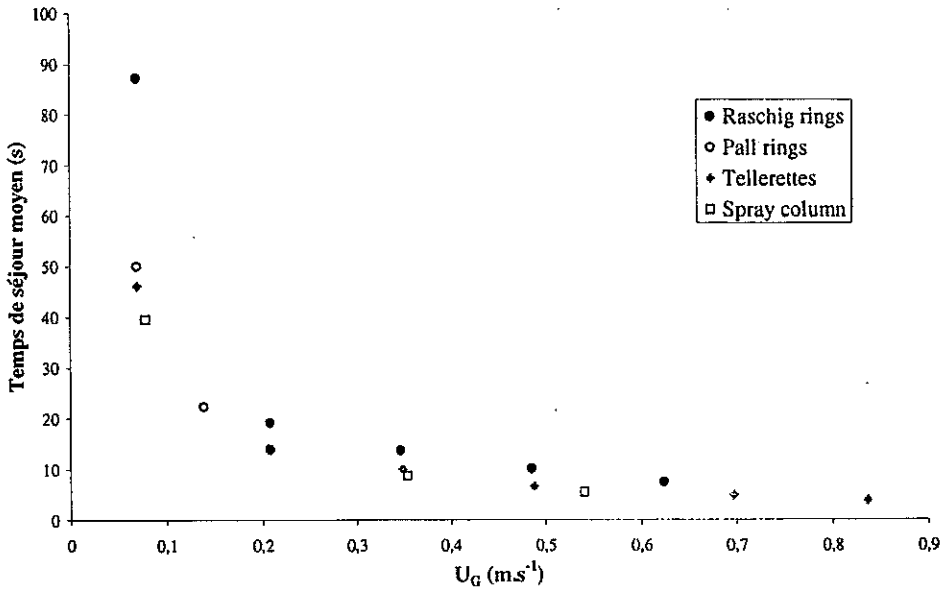

Figure 2. Mean residence time of gas according to the gas velocity and the packing (Liquid load: 0,560 $kg.m^{-2}.s^{-1}$).

The dispersion coefficients experimentally obtained in the spray column are more important than the calculated values: when experimental data were from $1.1.10^{-3}$ to $80.9.10^{-3}$ $m^2.s^{-1}$, the calculated dispersion values only range from $0.7.10^{-3}$ to $2.6.10^{-3}$ $m^2.s^{-1}$. The greatest deviations are observed for high values of superficial velocity of gas. These deviations between experimental and predicted values could be explained by the different column diameter. According to Shah *et al.* [3], the most important parameter, which induces a deviation from the plug flow, is the diameter of the reactor: there is usually more backmixing when the diameter increases.

As the dispersion factor affects the performances of deodorization, it is necessary to define the operating conditions leading to the lowest dispersion coefficient. Thus, for a given gas flow rate, the lower diameter and the lower ratio between liquid and gas should be reached. Moreover, the choice of a spray column or an absorber packed with a material offering a high bed voidage should be preferred, rather than a packed column with a lower bed voidage.

2. Liquid flow

The water flow was represented by a tanks-in-series with mass exchange model. This model involves four parameters: τ, J, t_m and K. They were defined following equations 6 to 8, and determined by fitting a theoretical curve to the experimental response. The DTS software (Progepi, Nancy, France) was used for the resolution of equations.

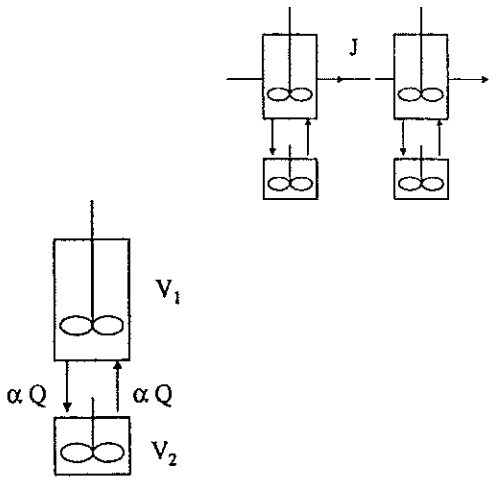

$$\tau = \frac{J.V_1}{Q} \qquad (6)$$

$$K = \frac{V_2}{V_1} \qquad (7)$$

$$t_m = \frac{V_2}{\alpha Q} \qquad (8)$$

The four-parameter model was validated by comparison of mean residence times [τ . (K+1)] with the first order statistical moments calculated from their corresponding E(t) curves following the equation (9).

$$\bar{t} = \frac{\int_0^\infty t.C.dt}{\int_0^\infty C.dt} = \frac{\sum_i t_i . C_i . \Delta t_i}{\sum_i C_i . \Delta t_i} \qquad (9)$$

Furthermore, calculated volumes [J . (V_1 + V_2)] were compared with water volumes h_t experimentally measured for each operating conditions. The difference between calculated and measured volumes does not exceed 5%, as shown in Figure 3 for gas-liquid column packed with Raschig rings.

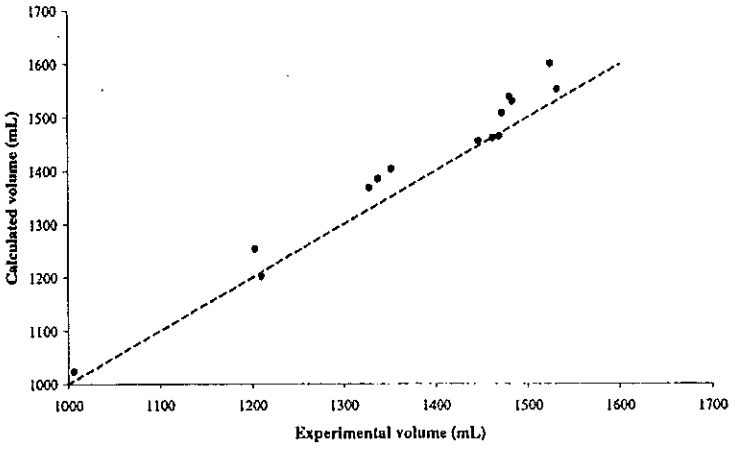

Figure 3. Comparison of the calculated and observed volumes in gas-liquid column packed with Raschig rings.

The values of mean residence time [τ . (K+1)], J and t_m for three absorber configurations (spray column and column packed with Raschig rings or tellerettes) and different operating conditions are reported in Table 3.

Table 3. Values of mean residence time [τ. (K+1)], J and t_m according to operating conditions and packing material

Liquid flow rate ($kg.m^{-2}.s^{-1}$)	U_G ($m.s^{-1}$)	Spray column			Raschig rings			Tellerettes		
		[τ. (K+1)]	J	t_m	[τ. (K+1)]	J	t_m	[τ. (K+1)]	J	t_m
0.400	0	-	-	-	125 s	22	29 s	67 s	8	22 s
	0.340	27s	11	7 s	130 s	16	30 s	72 s	11	24 s
	0.476	-	-	-	126 s	19	26 s	75 s	11	35 s
0.492	0	-	-	-	84 s	8	23 s	58 s	12	24 s
	0.340	20 s	6	6 s	96 s	10	31 s	60 s	9	27 s
	0.476	-	-	-	97 s	11	28 s	60 s	9	25 s
0.560	0	-	-	-	90 s	14	24 s	56 s	9	23 s
	0.340	22 s	9	7 s	95 s	10	42 s	54 s	8	23 s
	0.476	-	-	-	96 s	11	26 s	59 s	6	27 s
0.690	0	-	-	-	87 s	10	38 s	54 s	13	24 s
	0.340	25 s	16	6 s	92 s	17	28 s	53 s	11	19 s
	0.476	-	-	-	-	-	-	55 s	8	24 s

The influence of the liquid flow rate and of the packing is enlightened. The increase of liquid load and bed voidage lead to a reduction of the mean residence time. If the liquid flow rate contribution is easily revealed, the bed voidage impact is due to its effects on the liquid retention in the column. As it is shown in Table 1, the static liquid holdup per volume of packed bed is more important in the column packed with Raschig rings than with Tellerettes.

The variations of J and t_m were not as important as the variations of mean residence time for a given configuration of the contactor. The differences were only observed between the column packed with Raschig rings and the two other configurations: the dispersion was lower in the case of the column packed with Raschig rings. The parameter which represents the mean residence time in the stagnant phase of the liquid flow (t_m) increases with the static holdup in the column. The presence of this stagnant phase was responsible of the long tail of the DTS curves. Moreover, it should be noted that there was a stagnant phase in the spray column due to a part of liquid which was retained on the walls of the absorber.

The interest of this kind of model is to quantify the stagnant fraction of the liquid flow with the knowledge of K (ratio between stagnant and dynamic volumes). Indeed, this stagnant volume may not participate in the transfer operation as the global mass transfer coefficient K_G tends to zero with the liquid velocity. This parameter is also of great interest in the case of a mass transfer enhanced by a reaction in the liquid phase (pollutant degradation by the biomass). The performances could be optimised if mass transfer is not a limiting factor and is enhanced by a kinetic reaction.

3. Application to deodorization of a waste gas

High residence time of the dynamic phase and the low part of stagnant phase enhance the transfer rate. It is possible to increase the residence time by the choice of the minimum liquid flow rate in the absorber, but also by increasing the height of

the column. Moreover, a lower washing solution enhances the residence time in the activated sludge basin of the bioscrubber where the major part of the biodegradation step takes place. Then, the use of a packing characterized by high bed voidage reduces the fraction of stagnant liquid volume in the column.

A study of deodorization by bioscrubbing of an exhaust gas emitted by a pumping station was realised. The operating conditions and the design of the bioscrubber were defined according to the hydrodynamic behaviour characterization. Thus, a column packed over 1.20 m with Tellerettes, with inner diameter 0.302 m and height 3.20 m was used. The gas and liquid flows were respectively 300 $m^3.h^{-1}$ and 600 $L.h^{-1}$. The inlet concentrations of H2S (major odorous compound) range from 1 to 7 $mg.m^{-3}$. The elimination rates (40 to 80 %) were sufficient to obtain an entire deodorization of the effluent. Moreover, the parameters of the washing solution, as pH control between 8.5 and 9, were determined to optimize the transfer rate.

CONCLUSIONS

The study of RTD curves of air and liquid in a gas-liquid column allows the hydrodynamic parameters of each phase to be obtained with the use of models. The dispersion model was retained to represent the air flow. It results that the dispersion factor should not be neglected in such systems, as it affects the transfer performances. The liquid flow was represented by a tanks-in series with mass exchange model. This kind of model enables the determination of the fraction of active volume of the liquid which is involved in the transfer process.

From this work, the operating conditions and the designing of the bioscrubber leading to the optimal deodorization rate could be defined: low column diameter and liquid flow rate, choice of packing material with high bed voidage. It is then possible to propose a bioscrubber device for a specific odorous effluent.

ACKNOWLEDGEMENTS

Financial support provided by ADEME (Agence De l'Environnement et de la Maîtrise de l'Energie) is gratefully acknowledged.

REFERENCES

[1] Le Cloirec P., Humeau P., Baléo J.N., *Processes for biological purification of air loaded with volatile organic compounds*, Biodépol'99, Rennes, France, October 26 & 27 (1999), 25-41

[2] Laddha G.S., Krishnan T.R., Viswanathan S., Vedaiyan S., Degaleesan T.E., *Some performances characteristics of liquid phase spray columns*, AIChE J., 22 (1976), 456-462

[3] Shah Y.T., Stiegel G.J., Sharma M.M., *Backmixing in gas-liquid reactors*, AIChE J., 24 (1978),369-400

[4] Humeau P., Baléo J.N., Raynaud F., Bourcier J., Le Cloirec P., *Flow characterization in a gas-liquid column: application to a bioscrubber for the deodorization of waste gases*, Wat. Sci. Technol., 41 (2000), 191-198

[5] Froment G.F., Bischoff K.B., *Chemical reactor analysis and design*, Ed. John Wiley & Sons (2nd Ed.), New York (1990)

[6] Iliuta I., Larachi F., Grandjean B.P.A., *Residence time, mass transfer and back-mixing of the liquid in trickle flow reactors containing porous particles*, Chem. Eng. Sci., 54 (1999), 4099-4109

[7] Levenspiel O., *Chemical Reaction Engineering*, Ed. John Wiley & Sons (3rd Ed.), New York (1999)

HYDRODYNAMICS IN AN AERATED CHANNEL REACTOR : INFLUENCE OF AIR AND GAS FLOW RATES ON AXIAL DISPERSION

O. Potier, M.-N. Pons, J.-P. Leclerc, E. Renou

Laboratoire des Sciences du Génie Chimique, CNRS-ENSIC-INPL,
1, rue Grandville BP 451, 54001 Nancy, France

Abstract. The channel reactor is one of the most widespread reactors in waste water treatment plants (WWTPs). Its hydrodynamics have been studied in a pilot plant. The reactor is aerated from its floor by an air diffusion system. For large gas velocities like those used in WWTPs, the bubbles induce an upward motion of liquid near one of the fixed walls, thus creating vertical recirculation cells. To highlight these cells, local velocities of liquid are measured with a two-components laser Doppler anemometer. A correlation is obtained between these velocities and the axial dispersion coefficient measured by an RTD method. This correlation shows a link between the systemic and local approaches.

INTRODUCTION

Activated sludge process is the most widespread technique in biological waste water treatment. In the aerated reactor, micro-organisms grow and degrade the pollutants. This study deals with one type of these aerators, the channel reactor. Its section is rectangular and its length can be very large, although it can be folded in sections. The 3000 m^3 channel reactors of the Nancy-Maxéville plant are 100 meters long, but longer reactors can be found. An air diffusion system is fixed on its floor and provides oxygen to the micro-organisms. These reactors are of the cross flow type (horizontal flow for the liquid and vertical for the gas).

Due to their shape and size, there is definitely an effect of hydrodynamics on the efficiency of the pollution abatement, as concentration gradients are experimentally observed. The purpose of this study is to understand the channel reactor hydrodynamics in order to improve its design and its operation.

Experiments were carried out in a pilot channel reactor using two approaches : a systemic approach based on the measure of Residence Time Distribution (RTD) and a local approach with velocity measurements using a laser Doppler anemometer. The gas and liquid flow rates and the liquid height are the variable parameters of the experiments.

CHANNEL REACTOR HYDRODYNAMICS

1. Systemic approach

RTDs on the full-scale and the pilot plants show that the channel reactor hydrodynamics are well represented by a series of J complete mixed reactors (CMR) and by a plug flow reactor with axial dispersion model [1]. The influence of the liquid flow rate was studied by determining the number J of CMR for different

liquid space-time $\tau = V/Q_L$ where V is the volume and Q_L the liquid flow rate. By considering the equivalence relation between the Peclet number , $P \approx 2$ (J-1) [1], J is related to the residence time τ. As $P = \frac{uL}{D}$ with L, the reactor length, u, the average velocity ($u=\frac{L}{\tau}$) and D, the axial dispersion coefficient, then $P = \frac{L^2}{\tau D}$ and $J = \frac{L^2}{2\tau D} + 1$ [2]. If the axial dispersion coefficient remains constant, we obtain a linear relation between J and $1/\tau$: $J = \frac{K}{\tau} + 1$

This linearity has been experimentally verified on the pilot plant [3] and on the full scale plant [4]. We have shown that the axial dispersion coefficient remains constant if the agitation is governed by the aeration i.e. when the air flow rate is larger than the liquid flow rate. In this case, D depends only on the reactor geometry and on the air flow rate. The CMR in series model is very useful for waste water treatment simulations, but for design the axial dispersion coefficient becomes an important characteristic.

The influence of the air flow rate Q_G upon the axial dispersion coefficient has also been studied [5]:

$$D = a.Q_G^x \text{ with } 0.3 \leq x \leq 0.5$$

A similar law was proposed by Murphy and Boyko [6] for aerators, with exponent between 0.25 and 0.45.

2. Liquid circulation inside the channel reactor

The aeration system has an important effect on hydrodynamics. The bubbles rise into the reactor and drag up the liquid which must go down near the opposite wall in order to conserve the mass balance. Consequently vertical recirculation cells are induced.

Two types of aeration systems are mainly found : the in-line layout and the nozzle-floor layout. We use the first system in our pilot plant. It induces an important and global recirculation. (Fig. 1a). The second set-up induces a more local circulation due to the homogeneous repartition of the diffuser. (Fig. 1b) [7]. Abraham et al. [7] studied the circulation velocity of the liquid in an aeration tank without horizontal liquid velocity. They obtained a good correlation between the liquid circulation velocity U and the specific gas flow rate Q_G/L :

$$U = p\left(\frac{Q_G}{L}\right)^x$$

The exponent x varies between 0.33 and 0.50 according to the aerator geometry. It is interesting to note that the exponent varies in the same range than in the relation between the axial dispersion coefficient D and the gas flow rate Q_G. The constant p depends strongly on the ratio between the water height and the aerator width.

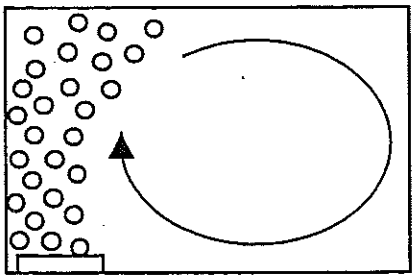

Figure 1a : in-line layout

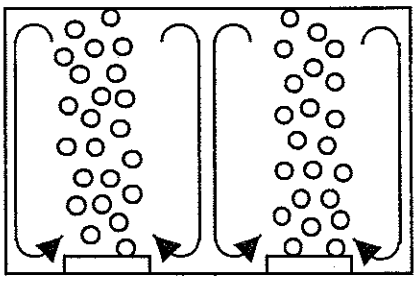

Figure 1b : nozzle-floor layout

3. Comparison with bubble columns

The bubble column hydrodynamics has been largely studied. These reactors present some similarity with the channel aerator: they are two-phase gas-liquid systems where the gas phase is dispersed into the continuous liquid phase inducing circulation cells. However the main difference is that aerators have liquid-gas cross flows, when bubble columns operate with parallel flows. Baird and Rice [8] studied the axial dispersion coefficient in bubble columns and derived from the Kolmogoroff's theory of isotropic turbulence and dimensional analysis the following correlation between the axial dispersion coefficient, the superficial gas velocity u_G and the reactor diameter d :

$$D = K\, d^{4/3} (u_G \cdot g)^{1/3}$$

where K is a dimensionless constant. Baird and Rice proposed a value of 0.35 for K. This relation is in agreement with a very large number of empiric correlations [9, 10, 11, 12], which describe the link between the axial dispersion coefficient and the column diameter and superficial velocity of gas. Krishna *et al.* [13] have showed that the radial distribution of the upflow liquid velocity compared to the velocity on the centerline of the column is independent of the column diameter and of the superficial velocity of the gas. The mere knowledge of this liquid velocity allows to characterise the entire liquid flow in the column. Many empirical correlations have also being proposed to relate the liquid velocity in the centerline of the column, the superficial velocity of the gas and the column diameter. Globally, for the axial dispersion coefficient, a relation of the type $D = K \cdot d \cdot u_L(0)$ can be obtained According to the authors, [10-13] K varies between 0.31 and 0.5.

EXPERIMENTAL DEVICE

1. Description of reactor pilot plant

The pilot channel, of width $W = 0.2$ m is built in transparent material (Plexiglass). Its total unfolded length is 3.60 meters. One wall of the reactor is fitted with stainless steel tubes in which holes have been drilled for air injection. The air flow rate is measured with a flowmeter and can be varied between 15 and 66 L/min.

2. Equipment and measurement methods

For the measurement of the Retention Time Distribution, tracing experiments have been carried out by injecting pulses of a solution of sodium chloride, the concentration of which is monitored with a conductimetric probe. The tracing

experiments are analysed using the software DTS 4.2. The experimental Peclet number and axial diffusion coefficient were determined by curve fitting.

Local velocities of liquid were measured with a two-components laser Doppler anemometer equipped with a RSA-1000L processor, which operates in the backward scattering mode. In fact the anemometer measures the velocities of pearly particles (Iriodine® 110, Merck) which have the same motion than the liquid. The anemometer takes 10000 data for each measurement point in the reactor. The average value is recorded. The data presented here refer to the y-axis component. The reflection of the laser beam over the steel tubes can be dangerous. Therefore no measurement was taken below 3 cm from the reactor floor neither below 1.5 cm of the surface because of the reflection of the laser onto the water surface.

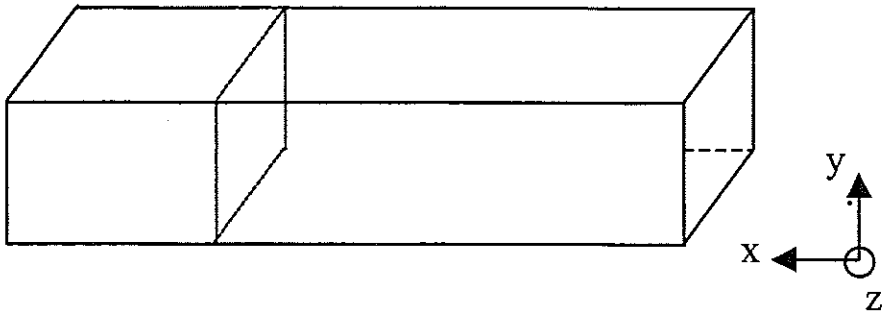

Figure 2 : Plane of anemometric measures (x: liquid flow direction)

3. Liquid velocity field

The air flow rate has been fixed at 35 L/min and the liquid space time to 36 minutes. Experiments have been performed to test the effect of the liquid flow rate and height. The flow pattern has been investigated in a vertical plane perpendicular to the liquid flow direction and in an horizontal plane situated at mid-depth in the liquid phase.

RESULTS

1. Velocity field for $H/W \approx 1$

The first tests have been conducted with a water depth H = 0.2 m, i.e. a channel shape factor H/W = 1.1. The obtained profile corresponds to what is expected with a recirculation loop (Figure 3).

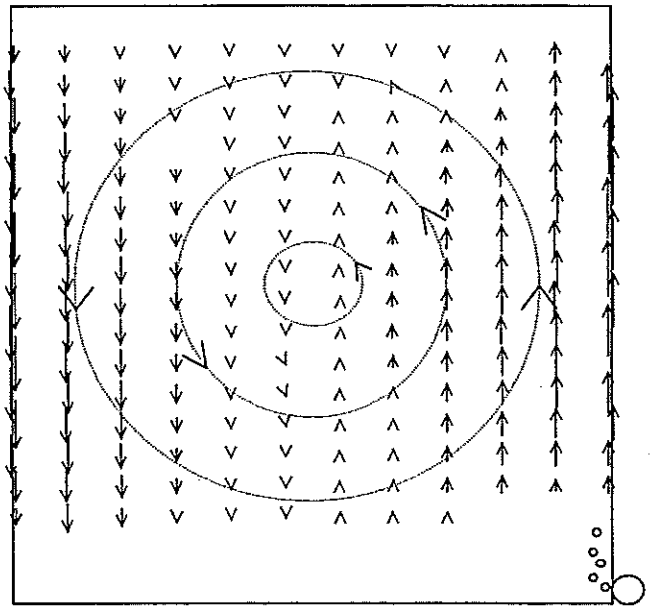

Figure 3 : Velocity field and recirculation loop in plane y-z for H/W = 1.1

2. Velocity field for $H/W \neq 1$

Several tests have been conducted for a water depth of 0.1 m, i.e. $H/W = 0.56$. The velocity field has been investigated according to a vertical plane and to a horizontal centre plane. Obviously the circulation loop is not so well developed (Figure 4). An downward flow is visible in the 2/3 of the reactor opposite to the air injection. The upward flow is located near the injectors and much faster than the liquid downward flow. The value of the upward velocity (0.2 m/s) is lower than what was obtained with $H = 0.2$ m which is due to the turbulence induced by the bubble disintegration at the liquid surface and to the very low height of the channel. The liquid surface is completely perturbed.

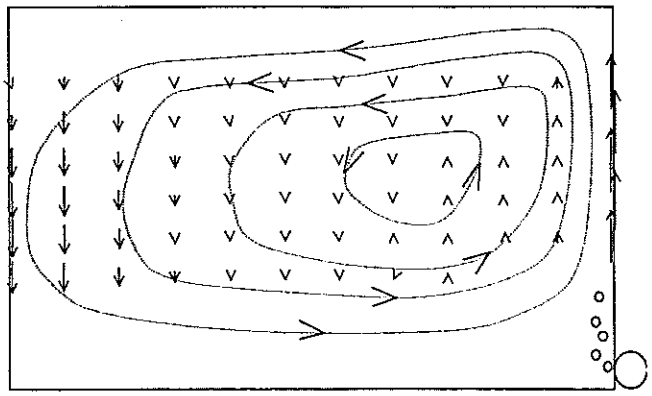

Figure 4 : Velocity field and recirculation loop in plane y-z for $H/W \neq 1$

For a better visualisation of the water displacement the velocity vectors have been plotted in Figure 4. The dotted line represents the water motion, as assumed from the measurements. The circulation loop is asymmetrical.

3. Correlations with the axial dispersion coefficient

When the circulation loop is circular (for $H/W \approx 1$) the velocity along the walls at mid-depth is vertical and the z-component, which cannot be measured here, is zero. The measured component is then equal to the maximal total circulation velocity. When the loop is not exactly circular, the maximal value of the vertical component should be found where the velocity is maximal and vertical.

3.1 Case $H/W \approx 1$

Three space times and five gas flow rates have been tested. The velocities at mid-depth and the maximal velocities are very similar. When the gas flow rate is high enough, D is almost independent of the liquid flow rate, as shown by Figure 5. The two points a little bit off the correlation on each graph correspond to the lowest gas velocity.

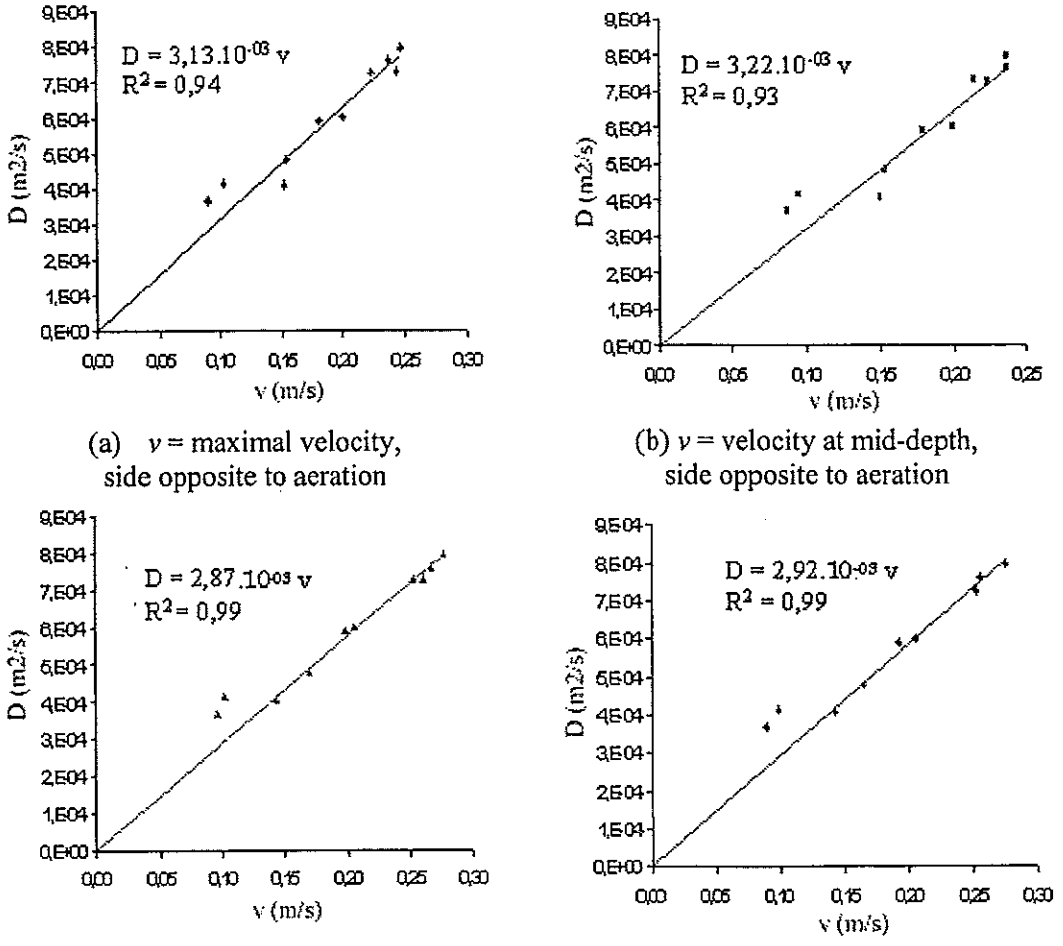

(a) v = maximal velocity, side opposite to aeration

(b) v = velocity at mid-depth, side opposite to aeration

(c) v = maximal velocity, on aeration side

(d) v = velocity at mid-depth, on aeration side

Figure 5: Correlation between the axial diffusion coefficient D measured by RTDs and the velocities extracted from the LDA data for H/W = 1.1

3.2. Case $H/W \neq 1$

Similar experiments have been performed for $H/W = 0.56$. No satisfactory correlation was obtained between D and the velocities on the side opposite to aeration (Table 1). On the aeration side, the data points are in agreement with the correlation obtained with $H/W \approx 1$. The discrepancies can be explained by the asymmetrical shape of the circulation loop: the offset of the loop centre on the aeration side means that the velocities measured on the opposite side are no more representative of the circulation. The very good correlation observed on the aeration side and the disagreement obtained in the opposite side is due to the importance of energy dissipation at the liquid surface where bubbles disintegrate.

Table 1: Correlations the case H/W = 0.56 between D and velocities

Velocity v	Correlations D (m^2/s) versus v (m/s)	Correlation coefficient
v = maximal velocity, on aeration side	$D = 2.878 \cdot 10^{-3} \cdot v$	0.99
v = maximal velocity, side opposite to aeration	$D = 3.244 \cdot 10^{-3} \cdot v$	0.45
v = velocity at mid-depth, on aeration side	$D = 2.964 \cdot 10^{-3} \cdot v$	0.95
v = velocity at mid-depth, side opposite to aeration	$D = 3.340 \cdot 10^{-3} \cdot v$	0.42

CONCLUSION

The liquid vertical velocity fields experimentally measured by LDA indicate that the circulation loops described by Roustan [7] exist in a channel aerator of shape factor $H/W \approx 1$. When this factor is smaller than 1, the circulation loop still exist but is asymmetrical.

A correlation has been obtained between the axial diffusion coefficient D and the maximal velocity observed on the aeration side (u_{max}) for two values of the shape factor:

$$D\left(m^2/s\right) = 0.0029 \cdot u_{\max}\left(m/s\right)$$

This correlation is not valid when the air flow rate is too small but this is not the case in general in aerated channels and carrousels in wastewater treatment plants. Further experiments are under way to examine the case of nozzle-floor injection systems and other H/W values..

REFERENCES

[1] Villermaux, J., *Génie de la réaction chimique conception et fonctionnement des réacteurs*, Tec&Doc. Lavoisier (1992).

[2] Potier O., *Etude des stations d'épuration des eaux usées urbaines par boues activées: modélisation de l'aérateur canal*, PhD, INPL, Nancy, (1993).

[3] Potier O., Pons M-N., Roche N., Leclerc J-P., Galdemas L., *Etude de l'hydrodynamique d'un aérateur canal à boues activées en régime variable, Récents Progrès en Génie des Procédés*, **12** (61) 367-372, (1998)

[4] Potier O., Pons M-N., Roche N., Leclerc J-P., Prost C., Hydrodynamics of activated sludge channel reactor, *Hungarian Journal of Industrial Chemistry*, 49-51 (1999).

[5] Loiseau V., *Etude de l'hydrodynamique d'un réacteur canal en fonction de ses caractéristiques géométriques et des paramètres de fonctionnement*, Diplôme d'Etude Approfondies, Institut National Polytechnique de Lorraine (1998).

[6] Murphy K., Boyko B., Longitudinal mixing in spiral flow aeration tanks, *Journal Sanit. Eng. Div. A.S.C.E.*, **96**, (SA2) 211-221 (1970).

[7] Roustan M., Line A., Rôle du brassage dans les procédés biologiques d'épuration, *Tribune de l'Eau*, N°5-6/96, 109-115 (1996).

[8] Baird M. H. I., Rice R. G., Axial dispersion in large unbaffled columns, *Chem. Eng. Journal*, **9**, 171-174 (1975).

[9] Deckwer W. D., *Bubble column reactors*, John Wiley and Sons, New-York (1992).

[10] Badura, R., Deckwer, W. D., Warnecke H. J., Langemann, H. Durchmischung in Blasensäulen. *Chem. Ing. Techn.* **46**, 399(1974).

[11] Joshi J. B., Sharma M. M., Liquid phase backmixing in sparged contactors, *Canadian Journal Chem. Eng.*, **56**, 116-119 (1978).

[12] Zehner, P., Impuls-, Stoff- und Wärmetransport in Blasensäulen Teil 1: Strömungsmodell der Blasensäule und Flüssigkeitsgeschwindigkeiten. *Verfahrenstechnik* **16**, 347-351 (1982).

[113] Krishna R., Urseanu M. I., Van Baten J. M., Ellenberger J., Influence of scale on the hydrodynamics of bubble columns operating in the churn-turbulent regime: experiments vs. Eulerian simulations, *Chem.. Eng. Sci.*, **54**, 4903-4911 (1999).

USE OF THE INDIUM 113 IN THE LABORATORY TO IMPROVE OUR KNOWLEDGE ON THE BEHAVIOR OF THE DISCHARGES OF MUDDY DREDGED MATERIAL

R. Boutin[1], P. Brisset[2]

[1]Service technique des travaux immobiliers et maritimes,15 rue de Laborde, 00309 Armées, FRANCE
[2]Commissariat à l'énergie atomique, Département des applications et de la métrologie, service des applications des radioéléments, BP52, 91193 Gif-sur Yvette Cedex, FRANCE

Abstract. Dredged materials in harbour waters, in order to maintain accessibility, are mainly composed of cohesive mud. Usually, they have to be rejected into the sea. On a theoritical point of view, the behavior of this kind of rejects still remains unclear, and subjected to many questions. Experiments are carried out in physical modelling flumes to study their behavior on a short time scale. Different types of wastes were studied. The sediment which is used is a natural mud from Le Havre sifted at 125 µm. The presence of cohesive fraction makes difficult the spatial follow-up of these materials Thanks to its labeling with indium 113m, the concentration of the turbid cloud in various places of the surface as well of the bottom can be seen with scintillation probes. 42 experiments were realized and 31 probes were mobilized

After a presentation of the experimental procedure, the methodology of treatment and analyses of the experimental data is described. Different results are also presented here.

We shall show that for the studied phenomena, the radioactive tracers are for our opinion one of best means of study.

INTRODUCTION

Approximately 400 millions tons of materials are dredged every year in the world for maintenance dredging. Environmental impact is on the base of the critics formulated against dredging or more precisely the harm it does. Impact analysis of the human activity on the environment is often hard due to the lack of knowledge. Several authors have described the behavior of the disposed material in free water (sea, lake, estuaries) by dumping or continue discharge [1-7]. They founded their analysis on different field observations. Their observations and interpretations show that if there is a consensus on the analysis which is made on general phenomena the divergence appear when we narrow down the observation. It is particularly true with fine sediment like mud and there is a need in knowledge.

Because of that, experiments are carried out in physical modelling flumes laboratory to improve our knowledge on the behavior of the discharges of muddy dredged material. Different types of wastes were studied. To follow these muddy sediments radioactive tracer techniques have been used.

RADIOACTIVE TRACER TECHNIQUE

1. A useful technique

Different tests showed that the classical measuring apparatus would not allow to obtain enough information on the development of phenomena because of the

presence of fine sediments. Probes with optical measure saturate quickly in the presence of mud and the technique of samplings is little precise and badly adapted. We turned then to the radioactive tracers, that as we are going to see, is perfectly adapted to our problem. Since the fifties, this one was widely developed by the French Atomic Energy Commission (Commissariat à l'Energie Atomique - CEA) to study sedimentary movements in the laboratory and in natural environment [8-14], notably for dredging problems [15-17].

2. Principle of radioactive technique

The tracer is used to label a population and to deduce properties of the population from the distribution of tracer data. Radioactivity is used to provide an immediate measurement of the tracer concentration at the point of mesurement. These time and space distributions of radioactivity measurements (counting rates) can be transformed in time and space distributions of tracer concentration from which tracer data treatment and modeling techniques provide the sediment behaviour.
Mixing the tracer within the mud provides after dumping informations concerning the transport in suspension and in the bottom.
In our case, a small quantity of particles of mud was labeled by a radioactive element, γ emitter. Labeling is directly realized by chemical adsorption. Radioactive element is distributed in an homogeneous way in the discharge.
The tracer used for experiments is the indium 113 m. It is produced by a Tin/ Indium generator constituted by a column to which Sn113 is fixed. This one is transformed in indium metastable (In113m) further to the reaction described by the equation 1. This radionuclide becomes stable by emitting a photon (391.70 keV-64.9%).

$$ {}^{113}_{50}Sn \xrightarrow{\beta^+} {}^{113m}_{49}In \xrightarrow{\gamma} {}^{113}_{49}In \qquad (1) $$

The tracer eluted from the generator is diluted and then injected gradually within the mixture to throw back, during the filling of the hopper (c.f. figure 1).

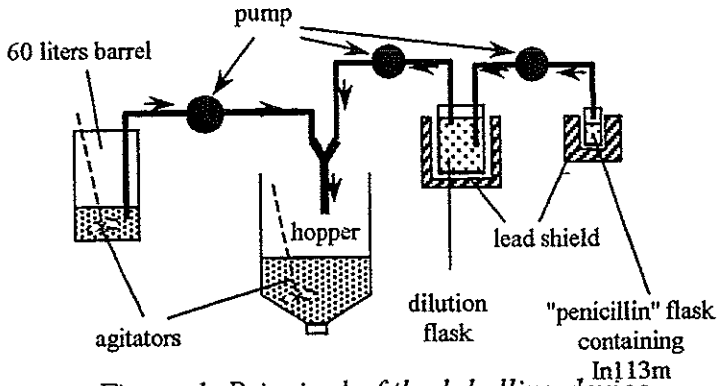

Figure 1. Principal of the labelling device

The operation of labeling must not modify either behavior hydrodynamics or the physico - chemical properties of the particles of mud. Labelling also must be stable in the time. This question was particularly studied by the CEA [18-23]. Different tests realized by the CEA / DAMRI in Saclay allowed to confirm the behavior of the labeled sediment.
The emission of photons allows to follow the particles during the discharge by scintillation probes.

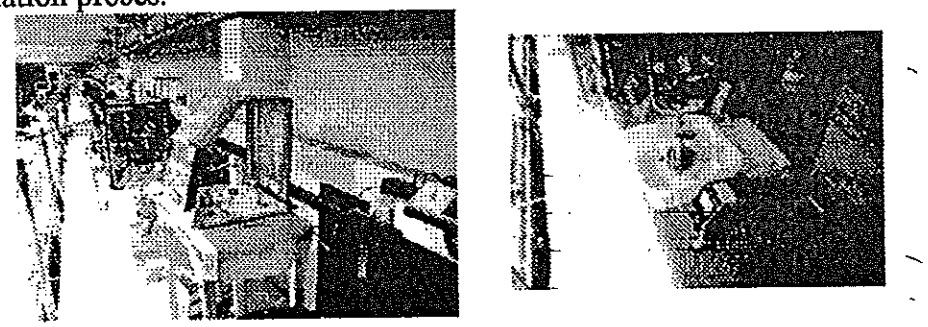

Figure 2. Apparatus for tracer preparation

EXERIMENTAL APPARATUS

1. Purpose and limitation

The studied domain brings in many factors (materials, physical, chemical, dynamic ...). The laboratory canal allows us to control the conditions of tests. The influence of initial concentration value of the rejection and the influence of speed of water flowing in the canal both have been studied. A simplified model at $1/25^{th}$ scale was used. We have showed [24] that the phenomena can be approximately scaled to the prototype (nature) as long as the flows conditions generated by the disposal are in the turbulent range and as long as the rejection can be considerate like a suspension.

2. Description of facility

The experiences were realized in the canal 5 at the research center of « Electricité de France » (EDF) at Chatou. The flume was 70 m long, 1,5 m wide and 1,5 m high. The tests were conducted with 1 m or 0,8 m depth (25 m or 20 m in nature) and the current had varied following the experiences from 0 to 20 $cm.s^{-1}$ (0 to 1 $m.s^{-1}$ in nature). Test with instantaneous or continuous discharge have been made. Figures 3 shows the disposal equipment for instantaneous discharge (dumping).
The disposal material used for experiments was natural mud taken from the port of Le Havre and sifted at 125µm. The dry matter initial concentration of the mud varied from $180g.l^{-1}$ to $420g.l^{-1}$. The volume of materials introduced in the flume was of approximately 44 liters. Different sections of the flume were equipped with measuring instruments in order to report the evolution of the discharge in space and time. Thanks to its marking with indium 113m, the concentration of the turbid cloud in various places of the surface as well as of the bottom could be seen with scintillation probes (30 were used). 42 experiments were realized.

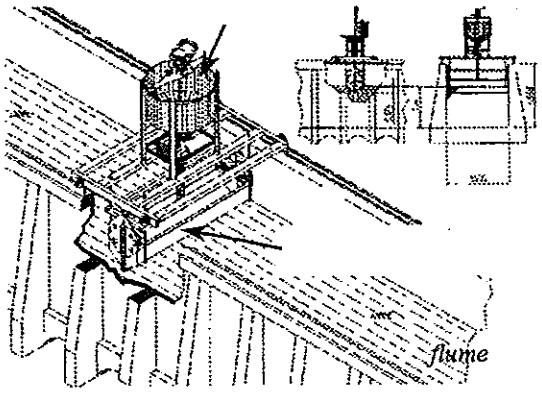

Figure 3. Disposal equipment

DATA PROCESSING

The developed computer tools allow the calculation of the concentration for every probe with information of time and place. After shaping of results, the flux going out of the domain of study is calculated in the entry and exit plans of the experimental zone. By difference with the quantity of rejected mud, the settling rate of materials is calculated.
After every test, the mass deposited at the bottom was measured in various points. By integration of these informations, the calculation of the quantity of mud deposited on the bottom is made. This result was compared to the settling rate calculus explained above.
Details of data processing are given in the reference [24]. Error calculus have been made for each estimated parameter.

RESULTS EXAMPLES

Tracer techniques, completed by data processing allow to obtain very good information.
Figure 4 shows an example of data supplied by probes placed in the canal near the bottom. In this test with current in the flume, there is erosion of the materials which has just settled. Concentration near the bottom is maintained by this erosion as shown on figure 4.
Figure 5 shows settling rate results obtain for instantaneous discharge tests (dumping). We have the same quality of data for tests with continuous discharge. With low initial concentration, the settling rate is very sensitive to the initial concentration and to the strength of current in the flume. When initial concentration is more than 300 $g.l^{-1}$ more than 80 % of materials stay in the close field whatever the speed in the flume.

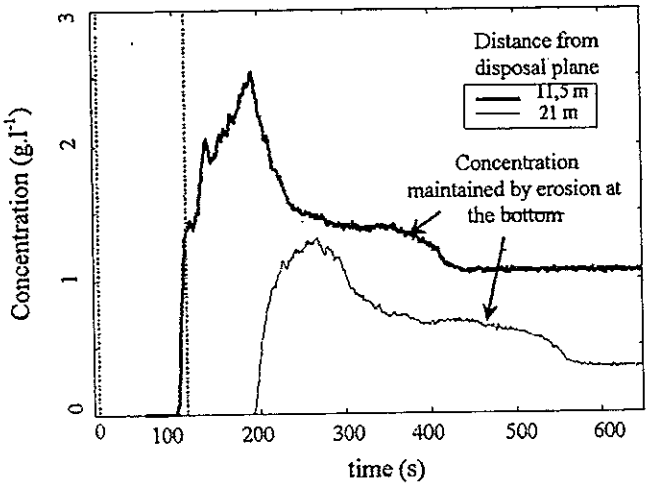

Figure 4. Concentration function of time, 5 cm near the bottom, test ssub9 at 274 g.l^{-1} , speed in the flume : 11,5 cm.s^{-1}

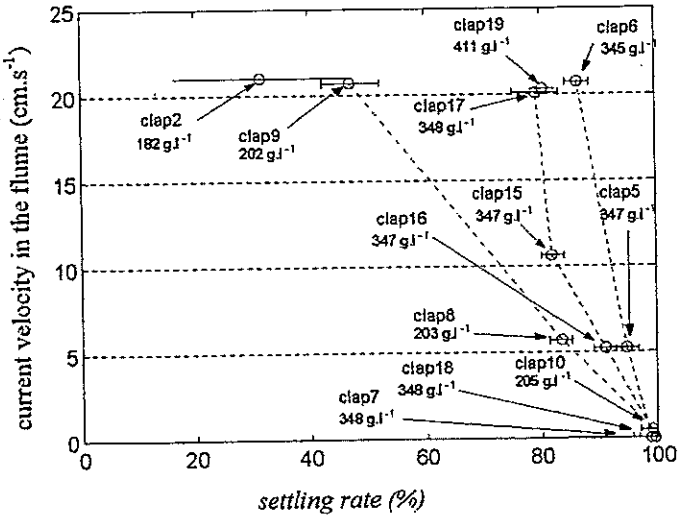

Figure 5. *Settling rate in function of the current velocity in the flume for dumping tests*

Figures 6 and 7 show examples of mapping of bottom deposition obtained after data processing. These figures allow us to understand how materials settle on the bottom. The figure 7, shows particularly the influence of the current in the canal on the deposition shape of the spot of deposit. There is movement of the center of gravity on the downstream side with the increase of the current in the flume. There is also modification of the shape of the spot. This last result is quite important because it is rarely taken into account.

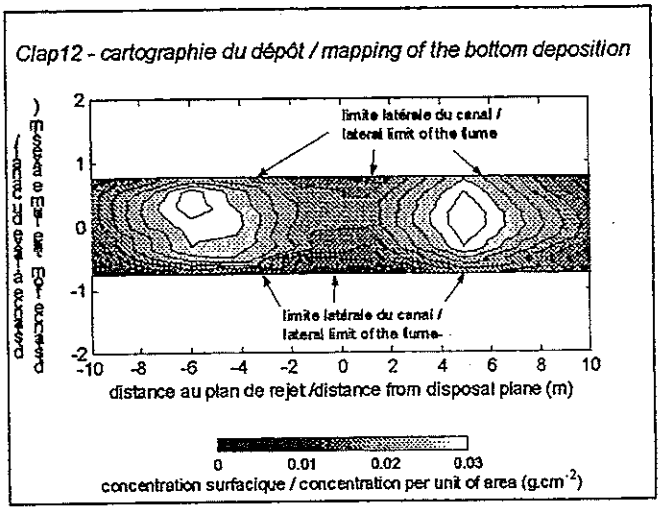

Figure 6. Mapping of bottom deposition for test clap12 at 204 g.l^{-1} , speed in the flume : 0 cm.s^{-1}

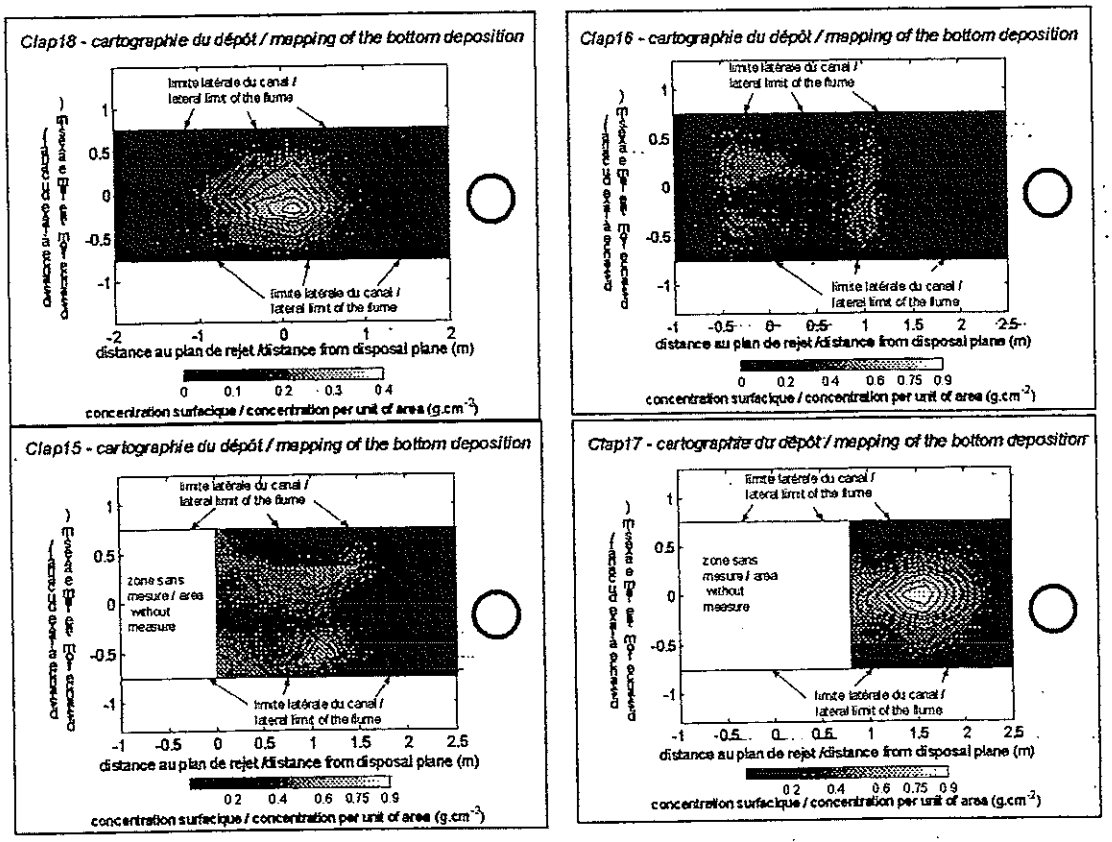

Figure 7. Mapping of bottom deposition for tests at 348 g.l^{-1} and for different speed in the flume
(Speed in the flume : a : 0 cm.s^{-1}, b : 5,2 cm.s^{-1}, c: 10,6 cm.s^{-1}, d : 20,1 cm.s^{-1})

CONCLUSION

The experimental device which was presented allows to reproduce in laboratory flume instantaneous or continuous discharges of dredged soil. Study concerned only muddy sediments. Because of these material, classical measuring apparatus of concentration is not adapted. Because of that, we decided to implement tracer techniques.
As we showed, this technics associated with data processing gives very good results. It allows to follow the spatial evolution of material in continue and so we can improve our understanding of phenomena.
These technics which can also be implemented in field condition is certainly one of the most adapted to follow muddy sediments.

THANKS

The experiments program were principally financed by the "mission pour le developpement de l'innovation participative" and the "Fond d'Intervention pour l'Environement" (FIE) of the French Ministry of Defense, by "le Groupe d'Etudes et d'Observations sur le Dragage et l'Environement" (GEODE) and by "le Centre d'Etudes Techniques Maritimes et Fluviales" (CETMEF). The "Service des Travaux Maritimes" and particularly "le Service Technique des Travaux Immobiliers et Maritimes" (STTIM) have also brought a very large contribution to the different phases of the study.

REFERENCES

[1] Bokuniewicz H.J., Gebert J., Gordon R.B., Higgins J.L., Kaminsky P., Pilbeam C.C., Reed M, Tuttle C., "*Field study of the mechanics of the placement of dredged material at open-water disposal sites*", New Haven, Connecticut (USA), Yale University for l'USAEWES. 318 p. TR D-78-7, 1978.
[2] Brandsma M.G., Divoky D.J., "*Development of models for prediction of short-term fate of dredged material discharged in the estuarine environment*", Pasadena, California, Tetra Tech Inc. for USAEWES. 133 p., Contract report D-76-5, 1976.
[3] Gordon R.B., "Dispersion of dredged spoil dumped in near-shore waters", Estuarine and coastal marine science, 1974, 2, pp 349-358, 1974.
[4] Koh R.C.Y., Chang Y.C., "*Mathematical model for dredged ocean disposal wastes*", Washington : National environmental research center, Corvalis for USEPA. 178 p. Report EPA-660/2-73-029, 1973.
[5] Krishnappan B.G., "*Dispersion of granular material dumped in deep water*", Burlington, Ontario : Environment Canada. 113 p. Scientific series n°55, 1975.
[6] Tola F., Caillot A., Courtois G., Gourlez P., Hoslin R., Massias J., Quesney M., Sauzay G., "Study of the evolution of dredged material discharges by means of radioactive tracers", International symposium of the use of isotope techniques in water resources development, Vienna, 30 march – 3 april 1987, pp 663 – 682. IAEA-SM-299/71, 1987.
[7] Truitt C.L., "*Environmental effect of dredging. Fate of dredged material during open-water disposal*", Vicksburg : USAWES. 12 p. EEDP-01-2, 1986.
[8] CAILLOT, A. Les techniques nucléaires utilisées en sédimentologie dynamique. Exemples d'applications aux estuaires. Saclay : CEA, 1986. 18 p. Rapport ORIS/SAR/S/86-132/C283.
[9] CAILLOT, A. Marquage radioactif des sédiments ou de leurs simulateurs. Panel hydrologie AIEA, Grenoble octobre 1965. Saclay : CEA, 1965. 7 p. Rapport DR/AR/65-23/AC/JJ.
[10] CAILLOT, A. Mesure en mer du déplacement des sédiments au moyen de traceurs radioactifs. Saclay : ORIS-SAR, 1981. 9 p + annexe. ORIS-SAR-S-81-7/C 160/AC.

[11] CAILLOT, A. Quelques emplois de traceurs radioactifs en milieu estuarien. Symposium eaux douces –eaux salées, association des sédimentologistes français, 20-21 janvier 1981. Saclay : CEA, 1981 15 p. Rapport ORIS/SAR/S/81-9/C 262/AC/MCM.
[12] CASTAIN, P, JOUANNEAU, J.M, KLINGUEBIEL, A. Mise au point d'une technique d'étude des transferts de vase en estuaire. Synthèse des mesures d'hydrologie. Bordeaux : CNEXO – Université Bordeaux I, IGBA, 1975. 70 p + annexes.
[13] COURTOIS, G. Les applications françaises des traceurs radioactifs en sédimentologie dynamique. Annales des mines, octobre 1969, p 39 – 56.
[14] HOURS, R, JAFFRY, P. Application des isotopes radioactifs à l'étude des mouvements des sédiments et des galets dans les cours d'eau et en mer. La Houille blanche, 1959, n°3, 30 p.
[15] BROSSARD, C, HELARD, J.P, MALHERBE, B, MONADIER, P, BRISSET, P, HOSLIN, R, MEYER, G, CAILLOT, A. Etudes et optimisation des travaux de dragage au moyen de la radioactivité. La houille blanche, 1992, n°4, p 309 – 314.
[16] TOLA, F, CAILLOT, A, COURTOIS, G, GOURLEZ, P, HOSLIN, R, MASSIAS, J, QUESNEY, M, SAUZAY, G. Study of the evolution of dredged material discharges by means of radioactive tracers. International symposium of the use of isotope techniques in water resources development, Vienna, 30 march – 3 april 1987, p 663 – 682. IAEA-SM-299/71.
[17] TOLA, F. Etude du rejet de produits de dragage à l'aide de traceurs radioactifs. Transfert et dispersion des fines particules en suspension et évolution dans le temps des sédiments déposés sur le fond. Société hydrotechnique de France, XVIII^{e} journée de l'hydraulique, Marseille, 11,12 et 13 sept 1984. 8 p. Q1 rapport n°15.
[18] BOUGAULT, H, CAILLOT, A, COURTOIS, G, JEANNEAU, B. Dépôts superficiels de radioéléments sur les sables et les vases. Isotopes in hydrology. Vienne : AIEA. 1967. p 233 – 262.
[19] BOUGAULT, H. *Etude de la sorption de quelques radioéléments artificiels par les sédiments pélitiques en vue de son application au marquage radioactif de ces matériaux.* Thèse Doct. Ing : Faculté des sciences de Paris, 1970. 90 p + figures.
[20] BRUN-COTTAN, J.C. *Influence du marquage radioactif sur les paramètres dynamiques des sédiments pélitiques.* Thèse géodynamique interne : Faculté des sciences de Paris, 1967, 111 p + figures
[21] COURTOIS, G. *Emploi des radioéléments en sédimentologie.* Saclay : CEA, 1967, 68 p, n°84, Série "Bibliographie".
[22] HOSLIN, R. *Le double marquage de la vase par le zinc et l'hafnium. Application : Etude du comportement du zinc et des mouvements sédimentaires dans le système Garonne-Gironde.* Thèse sédimentologie : Université de Paris-Sud, Centre d'Orsay, 1980, 157 p.
[23] MAGLOIRE, M. *Mesure de turbidité par des méthodes radioactives.* Thèse Doct. Ing : Université Paris VI, 1972, 83 p + figures.
[24] Boutin, R., 1999 : "Amélioration des connaissances sur le comportement des rejets en mer de produits de dragage de type vase." Thèse de doctorat en génie civil : INSA de Lyon, 527 p. (disponible sous la référence "Dragage et rejet en mer" aux presses de l'école nationale des ponts et chaussées, France- 2001).

SEDIMENTATION BASIN INVESTIGATION USING RADIOTRACERS

A.G. Chmielewski, A. Dobrowolski, A. Owczarczyk, J. Palige

Institute of Nuclear Chemistry and Technology, Dorodna 16, 03 – 195 Warsaw, POLAND

Abstract. Removal of suspended matter from sewage is one of the stages of sewage purification especially in biological treatment. The process is usually realized in two steps, preliminary sedimentation with biological sludge recirculation and secondary step where the sewage is finally clarified in a big settling basin. For prolongation of it exploitation time the sludge transport and sedimentation mechanism have to be known in detail. Using the tracer method the principal characteristics of a big sedimentation basin, 36000 m^3 capacity, were determined. As a tracer for sediment, the La – 140 radioisotope firmly absorbed on the sludge grains, was used. The labeled sediment spatial distribution as well as bathymetry were measured by mean of specially equipped boat. The residence time distribution of the sewage was also measured using fluoresceince as a tracer. The cross section of tank most convenient for location of any sludge removing system was determined.

INTRODUCTION

Removal of suspended matter from sewage is one of the stages of sewage purification, especially in biological treatment where the activated sludge is added to the system and should be removed from sewage before its discharge into the natural receiver.

The process is usually realized in two steps. Preliminary sedimentation with recirculation of biological sludge and secondary step where sewage are finally clarified in big settling basin. The accumulated sediment has been removed from the basin periodically after its filling during exploitation period. At that moment the parallel technological line should be ready to work.

It is technologically resonable to prolongate the sedimentation campaign time as much as possible. For this reason the sludge transport and sedimentation mechanism should be known in detail. Before design of any technical solution for partially removal of the accumulated sludge during the compain run, its best localization in the sediment basin plane should be find out. Therefore, the dynamic characteristics as well as distribution of sediment on bottom as effect of sedimentation process should be monitored during technological campaign. The best way for obtaining such data are tracer experiments.

TRACER SELECTION AND MEASUREMENT METHODOLOGY

As a tracer for sediment (biological activated sludge) the gamma – radioactive La – 140 has been selected. The $t_{1/2}$ = 40.2 h is sufficient for predicted time of experiment. The well known good sorption characteristics of La^{3+} ions on the sludge particle surface decided on applicability of sorption technique for tracing the sludge.

The portion of about 30 l of dense suspension of activated sludge suspended in sewage have been traced by the approximately 100 mCi La – 140 prepared as $La(NO_3)_3$ in acid aqueous solution. The tracer has been instantaneously injected to the sewage stream at the inlet of the sedimentation basin. The monitoring of labelled sediment bottom distribution started one day after injection (the time necessary for completion of sedimentation) and has been repeated at the next day (two days after injection). The same measurement schedule has been applied for all measurement sessions carried out in the course of technological campaign.

The two series of investigations have been carried out in the big settling basin (340x60x3 m) of the biological sewage treatment plant in petrochemical factory. The region of favourable sedimentation has been determined in two states of basin filling: first just after beginning of the campaign (filling with sediment about 15 %), second in the middle of campain (filling about 45 %). The detection of active sludge bottom distribution has been measured one day after injection by means of specially equipped boat (Figure 1).

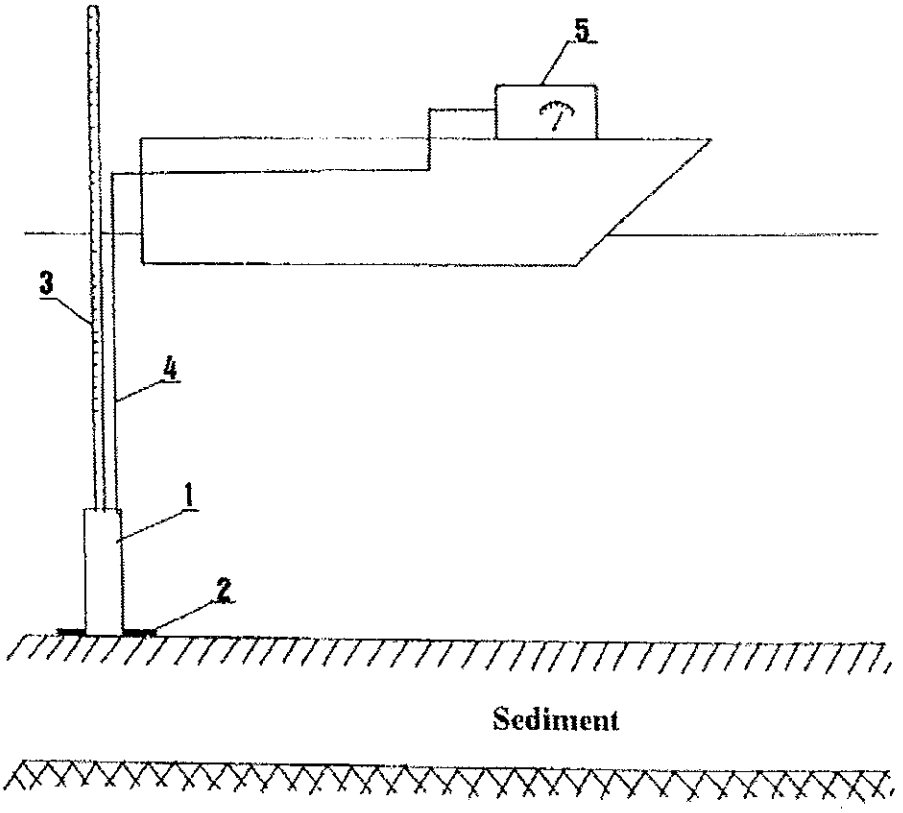

1. **Radiometric probe**
2. **Perfored plate**
3. **Calibrated rod of bathymeter**
4. **Cable**
5. **Radiometer**

Figure 1. Measuring boat equipment.

The waterproof radiometric probe with bathymetry unit have been used. The boat has been moved along the cross – sections localized in every 10 m along longitudinal axis of the basin (Figure 2).

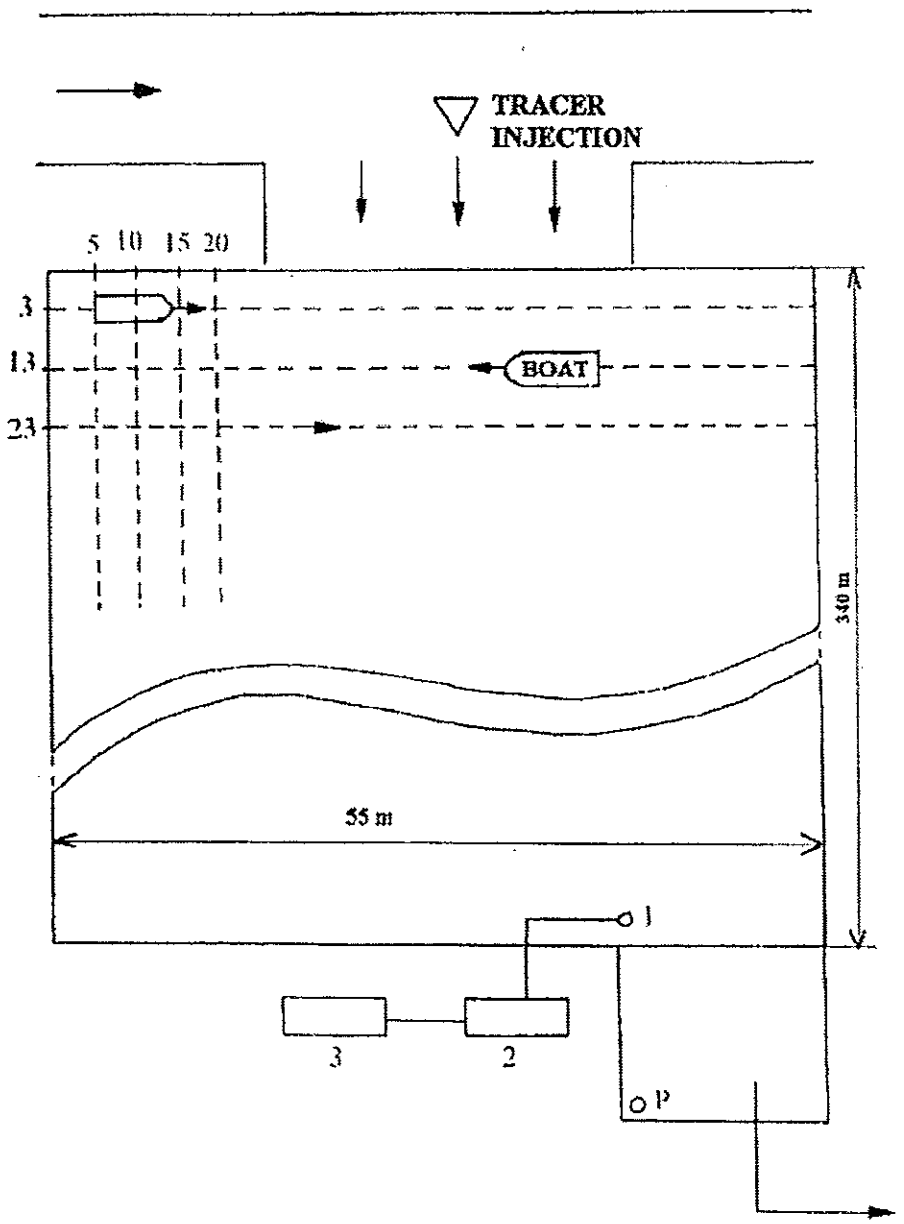

1. **Radiometric probe**
2. **Radiometer**
3. **Recorder**

P. Point of sampling

Figure 2. Measurements scheme.

The dynamics of sewage transport through sedimentation basin have been realized by uptake the sewage samples from the basin outlet and fluorometric measurement of RTD curve (residence time distribution) c = f(t) where c is the fluoresceine concentration in the sample.

MEAN SEDIMENTATION DISTANCE

The mean sedimentation distance is defined as the way along the basin axis, from inlet to the point in cross – section when the sludge particle with representative diameter (d_{50}) attain the bottom and leave the flow zone. The mean sedimentation distance of active sludge particles is independent on sediment accumulation in the basin during technological campaign.

If $t=H/u_c$ (1)

and $u_c=Q/F$ (2)

then $u_c.H=const$ (3)

If $L=u_c.t$ (4)

and $H=u_s.t$ (5)

then $L/H=u_c/u_s$ (6)

and $L=u_c.H/u_s$ (7)

where:
t– mean sedimentation time (hour),
H- -depth of the basin (m),
u_s – sedimentation velocity of representative particle (m/hour),
Q – sewage flow rate (m^3/hour),
F – cross section of basin (m^2),
u_c – sewage longitudinal velocity (m/hour),
L – mean sedimentation distance (m).

This cross – section is the best for localization of any technical solution for partially removal of the accumulated sediment. The example of bed bathymetry and tracer bed distribution (filling of 45 %) have been shown in Figures 3 and 4 respectively. The tracer distribution diagrams (cross – section summary of tracer activity vs. transport distance) obtained for 15 % of filling (Figure 5) and for 45 % of filling (Figure 6) shows that mean sedimentation distance was practicaly the same in the range 85 – 90 m from sewage inlet.

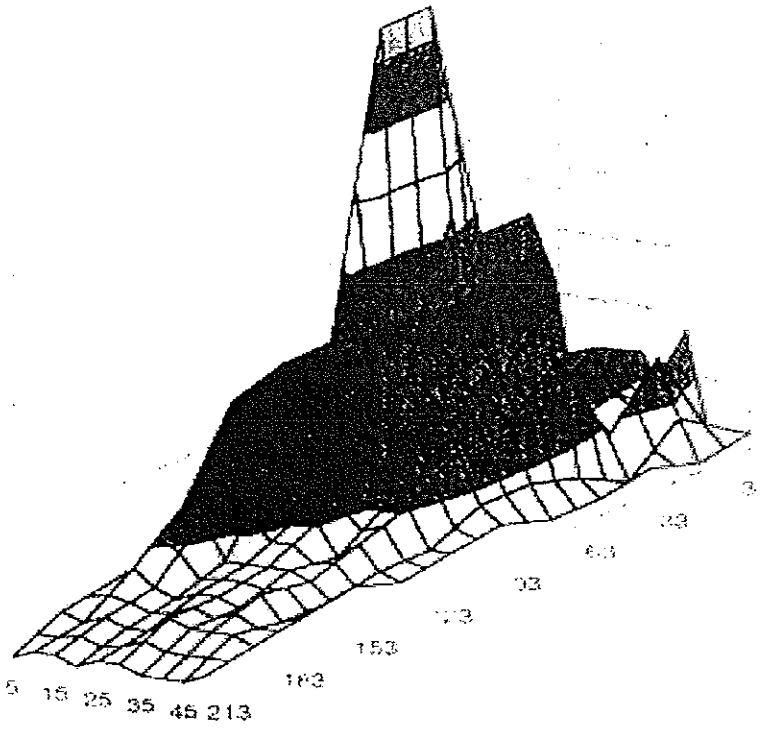

Figure 3. Sediment activity distribution .

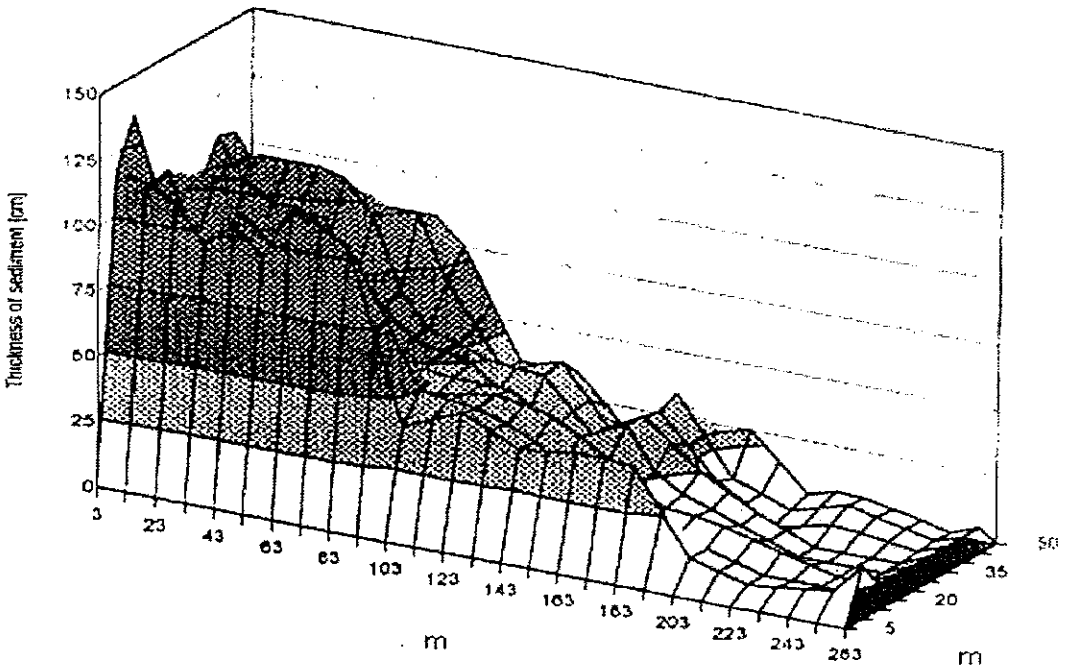

Figure 4. Bathymetry of sediment (measurement 1).

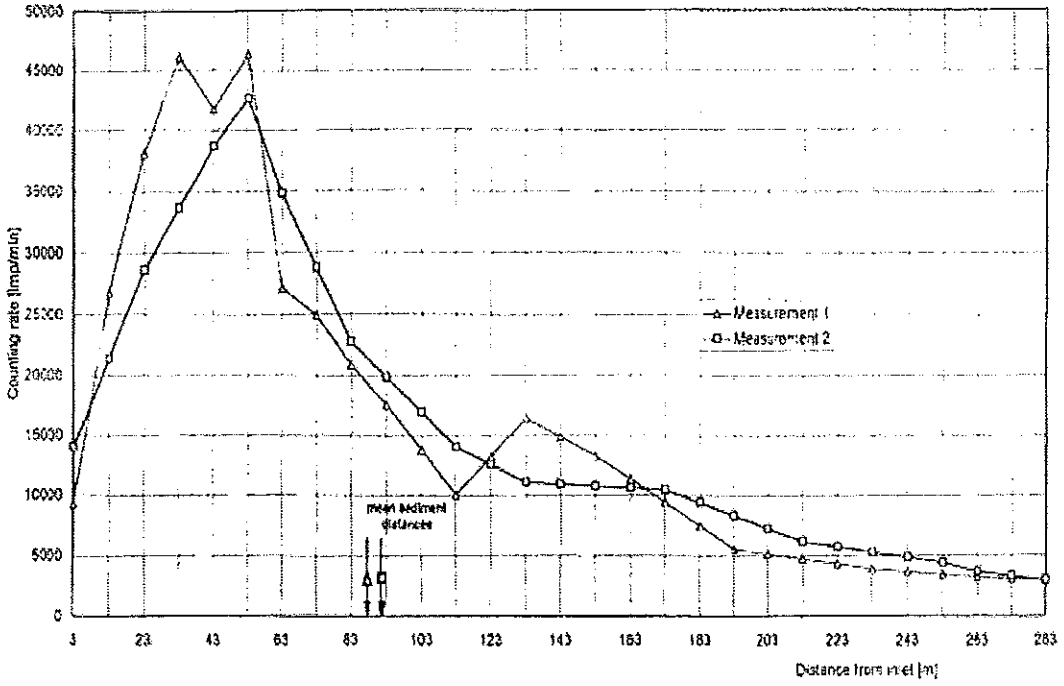

Figure 5. Sediment transport diagram – session 2.

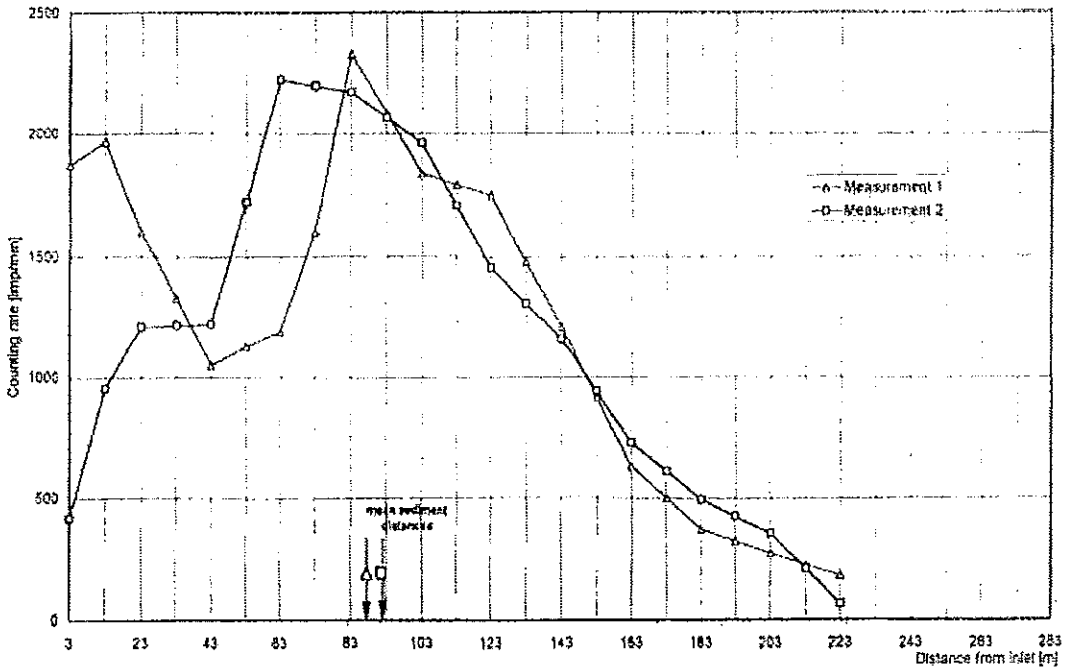

Figure 6. Sediment transport diagram – session 1.

CONCLUSIONS

It has been proved that most favourable sedimentation region localization is independent on sediment accumalation in basin. The cross – section mostly convenient for deposition of any sludge removing system without interruption of campaign have been determined.

ASSESSMENT OF SULPHUR EMISSION AT NORCEM'S CEMENT KILN BY USE OF ^{35}S-TRACER

D. Ø. Eriksen[1], L.-A. Tokheim[2], T. A. Eriksen[2], V. Martini[1] and C. Qvenild[1]

[1]Institute for Energy Technology, P.O. Box 40, N-2027 Kjeller, Norway
[2]Norcem AS, P.O. Box 38, N-3991 Brevik, Norway

Abstract. Although sulphur is not a major reacting species in making cement clinker, it is introduced as a pollutant in both the energy carrier (oil, coke, coal, household waste) and in the reactants (chalk, silica). Due to the huge amounts processed the total theoretical emission of sulphur, as SO_2 can be high. However, because of the kiln design and the presence of calcium and alkalis, sulphur is largely converted to sulphates and captured in the clinker product. In kiln no. 6 at Norcem's Brevik plant there are two sites, named primary and secondary, for injection of coal and coke, one in each end of the rotary kiln.

The objective of the study was to measure which portion of the sulphur introduced in the process from the coal and coke that escapes as SO_2, and how much sulphur will follow the clinker (solid phase)? Moreover, to see whether there is a difference in SO_2-emissions when the coal or coke is introduced in the primary and in the secondary injection site.

^{35}S-tracer in the form of yellow sulphur, α-S_8, absorbed in coke, was prepared by irradiating α-S_8 in a cold position with thermal neutrons in Institute for Energy Technology's (IFE) JEEP II nuclear reactor. The irradiated sulphur was dissolved in CS_2 and the solution was subsequently absorbed in finely grained coke.

Two injections were performed, one in the primary (3,8GBq) and one in the secondary site (3GBq).

The results showed clear differences depending on the injection site in the amount of sulphur emitted as SO_2 and also on how fast the sulphur would exit the kiln as part of the produced clinker. ^{35}S was detected in the exhaust gas only after the injection at the secondary site, but in minute amounts. Thus, the project was able to recommend that in order to avoid emission of SO_2 there is an advantage of injecting coal or coke at the primary site. Mass balance calculations gave more than 80% recovery of injected sulphur as ^{35}S.

INTRODUCTION

Although sulphur is not a major reacting species in making cement clinker it is introduced as a pollutant in both the energy carrier (oil, coke, coal, house-hold waste) and in the reactants (chalk, silica). Due to the huge amounts processed the total theoretical emission of sulphur, as SO_2 can be high. However, because of the special design of the kiln system (counter-current flow of gas and solids) and the presence of calcium and alkalis, most of the gaseous sulphur in the kiln or in the precalciner is converted to sulphates, which are eventually captured in the clinker product [1]. The chemical form of the sulphur in the fuels is not known, but is assumed to consist of a variety of compounds. Due to the high temperature in the kiln the chemical form of sulphur was considered of minor importance as all will be oxidised.

In rotary kiln no. 6 at Norcem's Brevik plant there are two sites, named primary and secondary, for injection of coal and coke, one in each end. There are two chimneys connected to this kiln, one on string 1 (Chimney 3) and one on string 2 (Aerofall chimney, downstream of the raw meal mill). Figure 1 illustrates the kiln system[1].

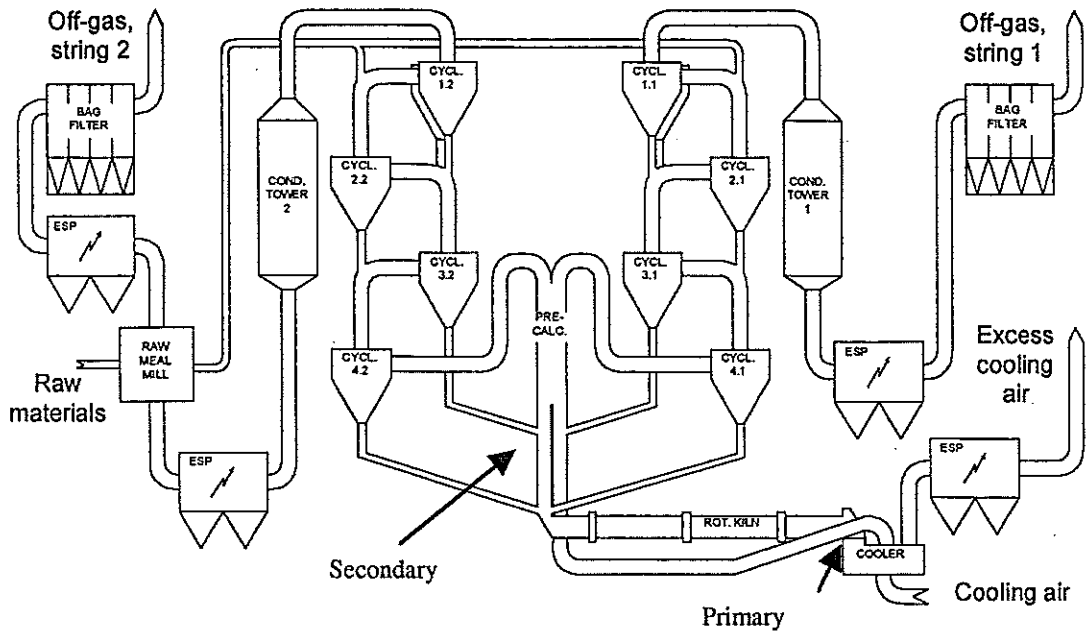

Figure 1. Kiln system at Norcem, Brevik. The figure shows the main units rotary kiln, precalciner, cyclone preheater and cooler, as well as gas conditioning towers and dust cleaning system. The injections sites are also indicated[1].

The objective of the study was twofold: To measure how much of the sulphur introduced in the process from the coal and coke that escapes as SO_2, and how much which follows the clinker (solid phase). Secondly, to see whether there is a difference in emission when introducing the coal or coke at the primary or at the secondary injection site.

To commit such a study, it was decided to absorb ^{35}S-labelled sulphur in coke, inject it into the kiln at the proper positions, to sample the exhaust gases in the two connected chimneys and in the produced clinker powder to measure the residence time, solid-gas distribution and the mass-balance.

It was expected from the standard production analyses that the concentration of SO_2 in the exhaust gas would be small (< 1 %). Thus, the amount of ^{35}S injected would have to be estimated with the purpose of detecting ^{35}S in the exhaust gas. In Table 1 typical gas emission rates during production of clinker at Norcem Brevik are given.

In order to perform tests with radioactive tracers outside IFE's laboratory, permission from the Norwegian Radiation Protection Agency (NRPA) was applied for and given.

Table 1. Typical rates of emission and production at Norcem Brevik.

Item	Rate	Item	Rate
Exhaust gas, Aerofall chimney	220 000 m^3/h STP	Clinker produced	150 tons/h
Exhaust gas,	150 000 m^3/h STP	Gas sampling	25 L/min STP

EXPERIMENTAL

1. Radioactivity

The necessary amount of ^{35}S to inject was estimated to 2,5 GBq based on a detection limit of 1 Bq/L, a gas emission of 350 000 m^3/h STP, gas-sampling of 25 L/min, 1 % sulphur emission and a response peak height of 100 Bq/L.

It was decided to irradiate elemental, yellow sulphur, α-S_8, in IFE's research reactor JEEP-II.

1.1. Irradiation

Due to dose exposure of operators it was desirable to reduce the amount of ^{32}P produced from the $^{32}S(n,p)^{32}P$ reaction. This reaction has threshold energy of 0,928 MeV[2], which means that epithermal neutrons are needed. Thus, an irradiation position with a very high ratio of thermal- to epithermal neutrons was chosen.

Portions of 50 g of α-S_8 were exposed to a thermal neutron flux of approximately $5 \cdot 10^{12}$ $cm^{-2}s^{-1}$ for 14 days. Also, the low temperature at the irradiation position (< 60 °C) avoided the transfer of rhombic α-S_8 to monoclinic β-S_8.

1.2. Production of the labelled ^{35}S-coke tracer

The irradiated sulphur was poured into a glass jar, CS_2 was added and the sulphur dissolved. Coke as powder was successively added so that the solution was totally absorbed. The CS_2 was then allowed to evaporate by exposure to air. The final radioactive coke was put into a polyethylene flask.

2. Injection of tracers

In the first test, Test 1, the secondary injection site was used. The polyethylene flask with the ^{35}S -impregnated coke was put directly into the hot zone by taping it to a wooden stick.

In the second test, Test 2, the primary site was used. Here the coke was poured into a cold pipe used for blowing coke and air into the kiln. The lid was closed and the coke blown into the hot zone within seconds.

3. Sampling

3.1. Gas sampling

Gas was extracted from the chimneys at a rate of 25 L/min by the means of a suction pump. The gas was bubbled through two flasks in series containing 700 mL 0,2M NaOH absorbing the gaseous oxides, i.e. CO_2, NO_2 and SO_2. Samples of 20 mL were taken from the first flask according to a predetermined sampling schedule. The second flask was used as an extra gas trap and was not sampled. In the first part

samples were taken every second minute. There were two alternating gas absorbing systems in parallel enabling a continuous gas-absorption.

The exhaust gas contained water vapour making the volume in the flasks increase. Thus, all flasks were weighed before and after the test to establish the average water condensation rate, which was shown to be 1,5 mL/min.

As the gas residence time in the kiln was assumed to be quite short, the gas sampling started immediately after the injection.

3.2. Sampling of clinker

Samples of 1 kg of hot freshly produced clinker was put into cans and left for cooling. Sampling continued for 15 hours with the highest sampling rate during the first four hours.

4. Measurements of ^{35}S

All determinations of ^{35}S were performed at IFE using a Quantulus Low-Level beta-spectrometer made by Wallac Oy, Finland.

4.1. Gas-absorbing solutions

10 mL of the sample solutions was mixed with 10 mL Optiphase Super mix liquid scintillator supplied by Wallac Oy, Finland. Each sample was corrected for quenching by use of the spectral quench parameter[3], SQP, inherent in the Quantulus system. The counting efficiency, ε_{SQP}, vs. SQP was measured in a separate laboratory experiment. It was found to be a linear function in the actual range. The used relation was: $\varepsilon_{SQP} = -1{,}7 + 0{,}003 \cdot SQP$.

Figure 2 shows two β-spectra containing only background and two containing additional activity of ^{35}S –spectra. In Figure 3 the net β-spectra of these two samples containing ^{35}S –spectra is shown. In addition, a spectrum from pure ^{35}S in CS_2 is shown proving that the extra activity in Figure 2 has the correct origin.

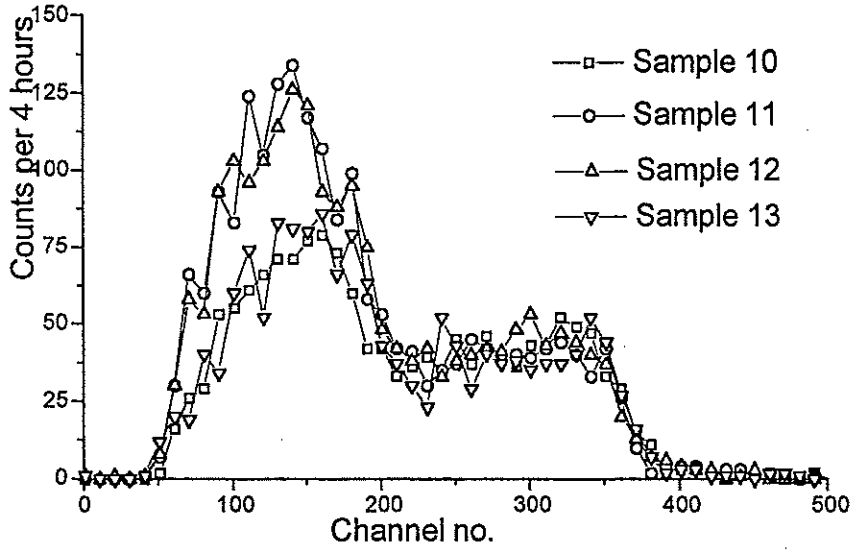

Figure 2. β-spectra of four samples from Test 1, Chimney 3, measured with Quantulus low-level liquid scintillation spectrometer.

The volume in the absorption bottle as a function of sampling time was calculated according to formula (1):

$$V_i(t_i) = V_0 - \sum_{k=1}^{i} v_k + K \sum_{k=1}^{i} \Delta t_k = V_0 - i\,?v_p + K \sum_{k=1}^{i} \Delta t_k \qquad (1)$$

where V_0 is the start volume in the absorption bottle, v_k=v_p is the sample volume extracted (20mL), K the condensation rate (1,5mL/min), and Δt_k the time interval between samples k-2 and k. The content given in Bq in the samples was calculated according to formula (2):

$$D_i(^{35}S) = R_i(^{35}S)V_i(t_i)/(\varepsilon_{SQP} v_p) \qquad (2)$$

where D_i denotes the disintegration rate (Bq) in sample i, R_i is the measured counting rate (counts per second, cps), and ε_{SQP} is counting efficiency (cps/Bq).

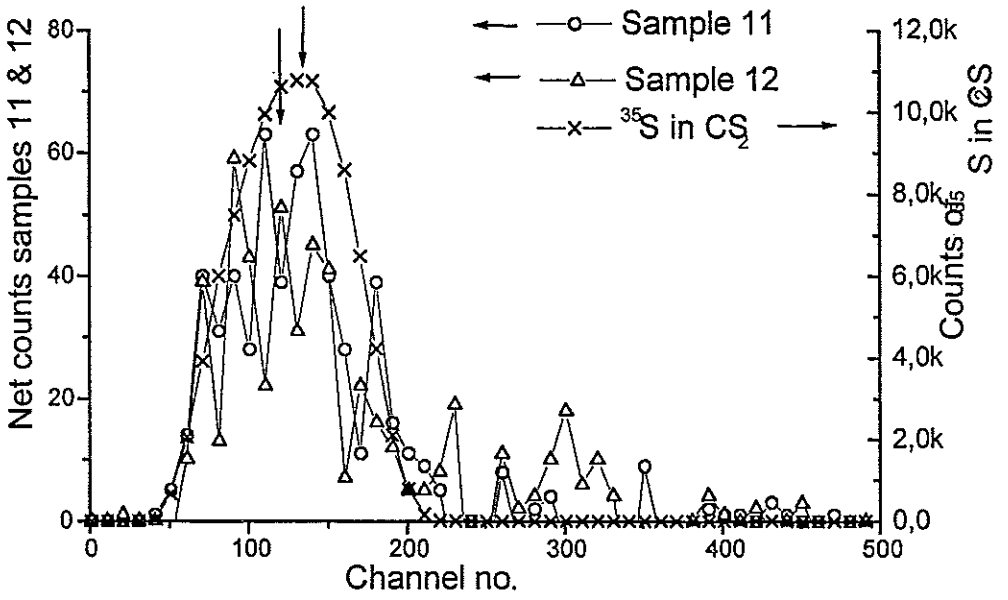

Figure 3. Net β-spectra of two samples from Test 1, Chimney 3, measured with Quantulus low-level liquid scintillation spectrometer. In addition a spectrum from pure ^{35}S in CS_2 is shown to prove that the extra activity in Figure 2 is the correct one. The difference in peak positions, indicated by the arrows, is due to different quenching in the different kind of samples.

4.2. ^{35}S in clinker

The clinker samples were inhomogeneous with respect to grain size distributions. All of the 1 kg samples were therefore crushed and run through a divider giving four fractions of 250 g. From one of these fractions 25 g were dissolved in HCl following a procedure used by Norcem for standard clinker analyses[4]. The dissolved sulphur as sulphate was then precipitated as $BaSO_4$. The solution was decanted, the precipitate was washed with 10 mL water and added to 10 mL Instagel liquid scintillator made by Packard Instruments B.V., The Netherlands.

In Figure 4 the production profiles for ^{35}S in clinker for the two tests are shown.

5. Determination of injected amounts of ^{35}S

In addition to the bulk samples (50 g of α-S_8) of sulphur, two packages of 1 g α-S_8 each were irradiated together with the bulk amounts. These sulphur samples were dissolved in 10 mL CS_2 and diluted to 50 mL with methanol. Aliquots from such diluted samples were used for standardisation of the injected amounts.

RESULTS AND DISCUSSION

No ^{35}S could be detected in the samples from the Aerofall chimney and from the Test 2 (primary injection site). Only two samples in Test 1 showed traces of ^{35}S. As the absorbing solutions accumulated sulphate from the exhaust gas a steady increase

in ^{35}S-activity was expected. However, when activity above the background only could be detected in samples 11 and 12, we conclude that we are close to the detection limit and that the dilution due to condensing water vapour and removal of samples brought the activity below detection level. Figure 3 proves that the activity above background comes from ^{35}S.

In Table 1 the average gas emissions from Chimney 3 and Aerofall chimney are listed. Assuming we are at the detection limit sampling the emissions in Chimney 3, then a gas flow 50 % higher than in the Aerofall chimney would make the ^{35}S-concentration far below detection limits. The Aerofall chimney has proven to release very little gases like SO_2[1].

The radioactive sulphur emitted as sulphate in the clinker is shown in Figure 4 as a function of time after injection. The measured values are normalised according to the production rate of clinker. Thus, the abscissa unit is given as MBq.

As seen from Figure 4, there is an immediate response when injecting at the primary site which is close to the clinker outlet, while the response in Test 1 is slower, but a pronounced peak after approximately 3 hours indicates that sulphur recycles inside the kiln system several times before it leaves the system along with the clinker, mainly as alkali sulphates [1]. In Test 2 this recycle effect is less pronounced.

The background may originate from several sources: traces of ^{40}K coming from the NaOH-added, ^{210}Pb in the exhaust gas due to the high temperature in the kiln, and radon and its daughters. The last ones are pollutants in the reacting silicates.

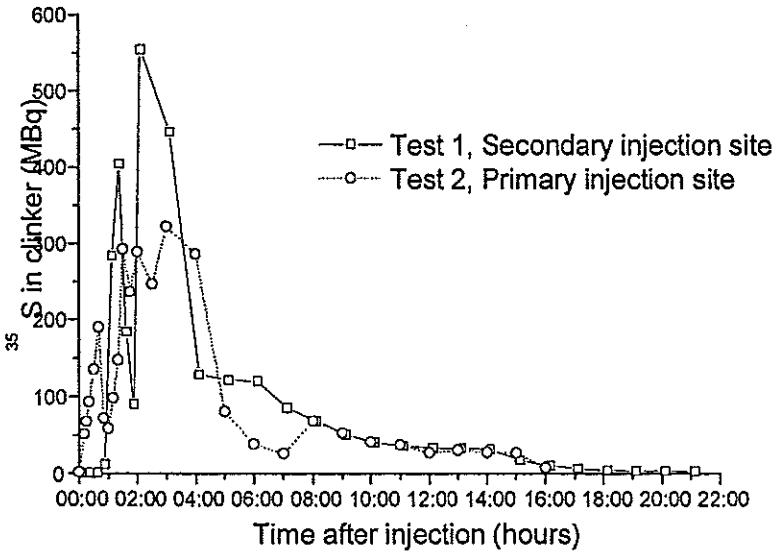

Figure 4. Responses (residence time distributions) of ^{35}S as sulphate produced in the clinker. The measured values are normalised according to the production rate of clinker. Thus, the abscissa unit is given as MBq.

CONCLUSION

From the ordinary process analyses it was known that the emission of sulphur was modest, i.e. < 1 % [1]. The tests performed showed that not more than 0,01% of the sulphur added to the process through coal or coke will leave as gas and only through Chimney 3. The Aerofall chimney emits less than Chimney 3, amounts below our detection limits.

A mass balance of recovered ^{35}S relative to injected showed that 80 - 95 % of injected activity was recovered in the clinker. This is considered very good since some sulphur has been shown to have a very long residence time in the kiln[1].

The residence time distribution of the sulphur showed a difference depending on the injection sites, a result which may be used for reduced emissions of sulphur to the environment.

REFERENCES

[1] L-A. Tokheim, *The impact of staged combustion on the operation of a precalciner cement kiln*, Dr.Eng. thesis, Telemark University College / Norwegian University of Technology and Science (1999)
[2] C. M. Lederer and V. S. Shirley (eds.) *Table of Isotopes, 7th ed.*, Wiley, New York (1978)
[3] P. Mäkinen, *Handbook of Liquid Scintillation Counting*, B.Sc. thesis, Turku Institute of Technology, Turku, Finland (1995)
[4] Clinker analysis, Handbook Norcem FoU-lab 9D/TH-2a, private communication Liv Margrethe Friberg

OF USE THE TC-99M IN STUDIES OF TREATMENT INDUSTRIAL OF WASTE IN PETROBRAS.

A. Dámera[1], A. Ferreira[2], M. Derivet[3], A. of Magalhaes [2], K. Ramos[1].

[1]Center of Attention to the Nuclear Activity.
Finlay Ave. Km. 2_, Puerto Principe, CP 70800 City of Camagüey, Cuba.
Telephones: 53 32 261657 (262273).
Fax: 53 32 2 96187
E. MAIL: damera@caonao.cmw.inf.cu
[2]Centro of Development of Nuclear Technology,
Rua Prof. Mario Werneck s/n. Campus UFMG, Pampulha 30123, Belo Horizon, Mines Gerais, Brazil.
[3] Cuban Institute of Sugar Investigations,
Remote 10154, Quivicán, Havana, Cuba.

Abstract. The industry of the petroleum has become the last decades in an user of Nuclear the Techniques. Due to the amplification of activities with this industry, in some of their technical and economic characteristics the possibilities of application of the nuclear techniques in the oil sector plows proportionally bigger and significant than it lives in many other sectors of the economy.
This work was carried out in the Station of Treatment Industrial Residual of (ETDI) of PETROBRAS. There is had ace objective to it determines the it cheats of real residence of the it mixes of residual inside the separators by means of the nuclear technique of tracer radioactive, using the Tc-99m.
This has to great economic and environmental relevance, because when obtaining the cheats of real residence experimentally in the separators, you dog compares with those obtained theoretically, that which allows to influence with precision on the system optimizing their operation and diminishing the magnitude of their possible negative environmental impact it lives.

INTRODUCTION

Cuba is among the countries that don't possess facilities for the radioisotopes production and it has appealed, in many cases, to the use of the generating isotopic of 99Mo/99mTc, employee habitually in nuclear medicine, as alternative for the application of the radiotracer techniques in the solution of diverse problems, it is interest to continue developing this technique. Our work was developed like part of a training in the Center of Development of Nuclear Technology (CDTN), Beautiful Horizon through a scholarship of the International Organization of Atomic Energy (OIEA).

The Station of Treatment of Residual Industrial (ETDI) of a refinery of petroleum he/she has the function of receiving, to store and to try the you discard liquids and gassy coming from diverse points of the refinery avoiding this way the contamination of the environment. In these moments the effluents that leave the separators has a high level of contamination, given by the little time of permanency that is given to this process and in other occasions the time is too big and it puts back the process of treatment of the residual ones considerably with the rising rise in the price of the same one.

For you discard them liquids the refinery where this was carried out this work it possesses 4 nets:

· RAC The net of polluted waters.
· RUM The net of oils of the new units.
· ROV The net of oils of the old units.
· ROC The net of oils of COKE.

These nets are in a box of flow and of this Water/Oil goes for the separators - old/new that has as function to separate Oil/Water for difference of densities. The separate oil is picked up in a box and pumped for recipients where this receives a specific preparation and then this is again a correspondent for the distillation units for its reproduction. The water after the separation continues for the flotation units.

Technique of radiotracer, theoretical foundation.

In general terms, the method of tracer used it is a technique to obtain information of a system or part of a system, by means of the observation of the behavior of a specific substance, - the tracer one - that has been added to the process. The method implied to mark with the tracer one, to make easily identifiable, a certain phase of the system denominated marked material.

The tracer one selected it fulfills the two fundamental requirements for the same one:

1. to behave exactly as the marked material, in the phase of the investigated process.
2. to possess a particular property that distinguishes it of the marked material, in such a way that can be easily detected in presence of other substances.

The radioisotopes or radiotracers are the tracer ones more universal and more practical. This owes it to the following main advantages:

a) The identity between the marked product and the tracer one can be achieved at atomic level (an atom of the tracer one or radioactive isotope will behave the same as a stable atom of the same element);

b) The detection of the radiotrazador can also reach atomic levels (for example, the radioisotopes of short life, with periods of 100 days or less, they can be detected in quantities so small as 10-16 or 10-17 grams).

As all the materials they are compound for atoms and one or more radioactive isotopes exist for most of the elements, one can, with appropriate synthesis methods, to prepare radiotracers for any product, from pure substances until complex molecules as those of the petroleum and their derived petrochemical.

In many continuous processes this interests to know the distribution of the time of permanency of a substance anyone, inside a reactor. This distribution is referred, generally, at the half time of residence, which is defined as the time average in which a given material remains inside the investigated system.

Suppose you that between you and you + Dt (for Dt spreading to zero) Xi molecules of a certain product enters in the volume Vo of a material processed in a reactor and it is wanted to know how many of those original molecules they will still

remain in the reactor after having lapsed a time t from the injection, if the material circulates with flow constant Q. In other words, it is to determine the function:

$$X(T) = F(XI, VO, Q, T)$$

keeping in mind that the dilution of Xi in Vo cannot be homogeneous.

The Fig. 1 illustrate this application and the interpretation of the results obtained in a particular case. The barycentric of the surface defined by the answer curve No(t), it coincides with the value of the half time of permanency Tm and the dispersion of the times of residence around Tm he/she gives idea of the treatment uniformity from the product to the exit of the reactor.

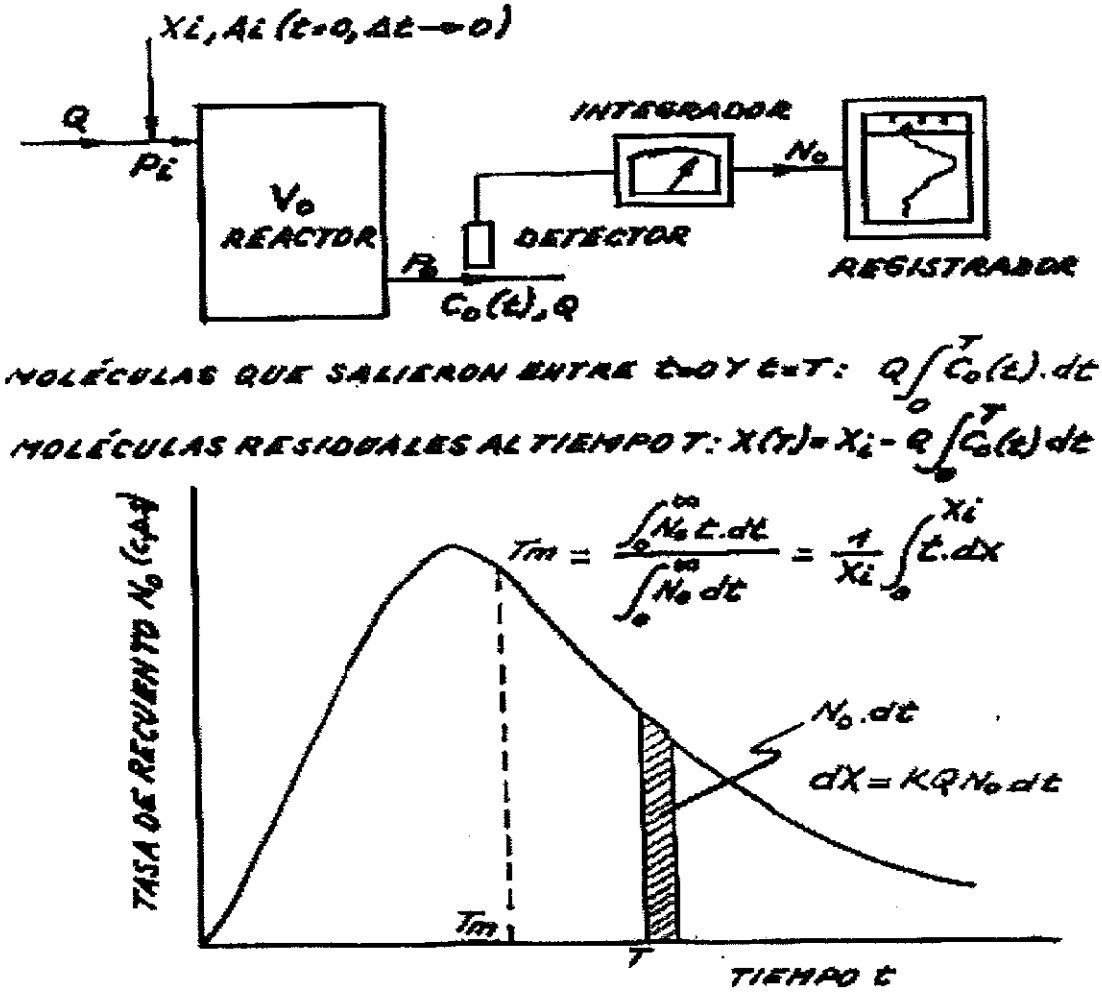

Fig. 1: Determination of the differential distribution of the time of residence of the injected molecules.

At world level they have been successfully employees tracer radioactive for the determination of hydrodynamic parameters. For obvious reasons for these ends isotopes of life half short and low toxicity are used only, what locates at the 99mTc as a potential candidate. However, besides the nuclear characteristics another series of requirements that should complete as radiotrazador exists. The most important in them is that during the study that is made, don't incorporate that is to say to a phase for which was not dedicated initially, that it is preservative.

OBTAINED RESULTS

The work carried out in the Station of Treatment of Residual Industrial (ETDI) of PETROBRAS, it consisted on determining the time of real residence of the mixture of residual inside the separators by means of the nuclear technique of tracer radioactive, using a generator of 99Mo (T_ = 67 h)----99mTc(T_ = 6h), for they were carried out it injections from 99mTc to the entrance of the 4 separators and a continuous detection was made <in site> of the same one, later on, all the obtained data were processed and finally the results were obtained (moments (used to determine the dispersion), the time of residence and the dispersion) following for each separator:

§ SEPARADOR #1
Number of data = 1101
MO = 1.9x10_ (Moment Order 0)
M1 = 2.7x10_ (Moment Order 1)
M2 = 5.5 x10_ (Moment Order 2)
TBAR = 1.4 hours (Time of residence)
S2 = 0.81 (Dispersion)
To see figure #2

§ SEPARADOR #2
Number of data = 410
MO = 1.2 x10_ (Moment Order 0)
M1 = 1.2 x10_ (Moment Order 1)
M2 = 1.4 x10_ (Moment Order 2)
TBAR = 1.0 hours (Time of residence)
S2 = 0.10 (Dispersion)
To see figure #3

§ SEPARADOR #3
Number of data = 716
MO = 4.7 x10_ (Moment Order 0)
M1 = 7.1 x10_ (Moment Order 1)
M2 = 1.2 x10_ (Moment Order 2)

TBAR = 1.5 hours (Time of residence)
S2 = 0.27 (Dispersion)
To see figure #4

§ SEPARADOR #4
Number of data = 665
MO = 5.4 x10_ (Moment Order 0)
M1 = 9.5 x10_ (Moment Order 1)
M2 = 1.8 x10_ (Moment Order 2)
TBAR = 1.8 hours (Time of residence)
S2 = 0.25 (Dispersion)
To see figure #5

CONCLUSIONS

Keeping in mind the obtained results of the mensurations and that the theoretical time of residence that should have each separator is of approximately TBAR = 2.0 hours we can conclude that:

- The separator #3 (TBAR = 1.5h) and 4 (TBAR = 1.8h) they have a quite acceptable behavior, because the times of residence obtained practically, approach to the theoretical values that should have therefore we understand that the process made in this separators of the ETDI is correct.

- The separators #1 (TBAR = 1.4h) and 2 (TBAR = 1.0h) they have a behavior that is not the most efficient possible, because the times of residence obtained practically, differ therefore of the theoretical values that should have, we understand that the process made in this separators of the ETDI can improve.

- In these moments the effluents that leave the separators #1y2 has a high level of contamination, given by the little time of permanency that is given to this process.

REFERENCES

- Radiochemistry Nuclear and Methods of Analysis, William D Ehman, Diane E. Vance. 1995.
- Theory and Technical of Tratamento of Water, Francisco Paes Leme, CETESB, Companhia of Tecnoligias of Environmental Saneamento Sao Paulo-Brazil. 1979.
- Parceria among or CDTN and or CENPES/PETROBRÁS, Virgílio L. Bomtempo, Rubens M. Moreira, Amenonia M. F. Paints, CDTN. Brazil. 1995.
- Estudo gives Dynamic of uma um Pilot Climbs Digestor Anaeróbico Using um Radio-active Tracador, A. M. F. Paints, R. M. Moreira, C. A. L. Chernicharo, CDTN, DESA/UFMG. Brazil.

- RADIOISOTOPE APPLICATIONS ON FLUIDIZED CATALYTIC CRACKING UNITS, J. S. CHARLTON, AUSTRALASIA.
- Current Status and Trends of Cooperation on Radiotracer and NCS Technologies, J. Thereska, IAEA, RIPC, Austria.
- Experiences of the Applications of the Nuclear Techniques in the Cuban Industry, J Griffith, Luis F. Desdín, R. Rodríguez. NURT-1997. Cuba.
- I project RLA/8/024-ARCAL XLIII Industrial Applications of the Technology of Tracer and Systems of Control Nucleónico", Peru, 1999.
- I study of the suitability of the 99mTc as radiotrazador for short-term hydrological studies, J.Domínguez, J. Borroto, E.Pérez, S.Calvo, G.Fernández, ISCTN, CUBA.1998.

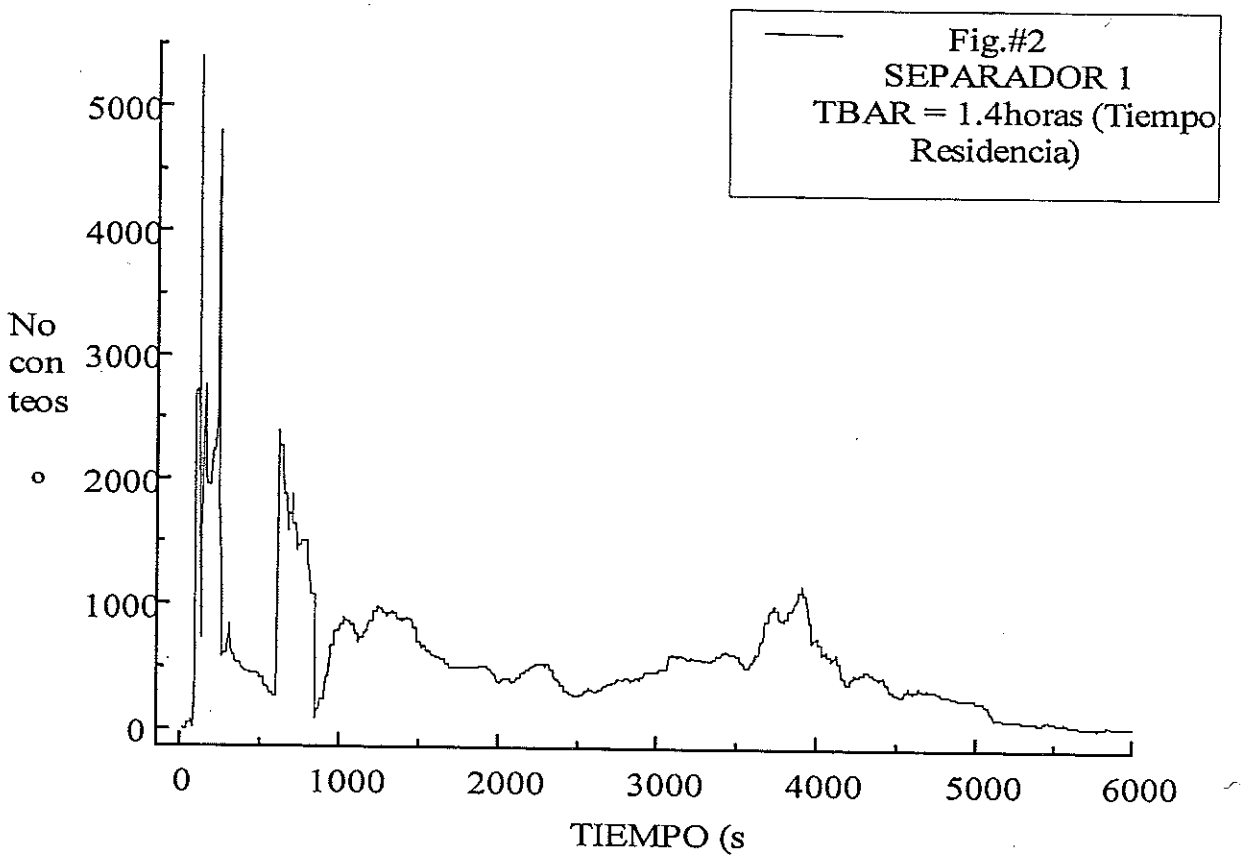

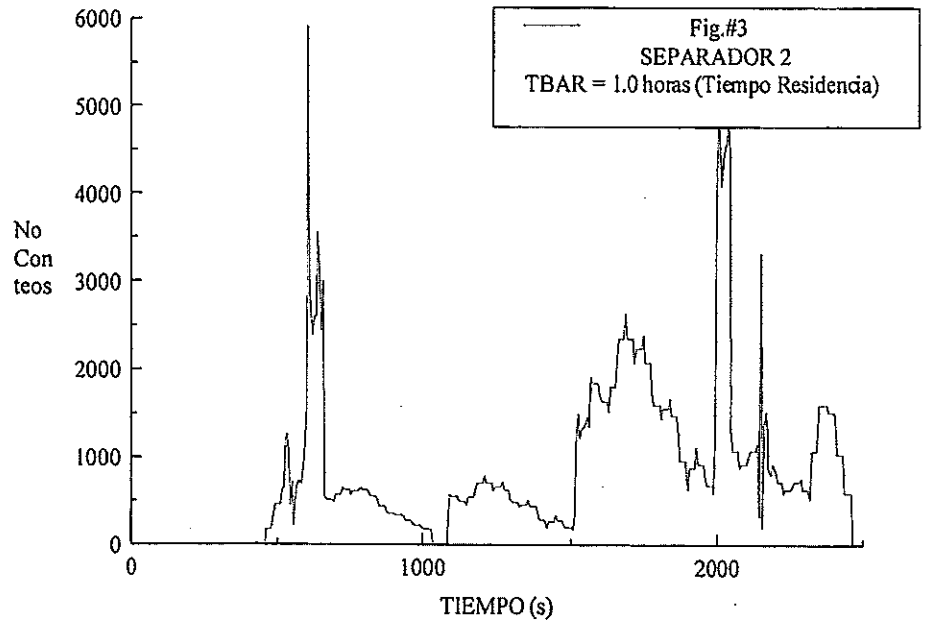
Fig.#3
SEPARADOR 2
TBAR = 1.0 horas (Tiempo Residencia)
No Conteos
6000
5000
4000
3000
2000
1000
0
0
1000
2000
TIEMPO (s)

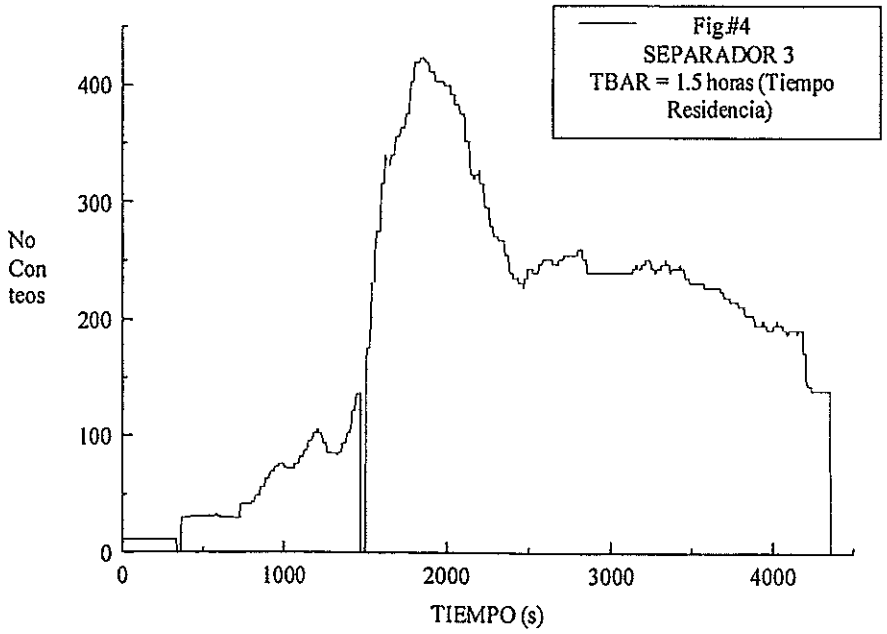
Fig#4
SEPARADOR 3
TBAR = 1.5 horas (Tiempo Residencia)
No Conteos
400
300
200
100
0
0
1000
2000
3000
4000
TIEMPO (s)

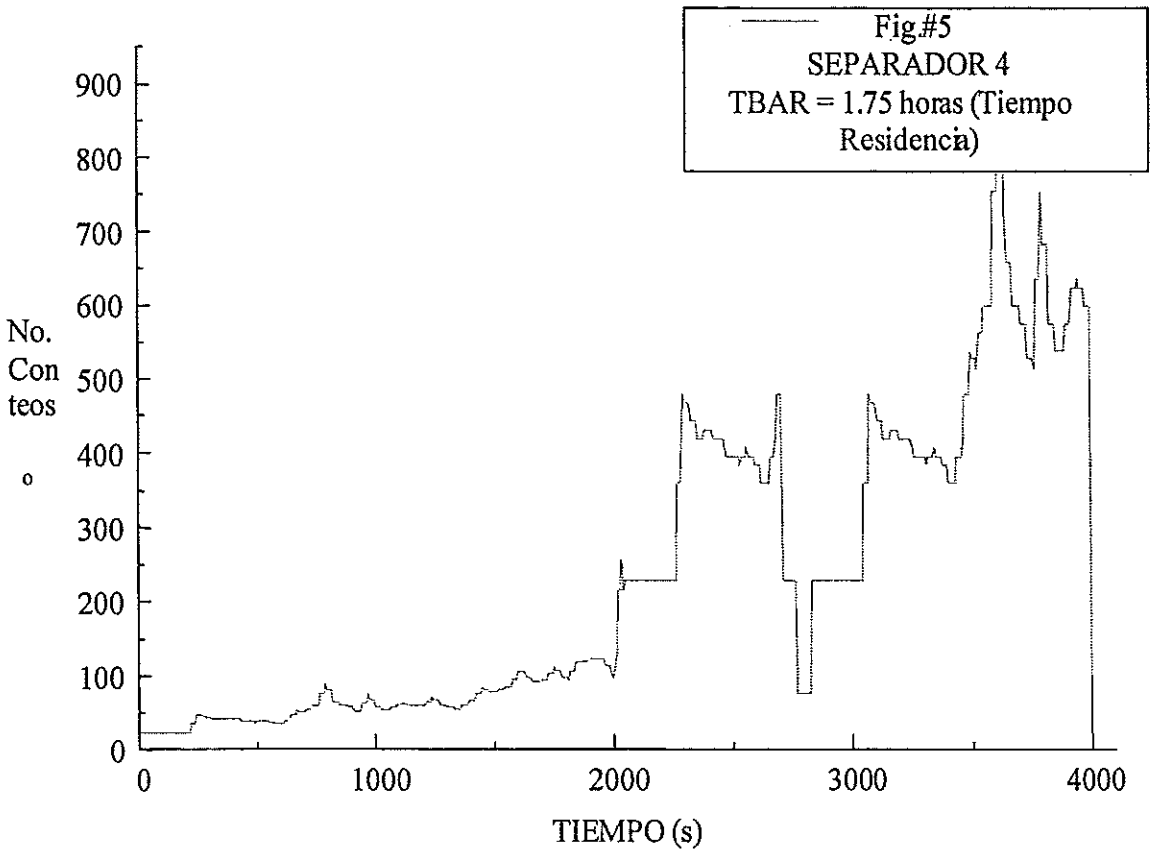
Fig.#5
SEPARADOR 4
TBAR = 1.75 horas (Tiempo Residencia)
No. Conteos
900
800
700
600
500
400
300
200
100
0
0
1000
2000
3000
4000
TIEMPO (s)

THE USE TRACER RADIOACTIVE IN THE STATION OF TREATMENT RESIDUAL OF IN THE OIL INDUSTRY

A. Dámera[1], A. Ferreira[2], M. Derivet[3], A. of Magalhaes [2], K. Ramos[1].

[1]Center of Attention to the Nuclear Activity.
Finlay Ave. Km. 2_, Port Prince, CP 70800 City of Camagüey, Cuba.
Telephones: 53 322 61657(62273).
Fax: 53 322 96187
E. MAIL: damera@caonao.cmw.inf.cu
[2]Centro of Development of Nuclear Technology,
Rua Prof. Mario Werneck s/n. Campus UFMG, Pampulha 30123, Belo Horizon, Mines Gerais, Brazil.
[3] Cuban Institute of Sugar Investigations,
Remote 10154, Quivicán, Havana, Cuba.

Abstract. The industry of the petroleum comes being in you finish them decades, an user of the Nuclear Techniques, overalls starting from the II World War, when sources radioactive and new techniques passed the investigators' disposition and technicians of the civil sector.
Due to the amplification of activities in some of the technical and economic characteristics of this industry the possibilities of application of the nuclear techniques are proportionally bigger and more important than in many other sectors of the economy.
This work was carried out in the Station of Treatment of Residual Industrial (ETDI) in PETROBRAS (Brazil).
The ETDI has the function of receiving, to store and to try the you discard liquids and gassy coming from diverse points of the refinery avoiding this way the contamination of the environment.
The work consisted on the determination of the time of residence inside the floculators and the floats, for it was used it the nuclear technique of radioactive radiotracer, concretely the Technetium 99 m.
This has a great economic and environmental importance, because when obtaining the time of real residence experimentally in the floculators and the floats, you can compare with those obtained theoretically and to influence on the system, optimizing their operation.

INTRODUCTION

With the use in convenient way of the properties of the radionuclides, substances that emit radiation, important information is obtained for the analysis, the address or the diagnosis, of chemical, biological and physical processes that lapse in teams and apparatuses or in the operation to great scale of an industrial sector.

The advantages of the methods that use radionuclides are given on one hand, for the capacity of the radiation especially the radiation of crossing the matter and for the other one for their simple and very effective detection. Not less important it is the property that the measured magnitude, the flow of particles as a result of a nuclear transformation, doesn't depend on physical conditions (pressure, temperature, or of the coloration of the means of mensuration).

The method of the indicators or tracer radioactive it offers information on the space to measure, the system that is studied, registering and evaluating the concentration

of the marked substance, that is to say of the tracer one that one adds to the system at the beginning of the experiment.

For example, during the evaluation of the material flow in a team for the one which this it happens, the tracer one is added radioactive to the entrance current. And its concentration that is proportional to the detected flow of particles is measured in the material current that leaves the system fig.1.

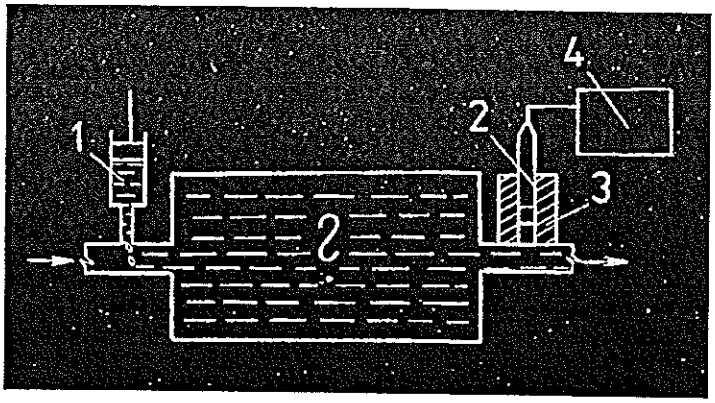

Figure.1 Method of the tracer Radioactive
1-dosificador of the tracer one
2-detecting of radiations,
3-blindaje of lead,
Registration 4-team.

Cuba is among the countries that don't possess facilities for the radioisotopes production and it has appealed, in many cases, to the use of the generating isotopic of 99Mo/99mTc, employee habitually in nuclear medicine, as alternative for the application of the radiotracer techniques in the solution of diverse problems, it is interest to continue developing this technique. Our work was developed like part of a training in the Center of Development of Nuclear Technology (CDTN), Beautiful Horizon through a scholarship of the International Organization of Atomic Energy (OIEA). The Station of Treatment of Residual Industrial (ETDI) of a refinery of petroleum he/she has the function of receiving, to store and to try the you discard liquids and gassy coming from diverse points of the refinery avoiding this way the contamination of the environment

OBTAINED RESULTS

The work carried out in the Station of Treatment of Residual Industrial (ETDI) of PETROBRAS, it consisted on determining the time of real residence of the mixture of residual inside the 2 floats and the 2 floculators by means of the nuclear technique of

tracer radioactive, using a generator of 99Mo (T_ = 67 h)----99mTc(T_ = 6h), for they were carried out it injections from 99mTc to the entrance of the floats and floculators and a continuous detection was made <in situ> of the same one, later on, all the obtained data were processed and finally the results moments were obtained (used to determine the dispersion), the time of residence and the following dispersion for each one:

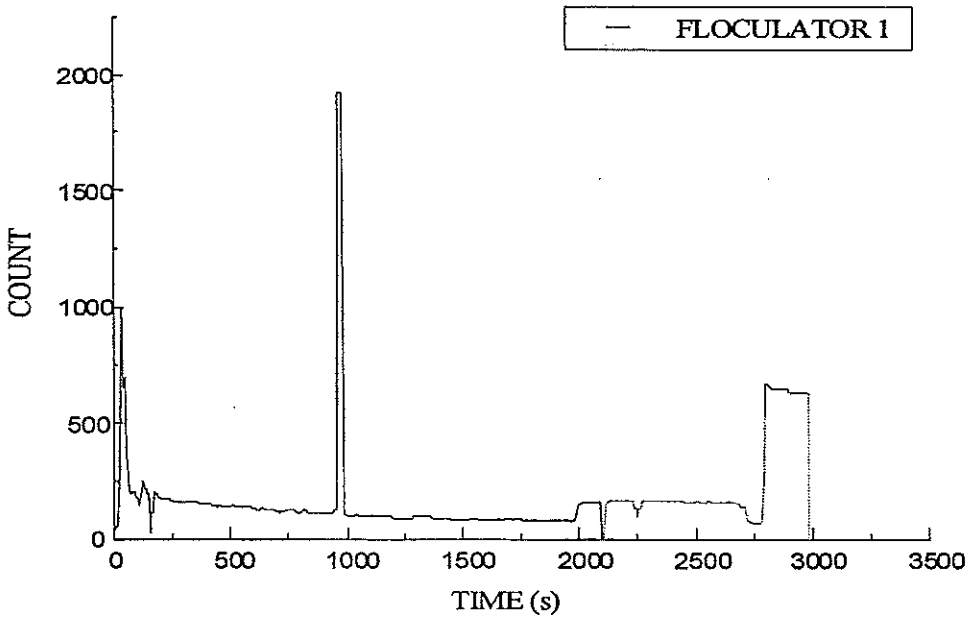

Figure 2
FLOCULATOR #1
Number of data = 1101
MO = 6.2 x10_ (Moment Order 0)
M1 = 1.3 x10_ (Moment Order 1)
M2 = 3.6 x10_ (Moment Order 2)
TBAR = 2.0 hours(Time of residence)
S2 = 1.4 (Dispersion)

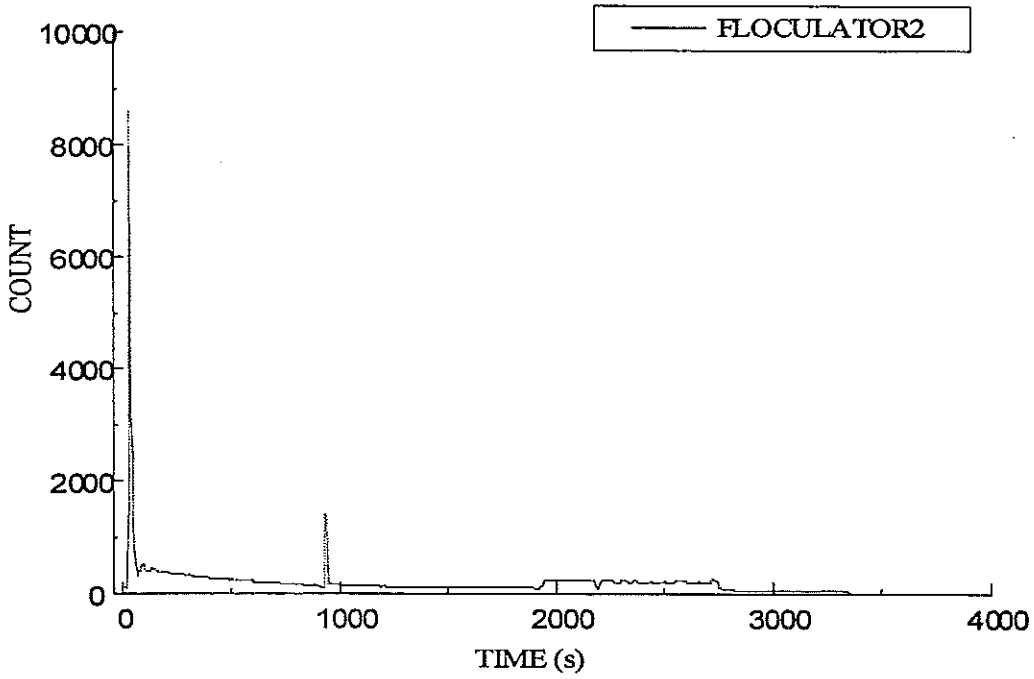

Figure 3
FLOCULATOR #2
Number of data = 1100
MO = 7.3 x10_ (Moment Order 0)
M1 = 2 ..1 x10_ (Moment Order 1)
M2 = 7.2 x10_ (Moment Order 2)
TBAR = 2.9 hours (Time Residence)
S2 = 1.1 (Dispersion)

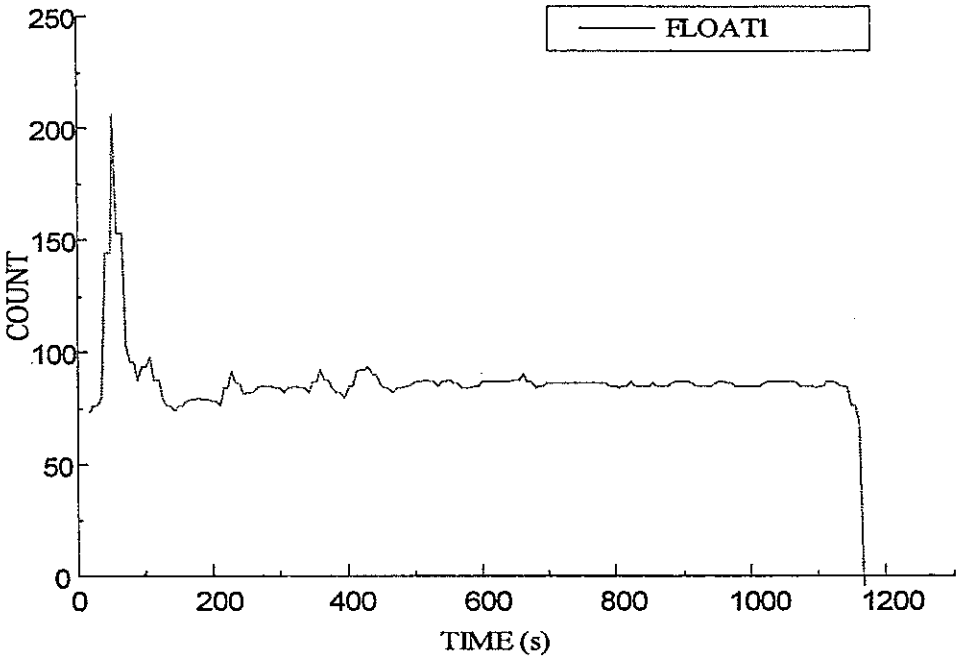

Figure 4
Float #1
Number of data = 346
MO = 1.0 x10_ (Moment Order 0)
M1 = 6.8 x10_ (Moment Order 1)
M2 = 5.5 x10_ (Moment Order 2)
TBAR = 0.6 hours (Time Residence)
S2 = 0.1 (Dispersion)

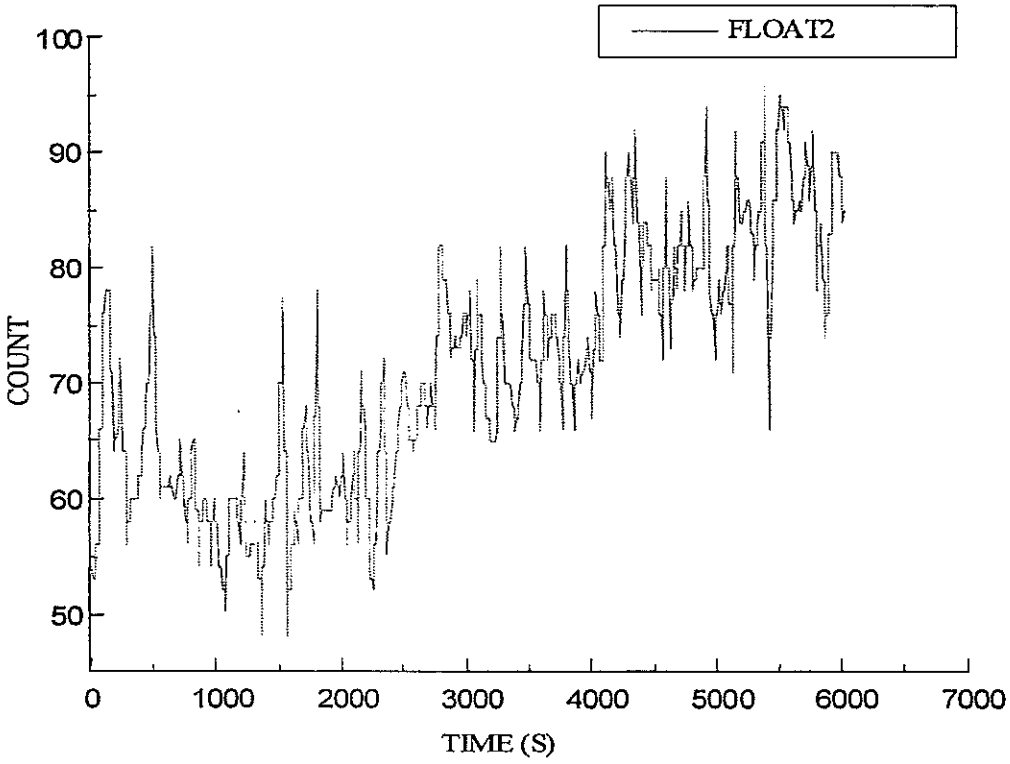

Figure 5
Float #2
Number of data = 6821
MO = 1.8 x10 (Moment Order 0)
M1 = 2.2 x10^4 (Moment Order 1)
M2 = 3.6 x10^5 (Moment Order 2)
TBAR = 12.2 hours (Time Residence)
S2 = 4.3 (Dispersion)

CONCLUSIONS

Keeping in mind the obtained results of the mensurations and that the theoretical time of residence that should have each floculator and each float is of approximately TBAR = 2.0 hours we can conclude that:

- The floculator #1 (TBAR = 2.0h) and 2 (TBAR = 2.9h) they have a quite acceptable behavior, because the times of residence obtained practically, approach to the theoretical values that should have therefore we understand that the process made in this floculators of the ETDI is correct, overalls the #1 coincide exactly with the theoretical one.
- The floats #1 (TBAR = 0.6h) and 2 (TBAR = 12.2h) they have a behavior that is not the most efficient, because the times of residence obtained practically, differ therefore of the theoretical values that should have, we understand that the process made in this floats of the ETDI can improve, overalls the float #2 which has a considerable deviation of its good value.

REFERENCES

- Radiochemistry Nuclear and Methods of Analysis, William D Ehman, Diane E. Vance. 1995.
- Theory and Technical of Tratamento of Water, Francisco Paes Leme, CETESB, Companhia of Tecnoligias of Environmental Saneamento Sao Paulo-Brazil. 1979.
- Parceria among or CDTN and or CENPES/PETROBRÁS, Virgílio L. Bomtempo, Rubens M. Moreira, Amenonia M. F. Paints, CDTN. Brazil. 1995.
- Estudo gives Dynamic of uma um Pilot Climbs Digestor Anaeróbico Using um Radio-active Tracador, A. M. F. Paints, R. M. Moreira, C. A. L. Chernicharo, CDTN, DESA/UFMG. Brazil.
- RADIOISOTOPE APPLICATIONS ON FLUIDIZED CATALYTIC CRACKING UNITS, J. S. CHARLTON, AUSTRALASIA.
- Current Status and Trends of Cooperation on Radiotracer and NCS Technologies, J. Thereska, IAEA, RIPC, Austria.
- Experiences of the Applications of the Nuclear Techniques in the Cuban Industry, J Griffith, Luis F. Desdín, R. Rodríguez. NURT-1997. Cuba.
- I project RLA/8/024-ARCAL XLIII Industrial Applications of the Technology of Tracer and Systems of Control Nucleónico", Peru, 1999.
- I study of the suitability of the 99mTc as radiotrazador for short term hydrological studies, J.Domínguez, J. Borroto, E.Pérez, S.Calvo, G.Fernández, ISCTN, CUBA.1998.

SIMULATION OF AIR FLOW DISTRIBUTION IN ROOMS BY A SYSTEMIC APPROACH

S. Soares[1], J.C. Laborde[1], S. Domenech[2], P. Floquet[2]

[1]Institut de Protection et de Sûreté Nucléaire, Département de Protection et d'Etude des Accidents,
Service d'Etudes et de Recherches en Aérocontamination et en Confinement
CEA/Saclay – Bât. 389 – 91191 Gif-sur-Yvette Cedex, France
[2]Laboratoire de Génie Chimique de Toulouse, UMR 5503 CNRS
INP-ENSIGC – 18, chemin de la loge – 31078 Toulouse Cedex, France

Abstract. In order to achieve a satisfactory level of hygiene and comfort in premises and to assess the pollutant transfers, it is necessary to control the air flow distribution. The research on air distribution in rooms involves full-scale experiments, scale-model experiments and Computational Fluid Dynamics (CFD) tools. An intermediate approach between predictive numerical simulation and experimental determination of aerodynamic parameters is the systemic approach.

The paper proposed presents the main features of the IDTS code recently developed and based on the principles of the systemic approach. A model is built from a combination of elementary systems representing basic flows as piston, mixing flow, recirculation, short circuiting; each elementary system is characterized by specific parameters such as the residence time and the volume of the unitary system. The adjustment of the model is derived from the comparison of the responses to a signal injected into the model with a tracer emission realized at the room inlet; these responses depend on the internal fluid flow patterns. The difficulty consists in finding quickly the most representative adjustment and the associated parameters. The code IDTS is constituted then by two main subroutines, whose functions are described: a subroutine in order to solve the algebra differential equations characterizing the unitary systems, and a subroutine in order to optimise the structural adjustment design respecting some defined numerical and physical constraints.

Furthermore, the computational tool has been tested from a ventilated laboratory enclosure (2 300 m^3 volume). Helium stimulus corresponding to pulse is realized in the blowing duct, and the helium concentration is monitored at the exhaust duct of the test enclosure. The experimental results are then analysed and compared with the IDTS identifications.

The IDTS code thus constitutes a computer-aided design tool of flow models to improve the knowledge about the gaseous transfers in a ventilated indoor space. So, a preliminary qualification from several experimental data has been achieved and is quite encouraging.

INTRODUCTION

The control of the airborne contamination transfers linked to the operators protection and to the facilities safety is an essential feature in the nuclear industry, particularly to prevent radiological risk. So, it is necessary to have tools in order to assess airborne contamination transfers inside a ventilated enclosure, since the ventilation constitutes a system of contamination containment.

The systemic approach concept aims at interpreting Residence Time Distribution (called RTD) in a room, whose theory is commonly used to describe flow patterns in a wide variety of applications. It appears to be of great interest, specially when the predictive method based on CFD codes is difficult to be used, particularly in the case of large and cluttered systems. Furthermore, this approach leads to more integrated results, giving a physical significance to the flow model within reasonable CPU times.

GENERAL PRINCIPLES

1. General structure of the code

The establishment of a RTD model lies on the comparison of a simulated response of a proposed model to a stimulus, with an experimental curve obtained generally through the response of the system to a tracer release, classically helium in ventilated premises. The problem can be formulated as a two levels identification problem: a structural identification problem and a parametric identification one. As a consequence, in the IDTS code [1], the modeling is split into two algorithmic loops as shown in figure 1: an inner loop performing the parametric identification for a given structure, and an outer loop performing the evolution and the choice of the model structures.

The parameter identification step for a fixed model structure consists in a constrained nonlinear least square minimization problem solved by a general successive quadratic procedure. The objective function j(p) is then given by (1).

$$j(p)=\frac{1}{n_t}\sum_i\left[y_{exp}(t_i)-y_{mod}(t_i)\right]^2 \qquad (1)$$

n_t is the number of experimental sampling points, y_{exp} the experimental response, y_{mod} the model response, t_i the time and p the vector of the model parameters, constituted by the volumes and the flow rates of the unitary models.

Concerning the structural identification, two evolutionary procedures based either on Simulated Annealing (SA) or on Genetic Algorithms (Gas) are performed to tackle the combinational aspect of the problem. The objective function j(M) considered for a structure M is given by (2).

$$j(M)=j(M,\hat{p})+\rho.dim(p) \qquad (2)$$

$j(M,\hat{p})$, representing the least square criterion for optimal parameters $\hat{p}$, is added to a penalty term, ρ.dim(p), related to the complexity of the model via the number of parameters included in the model (dim(p)) and a weighting factor ρ.

In addition, there is another physical constraint, specific to most ventilated rooms, relative to the exchanges between zones: whatever the zone in which the emission of pollutant takes place, the latter has to be detected in all other zones. This has been taken into account in adding an optional factor β in the previous expression of the objective function. The new criterion considered is then given by (3).

$$j(M)=(j(M,\hat{p})+\rho.dim(p)).(1+nb\_viol.\beta) \qquad (3)$$

nb_viol represents the total number of impossible exchanges between every couple of zones of the structure.

The structures are coded into a hierarchical unique decomposition of the flow diagrams. The models are then represented through a flow system made up with

ideal components (piston flow reactor or PFR, continuous stirred tank reactor or CSTR) connected by flow mixers, flow splitters and recycle loops. Leaks, infiltrations or short-circuits can also be introduced. The elementary building blocks are linear cascade, recycling loop and parallel distribution.

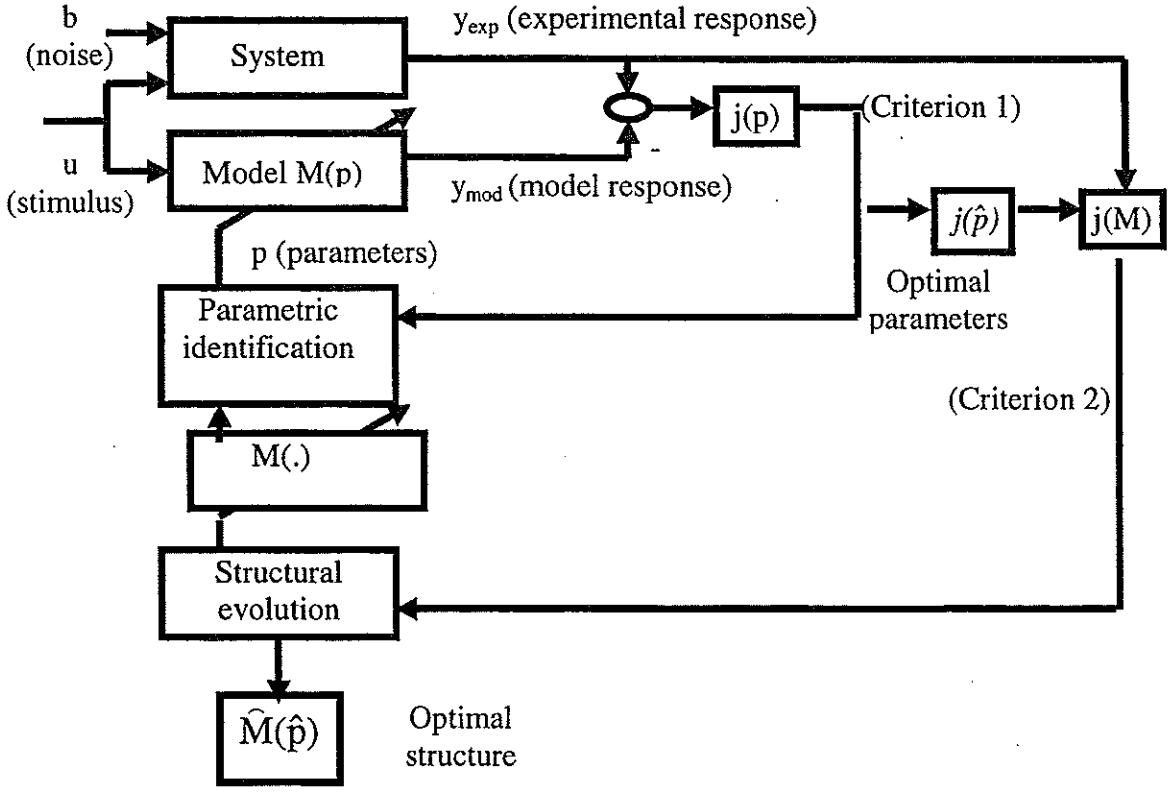

Figure1. Structure of the general identification strategy

2. Genetic algorithms procedure

As the Simulated Annealing procedure has been already presented [2], only the GAs one is here detailed. Theoretically developed by Holland [3], GAs are procedures based on the mimesis of the mechanics of natural selection and genetics (see Table 1). It computes a set of individuals, called population, evolving through a set of biologically inspired operators (selection, cross-over, mutation) constituting the reproduction scheme. In this way, new individuals are generated from parents; only the most suited elements of a population can survive and generate offspring, thus transmitting their biological heredity to new generations.

Table1. Analogies between natural genetics and GAs

Natural genetics		Genetic Algorithms
Individual	⟷	Coding of structures
Gene	⟷	Elementary building block
Population	⟷	Set of candidate structures
Generations	⟷	Algorithm iterations

The offspring generation is obtained from the parent one in accordance to the classical scheme below:

- Generation of the initial population
- Estimation of the fitness of the initial population
- While the number of generations is not reached, do:
  Generate the offspring population
  → selection of individuals surviving
  → synthesis of offspring obtained through cross-over
  → mutation of individuals

The fitness F_i of each individuals (or structure M_i) contained in a population of N_{pop} individuals is directly derived from the initial objective function $j(M_i)$.

$$1/F_i = j(M_i)/\left(\sum_{k=1}^{N_{pop}} j(M_k)/N_{pop}\right) \tag{4}$$

The selection process provides a fixed percentage of individuals that survive in the new generation. The selection is performed on a classical roulette wheel. The probability p_i that the individual M_i survives is given by (5).

$$p_i = F_i/\left(\sum_{j=1}^{N_{pop}} F_j\right) \tag{5}$$

After determining the surviving individuals, the population is completed with new individuals obtained through cross-over mechanisms performed on two parents randomly coupled, using the same probability p_i as in the selection procedure; a classical one point permutation operation has been here retained. The mutation operation is then performed on the entire population with a fixed probability; it consists in the replacement of one decomposition module with another one. The optimized set of parameters are: a population of N_{pop} = 20 individuals, a cross-over ratio equal to 0.6, a mutation one equal to 0.1, and a number of generations equal to 50.

APPLICATION TO A VENTILATED ENCLOSURE

1. Presentation of the experiment

A real ventilated room (2 311 m^3) has been used as an application of the IDTS computational tool. The exhaust system (figure 2) is constituted by four openings situated near the bottom, and the blowing one (figure 3) is constituted by sixteen openings situated near the ceiling of the enclosure. The global air flow rate is about 11 000 $m^3.h^{-1}$.

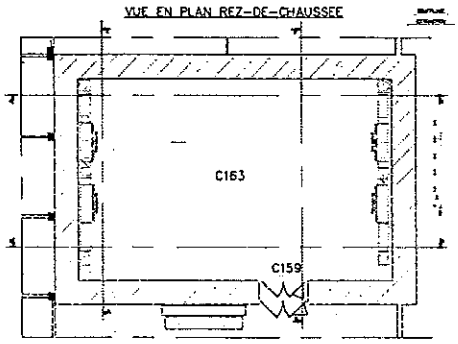

Figure 2. Upon view of the ventilated room

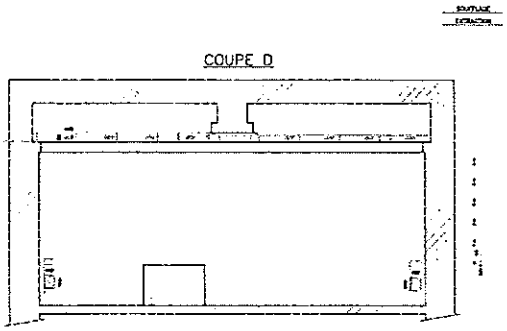

Figure 3. Front view of the ventilated room

A pulse of pure helium is generated in the blowing duct, and the response of the ventilated enclosure to this stimulus is measured by a specific analyzer (mass spectrometer) in the exhaust duct. The RTD curve, called E(t), resulting is represented on figure 4.

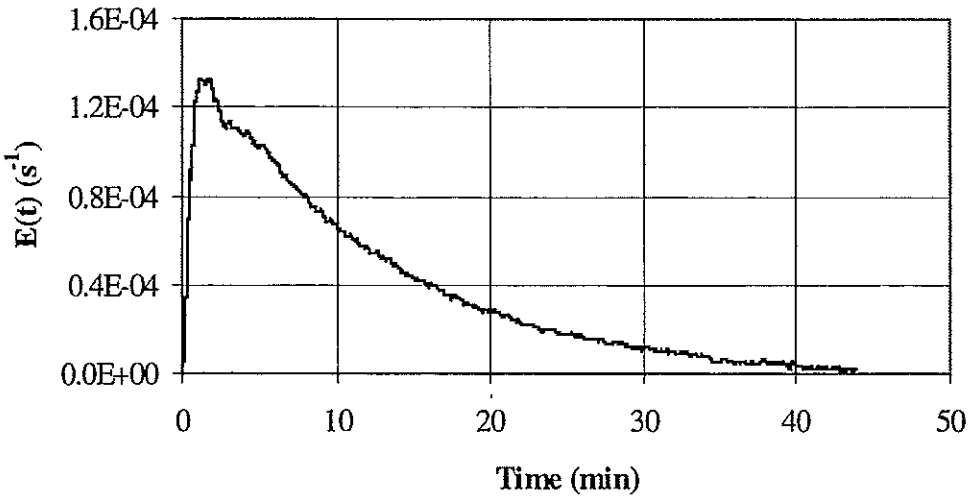

Figure 4. Experimental RTD curve

2. Parametric identification

The first stage of our analysis consists in two parametric identifications, based on two different structures. The first one corresponds to a "two zones model", commonly used in nuclear ventilation expertises. The second one has been obtained by structural identification, but from another room [4]. It has been nevertheless retained, because of the similarity between the blowing and exhaust openings positions of both enclosures. In addition, the both RTD curves have similar characteristics. This model comprises two recirculations: a secondary one, constituted by a CSTR and a PFR in series, and a main one, constituted by a CSTR alone.

The results of the parametric optimization (on volumes and flow rates) for both structures are presented figures 5 and 6; the comparison between the responses of each model and the experimental curve is then realized (cf. figure 7).

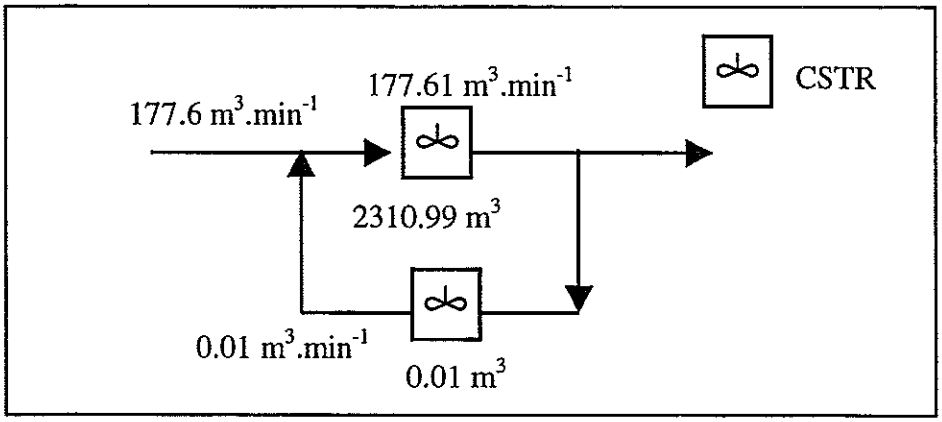

Figure 5. Two zones-model

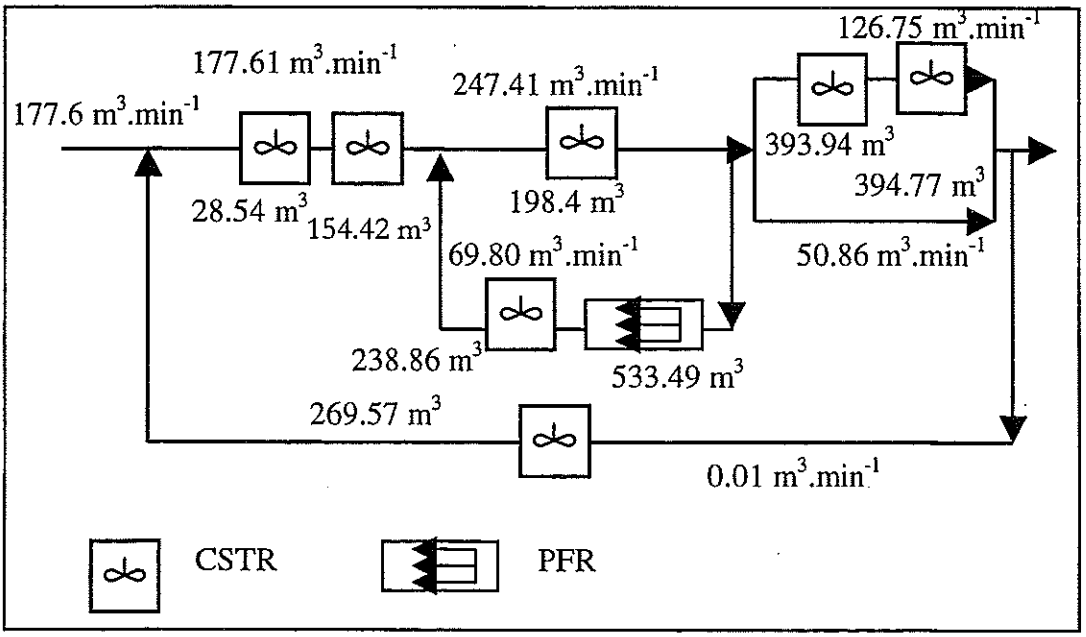

Figure 6. Other model

It is obvious that the "two zones model" cannot represent correctly the air flow patterns inside the enclosure: the flow rate and the volume of the CSTR corresponding to the recirculation are equal to the minimal bound. The optimized model is then closed to an unique CSTR. As to the other model, it seems to be quite satisfactory: the resulting RTD curve shows a first peak, closed to the experimental one, and a second one, more attenuated. Nevertheless, the structure could be improved.

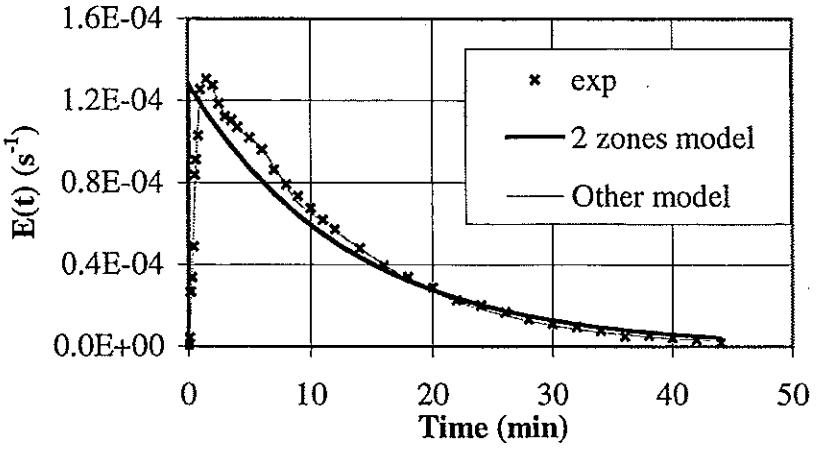

Figure 7. Comparison between experiment and models in case of parametric identification

3. Structural identification

The second stage of the analysis consists in structural identifications. Among the structures proposed by the code, only one has been retained as the most physically probable; it is presented figure 8. The comparison between the experimental curve and the simulated one corresponding to the structure retained is presented figure 9.

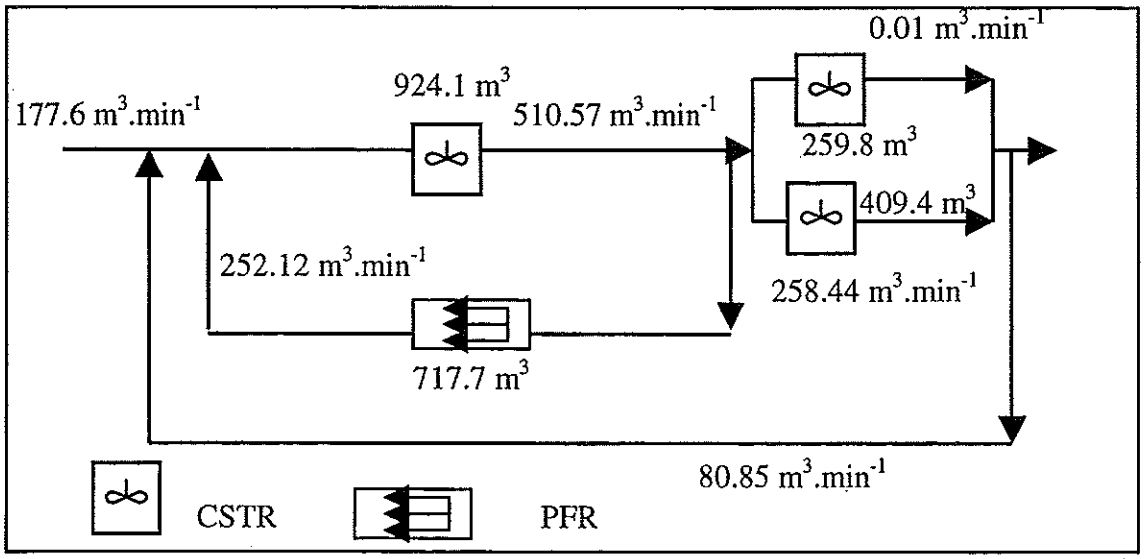

Figure 8. Model obtained by structural identification

The model then obtained is very similar to the one used in the parametric identification. It comprises also two recirculations: one is constituted by a PFR alone, and the main one is constituted by a short-circuit. This structure leads to a RTD curve close to the experimental one, and is quite satisfactory, from a physical point of view.

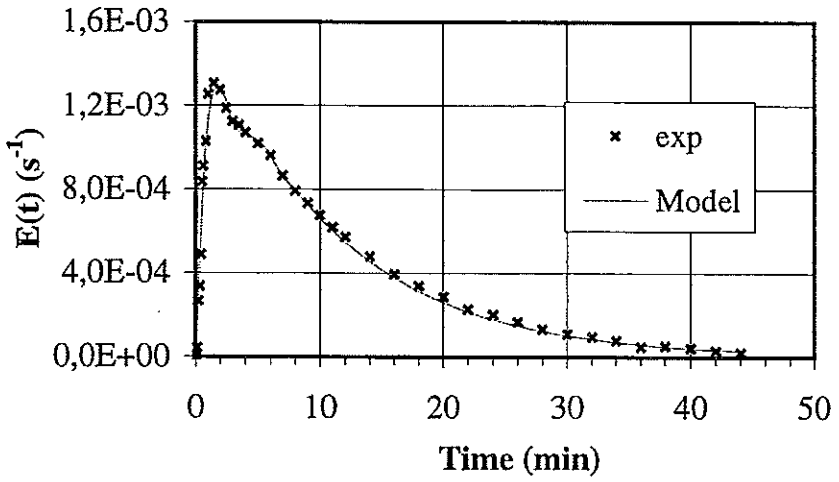

Figure 9. Comparison between experiment and model obtained by structural identification

CONCLUSION

The computational package IDTS presented in this paper constitutes an useful and innovative tool to elaborate residence times distribution models in order to characterize flow patterns and associated transfers. An application on a real ventilated enclosure has been realized. The results obtained by parametric and structural identification are quite satisfactory and propose models whose RTD curve is closed to the experimental one. Works are in progress in order to try to associate physical zones inside the room, where a contamination source is located for instance, with the zones of the structure obtained by the code.

REFERENCES

[1] Laquerbe C., *Modelisation of the air flow in a ventilated enclosure by a systemic approach*, INP Toulouse Thesis, France (1999)

[2] Drécourt S., Laborde J.C., Domenech S., Floquet F., Laquerbe C., Viguier D., *Développement d'un outil de calcul appliqué à la caractérisation d'une ventilation par traçage et basé sur l'approche systémique*, Congrès Traceurs et méthodes de traçage, France (1999)

[3] Holland J., *Adaptation in natural and artificial systems*, MIT Press, Cambridge (1975)

[4] Soares S., Domenech S., Laborde J.C., Laquerbe C., Ricciardi L., *Simulation of air flow distribution in rooms by a systemic approach*, Air Distribution in Rooms ROOMVENT (2000)

TRACER METHODS APPLIED TO ON-SITE WASTEWATER TREATMENT FACILITIES

A.Bennachera, C.Beck

Laboratoire des Systèmes Hydrauliques Urbains, ENGEES, 1, quai Koch, 67070 Strasbourg, FRANCE.

Abstract. Tracer methods, currently used in chemical engineering domains, may also be used to study on-site wastewater treatment process. In this case, these tools are useful to characterise global hydraulic patterns and suspended particles transportation. As most units are under ground and cannot be easily observed, an advantage of tracing techniques is also that they only need an injection and a sampling point at the exit.

The aim of our study on pretreatment systems as septic tanks was to get data on hydraulics and performance of existing units, to rely this results to geometric design and, if possible, to propose new design features to improve the system efficiency.

Key words: on-site wastewater treatment, septic tank, tracer studies, RTD, mixing, hydraulics, modelling.

INTRODUCTION

On-site wastewater treatment techniques are primarily used in rural zones or in suburban areas.

In France, 22 million permanent inhabitants and 14 million seasonal inhabitants are distributed in the 34 400 rural communes classified within the meaning of the code of the communes [1] [2] [3].

11 millions inhabitants of the " rural " population are directly concerned by on-site wastewater treatment, which accounts for 30% of this population.

Generally, an on-site wastewater treatment system is made of a pretreatment by septic tank, which receive both waters coming from toilets and from domestic activities, and an aerobic treatment by an underground spreading in the original or reconstituted ground.

Septic tank has as a role to prepare domestic effluents for their purification by the device of treatment located at its downstream. It ensures the anaerobic digestion of the solid and floating matters constituting sludge and the cap of greases. But its most significant role is the retention of the suspended matter responsible for the clogging of the spreading system [4] [5]. So the septic tank is a decanter whose correct operation depends mainly on its hydraulic characteristics and its geometry [6] [7].

Figure 1 below represents a typical diagram of a septic tank. The principal differences between the devices proposed by the various manufacturers in France or Europe are mainly linked to the design of the output or entry devices, with or without internal walls of different configurations. The geometrical forms are mainly parallelipipedic shapes or more or less cylindrical forms, depending on the manufacturing techniques and on raw materials employed (concrete, fiber glass, plastics...) [8] [9].

At the lawful level [10], the decree of May 6 specifies the main technical devices authorized in France and gives bases of dimensioning for the works (essentially minimum volumes or water height on the basis of the number of rooms).

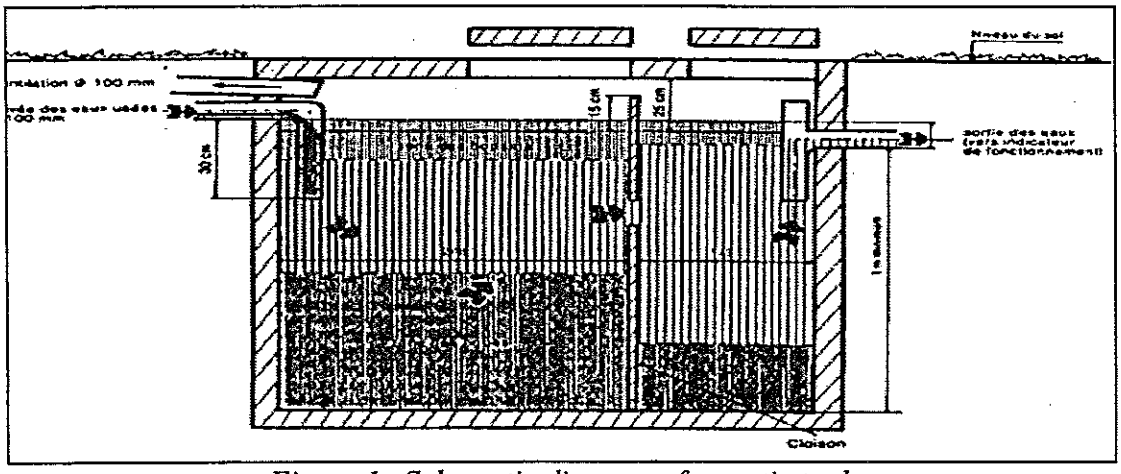

Figure 1. Schematic diagram of a septic tank

In complement, the DTU 64.1 sets the standards and specifies the code of practice which must be applied to the autonomous cleansing works[11].

Thus, in France, the dimensioning of the pretreatment works is based on the number of principal rooms of the house, with a minimum volume of 3 m^3.

The other imposed characteristics relate to the height of water, at least of 1 m, but no precision is given concerning inside septic tank configuration.

From an hydraulic point of view, an improvement of the pits geometry can provide a more effective decantation. Should then be adopted techniques aiming :

- to reduce turbulences responsible for the handing-over in suspension of the elutriated particles and the drive of the cap of grease towards the treatment device;
- to suppress short circuits which lead to the clogging of the spreading system or of the prefilter;
- to obtain a sufficient residence time to maximize the capture of the suspended matter inside the septic tank.

The goal of our study is to characterize hydraulic operation of an "all water" pit according to its initial geometrical design.

MATERIALS AND METHODS

1. Methods of measurement

Usually, the hydrodynamic study of the decantation works consists in the determination of speed profiles and utilizing the Navier-Stokes equations. Such an operation requires significant means of calculation and can prove less convincing if the aim of the study is not the search for an analytical approach of the hydrodynamics of the system [12].

Tracing techniques, commonly used in the field of chemical engineering, were used preferentially to characterize in a total way the hydraulic behavior of the works by the experimental measurement of the residence times distribution (RTD).

2. Interest of the RTD measurement

The RTD is a particular characteristic of the system. It relies any disturbance at the entry to an associated answer at the output of the work. Obtaining the RTD curves

allows the construction of a flow model and to thereafter forecast the performances of the reactor.

The total flow in a work is the result of the flows in various zones where the conditions are particular.

The observation of the RTD curves can give a precise idea on the anomalies of flow and makes it possible thereafter to bring judicious solutions leading to the improvement of the geometry of the work.

3. Implementation of the tracing method

The tracing method consists in causing a tracer concentration disturbance at the entry of the pit and following according to time the variations of concentration at the exit. The tracer must have the same flow properties as the molecules of the fluid. It must be injected through a weak section to ensure its good mixing and to take into account weighting in flow [13].

In our case, the injection is similar to a pulse. The tracer is injected instantaneously at the entry of the system, without disturbing the flow and with a not too high concentration, in order to avoid the appearance of transitory currents of convection, resulting from the difference of density between the injected solution and that of the fluid.

The tracer employed is the lithium chloride (LiCl), because it has the following advantages [14] :

- A very low detection and measurement limit;
- No-toxicity;
- Presence at very low concentration in drinking waters and urban waste water.

The system being fed with a known flow, samples are taken at exit at regular time step and are analyzed by atomic absorption spectrometry in the flame.

4. Experimental setup

The experimental device is a laboratory pilot built with the aim to study hydraulic patterns of two types of "all water" pit (rectangular and cylindrical), considering the works as simple tanks crossed by given clear water flows.

4.1. Description of the pilot

The general outline of the pilot is represented on Figure 2; it comprises:

- A clear water supply (tap water), directly on the network;
- A flow measurement and controlling device: a membrane valve and a needle valve associated with two flowmeters (range 25-160 l/h and 0.4-6.4 m^3/h);
- A volumetric pump (max. flowrate =2 l/h), for the tracer injection at the input of the "all water" pit
- A rectangular "all water" pit of 3.45 m^3 volume;
- A cylindrical pit of 4 m^3 volume in parallel with the rectangular pit;
- A whole of programmable automatic samplers.

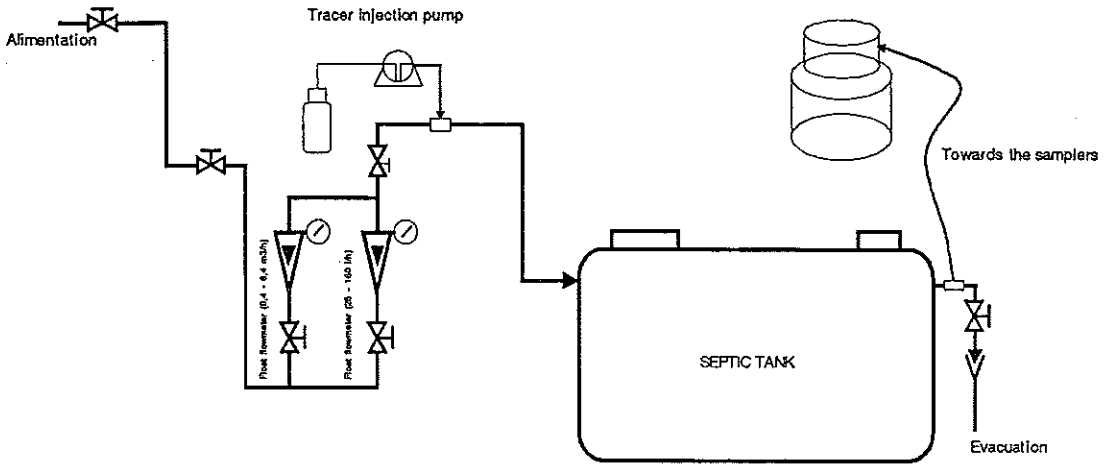

Figure 2. Schematic diagram of the laboratory pilot

4.2. Description of the studied pits

The geometrical characteristics of the two "all water" pits studied are given in table 1:

Table 1 : Geometrical characteristics of the pits

	Length (m)	Width (m)	Height (m)	Diameter in./out (mm)
Rectangular	2.65	0.89	1.61	110
Cylindrical	2.65	1.48	1.33	110

The two pits are connected in parallel, being fed continuously. One changes the flow each time that one begins a new handling, in order to cover all the load range the pit can receive. Under real operating conditions, flowrates of water that the pit receives are extremely variable, between zero and a peak value of approximately 1.5 l/s.

5. Determination of the RTD

Taking at the moment t=0 a quantity M of a tracer of concentration C injected at the entry of the work, following the evolution of the concentration c(t) on the outlet of the work, one then obtains the curve of residence times distribution. Let us normalize by surface, one will obtain the E(t) function which is given by the relation:

$$E(t) = \frac{C(t)}{\int_0^{\infty} C(t)dt} \qquad (1)$$

With :

$$\int_0^{\infty} E(t)dt = 1 \qquad (2)$$

The RTD can be described by some of its characteristics[13], called moment, which makes it possible to reach parameters such as the average value of the distribution, its dispersion, etc.

The n order moment around the origin is defined by:

$$\mu_n = \int_0^{\infty} t^n E(t)\,dt = \frac{\int_0^{\infty} t^n c(t)\,dt}{\int_0^{\infty} c(t)\,dt} \qquad (3)$$

What gives :

$$\mu_0 = \int_0^{\infty} E(t)\,dt = 1 \qquad (4)$$

$$\mu_1 = \int_0^{\infty} tE(t)\,dt = \tau = \frac{V}{Q} \qquad (5)$$

V being the accessible volume by the fluid, and Q the rate of feed.

The interpretation of the results obtained was made by the observation of the obtained curves shapes, by calculation of the moments values, and by comparison between the experimental curves and those obtained by simulation of various models with software " DTS " v3.1 (Progepi/Sysmatec).

RESULTS AND DISCUSSION

1. Comportment of the rectangular septic tank

1.1. Experimental results

Figure 3 shows the result of a tracing test on the rectangular pit presented at the § 4.2 (nominal volume =3450 l). The pit was fed continuously with a constant flow of 50 l/h during 207 H (approximately 3 times average residence time).

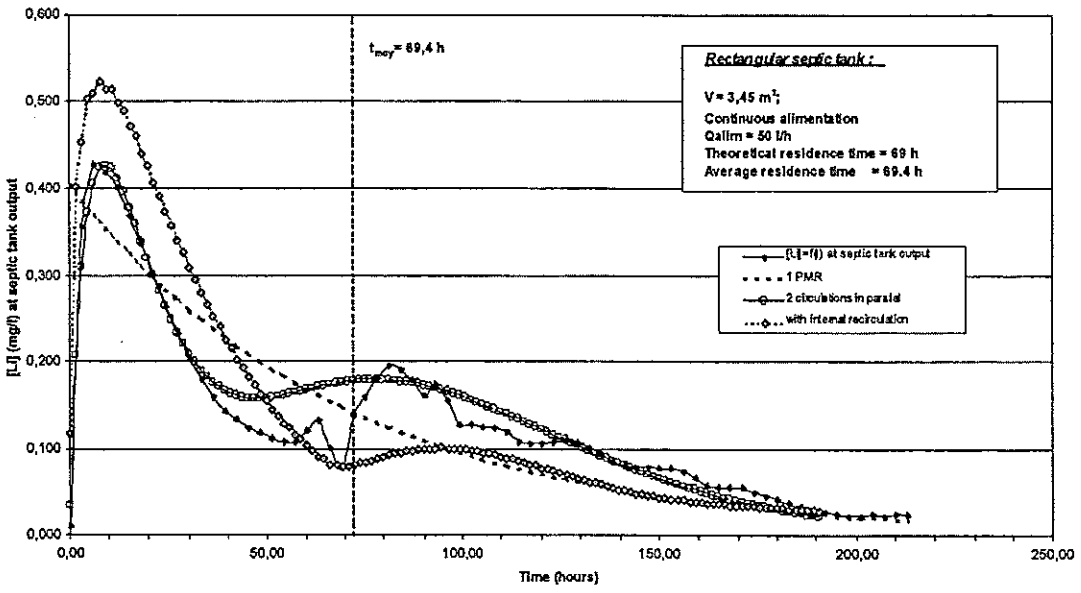

Figure 3. Rectangular pit : experimental tracing test result

One notices on this curve the existence of a first peak of concentration, 6 h after the injection of the tracer, and a second less significant peak after 81 h of the

beginning of handling. While basing oneself on the curve of RTD, one could establish his principal characteristics (average residence time, moments and the variance) which are reported in the table (2):

Tableau 2. Characteristics of the RTD test on the rectangular pit

Average residence time (h)	69.4
μ_0	68.9
μ_1	69.4
μ_2	7766.1
σ	2946.4

1.2. Interpretation

The internal configuration of the pit schematically includes a plunging entry with a bent tube and an exit of the same type, with a tube of larger diameter. Because of its manufacturing process and for reason of mechanical resistance, the tank also includes reinforcements which constitute two internal partitions located at each third length (see figure 4).

Figure 4 : Internal configuration of the rectangular pit

The presence of two peaks (figure 3) could be a sign of the existence of two parallel layers of flow, or of internal recirculations, these undoubtedly related to the presence of the transverse walls.

Our first attempts at modeling, led us to test various combinations of elementary reactors, respectively:

- *model 1:* two branches of flow in parallel, each one represented by an association of several perfectly mixed reactors (PMR) in series
- *model 2:* a branch of flow represented by a series of perfectly mixed reactors in series, and a recirculation branch represented by a pure delay.

Although the representation by these models is not optimized yet, those make it possible to give a first approach of internal circulations inside the tank while reasoning by analogy. In our case one can then make the assumption of the presence of internal recirculations and/or of various ways of parallel flow which will be able to harm the correct operation of the system, in particular by impact on the decantation.

2. Comportment of the cylindrical pit

2.1. Results

The same procedure was carried out on an "all water" pit of cylindrical type of a volume of 4000 l. The pit was fed continuously with a constant flow equal to 50 l/h during 240 hours of total time.

Figure 5 represents the RTD curve obtained. On this curve, one observes a significant trail which could be linked to a dead zone where the flow should very slow or quite equal to zero.

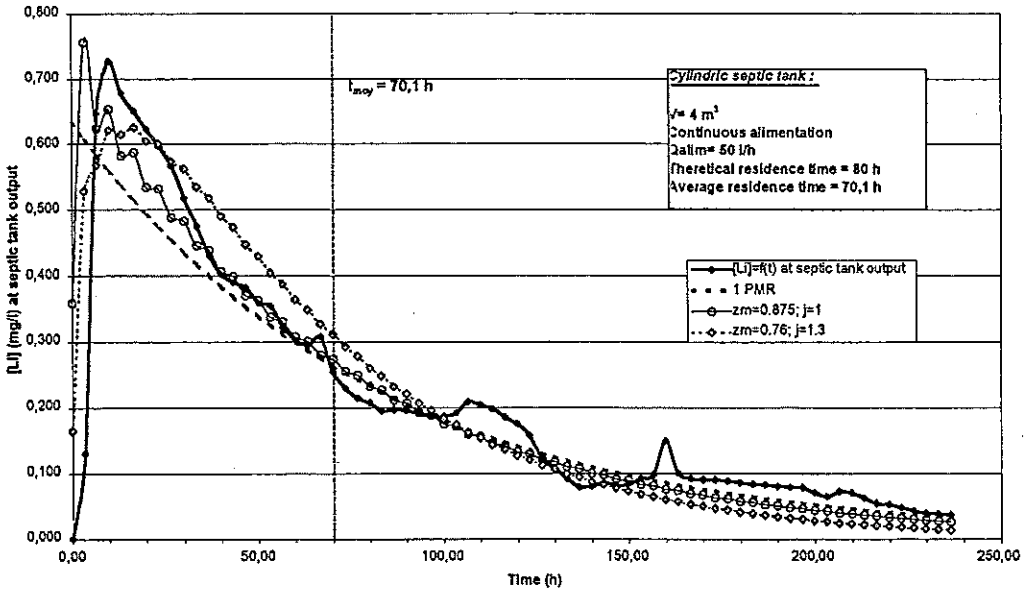

Figure 5. Cylindrical pit : experimental tracing test result

Main characteristics of the RTD curve are reported in table 3.

Tableau 3. Characteristics of the RTD test on the cylindrical pit

Average residence time (h)	0.86
μ_0	1.00
μ_1	0.86
μ_2	1.32
σ	0.58

2.2. Interpretation

Contrary to the rectangular pit, the cylindrical pit comprises entries and exits bent, but not internal walls.

The obtained curves are close to those which one would have for a perfectly mixed reactor (PMR). One can in addition note an experimental average residence time (70 h) weaker than the theoretical residence time (80 h). The peak observed at the beginning of the curve is in addition higher than for a PMR (gone up faster in concentration), which lets suppose the presence of a died zone, possibly of preferential flows, even of short-circuits.

One notes that the difference between the theoretical residence time T and the average residence time is 10 h, which leads to a stagnating volume of 500 l.

Different models, built from combinations of several PMR, with a more or less significant fraction of died zone, were tested. Although none of them permitted to describe with precision the real behavior of the work, one can note the absence of demonstrations of recirculations on the curves, which lets suppose better conditions of flow for the decantation in the case with the cylindrical pit, not partitioned.

CONCLUSIONS / PERSPECTIVES

The use of a tracing technique with lithium chloride was validated to characterize the RTD of various pretreatment works dedicated to autonomous cleansing. The tracing technique with the use of lithium permitted to have a general idea on the operation of these works and to evaluate the impact of various types of interior installations. The study of the hydraulic aspects and decantation is to be continued with wastewater on an arranged site, associated in addition to local velocity measurements and to a digital simulation of the flows.

SPECIAL THANKS

This study was carried out within the framework of a study convention with the company Sotralentz, French manufacturer of wastewater treatment equipment, with the collaboration of the LEGTA (Lycée d'Enseignement Général et Technologique Agricole) at Obernai and the ENSAIS (Ecole Nationale Supérieure des Arts et Industries de Strasbourg) in Strasbourg.

REFERENCES

[1] Environnement et Techniques, *Etat de l'assainissement non collectif en France*, N° 182, December 1998.

[2] Lesavre, J., Alexandre, O., *Assainissement autonome-assainissement groupé : Aspects techniques et économiques des différentes filières, Agence de l'eau Seine-Normandie, Cemagref-ENGEES*

[3] Agence de l'Eau Artois Picardie, *L'assainissement non collectif, une technique adaptée à l'habitat dispersé*, July 1997.

[4] Agence de Bassin Loire Bretagne, *L'assainissement individuel. Principes et techniques*, Etude inter-agences, 1980.

[5] Direction Départementale de l'Equipement, *Guide de l'assainissement non collectif*, January 1998.

[6] Garancher J. *L'assainissement autonome individuel et collectif*, Edition du MONITEUR, 1986.

[7] Hamou B., *Assainissement autonome, épuration des eaux usées des bâtiments d'habitation*, Centre d'assistance technique et de documentation, July 1982.

[8] Blanic R. et Benneton J.P., *Caractérisation d'effluents d'assainissement individuel et essai de matériels*, T.S.M, November 1989.

[9] Tribune de l'Eau. *Assainissement individuel et autonome*, N° 6, November/December 1992.

[10] Ministère de l'Aménagement du Territoire et de l'Environnement, *Recueil de textes réglementaires sur l'assainissement*, CERTU, January 1998.

[11] AFNOR. *Document Technique Unifié* (DTU 64.1), August 1998.

[12] Villermaux, J., *Génie de la réaction chimique*, Ed. TEC&DOC-LAVOISIER, (1993), 167.

[13] Sardin M., *Systèmes à paramètres distribués et systèmes à paramètres localisés équivalents*, DEA course, ENGEES, 1999.

[14] Bendounan, R., *Hydrodynamique et performances d'un décanteur primaire de station d'épuration des eaux usées urbaines*, phD thesis, INPL, 1995.

[15] Valiron, *Mémento de gestionnaire de l'alimentation en eau et de l'assainissement*, 1994.

[16] Vasel J. L. et Evrard V., *Assainissement en zone rurale*, Text of a seminar organized at FUL, Arlon (Belgium), May 23-31, 1996

B B5 - FOOD ENGINEERING AN BIO-ENGINEERING

STUDY OF THE SUGAR INGOT FLOW-PATTERNS IN THE NOTRE-DAME REFINERY SILO IN OREYE

N. Job[1], A. Dardenne[2], J.P. Pirard[1]

[1] Université de Liège, Institut de Chimie B6a, Laboratoire de Génie chimique, B-4000 Liège, BELGIUM
[2] Raffinerie Tirlemontoise S.A.-Tiense Suikerraffinaderij N.V., 1, Aandorenstraat B-3300 Tienen, BELGIUM

Abstract. The silo installed at the Notre-Dame Refinery in Oreye was designed for a plug flow pattern of Höweler sugar ingots introduced at its top in order to ensure effective drying of the sugar. Because of excessive moisture content in the extracted ingots, the Notre-Dame Refinery called into question the quality of ingot flowing in the silo. The silo flow-pattern was studied by introducing as a tracer sugar lumps layered at the top of the silo filled with 388 tons of sugar ingots. The tracer concentration was measured in samples collected at the silo outlet. Ingots and tracer in each sample were separated and weighed. The results show that the silo flow-pattern is not plug flow type in its whole volume. Only the central volume, corresponding to an internal cylinder whose diameter is roughly equal to the diameter of the small base of the truncated cone, flows whereas the external residual volume remains motionless and can be considered as a dead zone. The tracer test also enabled detecting preferential flow patterns in the silo. This study has led to improving the internal silo equipment.

INTRODUCTION

The silo installed at the Notre-Dame Refinery in Oreye was designed for a plug flow pattern of Höweler sugar ingots introduced at its top to ensure effective drying of the sugar. Because of excessive moisture content in the extracted ingots, the Notre-Dame refinery questioned the quality of ingot flowing in the silo. The silo flow-pattern was then studied by the tracer method.

The silo geometry could be divided into two parts : an upper cylinder (10 m in diameter and 4.60 m in height), and a lower truncated cone (10 m in diameter in its larger base, 6.40 m in diameter in its smaller base and 4.30 m in height). The sugar was extracted at the bottom of the silo using a 3-m long blade unloader, which was supposed to ensure a plug flow pattern of the Höweler ingots. Inside the bottom part of the silo, a metal cone, 3.30 m in height and 3.90 m in diameter, carried the sugar to the unloader end.

The tracer test performed here consists of a single experiment intended to quickly solve a practical industrial problem. To our knowledge, no previous similar test has been carried out. The experiment enabled to show that the silo flow-pattern is not plug flow type in its whole volume. Only the central volume, corresponding to an internal cylinder whose diameter was roughly equal to the diameter of the small base of the truncated cone, flowed whereas the external residual volume remained motionless and could be considered as a dead zone. The tracer test also enabled detecting preferential flow patterns in the silo. This study has led to improving the internal silo equipment.

EXPERIMENTAL

After complete emptying, the silo was filled with 388 tons of Höweler sugar ingots according to the profile shown in figure 1a. This profile displays a central cone whose tip was also filled with Höweler ingots so that the smaller base of the obtained truncated cone was 2 m in diameter. The remaining truncated cone, filled with 10 tons of sugar lumps, formed a tracer layer (truncated cone : 1.48 m height, 2 m in its smaller base, 5.1 m in its larger base). The sugar was then extracted at the rate of 50 tons a day. The extraction and filling rates per hour could fluctuate. So it was scheduled to restore the maximum level every morning at the same hour, just before measuring the silo profile.

In order to standardise the results, the considered variable was the number of blade unloader revolutions, not time. A complete unloader revolution was estimated to correspond to the extraction of 4.09 tons of sugar. For every revolution, 5 samples of sugar were taken from 5 equidistant positions of the unloader, in order to gather complete data on silo flow patterns. The first sample-taking corresponds to the appearance of the first sugar lumps.

The samples were taken by stopping the conveyor belt for a few minutes and removing all the accessible sugar. Ingots and tracer in each sample were manually separated and weighed. Fine and unclassified lumps were separated, but make up a very small part of the collected sugar. Table 1 shows the weight percentage of tracer in the extracted sugar for every unloader position. After the first tracer appearance, 10 unloader revolutions were necessary to recover 95% of the sugar lumps. Afterwards, the samples were taken every 3 positions of the unloader. The measurements were stopped after 13 revolutions.

RESULTS

The tracer appeared between 32 and 33 unloader revolutions. The quantity of sugar extracted before the tracer appearance was estimated to be 131.6 tons, which corresponds to 174 m^3 of sugar and to 32.2 unloader revolutions.

Results are shown on table 1. Each line of the table represents one unloader revolution (from 33^{rd} to 46^{th}), and each column represents one blade unloader position. Concentration maxima for each unloader position are surrounded with a rectangle, and minima are in bold. The last column gives the mean sugar lump percentage for each unloader revolution, and the sum of the columns is calculated (above every column). The tracer mass balance is quite correct as 9.96 tons out of 10 are recovered at the silo outlet.

The main basic data are grouped on table 2, and the geometric dimensions (measured and calculated) are shown on figures 1a and 1b.

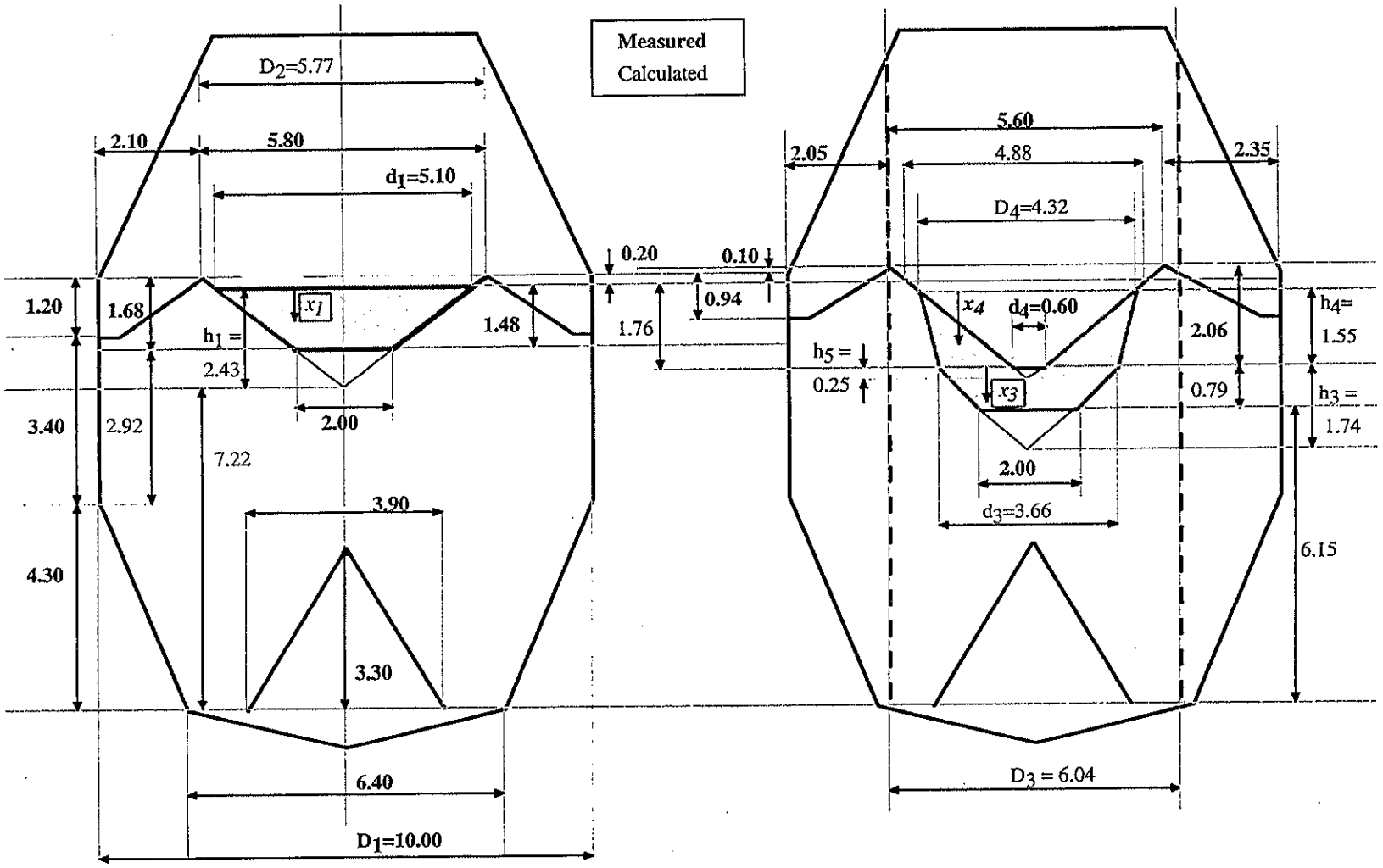

Fig. 1a. Initial state

Fig. 1b. State after crater formation

Table 1. Global results

position	1	2	3	4	5		
Σ columns						396.8	min. not included
before min.	103.9	84.8	125.6	45.5	37.1	436	min. included
unloader			sugar lump concentration				mean
revolution nr			(% weight)				concentration (%)
33	12.0	2.3	2.9	3.9	15.3		7.28
34	13.7	5.4	9.1	13.3	21.8		12.66
35	37.2	32.7	4.5	28.3	**7.8**		22.10
36	40.9	19.1	6.1	**8.8**	33.9		21.76
37	**4.8**	25.3	50.5	29.3	57.9		33.56
38	32.1	**4.4**	52.5	21.5	44.7		31.04
39	34.4	48.3	**13.4**	47.6	65.6		41.86
40	12.6	50.0	21.4	26.9	43.9		30.96
41	8.4	55.5	7.7	29.1	26.5		25.44
42	3.3	6.7	10	3	10.6		6.72
							mean : 23.33
% tracer	17.0	21.4	15.3	18.1	28.1		
43			3.9				3.9
44	8.0			2.2			5.1
45		4.3					4.3
							mean : 4.43
mass balance upon 12.2 revolutions						9.96 tons of extracted tracer	

Table 2. Data

specific mass of Howeler ingots	0.75	tons/m³
specific mass of sugar lumps	0.633	tons/m³
introduced tracer mass	10	tons
ingot mass at the beginning of the experiment	388	tons
extraction rate	4.09	tons/unloader revolution

DISCUSSION

The experimental tracer concentration versus the number of unloader revolutions is shown on figure 2. This curve was compared to those calculated from three models : plug flow type, central chimney flow type and chimney with crater formation flow type. The theoretical curves corresponding to the last two models are also shown on figure 2.

1. Plug flow type

Referring to figure 1a, the quantity of sugar to be extracted before the tracer appears corresponds to a volume that includes two parts : the bottom part of the silo (truncated cone, metallic distribution cone excluded) and one cylinder (10 m in diameter and 2.92 m in height). This volume (447 m³) corresponds to 336 tons of sugar, i.e. 82 unloader revolutions. In order to extract all of the introduced tracer, a cylindrical volume (10 m in diameter and 1.48 m high) must then be eliminated. 21 additional unloader revolutions are necessary to complete the tracer extraction.

From revolution 82 to 103, the tracer concentration is :

$$C_1(\%) = 100\frac{d_1^2}{D_1^2}\left(1-\frac{2x_1}{h_1}+\frac{x_1^2}{h_1^2}\right) \qquad x_1 \in [1{,}48-0]$$

The tracer test indubitably shows that the silo flow pattern is not plug flow type, as it was designed for. A silo running in a plug flow regime would result in the tracer appearing after 82 unloader revolutions, with a concentration of 4%. The last sugar lumps would have disappeared after 103 revolutions, with a concentration of 26%. On the contrary, the first sugar lumps already appear during the 33rd revolution, and the average concentration exceeds 40% during the 39th revolution. After 45 unloader revolutions, the sugar lump concentrations fall below 5% and more than 95% of the tracer is recovered.

2. Central chimney flow type

As the theoretical residence time of the plug flow type model largely exceeds the experimental one, one could imagine that only the central part of the silo flows, whereas the external ring remains motionless and can be considered as a dead zone.

Experimentally, the quantity of sugar extracted before the tracer appearance amounts to 131.6 tons of Höweler ingots (=157.4 m³). This quantity requires 32.2 unloader revolutions. Assuming that a central chimney flows according to a plug flow pattern, the volume of this chimney is the extracted sugar volume increased by the distribution cone volume (=13.2 m³). The height of the chimney is related to the distance between the silo bottom and the smaller base of the truncated cone originally filled with the tracer (=7.22 m). A chimney diameter of 5.77 m can then be calculated.

The sugar quantity to be extracted before recovering the entire tracer makes a 1.48 m in height, 10 m in diameter cylinder whose volume (38.7 m³) corresponds to 29 tons of sugar extracted by 7.1 unloader revolutions. From revolution 32.2 to 39.3, the tracer concentration is :

$$C_2(\%) = 100\frac{d_1^2}{D_2^2}\left(1-\frac{2x_1}{h_1}+\frac{x_1^2}{h_1^2}\right) \qquad x_1 \in [1.48-0]$$

The obtained theoretical curve is shown in figure 2. According to this model, the tracer would appear during the 33rd revolution with a concentration of 12%, and the

last sugar lumps would be recovered after 39 revolutions with a concentration of 78%. This model does not account for the long tracer tail experimentally observed.

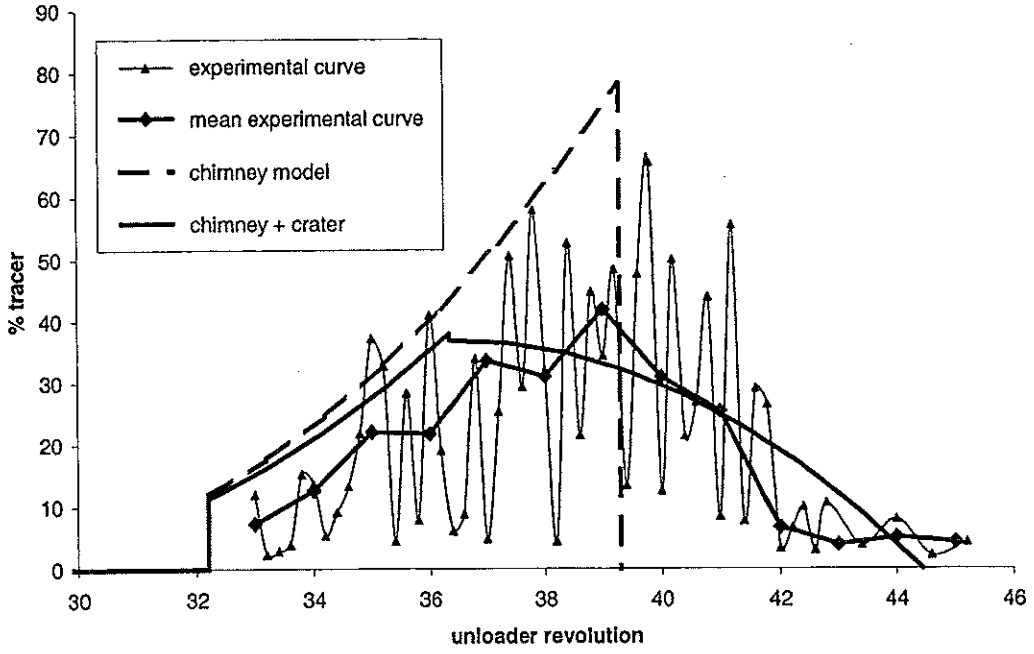

Fig.2. Experimental and simulation curves : chimney flow type and chimney with crater formation flow type

3. Chimney with crater formation flow type

Comparison between sugar profiles at the beginning of the experiment (fig.1a) and when the silo runs in normal working conditions (fig.1b) shows that the sugar level does not decrease systematically. A crater is first formed in the centre of the silo. One can then assume that the working behaviour passes through 2 phases : crater formation followed by systematic sugar drop.

During the crater formation, the tracer, which originally settled following a truncated cone would evolve into a rather complicated shape (fig.1b). The bottom part of the original tracer truncated cone would drop without any modification, whereas the upper part would spread on the crater walls. Considering this new geometry, the tracer concentration profile at the outlet must go through a maximum : the concentration increases during the extraction of the unchanged truncated cone, and must decrease during the extraction of the sugar spread on the crater walls.

The tracer mass balance points out that the total quantity of sugar extracted between the 33-1 sample and the 42-5 sample (quantity extracted by 10 unloader revolutions) corresponds to 9.54 tons of tracer. The quantity extracted before the concentration minimum is 3.24 tons (5.12 m^3 of tracer) and could correspond to the truncated cone that systematically drops without getting out of shape. The smaller base of this truncated cone is still 2 m in diameter and one can calculate its larger base diameter (3.66 m) and its height (0.79 m). These dimensions are transferred to figure 1b.

The crater (truncated cone) is 2.06 m in height, 5.6 m and 0.60 m in diameter respectively for its larger base and smaller base. According to the original and the regular situations of working, the horizontal tracer level goes down 1.76 m between the beginning of the experiment and the end of the crater formation. The crater formation needs to extract a sugar volume corresponding to another truncated cone whose height and smaller diameter are 0.6 m and 1.76 m respectively. One can calculate that this truncated cone's larger diameter equals 4.88 m, and that its volume is 12.5 m³, which corresponds to 9.37 tons of sugar. Thus, 9.37 tons of sugar must be extracted (by 2.3 unloader revolutions) to form the crater and to reach the steady-state flow rate. When the crater is formed, 162.9 tons of sugar remain to be extracted before any tracer appearance. This requires 29.9 unloader revolutions. Then, 32.2 unloader revolutions are actually needed before the first sugar lumps appear.

When the steady state is reached, the sugar flows following a chimney, and the flow-pattern is supposed to be plug flow type. The volume of this chimney amounts to the volume of sugar that remains to be extracted before the tracer appearance increased by the distribution cone volume (= 176.1 m³). Chimney sizes are respectively 6.15 m in height and 6.04 m in diameter.

The total volume to be extracted to eliminate the bottom tracer truncated cone corresponds to a cylinder 0.79 m in height and 6.04 m in diameter. Its volume (22.64 m³) is extracted by 4.15 unloader revolutions. From revolution 32.2 to 36.35, the tracer concentration at the outlet is then :

$$C_3(\%) = 100\frac{d_3^2}{D_3^2}\left(1-\frac{2x_3}{h_3}+\frac{x_3^2}{h_3^2}\right) \qquad x_3 \in [0.79-0]$$

After the concentration maximum, the remaining tracer mass to be extracted is 6.76 tons, which corresponds to 10.68 m³. This tracer volume is related to the difference between two truncated cones : the sizes of the first one are 3.66 m, D_4 and h_4 for its smaller base, larger base and height respectively. The sizes of the second one are 0.60 m, D_4 and h_4 for its smaller base, larger base and height respectively (fig.1b). Calculation shows that D_4 and h_4 are respectively 4.32 m and 1.55 m. The volume of sugar to be extracted thus represents a chimney 1.55-m high, 6.04 m in diameter, i.e. 44.41 m³ of sugar extracted by 8.1 unloader revolutions. The tracer concentration at the outlet from revolution 36.15 to 44.45 is then calculated to be :

$$C_4(\%) = 400\frac{(d_3-d_4)x_4}{2h_4D_4^2}\left(\frac{(d_3-d_4)x_4}{2h_4}+D_4-\frac{D_4x_4}{h_4+h_5}\right) \qquad x_4 \in [1.55-0]$$

The tracer concentration profile given by this model is shown in figure 2. According to this model, the tracer is completely recovered after 44.45 unloader revolutions, and the theoretical tracer concentration reaches a maximum of 38%, which agrees rather well to the experimental measurements.

4. Local flow anomalies

The analysis of the measurements carried out for every unloader position enables detecting local anomalies in the silo working. The evolution of the tracer concentration with regard to the revolution number shows that, for every position of the unloader, the concentration increases, reaches a maximum, drops steeply, reaches a maximum again and then decreases progressively to tend to zero. In our opinion, these minima are completely accidental. During the crater formation, the silo supply was kept continuous with a rate of about 2 tons/hour. A small fraction of these ingots could have been trapped inside the tracer. Therefore, the tracer was accidentally labelled. The minima (in bold in table 1) appear at different revolution numbers for every position : the minimum appears firstly at position 5 (33rd revolution) and lastly at position 3 (39th). It must be noted that position 3 is opposite to position 5. This enable deducing that the dropping rate is 10% higher in position 5 than in position 3. The tracer mass balance also shows a preferential way of flowing: 28.1% of the tracer was collected in position 5, even though the mean is 18%. Another clue is that the crater is not completely regularly formed but slightly eccentric.

CONCLUSIONS

This tracer test shows that the silo flow pattern is not plug flow type : for a capacity of 400 tons, only 150 actually flow, whereas 250 remain completely motionless. The mobile part of the loading flows following a chimney which is about 6 m in diameter. At the beginning of the extraction, a central crater is first formed and remains during extraction. This phenomenon futher reduces the effective capacity of the silo which drops to 130 tons if the purpose is to ensure a sufficient drying of all ingots. The sugar flow pattern following the central chimney is not regular. The maximum extraction rate appears in the area corresponding to position 5 of the unloader. The useful volume of the silo is shown on figure 1b (dotted line).

IDENTIFICATION BY FLUORESCENT TRACERS OF THE SPECIFIED RISK MATERIALS IN THE MEAT AND BONE MEAL INDUSTRY

J.P. Chanet[1], J.P. Frencia[2], G. Beaudoing[3], M. Berducat[1]

[1] Cemagref, UR TSCF, 24 Av. des Landais, BP 50085, 63172 Aubière Cedex, France.
[2] ADIV, 2 rue Chappe, 63039 Clermont-Ferrand Cedex 2, France.
[3] CEA, DTA/DAMRI/SAT, 17 rue des Martyres, 38054 Grenoble Cedex, France.

Abstract. For the by-products resulting from ruminant, the French regulation imposes the following constraints: I) separation of specified risk materials from the materials which can be used for animals feed, in particular by separating their circuits of collection and processing; II) denaturation of specified risk materials, then incineration after their transformation into Meat and Bone Meal. The markers currently used to denature specified risk materials do not resist to the thermal treatment of the transformation process into Meat and Bone Meal intended to be incinerated. We have developed an identification and marking system of specified risk materials containing fluorescent tracers. This marking resists to the thermal treatment and allows a detection of the marked materials throughout process of transformation. This method was developed in laboratory and was validated on an experimental device.

INTRODUCTION

In France, before the total Meat and Bone Meal (MBM) ban for animal feeding, at the end of 2000th, only meat wastes coming from animals suitable for human consumption could be used for the manufacture of MBM. Moreover, the specified risk offals of bovine and ovine/caprine, just as the sanitary seized products and the animals died in the farms, must be collected separately and intended for the incineration.

The regulation defines two categories of by-products in the slaughterhouses and the cutting rooms:

- Specified Risk Materials (SRM) (central nervous system of the cattle, sheep and goats, thymus, spleen, tonsils and intestines) which are intended for the incineration after transformation into MBM;
- the products which can be transformed into MBM for the feeding of animals other than the ruminants, or used in the petfood.

The French regulation is based on the principle of separation of the collection and of the processing chains right from the slaughterhouse.
In order to offer more significant guarantees with regard to the separation of the various categories of products and to avoid accidental or intentional mixtures, the regulation recommends a denaturation of the SRM.

A memorandum of the Ministery of Agriculture (DGAL/SDHA/N.97/N°8143) of September 11, 1997 stipulates that the colouring or the denaturation of high risk wastes intended for the incineration is mandatory in order to identify them throughout the elimination chain. This note also fixes the list of the products which are allowed to carry out colouring or denaturation and precises that this list can be modified on the initiative of the veterinary services. It should be noted that the annual production of SRM in France is about 500 000 tons out of approximately 2,5 million tons of meat waste.

Moreover, the products used (tartrazine, flour of alfalfa, purple of methyl, cresyl and the dyer patent blue) ensure only short-term marking, i.e. at the first steps of the transformation processing. Indeed, these products do not resist to thermal processing. Thus, the marking and the traceability of the SRM disappear after cooking, i.e. at a stage where the original products are not identifiable any more on the anatomical point of vue.

The techniques which are available to detect the origin of the components of the MBM are expensive and heavy to implement [1]. Thus the work carried out postulate that, in order to obtain a perfect separation of the SRM, it is necessary to have a marker which can be applied at the slaughterhouse and which can be detected in the MBM as well as in the tallow.

CHOICE OF A TRACER

1. Specifications of the tracer

The SRM are collected in the slaughterhouses, then transported towards the rendering plants where they are transformed into MBM according to the following process [2]:

- Operation of grinding: at various levels of the manufacturing of the MBM, the materials are crushed to decrease the size of the particles and thus to contribute to the optimization of some parameters such as the diffusion of heat, water and fat at the stages of drying and pressing. Moreover each type of MBM must match criterias defined by standards (size of the particles < 50 mm, lipid level...),
- Operation of drying / cooking: the materials are introduced into an oil bath at high temperature (150 °C) which causes the desorption and the evaporation of the water that they contain. When the materials are dehydrated, the temperature of the oil bath causes a cooking.
- Operation of pressing: according to the content of fat desired for a type of MBM, the cooked materials pass in a press which allows the extraction of fat. In the case of MBM with low content of fat, a degreasing is completed by action of an alcane (hexane used in the oil-works).
- Operation of sterilization: the regulation imposes a sterilization of the MBM with the following scale: 20 minutes with 133 °C under 3 absolute bars.

Once transformed into MBM, the SRM are transported towards the incinerators after possibly a time of storage.

All these stages are sources of constraint for the tracer and Table 1 shows the various characteristics which an effective tracer must have.

Table 1. Characteristic of the tracer

Characteristics	Stage of the process
Contact food	Slaughterhouse
Absence of toxicity	Slaughterhouse – Rendering
Cleanable	Slaughterhouse – Transport – Rendering
Limited polluting load	Slaughterhouse – Transport – Rendering
Low cost	Slaughterhouse – Rendering
Visually detectable	Slaughterhouse
Strong inking on all materials Resisting to scrubbing, solvents	Slaughterhouse – Storage – Transport – Rendering
No suspension setting in the environment of the plants	Slaughterhouse – Rendering
Easy to use for the operator	Slaughterhouse – Rendering
Not damageable (microbiological, chemical)	Storage – Transport
Not aggressive for the equipments	Rendering
Resisting to the processing	Rendering
Resisting to cooking & sterilization	Rendering
Not very magnetic	Rendering
Low detection threshold	Slaughterhouse – Transport – Rendering
Able to be incinerated	Site of incineration

2. Choice of a tracer

Various solutions to trace wastes are possible: fluorescent tracers, radioactive tracers, magnetic tracers [3-8]. But the specifications of the tracer previously exposed reduce the choice to the fluorescent tracers. The magnetic tracers can cause disturbance and disappear at the iron detector of the rendering plant; as for the radioactive tracers, they are not well adapted to an industrial application because of their implementation constraints.

The list of the compounds which can be used as fluorescent tracers is long [9]: fluorescent pyranine, rhodamine, inks, paintings, eosine, fluorescein... Within the framework of our study, several of them were tested. Products were marked and processed into MBM. A qualitative analysis of marking (visual monitoring) was carried out and only two tracers were retained: rhodamine B and pyranine. The other products disappear during the process and the MBM are not fluorescent.

We then retained only the pyranine [10] because its capacity of fluorescence is higher than that of rhodamine B at the end of the process.

STUDY OF THE PYRANINE FIXATION

1. Materials and Methods

The purpose of this experimental protocol is to measure the capacity of animal material making up the MBM (lean meat, bone, brain, fat, bowels) to fix the tracer. To be placed under the optimum conditions for marking, a soaking method is used. It ensures a maximum contact between the tracer and the material.

Each experiment is carried out on material samples of 100 g, for a volume of solution in tracer of 1 l. The concentration in tracer was fixed at 0,005 g/l, because of detection limits, and optimal marking conditions. Marking is measured in an indirect way. The system of acquisition records the variations of quantity of tracer in the solution. The quantity of disappeared tracer corresponds to the tracer fixed on the material.

Figure 1 presents the diagram of the installation used to measure the fixation of the tracer on the various kinds of materials which compose the high risk MBM.

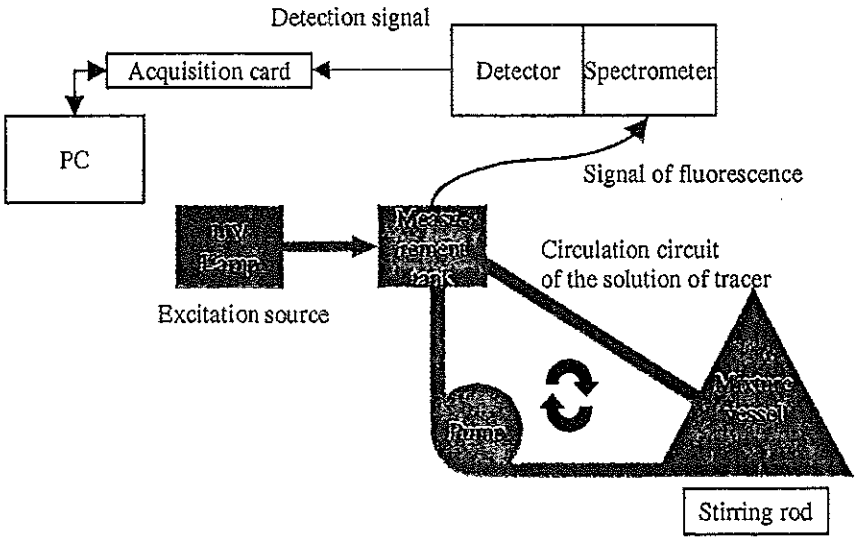

Figure 1 : Measurement device

A pump (Steriflow model 600) ensures the circulation of the tracer solution. The aspiration is made at the level of the mixture vessel, and the exhaust pipe leads the solution to the bottom of the measurement tank. Under the experimental conditions, the flow of the pump is about 100 l/h. The junctions between the mud of mixture, the pump and the measurement tank are ensured by flexible and transparent plastic pipes of small diameter (2 mm).

In order to generate a continuous spectrum of wavelengths which contain the wavelengths of excitation of the selected tracers, a high pressure lamp Xénon Mercury of a power of 200 W (ORIEL, model 66057), supplied with a variable power generator in the range 50-200 W (ORIEL, model 68806) is used.

The guiding of the fluorescence signal from the measurement tank to the spectrometer is ensured by an optical fibre (ORIEL, model 77553). The spectrometer used (ORIEL, model MultiSpec^{TM} 77400) is coupled with a PDA (Photo Diode Array) detector (ORIEL, model InstaSpec^{TM}II), allowing the detection of all the wavelengths between 200 and 750 nm.

This spectrometric method has the advantage of measuring all the wavelengths coming from the fluorescence of the tracer, unlike the traditional spectrometry which allows the analysis of only one wavelength at the same time.

The PDA detector is connected to an acquisition card and a PC which performs the recording. The data are analysed by the software provided by the manufacturer.

The solution of pyranine used is prepared by putting the tracer powder in distilled water. The concentration unit used is the gram per litre (g/l), owing to the fact that the purity rate of the powders is not known accurately (about 90 %). The quantity of material needed for the preparation of the solution is weighed on a balance. The glassware is privileged insofar as glass is inert to the tracer sorption, avoiding, by this way, a loss of masses during the preparation of solutions.

The animal material is very heterogeneous. It is impossible to find two pieces having the same characteristics, and so, it is difficult to speak about representativeness of the samples. This heterogeneity could be the expression of a different rate of sorption in tracer for several samples from a same batch. Each sample represents a material mass of 100 grams. The materials are cut out, with a knife, in cubes of 1 cm size. Some materials such as the bowels or the bones are difficult to dimension, and their cutting is more approximate. Although the meat cubes are cut most precisely possible, the product are not a rigid structure and consequently becomes deformed and then not preserving a constant surface offered to the tracer.

The tissues used for the samples preparation, can be preserved in a refrigerator at the temperature of 0-1 °C, to avoid any microbial development. It is important that the materials are not stored at negative temperatures, because a freezing/unfreezing would involve a modification of the structure (for the thin one: bursting of the sarcomeres, water loss), and consequently one would move away from the real conditions of the meat state at the various marking stages.

2. Fixing of the pyranine

MBM is made of 5 types of materials: the lean, the fat, nervous tissues, bowels and bones. Each type of material was studied separately.

The tracer is rather well on the lean (see Table 2). The variations of fixation intra and inter muscles are relatively weak, and show the homogeneity of marking on the lean material. The repeatability of fixing was shown within a same muscle, and for two different muscles.

The fixation obtained for the bowels and nervous tissues is of medium quality because of a noise effect coming from the breaking up of these materials during the experiment. One can note that the fixed quantities of tracer are lower than those obtained on the lean meat (see Table 2).

For the fat and the bones, the device has not allowed to measure the quantities of tracer which were fixed: in the case of the fat, the materials have involved a dirtying of the measuring cell which did not allow a correct measurement; as regard the bones, one notes that the tracer is not fixed.

Table 2. Fixing of the pyranine according to the type of product for a concentration in tracer of 5 mg/l

Kind of product	Tracer fixed in 15 mn
Lean	70 %
Bowels	30 %
Nervous tissues	40 %
Fat – Bone	Not measured

IMPLEMENTATION OF THE TRACER

In order to have conditions closer to reality, tests were carried out to validate a marking by spraying. A marking with a concentration of 10 mg/l in immersion is equivalent to a marking by spraying with a concentration of 10 g/l. This concentration was validated on lean materials with the complete cycle of the process: cooking, sterilization, pressing. The materials were sprayed with the solution during 2 minutes.

To see if the operations order, cooking and sterilization, has an influence on the marking, wastes were marked then processed with different operation order. One thus could note that the chronology has not influenced the marking quality.

The first means to see if a MBM is made from marked products is visual. Under a UV lighting, the marked MBM emits a green/yellow light characteristic of pyranine marking (see Figure 2).

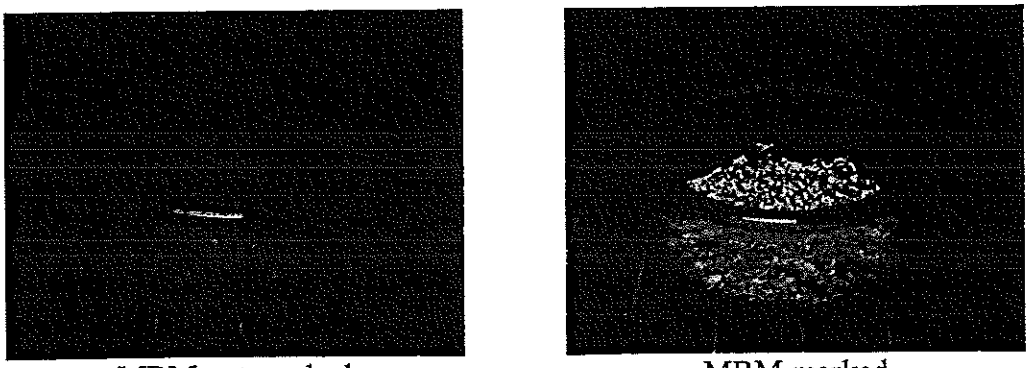

MBM not marked MBM marked

Figure 2. Difference between not marked and marked MBM

One can also use a radiometer in order to quantify the light emitted by the MBM. The radiometer is a device equipped with a photosensitive cell which reacts to a specified wavelength. When this cell is excited by a light radiation having the good wavelength, an electric tension appears on the radiometer terminal. In the case of the marked MBM, an excitation of the MBM by a UV lamp results in an emitting light (wavelength of 510 nm) coming from the pyranine fluorescence: this radiation can then be measured by the sensor.

Tests were carried out in order to measure in a quantitative way the evolution of marking in time. Two samples of MBM of 300 g, one marked and the other not, were dried. The two samples were then exposed to the sun light during several days

in order to see if it exists a degradation of marking. Measurements with a radiometer were made at days 1, 2, 4, 7, 14, 21. The Figure 3 presents the results obtained.

This experiment shows that the intensity of light emitted by marked MBM at wavelength of the pyranine is three times higher than that of the not marked MBM. Also the marking has an excellent holding in time (see Figure 3).

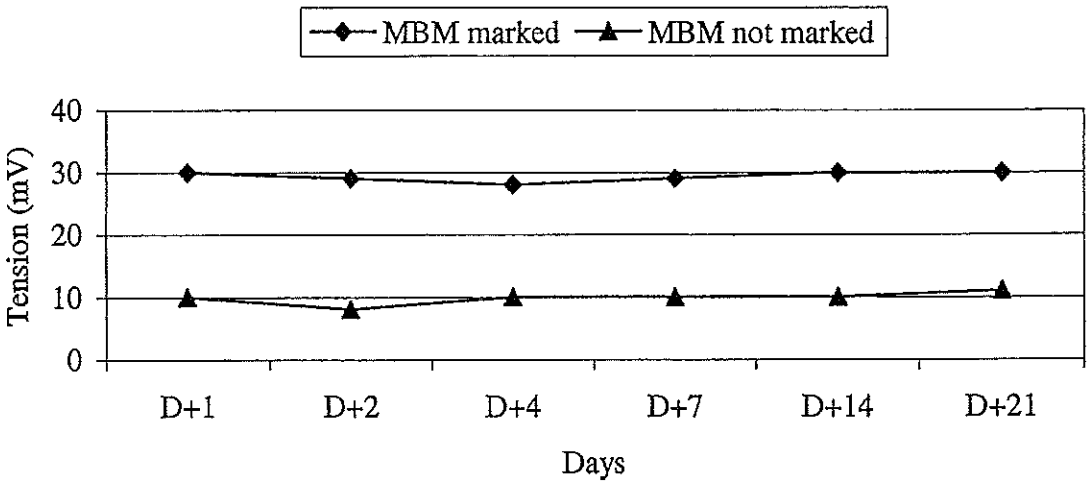

Figure 3. Evolution of marking in time

CONCLUSION

The objective of this study was to show the feasibility of marking the Specific Risk Materials at the slaughterhouse with a tracer and the ability to detect the tracer in the Meat and Bones Meal obtained after the transformation process. The redaction of the specification of the tracer which can ensure this traceability allowed the selection of fluorescence tracers. They are able to resist to the constraints of the MBM manufacturing process.

Preliminary tests show it is possible to select two tracers whose characteristics and performance towards the process constraints allow their detection in MBM: rhodamine B and the pyranine. The pyranine was privileged for its higher fluorescent capacity.

The study of the pyranine fixation on the various kinds of materials entering in the composition of the MBM was considered. The results are encouraging in the sense that the pyranine is fixed satisfactorily on all the materials, except the bones, but they are not high risks products. The detection of the pyranine is possible at all the stages of the process as well visually by an operator as using an automatic device of radiometer type. Moreover the tracer keeps its capacity of fluorescence in time.

In a new phase of the project, it will be necessary to carry out other tests such as detection on a mixture of marked MBM with not marked MBM or vegetable meal in order to quantify the minimal detection threshold in the event of cross contamination. A test on factory site will be also essential to validate the functioning of the method as well as the optimum quantity of pyranine estimated during the previous experiments.

REFERENCES

[1] Shilton N., Colgan S., *An investigation into traceability strategy for meat and bone meal*, Report of Agriculture and Food Department, University of Dublin (2000).
[2] Dametto H., *Identification par traceurs et détection des produits à hauts risques dans la filière farines de viandes et d'os : cahier des charges traceur*, Report of ADIV, Clermont-Ferrand (1998).
[3] Mabit J., Riou Y., Novales B., Legrand J., *Choix des traceurs pour la détermination des temps de séjour des faines dans les conditionneurs*, Traceurs et Méthodes de Traçage, Nancy (1198), 189-194.
[4] Cai S.S., Stark J. D., *Evaluation of five fluorescent dyes and triethyl phosphate as atmospheric tracers of agricultural sprays*, J. Environ. Sci. Health, B32(6) (1997), 969-983.
[5] Poirier G., Desjardin R., Brière F., Dagenais D., *Mesure en continu de débits d'eaux usées à l'aide d'un traceur fluorescent, la Rhodamine WT*, Sciences et Techniques de l'eau, Vol.20 n°2 (1997), 127-130.
[6] Davis S. N., Thompson G. M., Bentley H. W., Stiles G., *Ground-Water Tracers – A Short Review*, Ground Water, Vol. 18 (1980), 14-23.
[7] Girma J.P., Développement de nouvelles méthodes de marquage radioactive des composes d'intérêt biologique, Thèse Paris 6 (1994).
[8] Buron M.P., Elaboration, caractérisation structurale et morphologique, propriétés magnétiques de pigments composites ferrites de cuivre-magnétite, ferrites de cobalt-magnétite, Thèse Toulouse 3 (1996).
[9] Viriot M. L., André J. C., *Fluorescent dyes: a search for new tracers for hydrology*, Analusis Vol. 17 n°3 (1989), 97-111.
[10] Bayer, Pyranin 120, Fiche de données techniques société Bayer (1997).

A BIOCHEMICAL TRACER DETECTION TO QUANTIFY THE INTENSITY OF THERMAL PROCESSING AND TO OPTIMISE FOOD QUALITY

S.C. Eliot-Godéreaux, A. Goullieux, M. Quéneudec t'Kint

Transfer and Reactivity in Condensed Media Laboratory, IUT Amiens, 80025 Amiens cedex 1, FRANCE

Abstract. This study aimed to develop a new time-temperature integrator (TTI) to quantify the effects of high temperature short time (HTST) processing on food quality. A product of non enzymatic browning was selected as a potential tracer and its formation was studied in a glucose-serine model system. The formation kinetic of the tracer was modelled as a function of temperature and time of thermal treatment applied. Three models described well the time and temperature dependence of the tracer formation and fitted well with experimental data. These models were validated by comparing the intensity of thermal treatments applied in a laboratory-scale ohmic heating process to the predicted intensity given by the tracer. The best model resulted in an average absolute error inferior to 15%. The tracer was then used in an industrial continuous ohmic heating installation to estimate quantitatively the thermal effect of processing in various experimental conditions of flow rate and holding tube. This method offers new perspectives for HTST process optimisation and control of food quality.

INTRODUCTION

Food thermal processing requires optimisation in order to maximise the microbiological quality of the product and to minimise sensorial or nutritional degradation induced. To estimate the lethality delivered to a food product during processing, current methods rely on destruction kinetics of micro-organisms (*Bacillus stearothermophilus* spores[1,2]) or other substances such as enzymes[3] or salts[4]. In the first case, destruction occurs very quickly at high temperatures and the response is only qualitative (minimum sterilising value); in the second case, destruction rate is very low and very precise analytical methods have to be used.

Some researchers[5] suggested the use of compounds thermally produced in foods to quantify the effect of thermal processing. A chemical tracer, nitrophenolate ion, produced by hydrolysis of p-nitrophenol β-D-glucopyranoside in a borate buffer at pH 11, was developed[6]. This ion formation kinetic was modelled and used to quantify the effect of thermal processing on food quality. This TTI appeared to be a good predictor of the cook value for conditions not exceeding F_0= 10 min, beyond which hydrolysis was completed. This sterilisation level is unfortunately very quickly attained in HTST processing.

Among the numerous compounds issued of non enzymatic browning (Maillard reaction), 2,3-dihydro-3,5-dihydroxy-6-methyl-4(H)-pyran-4-one was identified[7] and this molecule formation was correlated (at low temperatures) with the lethality endured by food products, estimated from the reduction of *B. stearothermophilus* spores[8,9]. The rate of Maillard reaction is however known to be affected by many factors and the reaction scheme used was simplified in this study to avoid any external interaction susceptible to interfere with the formation kinetic of the tracer[10].

This study aimed at characterising a new tracer, at modelling its formation kinetic at high temperatures, and then at using it as a TTI to quantify the thermal treatment endured by food products in various configurations of a continuous ohmic heating installation.

MATERIAL AND METHODS

1. Samples preparation and identification of the tracer

An aqueous solution containing 15% (w/v) D-glucose and an equimolar quantity of serine was prepared with Ultra High Quality (UHQ) grade water. Volumes of 1 ml of the solution were placed in glass flasks: 4 mL capacity for the modelling phase, 1.5 mL capacity for the validation and prediction phases (Spectrophysics, Alltech, Templemars, France), closed with phenolic caps and teflon gaskets.

The chemical identity of the biochemical tracer was determined during preliminary experiments. Several samples of the glucose-serine mixture, previously heated in various temperature and time conditions, were analysed by gas chromatography-mass spectrometry[7]. The mass spectrum obtained was similar to the one attributed to 2,3-dihydro-3,5-dihydroxy-6-methyl-4(H)-pyran-4-one. Analyses concluded that this molecule was the major product of the reaction.

Samples were scanned in the 240-460 wavelength range. A peak was systematically observed around 285 nm confirming that a spectrophotometric detection at 285 nm wavelength can be used for 2,3-dihydro-3,5-dihydroxy-6-methyl-4(H)-pyran-4-one determination[5].

2. Thermal treatment of samples

2.1 Kinetic modelling

Thermal treatments, performed in triplicates, were carried out in a dry bath (Bioblock Scientific) at temperatures ranging from 100°C to 148°C and for sets of time varying between 1.5 and 120 min.

2.2 Kinetic validation

Thermal treatments, performed in duplicates, were carried out in a 5 kW laboratory-scale ohmic heating cell[11] at the same temperatures as previously and for sets of time ranging between 6 and 90 min. Five to seven glass flasks were suspended in the cell and 1 L of a brine solution (0.5% w/w NaCl) was added as conducting fluid (Figure 1).

2.3 Prediction of thermal treatment intensity

The tracer was used to determine the intensity of thermal treatments endured by food products in a continuous ohmic heating installation (APV Baker, Crawley, UK). A syringe was specially designed and manufactured (MEGECO, Cotenchy, France) for tracer injection at the bottom of the ohmic column (Figure 2). The installation was studied with 3 different configurations: not intense (high flow rate, short holding section), very intense (low flow rate, long holding section) and intermediate. 15 to 20 flasks were injected for each experimental run.

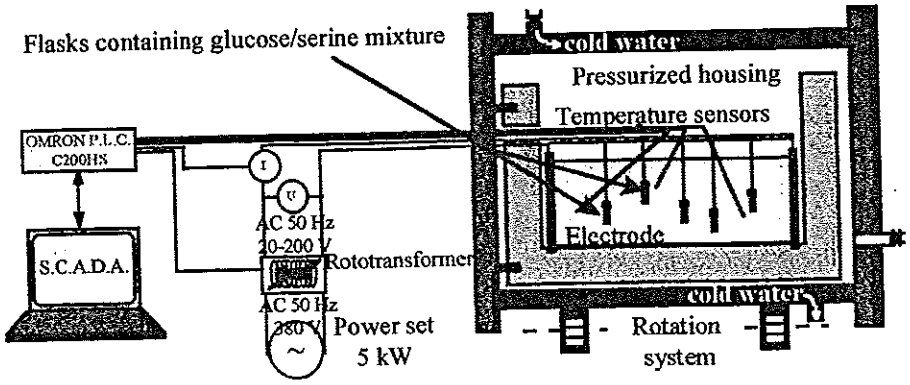

Figure 1. Schematic description of the laboratory-scale ohmic heating device

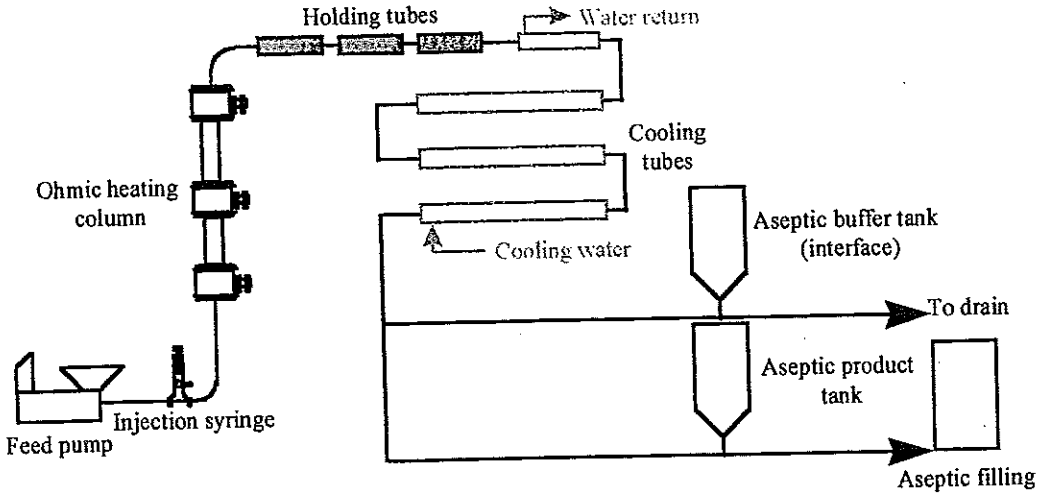

Figure 2. Schematic diagram of the APV ohmic heating installation

3. Tracer formation quantification

Aliquots of heated mixtures were recovered after thermal treatment and were centrifuged at 12,000 x g at 4°C for 12 min (Sigma 2 K 15, Bioblock Scientific) to reduce any potential deposit susceptible to interfere with subsequent measurements. Absorbance measurements at 285 nm were then performed with a Beckman DU 640 UV-Visible spectrophotometer (Beckman Instrument Inc., Fullerton, California, USA). Samples were diluted with UHQ grade water in order to obtain absorbance signals on scale. For each sample, the mean value of triplicate measurements was recorded.

4. Statistical treatment of data

Experimental data were fitted to different kinetic models using Sigmaplot® 5.0 software (SPSS Science Software Gmb, Erkrath, Germany). The models presented were all found significant at a 99% level.

RESULTS AND DISCUSSION

1. Experimental data

The changes in absorbance at 285 nm of the heated glucose/serine mixture as a function of heating time at 100, 112, 133 and 148°C are reported in figure 3. Error bars on graphs represent the standard deviation of measurements. Absorbance values measured in heated samples increase with heating duration at each of the temperature studied. The shape of the curve is similar in every case and seems to follow exponential or power law model. No slowing tendency of the reaction was observed. Absorbance values increase very quickly with increasing temperature of reaction as well: those recorded with samples heated at 148°C reach, after few minutes, levels far greater than those measured with samples heated at 100°C for long times. The kinetic of the reaction looks very long at this last temperature, and seems to indicate that the reaction may be negligible below this temperature. Temperature and time effects were found highly significant by ANOVA ($p<0.0001$).

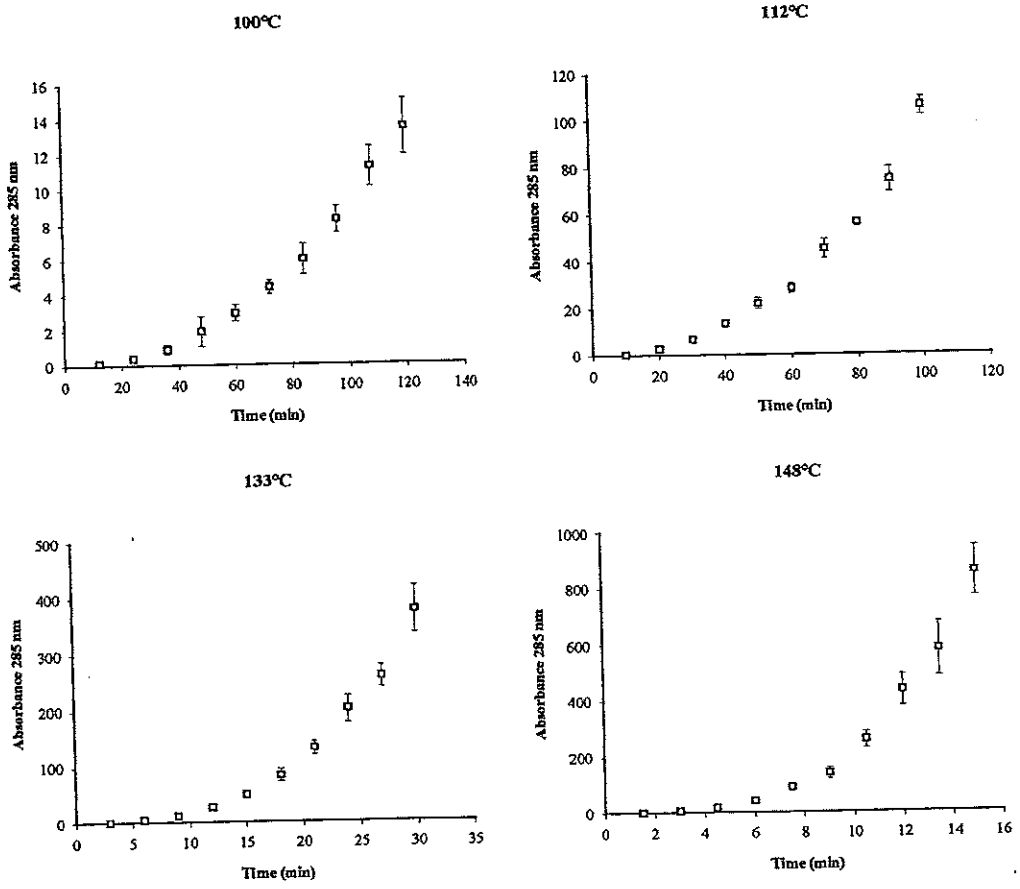

Figure 3. Absorbance measurements at 285 nm of glucose/serine heated mixture

2. Kinetic modelling

Experimental data were first compared to theoretical models and the model parameters were calculated for each level of temperature. The correlation of these parameters with temperature was then found and the general law representing absorbance changes with temperature and time was finally expressed. Four kinetic models, 2 or 3 parameters exponential law or power law, were fitted to experimental data. The 3 parameters power law model was not found significant with some experimental data and the only three other models are described. The regression between theoretical expression and experimental data was found very significant by ANOVA ($p<0.0001$) and the correlation coefficient of the regression equation was >99%.

$$A_{285} = x_1 e^{y_1 t} \quad (1)$$

$$A_{285} = x_2 e^{y_2 t} + z_2 \quad (2)$$

$$A_{285} = x_3 t^{y_3} \quad (3)$$

It was noted that parameters x_i, y_i et z_i vary logically with temperature (data not shown) and the best correlation was searched. The correlations expressions and the corresponding parameters values x_i, y_i et z_i are detailed in table 1.

Table 1. Correlation between the models parameters and temperature

Model	Correlation	R	Parameter	Value ± standard error
1	$x_1 = x_1' + aT$	0.997	x_1'	-24.81 ± 1.64
			a	0.254 ± 0.013
	$y_1 = Ae^{-\frac{E_a}{R(T+273.15)}}$	0.995	A	$32.63\ 10^6 \pm 0.76\ 10^6$
			E_a	$65.13\ 10^3 \pm 0.17\ 10^3$
2	$x_2 = x_2' + bT$	0.999	x_2'	-46.64 ± 1.27
			b	0.49 ± 0.01
	$y_2 = Ce^{-\frac{c}{T+273.15}}$	0.993	C	$29.65\ 10^6 \pm 0.80\ 10^6$
			c	7866.3 ± 25.7
	$z_2 = De^{dT} + z_2'$	0.999	D	-2.84 ± 0.53
			d	0.022 ± 0.001
			z_2'	23.60 ± 2.24
3	$x_3 = Fe^{fT}$	0.999	F	$2.35\ 10^{-9} \pm 0.05\ 10^{-9}$
			f	0.1194 ± 0.0002
	$y_3 = y_3' + gT$	0.997	y_3'	-0.128 ± 0.161
			g	0.0230 ± 0.0013

With the first model (first order kinetic), an activation energy of 65 kJ.mol^{-1} was obtained for the reaction between glucose and serine in these experimental conditions, which is equivalent to a z-value of 44.2 ± 4.5°C. This value is of the same magnitude order as activation energies of Maillard reactions obtained for various sugar / amino function systems[12, 13, 14]. The resulting z value indicates that the absorbance measurement constitutes a good indicator of the cooking level endured by the system. Finally, the variation of absorbance (A_{285}) as a function of temperature (T in °C) and time (t in min) of heating can be modelled by the three following models, whose constants are given in table 1.

$$A_{285} = (x_1' + aT)e^{Ate^{-\frac{E_a}{R(T+273.15)}}} \quad (4)$$

$$A_{285} = (x_2' + bT)e^{Cte^{-\frac{c}{T+273.15}}} + De^{dT} + z_2' \quad (5)$$

$$A_{285} = Fe^{fT}t^{(y_3' + gT)} \quad (6)$$

3. Comparison between experimental data and predicted values

Theoretical values of absorbance given by the three models were compared to experimental values measured (Figure 4).

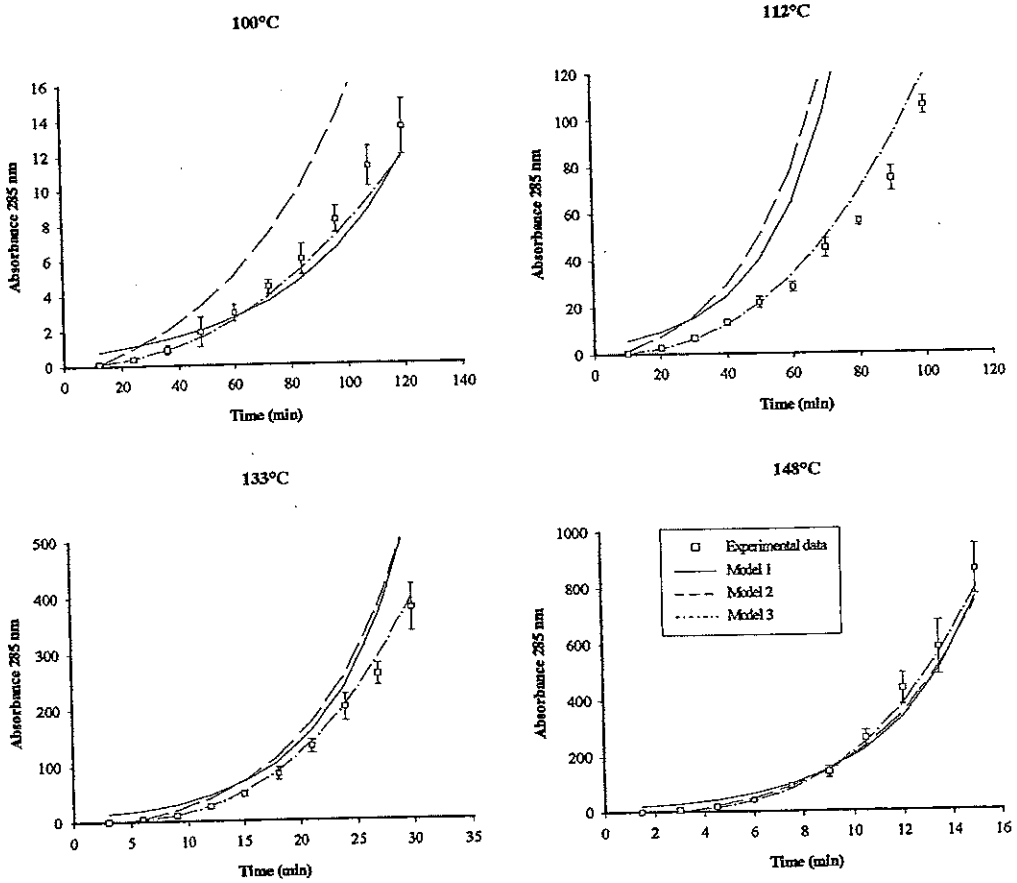

Figure 4. Comparison between experimental data and predicted values

Excepted predictions observed at 112°C, the predicted values of model 1 are relatively close to experimental data. Values predicted by the second model are overestimated in most cases, particularly at low temperatures. The predictions of model 3 closely fit to experimental data, even at 112°C. Predictions are more reliable at high temperatures, where they are closer to experimental data for all 3 models.

4. Validation of kinetic modelling

New thermal treatments were applied to the glucose-serine system in a laboratory-scale ohmic heating installation. Equations 4, 5 and 6 were used to calculate, from the absorbance value and the experimental temperature of reaction, a theoretical duration of the thermal treatment applied. This theoretical value was then compared to the experimental time of treatment.

Predictions given by the first and the second models were rather mediocre at low and high temperature but were improved at 133°C (data not shown). Model 3 appeared as the most interesting model, with a mean prediction error below 15%. The tracer can thus be used to get a prediction of the intensity of thermal processing in a continuous ohmic heating installation.

5. Quantification of thermal treatments intensities

A product composed of 15% (w/w) potato cubes (precooked 15 min at 75°C with 5% NaCl) and 85% of a starch solution (7% Thermtex, 0.35% NaCl or 5% Colflo 67, 0.37% NaCl) was used for experiments in the continuous ohmic installation. 125 to 160 kg of the product were processed for each trial. Experimental conditions used are described in table 2. Flasks were injected in the installation during processing and were collected at the exit of the product tank at the end of trials (cleaning phase). From the absorbance measurement on collected mixtures and from the experimental temperature in the holding section, it was possible to estimate a theoretical duration of the global thermal treatment endured by the product in the installation using equation 6. The range of predictions given by numerous tracers are detailed for each experimental run in table 2.

Predictions bring out the intensity of thermal treatment applied and the hierarchy induced by the choice of experimental variables. The thermal treatment applied during the first run is confirmed as being the less intense. The severity of the second trial is confirmed and the intensity of the third experiment is referred to as intermediate. The predicted intensities of thermal treatments applied are however far more severe than expected from the residence time in the holding section estimation (sterilising value). The tracer reveals that the thermal effect endured by the product is probably not restricted to the holding section. Both heating and cooling sections may significantly contribute to the global thermal treatment. The range of predictions of thermal treatments duration is expanded on several minutes scale. This heterogeneous nature of the thermal treatment applied confirms previous observations: the great dispersion of passage time distribution for particles in the ohmic column[15], which was assumed to be responsible for overcooking of particles during particles/liquid sterilisation.

Table 2. Experimental conditions used and predictions given by tracers

Trial	1	2	3
Electrical conductivity at 65°C ($S.m^{-1}$)	1,51	1,67	1,6
Flow rate (kg/h)	119	100	115
Holding temperature (°C): Tref	132	130	132
Holding volume (L)	1,43	2,69	2,06
Holding time (min)[a]	0,73	1,64	1,09
Sterilising value at Tref (min)	0,7	1,6	1,1
Absorbance (285 nm)	0,10-1,73	2,1-4,8	0,73-6,8
Predicted intensity (min) at Tref	1,8-5,0	5,9-7,9	3,7-7,9

[a] Calculation based on a plug flow assumption

CONCLUSION

A biochemical tracer was characterised and its formation kinetic was studied and modelled in order to use it as a TTI to evaluate the intensity of thermal treatments applied in a continuous ohmic heating installation. This TTI appeared to be a good predictor of the cooking effect endured by food products. It may also be used to characterise other thermal processes. The perspectives of this work are interesting because it may be possible to change the formation kinetic of the tracer, by simply changing the reactants concentration, and to attain different TTI. The use of double or triple response TTI systems makes then possible to evaluate the impact of a thermal process on a particular target substance.

REFERENCES

[1] Jonsson, U., Snygg, B.G., Härnulv, B.G., Zachrisson, T., J. Food Sci., 42(5) (1977), 1251-1252, 1263
[2] David, J.R.D., Merson, R.L., J. Food Sci., 55(2) (1990), 488-493, 515
[3] Van Loey, A., Hendrickx, M., Ludikhuyze, L., Weemaes, C., Haentjens, T., De Cordt, S., Tobback, P., J. Food Prot., 59(3) (1996), 261-267
[4] Berry, M.F., Singh, R.K., Nelson, P.E., J. Food Proc. Preserv., 13 (1989), 475-488
[5] Kim, H.-J., Taub, I.A., Choi, Y.-M., Prakash, A., *Chemical markers for processed and stored products.*, Ed. Lee T.C., Kim H.-J., ACS Symposium Series 631 (1995)
[6] Williams, A., Adams, J.B., *7th International Congress on Engineering and Food*, Ed. Jowitt R., Brighton, Sheffield Academic Press, Sheffield (1997)
[7] Kim, H.-J., Taub, I.A., Food Technol., 47(1) (1993), 91-97, 99
[8] Kim, H.-J., Choi, Y.-M., Yang, A.P.P., Yang, T.C.S., Taub, I.A., Giles, J., Ditusa, C., Chall, S., Zoltai, P., J. Food Proc. Preserv., 20(1) (1996), 41-58
[9] Ramaswamy, H.S., Awuah, G.B., Kim, H.-J., Choi, Y.-M., J. Food Proc. Preserv., 20 (1996), 235-249
[10] Eliot-Godéreaux, S.C., *Contribution à l'optimisation du traitement de produits alimentaires par chauffage ohmique*, Thèse de Doctorat, Université de Technologie de Compiègne (2000)
[11] Goullieux, A., Pain, J.-P., Baudez, P., *7th International Congress on Engineering and Food*, Ed. Jowitt R., Brighton, Sheffield Academic Press, Sheffield (1997)
[12] Bates, L., Ames, J.M., McDougall, D.B., Taylor, P.C., J. Food Sci., 63(6) (1998), 991-996.
[13] Ibarz, A., Pagán, J., Garza, S., J. Food Eng., 39 (1999), 415-422.
[14] Garza, S., Ibarz, A., Pagán, J., Giner, J., Food Res. Int., 32 (1999), 335-343.
[15] Eliot-Godéreaux, S.C., Fairhurst, P.G., Goullieux, A., Pain, J.-P., J. Food Eng., 47(1) (2001), 11-22

Assessment of the bioavailability of heavy metals in soils using isotopic exchange kinetics method

G. ECHEVARRIA, E. GERARD, S. SHALLARI, S. MASSOURA, C. SCHWARTZ
and J.-L. MOREL
Laboratoire Sols et Environnement ENSAIA-INRA
2, avenue de la Forêt de Haye, BP 172, 54 505 Vandœuvre-lès-Nancy cedex, France

Introduction

Soils contaminated by heavy metals represent a threat for the environment and the human food chain. It is therefore crucial to evaluate the potential risk of dissemination of metals in the environment. Among the possible ways of food chain contamination is the soil-to-plant transfer, which can be decomposed in three main processes: i) exchange between the metal soluble fraction and the labile fractions in the solid phase, ii) transport in the soil medium (mainly diffusion in the case of metals) and, iii) absorption at the root surface. The first process can be defined as bioavailability or phytoavailability (Echevarria *et al.*, 1998; Gérard *et al.*, 2000). Bioavailability itself can be described as a combination of three capital properties of a given metal in a soil (Echevarria *et al.*, 1998): the intensity factor (concentration of the free metal in solution), the quantity factor (quantity of the metal able to exchange with the free ion fraction in solution over a given time) and the capacity factor which expresses the buffer power between the quantity factor and the intensity factor.

The isotopic exchange kinetics method gives access to these three factors in short-term assessments and therefore allows to predict the long-term transfers of metals to the plant. The method is based on the use of a radioisotope of the metal (Cd, Ni or Zn) to determine both the size of the metal pools in the solid phase that are able to exchange with the free metal ion fraction in solution and their time of exchange. Parallel pot experiments with plants in which metals in soils had been labelled confirmed the long term validity of this method since the metal taken up from the plant came exclusively from the isotopically exchangeable pool (Echevarria *et al.*, 1998). Moreover, it has been demonstrated that, despite their metal accumulation pattern, plants from metal excluders to hyperaccumulators take up metals from the same isotopically-exchangeable pools (Gérard *et al.*, 2000 ; Shallari *et al.*, 2000).

The aim of this paper was to investigate the potential risk of food chain contamination of soils from urban and industrial sites by nickel and cadmium. Therefore, the isotopic exchange kinetics method, which allows to understand the potential transfer from soil to plant of these two metals, was carried out on soil samples from agricultural, urban and industrial areas contaminated by mining, smelting and other metal-industry activities.

Materials and methods

Soils. Samples were collected in the upper horizon (0-20 cm) of eight soils (Table 1).

- One industrial soil from the nickel-mining area of Prrenjas (Albania) developed on serpentine ore containing more than 1 000 mg Ni kg^{-1}.
- Two oxisols from New Caledonia (France) close to a mining area which are devoted to food production and contain several thousands of mg kg^{-1} of total nickel, one of them showing waterlogging conditions
- Four limed silt loam luvisols with similar properties from a series located in northern France (Région Nord-Pas de Calais) showing a gradient of distance from a lead and zinc smelter and consecutively a gradient of contamination due to atmospheric deposition of industrial particles bearing Cd, Pb and Zn, exhibiting a total Cd content of 0.6, 8.9, 15.1 and 25.4 mg kg^{-1}.
- One acidic luvisol from the immediate vicinity of a brownfield in France showing high levels of cadmium and zinc.

Soil samples were air-dried and sieved with a 5-mm mesh.

Table 1: Selected characteristics of the eight soils

Soil	Soil type	Land use	Soil pH (water)	Total Ni (mg kg^{-1})	Total Cd (mg kg^{-1})
1	Industrial serpentine	gardening	8.3	1 316	-
2	Oxisol	agriculture	5.6	6 280	-
3	Oxisol, waterlogged	agriculture	6.1	9 420	-
4	Luvisol	agriculture	8.2	-	0.6
5	Luvisol	agriculture	7.9	-	8.9
6	Luvisol	agriculture	8.1	-	15.1
7	Luvisol	Brownfield	7.8	-	25.4
8	Acidic luvisol	Brownfield	6.2	-	20.3

Isotopic exchange kinetics (IEK). Soil samples were air-dried and sieved (through a 2-mm mesh) before performing IEK. A soil-water slurry (soil:solution ratio of 1:10) was equilibrated at room temperature for 17 h, and 1 mL of a $^{63}Ni^{2+}$ solution or of a $^{109}Cd^{2+}$ solution was injected into the suspension (details of the procedures are given in Echevarria et al., 1998 for nickel and in Gérard et al., 2000 for cadmium). Aliquots were sampled at several times from 1 min up to 100 min, and filtrated through cellulose nitrate (0.2-µm porosity, Sartorius). Radioactivity was counted by liquid scintillation spectrometry for ^{63}Ni and by gamma-counting spectrometry for ^{109}Cd, and stable metals were measured in solution (ICP-AES) after filtration of each aliquot. IEK were run in five replicates on each soil.

The radioactivity of the ^{63}Ni or of the ^{109}Cd isotope in solution, r_t, decreases as a function of time following Equation 3. as previously demonstrated (Echevarria et al., 1998; Gérard et al., 2000):

$$r_t/R_S = r_1/R_S[t + (r_1/R_S)^{1/n}]^{-n} + Metal_S/Metal_T$$

where r_t is the radioactivity in solution, R_S the total radioactivity added to the system, $Metal_S$ the total amount of Metal in solution (Ni_S or Cd_S in mg kg^{-1}) per

gram of soil, and $Metal_T$ the total amount of metal per kg of soil (Ni_T or Cd_T in mg kg^{-1}). For both metals, it is possible to calculate for each time t the isotopically exchangeable amount of the metal i.e. E_t (Echevarria et al., 1998; Gérard et al., 2000).

The following parameters were calculated from the IEK which fully describe the bioavailability of Ni and Cd in the soils (see details in Echevarria *et al.*, 1998): intensity factor (concentration in solution, in mg l^{-1}), quantity factor (Cd or Ni exchangeable within one minute and within 3 months, E_{1min} and E_{3mo}, in mg kg^{-1}) and capacity factor (E_{1min}/Concentration in solution, in l kg^{-1}).

Results and discussion

Nickel – Bioavailability of Ni in soils from mining areas or from agricultural soils developed on mineralised areas is usually very low in terms of percentage of total Ni (Table 2). Very often the pedological conditions have a very strong influence on the bioavailability parameters of Ni in soils (Echevarria et al., 2000). In the case of the two New Caledonian soils, the higher bioavailability in soil 3 is explained by the presence of strong hydromorphic conditions in this downslope soil whereas soil 2 is upslope and does not show any sign of hydromorphy (Becquer et al., 1995). Low E_h conditions in the second soil lead to an increase of the solubility of Ni (C_{Ni}) and also of the isotopically-exchangeable Ni. Crops grown on the two soils (especially maize) shown signs of heavy toxicity in soil 3 and no toxicity on soil 2 even though both soils display very high amounts of total Ni. Soil 1 does not show signs of high Ni toxicity either. Several associated metals (such as Cr) may be more toxic than Ni on soil 1. Therefore, agriculture shows no particular problem of Ni transfer on soil 2, whereas it should be avoided on soil 3. Phytoextraction and efficient soil drainage could be a suitable solution for soil 3. The quantity factor (i.e. E_{1min}) in soils 2 and 3 was similar to the amount of Ni extracted by DTPA as well as in the case of many other soils from the same catena, thus confirming the information supplied by IEK experiments.

Table 2: Parameters expressing bioavailability of Ni or Cd in the eight soils

Nickel	Ni_T (mg kg^{-1})	C_{Ni} (mg L^{-1})	E_{1min} (mg kg^{-1})	E_{3mo} (mg kg^{-1})	E_{1min}/C_{Ni} (L kg^{-1})
Soil 1	1 316	0.040	4.3	44.5	109
Soil 2	6 280	0.012	2.2	183.2	181
Soil 3	9 420	0.179	31.2	721.3	174
Cadmium	Cd_T (mg kg^{-1})	C_{Cd} (µg L^{-1})	E_{1min} (mg kg^{-1})	E_{3mo} (mg kg^{-1})	E_{1min}/C_{Cd} (L kg^{-1})
Soil 4	0.6	0.1	0.04	0.43	400
Soil 5	8.9	2.5	0.93	6.5	372
Soil 6	15.1	3.7	1.7	8.3	459
Soil 7	25.4	3.8	2.0	11.6	526
Soil 8	20.3	18.0	5.5	16.1	306

Cadmium – The IEK experiments allowed the measurement of the size of the isotopically-exchangeable pool, that is the phytoavailable pool of soil Cd. Despite high pH values, Cd was easily exchangeable in the four soils. Most Cd was phytoavailable within 30 d, and more than 50% was available within 90 d. This makes Cd a metal that behaves differently than Ni. As for Ni the solubility (C_{Cd}) is strongly influenced by as shown by soils. But whereas exchangeable Ni is also

strongly influenced by soil pH, exchangeable Cd seems to remain high even after a strong liming at pH values higher than 8. Soils 7 and 8 which are from the same pedological origin (except that soil 7 was limed) show this fact rather clearly. These findings have important implications in the concept of phytoextraction, a means promoted to decontaminate the soils polluted by metals.

Phytoextraction could be a means to treat these soils, in particular these Cd-contaminated soils for which, liming is not sufficient to reduce the risk of food-chain contamination. Hence, the amount of metal extracted from the soil to meet a standard based on the total metal concentration is not a satisfactory criterion to assess the actual efficiency of soil remediation of Cd. The IEK method could also be a suitable tool to determine the required number of cultures of hyperaccumulating plants to significantly reduce the risk of metal transfer to plants (Gérard et al., 2000; Shallari et al., 2000).

Conclusion

IEK have been successfully used to assess metal bioavailability in natural and anthropogenic metal-rich soils and have succeeded in predicting metal transfer to plants, especially to hyperaccumulators (Gérard *et al.*, 2000 ; Shallari *et al.*, 2000). This method allows to characterise the three main characteristics of bioavailability of metals in soils, i.e. intensity, quantity and capacity. The latter being the most difficult to assess with traditionnal chemical extraction procedures. A further step in improving the method would be to characterise for each soil sample the part of the metal in solution which is actually under the form M^{2+} rather than assuming that the total metal in solution is M^{2+}. It is therefore possible to assess the risk associated with the presence of metals in urban and industrial soils and also to evaluate the management practices on these areas. Their use has also allowed to assess the effect of management practices on contaminated agricultural, urban and industrial soils (i.e. liming, sewage sludge applications, phytoextraction). The effect of such practices is often a combined effect directly on the solubility of the metals (intensity), on the increase or decrease of the exchangeable pool (quantity) and on the decrease or increase of the capacity (Echevarria *et al.*, 2000).

References

Becquer T., Bourdon E, Pétard, 1995. Disponibilité du nickel le long d'une toposéquence de sols développés sur roches ultramafiques de Nouvelle-Calédonie. C. R. Acad. Sci. Paris, 321 IIa, 585-592.

Echevarria G., Morel J.L., Fardeau J.C. Leclerc-Cessac E., 1998. Assessment of phytoavailability of nickel in soils. J. Environ. Qual., 27:1064-1070.

Echevarria G., Massoura S., Morel J.L., 2000. Biodisponibilité du nickel après épandage de boues urbaines (Poster presentation). *In* 6èmes Journées de l'AFES : Les enjeux actuels de l'anthropisation des sols, Nancy 25-28 april 2000.

Gerard E., Echevarria G., Sterckeman T. Morel J.L., 2000. Available pools of Cd for three plant species varying in accumulation pattern. J. Environ. Qual., 29:1117-1123.

Shallari S., Echevarria G., Schwartz C. Morel J.L., 2000. Availability of nickel in soils for the hyperaccumulator *Alyssum murale* (Waldst. & Kit.). South African Journal of Science, *in press*.

FORMULATION OF FLOW MODEL IN LOW GRADE MASSECUITE FLUIDS IN SUGAR CRYSTALLIZATION PROCESS.

Griffith, M.J.

Instituto Cubano de Investigaciones Azucareras (ICINAZ), Cuba.

Abstract. A new approach for the normalisation of RTD curve obtained in tracer experiments performed at a low-grade massecuite crystallizer is described.
Taking in account the non-Newtonian behaviour of massecuite fluids, the discrete measurement of viscosity during the tracer experiment (Tc-99m) was used to smooth off the fluctuations observed in the original RTD curve, due the variation of this parameter.
Employing different software, a new flow model, based in the normalisation by viscosity is proposed. The normalised RTD curve better describes the hydrodynamic behaviour of the massecuite fluid within the exhaustion crystallizer.

INTRODUCTION

The crystallizer station in a raw sugar factory represents the last opportunity to recover sugar from solution before it is lost to final molasses The greatest complication in operating this type of low-grade exhaustion crystallizer is in setting the cooling profile. At low temperature, the solubility of sucrose is lower, but the growth kinetics are much slower, There exists an optimum cooling profile which will maximise the exhaustion of massecuite for a given residence time [1]. At the same time, with the decreasing of the temperature, generally an increase of massecuite viscosity is observed that becomes the mayor constraint to molasses exhaustion.

Several works concerning the efficiency and the optimization of crystallization processes in the sugar industry have been reported in the last few years [2-5] through the analysis of the RTD curves obtained by tracer techniques. Conventional methods to study crystal growth rates in high grade massecuite in vacuum pans [6] so as the modeling of low grade cooling crystallizer using computational fluid dynamics [3], illustrate that this subject, due its complexity is in the scope of many researchers in this field.

Taking in account this last statement, in the present report we have centered our attention in the searching of certain correlation between the pattern flux in an exhaustion low-grade continuous crystallizer and the massecuite viscosity. The final objective is to formulate the flow model in a high viscous non-Newtonian material as the massecuite is following a procedure close to that described by Nieme [7] for the expression of RTD in Z domain in transient conditions. As a first attempt, for flow model simplification, steady conditions must be continuously checked in order to perform the normalisation of the response curve only as a function of the viscosity variations in the system.

EXPERIMENTAL

1. The Air-Swept exhaustion crystallizer.

ICINAZ has developed an air-swept crystallizer for the processing of low-grade massecuite. The new technology relies on evaporative and convective cooling of massecuite fluid by direct contact with air, with significant emphasis to maximise the evaporative cooling.

The installation is a simple 500 cubic feet vessel divided in three compartments equipped with an special stirrer device that involves a series of buckets to pick up and tip sheets of massecuite through a carefully controlled flow of air (counter stream). The use of direct contact cooling with air avoids some of the major problems of water-cooled crystallizers, the high initial cost of providing the cooling surface, and then the problem of maintaining that cooling surface in a corrosive environment. In each compartment they are installed resistance thermometers for cooling profile determination. The massecuite fluid exit the unit through a gate that can be adjusted up and down for flow control. The lubrication of molasses is performed manually in correspondence with the power consumption of the motor stirrer device.

The crystallizer is fed by a constant massecuite flow rate, coming from a holding batch agitated vessel that "iron out" the flow fluctuations from individual pan drops. The aim of this active receiver is to perform a good mixing between the massecuite and the lubricated molasses, in order to feed the air-swept crystallizer with an homogeneous mixture, according to the parameters of temperature, viscosity and massecuite purity required in the design of this new type of crystallizer. According to the volume and the normal flow rate of massecuite it is expected that the average residence time of the unit will be in range of 2 hours, time relative short in comparison with the conventional Blanchard crystallizer widespread over almost all the sugar factories in Cuba.

2.**Viscosity measurements.**

During the trials, temperature of the inlet massecuite so as from the taken samples was continuously measured. Samples (1.5 Kg of massecuite) were immediately centrifuged in a laboratory basket centrifuge without any water wash using a standard procedure [8]. A part of the mother liquor (molasses) was stored for purity analysis.

The viscosity (really the consistency) was determined in the separated molasses and massecuite samples, at the same temperature as in the fluid during the test

The Brookfield Digital Rheometer Model DV-III was used for all viscosity measurements. For massecuite the disc spindle technique as recommended in [9] was employed, meanwhile that for the molasses the same technique or the cylindrical sample adapter was used over a range of shear rates. This technique allowed the consistency (K) and flow index (n) of the material to be determined.

3.**RTD studies at the Air-swept crystallizer.**

^{99m}Tc from radioisotope generator ^{99}Mo/^{99m}Tc was used for RTD studies. The tracer was thoroughly mixed with 1 Kg of massecuite before injection into the system to insure that the tracer would correctly represent the highly viscous massecuite flow. Injection was made manually with the stream inlet of the massecuite pumped from the holding vessel. The duration of this operation was always lower than 1% of the

mean residence time, for purpose of analysis, the injection was assumed to approximate a delta function input.

Sampling method at the outlet so as several detectors (3) attached to the wall of the equipment, were used to record the activity passing by the measuring points.

Home made software (Beam) so as commercial DTR8 [10] and DTSPRO [11] were used to obtain RTD curves and for modelling.

Three trials were carried out under different experimental conditions (specially varying the height of the exit gate), in order to establish certain correspondence between residence time and pattern flux with the drop of purity in the exhausted mother liquor (molasses). Discrete samples were drawn out at the inlet and outlet of the crystallizer for purity analysis and viscosity measurements. Cooling profile as a measure of the massecuite exhaustion was also carried out.

The power draw of the drive motor was continuously monitored and if it rises too high, lubrication molasses was added manually to the vessel. An attempt to find a correlation between values of power draw and the apparent viscosity in discrete samples, gave non precisely results, the high measuring range in kW of the power consumption in our case did not reflect small variations of the apparent viscosity. It seems that an electric compensation has to be coupled to this device in order to establish the well-known correspondence [12].

The preliminary results achieved in these trials, using home made software BEAM for statistical parameter evaluation of RTD curves were as follow:

In the first trial, operating the exit gate normally at a 400mm height, residence time was in order of 97-99 min. and the pattern flux was close to an ideal plug flow (number of tank =64- 68). The power draw was always below the fixed value (26 kW) and the temperature of the massecuite at the exit was 43°C. Nevertheless that the pattern flux approach the desired plug flow model, the drop of purity of the mother liquor was poor (below 2 units). There was practically no difference between the residence time of the massecuite and its separated molasses.

The second trial was performed with the exit gate situated at 500mm height (more narrow the aperture for massecuite exit). An increase in the residence time was observed (110-120 min.) and the pattern flux was close to a dispersed plug flow (n = 12-15). During this trial a clear difference between residence time of massecuite (207 min.) and its separated molasses (194 min) was achieved indicating, as it has been pointed out in our early work [13], that an exhaustion process had took place in the system.

The third trial was carried out without the previous cooling at the active receiver, with the exit gate installed at the 600mm height. Residence time increased up to 135-145 min and the pattern flux was a little far from the dispersed plug flow (n=6-8) with the evidence of some backmixing.

Purity variation of mother liquor at the inlet had a clear diminution with time and purity drop in the mother liquor at the outlet increased up to 6 units (in comparison with the mother liquor at the inlet). This fact was also reflected by the difference between residence time of massecuite (216 min) and its separated molasses(198 min) and by the exponential dependence of the cooling profile. Table.1 resumes the main results in RTD studies during these trials.

Table 1. Pattern flux and residence time in the Air-Swept crystallizer.

Trial	Residence Time (experimental), min	Residence Time (model), min	Tank in series model (n)	Gate height, mm	Purity drop mother liquor (units)
1st	99	92	64	400	1,91
2nd	112	116	12	500	4,39
3rd	139	149	6	600	5,87

4. **Modeling process.**

Two software (DTR8 and DTSPRO), were employed for modeling process of the RTD curves obtained during the trials. Statistic parameters are in good agreement with the previous results obtained by the BEAM analyzer software (Table2.).

Table 2. Statistic parameters RTD curve by different software.

Parameters	DTR8	DTSPRO	BEAM
Residence time, Exp. (min)	99,28	99,84	98,78
Residence time, model (min.)	91,38	92,17	91,00
Variance	417,69	425	406,83
Peclet	130	130	132
% Dead time	7,9	7,7	7,9

The best fit was obtained with the DTSPRO software for the model that compromises a plug flow reactor (PFR) in parallel with a plug flow reactor with axial dispersion (PFRAD) (Fig. 1)

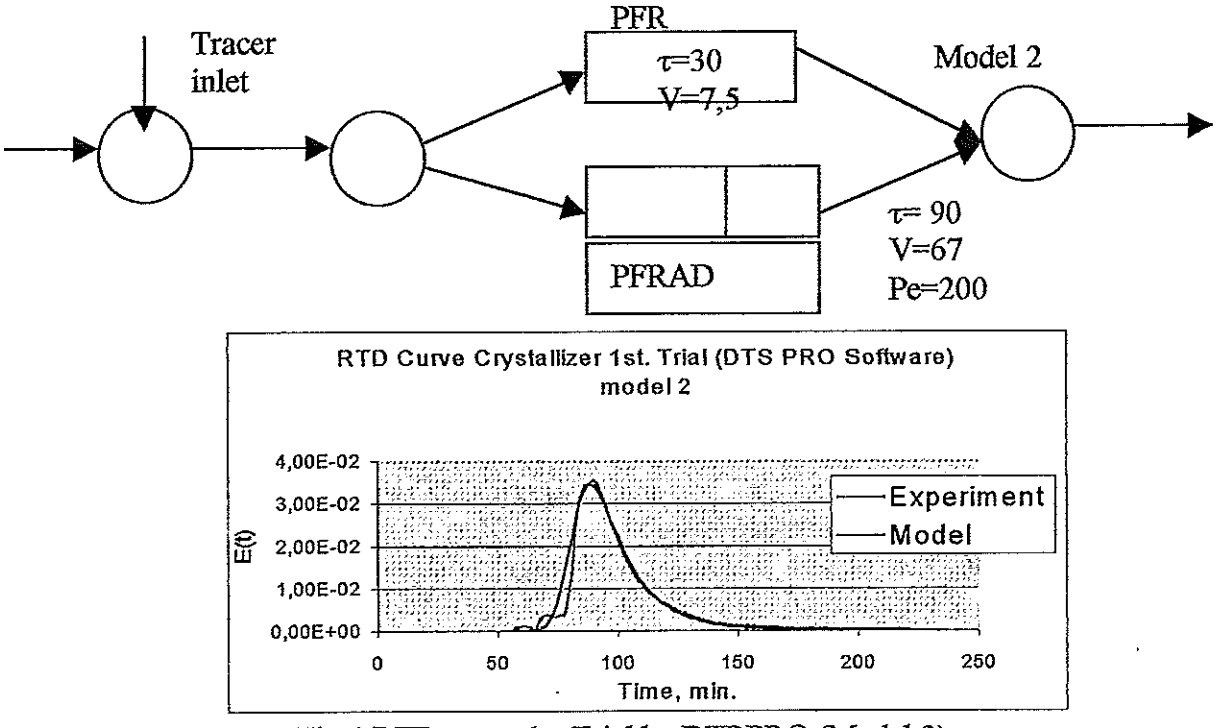

Fig.1 RTD curve 1st Trial by DTRPRO (Model 2)

Taking in account that during this first trial, viscosity values in the discrete taken samples were practically constant (no lubrication molasses was added) and therefore no normalization by this parameter was done, the presence of two parallel flows with different residence time, may be the results of some retention of the fluid provoked by the narrow aperture of the gate, that does not allow the exit, at the same time of the whole massecuite fluid.

The picture was quite difference in the case of the second experiment. It was practically impossible to fit by both software's an adequate model for the experimental curve (Fig2).

Fig.3 reflects the variation that "suffers" the viscosity during this trial

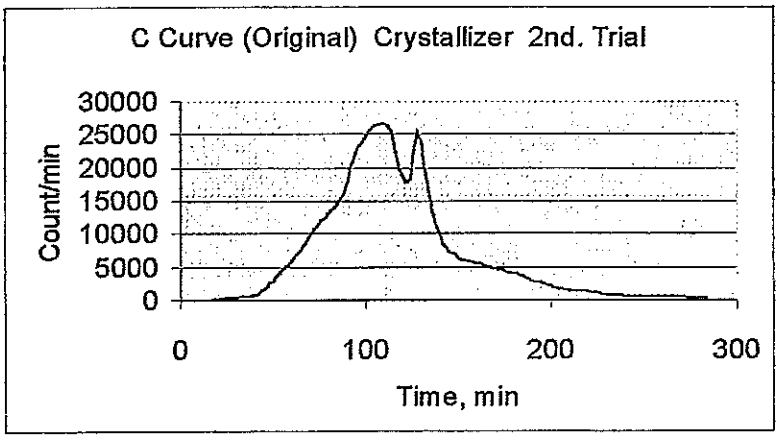

Fig.2 Original C Curve 2nd trial

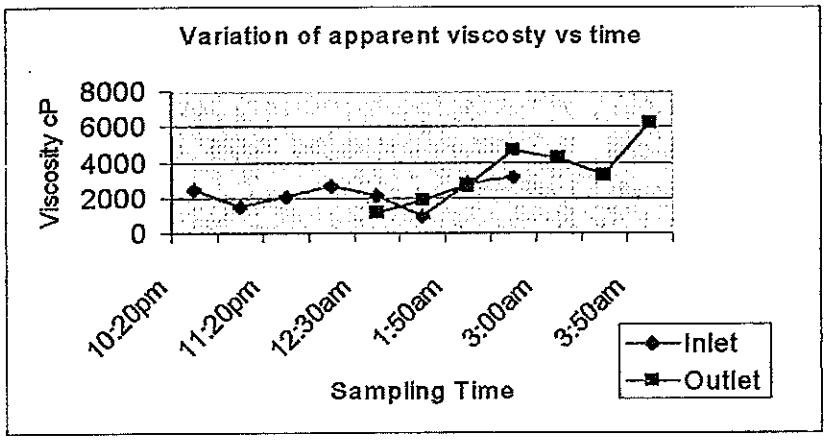

Fig.3 Variation of apparent viscosity 2nd trial.

Taking in account these variations, the original curve was adjusted using the DTSPRO software (DTR8 does not have this possibility) according again to a model that reflects two plug flow reactor with axial dispersion in parallel (Fig.4). The new approach consists in the normalization of the original RTD curve by the measuring viscosity values. Statistic parameters after optimization (iterations = 300; precision = 0.1) are shown in table3. For the sake of simplicity, viscosity values were taken

divided by 10^3 to achieve the same order in the normalized RTD curve as in the original.

Table 3. Statistic parameters two parallel plug flow reactor for the 2nd trial.

Parameters	Subsystem1	Subsystem2
Flow (%)	60	40
Residence time, min	95	105
Volume	57	42,29
Peclet	11,23	94,5

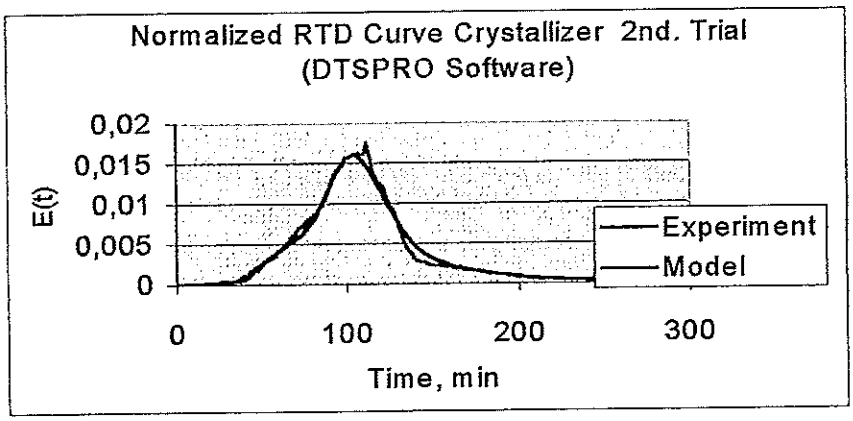

Fig 4 Normalized RTD Curve 2nd trial by DTSPRO software.

The original C Curve for the 3rd trial was still more complicated. The normalization by viscosity values achieved during this assay, "iron" the fluctuations derived from the variations of this parameter, but can not eliminate or fix the bad operation of the crystallizer that was detected and cause that we were far from the steady conditions required for these experiments.

The best fit was obtain for the model described below, that compromises an initial plug flow reactor (reflects the inlet of the pumped massecuite), follow by two parallel path or subsystems, in one of them a plug flow reactor connected to a perfect mixing cell in series with backmixing, and in other path a plug flow reactor connected directly to the exit.

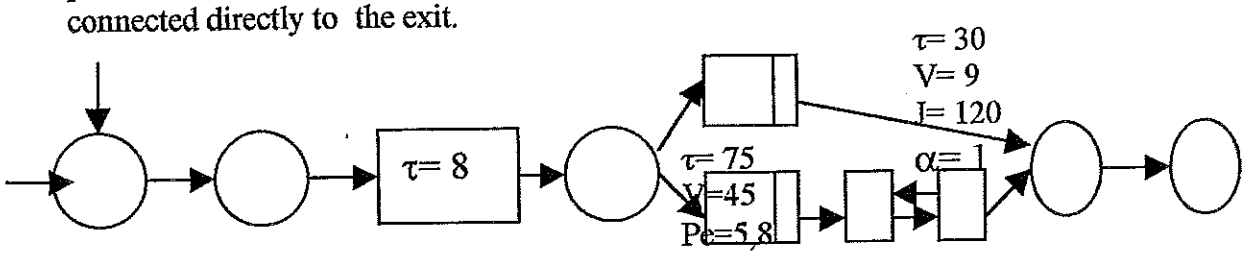

The presence of the backmixing reactor takes in account, that when the exit gate is situated at 600-mm height, the aperture is narrower and a great part of the fluid is forced to recirculate several times before leaving the unit. This effect enlarges residence time and mixing as it is reflected in table 1.

DISCUSSION

Results obtained in the present work show, that in steady conditions, pattern flux within an exhaustion crystallizer is seriously affected by the variation of viscosity that practically always take place, either by the cooling process that suffer the massecuite fluid, or by lubrication of molasses that is added, in order to increase mixing and therefore enhanced the deposition of sucrose, from the mother liquor to the formed crystal.

Nowadays, little attempt has been done in order to correlate the pattern flux in an exhaustion crystallizer with the high viscosity that normally exhibit the massecuite fluid (non Newtonian pseudoplastic behavior),and some conclusions related to the flow model of this unit, that have not take in account this fact, may be not sustainable.

The normalization of the original RTD curves by the viscosity, really "iron" some fluctuations derived from the variation of this parameter during the trial. Unfortunable we did not find, as in [12] a direct correlation between power draw of the motor and the viscosity value obtained in discrete samples, this could have improve the normalization process, allowing to have in each moment a value proportional to viscosity variations.

From the other hand, the statement that the massecuite fluid in an exhaustion crystallizer must account for an ideal plug flow [2] is not sustainable for short residence time in this unit.

Some authors [3-5] have found that in some cases the best results are obtained when some degree of mixing (axial and radial) is present in the massecuite fluid. In the this work, results show that the greatest increase in purity drop was obtained in the third trial where the flow model compromising two parallel path with dispersed plug flow reactors, showed an overall Peclet number lower than 8, indicating that a high degree of mixing was taken place in the process. In all cases where some purity drop was reached, the pattern flux shows at least two parallel paths or subsystems with different Peclet number, one of them indicating the presence of axial dispersion in the system

Finally once again, during these trials was detected a remarkable difference between residence time of massecuite packet and its separated mother liquor (molasses) at there arrive to the exit of the unit. The difference is more pronounced when a greater purity drop of the mother liquor is present. It is not easy to explain this phenomenon, but it has some relation with the exhaustion process that is taken place within the crystallizer.

As we have pointed out in early works [13] this fact reflects that the mother liquor, after some deposition of sucrose to the formed crystal, moves a little ahead from the massecuite packet to which initially it was linked. If this process is repeated infinite time, the exhausted molasses will exit early the unit than the "father" massecuite packet, and as a result the residence time of molasses will be smaller than that for the massecuite packet.

Tracers, specially radiotracers, due that they do not participate in crystal formation staying completely in the liquid phase (mother liquor), give the possibility to follow this process and can be used to evaluate the exhaustion characteristic of

any type of crystallizer by the continuous measurement of the residence time of massecuite and its separated molasses.

CONCLUSIONS

1. Pattern flux in an low-grade exhaustion crystallizer, in certain degree, depends on the viscosity of the massecuite fluid (really the molasses) in the system.
2. In steady conditions, the normalization by viscosity can smooth the fluid fluctuations observed in RTD curve of a low-grade crystallizer, allowing the possibility to find a proper model that can describe the behavior of the non-Newtonian massecuite fluid.
3. An adequate purity drop can be achieved in short residence time low-grade crystallizer, with the presence of certain degree of mixing (axial and radial) in the pattern flux. In this case at least two parallel paths or subsystems are always present.
4. There is a direct relation of the purity drop in mother liquor in a low-grade crystallizer with the difference in residence time between massecuite packet and its separated molasses.
5. From the above conclusion it follows, that tracers specially Tc-99m, taking in account they do not participate in crystal formation staying all the time in the liquid phase, could be use as an effective method for the evaluation of the exhaustion characteristics of any type of low-grade crystallizer.

REFERENCES

[1] Tait, P. J., et al., Performance trials on the STG-FCB air-swept crystallizer. Proc. Aust. Soc. Sugar Cane Technol. 20(1998),491-497.

[2] Smith, S. W., Basson, J. K.., Smith, I. A.., Radioactive tracer investigation of the flow characteristics in sugar crystallizers. Int. J. Appl. Radiat. Isotopes. 28,(1977), 839-845.

[3] Sima, M.A,. Harris J.A.,. Modeling of a low-grade vertical cooling crystallizer using Computational Fluid Dynamics. Proc. Australian Soc. of Sugar Cane Technol. 19 Conf. (1997) 448-455.

[4] Broadfoot, R., Steindl, R. J. , A model of cooling crystallization of low grade Massecuite. SRI Technical Report,. 212(1997).

[5] Brown, D.T., Alexander, K., Boysan, F., Crystal growth measurement and modeling of fluid flow in a crystallizer. Zuckerind 117(1992)., 35-39.

[6] Miller, K.F.., Broadfoot,, R., Crystal growth rates in high-grade massecuite boiling. Proc. Australian Soc. of Sugar Cane Technol. 19 Conf (1997), 440-447.

[7] Niemi, A., Zenger, K., Thereska, J-. Griffith, J., Tracer testing of processes under variable flow and volume. Nukleonika, 43(1998), 73-94.

[8] Analytical Method Manual for unified control ICINAZ, MINAZ, Cuba (1996).

[9] Broadfoot, R., Miller, K.F.., McLaughlin, R.L., Rheology of high grade massecuite. Proc. Aust. Soc. Sugar Cane Technol. 20(1998), 388-397.

[10] Maggio, G.E., Programa DTR8. Manual de Operación. NOLDOR SRL. Argentina (1998).

[11] Leclrec, J.P., DTSPRO. Software for interpretation of tracer experiments in industrial processes using systemic approach. Examples of Applications. Recent Developments Research Projects. PROGEPI, France (1999).

[12]. Attard, R. G.., Doyle, C. D., Additional heavy-up module to the reacecourse low- grade continuous pan. Proc. Aust. Soc. Sugar Cane Technol 20(1998), 357-361.

[13] Griffith, J. M., Second year report activity research contract. Cub 10050, Krakow, Poland,(1999).